frontiers | Research Topics

Molecular mechanisms and pathways in cerebellar function

Edited by
Catarina Osorio, Lilian Kisiswa and Alanna J. Watt

Coordinated by
Etsuko Shimobayashi

Published in
Frontiers in Molecular Neuroscience

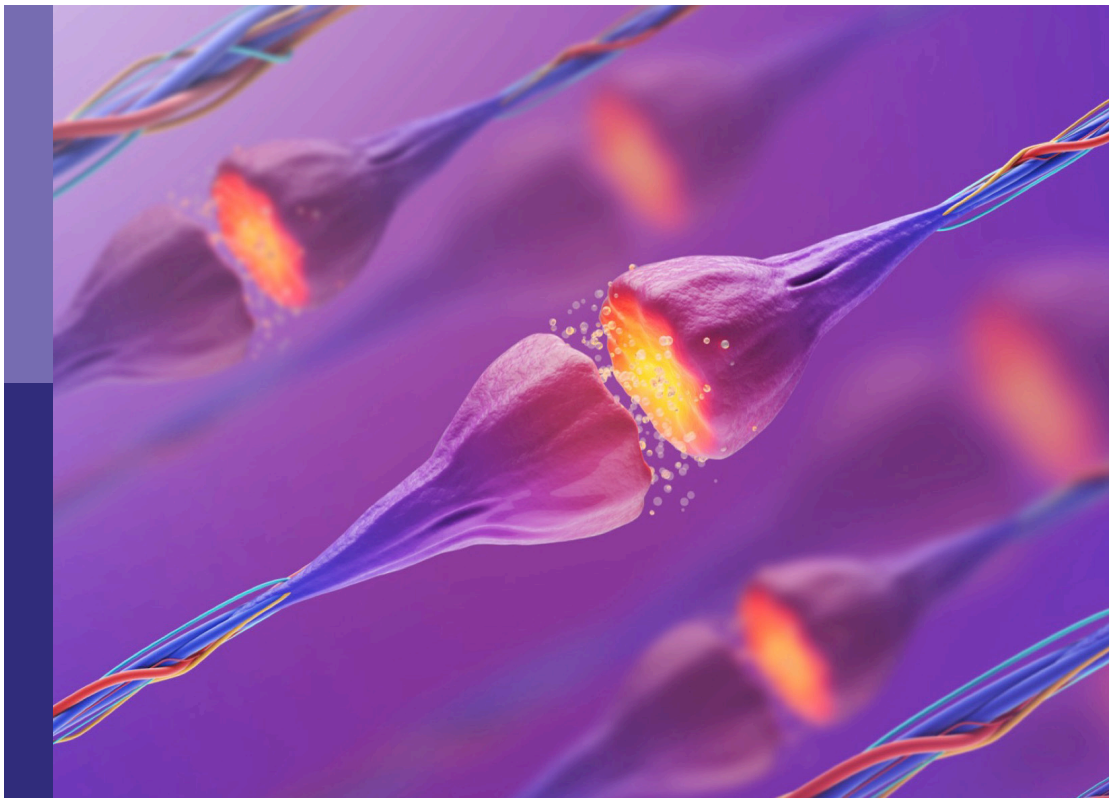

ISSN 1664-8714
ISBN 978-2-8325-3219-5
DOI 10.3389/978-2-8325-3219-5

About Frontiers

Frontiers is more than just an open access publisher of scholarly articles: it is a pioneering approach to the world of academia, radically improving the way scholarly research is managed. The grand vision of Frontiers is a world where all people have an equal opportunity to seek, share and generate knowledge. Frontiers provides immediate and permanent online open access to all its publications, but this alone is not enough to realize our grand goals.

Frontiers journal series

The Frontiers journal series is a multi-tier and interdisciplinary set of open-access, online journals, promising a paradigm shift from the current review, selection and dissemination processes in academic publishing. All Frontiers journals are driven by researchers for researchers; therefore, they constitute a service to the scholarly community. At the same time, the *Frontiers journal series* operates on a revolutionary invention, the tiered publishing system, initially addressing specific communities of scholars, and gradually climbing up to broader public understanding, thus serving the interests of the lay society, too.

Dedication to quality

Each Frontiers article is a landmark of the highest quality, thanks to genuinely collaborative interactions between authors and review editors, who include some of the world's best academicians. Research must be certified by peers before entering a stream of knowledge that may eventually reach the public - and shape society; therefore, Frontiers only applies the most rigorous and unbiased reviews. Frontiers revolutionizes research publishing by freely delivering the most outstanding research, evaluated with no bias from both the academic and social point of view. By applying the most advanced information technologies, Frontiers is catapulting scholarly publishing into a new generation.

What are Frontiers Research Topics?

Frontiers Research Topics are very popular trademarks of the *Frontiers journals series*: they are collections of at least ten articles, all centered on a particular subject. With their unique mix of varied contributions from Original Research to Review Articles, Frontiers Research Topics unify the most influential researchers, the latest key findings and historical advances in a hot research area.

Find out more on how to host your own Frontiers Research Topic or contribute to one as an author by contacting the Frontiers editorial office: frontiersin.org/about/contact

Molecular mechanisms and pathways in cerebellar function

Topic editors
Catarina Osorio — Erasmus Medical Center, Netherlands
Lilian Kisiswa — Aarhus University, Denmark
Alanna J. Watt — McGill University, Canada

Topic coordinator
Etsuko Shimobayashi — University of Basel, Switzerland

Citation
Osorio, C., Kisiswa, L., Watt, A. J., Shimobayashi, E., eds. (2023). *Molecular mechanisms and pathways in cerebellar function*. Lausanne: Frontiers Media SA. doi: 10.3389/978-2-8325-3219-5

Table of contents

frontiers | Frontiers in Molecular Neuroscience

TYPE Editorial
PUBLISHED 28 July 2023
DOI 10.3389/fnmol.2023.1258215

OPEN ACCESS

EDITED AND REVIEWED BY
Jean-Marc Taymans,
Institut National de la Santé et de la Recherche Médicale (INSERM), France

*CORRESPONDENCE
Catarina Osório
✉ c.osorio@erasmusmc.nl
Lilian Kisiswa
✉ liki@biomed.au.dk

RECEIVED 13 July 2023
ACCEPTED 17 July 2023
PUBLISHED 28 July 2023

CITATION
Osório C, Watt AJ and Kisiswa L (2023) Editorial: Molecular mechanisms and pathways in cerebellar function.
Front. Mol. Neurosci. 16:1258215.
doi: 10.3389/fnmol.2023.1258215

Editorial: Molecular mechanisms and pathways in cerebellar function

Catarina Osório[1]*, Alanna J. Watt[2] and Lilian Kisiswa[3,4,5]*

[1]Erasmus Medical Center, Rotterdam, Netherlands, [2]Department of Biology, McGill University, Montreal, QC, Canada, [3]Department of Biomedicine, Aarhus University, Aarhus, Denmark, [4]Danish Research Institute of Translational Neuroscience (DANDRITE)–Nordic EMBL Partnership for Molecular Medicine, Aarhus University, Aarhus, Denmark, [5]The Danish National Research Foundation Center, PROMEMO, Aarhus University, Aarhus, Denmark

KEYWORDS

neurodevelopment, signaling pathways, plasticity, cerebellar disorders, cerebellar therapies

Editorial on the Research Topic
Molecular mechanisms and pathways in cerebellar function

The cerebellum contains the majority of the neurons found in the central nervous system. This neuronal richness poses a challenge for the correct wiring of the cerebellar neurocircuits that are a prerequisite for a properly functioning cerebellum. These circuits underlie a wide range of functions such as motor learning, balance, and coordination, as well as cognitive and emotional processes. Strikingly, the human cerebellum has a prolonged developmental period, which increases the risk for both genetic and environmental disruptions, and consequently neurological disorders. Hence, a deeper knowledge on the fundamental molecular and cellular processes governing cerebellar development is imperative, and may eventually provide a springboard for novel treatments. With this Research Topic we provide a platform to bring together the latest findings focused on the molecular and cellular mechanisms underlying cerebellar development, function and disease.

The molecular mechanisms driving cerebellar developmental programs are not fully understood. However, studies from several groups are now elucidating these mechanisms and pathways. Focusing on the granule cells (GCs), Kim et al. summarize the GCs-related molecules involved in cerebellar development. GCs constitute more than 50% of the brain's neurons, hence their development influence not only the size and foliation of the cerebellum but also the development of other neurons. Kim et al. proposed several research directions to further investigate how GCs regulate the assembly of the cerebellar network. Importantly, combining neurodevelopmental studies with behavioral assays allows for a better understanding on the impact specific molecules have in the maturation and function of the cerebellum. For instance, the absence of the neurotrophin receptor p75 ($p75^{NTR}$) from granule cell precursors (GCPs) increases their rate of proliferation. Consequently, mice with an excess of GCs performed poorer in the eyeblink conditioning, a cerebellar-dependent motor learning task. Building on their previous work, Zanin et al. tested the same $p75^{NTR}$ model for non-motor behaviors. These animals displayed high levels of anxiety, lack of preference on social novelty and social disengagement. Overall, deletion of $p75^{NTR}$ from GCPs during development was sufficient to perturb social behavior. The involvement of $p75^{NTR}$ suggests that the neurotrophins play an important role in cerebellar development.

This is further supported in a systematic review by Boxy et al. that detailed how each trophic factor participate in the survival, migration, differentiation, synaptogenesis, and maintenance of the cerebellum. They provide examples on how disruption of their signaling pathways contribute for neurodevelopment disorders with a cerebellar component. These articles highlight the need to understand how disruptions in signaling pathways lead to brain abnormalities so better therapeutic strategies can be developed.

A mechanistic study presented by Okuno et al. focused on the assembly of cerebellar neuronal networks. The climbing fiber to Purkinje cell (PC) synapse is a well-established model for synaptogenesis: it develops from early multi-innervating climbing fibers to the selective strengthening of one climbing fiber input, and finally to synapse elimination of extra climbing fibers. Perturbations in any of these steps can have dramatic consequences on cerebellar connectivity. Okuno et al. report the receptor-type tyrosine-protein phosphatase delta (PTPδ) as a novel presynaptic organizer in the cerebellum. Using a combination of mouse genetics, molecular and systems neurosciences approaches, they showed that PTPδ is required for both motor function as well as during development for climbing fiber translocation, synaptic transmission and maintenance predominantly in the anterior cerebellum. It is important to recognize that the cerebellum is not a homogeneous structure and many studies have revealed molecular, cellular, physiological and functional regional differences. However, the mechanisms underlying these emerging differences during development are still unclear. In this topic, Dorigo et al. used zebrafish as a developmental model to shed light on the origins of cerebellar functional domains. Pharmacological as well as optogenetic silencing of PC activity disrupted the development of functional regionalization of the PC layer. The authors propose an activity-driven maturation for cerebellar connectivity in which PC physiological response develops alongside their functional regionalization.

Given the importance of proper developmental programs in establishing cerebellar neuronal connections, alterations in the molecular composition of neuronal circuits can result in cerebellar diseases. A stellar example of disorders caused by impairment in neurocircuits are the spinocerebellar ataxias (SCAs) that comprises of a group of degenerative diseases originated by a wide range of mutations. Kapfhammer and Shimobayashi summarized the evidence that mutation in Protein kinase C gamma (PKCγ) results in a constitutive active protein and this alters PC function and signaling, which in turn impairs cerebellar circuits causing SCA. Disruptions in cerebellar circuitry was further demonstrated in Piasecki et al. where they showed that ataxin-3 containing 150 CAG repeats leads to impaired ataxin-3 interactome. Loss of ataxin-3/Camk2 interaction impeded the transport of mitochondria to axons. Insufficient axonal mitochondrial transport reduces local energy supply leading to axonal degeneration. Additionally, Gorski et al. reported that mutation in cystatin B (*CSTB*) gene leads to mitochondria dysfunction that perturbs synaptic function resulting in ataxia. Impairment in mitochondrial function is extended to other forms of ataxia. Chen et al. identified a patient carrying a novel homozygous senataxin (*SETX*) mutation that causes autosomal recessive inherited ataxia with oculomotor apraxia type 2. Non-functioning *SETX* gene causes protein aggregation and accumulation of defective mitochondria, which subsequently results in neurite degeneration that alters the cerebellar circuit. Data on the molecular signatures that drive impairment in cerebellar circuits described here may eventually give rise to novel therapeutic interventions in SCA patients.

Indeed, Ding et al. reviewed the basis and prospect of therapies for SCAs focusing on the potential use of RNA interference (RNAi) and extracellular vesicles (EVs). They proposed a novel therapeutic strategy that combines RNAi and EVs for the treatment of SCAs. Although RNAi treatment has been explored in patients and mouse models of SCAs with some success, RNAi poor stability *in vivo* and toxicity caused by excess of RNAi makes the use of RNAi technology alone insufficient for treating SCA patients. Therefore, packing EVs with RNAi may be a good strategy to increase RNAi stability and reduce toxicity *in vivo* resulting in an increased potential of gene therapy for the treatment of these diseases. Other cerebellar-related disorders such as Down Syndrome (DS) also exhibit mitochondrial dysfunction and impairment in neuronal circuits. DS caused by overexpression of dual specific tyrosine-phosphorylation-regulated kinase 1A show alteration in the cerebellar proteome indicating mitochondrial dysfunction that could be rescued by green tea extract containing epigallocatechin-3-gallate as evidenced in Ortega et al.. Taken together, these articles elucidate molecular mechanisms of mitochondrial dysfunction altering cerebellar network associated with cerebellar malfunction. This knowledge may aid the development of therapies that can halt disease progression and eventually provide relief to patients.

Once the cerebellar network is established, it requires maintenance across the lifespan of an animal. Butler et al. demonstrated that subjecting the developing cerebellum to hemorrhagic injury, leads to reduced number of cerebellar neurons but this did not alter the behaviors of the animals suggesting compensatory robustness in the network. Furthermore, the dynamic nature of neurocircuits suggests that there are mechanisms in place to ensure that circuit function is maintained in adulthood. Although, factors required for maintenance of healthy cerebellar circuits are partially known, van't Sant et al. provided additional evidence that dietary restriction promotes expression of genes that contributes to maintenance of these circuits.

Overall, a proper functioning cerebellum requires correct wiring of circuits that are built by a combination of molecular neurodevelopmental programs and mechanisms that maintain these circuits. This Research Topic provides a glimpse of the molecular mechanisms responsible for the development of cerebellar circuits and their preservation in adulthood. These studies emphasize the need for further studies to understand the formation and maintenance of cerebellar wiring and elucidate what goes wrong in cerebellar-related disorders. This knowledge will provide a foundation for development of therapeutic interventions for cerebellar diseases.

Author contributions

All authors listed have made a substantial, direct, and intellectual contribution to the work and approved it for publication.

Acknowledgments

We would like to thank Dr. Etsuko Shimobayashi from University of Basel, Switzerland, for coordination of the Research Topic.

Conflict of interest

The authors declare that the research was conducted in the absence of any commercial or financial relationships that could be construed as a potential conflict of interest.

Publisher's note

All claims expressed in this article are solely those of the authors and do not necessarily represent those of their affiliated organizations, or those of the publisher, the editors and the reviewers. Any product that may be evaluated in this article, or claim that may be made by its manufacturer, is not guaranteed or endorsed by the publisher.

frontiers | Frontiers in Molecular Neuroscience

TYPE Mini Review
PUBLISHED 13 October 2022
DOI 10.3389/fnmol.2022.1043947

OPEN ACCESS

EDITED BY
Andrei Surguchov,
University of Kansas Medical Center,
United States

REVIEWED BY
Irina G. Sourgoutcheva,
University of Kansas Medical Center,
United States

*CORRESPONDENCE
Xuehong Liu
liuxueh6588@126.com

†These authors have contributed equally to this work

SPECIALTY SECTION
This article was submitted to Brain Disease Mechanisms, a section of the journal Frontiers in Molecular Neuroscience

RECEIVED 14 September 2022
ACCEPTED 21 September 2022
PUBLISHED 13 October 2022

CITATION
Ding Y, Zhang Y and Liu X (2022) Combinational treatments of RNA interference and extracellular vesicles in the spinocerebellar ataxia. *Front. Mol. Neurosci.* 15:1043947. doi: 10.3389/fnmol.2022.1043947

Combinational treatments of RNA interference and extracellular vesicles in the spinocerebellar ataxia

Yingying Ding[1,2†], Yong Zhang[1†] and Xuehong Liu[1*]

[1]Department of Histology and Embryology, Medical College, Shaoxing University, Shaoxing, Zhejiang, China, [2]Department of Clinical Medicine, Affiliated Hospital of Hangzhou Normal University, Hangzhou, China

Spinocerebellar ataxia (SCA) is an autosomal dominant neurodegenerative disease (ND) with a high mortality rate. Symptomatic treatment is the only clinically adopted treatment. However, it has poor effect and serious complications. Traditional diagnostic methods [such as magnetic resonance imaging (MRI)] have drawbacks. Presently, the superiority of RNA interference (RNAi) and extracellular vesicles (EVs) in improving SCA has attracted extensive attention. Both can serve as the potential biomarkers for the diagnosing and monitoring disease progression. Herein, we analyzed the basis and prospect of therapies for SCA. Meanwhile, we elaborated the development and application of miRNAs, siRNAs, shRNAs, and EVs in the diagnosis and treatment of SCA. We propose the combination of RNAi and EVs to avoid the adverse factors of their respective treatment and maximize the benefits of treatment through the technology of EVs loaded with RNA. Obviously, the combinational therapy of RNAi and EVs may more accurately diagnose and cure SCA.

KEYWORDS

extracellular vesicle, RNA interference, miRNA, siRNA, shRNA, spinocerebellar ataxia, neurodegenerative disease, combinational treatment

Introduction

Spinocerebellar ataxia (SCA) is a group of progressive neurodegenerative diseases (NDs) with autosomal dominant inheritance. They are divided into 48 subtypes according to the time sequence of discovery of the pathogenic gene loci. SCA has different clinical features, and ataxia is their core symptom (Chen H. Y. et al., 2021; Shin et al., 2021). The pathologically extended cytosine adenine guanine (CAG) repeat sequences encoded by poly-glutamine (polyQ) are their common pathogenesis, which leads to the misfolding and aggregation of translated protein and causes neuronal death (Shin et al., 2021). The prevalence of SCA is approximately 3/100,000 that varies in

different subtypes and regions (Gómez et al., 2022). Currently, there are only several symptomatic treatments for SCA, which cannot prevent or delay the progression of SCA with severe complications. Patients usually die because brain stem lesions, pulmonary infection and respiratory failure within 10–30 years after diagnosis (Pérez Ortiz and Orr, 2018; Cendelin et al., 2022). Thyroid-stimulating hormone releasing hormone (TRH) can improve the symptoms (Shimizu et al., 2020). However, its complications such as headache and nausea occur in about 50% patients (Ghanekar et al., 2022). Aripiprazole improves dyskinesia but has significant side effects, such as anxiety, nausea, and dizziness (Jalles et al., 2022). The complex pathogenic mechanism and differences between subtypes, patients show the inadequacy of symptomatic treatment (Yap et al., 2022b).

Gene therapies, including RNA interference (RNAi), antisense oligonucleotides, and gene editing technology, are hoped to cure SCA by correcting the pathogenic genes (Vázquez-Mojena et al., 2021). RNAi is the most popular and effective way in preclinical trials mediated by microRNAs (miRNAs), small interfering RNAs (siRNAs), and short hair protein RNAs (shRNAs) (Costa, 2020). Repeat-targeting shRNAs specifically silence the expression of extended CAG repeats (Kotowska-Zimmer et al., 2020). Adeno-associated virus (AAV) loads with microRNA against ataxin (ATXN) 3 to restore the neuronal signaling and physiological functions in SCA3 mice (Nobre et al., 2022). Long-term and persistent RNAi reduces the cerebellar lesions and axonal demyelination in SCA3 mice by lowering the level of ATXN3 (Costa et al., 2020). However, RNAi has disadvantages such as carrier selection, poor stability *in vivo*, off-target effect and toxicity caused by excess effect (Vázquez-Mojena et al., 2021; Wang et al., 2022). Extracellular vesicles (EVs) as carriers have long plasma half-life, strong stability *in vivo* and can target the injury site (Sun et al., 2010; Huang et al., 2020). miRNA is an important component of EVs, which can treat SCA. Mesenchymal stem cell (MSC)-derived exosomes can alleviate the damage to Purkinje fibers and myelin sheath, motor function and neuroinflammation in SCA3 mice (You et al., 2020; Tao et al., 2021). The miRNA in EVs can be biomarkers of SCA3, revealing the subtypes and progression of SCA3 (Hou et al., 2019). Obviously, the combination of RNAi and EVs can avoid the adverse factors of RNAi or EVs treatment alone to maximize the benefits of treatment. The combinational therapy of RNAi and EVs is a brand new idea. It may more accurately diagnose and cure SCA, which still needs our in-depth research.

RNA interference

RNA interference is a process, which is mediated by double-stranded RNA (dsRNA) and leads to the silence of target genes (mRNA) containing complementary sequences and inhibition of related protein production (Kara et al., 2022). dsRNAs in the process include miRNAs, siRNAs and shRNAs (Costa, 2020). The pathogenesis of NDs remains unknown. However, their pathological features are the deposition of misfolded protein such as amyloid-β, alpha-synuclein, tau and prion proteins. RNAi can completely eliminate or alter the synthesis of target protein (Khan et al., 2022). RNAi can treat SCA by silencing the specific genes and assisting in the diagnosis and condition monitoring of SCA.

microRNAs

microRNAs are single-stranded non-coding RNAs, about 19–25 nucleotides in length. They are RNAi silencing trigger that binds to a specific region of 3′ untranslated region of messenger RNA, silences the target gene by altering RNA stability to inhibit the corresponding protein synthesis (Wei et al., 2021). miRNAs are divided into artificial synthesis miRNAs and natural synthesis miRNAs. Artificial miRNAs can target disease genes (Saad et al., 2021). They are important for brain development and homeostasis (Penning et al., 2021). The imbalance of miRNAs is closely related to the pathogenesis of NDs, which may be the biomarkers. The expressions of Hsa-miR-204-3p and hsa-miR-873-3p are significantly increased, and the expression of hsa-miR-6840-5p is decreased in the patients of progressive supranuclear palsy (Nonaka et al., 2022). The expressions of miR-132-5p, miR-138-5p, and miR-129-5p are reduced in the brain of Alzheimer's disease (AD) patients (Dobricic et al., 2022). MIR-144 expression is significantly increased in Multiple Sclerosis (MS) patients (Roshani et al., 2021). miR-181 can be a potential biomarker for the prognosis of amyotrophic lateral sclerosis (ALS). Patients with low miR-181 content have a longer survival time (Magen et al., 2021).

microRNAs are important for the treatment of NDs. The increased serum miR-485-3p can be a diagnostic marker for AD. Knocking out miR-485-3p reduces neuro-inflammation and improves neuronal viability, which is conducive to protect neurons in AD patients (Yu et al., 2021). Injection of AAV encoding miRNA targets to the superoxide dismutase 1 and immunosuppressive agents to improve sensory dysfunction and delay disease progression in an ALS patient (Mueller et al., 2020). miRNA inhibits the effect of stress on visual transduction and reduces the retinal inflammation to treat the age-related macular degeneration (Chu-Tan et al., 2021).

microRNAs are potential in the diagnosis, treatment and monitoring of SCA. Three miRNAs interact with ATXN3-3′UTR (miR-9, mir-181a, and mir-494) that are overexpressed in SCA3 patients (Carmona et al., 2017). The injection of AAV expressing miR760 reduces ATXN1 levels *in vivo* and improves motor disharmony in the cerebellum of SCA1 mice (Nitschke et al., 2020). miR-32 and miR-181c target the 3′UTR of ATXN3 and inhibit the expression of ATXN3 to reduce the

polyQ-mediated cytotoxicity (Krauss et al., 2019). AAV5-loaded miRNA ATXN3 specifically decreases the ATXN3 mRNA and protein in SCA3 mice and cell models (Martier et al., 2019). The lowest effective dose, the maximum tolerated dose and the toxicity threshold that can improve SCA1 to guide the clinical application of RNAi in the treatment of SCA1 (Keiser et al., 2016).

Small interfering RNAs (siRNAs)

Small interfering RNAs are short dsRNAs of 20 to 25 base pairs produced by RNAse III family cutting long dsRNAs. They silence the post-transcription genes by interfering with the expression of specific genes through complementary nucleotides (Jiang et al., 2021; Akhilesh et al., 2022). In mammals, siRNAs only come from synthetic sources (Wang et al., 2021).

Small interfering RNAs participate in various biological mechanisms, including the proliferation, growth and differentiation of cells, as well as the arrangement of heterochromatin in nucleus (Mishra et al., 2022). SiRNA-mediated glycogen synthase kinase (GSK)3β silencing improves the cognitive function and relieves the progression of AD by eliminating the deposition of neurofibrils and amyloid plaques (Gupta et al., 2022). SiRNA restores the normal expression of schwann cells in Charcot-Marie-tooth disease type 1a mice, electrophysiological activity of motor nerves and muscular function. However, long-term treatment produces off-target and toxic side effects (Boutary et al., 2021). Anti-Huntington (HTT) siRNAs effectively reduce the expression of HTT gene and slow the disease's progression in mice with Huntington's disease (HD) (Sava et al., 2020).

CAG-siRNA specifically silences the alleles of estrogen receptor with CAG repeats in fibroblasts, inhibits the generation of polyQ protein in the central nervous system to treat the SCA, spinal cord and medullary atrophy, HD, dentatered-globus pallidus atrophy, etc., (Hirunagi et al., 2021). Intravenous siRNAs reduce the Axin-3 expression, alleviate the dyskinesia and improve the striatal and cerebellar lesions in SCA3 mice (Conceição et al., 2016).

Short hairpin RNAs (shRNAs)

Short hairpin RNA consists of two complementary 19–22 bp RNA sequences linked by a short loop consisting of 4–11 nt. It is similar to the hairpin in naturally synthesize miRNA, so it is called the short hairpin RNA (Moore et al., 2010). Although shRNAs are exogenous RNAs (Sheng et al., 2020), they can be assimilated into endogenous RNA pathways with greater efficiency than siRNAs (Gorabi et al., 2020).

Short hairpin RNAs inhibit the expressions of SNCA and endogenous α-synuclein to protect nerves and reduce dyskinesia in the substantia nigra of Parkinson's disease (PD) rats (Nakamori et al., 2019). shRNAs convert the midbrain astrocytes into dopaminergic neurons to improve the motor dysfunction in PD (Qian et al., 2020). shRNAs target the glutamate N-methyl-d-aspartate receptor subunit (GluN) 3A inhibition to prevent the loss of dendritic spines and improve the locomotor performance in HD mice (Marco et al., 2018). shRNAs carry out spindle pole body component (SPC) 25 to pass through the blood-brain barrier (BBB), reduce the proliferation of microglia, and slow the disease progression in AD mice (Cui et al., 2021). For SCA3 and SCA7, shRNAs reduce the Axin-3 in mutant cells by 60%, and the expressions and aggregations of toxic mutant ataxin-7 proteins. The normal proteins are unchanged and stored in the non-aggregated diffuse cells (Scholefield et al., 2009; Kotowska-Zimmer et al., 2020). shRNAs restore the cerebellar morphology of SCA1 mice and improve the motor coordination of Purkinje cells (Xia et al., 2004).

The currently RNAi drugs only include N-acetylgalactosamine-siRNA conjugates (givosiran, inclisiran, and lumasiran), which targets to hepatocyte and siRNA drugs (vutrisiran and onpattro) that can treat the familial amyloid polyneuropathy (Kulkarni et al., 2021; Holm et al., 2022). Although RNAi shows the different ways of gene silencing in each ND, it seems to be a general treatment for them. However, it suffers from endosome escape, off-target effect, unclear targeting specificity, and short half-life (the half-life is only a few minutes due to rapid degradation by nucleases) (Aigner, 2019; Setten et al., 2019). Conventional RNAi vectors have shortcomings. Adenoviral vectors themselves can be toxic (Keiser et al., 2021). Liposomes have a short half-life due to the hydrolysis and oxidation of phospholipids and are vulnerable to temperature. Composite nanoparticle are cytotoxic which may destroy the genetic material of a body (Hernández-Soto and Chacón-Cerdas, 2021). The aforementioned disadvantages of RNAi make it difficult to treat SCA alone.

Extracellular vesicles

Extracellular vesicles have target specificity, long plasma half-life and wide distribution, and can cross the BBB. Their contents such as miRNAs can assist in the diagnosis and prognosis of NDs. Neurotrophic factors (NTFs), heat shock proteins, vascular endothelial growth factors and other factors can restore neuronal activity and maintain protein homeostasis.

The general position of extracellular vesicles

Extracellular vesicles are nano-sized vesicles released by various cells and surrounded by phospholipid membranes (Ye et al., 2022). EVs contain abundant DNA, proteins, lipids,

mRNA and small non-coding RNA, including miRNAs (account for half of the content of EVs), which are not affected by extracellular proteases and nucleases (Cuomo-Haymour et al., 2022; Zhu et al., 2022). According to the mechanism and diameter of the production, they are divided into exosomes (50–150 nm), microbubbles (100–1,000 nm) and apoptotic bodies (100–5,000 nm). Their functions are related to the originating cells (Mathieu et al., 2019).

As a novel carrier, EVs have high biocompatibility to avoid the adverse immune reactions, targeting specificity, low toxicity, long plasma half-life, source diversity, and can be easy to cross the BBB to overcome the shortcomings of conventional carriers and RNAi (Zhang et al., 2019; O'Brien et al., 2020; Herrmann et al., 2021).

Extracellular vesicles are important in the treatment of NDs (**Table 1**). Stem cell-derived EVs have neuroprotective and immunomodulatory effects (Niu et al., 2020; Garcia-Contreras and Thakor, 2021). EVs derive from MSCs and anti-inflammatory immune cells that can reduce the inflammatory damage and cell stress (Thome et al., 2022). The exosomes of human amniotic fluid MSCs can treat the inflammation-related neurological diseases by reducing inflammation caused by microglia and improving neurotoxicity (Zavatti et al., 2022). EV-mediated the delivery of DnaJ Homolog Subfamily B Member 6 (DNAJB6) molecular chaperone inhibits the aggregation of polyQ and HTT proteins to delay the onset of HD (Joshi et al., 2021). EVs derive from neural stem cells that target the functional substances to protect damaged neurons by resisting oxidation, apoptosis and inflammation (Lee et al., 2022). Most of the data on the treatment of EVs are concentrated in preclinical trials, but many clinical trials have proved the potential of EVs in diagnosis and monitoring.

Extracellular vesicles can assist in the diagnosis and monitoring of NDs (**Table 2**). The α-globin, β-globin, δ-globin, α-1-antichymotrypsin, beta-2-glycoprotein 1 and complement component C9 are increased, and apolipoprotein C-III is decreased in the neuron-derived exosomes of AD patients (Arioz et al., 2021; Soares Martins et al., 2022). The number of α-syn-carrying EVs in cerebrospinal fluid (CSF) and plasma of PD patients are significantly increased, which is positively correlated with the severity (Agliardi et al., 2021; Hong et al., 2021). Concentrations of syntaxin-1A (STX-1A) and vesicle associated membrane protein 2 (VAMP-2) are significantly reduced in PD (Agliardi et al., 2021). The concentration of toll-like receptor (TLR) 3 is decreased and TLR4 is increased in EVs from MS patients (Bhargava et al., 2019). The increased expressions of Junctional Adhesion Molecule A (JAM-A), TNF-R2, and Chitinase 1 lead to increase platelet activation, angiogenesis, motor neuron destruction and microglia activation in the EVs of ALS patients (Czubak-Prowizor et al., 2022; Sjoqvist and Otake, 2022). In the clinical trial of exenatide for PD, neuron-derived EVs, as biomarkers, have potential in examining the molecular mechanisms of patients' motor function changes (Athauda et al., 2019).

The use of extracellular vesicles in spinocerebellar ataxia

Extracellular vesicles, as an important communication tool, can transmit the pathogenic gene, misfold, and aggregate proteins between cells, thus participating in the pathophysiology of NDs (Surgucheva et al., 2012). Other propagation mechanisms include soluble oligomers, synaptic connections, and nano tunnel tube (Takeuchi and Nagai, 2022; **Figure 1**). As EVs contain miRNAs, proteins and other components, their changes can reflect the condition of SCA (Cuomo-Haymour et al., 2022). There are few studies in the biomarkers of EVs in SCA compared to AD, PD, and ALS. Only one study of miRNA in the EVs is described below. None of the studies about protein biomarkers has demonstrated that they are in EVs. Both neurofilament medium (NFL) and myelin basic protein levels decrease in the cerebellar cortex of SCA3 patients, indicating axonal damage and myelin formation disorders (Paul et al., 2018). Increased levels of staufen 1 are associated with the abnormal metabolism of RNA due to ATXN2 mutations in the brain tissue of SCA2 patients (Yang et al., 2021). The traditional diagnostic methods for SCA include three aspects: (1) MRI can only show the pathological changes of extensive atrophy of the brain and thinning of the cortex, which lacks the functional changes corresponding to the pathological changes. Meanwhile, MRI is very expensive (Yap et al., 2022a). (2) The diagnosis of symptomatology is easily affected by subjectivity. (3) Genetic examination: The gene loci of mutations in different subtypes are different. For example, SCA1, SCA2, SCA3, SCA6, SCA7, SCA12, and SCA19/22 are, respectively, related to the CAG repeated amplification in ATXN1, ATXN2, ATXN3, CACNA1A, ATX7, PPP2R2B, and potassium voltage gated channel, Shal-related family, member 3 (KCND3) genes on different chromosomes (Li M. et al., 2022; Lian et al., 2022).

Extracellular vesicles can transmit NTFs, heat shock proteins, and others to promote the damaged neurons and maintain the stability and activity of proteins (Backe et al., 2022; Harrell et al., 2022; Van den Broek et al., 2022). The proteins encoded by polyQ are the key to the pathogenesis of SCA, and Heat shock protein (HSP) 70 can promote the synthesis of correctly folded proteins and the degradation of misfolded proteins, prevent the aggregation of abnormal proteins and disaggregate the aggregation of abnormal proteins (Johnson et al., 2020; Serlidaki et al., 2020). MSCs-derived exosomes reduce the loss of purkinje cells and cerebellar myelin sheaths, alleviate neuroinflammation and improve the locomotor function in SCA3 mice [19] (You et al., 2020). MSC-conditioned medium (simulates EVs) significantly reduces the motor disharmony and neuronal degeneration in SCA1 mice,

TABLE 1 Clinical treatment of EVs in the neurodegenerative diseases.

Sources of EVs	Diseases	Species	Treatment options	Outcomes	References
Human bone marrow-derived mesenchymal stem cell (MSC)	Status epilepticus	Mouse	EVs derived from human bone marrow-derived MSCs are administered intranasally (15 μg, ~7.5 × 109)	Inflammatory response, abnormal neurogenesis, memory and cognitive deficits are significantly inhibited.	Long et al., 2017
Bone-marrow mesenchymal stem cells (BMSCs)	Alzheimer's disease (AD)	Mouse	BMSC-exos are administered intraventricular (0.5 μg per day)	Inflammatory response, glial cell over-activation are significantly improve and the expression of BDNF is significantly increased.	Liu S. et al., 2022
GDNF transfected macrophages	Parkinson disease (PD)	Mouse	PD mice are intranasally dosed with EV-GDNF three times per week (3 × 109 particles/10 μl/mouse)	The activity of mice significantly improved, neurons increased, inflammatory response decreased, and no significant toxic reactions are observed.	Zhao et al., 2022a
Blood from healthy volunteers	PD	Mouse	PD mice are given exosomes via tail vein (0.2 ml per mouse, four injections)	Motor coordination is restored with increased dopaminergic neuron production in the substantia nigra and striatum, and oxidative stress, neuroinflammation, and apoptosis are decreased.	Sun et al., 2020
Astrocyte	Traumatic brain injury (TBI)	Rat	Exosomes are injected into the lateral ventricles of each cerebral hemisphere of the rat (2 μl of 2,400 × -enriched exosomes)	Oxidative stress is reduced and the damaged mitochondria and neurons are restored.	Chen et al., 2020
Human MSC	TBI	Swine	Exosomes are injected through the left external jugular vein slowly (1 ml/min, 1 × 10 exosome particles in 5 ml lactated Ringer's)	Exosomes treatment significantly reduces brain swelling and lesion size, reduces brain biomarkers, and improves the integrity of the blood-brain barrier.	Williams et al., 2020
Serum from young mice	Huntington's disease (HD)	Cell	Young serum-exosomes are administered to the HD cell model. (200 μg/ml for 3 days)	The decrease of mHtt agglutinin and apoptosis signal makes more cells survive, less apoptosis and mitochondrial dysfunction recover.	Lee et al., 2021
Adipose-derived stem cells (ASCs)	Amyotrophic lateral sclerosis (ALS)	Mouse	Exosomes (6~8 × 108/ml) are administered intravenously and intranasally to the mice. (The iv dose was 100 μl or 10 μl).	Movement is improved with improved lumbar motor neurons, neuromuscular junctions and muscle function, and decreases glial cell activity.	Bonafede et al., 2020
ASCs from mice	ALS	Mouse	NSC-34 cells are inoculated in medium with or without 0.2 μg/ml exosomes.	Decreasing pro-apoptotic proteins, increasing anti-apoptotic proteins and cell viability provide neuroprotective effects	Bonafede et al., 2019

due to the inclusion of hepatocyte growth factor, fibroblast growth factor-2, insulin-like growth factor-1 and vascular endothelial growth factor (VEGF) (Suto et al., 2016). Studies have shown that VEGF can reduce ataxia and dendritic defects and even reverse cerebellar lesions in SCA1 (Hu et al., 2019).

Extracellular vesicles also face some challenges, which have been nowly solved. Endogenous EVs competing for binding sites and the clearance of macrophages can be solved by specifically modifying the surface of EVs (Zhang et al., 2022). EVs from the different sources have the different effects. Novel micro-nano technology tool can sensitively separate the different subsets of EVs (Chiang and Chen, 2019; Wang et al., 2020). Ultra-centrifugation, ultrafiltration, precipitation and size exclusion chromatography improve the separation and purification of EVs (Li M. et al., 2020). Membrane extrusion technology combine the surface composition of EVs with lipid materials to achieve mass production of EVs (Jhan et al., 2020).

The combinational therapeutic effect of RNA interference and extracellular vesicles in spinocerebellar ataxia

Extracellular vesicles not only can treat SCA, but also can be carriers of RNAi, which can make up for the deficiencies of RNAi. Treating SCA with the combination of EVs and RNAi

TABLE 2 EVs as the biological markers of neurodegenerative diseases.

Diseases	Species	Source of EVs	Contents of EVs	Significance of changes	References
AD	Human	Neuron-derived plasma EVs	High brain β-amyloid (Aβ)	It is suggested that cognitive function are impaired, entorhinal atrophy and amyloid deposition in cortex.	Li T. R. et al., 2022
AD	Human	Central nervous system-derived plasma EVs	NMDAR2A	It may be related to impaired synaptic function in the brain.	Tian et al., 2022
Chronic Traumatic Encephalopathy (CTE)	Human	CTE brain tissues	t-tau, p-tau, SNAP-25, PLXNA4	It is related to further development of the disease.	Muraoka et al., 2021b
CTE	Human	Plasma	COL6A3, RELN and COL6A1	They, respectively, indicate impaired sciatic nerve, increased tau phosphorylation, and rarefaction of white matter.	Muraoka et al., 2021a
PD	Human	Neuron-derived plasma EVs	α-synuclein, Phosphorylated Tau (T181)	They indicate that PD patients have cognitive impairment, which can predict the cognitive prognosis.	Blommer et al., 2022
PD	Human	Plasma	Neurofilament light chain (NfL)	NfL may be related to the degree of dyskinesia in PD patients, especially in terms of akinetic rigidity.	Chung et al., 2020
Huntington's disease (HD)	Human and Mouse	Cerebrospinal fluid (CSF)	SG-nucleating Ras GTPase-activating protein-binding protein 1 (G3BP1)	It is related to the pathogenesis of HD. The increased production in cortex and hippocampal pyramidal neurons may be related to the memory impairment of HD patients.	Sanchez et al., 2021
ALS	Human	CSF and plasma	neurofilament light chain (NfL), TAR DNA-binding protein 43 (TDP-43), and total	All of them can be used as sensitive biomarkers for the diagnosis of ALS. NFL can predict disease progression	Kasai et al., 2019
Sporadic Creutzfeldt-Jakob disease (sCJD)	Human	CSF	tau (t-tau) 14-3-3β,14-3-3γ NfL, neuron-specific enolase, RT-QuIC, S100B, t-tau	RT-QuIC is the most accurate biomarkers. RT-QuIC and NfL are the most sensitive diagnostic marker.	Rübsamen et al., 2022
Epilepsy	Human and Mouse	Serum	coagulation factor IX (F9) and thrombospondin-1 (TSP-1)	F9 may be associated with excitatory toxicity, apoptosis, and coagulation abnormalities. TSP-1 may be related to abnormally high excitability.	Lin et al., 2020

is a promising direction. The miRNAs and proteins contained in EVs will undergo corresponding significant changes, making them biomarkers to assist the diagnosis and monitoring of SCA.

A novel RNA interference delivery carrier – Extracellular vesicles

Several cells can self-secrete miRNAs through paracrine and transport them to the receptor cells, and then change the expression of target genes, such as macrophages, microglia, oligodendrocytes, astrocytes, schwann cells and so on (Loch-Neckel et al., 2022; Zhu et al., 2022). Astrocyte-derived exosomes carrying miR-17-5p reduce oxidative stress, inflammatory, cerebral infarction and neurological disorders in hypoxic-ischemic brain injured rats (Du et al., 2021). Microglia secretes the exosomes containing miR-190b to inhibit neuronal apoptosis by targeting autophagy-related protein 7 to regulate autophagy (Pei et al., 2020). M2 microglia secretes the exosomes containing miR-124 to target ubiquitin-specific protease 14 to promote neuronal survival and mitigate ischemic brain injury (Song et al., 2019). Fibroblasts secrete the exosomes containing miR-673-5p to stimulate myelin gene expression by activating the tuberous sclerosis complex 2/mTOR complex 1/sterol-regulatory element binding protein 2 axis in Schwann cells and peripheral myelin formation (Zhao et al., 2022b). It is

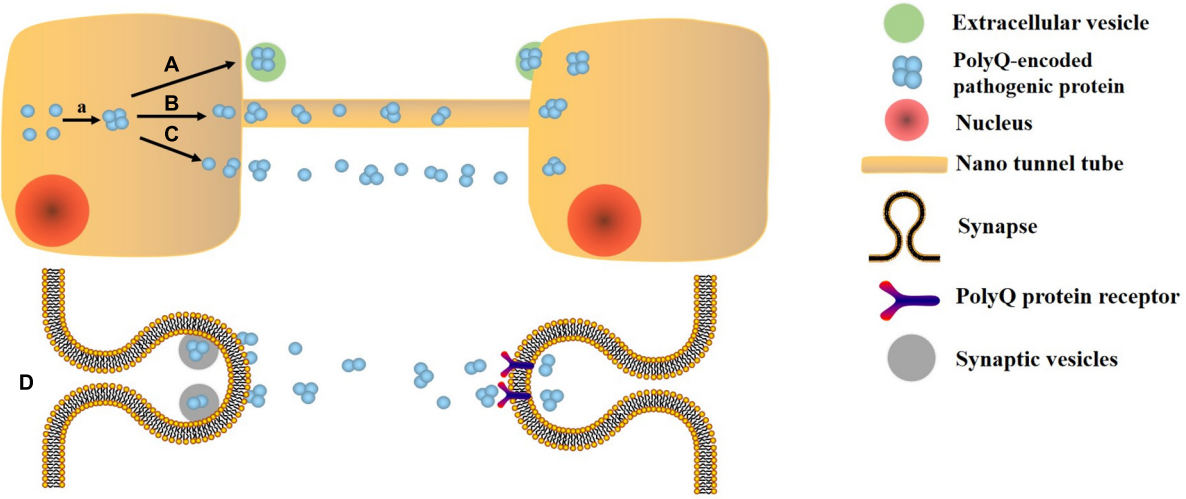

FIGURE 1
Transmission mechanism of polyQ protein. a. Error folding and aggregation of polyQ encoded protein. A. Extracellular vesicle pathway. B. Nano tunnel tube approach: the polyQ protein is exchanged by a tunnel-like membrane-derived structure that connects two cells. C. Soluble oligomer: due to its high solubility and small size, PolyQ protein may be able to escape from cells and diffuse to other cells. D. Synaptic connection: the polyQ protein is transmitted between neurons with high transmission efficiency.

infeasible to implant them directly to patients. On the one hand, they may contain pathogenic substances. The transmission of astrocyte-derived EVs carrying casein kinase 1 increases the formation of Aβ Aand promotes inflammatory response by targeting the related neurons, which is the pathogenesis of AD (Li Z. et al., 2020). EVs can spread α-synuclein in the brain and accelerate the progress of PD [126] (Longoni et al., 2019). On the other hand, as there are 48 subtypes of SCA having the different genetic changes which require the different types of RNAi (Chen H. Y. et al., 2021; Shin et al., 2021). The composition and function of EVs are related to its secretory cells and their environments. The MSC-derived EVs in an inflammatory environment reduce inflammatory response more than the normal MSC-derived EVs (Mathieu et al., 2019; Liu Y. et al., 2022). Hypoxia-treated exosomes improve the inflammatory responses and synaptic functions by increasing the production of miR-21 to improve the cognitive and memory disorders (Cui et al., 2018). Therefore, we should select the metrocyte that can alleviate nerve damage and movement disorder, and appropriately stimulate the metrocyte to maximize the therapeutic value of EVs derived from it.

The desired RNAi can be loaded into the isolated and purified EVs. Electroporation is the most common and optimal technology. Each EV is probably loaded with 3,000 miRNA molecules (Batrakova and Kim, 2015; Pomatto et al., 2022). Incubation is a simple method while maintaining the integrity and stability of the EVs. It is achieved by incubating EVs with miRNA in Roswell Park Memorial Institute (RPMI) medium at 37°C for 1 h (Tapparo et al., 2021). Ultrasound damages the integrity of EVs membranes, in which drugs, protein and nanoparticles are loaded, and then membranes are recovered by incubation (Li Y. J. et al., 2020). Under the cross substitution of heat shock and freezing, $CaCl_2$ mediates the loading of miRNA into the exosomes without losing activity and with high efficiency (Rezaei et al., 2021). Although the method of encapsulating RNAi in EVs has not been tested in SCA, many studies have proved the feasibility in NDs, autoimmune diseases, tumors, cardiovascular diseases, etc. The EVs-derived from human neural stem cells attenuate the neuroinflammation and ROS-induced apoptosis, and promote the survival of dopaminergic neurons in PD, which may be related to the specific miRNA-embedded in EVs (Lee et al., 2022). Increasing the paracrine miR-146a of cortical astrocytes eliminate their phenotypic abnormalities through pre-miR-146a or dipeptidyl vinyl sulfone and play a neuro-glial repair role in ALS (Barbosa et al., 2021). Exosomes-loaded with miRNA-22 improve AD by inhibiting the pyroptosis and neuroinflammation (Zhai et al., 2021). The miRNA-encapsulated in exosomes control the target genes (nuclear factor kappa-B (NF-κB), signal transducer and activator of transcription (STAT) 1, and phosphatidylinositol 3 kinase/protein kinase B (PI3K/Akt), etc.) in the regulatory signaling pathway in immune response to treat the autoimmune diseases (Matsuzaka and Yashiro, 2022). Exosomes-loaded with miR-145-5p reduce the growth of pancreatic ductal adenocarcinoma (PDAC) by inhibiting the proliferation and invasion of PDAC cells (Ding et al., 2019). Exosomes carrying mir-6785-5P inhibit the angiogenesis and metastasis by inhibiting the inhibin subunit beta A in gastric cancer (Chen Z. et al., 2021). Cardiac progenitor cell-derived exosomes containing miR-146, miR-210, and miR-132 reduce

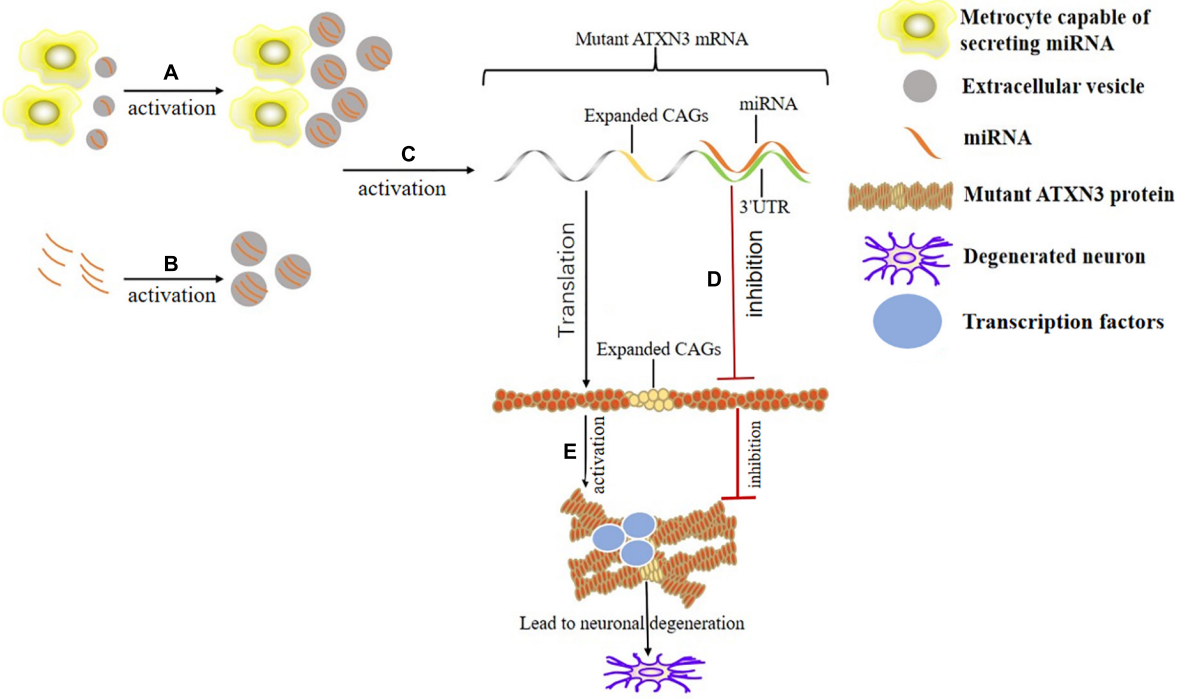

FIGURE 2
Mechanism of the binding of EVs and miRNA in the treatment of SCA3. **(A)** Appropriately stimulate the specific metrocyte (such as hypoxia treatment) to maximize the therapeutic value of EVs derived from it. **(B)** Load the desired miRNA into the isolated and purified EVs through electroporation, incubation or ultrasound, etc. **(C)** EVs with specific miRNA acts on corresponding miRNA sites (there are 1,137 known sites presently) in the 3'UTR of mutant ATXN3 mRNA. **(D)** The mutated ATXN3 mRNA that binds to the miRNA in the 3'UTR region is degraded or its translation is inhibited. **(E)** Misfolding and aggregation of the mutated ATXN3 protein occur. Transcription factors are adsorbed by protein aggregates, interfering with the expression and biogenesis of normal miRNA. Eventually the neurons degenerate.

the infarct size and improve the cardiac functions in infarcted hearts (Cervio et al., 2015; **Figure 2**).

A novel spinocerebellar ataxia biomarker – RNA interference in extracellular vesicles

The onset and progression are vary significantly among SCA patients. Biomarkers can sensitively monitor the SCA progression that is needed (Borgonio-Cuadra et al., 2019). Conventional diagnostic methods for SCA have shortcomings and cannot accurately monitor the disease progression. Existing measurements of protein biomarkers such as NfL in CSF and blood fail to locate the site of injury (Yap et al., 2022a). Ataxin-3 produced by polyQ amplification in plasma is highly stable only for 1 year (Hübener-Schmid et al., 2021). The protein biomarkers in EVs may specifically concentrate at the injured site and remain stable for longer time unaffected by proteolytic enzymes.

The miRNA in exosomes directly reflect the physiological conditions of brain, which are highly expressed in brain and body fluids, such as serum, plasma and CSF (Mori et al., 2019). Furthermore, a DNA-assembled advanced plasmonic architecture-based plasmonic biosensor is sensitive and accurate enough to detect miRNA in exosomes for clinical applications (Song et al., 2022). The miRNAs in the SCA patients undergo the specific changes with low stability. Loading miRNA in EVs may protect them from nuclease-rich environments (Borgonio-Cuadra et al., 2019). The miR-7014 in EVs of SCA3 patients is downregulated in plasma and upregulated in CSF (Hou et al., 2019). Although there is only one case of RNAi in EVs as SCA biomarkers, its feasibility has been confirmed in cancer, autoimmune diseases, kidney diseases, and NDs. miR-320a and miR-4433b-5p in EVs can differentiate breast cancer from the control population (Carvalho et al., 2022). Blood-derived EVs show that the level of miRNA-146a is reduced in the systemic lupus erythematosus patients, as oppose to urine-derived EVs (Zhou et al., 2022). Renal function is negatively correlated with the levels of miRNA-12136 and miRNA-483-5p (Sun et al., 2022). Expression of miR-16-5p, -331-3p, -409-3p, and -454-3p increase 1.5-fold in the CSF-derived EVs in AD patients (Sandau et al., 2022). The combination of miR-125b and -361 in exosomes can distinguish AD patients from healthy control with an accuracy rate of 99.52% (Song et al., 2022). MS patients show the upregulation of miR-21-5p and the

downregulation of miR-6735-3p, miR-6833-5p, and miR-510-3p in the EVs (Cuomo-Haymour et al., 2022). Hsa-miR-374a-5, -374b-5p,-199a-3p, -28-5p, -22-5p, and -151a-5p are potential biomarkers for the diagnosis of PD at different stages (He et al., 2021). Therefore, RNAi in EVs can assist in the diagnosis and monitoring of NDs.

There are still some limitations in the research of RNAi biomarkers in EVs. Most studies on biomarkers are conducted in SCA3 because it is the most common hypotype. Most RNAi studies have focused on miRNA because it accounts for half of the EVs content. Since SCA is a rare disease, the sample size of cases is insufficient, leading to the possibility of biased results. EVs and RNAi are affected by many factors *in vitro* and *in vivo*, so currently they can only serve as reference indicators for the diagnosis and monitoring of SCA.

Conclusion and future prospect

At present, symptomatic treatment is the only clinical treatment for SCA that has many side effects and limited efficacy. Gene therapy is the most popular potential treatment for SCA, and RNAi is the most effective among it. Many studies have shown that EVs and RNAi work well in SCA cells, animal models, and patients. In particular, the combination of them can make up for their deficiencies. The therapeutic effect, target specificity, stability and plasma half-life of EVs containing RNAi secreted by cells or EVs loaded with specific RNAi are significantly improved. They also have potential in the diagnosis and condition monitoring of SCA. Changes of RNAi in patients' EVs may reflect disease progression. However, there are few studies on the combination treatment, diagnosis and monitoring for SCA. In addition, most of them are animal and cell experiments, which do not eliminate the influence of sample size, gender, age, and race of the experimental subjects. Most studies have focused on SCA3 and miRNA while ignoring other subtypes of SCA and RNAi. Therefore, the combination of RNAi and EVs is a new therapeutic way for SCA, further in-depth clinical studies on large-scale multiple subtypes of RNAi and EVs are needed.

Author contributions

XL and YD designed the study. YD, YZ, and XL prepared the first draft of the manuscript and revised the manuscript. All authors agreed to publish this article and approved the final manuscript.

Conflict of interest

The authors declare that the research was conducted in the absence of any commercial or financial relationships that could be construed as a potential conflict of interest.

Publisher's note

All claims expressed in this article are solely those of the authors and do not necessarily represent those of their affiliated organizations, or those of the publisher, the editors and the reviewers. Any product that may be evaluated in this article, or claim that may be made by its manufacturer, is not guaranteed or endorsed by the publisher.

References

Agliardi, C., Meloni, M., Guerini, F. R., Zanzottera, M., Bolognesi, E., Baglio, F., et al. (2021). Oligomeric α-Syn and SNARE complex proteins in peripheral extracellular vesicles of neural origin are biomarkers for Parkinson's disease. *Neurobiol. Dis.* 148:105185. doi: 10.1016/j.nbd.2020.105185

Aigner, A. (2019). Perspectives, issues and solutions in RNAi therapy: The expected and the less expected. *Nanomedicine (Lond)* 14, 2777–2782. doi: 10.2217/nnm-2019-0321

Akhilesh, Uniyal, A., Gadepalli, A., Tiwari, V., Allani, M., Chouhan, D., et al. (2022). Unlocking the potential of TRPV1 based siRNA therapeutics for the treatment of chemotherapy-induced neuropathic pain. *Life Sci.* 288:120187. doi: 10.1016/j.lfs.2021.120187

Arioz, B. I., Tufekci, K. U., Olcum, M., Durur, D. Y., Akarlar, B. A., Ozlu, N., et al. (2021). Proteome profiling of neuron-derived exosomes in Alzheimer's disease reveals hemoglobin as a potential biomarker. *Neurosci. Lett.* 755:135914. doi: 10.1016/j.neulet.2021.135914

Athauda, D., Gulyani, S., Karnati, H. K., Li, Y., Tweedie, D., Mustapic, M., et al. (2019). Utility of neuronal-derived exosomes to examine molecular mechanisms that affect motor function in patients with Parkinson disease: A secondary analysis of the Exenatide-PD trial. *JAMA Neurol.* 76, 420–429. doi: 10.1001/jamaneurol.2018.4304

Backe, S. J., Sager, R. A., Regan, B. R., Sit, J., Major, L. A., Bratslavsky, G., et al. (2022). A specialized Hsp90 co-chaperone network regulates steroid hormone receptor response to ligand. *Cell Rep.* 40:111039. doi: 10.1016/j.celrep.2022.111039

Barbosa, M., Gomes, C., Sequeira, C., Gonçalves-Ribeiro, J., Pina, C. C., Carvalho, L. A., et al. (2021). Recovery of depleted miR-146a in ALS cortical astrocytes reverts cell aberrancies and prevents paracrine pathogenicity on microglia and motor neurons. *Front. Cell Dev. Biol.* 9:634355. doi: 10.3389/fcell.2021.634355

Batrakova, E. V., and Kim, M. S. (2015). Using exosomes, naturally-equipped nanocarriers, for drug delivery. *J. Control Release* 219, 396–405. doi: 10.1016/j.jconrel.2015.07.030

Bhargava, P., Nogueras-Ortiz, C., Chawla, S., Bæk, R., Jørgensen, M. M., and Kapogiannis, D. (2019). Altered levels of toll-like receptors in circulating extracellular vesicles in multiple sclerosis. *Cells* 8:1058. doi: 10.3390/cells8091058

Blommer, J., Pitcher, T., Mustapic, M., Eren, E., Yao, P. J., Vreones, M. P., et al. (2022). Extracellular vesicle biomarkers for cognitive impairment in Parkinson's disease. *Brain* awac258. doi: 10.1093/brain/awac258

Bonafede, R., Brandi, J., Manfredi, M., Scambi, I., Schiaffino, L., Merigo, F., et al. (2019). The anti-apoptotic effect of ASC-Exosomes in an in vitro ALS model and their proteomic analysis. *Cells* 8:1087. doi: 10.3390/cells8091087

Bonafede, R., Turano, E., Scambi, I., Busato, A., Bontempi, P., Virla, F., et al. (2020). Exosomes ameliorate the disease progression in SOD1(G93A) murine model underlining their potential therapeutic use in human ALS. *Int. J. Mol. Sci.* 21:3651. doi: 10.3390/ijms21103651

Borgonio-Cuadra, V. M., Valdez-Vargas, C., Romero-Córdoba, S., Hidalgo-Miranda, A., Tapia-Guerrero, Y., Cerecedo-Zapata, C. M., et al. (2019). Wide profiling of circulating MicroRNAs in spinocerebellar ataxia type 7. *Mol. Neurobiol.* 56, 6106–6120. doi: 10.1007/s12035-019-1480-y

Boutary, S., Caillaud, M., El Madani, M., Vallat, J. M., Loisel-Duwattez, J., Rouyer, A., et al. (2021). Squalenoyl siRNA PMP22 nanoparticles are effective in treating mouse models of Charcot-Marie-Tooth disease type 1 A. *Commun. Biol.* 4:317. doi: 10.1038/s42003-021-01839-2

Carmona, V., Cunha-Santos, J., Onofre, I., Simões, A. T., Vijayakumar, U., Davidson, B. L. et al. (2017). Unravelling endogenous MicroRNA system dysfunction as a new pathophysiological mechanism in machado-joseph disease. *Mol. Ther.* 25, 1038–1055. doi: 10.1016/j.ymthe.2017.01.021

Carvalho, T. M., Brasil, G. O., Jucoski, T. S., Adamoski, D., de Lima, R. S., Spautz, C. C., et al. (2022). MicroRNAs miR-142-5p, miR-150-5p, miR-320a-3p, and miR-4433b-5p in serum and tissue: Potential biomarkers in sporadic breast cancer. *Front. Genet.* 13:865472. doi: 10.3389/fgene.2022.865472

Cendelin, J., Cvetanovic, M., Gandelman, M., Hirai, H., Orr, H. T., Pulst, S. M., et al. (2022). Consensus paper: Strengths and weaknesses of animal models of spinocerebellar ataxias and their clinical implications. *Cerebellum* 21, 452–481. doi: 10.1007/s12311-021-01311-1

Cervio, E., Barile, L., Moccetti, T., and Vassalli, G. (2015). Exosomes for intramyocardial intercellular communication. *Stem Cells Int.* 2015:482171. doi: 10.1155/2015/482171

Chen, H. Y., Hsu, C. L., Lin, H. Y., Lin, Y. F., Tsai, S. F., Ho, Y. J., et al. (2021). Clinical and functional characterization of a novel STUB1 frameshift mutation in autosomal dominant spinocerebellar ataxia type 48 (SCA48). *J. Biomed. Sci.* 28:65. doi: 10.1186/s12929-021-00763-1

Chen, W., Zheng, P., Hong, T., Wang, Y., Liu, N., He, B., et al. (2020). Astrocytes-derived exosomes induce neuronal recovery after traumatic brain injury via delivering gap junction alpha 1-20 k. *J. Tissue Eng. Regen. Med.* 14, 412–423. doi: 10.1002/term.3002

Chen, Z., Xie, Y., Chen, W., Li, T., Chen, X., and Liu, B. (2021). microRNA-6785-5p-loaded human umbilical cord mesenchymal stem cells-derived exosomes suppress angiogenesis and metastasis in gastric cancer via INHBA. *Life Sci.* 284:119222. doi: 10.1016/j.lfs.2021.119222

Chiang, C. Y., and Chen, C. (2019). Toward characterizing extracellular vesicles at a single-particle level. *J. Biomed. Sci.* 26:9. doi: 10.1186/s12929-019-0502-4

Chung, C. C., Chan, L., Chen, J. H., Bamodu, O. A., and Hong, C. T. (2020). Neurofilament light chain level in plasma extracellular vesicles and Parkinson's disease. *Ther. Adv. Neurol. Disord.* 13:1756286420975917. doi: 10.1177/1756286420975917

Chu-Tan, J. A., Cioanca, A. V., Feng, Z. P., Wooff, Y., Schumann, U., Aggio-Bruce, R., et al. (2021). Functional microRNA targetome undergoes degeneration-induced shift in the retina. *Mol Neurodegener.* 16:60. doi: 10.1186/s13024-021-00478-9

Conceição, M., Mendonça, L., Nóbrega, C., Gomes, C., Costa, P., Hirai, H., et al. (2016). Intravenous administration of brain-targeted stable nucleic acid lipid particles alleviates Machado-Joseph disease neurological phenotype. *Biomaterials* 82, 124–137. doi: 10.1016/j.biomaterials.2015.12.021

Costa, M. D. C. (2020). Recent therapeutic prospects for Machado-Joseph disease. *Curr. Opin. Neurol.* 33, 519–526. doi: 10.1097/WCO.0000000000000832

Costa, M. D. C., Radzwion, M., McLoughlin, H. S., Ashraf, N. S., Fischer, S., Shakkottai, V. G., et al. (2020). In vivo molecular signatures of cerebellar pathology in spinocerebellar ataxia type 3. *Mov. Disord.* 35, 1774–1786. doi: 10.1002/mds.28140

Cui, F., Xu, Z., Lv, Y., and Hu, J. (2021). Role of spindle pole body component 25 in neurodegeneration. *Ann. Transl. Med.* 9:1432. doi: 10.21037/atm-21-4064

Cui, G. H., Wu, J., Mou, F. F., Xie, W. H., Wang, F. B., Wang, Q. L., et al. (2018). Exosomes derived from hypoxia-preconditioned mesenchymal stromal cells ameliorate cognitive decline by rescuing synaptic dysfunction and regulating inflammatory responses in APP/PS1 mice. *FASEB J.* 32, 654–668. doi: 10.1096/fj.201700600R

Cuomo-Haymour, N., Bergamini, G., Russo, G., Kulic, L., Knuesel, I., Martin, R., et al. (2022). Differential expression of serum extracellular vesicle miRNAs in multiple sclerosis: Disease-Stage specificity and relevance to pathophysiology. *Int. J. Mol. Sci.* 23:1664. doi: 10.3390/ijms23031664

Czubak-Prowizor, K., Babinska, A., and Swiatkowska, M. (2022). The F11 Receptor (F11R)/Junctional Adhesion Molecule-A (JAM-A) (F11R/JAM-A) in cancer progression. *Mol. Cell Biochem.* 477, 79–98. doi: 10.1007/s11010-021-04259-2

Ding, Y., Cao, F., Sun, H., Wang, Y., Liu, S., Wu, Y., et al. (2019). Exosomes derived from human umbilical cord mesenchymal stromal cells deliver exogenous miR-145-5p to inhibit pancreatic ductal adenocarcinoma progression. *Cancer Lett.* 442, 351–361. doi: 10.1016/j.canlet.2018.10.039

Dobricic, V., Schilling, M., Schulz, J., Zhu, L. S., Zhou, C. W., Fuß, J., et al. (2022). Differential microRNA expression analyses across two brain regions in Alzheimer's disease. *Transl. Psychiatry* 12:352. doi: 10.1038/s41398-022-02108-4

Du, L., Jiang, Y., and Sun, Y. (2021). Astrocyte-derived exosomes carry microRNA-17-5p to protect neonatal rats from hypoxic-ischemic brain damage via inhibiting BNIP-2 expression. *Neurotoxicology* 83, 28–39. doi: 10.1016/j.neuro.2020.12.006

Garcia-Contreras, M., and Thakor, A. S. (2021). Human adipose tissue-derived mesenchymal stem cells and their extracellular vesicles modulate lipopolysaccharide activated human microglia. *Cell Death Discov.* 7:98. doi: 10.1038/s41420-021-00471-7

Ghanekar, S. D., Kuo, S. H., Staffetti, J. S., and Zesiewicz, T. A. (2022). Current and emerging treatment modalities for spinocerebellar ataxias. *Expert Rev. Neurother.* 22, 101–114. doi: 10.1080/14737175.2022.2029703

Gómez, R., Tapia-Guerrero, Y. S., Cisneros, B., Orozco, L., Cerecedo-Zapata, C., Mendoza-Caamal, E., et al. (2022). Genetic distribution of five spinocerebellar ataxia microsatellite loci in mexican native american populations and its impact on contemporary mestizo populations. *Genes (Basel)* 13:157. doi: 10.3390/genes13010157

Gorabi, A. M., Kiaie, N., Aslani, S., Jamialahmadi, T., Johnston, T. P., and Sahebkar, A. (2020). Prospects for the potential of RNA interference in the treatment of autoimmune diseases: Small interfering RNAs in the spotlight. *J Autoimmun.* 114:102529. doi: 10.1016/j.jaut.2020.102529

Gupta, S., Singh, V., Ganesh, S., Singhal, N. K., and Sandhir, R. (2022). siRNA Mediated GSK3β knockdown targets insulin signaling pathway and rescues Alzheimer's disease pathology: Evidence from in vitro and in vivo studies. *ACS Appl. Mater. Interfaces* 14, 69–93. doi: 10.1021/acsami.1c15305

Harrell, C. R., Volarevic, V., Djonov, V., and Volarevic, A. (2022). Therapeutic potential of exosomes derived from adipose tissue-sourced mesenchymal stem cells in the treatment of neural and retinal diseases. *Int. J. Mol. Sci.* 23:4487. doi: 10.3390/ijms23094487

He, S., Huang, L., Shao, C., Nie, T., Xia, L., Cui, B., et al. (2021). Several miRNAs derived from serum extracellular vesicles are potential biomarkers for early diagnosis and progression of Parkinson's disease. *Transl. Neurodegener.* 10:25. doi: 10.1186/s40035-021-00249-y

Hernández-Soto, A., and Chacón-Cerdas, R. (2021). RNAi crop protection advances. *Int. J. Mol. Sci.* 22:12148. doi: 10.3390/ijms222212148

Herrmann, I. K., Wood, M. J. A., and Fuhrmann, G. (2021). Extracellular vesicles as a next-generation drug delivery platform. *Nat. Nanotechnol.* 16, 748–759. doi: 10.1038/s41565-021-00931-2

Hirunagi, T., Sahashi, K., Tachikawa, K., Leu, A. I., Nguyen, M., Mukthavaram, R., et al. (2021). Selective suppression of polyglutamine-expanded protein by lipid nanoparticle-delivered siRNA targeting CAG expansions in the mouse CNS. *Mol. Ther. Nucleic Acids* 24, 1–10. doi: 10.1016/j.omtn.2021.02.007

Holm, A., Hansen, S. N., Klitgaard, H., and Kauppinen, S. (2022). Clinical advances of RNA therapeutics for treatment of neurological and neuromuscular diseases. *RNA Biol.* 19, 594–608. doi: 10.1080/15476286.2022.2066334

Hong, Z., Tian, C., Stewart, T., Aro, P., Soltys, D., Bercow, M., et al. (2021). Development of a sensitive diagnostic assay for parkinson disease quantifying α-synuclein-containing extracellular vesicles. *Neurology* 96, e2332–e2345. doi: 10.1212/WNL.0000000000011853

Hou, X., Gong, X., Zhang, L., Li, T., Yuan, H., Xie, Y., et al. (2019). Identification of a potential exosomal biomarker in spinocerebellar ataxia Type 3/Machado-Joseph disease. *Epigenomics* 11, 1037–1056. doi: 10.2217/epi-2019-0081

Hu, Y. S., Do, J., Edamakanti, C. R., Kini, A. R., Martina, M., Stupp, S. I., et al. (2019). Self-assembling vascular endothelial growth factor nanoparticles improve function in spinocerebellar ataxia type 1. *Brain* 142, 312–321. doi: 10.1093/brain/awy328

Huang, Y., Li, R., Ye, S., Lin, S., Yin, G., and Xie, Q. (2020). Recent advances in the use of exosomes in Sjögren's syndrome. *Front. Immunol.* 11:1509. doi: 10.3389/fimmu.2020.01509

Hübener-Schmid, J., Kuhlbrodt, K., Peladan, J., Faber, J., Santana, M. M., Hengel, H., et al. (2021). Polyglutamine-Expanded Ataxin-3: A target engagement marker for spinocerebellar ataxia Type 3 in peripheral blood. *Mov. Disord.* 36, 2675–2681. doi: 10.1002/mds.28749

Jalles, A., Vieira, C., Pereira-Sousa, J., Vilasboas-Campos, D., Mota, A. F., Vasconcelos, S., et al. (2022). Aripiprazole offsets mutant ATXN3-Induced motor dysfunction by targeting dopamine D2 and serotonin 1A and 2A receptors in C. elegans. *Biomedicines* 10:370. doi: 10.3390/biomedicines10020370

Jhan, Y. Y., Prasca-Chamorro, D., Palou Zuniga, G., Moore, D. M., Arun Kumar, S., Gaharwar, A. K., et al. (2020). Engineered extracellular vesicles with synthetic lipids via membrane fusion to establish efficient gene delivery. *Int. J. Pharm.* 573:118802. doi: 10.1016/j.ijpharm.2019.118802

Jiang, Q., Yue, S., Yu, K., Tian, T., Zhang, J., Chu, H., et al. (2021). Endogenous microRNA triggered enzyme-free DNA logic self-assembly for amplified bioimaging and enhanced gene therapy via in situ generation of siRNAs. *J. Nanobiotechnol.* 19:288. doi: 10.1186/s12951-021-01040-x

Johnson, S. L., Ranxhi, B., Libohova, K., Tsou, W. L., and Todi, S. V. (2020). Ubiquitin-interacting motifs of ataxin-3 regulate its polyglutamine toxicity through Hsc70-4-dependent aggregation. *Elife* 9:e60742. doi: 10.7554/eLife.60742

Joshi, B. S., Youssef, S. A., Bron, R., de Bruin, A., Kampinga, H. H., and Zuhorn, I. S. (2021). DNAJB6b-enriched small extracellular vesicles decrease polyglutamine aggregation in in vitro and in vivo models of Huntington disease. *iScience* 24:103282. doi: 10.1016/j.isci.2021.103282

Kara, G., Calin, G. A., and Ozpolat, B. (2022). RNAi-based therapeutics and tumor targeted delivery in cancer. *Adv. Drug Deliv. Rev.* 182:114113. doi: 10.1016/j.addr.2022.114113

Kasai, T., Kojima, Y., Ohmichi, T., Tatebe, H., Tsuji, Y., Noto, Y. I., et al. (2019). Combined use of CSF NfL and CSF TDP-43 improves diagnostic performance in ALS. *Ann. Clin. Transl. Neurol.* 6, 2489–2502. doi: 10.1002/acn3.50943

Keiser, M. S., Monteys, A. M., Corbau, R., Gonzalez-Alegre, P., and Davidson, B. L. (2016). RNAi prevents and reverses phenotypes induced by mutant human ataxin-1. *Ann. Neurol.* 80, 754–765. doi: 10.1002/ana.24789

Keiser, M. S., Ranum, P. T., Yrigollen, C. M., Carrell, E. M., Smith, G. R., Muehlmatt, A. L., et al. (2021). Toxicity after AAV delivery of RNAi expression constructs into nonhuman primate brain. *Nat. Med.* 27, 1982–1989. doi: 10.1038/s41591-021-01522-3

Khan, I., Preeti, K., Fernandes, V., Khatri, D. K., and Singh, S. B. (2022). Role of MicroRNAs, aptamers in neuroinflammation and neurodegenerative disorders. *Cell Mol. Neurobiol.* 42, 2075–2095. doi: 10.1007/s10571-021-01093-4

Kotowska-Zimmer, A., Ostrovska, Y., and Olejniczak, M. (2020). Universal RNAi triggers for the specific inhibition of mutant huntingtin, Atrophin-1, Ataxin-3, and Ataxin-7 expression. *Mol. Ther. Nucleic Acids* 19, 562–571. doi: 10.1016/j.omtn.2019.12.012

Krauss, S., Nalavade, R., Weber, S., Carter, K., and Evert, B. O. (2019). Upregulation of miR-25 and miR-181 family members correlates with reduced expression of ATXN3 in lymphocytes from SCA3 patients. *Microrna* 8, 76–85. doi: 10.2174/2211536607666180821162403

Kulkarni, J. A., Witzigmann, D., Thomson, S. B., Chen, S., Leavitt, B. R., Cullis, P. R., et al. (2021). The current landscape of nucleic acid therapeutics. *Nat. Nanotechnol.* 16, 630–643. doi: 10.1038/s41565-021-00898-0

Lee, E. J., Choi, Y., Lee, H. J., Hwang, D. W., and Lee, D. S. (2022). Human neural stem cell-derived extracellular vesicles protect against Parkinson's disease pathologies. *J. Nanobiotechnol.* 20:198. doi: 10.1186/s12951-022-01356-2

Lee, M., Im, W., and Kim, M. (2021). Exosomes as a potential messenger unit during heterochronic parabiosis for amelioration of Huntington's disease. *Neurobiol. Dis.* 155:105374. doi: 10.1016/j.nbd.2021.105374

Li, M., Liu, F., Hao, X., Fan, Y., Li, J., Hu, Z., et al. (2022). Rare KCND3 Loss-of-Function mutation associated with the SCA19/22. *Front. Mol. Neurosci.* 15:919199. doi: 10.3389/fnmol.2022.919199

Li, M., Zhou, H., Yang, C., Wu, Y., Zhou, X., Liu, H., et al. (2020). Bacterial outer membrane vesicles as a platform for biomedical applications: An update. *J. Control Release* 323, 253–268. doi: 10.1016/j.jconrel.2020.04.031

Li, T. R., Yao, Y. X., Jiang, X. Y., Dong, Q. Y., Yu, X. F., Wang, T., et al. (2022). β-Amyloid in blood neuronal-derived extracellular vesicles is elevated in cognitively normal adults at risk of Alzheimer's disease and predicts cerebral amyloidosis. *Alzheimers Res. Ther.* 14:66. doi: 10.1186/s13195-022-01010-x

Li, Y. J., Wu, J. Y., Wang, J. M., Hu, X. B., Cai, J. X., and Xiang, D. X. (2020). Gemcitabine loaded autologous exosomes for effective and safe chemotherapy of pancreatic cancer. *Acta Biomater.* 101, 519–530. doi: 10.1016/j.actbio.2019.10.022

Li, Z., Moniruzzaman, M., Dastgheyb, R. M., Yoo, S. W., Wang, M., Hao, H., et al. (2020). Astrocytes deliver CK1 to neurons via extracellular vesicles in response to inflammation promoting the translation and amyloidogenic processing of APP. *J. Extracell. Vesicles* 10:e12035. doi: 10.1002/jev2.12035

Lian, M., Limwongse, C., Yoon, C. S., Lee, C. G., Law, H. Y., and Chong, S. S. (2022). Single-Tube screen for rapid detection of repeat expansions in seven common spinocerebellar ataxias. *Clin. Chem.* 68, 794–802. doi: 10.1093/clinchem/hvac011

Lin, Z., Gu, Y., Zhou, R., Wang, M., Guo, Y., Chen, Y., et al. (2020). Serum exosomal proteins F9 and TSP-1 as potential diagnostic biomarkers for newly diagnosed epilepsy. *Front. Neurosci.* 14:737. doi: 10.3389/fnins.2020.00737

Liu, S., Fan, M., Xu, J. X., Yang, L. J., Qi, C. C., Xia, Q. R., et al. (2022). Exosomes derived from bone-marrow mesenchymal stem cells alleviate cognitive decline in AD-like mice by improving BDNF-related neuropathology. *J. Neuroinflammation* 19:35. doi: 10.1186/s12974-022-02393-2

Liu, Y., Zhang, Z., Wang, B., Dong, Y., Zhao, C., Zhao, Y., et al. (2022). Inflammation-Stimulated MSC-Derived small extracellular vesicle miR-27b-3p regulates macrophages by targeting CSF-1 to promote temporomandibular joint condylar regeneration. *Small* 18:e2107354. doi: 10.1002/smll.202107354

Loch-Neckel, G., Matos, A. T., Vaz, A. R., and Brites, D. (2022). Challenges in the development of drug delivery systems based on small extracellular vesicles for therapy of brain diseases. *Front. Pharmacol.* 13:839790. doi: 10.3389/fphar.2022.839790

Long, Q., Upadhya, D., Hattiangady, B., Kim, D. K., An, S. Y., Shuai, B., et al. (2017). Intranasal MSC-derived A1-exosomes ease inflammation, and prevent abnormal neurogenesis and memory dysfunction after status epilepticus. *Proc. Natl. Acad. Sci. U.S.A.* 114, E3536–E3545. doi: 10.1073/pnas.1703920114

Longoni, B., Fasciani, I., Kolachalam, S., Pietrantoni, I., Marampon, F., Petragnano, F., et al. (2019). Neurotoxic and neuroprotective role of exosomes in Parkinson's disease. *Curr. Pharm. Des.* 25, 4510–4522. doi: 10.2174/1381612825666191113103537

Magen, I., Yacovzada, N. S., Yanowski, E., Coenen-Stass, A., Grosskreutz, J., Lu, C. H., et al. (2021). Circulating miR-181 is a prognostic biomarker for amyotrophic lateral sclerosis. *Nat. Neurosci.* 24, 1534–1541. doi: 10.1038/s41593-021-00936-z

Marco, S., Murillo, A., and Pérez-Otaño, I. (2018). RNAi-Based GluN3A silencing prevents and reverses disease phenotypes induced by mutant huntingtin. *Mol. Ther.* 26, 1965–1972. doi: 10.1016/j.ymthe.2018.05.013

Martier, R., Sogorb-Gonzalez, M., Stricker-Shaver, J., Hübener-Schmid, J., Keskin, S., Klima, J., et al. (2019). Development of an AAV-Based MicroRNA gene therapy to treat Machado-Joseph disease. *Mol. Ther. Methods Clin. Dev.* 15, 343–358. doi: 10.1016/j.omtm.2019.10.008

Mathieu, M., Martin-Jaular, L., Lavieu, G., and Théry, C. (2019). Specificities of secretion and uptake of exosomes and other extracellular vesicles for cell-to-cell communication. *Nat. Cell Biol.* 21, 9–17. doi: 10.1038/s41556-018-0250-9

Matsuzaka, Y., and Yashiro, R. (2022). Immune modulation using extracellular vesicles encapsulated with MicroRNAs as novel drug delivery systems. *Int. J. Mol. Sci.* 23:5658. doi: 10.3390/ijms23105658

Mishra, N., Ashique, S., Garg, A., Rai, V. K., Dua, K., Goyal, A., et al. (2022). Role of siRNA-based nanocarriers for the treatment of neurodegenerative diseases. *Drug Discov. Today* 27, 1431–1440. doi: 10.1016/j.drudis.2022.01.003

Moore, C. B., Guthrie, E. H., Huang, M. T., and Taxman, D. J. (2010). Short hairpin RNA (shRNA): Design, delivery, and assessment of gene knockdown. *Methods Mol. Biol.* 629, 141–158. doi: 10.1007/978-1-60761-657-3_10

Mori, M. A., Ludwig, R. G., Garcia-Martin, R., Brandão, B. B., and Kahn, C. R. (2019). Extracellular miRNAs: From biomarkers to mediators of physiology and disease. *Cell Metab.* 30, 656–673. doi: 10.1016/j.cmet.2019.07.011

Mueller, C., Berry, J. D., McKenna-Yasek, D. M., Gernoux, G., Owegi, M. A., Pothier, L. M., et al. (2020). SOD1 suppression with adeno-associated virus and MicroRNA in familial ALS. *N. Engl. J. Med.* 383, 151–158. doi: 10.1056/NEJMoa2005056

Muraoka, S., Lin, W., Takamatsu-Yukawa, K., Hu, J., Ikezu, S., DeTure, M. A., et al. (2021b). Enrichment of phosphorylated tau (Thr181) and functionally interacting molecules in chronic traumatic encephalopathy brain-derived extracellular vesicles. *Aging Dis.* 12, 1376–1388. doi: 10.14336/AD.2020.1007

Muraoka, S., DeLeo, A. M., Yang, Z., Tatebe, H., Yukawa-Takamatsu, K., Ikezu, S., et al. (2021a). Proteomic profiling of extracellular vesicles separated from plasma of former national football league players at risk for chronic traumatic encephalopathy. *Aging Dis.* 12, 1363–1375. doi: 10.14336/AD.2020.0908

Nakamori, M., Junn, E., Mochizuki, H., and Mouradian, M. M. (2019). Nucleic Acid-Based therapeutics for Parkinson's disease. *Neurotherapeutics* 16, 287–298. doi: 10.1007/s13311-019-00714-7

Nitschke, L., Tewari, A., Coffin, S. L., Xhako, E., Pang, K., Gennarino, V. A., et al. (2020). miR760 regulates ATXN1 levels via interaction with its 5' untranslated region. *Genes Dev.* 34, 1147–1160. doi: 10.1101/gad.339317.120

Niu, Y., Wang, X., Li, M., and Niu, B. (2020). Exosomes from human umbilical cord Mesenchymal stem cells attenuates stress-induced hippocampal dysfunctions. *Metab. Brain Dis.* 35, 1329–1340. doi: 10.1007/s11011-019-00514-0

Nobre, R. J., Lobo, D. D., Henriques, C., Duarte, S. P., Lopes, S. M., Silva, A. C., et al. (2022). miRNA-Mediated Knockdown of ATXN3 alleviates molecular disease hallmarks in a mouse model for spinocerebellar ataxia type 3. *Nucleic Acid Ther.* 32, 194–205. doi: 10.1089/nat.2021.0020

Nonaka, W., Takata, T., Iwama, H., Komatsubara, S., Kobara, H., Kamada, M., et al. (2022). A cerebrospinal fluid microRNA analysis: Progressive supranuclear palsy. *Mol. Med. Rep.* 25:88. doi: 10.3892/mmr.2022.12604

O'Brien, K., Breyne, K., Ughetto, S., Laurent, L. C., and Breakefield, X. O. (2020). RNA delivery by extracellular vesicles in mammalian cells and its applications. *Nat. Rev. Mol. Cell Biol.* 21, 585–606. doi: 10.1038/s41580-020-0251-y

Paul, S., Dansithong, W., Figueroa, K. P., Scoles, D. R., and Pulst, S. M. (2018). Staufen1 links RNA stress granules and autophagy in a model of neurodegeneration. *Nat. Commun.* 9:3648. doi: 10.1038/s41467-018-06041-3

Pei, X., Li, Y., Zhu, L., and Zhou, Z. (2020). Astrocyte-derived exosomes transfer miR-190b to inhibit oxygen and glucose deprivation-induced autophagy and neuronal apoptosis. *Cell Cycle* 19, 906–917. doi: 10.1080/15384101.2020.1731649

Penning, A., Tosoni, G., Abiega, O., Bielefeld, P., Gasperini, C., De Pietri Tonelli, D., et al. (2021). Adult neural stem cell regulation by small non-coding RNAs: Physiological significance and pathological implications. *Front. Cell Neurosci.* 15:781434. doi: 10.3389/fncel.2021.781434

Pérez Ortiz, J. M., and Orr, H. T. (2018). Spinocerebellar ataxia type 1: Molecular mechanisms of neurodegeneration and preclinical studies. *Adv. Exp. Med. Biol.* 1049, 135–145. doi: 10.1007/978-3-319-71779-1_6

Pomatto, M. A. C., Negro, F., and Camussi, G. (2022). Optimized protocol for plasma-derived extracellular vesicles loading with synthetic miRNA mimic using electroporation. *Methods Mol. Biol.* 2504, 219–230. doi: 10.1007/978-1-0716-2341-1_16

Qian, H., Kang, X., Hu, J., Zhang, D., Liang, Z., Meng, F., et al. (2020). Reversing a model of Parkinson's disease with in situ converted nigral neurons. *Nature* 582, 550–556. doi: 10.1038/s41586-020-2388-4

Rezaei, R., Baghaei, K., Amani, D., Piccin, A., Hashemi, S. M., Asadzadeh Aghdaei, H., et al. (2021). Exosome-mediated delivery of functionally active miRNA-375-3p mimic regulate epithelial mesenchymal transition (EMT) of colon cancer cells. *Life Sci.* 269:119035. doi: 10.1016/j.lfs.2021.119035

Roshani, F., Delavar Kasmaee, H., Falahati, K., Arabzade, G., Sohan Forooshan Moghadam, A., and Sanati, M. H. (2021). Analysis of Micro-RNA-144 expression profile in patients with multiple sclerosis in comparison with healthy individuals. *Rep. Biochem. Mol. Biol.* 10, 396–401. doi: 10.52547/rbmb.10.3.396

Rübsamen, N., Pape, S., Konigorski, S., Zapf, A., Rücker, G., and Karch, A. (2022). Diagnostic accuracy of cerebrospinal fluid biomarkers for the differential diagnosis of sporadic Creutzfeldt-Jakob disease: A (network) meta-analysis. *Eur. J. Neurol.* 29, 1366–1376. doi: 10.1111/ene.15258

Saad, N. Y., Al-Kharsan, M., Garwick-Coppens, S. E., Chermahini, G. A., Harper, M. A., Palo, A., et al. (2021). Human miRNA miR-675 inhibits DUX4 expression and may be exploited as a potential treatment for facioscapulohumeral muscular dystrophy. *Nat. Commun.* 12:7128. doi: 10.1038/s41467-021-27430-1

Sanchez, I. I., Nguyen, T. B., England, W. E., Lim, R. G., Vu, A. Q., Miramontes, R., et al. (2021). Huntington's disease mice and human brain tissue exhibit increased G3BP1 granules and TDP43 mislocalization. *J. Clin. Invest.* 131:e140723. doi: 10.1172/JCI140723

Sandau, U. S., McFarland, T. J., Smith, S. J., Galasko, D. R., Quinn, J. F., and Saugstad, J. A. (2022). Differential effects of APOE genotype on MicroRNA cargo of cerebrospinal fluid extracellular vesicles in females with Alzheimer's disease compared to males. *Front. Cell Dev. Biol.* 10:864022. doi: 10.3389/fcell.2022.864022

Sava, V., Fihurka, O., Khvorova, A., and Sanchez-Ramos, J. (2020). Enriched chitosan nanoparticles loaded with siRNA are effective in lowering Huntington's disease gene expression following intranasal administration. *Nanomedicine* 24:102119. doi: 10.1016/j.nano.2019.102119

Scholefield, J., Greenberg, L. J., Weinberg, M. S., Arbuthnot, P. B., Abdelgany, A., and Wood, M. J. (2009). Design of RNAi hairpins for mutation-specific silencing of ataxin-7 and correction of a SCA7 phenotype. *PLoS One* 4:e7232. doi: 10.1371/journal.pone.0007232

Serlidaki, D., van Waarde, M. A. W. H., Rohland, L., Wentink, A. S., Dekker, S. L., Kamphuis, M. J., et al. (2020). Functional diversity between HSP70 paralogs caused by variable interactions with specific co-chaperones. *J. Biol. Chem.* 295, 7301–7316. doi: 10.1074/jbc.RA119.012449

Setten, R. L., Rossi, J. J., and Han, S. P. (2019). The current state and future directions of RNAi-based therapeutics. *Nat. Rev. Drug Discov.* 18, 421–446. doi: 10.1038/s41573-019-0017-4

Sheng, P., Flood, K. A., and Xie, M. (2020). Short hairpin RNAs for strand-specific small interfering RNA production. *Front. Bioeng. Biotechnol.* 8:940. doi: 10.3389/fbioe.2020.00940

Shimizu, T., Tsutsumi, R., Shimizu, K., Tominaga, N., Nagai, M., Ugawa, Y., et al. (2020). Differential effects of thyrotropin releasing hormone (TRH) on motor execution and motor adaptation process in patients with spinocerebellar degeneration. *J. Neurol. Sci.* 415:116927. doi: 10.1016/j.jns.2020.116927

Shin, H. R., Moon, J., Lee, W. J., Lee, H. S., Kim, E. Y., Shin, S., et al. (2021). Serum neurofilament light chain as a severity marker for spinocerebellar ataxia. *Sci. Rep.* 11:13517. doi: 10.1038/s41598-021-92855-z

Sjoqvist, S., and Otake, K. (2022). A pilot study using proximity extension assay of cerebrospinal fluid and its extracellular vesicles identifies novel amyotrophic lateral sclerosis biomarker candidates. *Biochem. Biophys. Res. Commun.* 613, 166–173. doi: 10.1016/j.bbrc.2022.04.127

Soares Martins, T., Marçalo, R., da Cruz, E., Silva, C. B., Trindade, D., Catita, J., et al. (2022). Novel exosome biomarker candidates for Alzheimer's disease unravelled through mass spectrometry analysis. *Mol. Neurobiol.* 59, 2838–2854 doi: 10.1007/s12035-022-02762-1

Song, S., Lee, J. U., Jeon, M. J., Kim, S., and Sim, S. J. (2022). Detection of multiplex exosomal miRNAs for clinically accurate diagnosis of Alzheimer's disease using label-free plasmonic biosensor based on DNA-Assembled advanced plasmonic architecture. *Biosens. Bioelectron.* 199:113864. doi: 10.1016/j.bios.2021.113864

Song, Y., Li, Z., He, T., Qu, M., Jiang, L., Li, W., et al. (2019). M2 microglia-derived exosomes protect the mouse brain from ischemia-reperfusion injury via exosomal miR-124. *Theranostics* 9, 2910–2923. doi: 10.7150/thno.30879

Sun, D., Zhuang, X., Xiang, X., Liu, Y., Zhang, S., Liu, C., et al. (2010). A novel nanoparticle drug delivery system: The anti-inflammatory activity of curcumin is enhanced when encapsulated in exosomes. *Mol. Ther.* 18, 1606–1614. doi: 10.1038/mt.2010.105

Sun, I. O., Bae, Y. U., Lee, H., Kim, H., Jeon, J. S., Noh, H., et al. (2022). Circulating miRNAs in extracellular vesicles related to treatment response in patients with idiopathic membranous nephropathy. *J. Transl. Med.* 20:224. doi: 10.1186/s12967-022-03430-7

Sun, T., Ding, Z. X., Luo, X., Liu, Q. S., and Cheng, Y. (2020). Blood exosomes have neuroprotective effects in a mouse model of Parkinson's disease. *Oxid. Med. Cell. Longev.* 2020:3807476. doi: 10.1155/2020/3807476

Surgucheva, I., Sharov, V. S., and Surguchov, A. (2012). γ-Synuclein: Seeding of α-synuclein aggregation and transmission between cells. *Biochemistry* 51, 4743–4754. doi: 10.1021/bi300478w

Suto, N., Mieda, T., Iizuka, A., Nakamura, K., and Hirai, H. (2016). Morphological and functional attenuation of degeneration of peripheral neurons by mesenchymal stem cell-conditioned medium in spinocerebellar ataxia type 1-Knock-in Mice. *CNS Neurosci. Ther.* 22, 670–676. doi: 10.1111/cns.12560

Takeuchi, T., and Nagai, Y. (2022). Emerging roles of extracellular vesicles in polyglutamine diseases: Mutant protein transmission, therapeutic potential, and diagnostics. *Neurochem. Int.* 157:105357. doi: 10.1016/j.neuint.2022.105357

Tao, L., Xu, C., Shen, W., Tan, J., Li, L., Fan, M., et al. (2021). HIPK3 inhibition by exosomal hsa-miR-101-3p is related to metabolic reprogramming in colorectal cancer. *Front. Oncol.* 11:758336. doi: 10.3389/fonc.2021.758336

Tapparo, M., Pomatto, M. A. C., Deregibus, M. C., Papadimitriou, E., Cavallari, C., D'Antico, S., et al. (2021). Serum derived extracellular vesicles mediated delivery of synthetic miRNAs in human endothelial cells. *Front. Mol. Biosci.* 8:636587. doi: 10.3389/fmolb.2021.636587

Thome, A. D., Thonhoff, J. R., Zhao, W., Faridar, A., Wang, J., Beers, D. R., et al. (2022). Extracellular vesicles derived from ex vivo expanded regulatory T cells modulate in vitro and in vivo inflammation. *Front. Immunol.* 13:875825. doi: 10.3389/fimmu.2022.875825

Tian, C., Stewart, T., Hong, Z., Guo, Z., Aro, P., Soltys, D., et al. (2022). Alzheimer's disease neuroimaging initiative. Blood extracellular vesicles carrying synaptic function- and brain-related proteins as potential biomarkers for Alzheimer's disease. *Alzheimers Dement.* doi: 10.1002/alz.12723

Van den Broek, B., Wuyts, C., Sisto, A., Pintelon, I., Timmermans, J. P., Somers, V., et al. (2022). Oligodendroglia-derived extracellular vesicles activate autophagy via LC3B/BAG3 to protect against oxidative stress with an enhanced effect for HSPB8 enriched vesicles. *Cell Commun. Signal.* 20:58. doi: 10.1186/s12964-022-00863-x

Vázquez-Mojena, Y., León-Arcia, K., González-Zaldivar, Y., Rodríguez-Labrada, R., and Velázquez-Pérez, L. (2021). Gene therapy for polyglutamine spinocerebellar ataxias: Advances, challenges, and perspectives. *Mov. Disord.* 36, 2731–2744. doi: 10.1002/mds.28819

Wang, P., Zhou, Y., and Richards, A. M. (2021). Effective tools for RNA-derived therapeutics: siRNA interference or miRNA mimicry. *Theranostics* 11, 8771–8796. doi: 10.7150/thno.62642

Wang, S., Khan, A., Huang, R., Ye, S., Di, K., Xiong, T., et al. (2020). Recent advances in single extracellular vesicle detection methods. *Biosens. Bioelectron.* 154:112056. doi: 10.1016/j.bios.2020.112056

Wang, W., Zhou, P., Wang, X., Chen, F., Christensen, E., Thompson, J., et al. (2022). Efficient and precise processing of the optimized primary artificial MicroRNA in a Huntingtin-Lowering Adeno-Associated viral gene therapy in vitro and in mice and nonhuman primates. *Hum. Gene Ther.* 33, 37–60. doi: 10.1089/hum.2021.221

Wei, X. C., Xia, Y. R., Zhou, P., Xue, X., Ding, S., Liu, L. J., et al. (2021). Hepatitis B core antigen modulates exosomal miR-135a to target vesicle-associated membrane protein 2 promoting chemoresistance in hepatocellular carcinoma. *World J. Gastroenterol.* 27, 8302–8322. doi: 10.3748/wjg.v27.i48.8302

Williams, A. M., Bhatti, U. F., Brown, J. F., Biesterveld, B. E., Kathawate, R. G., Graham, N. J., et al. (2020). Early single-dose treatment with exosomes provides neuroprotection and improves blood-brain barrier integrity in swine model of traumatic brain injury and hemorrhagic shock. *J. Trauma Acute Care Surg.* 88, 207–218. doi: 10.1097/TA.0000000000002563

Xia, H., Mao, Q., Eliason, S. L., Harper, S. Q., Martins, I. H., Orr, H. T., et al. (2004). RNAi suppresses polyglutamine-induced neurodegeneration in a model of spinocerebellar ataxia. *Nat. Med.* 10, 816–820. doi: 10.1038/nm1076

Yang, L., Shao, Y. R., Li, X. Y., Ma, Y., Dong, Y., and Wu, Z. Y. (2021). Association of the level of neurofilament light with disease severity in patients with spinocerebellar ataxia type 2. *Neurology* 97, e2404–e2413. doi: 10.1212/WNL.0000000000012945

Yap, K. H., Azmin, S., Che Hamzah, J., Ahmad, N., van de Warrenburg, B., and Mohamed Ibrahim, N. (2022b). Pharmacological and non-pharmacological management of spinocerebellar ataxia: A systematic review. *J. Neurol.* 269, 2315–2337. doi: 10.1007/s00415-021-10874-2

Yap, K. H., Abdul Manan, H., Yahya, N., Azmin, S., Mohamed Mukari, S. A., and Mohamed Ibrahim, N. (2022a). Magnetic resonance imaging and its clinical correlation in spinocerebellar ataxia type 3: A systematic review. *Front. Neurosci.* 16:859651. doi: 10.3389/fnins.2022.859651

Ye, C., Zheng, F., Xu, T., Wu, N., Tong, Y., Xiong, X. Q., et al. (2022). Norepinephrine acting on adventitial fibroblasts stimulates vascular smooth muscle cell proliferation via promoting small extracellular vesicle release. *Theranostics* 12, 4718–4733. doi: 10.7150/thno.70974

You, H. J., Fang, S. B., Wu, T. T., Zhang, H., Feng, Y. K., Li, X. J., et al. (2020). Mesenchymal stem cell-derived exosomes improve motor function and attenuate neuropathology in a mouse model of Machado-Joseph disease. *Stem Cell Res. Ther.* 11:222. doi: 10.1186/s13287-020-01727-2

Yu, L., Li, H., Liu, W., Zhang, L., Tian, Q., Li, H., et al. (2021). MiR-485-3p serves as a biomarker and therapeutic target of Alzheimer's disease via regulating neuronal cell viability and neuroinflammation by targeting AKT3. *Mol. Genet. Genomic Med.* 9:e1548. doi: 10.1002/mgg3.1548

Zavatti, M., Gatti, M., Beretti, F., Palumbo, C., and Maraldi, T. (2022). Exosomes derived from human amniotic fluid mesenchymal stem cells preserve microglia and neuron cells from Aβ. *Int. J. Mol. Sci.* 23:4967. doi: 10.3390/ijms23094967

Zhai, L., Shen, H., Sheng, Y., and Guan, Q. A. D. M. S. C. (2021). Exo-MicroRNA-22 improve neurological function and neuroinflammation in mice with Alzheimer's disease. *J. Cell Mol. Med.* 25, 7513–7523. doi: 10.1111/jcmm.16787

Zhang, Q., Higginbotham, J. N., Jeppesen, D. K., Yang, Y. P., Li, W., McKinley, E. T., et al. (2019). Transfer of functional cargo in exomeres. *Cell Rep.* 27, 940.e–954.e. doi: 10.1016/j.celrep.2019.01.009

Zhang, Y., Liu, Q., Zhang, X., Huang, H., Tang, S., Chai, Y., et al. (2022). Recent advances in exosome-mediated nucleic acid delivery for cancer therapy. *J. Nanobiotechnol.* 20:279. doi: 10.1186/s12951-022-01472-z

Zhao, Y., Haney, M. J., Fallon, J. K., Rodriguez, M., Swain, C. J., Arzt, C. J., et al. (2022a). Using extracellular vesicles released by GDNF-Transfected macrophages for therapy of parkinson disease. *Cells* 11:1933. doi: 10.3390/cells11121933

Zhao, Y., Liang, Y., Xu, Z., Liu, J., Liu, X., Ma, J., et al. (2022b). Exosomal miR-673-5p from fibroblasts promotes schwann cell-mediated peripheral neuron myelination by targeting the TSC2/mTORC1/SREBP2 axis. *J. Biol. Chem.* 298:101718. doi: 10.1016/j.jbc.2022.101718

Zhou, Z. R., Chen, X., Lv, J., Li, D. W., Yang, C. D., Liu, H. L., et al. (2022). A plasmonic nanoparticle-embedded polydopamine substrate for fluorescence detection of extracellular vesicle biomarkers in serum and urine from patients with systemic lupus erythematosus. *Talanta* 247:123620. doi: 10.1016/j.talanta.2022.123620

Zhu, Y., Zhang, X., Yang, K., Shao, Y., Gu, R., Liu, X., et al. (2022). Macrophage-derived apoptotic vesicles regulate fate commitment of mesenchymal stem cells via miR155. *Stem Cell Res. Ther.* 13:323. doi: 10.1186/s13287-022-03004-w

frontiers | Frontiers in Molecular Neuroscience

TYPE Original Research
PUBLISHED 10 November 2022
DOI 10.3389/fnmol.2022.1019974

OPEN ACCESS

EDITED BY
Aruna Sharma,
Uppsala University, Sweden

REVIEWED BY
Amjad Khan,
Université de Strasbourg, France
Mariana Santos,
Universidade Do Porto, Portugal

*CORRESPONDENCE
Bo Shen
shenb@enzemed.com
Yuanlin Zhou
zyl@enzemed.com

SPECIALTY SECTION
This article was submitted to Brain Disease Mechanisms, a section of the journal Frontiers in Molecular Neuroscience

RECEIVED 15 August 2022
ACCEPTED 26 September 2022
PUBLISHED 10 November 2022

CITATION
Chen S, Du J, Jiang H, Zhao W, Wang N, Ying A, Li J, Chen S, Shen B and Zhou Y (2022) Ataxia with oculomotor apraxia type 2 caused by a novel homozygous mutation in SETX gene, and literature review. *Front. Mol. Neurosci.* 15:1019974. doi: 10.3389/fnmol.2022.1019974

Ataxia with oculomotor apraxia type 2 caused by a novel homozygous mutation in SETX gene, and literature review

Shuaishuai Chen[1], Juping Du[1], Huihua Jiang[2], Weibo Zhao[3], Na Wang[1], Anna Ying[2], Jun Li[1], Shiyong Chen[1], Bo Shen[1]* and Yuanlin Zhou[2]*

[1]Department of Clinical Laboratory, Taizhou Hospital of Zhejiang Province Affiliated to Wenzhou Medical University, Linhai, China, [2]Department of Neurology, Taizhou Hospital of Zhejiang Province Affiliated to Wenzhou Medical University, Linhai, China, [3]Department of Orthopedics, Taizhou Hospital of Zhejiang Province Affiliated to Wenzhou Medical University, Linhai, China

Objectives: Autosomal recessive inherited ataxia with oculomotor apraxia type 2 (AOA2), caused by *SETX* gene mutations, is characterized by early-onset, progressive cerebellar ataxia, peripheral neuropathy, oculomotor apraxia and elevated serum α-fetoprotein (AFP). This study aimed to expand and summarize the clinical and genetic characteristics of *SETX* variants related to AOA2.

Methods: The biochemical parameters, electromyogram and radiological findings of the patient were evaluated. Whole-exome sequencing (WES) was performed on the patient using next-generation sequencing (NGS), the variants were confirmed by Sanger sequencing and the pathogenicity of the variants was classified according to the American College of Medical Genetics and Genomics/Association for Molecular Pathology (ACMG/AMP) guidelines. We reviewed 57 studies of AOA2 patients with *SETX* mutations and collected clinical and genetic information.

Results: The patient was a 40-year-old Chinese woman who primarily presented with numbness and weakness of the lower limbs in her teenage years. She had elevated AFP, increased serum follicle-stimulating hormone (FSH) and luteinizing hormone (LH) and decreased anti-Müllerian hormone (AMH) levels. We identified a novel homozygous missense mutation of the *SETX* gene, c.7118 C>T (p. Thr2373Ile), in the patient via Whole-exome and Sanger sequencing. The variant was located in the DNA/RNA helicase domain and is highly conserved. The protein prediction analysis verified the *SETX* variant as a damaging alteration and ACMG/AMP guidelines classified it as likely pathogenic. Through a literature review, we identified 229 AOA2 cases with *SETX* variants, and among the variants, 156 *SETX* variants were exonic. We found that 107 (46.7%) patients were European, 50 (21.8%) were African and 48 (21.0%) were Asian. Among the Asian patients, five from two families were Mainland Chinese. The main clinical features were cerebellar ataxia (100%), peripheral neuropathy (94.6%), cerebellar atrophy (95.3%) and elevated AFP concentration (92.0%). Most reported *SETX* mutations in AOA2 patients were missense, frameshift and nonsense mutations.

Conclusion: We discovered a novel homozygous variant of the *SETX* gene as a cause of AOA2 in the current patient and expanded the genotypic spectrum of AOA2. Moreover, the clinical features of AOA2 and genetic findings in *SETX* were assessed in reported cohorts and are summarized in the present study.

KEYWORDS

ataxia with oculomotor apraxia type 2, *SETX* gene, early-onset menopause, Whole-exome sequencing, clinical and genetic spectrum

Introduction

Hereditary autosomal recessive cerebellar ataxias (ARCAs) are neurodegenerative diseases with many different phenotypes (Le Ber et al., 2005; Chiang et al., 2022). Ataxia with oculomotor apraxia type 2 (AOA2) (also known as spinocerebellar ataxia with axonal neuropathy-2 (SCAN2), Online Mendelian Inheritance of Man (OMIM) #606002) is one type of ARCA with a worldwide distribution. The main clinical manifestations of AOA2 include early-onset, progressive cerebellar ataxia, peripheral axonal sensorimotor neuropathy, oculomotor apraxia (OMA) and cerebellar atrophy. Laboratory assays of AOA2 patients frequently reveal elevated serum α-fetoprotein (AFP) concentrations (Anheim et al., 2009; Nanetti et al., 2013).

AOA2 is caused by mutations in the *SETX* gene (OMIM #608465) located on chromosome 9q34 (Nanetti et al., 2013). Human *SETX* encodes a 2677-amino acid protein named senataxin, which was mainly located in the nucleoplasm, and contains an N-terminal protein interaction domain and a DNA/RNA helicase in the C-terminal (Moreira et al., 2004; Suraweera et al., 2007; Yuce and West, 2013). As a large DNA/RNA putative helicase protein, senataxin shows homology to the yeast splicing endonuclease 1 protein (Sen1p) (Moreira et al., 2004). Senataxin is involved in the regulation of transcription, protecting genome integrity against the DNA damage response and oxidative stress and autophagy (Tariq et al., 2018; Richard et al., 2021). Moreover, mutations in the *SETX* gene are also associated with an autosomal dominant inheritance form of the juvenile amyotrophic lateral sclerosis 4 (ALS4) (OMIM 602433).

In this study, we report the clinical and genetic characterizations of an AOA2 patient with early menopause. A new homozygous mutation in *SETX* was identified in the patient. To the best of our knowledge, there were few reports about AOA2 in Mainland China. Additionally, we reviewed 57 studies that reported AOA2 patients with *SETX* mutations from 2004 to 2022 to identify the clinical and genetic spectrum of AOA2 caused by *SETX* mutations and summarize the relevant clinical symptoms of AOA2 patients.

Materials and methods

Ethics statement

The study was approved by the Ethics Committee of Taizhou Hospital of Zhejiang Province Affiliated to Wenzhou Medical University. The family members signed informed consent prior to sample collection and gene testing.

Study subjects and clinical examinations

Clinical assessment of the proband and her parents was performed by neurologists, including physical and neurological examinations. The proband was considered to have hereditary peripheral neuropathy, as she had progressive gait disturbance and muscle atrophy. The blood samples and pedigree were collected from the family after obtaining informed consent. The levels of laboratory indicators, such as serum α-fetoprotein (AFP), creatine kinase (CK), albumin, immunoglobulin, follicle-stimulating hormone (FSH), luteinizing hormone (LH) and anti-Müllerian hormone (AMH), were measured. Electromyography (EMG) and nerve conduction studies (NCSs) were evaluated. Brain magnetic resonance imaging (MRI) of the proband was performed on a GE Signa TwinSpeed 1.5T Medical System. Cognitive function was assessed using the Montreal Cognitive Assessment (MoCA) and Mini-Mental State Examination (MMSE) by neuro physicians.

Genetic testing and data analysis

Genomic DNA was isolated from the peripheral blood of the proband and her parents and used for DNA library preparation. Sequencing library construction was performed using Agilent SureSelect Human All ExonV6 kits (60 M capture, Agilent Technologies, Santa Clara, CA, USA) according to the manufacturer's instructions. Products were purified by an AMPure XP system (Beckman Coulter, Beverly, MA, USA) and quantified on an Agilent 2100 system. Whole-exome sequencing (WES) was performed by using next-generation

sequencing (NGS) techniques on an Illumina NovaSeq 6000 Sequencing System with 150 bp paired-end sequences. The DNA sequence was referred to the UCSC hg19/GRCh37 (University of California Santa Cruz version hg19/Genome Reference Consortium Human Build 37) human reference sequence, and alignment analysis was performed by Burrows–Wheeler Aligner (BWA) v0.7.1. The variation annotation database includes RfeSeq (NCBI Reference Sequence Database) (https://www.ncbi.nlm.nih.gov/refseq/rsg/), Single Nucleotide Polymorphism Database (dbSNP, https://www.ncbi.nlm.nih.gov/snp/), 1000 Genomes Project (https://www.internationalgenome.org/) and the Genome Aggregation Database (gnomAD, http://gnomad-sg.org/). The pathogenicity and clinical significance of the variants were analyzed using databases such as ClinVar (https://www.ncbi.nlm.nih.gov/clinvar/), the Human Gene Mutation Database (HGMD, https://www.hgmd.cf.ac.uk/ac/index.php) and OMIM (Online Mendelian Inheritance in Man, https://www.omim.org/). The functionally predicted impact of the missense variant was evaluated by MutationTaster (https://www.mutationtaster.org/), SIFT (Sortin Intolerant from Tolerant, https://sift.bii.a-star.edu.sg/), Polyphen2 (Polymorphism Phenotyping v2, http://genetics.bwh.harvard.edu/pph2/), REVEL (Rare Exome Variant Ensemble Learner, https://sites.google.com/site/revelgenomics/) and ClinPred (https://sites.google.com/site/clinpred/). Furthermore, the variants identified from proband were confirmed by Sanger sequencing on herself and her parents using Applied Biosystems ABI 3730xl sequencer, the primer sequences were as follows: *SETX* forward (5′-GGCCAAGATTGCACCAAGAT-3′) and reverse (5′-AACTGAGATCGCGCCACT-3′); *MME* forward (5′-GGTTGTGACTGAGACCTGTCAA-3′) and reverse (5′-AGTAAGCGTGAGCGCACTA-3′). The pathogenicity of new variants was classified according to the American College of Medical Genetics and Genomics/Association for Molecular Pathology (ACMG/AMP) guidelines (Richards et al., 2015).

In silico analysis

To analyze the evolutionary conservation of *SETX* candidate variant, the gene and protein sequences of nine different species were derived from HomoloGene database (https://www.ncbi.nlm.nih.gov/homologene/?term=) and the alignment was performed by DNAMAN software (Version 9), including *Homo sapiens* (NM_015046.7, NP_055861.3), *Pan troglodytes* (XM_520331.4, XP_520331.2), *Macaca mulatta* (XM_002799947.1, XP_002799993.1), *Canis lupus familiaris* (XM_005625198.1, XP_005625255.1), *Bos taurus* (XM_002691649.3, XP_002691695.3), *Mus musculus* (NM_198033.2, NP_932150.2), *Rattus norvegicus* (XM_006233886.1, XP_006233948.1), *Gallus gallus* (XM_004945911.1, XP_004945968.1) and *Danio rerio* (XM_685853.6, XP_690945.5). The potential influence of the detected variant on the secondary structure of senataxin was evaluated by SOPMA (Self-Optimized Prediction method with Alignment, https://npsa-prabi.ibcp.fr/cgi-bin/npsa_automat.pl?page=npsa_sopma.html), and the three-dimensional (3D) structure was determined by SWISS-Model (https://swissmodel.expasy.org/) and visualized by PyMOL (Python-enhanced molecular graphics system) software (Version 2.6.0).

Results

Clinical manifestation of the proband

The proband (II-1) was a 40-year-old Chinese woman born to a non-consanguineous couple. She had normal developmental milestones, and her family history was unremarkable. Her lower limbs started to numb and weaken at the age of 16, and then she dropped out of school at the senior high school stage. The patient subsequently obtained employment in an optical factory, and her hips became numb and immobile after long periods of sitting. Later, she developed progressive gait disturbance and muscle atrophy in both lower extremities.

Physical and neurological examinations were performed at our hospital when the patient was 40 years old and revealed gait disturbances, cerebellar ataxia, peripheral neuropathy, hand dystonia, severe pes cavus and early-onset menopause but no oculomotor apraxia, head tremor or dysarthria. Sensory and motor examinations revealed absent tendon reflexes, deep sensory loss, muscular atrophy of both lower limbs and significant muscle weakness in the distal upper and lower limbs. The patient demonstrated no obvious cognitive impairment, with MMSE and MoCA scores of 27 (normal $>$ 26 points) and 23 points (normal $\geq$ 25 points), respectively. Moreover, the patient required assistance with walking.

Brain magnetic resonance imaging (MRI) showed a few lacunar foci in the subcortex of bilateral frontal lobe and mild degeneration of white matter, while without cerebellar and brainstem atrophy (Figures 1B,C). Nerve conduction studies (NCSs) showed that the compound muscle action potential (CMAP) amplitudes of partial motor nerves were decreased and that sensory nerve action potentials (SNAPs) were absent. Electromyography (EMG) showed multiple peripheral nerve damages involving some nerves of the upper and lower limbs and motor sensory axonal changes with myelin sheath damage. The laboratory assays indicated elevated serum AFP at 9.15 ng/mL (normal range $<$7.0 ng/ml), creatine kinase (CK) at 188 U/L (normal range 26–140 U/L), lipoprotein (a) at 696 mg/L (normal range $<$300 mg/L) and high-density lipoprotein cholesterol (HDL-C) at 1.68 mmol/L (normal range 1.03–1.55 mmol/L), while the levels of albumin, total cholesterol and immunoglobulins were normal. In addition, the serum sex hormone test showed that serum follicle-stimulating hormone (FSH) and luteinizing hormone (LH) were

10.3389/fnmol.2022.1019974

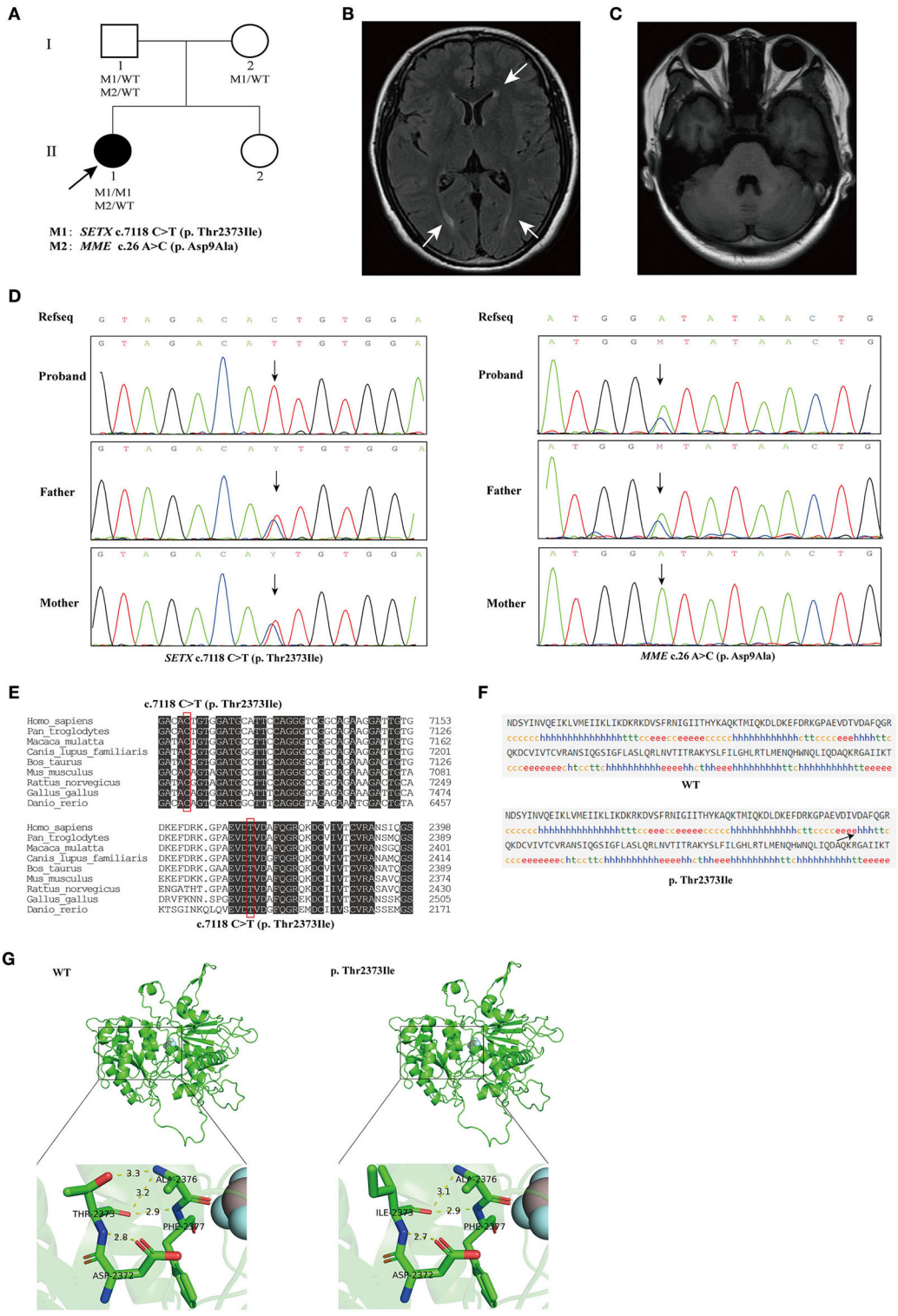

FIGURE 1
(A) The pedigree of the family. The black arrow indicates the proband that subjected for Whole-exome sequencing (WES). **(B)** Brain magnetic resonance imaging (MRI) of the proband, showing mild degeneration of white matter (white arrows). **(C)** Brain MRI of the proband, showing normal cerebellum. **(D)** Sequencing results showed that the homozygous variant c.7118C>T (p. Thr2373Ile) of *SETX* was inherited from both of the proband's parents (left), and the c.26A>C (p. Asp9Ala) variant in *MME* was inherited from the proband's father (right). **(E)** Conservation analysis of *SETX* c.7118C>T (p. Thr2373Ile) variant. **(F)** Secondary structures of wild-type and *SETX* p. Thr2373Ile variant were analyzed by SOPMA (Self-Optimized Prediction method with Alignment) online. h, α-helix; e, extended strand, arrow indicates change in secondary structure. **(G)** Prediction of the change in the three-dimensional (3D) structure of senataxin by *SETX* c.7118C>T (p. Thr2373Ile) variant.

39.41 and 15.7, respectively (interpreted as postmenopausal) and a decreased level of anti-Müllerian hormone (AMH) at 0.030 ng/ml (normal range 0.147–7.490 ng/ml). The clinical characteristics, laboratory indicators and molecular findings of the proband are shown in Table 1.

Genetic findings

The pedigree of the family is presented in Figure 1A. We performed next-generation sequencing (NGS) analysis for the proband. As a result, a novel homozygous missense variant in the *SETX* gene (NM_015046.7, exon 24, c.7118 C>T) and a heterozygous missense variant in the *MME* gene (NM_007289.3, exon 2, c.26 A>C) were identified. The c.7118 C>T variant in *SETX* caused a change of amino acid 2373 from threonine to isoleucine (p. Thr2373Ile), and the c.26 A>C variant in *MME* caused a change of amino acid 9 from aspartic acid to alanine (p. Asp9Ala). Sanger sequencing was performed to verify the variants on her parents (Figure 1D). The result indicated that both her parents were heterozygous carriers for the c.7118 C>T (p. Thr2373Ile) variant in the *SETX* gene, and her father was heterozygous for the c.26 A>C (p. Asp9Ala) variant in *MME*. However, the parents did not show any *SETX*- or *MME*-caused manifestations.

Heterozygous mutation in *MME* are associated with the Charcot–Marie–Tooth disease type 2T (CMT2T) (OMIM 617017) and spinocerebellar ataxia 43 (SCA43) (OMIM 617018), which both have a late-onset age and neither of them has symptoms of early menopause (Higuchi et al., 2016). The proband's father (I-1) was heterozygous for the *MME* c.26A > C variant and was not affected. The *MME* variant was of uncertain significance according to the ACMG/AMP guidelines as the criteria for pathogenic and benign are contradictory (BS4, PM2). Evaluating the clinical symptoms and family history, we considered that the c.26 A>C (p. Asp9Ala) variant in the *MME* gene may not be pathogenic in the proband in this study.

The homozygous or compound heterozygous mutations in *SETX* are associated with AOA2. The *SETX* p. Thr2373Ile variant has not been reported in the gnomAD, ClinVar and HGMD databases. Furthermore, no patient with the variant has been reported to date. The variant had a REVEL score of 0.948 and a ClinPred score of 0.9992; MutationTaster, SIFT and Polyphen2 predicted that this novel variant in the *SETX* gene was pathogenic. Conservative analysis showed that a threonine at position 2373 of *SETX* was evolutionarily highly conserved among various species (Figure 1E). The secondary structure of *SETX* was changed by p. Thr2373Ile variant (Figure 1F). Moreover, the three-dimensional (3D) protein structure models showed that one of the hydrogen bonds formed between Thr2373 and Ala2376 disappeared after Thr2373Ile variant, which may affect the protein spatial structure (Figure 1G). Additionally, an AOA2 patient with compound heterozygous

TABLE 1 Clinical and molecular characteristics of patients with SETX p. Thr2373 mutation.

Variables	Current study	Bernard et al. (2008)
Sex/Age/Age at onset (year)	F/40/16	F/21/17
Initial symptom	Lower limb weakness	Ataxia
Clinical symptoms		
Cerebellar ataxia	Yes	Yes
Oculomotor apraxia	No	No
Deep Tendon reflexes	Absent	No
Distal weakness	Yes	N/A
Deep sensory loss	Yes	N/A
Muscle atrophy	Lower limbs	No
Dystonia	Yes	Yes
Head tremor	No	N/A
Pes cavus	Yes	N/A
Cognitive impairment	No	No
Others	Menopause	Mild spastic paraparesis
Neurophysiology		
Peripheral neuropathy	Yes	Yes
Nerve conduction study	Sensorimotor neuropathy	N/A
Brain MRI		
Cerebellar atrophy	No	Yes
Leukoaraiosis	Mild	No
Biochemistry		
AFP (ng/ml)	9.15 (<7 ng/ml)	34 (<5 ng/ml)
CK (U/L)	188 (26–140 U/L)	263 (<171 U/L)
HDL-C (mmol/L)	1.68 (1.03–1.55 mmol/L)	N/A
Lp (a) (mg/L)	696 (<300 mg/L)	N/A
FSH (mIU/ml)	39.41 (Postmenopausal: 26.72–133.41 mIU/ml)	N/A
LH (mIU/ml)	15.7 (Postmenopausal: 5.61–61.99 mIU/ml)	N/A
AMH (ng/ml)	0.030 (0.147–7.490 ng/ml)	N/A
Mutation		
Nucleotide changes	c.7118C>T	c.6620A > T/c.7117A > C
Protein change	p. Thr2373Ile	p. Asp2207Val/p. Thr2373Pro
Mutation type	Homozygous	Compound heterozygous

AFP, α-fetoprotein; CK, creatine kinase; HDL-C, High-density lipoprotein cholesterol; Lp(a), Lipoprotein (a); FSH, Follicle-stimulating hormone; LH, Luteinizing hormone; AMH, anti-Müllerian hormone; N/A, not available.

mutations of c.6620 A > T (p. Asp2207Val) and c.7117 A>C (p. Thr2373Pro) in *SETX* gene was reported previously, one variant site was adjacent to c.7118 C>T and encoded the same amino acid 2373 (Table 1) (Bernard et al., 2008). According to the ACMG/AMP guidelines, the *SETX* c.7118 C>T variant was classified as likely pathogenic (PP3+PP4+PM2+PM5). Combining the clinical manifestations and genetic findings of the proband, we considered the proband as an AOA2 caused by a novel homozygous *SETX* missense mutation.

Discussion

AOA2 is characterized by progressive cerebellar ataxia associated with peripheral neuropathy, cerebellar atrophy and elevated AFP concentrations (Anheim et al., 2009). In the present study, we report an AOA2 patient with a novel homozygous *SETX* mutation c.7118 C>T (p. Thr2373Ile). The patient's age of onset was 16 years, when she presented with numbness and weakness of the lower limbs. Then, she developed progressive gait disturbance accompanied by muscle atrophy of the lower limb extremities. She was characterized by cerebellar ataxia, hand dystonia, severe pes cavus, absent tendon reflexes, deep sensory loss and early-onset menopause. The pathogenicity of the *SETX* variant was confirmed by clinical symptoms, human genome variation database analysis and functional prediction. According to the ACMG guidelines, the *SETX* variant was categorized as a likely pathogenic variant.

Senataxin contains an N-terminal protein interaction domain and a DNA/RNA helicase in the C-terminal and is implicated in transcription, RNA processing, DNA damage responses and neurodevelopment (Yuce and West, 2013; Groh et al., 2017; Richard et al., 2021). Richard et al. (2021) found that *SETX* knockdown reduced transcripts encoding RNA-binding proteins and caused the accumulation of defective mitochondria and protein aggregates. Pathogenic variants of *SETX* cause two neurological diseases, AOA2, an autosomal recessive disorder, and ALS4, an autosomal dominant motor neuron disorder (Hadjinicolaou et al., 2021). *SETX* gene mutations were first reported as a cause of AOA2 by Moreira et al. (2004), they described 15 affected families with onset ages of 10–22 years who presented with gait ataxia, sensory motor neuropathy, cerebellar atrophy and high AFP levels; 15 variants in the *SETX* gene were identified, comprising five missense mutations, four nonsense mutations and six frameshift mutations (Moreira et al., 2004).

We reviewed 57 studies on AOA2 patients with *SETX* variants conducted from 2004 to 2022 (Supplementary material). Among the variants, 156 homozygous or compound heterozygous variants in *SETX* genes were exonic (Figure 2A), comprising 70 missense mutations, 24 nonsense mutations, 57 frameshift mutations and 5 codon mutations. Among these mutations, 59 were located in the DNA/RNA helicase domain. Four studies were excluded because the patients' clinical features were unclear. Finally, we summarized the main clinical manifestations of 229 affected patients with *SETX* variants. The origin distribution of the patients is shown in Figure 2C. Nearly half of the patients (107, 46.7%) were European, 50 (21.8%) were African, 48 (21.0%) were Asian and 24 were American. Among the Asian patients, most of them were Pakistani (13 cases) and Japanese (11 cases), while 5 cases from two families were Mainland Chinese. The main clinical symptoms included cerebellar ataxia (100%), peripheral neuropathy (94.6%), cerebellar atrophy (95.3%), elevated AFP concentration (92.0%), oculomotor apraxia (OMA) (34.1%) and pes cavus (34.3%), while dystonia (27.4%), head tremor (24.2%), chorea (14.3%) and cognitive impairment (9.5%) were less frequent (Figure 2B). Furthermore, eight female patients had early menopause, and one had polycystic ovarian syndrome, two male patients had azoospermia and were infertile.

Our patient showed several clinical symptoms, including cerebellar ataxia, peripheral neuropathy, hand dystonia, pes cavus and elevated AFP, without oculomotor apraxia (OMA) and cerebellar atrophy. As reported, oculomotor apraxia (OMA) is not a basic feature in AOA2 patients. For example, Tazir et al. (2009) reported 19 patients with *SEXT* variants, all assessed patients had ataxia and elevated AFP concentrations, 80% of the affected patients presented with cerebellar dysarthria, 90% had sensory motor neuropathy, including muscular weakness and amyotrophy of distal lower limbs, and only 32% of the patients showed OMA. Nanetti et al. (2013) described 13 Italian patients who carried *SETX* variants. All these patients presented with gait unsteadiness, dysarthria, nystagmus, slow saccades, sensorimotor neuropathy and cerebellar atrophy of the vermis. Twelve patients had pes cavus, while none had symptoms of OMA and cognitive impairment (Nanetti et al., 2013). Duquette et al. (2005) studied 23 French-Canadian-affected AOA2 patients, who shared symptoms of gait ataxia, dysarthria, distal amyotrophy and saccadic pursuit, while none had OMA.

To the best of our knowledge, there were few reports of AOA2 patients in Mainland China. In 2016, two affected cases in one family from China with compound heterozygous variants, c.3190 G>T (p. E1064*) and c.4883 C>G (p. S1628*) of the *SETX* gene were identified, and both patients had early onset of unsteady gait, dysarthria, sensorimotor neuropathy, elevated serum AFP level and cerebellar atrophy (Lu et al., 2016). We observed a novel missense variant c.7118 C>T (p. Thr2373Ile) in exon 24 of the *SETX* gene on the proband, the variant identified in the present study affects the DNA/RNA helicase domain and may cause damage to helicase function, and the affected amino acid was fully conserved among several species. The C-terminal DNA/RNA helicase domain of the protein ranges from 1931 to 2456 amino acids. Studies have shown that variants located in the domain may cause AOA2 through the loss of function of senataxin (Ghrooda

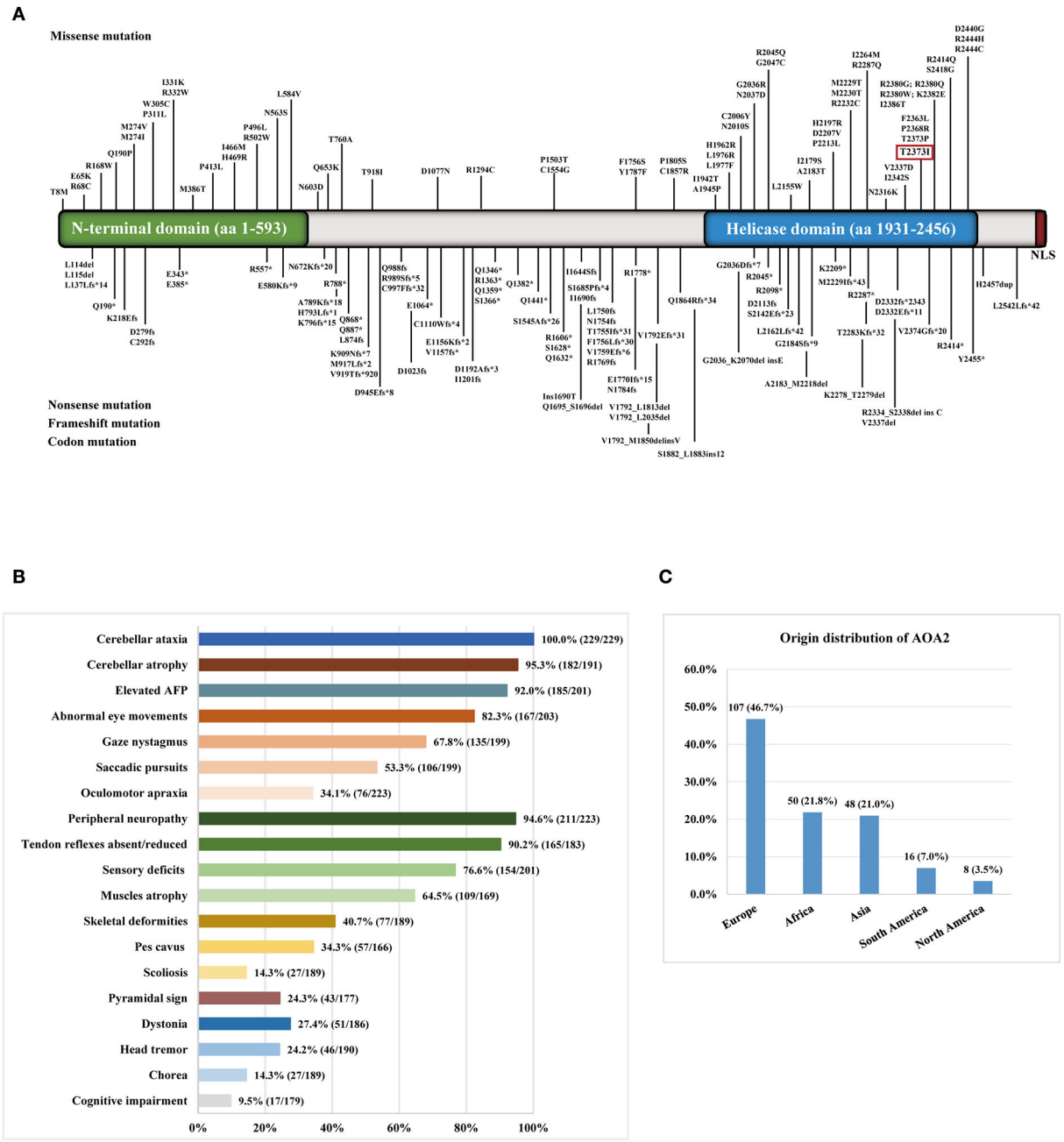

FIGURE 2
(A) Distribution of *SETX* gene variants in ataxia with oculomotor apraxia type 2 (AOA2) patients throughout exons. The variant in the red box was detected in the present study. **(B)** The clinical symptoms of AOA2 patients with *SETX* variants. **(C)** The origin distribution of the AOA2 patients.

et al., 2012; Davis et al., 2013). Bernard et al. reported an AOA2 patient with compound heterozygosity of c.6620 A>T (p. Asp2207Val) and c.7117 A>C (p. Thr2373Pro) in *SETX* gene, the mutation site (c.7117 A>C) was adjacent to c.7118 C>T and encoded the same amino acid at position 2373, enhancing the possibility that the variant in this study may pathogenic. She developed ataxia at 17 years of age and clinical symptoms including cerebellar ataxia, mild spastic paraparesis, neuropathy, cerebellum atrophy and elevated serum AFP, without oculomotor apraxia, dystonia and cognitive impairment (Bernard et al., 2008).

Moreover, the present patient also experienced early menopause at 39 years old due to hypogonadism with FSH and LH levels in the postmenopausal range and low anti-Müllerian

hormone (AMH) levels. Several previous studies have revealed that *SETX* may be related to hypogonadism, spermatogenesis and premature ovarian failure. The major clinical symptoms of nine previously reported AOA2 patients, who were affected by premature ovarian failure or azoospermia, are summarized in Supplementary Table S1. Subramanian et al. showed that *SETX* plays an important role in preventing premature ovarian failure in mice by maintaining the integrity of oocyte DNA. They found that *SETX* deficiency leads to an early-onset decline in female fertility by affecting DNA damage, a premature decline in ovarian follicle numbers and impaired meiotic maturation (Subramanian et al., 2021). Lynch et al. (2007) reported the case of a 21-year-old woman with primary ovarian failure, and her levels of serum FSH and LH indicated that she was postmenopausal; the homozygous mutation of *SETX* c.6292 C>T (p. Arg2098*) was then confirmed in the patient (Lynch et al., 2007). Mancini et al. (2015) reported the cases of three sisters from an Italian family with the *SETX* variant p. Arg2098* who had all experienced early menopause in their thirties. These patients also demonstrated severe ataxia, saccadic pursuit, sensory motor neuropathy, kyphoscoliosis, head/hand tremor, chorea/myoclonia and vermian atrophy (Mancini et al., 2015). Gazulla et al. (2009) reported the case of a 37-year-old woman with AOA2 with a Val919Thrfs*920 homozygous variant in *SETX*. She had been experiencing recurrent amenorrhea for several years, with decreased 17-estradiol and elevated FSH, which was consistent with postmenopausal levels (Gazulla et al., 2009). Furthermore, two AOA2 cases with compound heterozygous variants of p. Met917Leufs*2/p. Met2230Thr and homozygous variant of p. Ser2142Glufs*23 in *SETX* genes were reported, and both had azoospermia and primary infertility. The role of *SETX* in azoospermia and infertility was subsequently determined by histopathological examinations of testes from AOA2 patients and *SETX* knockdown mice (Becherel et al., 2019; Catford et al., 2019).

However, there were several limitations of the present study. As the patient had not sought medical treatment at our hospital before, her past medical history and examination results were unclear, and the progression of her clinical symptoms was different to determine. Although we considered the *MME* p. Asp9Ala variant was not the cause of the patient's disease based on her onset age, clinical symptoms and family history, more family verification and functional experiments are needed to confirm this finding. Although the pathogenicity of the novel *SETX* variant identified is explained by the clinical phenotype of the proband, her onset age, the pedigree analysis and bioinformatic predictions, further functional experiments are needed to determine the impact of the variant on the expression and function of senataxin.

In conclusion, we identified a novel homozygous mutation of the *SETX* gene in a Chinese woman. Our report may expand the clinical and genetic spectrum of AOA2. Moreover, the clinical features of AOA2 and genetic findings in *SETX* were assessed from reported cohorts and are summarized in the present study.

Data availability statement

The original contributions presented in the study are included in the article/Supplementary material and the sequencing data presented in the study are deposited in the Sequence Read Archive repository, accession number SRR21116234.

Ethics statement

The studies involving human participants were reviewed and approved by the Ethics Committee of Taizhou Hospital of Zhejiang Province Affiliated to Wenzhou Medical University. The patients/participants provided their written informed consent to participate in this study. Written informed consent was obtained from the individual(s) for the publication of any potentially identifiable images or data included in this article.

Author contributions

ShuC, JD, and YZ conceived the study. ShuC analyzed the data and wrote the manuscript. YZ and HJ provided the clinical samples. AY and WZ participated in the clinical data collection and clinical evaluations. ShuC, JD, NW, and BS performed the genetic analysis and bioinformatics analysis. ShiC and JL conducted the biochemical analysis. BS and YZ critically commented and revised the manuscript. All authors have read and approved the final version of the manuscript.

Acknowledgments

We would like to thank the patient and her family members for participating in our study. We also thank Dian Diagnostics for their excellent technical assistance.

Conflict of interest

The authors declare that the research was conducted in the absence of any commercial or financial relationships that could be construed as a potential conflict of interest.

Publisher's note

All claims expressed in this article are solely those of the authors and do not necessarily represent those

of their affiliated organizations, or those of the publisher, the editors and the reviewers. Any product that may be evaluated in this article, or claim that may be made by its manufacturer, is not guaranteed or endorsed by the publisher.

Supplementary material

The Supplementary Material for this article can be found online at: https://www.frontiersin.org/articles/10.3389/fnmol.2022.1019974/full#supplementary-material

References

Anheim, M., Monga, B., Fleury, M., Charles, P., Barbot, C., Salih, M., et al. (2009). Ataxia with oculomotor apraxia type 2: clinical, biological and genotype/phenotype correlation study of a cohort of 90 patients. *Brain* 132, 2688–2698. doi: 10.1093/brain/awp211

Becherel, O. J., Fogel, B. L., Zeitlin, S. I., Samaratunga, H., Greaney, J., Homer, H., et al. (2019). Disruption of spermatogenesis and infertility in ataxia with oculomotor apraxia type 2 (AOA2). *Cerebellum* 18, 448–456. doi: 10.1007/s12311-019-01012-w

Bernard, V., Stricker, S., Kreuz, F., Minnerop, M., Gillessen-Kaesbach, G., Zuhlke, C., et al. (2008). Ataxia with oculomotor apraxia type 2: novel mutations in six patients with juvenile age of onset and elevated serum alpha-fetoprotein. *Neuropediatrics* 39, 347–350. doi: 10.1055/s-0029-1214424

Catford, S. R., O'Bryan, M. K., McLachlan, R. I., Delatycki, M. B., and Rombauts, L. (2019). Germ cell arrest associated with aSETX mutation in ataxia oculomotor apraxia type 2. *Reprod. Biomed.* 38, 961–965. doi: 10.1016/j.rbmo.2018.12.042

Chiang, P. I., Liao, T. W., and Chen, C. M. A. (2022). Novel SETX mutation in a Taiwanese patient with autosomal recessive cerebellar ataxia detected by targeted next-generation sequencing and a literature review. *Brain Sci.* 12, 173. doi: 10.3390/brainsci12020173

Davis, M. Y., Keene, C. D., Swanson, P. D., Sheehy, C., and Bird, T. D. (2013). Novel mutations in ataxia telangiectasia and AOA2 associated with prolonged survival. *J. Neurol. Sci.* 335, 134–138. doi: 10.1016/j.jns.2013.09.014

Duquette, A., Roddier, K., McNabb-Baltar, J., Gosselin, I., St-Denis, A., Dicaire, M. J., et al. (2005). Mutations in senataxin responsible for Quebec cluster of ataxia with neuropathy. *Ann. Neurol.* 57, 408–414. doi: 10.1002/ana.20408

Gazulla, J., Benavente, I., Lopez-Fraile, I. P., Modrego, P., and Koenig, M. (2009). Sensorimotor neuronopathy in ataxia with oculomotor apraxia type 2. *Muscle Nerve* 40, 481–485. doi: 10.1002/mus.21328

Ghrooda, S., Borys, A., Spriggs, E., Hegde, M., and Mhanni, A. (2012). SETX gene novel mutations in a non-French Canadian with ataxia-oculomotor apraxia type 2. *Parkinsonism Relat. Disord.* 18, 700–701. doi: 10.1016/j.parkreldis.2012.01.022

Groh, M., Albulescu, L. O., Cristini, A., and Gromak, N. (2017). Senataxin: genome guardian at the interface of transcription and neurodegeneration. *J. Mol. Biol.* 429, 3181–3195. doi: 10.1016/j.jmb.2016.10.021

Hadjinicolaou, A., Ngo, K. J., Conway, D. Y., Provias, J. P., Baker, S. K., Brady, L. I., et al. (2021). De novo pathogenic variant in SETX causes a rapidly progressive neurodegenerative disorder of early childhood-onset with severe axonal polyneuropathy. *Acta Neuropathol. Commun.* 9, 194. doi: 10.1186/s40478-021-01277-5

Higuchi, Y., Hashiguchi, A., Yuan, J., Yoshimura, A., Mitsui, J., Ishiura, H., et al. (2016). Mutations in MME cause an autosomal-recessive Charcot-Marie-Tooth disease type 2. *Ann. Neurol.* 79, 659–672. doi: 10.1002/ana.24612

Le Ber, I., Brice, A., and Durr, A. (2005). New autosomal recessive cerebellar ataxias with oculomotor apraxia. *Curr. Neurol. Neurosci. Rep.* 5, 411–417. doi: 10.1007/s11910-005-0066-4

Lu, C., Zheng, Y. C., Dong, Y., and Li, H. F. (2016). Identification of novel senataxin mutations in Chinese patients with autosomal recessive cerebellar ataxias by targeted next-generation sequencing. *BMC Neurol.* 16, 179. doi: 10.1186/s12883-016-0696-y

Lynch, D. R., Braastad, C. D., and Nagan, N. (2007). Ovarian failure in ataxia with oculomotor apraxia type 2. *Am. J. Med. Genet. Part A.* 143A, 1775–1777. doi: 10.1002/ajmg.a.31816

Mancini, C., Orsi, L., Guo, Y., Li, J., Chen, Y., Wang, F., et al. (2015). An atypical form of AOA2 with myoclonus associated with mutations in SETX and AFG3L2. *BMC Med. Genet.* 16, 16. doi: 10.1186/s12881-015-0159-0

Moreira, M. C., Klur, S., Watanabe, M., Nemeth, A. H., Le Ber, I., Moniz, J. C., et al. (2004). Senataxin, the ortholog of a yeast RNA helicase, is mutant in ataxia-ocular apraxia 2. *Nat. Genet.* 36, 225–227. doi: 10.1038/ng1303

Nanetti, L., Cavalieri, S., Pensato, V., Erbetta, A., Pareyson, D., Panzeri, M., et al. (2013). SETX mutations are a frequent genetic cause of juvenile and adult onset cerebellar ataxia with neuropathy and elevated serum alpha-fetoprotein. *Orphanet J. Rare Dis.* 8, 123. doi: 10.1186/1750-1172-8-123

Richard, P., Feng, S., Tsai, Y. L., Li, W., Rinchetti, P., Muhith, U., et al. (2021). SETX (senataxin), the helicase mutated in AOA2 and ALS4, functions in autophagy regulation. *Autophagy* 17, 1889–1906. doi: 10.1080/15548627.2020.1796292

Richards, S., Aziz, N., Bale, S., Bick, D., Das, S., Gastier-Foster, J., et al. (2015). Standards and guidelines for the interpretation of sequence variants: a joint consensus recommendation of the American College of Medical Genetics and Genomics and the Association for Molecular Pathology. *Genet. Med.* 17, 405–424. doi: 10.1038/gim.2015.30

Subramanian, G. N., Lavin, M., and Homer, H. A. (2021). Premature ovarian ageing following heterozygous loss of Senataxin. *Mol. Hum. Reprod.* 27:gaaa080. doi: 10.1093/molehr/gaaa080

Suraweera, A., Becherel, O. J., Chen, P., Rundle, N., Woods, R., Nakamura, J., et al. (2007). Senataxin, defective in ataxia oculomotor apraxia type 2, is involved in the defense against oxidative DNA damage. *J. Cell Biol.* 177, 969–979. doi: 10.1083/jcb.200701042

Tariq, H., Imran, R., and Naz, S. A. (2018). Novel homozygous variant of SETX causes ataxia with oculomotor apraxia type 2. *J. Clin. Neurol.* 14, 498–504. doi: 10.3988/jcn.2018.14.4.498

Tazir, M., Ali-Pacha, L., M'Zahem, A., Delaunoy, J. P., Fritsch, M., Nouioua, S., et al. (2009). Ataxia with oculomotor apraxia type 2: a clinical and genetic study of 19 patients. *J. Neurol. Sci.* 278, 77–81. doi: 10.1016/j.jns.2008.12.004

Yuce, O., and West, S. C. (2013). Senataxin, defective in the neurodegenerative disorder ataxia with oculomotor apraxia 2, lies at the interface of transcription and the DNA damage response. *Mol. Cell. Biol.* 33, 406–417. doi: 10.1128/MCB.01195-12

frontiers | Frontiers in Molecular Neuroscience

TYPE Original Research
PUBLISHED 15 December 2022
DOI 10.3389/fnmol.2022.1015220

OPEN ACCESS

EDITED BY
Michel J. Simonneau,
École normale supérieure Paris-Saclay, France

REVIEWED BY
Tilmann Achsel,
Université de Lausanne, Switzerland
Pierre Billuart,
Institut National de la Santé et de la Recherche Médicale (INSERM), France

*CORRESPONDENCE
Mara Dierssen
✉mara.dierssen@crg.eu

†PRESENT ADDRESS
Mireia Ortega,
IDIBAPS (Institut d'Investigacions Biomèdiques August Pi i Sunyer), Barcelona, Spain

‡These authors have contributed equally to this work

SPECIALTY SECTION
This article was submitted to Brain Disease Mechanisms, a section of the Frontiers in Molecular Neuroscience

RECEIVED 09 August 2022
ACCEPTED 02 December 2022
PUBLISHED 15 December 2022

CITATION
Ortega M, De Toma I, Fernández-Blanco Á, Calderón A, Barahona L, Trullàs R, Sabidó E and Dierssen M (2022) Proteomic profiling reveals mitochondrial dysfunction in the cerebellum of transgenic mice overexpressing DYRK1A, a Down syndrome candidate gene.
Front. Mol. Neurosci. 15:1015220.
doi: 10.3389/fnmol.2022.1015220

Proteomic profiling reveals mitochondrial dysfunction in the cerebellum of transgenic mice overexpressing DYRK1A, a Down syndrome candidate gene

Mireia Ortega[1†‡], Ilario De Toma[1‡], Álvaro Fernández-Blanco[1], Anna Calderón[2], Lucía Barahona[2], Ramón Trullàs[2], Eduard Sabidó[1,3] and Mara Dierssen[1,3,4*]

[1]Centre for Genomic Regulation (CRG), The Barcelona Institute of Science and Technology, Barcelona, Spain, [2]Instituto de Investigaciones Biomédicas de Barcelona, IIBB/CSIC y Centro de Investigación Biomédica en Red, Barcelona, Spain, [3]Department of Experimental Sciences, Universitat Pompeu Fabra (UPF), Barcelona, Spain, [4]Centro de Investigación Biomédica en Red de Enfermedades Raras (CIBERER), Barcelona, Spain

Introduction: DYRK1A is a dual-specificity kinase that is overexpressed in Down syndrome (DS) and plays a key role in neurogenesis, neuronal differentiation and function, cognitive phenotypes, and aging. Dyrk1A has also been implicated in cerebellar abnormalities observed in association with DS, and normalization of Dyrk1A dosage rescues granular and Purkinje cell densities in a trisomic DS mouse model. However, the underlying molecular mechanisms governing these processes are unknown.

Methods: To shed light on the effects of Dyrk1A overexpression in the cerebellum, here we investigated the cerebellar proteome in transgenic Dyrk1A overexpressing mice in basal conditions and after treatment with green tea extract containing epigallocatechin-3-gallate (EGCG), a DYRK1A inhibitor.

Results and Discussion: Our results showed that Dyrk1A overexpression alters oxidative phosphorylation and mitochondrial function in the cerebellum of transgenic mice. These alterations are significantly rescued upon EGCG-containing green tea extract treatment, suggesting that its effects in DS could depend in part on targeting mitochondria, as shown by the partially restoration by the treatment of the increased mtDNA copy number in TG non-treated mice.

KEYWORDS

DYRK1A, cerebellum, mitochondria, oxidative phosphorylation system, Down syndrome, proteomics

1. Introduction

Trisomy of chromosome 21 causes Down syndrome (DS), the most common genetic cause of intellectual disability (Dierssen, 2012). DS individuals exhibit an overall reduction in brain size with a disproportionately greater reduction in cerebellar volume. Given that the cerebellum is a key regulator of motor control and motor learning, motor abnormalities in

DS including the coordination of voluntary movement, gait, posture, and speech are ascribed cerebellar abnormalities. The analysis of single-gene contributions to DS has revealed the Dual-Specificity Tyrosine-Phosphorylation-Regulated Kinase 1A (*DYRK1A*), a DS candidate gene located in the 21q22.2 human chromosome region (Duchon and Herault, 2016), as a good candidate to contribute to cerebellar DS phenotypes. DYRK1A is expressed at high levels in the cerebellum (Martí et al., 2003), and mouse models with altered *Dyrk1A* expression exhibit altered motor abilities (Altafaj et al., 2001; Fotaki et al., 2002; Martínez de Lagrán et al., 2004). Overexpression of human *Dyrk1A* in post-mitotic cerebellar Purkinje neurons in zebrafish resulted in a structural disorganization of the Purkinje cells in cerebellar hemispheres and a compaction of this cell population that could be rescued by a novel selective DYRK1A inhibitor, KuFal194 (Buchberger et al., 2021). Similarly, normalization of the dosage of Dyrk1A in the partial trisomic Ts65Dn DS mouse model (Ts65Dn +/+/− with only two copies of Dyrk1A), rescues granular and Purkinje cell densities and the size of the granular and molecular layers (García-Cerro et al., 2018). Interestingly, *in vitro* studies have shown that bioenergetic dysfunction contributes to the reduced neurogenesis in progenitor cells from Ts65Dn, that is rescued by polyphenol 7,8-dihydroxyflavone (Valenti et al., 2021) suggesting a critical role of mitochondrial dysfunction in neurodevelopmental alterations in DS (Valenti et al., 2017). Indeed, we have previously shown that green tea extract containing epigallocatechin-3-gallate (EGCG), the main polyphenol in green tea, rescued the proteomic hippocampal alterations in both trisomic and *Dyrk1A* overexpressing transgenic (TG) mice (De Toma et al., 2019, 2020).

To elucidate putative mechanisms of the role of *Dyrk1A* in the cerebellum, here we explored the proteome changes induced by its overexpression in TG mice, and their possible restoration upon treatment with green tea extract containing EGCG, which has DYRK1A kinase inhibitor properties. We detected important proteomic alterations in TG cerebellum with over 200 proteins showing changes in abundance. The most significant changes indicate mitochondrial dysfunction as a crucial factor in the pathogenesis of cerebellar dysfunction in TG mice. Interestingly, treatment with green tea extracts rescued the level of many proteins, especially those involved in mitochondrial function. Thus, we also explored whether mitochondrial malfunction in a neuron-rich area of the cerebellum of TG mice could be recovered upon treatment with green tea extract containing EGCG. Our findings suggest that increased mtDNA copy numbers in TG non-treated mice are partially restored by EGCG-containing green tea extract.

2. Materials and methods

2.1. Animal models

All the experiments were performed using 2-month male wild-type (WT) and transgenic mice overexpressing Dyrk1A (TG). We selected this stage because most of the alterations found in TgDyrk1a mice such as memory and motor deficits (Altafaj et al., 2001) are already present at 2 months. Neuronal alterations such as reduced dendritic arborizations, reduction of neurite outgrowth, synaptogenesis, and spontaneous activity have also been described at this stage (Martínez de Lagran et al., 2012). Mice were obtained by crossing TG male mice with C57BL6/SJL WT female mice. Mice were reared in standard cages (20 × 12 × 12 cm Plexiglas cage) in groups of 2–3 animals and maintained under a 12-h light–dark cycle (8:00 h to 22:00 h) in controlled environmental conditions of humidity (60%) and temperature (22 ± 1°C) with *ad libitum* access to food and water. All procedures were approved by the local ethical committee (Comité Ético de Experimentación Animal del PRBB (CEEA-PRBB; MDS 0035P2), and met the guidelines of the local (law 32/2007) and European regulations (EU directive e no. 86/609, EU decree 2001-486) and the Standards for Use of Laboratory Animals no. A5388-01 (NIH). The CRG is authorized to work with genetically modified organisms (A/ES/05/I-13 and A/ES/05/14). Animal del PRBB (CEEA-PRBB); MDS 0035P2), and met the guidelines of the local (law 32/2007) and European regulations (EU directive e no. 86/609, EU decree 2001-486) and the Standards for Use of Laboratory Animals no. A5388-01 (NIH). The CRG is authorized to work with genetically modified organisms (A/ES/05/I-13 and A/ES/05/14).

2.2. EGCG-containing green tea extract treatment

One month-old TG or WT mice were assigned using a simple randomization to either control conditions or a treatment consisting on green tea extract containing 45% EGCG for 30 days. Green tea leaf extract was used to create a green tea extract with 45% EGCG, which was then used to make new EGCG solutions every 2 days to be added to drinking water (EGCG dosage: 0.326 mg/ml, 0.65 mg per day, and 30 mg/kg per day; Mega Green Tea Extract, Decaffeinated, Life Extension, Fort Lauderdale, FL; EGCG content 326.25 mg per capsule).

2.3. Mass-spectrometry-based proteomics

Mice were sacrificed, and the dissected cerebelli were frozen at −80°C. For the experiments, tissues were homogenized with a RIPA-modified buffer (50 mM tris-HCl pH 7.5, 150 mM NaCl, 1 mM EDTA, 1% NP-40, 0.1% sodium deoxycholate with the addition of 5 mM b-glycerophosphate, 10 mM sodium fluoride, 10 mM sodium orthovanadate, and protease inhibitors from the Complete Protease Inhibitor Cocktail Roche). Samples were sonicated using Bioruptor® (Diagenode) for 5 min with 30 on/off cycles, maintaining the samples on ice, and were centrifuged for 10 min 10,000 rpm at 4°C. Proteins from the supernatants were precipitated overnight at −20°C by adding a volume of ice-cold acetone in six-fold excess. The acetone-precipitated proteins were solubilized in a denaturation

buffer (6 M urea and 200 mM ammonium bicarbonate in water). Final protein content was quantified using the BCA assay (Pierce). Proteins were reduced with dithiothreitol (DTT, 10 mM, 37°C, 60 min), and alkylated with iodoacetamide (IAM, 20 mM, 25°C, 30 min). Then samples were diluted with 200 mM ammonium bicarbonate up to 2 M urea, digested overnight with Lys-C at 37°C, and then diluted two-fold again and digested overnight with trypsin at 37°C. Peptides were desalted using a C18 MicroSpin 300A silica column (The Nest Group, Inc.), evaporated to dryness using a SpeedVac, and dissolved in 30 µl of 0.1% formic acid in water.

2.4. Liquid chromatography–tandem mass spectrometry

For each sample, 1 µg of tryptic peptides from digested cerebellar tissue was injected in an LTQ-Orbitrap Velos Pro mass spectrometer (Thermo Fisher Scientific) coupled to a nano-LC (EASY-nLC, Proxeon). Nano-LC was equipped with a reversed-phase chromatography column of 25 cm with an inner diameter of 75 µm, packed with 3 µm C18 particles (Nikkyo Technos, NTCC-360/75-3-25L), and a Nano Trap Column Acclaim PepMap100 100 µm × 2 cm C18, 5 µm, 100A (Thermo, 164,199). Chromatographic gradients started at 93% of buffer A and 7% of buffer B with a flow rate of 250 nl/min during 5 min and linearly changed to 65% buffer A and 35% buffer B after 240 min. After each analysis, the column was washed for 16 min with 90% buffer A and 10% buffer B (Buffer A: 0.1% formic acid in water. Buffer B: 0.1% formic acid in acetonitrile). The mass spectrometer was operated in positive ionization mode with the nanospray voltage set at 2.2 kV and the source temperature at 250°C. Ultramark 1621 for the FT mass analyzer was used for external calibration prior to the analyses. The background polysiloxane ion signal at m/z 445.1200 was used as lock mass. The instrument was operated in data-dependent acquisition (DDA) mode with 1 microscan at resolution of 60,000 at 400 m/z and survey scans were recorded over a mass range of m/z 350–2,000 with detection in the Orbitrap mass analyzer. Auto gain control (AGC) was set to 10^6, dynamic exclusion was set at 60 s, and the charge-state filter disqualifying singly charged peptides for fragmentation was activated. Following each survey scan, the top 20 most intense ions with multiple charged ions above a threshold ion count of 5,000 were selected for fragmentation at normalized collision energy of 35%. Fragment ion spectra produced *via* collision-induced dissociation (CID) were acquired in the linear ion trap, AGC was set to 5×10^4, and isolation window of 2.0 m/z, activation time of 0.1 ms, and maximum injection time of 100 ms were used.

2.5. Mass spectrometry data analysis

Acquired mass spectra were processed using the MaxQuant computational platform version 1.5.2.8 (Cox and Mann, 2008). The MS2 spectra were searched by using the Andromeda search engine (Cox et al., 2011) against the UniProt sequence database for Mus musculus (17,263 forward entries; version from July 2015). The search included cysteine carbamidomethylation as a fixed modification, and N-terminal protein acetylation and methionine oxidation as variable modifications. We allowed a maximum of two miscleavages, 4.5 ppm as mass tolerance for precursor ions, and 0.5 Da as mass tolerance for fragment ions. FDR was set to 1% at the peptide and protein level, and protein identification required at least one unique or razor peptide per protein group. The MaxQuant algorithm was used to retrieve extracted ion currents (XICs) per peptide feature for quantification purposes. Areas under the curve for each peptide were calculated and later used to estimate protein intensities during the statistical analysis. Statistical analysis was performed using the R package MSstats version 2.6.0 (Choi et al., 2014). One of the five biological replicates of the TG.NT group was excluded from the analysis, because the number of peptides identified was substantially lower (e.g., 1,000 peptides) than the average of peptides identified in the whole experiment. To ensure high confidence in our quantitative data, only peptides observed at least in three of the five biological replicates (or at least in two when we remained only with four biological replicates), were used, and no imputation of missing values was performed.

2.5.1. Differentially expressed proteins

Downstream bioinformatics analysis was performed on proteins that showed a significant change in abundance with a Benjamini adjusted *p*-value lower than 0.05 and a log2(Fold Change) (log2FC) >0.3 or lower than −0.3. The proteins preferentially detected present in one condition of the ones compared were added to the lists of differentially abundant proteins. A peptide was defined as "absent" when it was detected in <3 out of 5 biological replicates for a given condition (or <2 out of 4 biological replicates for the TG.NT group). Since blood contamination is a common problem in sample collection from dissected tissues, proteins belonging to the GO-term cell component "blood microparticle" were filtered out from all datasets before proceeding with downstream analyses.

We calculated the following contrasts for each of the three treatments were calculated (TG: TG mice; WT: wild-type mice; NT: not treated mice):

TG.NT-WT.NT (deregulated proteins in untreated TG mice)

TG.EGCG-TG.NT (proteins responding to the treatments in TG mice)

WT.EGCG-WT.NT (proteins responding to the treatments in WT mice)

(TG.EGCG-TG.NT) − (WT.EGCG-WT.NT) (interaction: proteins responding differently to the treatments in TG compared to WT mice)

For each protein whose abundance was significantly changing in the TG.NT-WT.NT contrasts we first calculated the genotype gap as the log2-fold-change obtained in the contrast TG.NT-WT.NT. Thereafter, we computed the "treatment gap" as the fold change observed in the TG.EGCG - WT.NT contrast. We therefore

calculated the "percentage of recovery" based on the fraction of recovered abundance—in protein levels–after treatment—given by the difference between the genotype gap and the treatment gap—on the genotype gap: (genotype gap) – (treatment gap)/(genotype gap).

Note that once WT.NT is set to 0 (log2(1) = 0):

* TG.NT-WT.NT contrast can be simplified by TG.NT – log2(1) = TG.NT-0 = TG.NT.

* TG.EGCG - WT.NT = Levels impaired at the basal state + levels after treatment = (TG.NT-WT.NT) + (TG.EGCG-TG.NT) = TG.NT-0 + TG.EGCG –TG.NT = TG.EGCG.

And so:

$$(TG.NT - TG.EGCG)/TG.NT == [(TG.NT\text{-}WT.NT) - (TG.NT\text{-}WT.NT) + (TG.EGCG+TG.NT)]/(TG.NT\text{-}WT.NT)$$

The fraction of recovery could go from 0 (no recovery) to 1 (100% recovery). A value >1 indicates overcorrection. A value <0 is an impairment.

We considered as "rescued protein" those proteins with a % of recovery from 50% to 150%; as "overcorrected proteins," the ones with a % of recovery higher than 150; "not sufficiently rescued" those proteins with a % of recovery between −50% and 50%; and "impaired proteins" those with a % of recovery < −50%.

With similar calculations, we computed the "percentage of impairment" by using instead of the TG.NT-WT.NT contrasts, its reverse WT.NT-TG.NT, in order to calculate how much the treatment in the wild type was reducing the differences between TG and WT.

2.5.2. DYRK1A interactors

DYRK1A interactors were taken from the mammalian verified targets present in (Aranda et al., 2011; Duchon and Herault, 2016; Guard et al., 2019; Roewenstrunk et al., 2019). The significance of the overlaps between DYRK1A targets and the differentially abundant proteins was assessed using a Fisher Exact Test.

2.5.3. Network analysis

The list of differentially abundant proteins was expanded to build a larger protein–protein interaction network including DYRK1A substrates and direct interactors. Specifically, for the disease network, we used the expanded list of proteins deregulated in the TG.NT-WT.NT contrast. For the expansion, we used a list of *bona fide* physical interactors mainly coming from the STRING (version 10; Szklarczyk et al., 2015) and an internal database from Interactome3d version 2017_01 (Mosca et al., 2013). We only considered interactions with a very high score (>0.9) in STRINGdb and IMEx index (Orchard, 2012; Orchard et al., 2012). Graph visualization was performed with the igraph R package using the Davidson Harel layout algorithm (Csardi and Nepusz, 2006).

2.5.4. Enrichment analyses

Protein identifiers were annotated using the R packages UniProt.ws and biomaRt (Durinck et al., 2009). We assessed the significance of the overlaps using a Fisher's exact test, *p*-values for the right tail are obtained directly using hypergeometric distribution considering as background the detected proteins for each contrast. For the Gene Ontology Enrichment analysis, we used the clusterProfiler R package (Yu et al., 2012).

2.5.5. Identification of significant hubs

We used the poweRlaw R package (Alstott et al., 2014) to analyze the heavy tail distribution of interactions. We compared the power-law, Poisson, exponential, and log-normal distribution. Thereafter, we used the fitted distribution for calculating the *p*-values associated to each protein corresponding to encountering by chance a higher number of interactions per protein than the given protein, setting the threshold to define hub at a $p < 0.05$.

2.5.6. Tissue-specific genes

Cerebellar-enriched proteins were detected using the TissueEnrich R package (Jain and Tuteja, 2019) processing RNA-Seq data across 17 mouse tissues (Mouse ENCODE Dataset; Shen et al., 2012).

We used TissueEnrich default parameters based on the algorithm from the HPA (Uhlén et al., 2015): genes with an expression level >1 TPM (Transcripts Per kilobase Million) or FPKM (Fragments Per Kilobase Million) that also have at least five-fold higher expression levels in a particular tissue (or group of tissues) compared to the average levels in all other tissues were defined as tissue enriched.

2.6. *cf*-mtDNA copy number and nuclear genomes using digital PCR

Quantification of mitochondrial DNA copy number per cell was performed with multiplex digital PCR as previously described (Podlesniy and Trullas, 2017). For the present studies we used two different primer pairs targeting opposite regions of the mtDNA molecule; one primer pair targeting the ND1 region (mtDNA-ND1: CTAGCAGAAACAAACCGGGC; CCGGCTGCGTATTCTACGTT), and another primer pair targeting the ND4 region (mtDNA-ND4: TAATCGCACATGGCCTCACA; GCTGTGGATCCGTTCGTAGT) of the mtDNA molecule. These primer pairs were selected with Primer-Blast for specific amplification of the mouse mtDNA reference sequence NC_005089.1.

The number of cells in the tissue homogenate was determined by quantification of diploid nuclear genomes with digital PCR by amplification of the single-copy nuclear gene BAX (forward, CACTGCCTTGGACTGTGTCT; reverse, CCTTTCCCCTTCCCCCATTC).

Results were expressed as mean ± standard deviation (SD). GraphPad Prism software v9 was used for statistical tests. Statistical analyses were performed using one-way analysis of variance (ANOVA) with Fisher's least significant difference (LSD) *post-hoc* tests. Differences were considered statistically significant at a value of $p < 0.05$.

10.3389/fnmol.2022.1015220

3. Results

3.1. Dyrk1a overexpression leads to protein dysregulation in the cerebellum disrupting mitochondrial function

We used label-free quantitative mass spectrometry-based proteomics (LC-MS/MS) to characterize the cerebellum proteome on whole protein extracts from TgDyrk1A (TG) and wild-type (WT) mice, treated or not with EGCG-containing green tea extract. In total, we quantified 3,608 proteins whose abundances were fitted into a linear model to evaluate changes related to the genotype, the treatment, and their interaction. We set a threshold of adjusted *p*-value (Benjamini-Hochberg correction) of 0.05 and a minimum absolute log2 fold change of 0.3 to consider a protein to be significantly changing (Table 1; Supplementary Figure S1; Vizcaíno et al., 2014). Out of the 3,608 quantified proteins, in the cerebellum of TG mice we found 90 significantly upregulated and 99 downregulated proteins (adjusted *p*-value <0.05; Table 1) with respect to WT. We also found proteins that were preferentially detected in one condition: 31 proteins were present exclusively in TG samples, and 53 proteins were exclusively detected in WT samples, thus making a total of 273 proteins with differential abundance. Among the proteins with altered abundance, 16 of them are known to be direct DYRK1A interactors or targets (Table 1). Gene ontology analysis of the deregulated proteins in the cerebellum of TG mice revealed a significant enrichment for "cytochrome complex," and in general in the oxidative phosphorylation system (OXPHOS; Figure 1A). We also observed that 16 of the differentially abundant proteins had previously been reported to be preferentially expressed in the cerebellum (Figure 1B; Jain and Tuteja, 2019). These proteins were enriched in categories that included myelination and axon ensheathment (Figure 1C).

In order to better understand the molecular pathways affected by DYRK1A overexpression in the cerebellum, we built a protein–protein interaction network with the proteins deregulated in TG cerebellum. A total of 139 proteins (out of the 273) were involved in known protein–protein interactions (PPI, STRING database score > 0.4), and those were established as *seed* proteins (Figure 2). Then, we added their 130 *bona fide* primary interactors previously reported in the STRING database, creating a final network of 269 interacting proteins and a total of 511 interactions.

The number of interactions per protein (node degree) in the network followed a log-normal right-skewed distribution (Supplementary Figures S1A,B). Using this distribution, we detected 18 "protein hubs," defined as those appearing in the 10% right tail of the node-degree distribution (Supplementary Figures S2A,B) with an average node degree of 12 (from 11 to 14). Of these 18 hub proteins, 12 were *seed* proteins of the TG network, while the others were primary interactors (Table 2). Moreover 5 of these hubs, Ndufs8 (NADH:Ubiquinone Oxidoreductase Core Subunit S8), Ndufb10 (NADH:Ubiquinone Oxidoreductase Subunit B10), Uqcrc2 (ubiquinol-cytochrome c

TABLE 1 Differentially abundant proteins in TG Dyrk1A mouse cerebellum.

	Detected proteins (*n*)	Upregulated (*n*)	Present in TG, absent in WT	Downregulated (*n*)	Absent in TG, present in WT	DYRK1A targets	DYRK1A targets (in first interactors)
TG.NT-WT.NT	3,608	90	31	99	53	Phb2, Eef1b2, Creb1, Plbd2, Wdr47, Sfpq, Eif2b1, Prkar1a, Eef1b	Fhl2, Prkaca, Traf2, Stat3, Psen1, Ywhag, Kpnb1, Smarca4, Myo1c
WT.EGCG-WT.NT	3,554	142	22	60	32	Prkaca, Tra2b, Prkacb, Creb1, Tanc1, Wdr26, Phyhip, Eif2b1, Srsf10, Sf3b1	Trp53, Egr2, Braf, Traf2, Stat3, Gli1, Ywhag, Notch1, Ywhab, Prkar1a, Gsk3b, Tp53
TG.EGCG-TG.NT	3,603	97	47	110	35	Anapc1, Tanc1, Plbd2, Srsf2, Srsf1, Tomm34, Srsf10	Egr2, Polr2a, App, Map1b, Grin2a, Traf2, Stat3, Gli1, Psen1, Mapk1, Notch1, Smarca4, Ablim1, Wasl, Ywhab, Myo1c, Ap3b1
(TG.EGCG-TG.NT)-(WT.EGCG-WT.NT)	3,443	122	23	70	11	Phb2, Ywhag, Srsf2, Srsf1, Eif2b1, Prkar1a	Fhl2, Prkaca, Egr2, Polr2a, Traf2, Stat3, Psen1, Kpnb1, Smarca4, Grb2, Rbl2, Wasl, Ywhab, Myo1c
Rescued by EGCG	123	NA	NA	NA	NA	Phb2, Eef1b2, Plbd2, Eef1b	Stat3, Psen1, Kpnb1, Myo1c

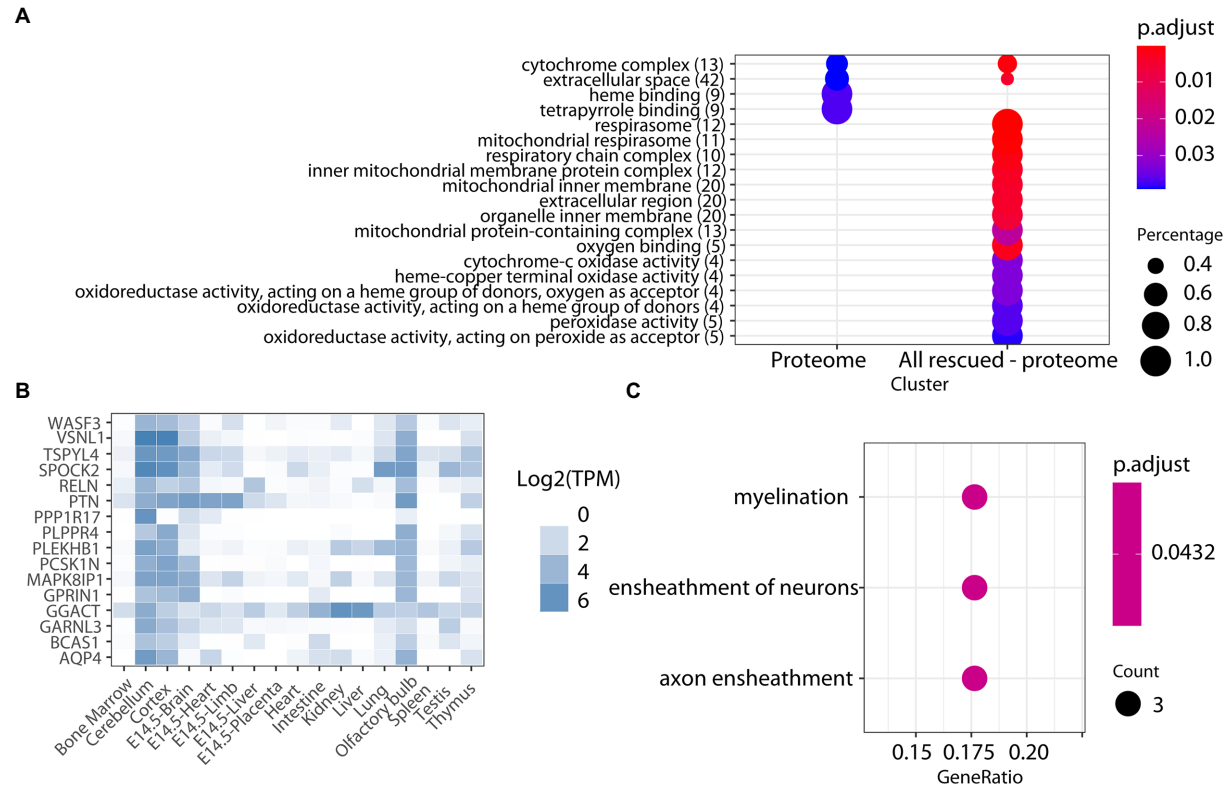

FIGURE 1
(A) Enrichment analysis for biological processes, molecular function, and cell components of proteins altered in the cerebellum of TG mice. The color-gradient indicates the adjusted *p*-value for the enrichment. Numbers in parentheses indicate the number of identified proteins in each category. Dot size corresponds to "protein count for each group"/"total protein count for each category." **(B)** Heatmap showing the expression across tissues (TPM, transcript per million) of the cerebellar proteins found to be differentially abundant in our study, showing their cerebellar enrichment. **(C)** Enrichment analysis on the cerebellar-enriched proteins using the GO annotations.

reductase complex (complex III) of the mitochondrial respiratory chain), Cyc1 (OXPHOS complex III) and Cox6c (OXPHOS complex IV), formed a cluster with most of their interactors in common. Interestingly, the hubs and ~10% of their common interactors were rescued by EGCG-containing green tea extract (Supplementary Figures S2C,D).

3.2. Green tea extracts partially rescue the molecular processes disrupted by DYRK1A overexpression

Next, we treated TG mice with green tea extract, which has inhibitory properties on DYRK1A kinase activity, and compared its cerebellar proteome to that of TG not-treated mice. We first analyzed rescued proteins, e.g., those with compromised abundances in TG mice that were restored to WT levels upon the treatment, and found that 50% of the original abundance level of 123 proteins (45% of those differentially abundant) were restored. For 70 of these proteins, the effect of the treatment was significant (TG_EGCG vs. TG_NT; Figure 3A). Rescued proteins were enriched in categories connected with mitochondria and oxidative phosphorylation. However, the treatment had a much wider effect on the proteome in TG mice, as it significantly changed the abundance of a total of 289 proteins. These proteins were also mainly involved in mitochondrial pathways connected to oxidative phosphorylation and the respirasome. Noteworthy, green-tea extract also affected 256 proteins in WT mice, of which only 50 were in common with TG-treated mice (Figure 3B). However, enrichment analysis of the proteins changing in WT upon green tea-extract treatment showed no enrichment in any significant categories, thus suggesting EGCG action was more meaningful in TG mice, as was also observed in previous work in the hippocampus (De Toma et al., 2019). We found 226 proteins with significant changes in abundance upon treatment in both genotypes (Figure 3C). However, those showed a divergent response to green-tea treatment, with protein abundance increased in one genotype and reduced in the other upon green-tea treatment (red dots in Figure 3D). These 226 proteins were enriched in the mitochondrial respirasome but also in "extracellular space" and in "serine-type endopeptidase inhibitor activity" (Figure 3E). Taking advantage of our previously published proteomic dataset of the hippocampus of the same type of mice, we could also compare the proteomic changes due to

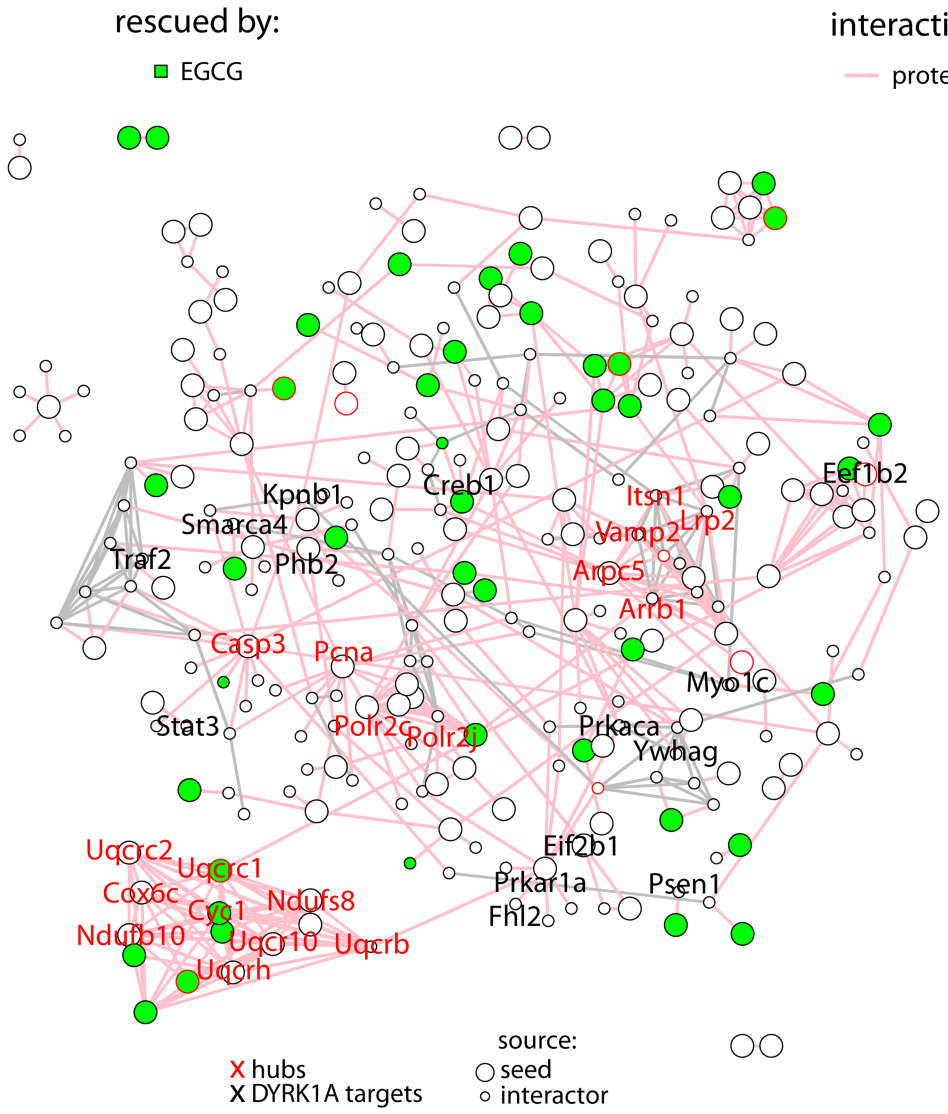

FIGURE 2
Protein–protein interaction network with the proteins differentially abundant in TG mice (*seed* proteins), represented as big nodes and their primary interactors (small nodes). Interactions between two *seed* proteins are depicted as pink edges. Interactions between interactors are shown in gray. Proteins rescued upon treatment are colored in green. The names of the hubs are depicted in red, the names of DYRK1A targets in black.

DYRK1A overexpression in both regions. In the hippocampus, changes were mainly related to antioxidant activity categories and involved a lower number of proteins in the hippocampus (98/2685 for the hippocampus (De Toma et al., 2019), versus 273/3608 in the cerebellum). Indeed, we detected significant overlaps of 14%–18% corresponding to 14 proteins differentially abundant both in the cerebellum and the hippocampus when looking at the genotype contrast and 15 in the treatment contrast in TG (Figure 4). However, when looking at the treatment contrast in WT, the overlap was not significant (5%, corresponding to 6 proteins), indicating that the proteins changing in WT upon EGCG-containing green tea extract treatment are less consistent, and thus, probably randomly deregulated.

3.3. Mitochondrial DNA copy number per cell in the Declive neuron-rich area of the cerebellum is increased in TG mice

In order to validate whether DYRK1A overexpression leads to mitochondrial dysfunction in TG mice, we measured the number of mitochondrial DNA (mtDNA) copy number and nuclear genomes in the different experimental groups. mtDNA copy number of ND1 ($p = 0.16$) and ND4 ($p = 0.13$) showed a tendency to be higher in TG mice compared to WT mice. mtDNA copies of ND1 ($p = 0.03$) and ND4 ($p = 0.02$) were significantly higher in TG mice compared to WT mice treated with EGCG (Figures 5A,B). TG mice treated with EGCG-containing green tea extract showed

TABLE 2 Protein hubs in TG Dyrk1A cerebellum network.

Interactions (*n*)	Value of *p*	Symbol	Uniprot ID	Description	Rescued	Seed
14	0.05806	Casp3	P70677	Caspase 3		Yes
13	0.06702	Vamp2	P63044	Vesicle-associated membrane protein 2		
13	0.06702	Uqcrb	Q9D855	Ubiquinol-cytochrome c reductase binding protein		
13	0.06702	Arpc5	Q9CPW4	Actin related protein 2/3 complex, subunit 5		Yes
13	0.06702	Uqcrh	P99028	Ubiquinol-cytochrome c reductase hinge protein	Yes	Yes
13	0.06702	Polr2c	P97760	Polymerase (RNA) II (DNA directed) polypeptide C		Yes
12	0.07788	Uqcrc1	Q9CZ13	Ubiquinol-cytochrome c reductase core protein 1	Yes	Yes
12	0.07788	Pcna	P17918	Proliferating cell nuclear antigen	Yes	Yes
12	0.07788	Polr2j	O08740	Polymerase (RNA) II (DNA directed) polypeptide J		
12	0.07788	Uqcr10	Q8R1I1	Ubiquinol-cytochrome c reductase, complex III subunit X		Yes
12	0.07788	Arrb1	Q8BWG8	Arrestin, beta 1		
12	0.07788	Itsn1	Q9Z0R4	Intersectin 1 (SH3 domain protein 1A)		
11	0.0912	Cox6c	Q9CPQ1	Cytochrome c oxidase subunit 6C	Yes	Yes
11	0.0912	Cyc1	Q9D0M3	Cytochrome c-1	Yes	Yes
11	0.0912	Uqcrc2	Q9DB77	Ubiquinol cytochrome c reductase core protein 2	Yes	Yes
11	0.0912	Ndufb10	Q9DCS9	NADH:ubiquinone oxidoreductase subunit B10	Yes	Yes
11	0.0912	Ndufs8	Q8K3J1	NADH:ubiquinone oxidoreductase core subunit S8	Yes	Yes
11	0.0912	Lrp2	A2ARV4	Low density lipoprotein receptor-related protein 2		
10	0.10771	Cox5a	P12787	Cytochrome c oxidase subunit 5A	Yes	Yes
10	0.10771	M6pr	P24668	Mannose-6-phosphate receptor, cation dependent		Yes
10	0.10771	Ndufa1	O35683	NADH:ubiquinone oxidoreductase subunit A1	Yes	Yes
10	0.10771	Csnk1d	Q9DC28	Casein kinase 1, delta		Yes
10	0.10771	Plk1	Q07832	Polo like kinase 1		
10	0.10771	Ikbkb	O88351	Inhibitor of kappaB kinase beta		
10	0.10771	Prkar1a	Q9DBC7	Protein kinase, cAMP dependent regulatory, type I, alpha		Yes
10	0.10771	Cttn	Q60598	Cortactin		
9	0.12845	Birc3	O08863	Baculoviral IAP repeat-containing 3		
9	0.12845	Crebbp	P45481	CREB binding protein		
9	0.12845	Cox4i1	P19783	Cytochrome c oxidase subunit 4I1	Yes	Yes
9	0.12845	Pacsin1	Q61644	Protein kinase C and casein kinase substrate in neurons 1		

(Continued)

10.3389/fnmol.2022.1015220

TABLE 2 (Continued)

Interactions (n)	Value of p	Symbol	Uniprot ID	Description	Rescued	Seed
9	0.12845	Pacsin3	Q99JB8	Protein kinase C and casein kinase substrate in neurons 3		Yes
9	0.12845	Xiap	Q60989	X-linked inhibitor of apoptosis		
9	0.12845	Pacsin2	Q9WVE8	Protein kinase C and casein kinase substrate in neurons 2		
9	0.12845	Birc2	Q62210	Baculoviral IAP repeat-containing 2		
9	0.12845	Creb1	Q01147	camp responsive element binding protein 1		Yes
8	0.1549	Tnfrsf1a	P25118	Tumor necrosis factor receptor superfamily, member 1a		
8	0.1549	Rpl28	P41105	Ribosomal protein L28		Yes
7	0.18922	Ranbp2	Q9ERU9	RAN binding protein 2		
7	0.18922	Prkaca	P05132	Protein kinase, cAMP dependent, catalytic, alpha		
7	0.18922	Mylk	Q6PDN3	Myosin, light polypeptide kinase		
7	0.18922	Rhoq	Q8R527	Ras homolog family member Q		
7	0.18922	Chuk	Q60680	Conserved helix-loop-helix ubiquitous kinase		
7	0.18922	Baiap2	Q8BKX1	Brain-specific angiogenesis inhibitor 1-associated protein 2	Yes	Yes
7	0.18922	Ndufs5	Q99LY9	NADH:ubiquinone oxidoreductase core subunit S5	Yes	Yes

reduced, albeit non-significant, mtDNA copy number of ND1 ($p = 0.11$) and ND4 ($p = 0.07$) compared to non-treated TG mice.

4. Discussion

DYRK1A is one of the most important candidate genes to explain Down syndrome (DS) neuropathology. DYRK1A immunostaining is found in the cerebellum (Martí et al., 2003), suggesting a possible involvement of this kinase in the cerebellar physiology and pathology, which might be involved in DS motor, and learning phenotypes. However, the proteomic modifications due to *Dyrk1A* overexpression in the cerebellum had not been yet explored. Using mass-spectrometry-based proteomic we detected important proteomic alterations in Tg*Dyrk1A* (TG) cerebellum with over 200 proteins showing changes in abundance, a much higher number than what was detected in the hippocampus (De Toma et al., 2019). The most significant changes indicate mitochondrial dysfunction as a crucial factor in the pathogenesis of cerebellar impairment in TG mice. Interestingly, treatment with green tea extracts rescued the level of numerous proteins, especially those involved in mitochondrial function.

Dyrk1A overexpression in the cerebellum of TG mice altered mitochondrial pathways with a significant enrichment for "cytochrome complex," and in general in the oxidative phosphorylation system (OXPHOS). In fact, oxidative stress and mitochondrial dysfunction are involved in DS and have been reported in *in vitro* and *in vivo* models of DS. The OXPHOS has five mitochondrial respiratory chain complexes (complexes I-V), complex I (NADH–ubiquinone oxidoreductase), complex II (succinate dehydrogenase), complex III (ubiquinone-cytochrome c oxidoreductase), complex IV (cytochrome C oxidase), and the ATP synthase. We detected a differential abundance of ubiquinol:cytochrome c oxidoreductase (complex III), ATP synthase (complex V), and NADH:ubiquinone oxidoreductase (complex I). In previous proteomic studies, complex III core protein 1 was significantly reduced in the temporal cortex of AD patients while complex V beta chain and protein levels of complex I 30-kDa subunit were significantly reduced in the cerebral cortex of adult (Kim et al., 2000), and fetal DS brain (Kim et al., 2000, 2001). Our results support previous findings from Valenti et al. who found that deficits in the OXPHOS system in DS fibroblasts and lymphoblastoid cells lead to energy deficit and a dramatic increased ROS production in mitochondria (Valenti et al., 2010, 2011), and the severe deficits in mitochondrial bioenergetics in hippocampal neural progenitor cells (NPCs) of Ts65Dn mice (Valenti et al., 2016). These disturbances of enzymes of the mitochondrial electron transport chain may lead to a reduction in mitochondrial energy production, altered mitochondrial morphology, and increased fragmentation (Piccoli et al., 2013) that could be linked to cerebellar hypoplasia (Guidi et al., 2011) in DS. In fact, deregulated mitochondrial oxidative phosphorylation complexes are an early marker of cognitive decline in DS and AD (Alldred

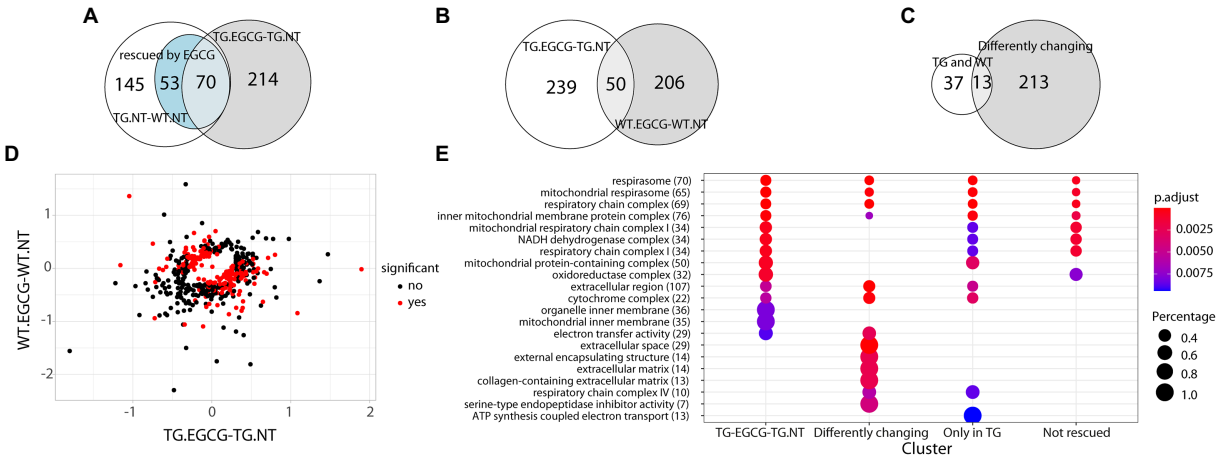

FIGURE 3
Dyrk1A overexpression extend beyond the network and differently affect wt and TgDYRK1A mice **(A)** Venn diagram showing the overlap between proteins changing their abundance in TG mice, protein changing upon EGCG-containing green tea extract treatment in TG mice, and the ones rescued. **(B)** Venn diagram showing the overlap between the proteins changing in TG mice upon treatment and the ones changing in WT. **(C)** Venn diagram showing the overlap between protein changing in both TG and WT mice upon EGCG-containing green tea extract treatment and the ones exhibiting a genotype-specific response to EGCG-containing green tea extract treatment **(D)** Plot comparing protein fold changes upon EGCG treatment in TG mice (*x*-axis), and wild-type mice (*y*-axis). Proteins with a significant interaction in the contrast *(TG.EGCG-TG.NT) – (WT. EGCG-WT.NT)*, where NT stands for "not treated," are indicated as red dots. **(E)** Enrichment analysis for biological processes, molecular functions, and cell components upon EGCG-containing green tea extract treatment in TG. The color-gradient indicates the adjusted *p*-value for the enrichment. Numbers in parentheses indicate the number of identified proteins in each category. Dot size corresponds to (protein count for each group)/(total protein count for each category). Only categories with an FDR<1% are shown.

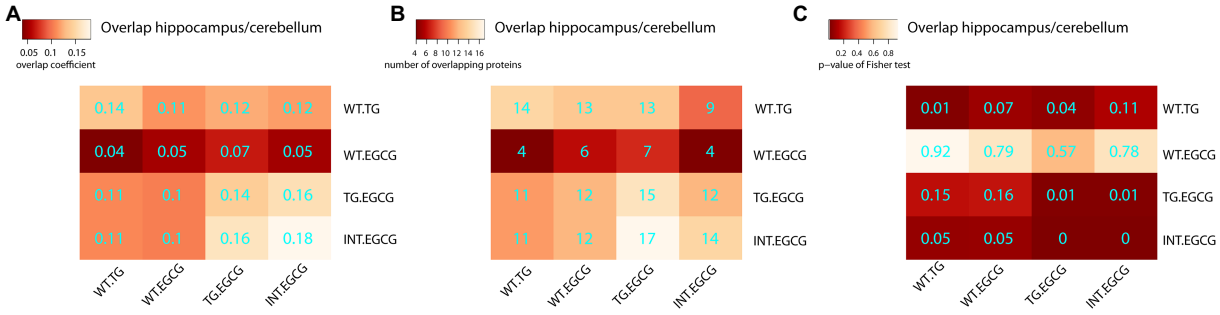

FIGURE 4
Overlaps of differentially abundant proteins across experimental conditions. Heatmap showing the overlap between differentially abundant proteins in the cerebellum and hippocampus. **(A)** The Szymkiewicz–Simpson overlap coefficient is depicted in cyan; **(B)** the number of overlapping proteins; **(C)** the *p*-values of the exact Fisher test. TG, TG mice. WT, wild-type mice. NT, not treated, EGCG treated with green tea extracts.

et al., 2021). Here, we tested if gene deregulation caused by the sole overexpression of *Dyrk1A* would influence mtDNA replication (Clayton, 1992). mtDNA is a double-stranded DNA molecule encoding for 13 structural peptide subunits of the oxidative phosphorylation system along with 24 RNA molecules required for mitochondrial protein synthesis (Anderson et al., 1981; Andrews et al., 1999). It has been described that mutations in mtDNA can cause defects in structural proteins, impair mitochondrial RNA synthesis, and cause deficiencies in the respiratory chain (Sommerville et al., 2014; Lightowlers et al., 2015). Other DS mouse models, such as Ts1Cje, show decreased mitochondrial membrane potential and ATP production, and increase reactive oxygen species, although few studies have explored the cerebellum. Moreover, irregular shaped mitochondria have been reported in cerebellar neurons from Ts16 mice (Bersu et al., 1998).

We found a trend to higher mtDNA copy number of ND1 and ND4 in TG mice compared to WT mice. Our findings suggest that *Dyrk1A* overexpression would increase mtDNA copy number contributing to mitochondrial dysfunction leading to the alterations previously reported at the cerebellar level (Altafaj et al., 2008) in TG mice. Supporting this possibility, it was recently reported that DYRK1A is able to activate mitochondrial import machinery (Walter et al., 2021).

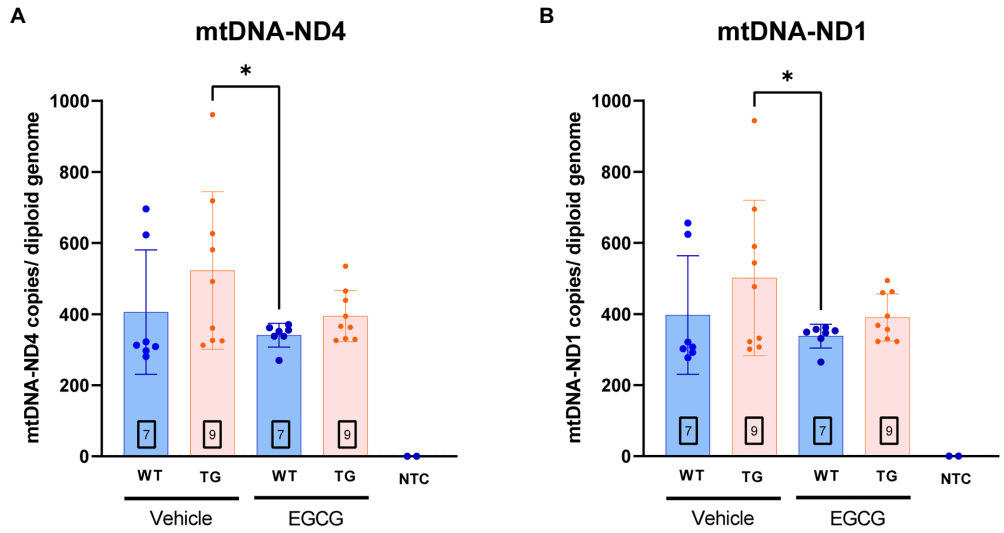

FIGURE 5
mtDNA copy number per cell is increased in TG mice. mtDNA copy number per cell in the Declive neuron-rich area of the cerebellum. Quantification of mitochondrial DNA copy number per diploid genome was performed with a multiplex digital PCR with different primer pairs targeting opposed regions of the mtDNA sequence: **(A)** the ND4 coding region and **(B)** the ND1 region. The n number of animals is within squares. Results are expressed as mean±SD. *p<0.05.

Remarkably, treatment with EGCG-containing green tea extract partially recovered the mtDNA copy number in TG mice. The stabilizing effect of EGCG on mtDNA copy number is consistent with previous findings showing that EGCG restored mtDNA copy number in hippocampal neuronal precursor cells (NPCs) from Ts65Dn mice (Valenti et al., 2016). In these cells, EGCG increased the number of mtDNA copies lowered by Ts65Dn to control levels (Valenti et al.). In contrast, the results reported here show that, in the cerebellum, EGCG lowers the number of mtDNA copies increased by Dyrk1A back to control levels. This difference is most likely due to brain region-specific regulation of mtDNA copy number. The amount of mtDNA copies per cell differs in almost one order of magnitude between the hippocampus and cerebellar cells (mtDNA) copy number relative to whole brain median = 0.7 vs. 0.09 (Fuke et al., 2011). Thus, Dyrk1A overexpression or Ts65Dn may alter mtDNA copy numbers differently in each brain region. Altered mtDNA copy number has been associated with different neurodegenerative disorders (Wei et al., 2017), and normalizing the number of mtDNA copies in different neurodegenerative diseases has been hypothesized to have a beneficial effect (Filograna et al., 2021). However, the mechanisms of brain region and cell-type specific regulation of mtDNA copy number are still unknown and further studies are necessary to determine the molecular mechanisms of selective vulnerability of neurodegeneration. Nonetheless, the present results suggest that Dyrk1a overexpression alters mtDNA copy number in the cerebellum and provide evidence to suggest that EGCG prevents alteration of mtDNA copy number set point in this brain region.

Treatment with EGCG-containing green tea extract also rescued the levels of 123 proteins (45%) to WT levels in TG mice. Rescued proteins were enriched in categories connected with mitochondria and oxidative phosphorylation. However, the effects of the treatment were mainly genotype-specific, as many proteins showed an opposite direction of change upon green-tea treatment in WT compared to TS (note the red dots in Figure 3D). These proteins were enriched in the mitochondrial respirasome but also in "extracellular space" and in "serine-type endopeptidase inhibitor activity" (see Figure 3E). Interestingly, comparing our previous proteomic study in the hippocampus, we observed that *Dyrk1A*-overexpression leads to region-specific proteomic dysregulation in the cerebellum.

In summary, our proteomic study revealed that *Dyrk1A* overexpression affects protein levels related with antioxidant activity and cerebellar proteins involved in oxidative phosphorylation system and cytochrome complex, suggesting a mitochondrial dysfunction. This was further emphasized by the increase of mtDNA copy number in TG cerebellum, which may explain mitochondrial dysfunction. EGCG-containing green tea extract treatment, which was already effective in rescuing the proteome alterations in the hippocampus, was also able to partially restore cerebellar protein levels and normalized the increased mtDNA levels that were found in non-treated TG mice.

Data availability statement

The datasets presented in this study can be found in online repositories. The names of the repository/repositories and accession number(s) can be found at: http://www.proteomexchange.org/, PXD030772 and directly at https://github.com/Ilarius/TgDyrk1A_protemics_cerebellum.

Ethics statement

The animal study was reviewed and approved by Comité Ético de Experimentación Animal del PRBB (CEEA-PRBB), Parc de Recerca Biomédica de Barcelona.

Author contributions

MO performed the proteomics experiment and made some of the analyses. IT performed the analyses, wrote the manuscript, and prepared all the figures. ÁF-B prepared the figures and did the validation experiments together with AC, LB, and RT. MD and ES conceived the project, supervised the experiments and analyses, and revised the manuscript. All authors contributed to the article and approved the submitted version.

Funding

This research was funded by the Agencia Estatal de Investigación (PID2019-110755RB-I00/AEI/10.13039/501100011033), the European Union's Horizon 2020 Framework Programme under grant agreement no 848077. This reflects only the author's view and the European Commission is not responsible for any use that may be made of the information it contains. Jerôme Lejeune Foundation (grant number 2002), NIH Blueprint for Neuroscience Research (grant number: 1R01EB 028159-01), Marató TV3 (#2016/20-30), and EU Joint Programme—Neurodegenerative Disease Research (Heroes AC170006). The CRG/UPF Proteomics Unit is part of the Spanish Infrastructure for Omics Technologies (ICTS OmicsTech), and it is supported by "Secretaria d'Universitats i Recerca del Departament d'Economia i Coneixement de la Generalitat de Catalunya" (2017SGR595). The CRG acknowledges the support of the Spanish Ministry of Science and Innovation to the EMBL partnership, the Centro de Excelencia Severo Ochoa, and the CERCA Programme/Generalitat de Catalunya. The CIBER of Rare Diseases (CIBERER) is an initiative of the ISCIII.

Conflict of interest

The authors declare that the research was conducted in the absence of any commercial or financial relationships that could be construed as a potential conflict of interest.

Publisher's note

Supplementary material

The Supplementary material for this article can be found online at: https://www.frontiersin.org/articles/10.3389/fnmol.2022.1015220/full#supplementary-material

References

Alldred, M. J., Lee, S. H., Stutzmann, G. E., and Ginsberg, S. D. (2021). Oxidative phosphorylation is Dysregulated within the Basocortical circuit in a 6-month old mouse model of down syndrome and Alzheimer's disease. *Front. Aging Neurosci.* 13:707950. doi: 10.3389/fnagi.2021.707950

Alstott, J., Bullmore, E., and Plenz, D. (2014). Powerlaw: a python package for analysis of heavy-tailed distributions. *PLoS One* 9:e85777. doi: 10.1371/journal.pone.0085777

Altafaj, X., Dierssen, M., Baamonde, C., Martí, E., Visa, J., Guimerà, J., et al. (2001). Neurodevelopmental delay, motor abnormalities and cognitive deficits in transgenic mice overexpressing Dyrk1A (minibrain), a murine model of Down's syndrome. *Hum. Mol. Genet.* 10, 1915–1923. doi: 10.1093/hmg/10.18.1915

Altafaj, X., Ortiz-Abalia, J., Fernández, M., Potier, M. C., Laffaire, J., Andreu, N., et al. (2008). Increased NR2A expression and prolonged decay of NMDA-induced calcium transient in cerebellum of TgDyrk1A mice, a mouse model of down syndrome. *Neurobiol. Dis.* 32, 377–384. doi: 10.1016/j.nbd.2008.07.024

Anderson, S., Bankier, T., Barrell, G., de Bruijn, H., Coulson, R., Drouin, J., et al. (1981). Sequence and organization of the human mitochondrial genome. *Nature* 290, 457–465. doi: 10.1038/290457a0

Andrews, M., Kubacka, I., Chinnery, F., Lightowlers, N., Turnbull, M., and Howell, N. (1999). Reanalysis and revision of the Cambridge reference sequence for human mitochondrial DNA. *Nat Gen* 23:147. doi: 10.1038/13779

Aranda, S., Laguna, A., and de la Luna, S. (2011). DYRK family of protein kinases: evolutionary relationships, biochemical properties, and functional roles. *FASEB J.* 25, 449–462. doi: 10.1096/fj.10-165837

Bersu, E. T., Ahmad, F. J., Schwei, M. J., and Baas, P. W. (1998). Cytoplasmic abnormalities in cultured cerebellar neurons from the trisomy 16 mouse. *Brain Res. Dev. Brain Res.* 109, 115–120. doi: 10.1016/s0165-3806(98)00070-4

Buchberger, A., Schepergerdes, L., Flaßhoff, M., Kunick, C., and Köster, R. W. (2021). A novel inhibitor rescues cerebellar defects in a zebrafish model of down syndrome-associated kinase Dyrk1A overexpression. *J. Biol. Chem.* 297:100853. doi: 10.1016/j.jbc.2021.100853

Choi, M., Chang, C.-Y., Clough, T., Broudy, D., Killeen, T., MacLean, B., et al. (2014). MSstats: an R package for statistical analysis of quantitative mass spectrometry-based proteomic experiments. *Bioinformatics* 30, 2524–2526. doi: 10.1093/bioinformatics/btu305

Clayton, D. (1992). Transcription and replication of animal mitochondrial DNAs. *Int. Rev. Cytol.* 141, 217–232. doi: 10.1016/S0074-7696(08)62067-7

Cox, J., and Mann, M. (2008). MaxQuant enables high peptide identification rates, individualized p.p.b.-range mass accuracies and proteome-wide protein quantification. *Nat. Biotechnol.* 26, 1367–1372. doi: 10.1038/nbt.1511

Cox, J., Neuhauser, N., Michalski, A., Scheltema, R. A., Olsen, J. V., and Mann, M. (2011). Andromeda: a peptide search engine integrated into the MaxQuant environment. *J. Proteome Res.* 10, 1794–1805. doi: 10.1021/pr101065j

Csardi, G., and Nepusz, T. (2006). The igraph software package for complex network research. *Inter J. Complex Syst.* 1695, 1–9.

De Toma, I., Ortega, M., Aloy, P., Sabidó, E., and Dierssen, M. (2019). DYRK1A overexpression alters cognition and neural-related proteomic pathways in the hippocampus that are rescued by green tea extract and/or environmental enrichment. *Front. Mol. Neurosci.* 12:272. doi: 10.3389/fnmol.2019.00272

De Toma, I., Ortega, M., Catuara-Solarz, S., Sierra, C., Sabidó, E., and Dierssen, M. (2020). Re-establishment of the epigenetic state and rescue of kinome deregulation in Ts65Dn mice upon treatment with green tea extract and environmental enrichment. *Sci. Rep.* 10:16023. doi: 10.1038/s41598-020-72625-z

Dierssen, M. (2012). Down syndrome: The brain in trisomic mode. *Nat. Rev. Neurosci.* 13, 844–858. doi: 10.1038/nrn3314

Duchon, A., and Herault, Y. (2016). DYRK1A, a dosage-sensitive gene involved in neurodevelopmental disorders, is a target for drug development in down syndrome. *Front. Behav. Neurosci.* 10:104. doi: 10.3389/fnbeh.2016.00104

Durinck, S., Spellman, P. T., Birney, E., and Huber, W. (2009). Mapping identifiers for the integration of genomic datasets with the R/bioconductor package biomaRt. *Nat. Protoc.* 4, 1184–1191. doi: 10.1038/nprot.2009.97

Filograna, R., Mennuni, M., Alsina, D., and Larsson, N. G. (2021). Mitochondrial DNA copy number in human disease: the more the better? *FEBS Lett.* 595, 976–1002. doi: 10.1002/1873-3468.14021

Fotaki, V., Dierssen, M., Alcántara, S., Martínez, S., Martí, E., Casas, C., et al. (2002). Dyrk1A haploinsufficiency affects viability and causes developmental delay and abnormal brain morphology in mice. *Mol. Cell. Biol.* 22, 6636–6647. doi: 10.1128/MCB.22.18.6636-6647.2002

Fuke, S., Kubota-Sakashita, M., Kasahara, T., Shigeyoshi, Y., and Kato, T. (2011). Regional variation in mitochondrial DNA copy number in mouse brain. *Biochim et Biophy Acta (BBA)-Bioenergetics* 1807, 270–274. doi: 10.1016/j.bbabio.2010.11.016

García-Cerro, S., Vidal, V., Lantigua, S., Berciano, M. T., Lafarga, M., Ramos-Cabrer, P., et al. (2018). Cerebellar alterations in a model of down syndrome: the role of the Dyrk1A gene. *Neurobiol. Dis.* 110, 206–217. doi: 10.1016/j.nbd.2017.12.002

Guard, S. E., Poss, Z. C., Ebmeier, C. C., Pagratis, M., Simpson, H., Taatjes, D. J., et al. (2019). The nuclear interactome of DYRK1A reveals a functional role in DNA damage repair. *Sci. Rep.* 9:6539. doi: 10.1038/s41598-019-42990-5

Guidi, S., Ciani, E., Bonasoni, P., Santini, D., and Bartesaghi, R. (2011). Widespread proliferation impairment and hypocellularity in the cerebellum of fetuses with down syndrome. *Brain Pathol.* 21, 361–373. doi: 10.1111/j.1750-3639.2010.00459.x

Jain, A., and Tuteja, G. (2019). TissueEnrich: tissue-specific gene enrichment analysis. *Bioinformatics* 35, 1966–1967. doi: 10.1093/bioinformatics/bty890

Kim, S. H., Fountoulakis, M., Dierssen, M., and Lubec, G. (2001). Decreased protein levels of complex I 30-kDa subunit in fetal down syndrome brains. *J. Neural Transm. Suppl.* 61, 109–116. doi: 10.1007/978-3-7091-6262-0_9

Kim, S. H., Vlkolinsky, R., Cairns, N., and Lubec, G. (2000). Decreased levels of complex III core protein 1 and complex V beta chain in brains from patients with Alzheimer's disease and down syndrome. *Cell. Mol. Life Sci.* 57, 1810–1816. doi: 10.1007/pl00000661

Lightowlers, N., Taylor, W., and Turnbull, M. (2015). Mutations causing mitochondrial disease: what is new and what challenges remain? *Science* 349, 1494–1499. doi: 10.1126/science.aac7516

Martí, E., Altafaj, X., Dierssen, M., de la Luna, S., Fotaki, V., Alvarez, M., et al. (2003). Dyrk1A expression pattern supports specific roles of this kinase in the adult central nervous system. *Brain Res.* 964, 250–263. doi: 10.1016/s0006-8993(02)04069-6

Martínez de Lagrán, M., Altafaj, X., Gallego, X., Martí, E., Estivill, X., Sahún, I., et al. (2004). Motor phenotypic alterations in TgDyrk1a transgenic mice implicate DYRK1A in down syndrome motor dysfunction. *Neurobiol. Dis.* 15, 132–142. doi: 10.1016/j.nbd.2003.10.002

Martínez de Lagran, M., Benavides-Piccione, R., Ballesteros-Yañez, I., Calvo, M., Morales, M., Fillat, C., et al. (2012). Dyrk1A influences neuronal morphogenesis through regulation of cytoskeletal dynamics in mammalian cortical neurons. *Cereb. Cortex* 22, 2867–2877. doi: 10.1093/cercor/bhr362

Mosca, R., Céol, A., and Aloy, P. (2013). Interactome3D: adding structural details to protein networks. *Nat. Methods* 10, 47–53. doi: 10.1038/nmeth.2289

Orchard, S. (2012). Molecular interaction databases. *Proteomics* 12, 1656–1662. doi: 10.1002/pmic.201100484

Orchard, S., Kerrien, S., Abbani, S., Aranda, B., Bhate, J., Bidwell, S., et al. (2012). Protein interaction data curation: the international molecular exchange (IMEx) consortium. *Nat. Methods* 9, 345–350. doi: 10.1038/nmeth.1931

Piccoli, C., Izzo, A., Scrima, R., Bonfiglio, F., Manco, R., Negri, R., et al. (2013). Chronic pro-oxidative state and mitochondrial dysfunctions are more pronounced in fibroblasts from down syndrome foeti with congenital heart defects. *Hum. Mol. Genet.* 22, 1218–1232. doi: 10.1093/hmg/dds529

Podlesniy, P., and Trullas, R. (2017). Absolute measurement of gene transcripts with Selfie-digital PCR. *Sci. Rep.* 7:8328. doi: 10.1038/s41598-017-08270-w

Roewenstrunk, J., Di Vona, C., Chen, J., Borras, E., Dong, C., Arató, K., et al. (2019). A comprehensive proteomics-based interaction screen that links DYRK1A to RNF169 and to the DNA damage response. *Sci. Rep.* 9:6014. doi: 10.1038/s41598-019-42445-x

Shen, Y., Yue, F., McCleary, D. F., Ye, Z., Edsall, L., Kuan, S., et al. (2012). A map of the cis-regulatory sequences in the mouse genome. *Nature* 488, 116–120. doi: 10.1038/nature11243

Sommerville, W., Chinnery, F., Gorman, S., and Taylor, W. (2014). Adult-onset mendelian PEO associated with mitochondrial disease. *J. Neuromuscul. Dis.* 1, 119–133. doi: 10.3233/JND-140041

Szklarczyk, D., Franceschini, A., Wyder, S., Forslund, K., Heller, D., Huerta-Cepas, J., et al. (2015). STRING v10: protein-protein interaction networks, integrated over the tree of life. *Nucleic Acids Res.* 43, D447–D452. doi: 10.1093/nar/gku1003

Uhlén, M., Fagerberg, L., Hallström, B. M., Lindskog, C., Oksvold, P., Mardinoglu, A., et al. (2015). Proteomics. Tissue-based map of the human proteome. *Science* 347:1260419. doi: 10.1126/science.1260419

Valenti, D., De Bari, L., De Rasmo, D., Signorile, A., Henrion-Caude, A., Contestabile, A., et al. (2016). The polyphenols resveratrol and epigallocatechin-3-gallate restore the severe impairment of mitochondria in hippocampal progenitor cells from a down syndrome mouse model. *Biochim. Biophys. Acta* 1862, 1093–1104. doi: 10.1016/j.bbadis.2016.03.003

Valenti, D., Manente, G. A., Moro, L., Marra, E., and Vacca, R. A. (2011). Deficit of complex I activity in human skin fibroblasts with chromosome 21 trisomy and overproduction of reactive oxygen species by mitochondria: involvement of the cAMP/PKA signalling pathway. *Biochem. J.* 435, 679–688. doi: 10.1042/BJ20101908

Valenti, D., Rossi, L., Marzulli, D., Bellomo, F., De Rasmo, D., Signorile, A., et al. (2017). Inhibition of Drp 1-mediated mitochondrial fission improves mitochondrial dynamics and bioenergetics stimulating neurogenesis in hippocampal progenitor cells from a down syndrome mouse model. *Biochim. Biophys. Acta Mol. basis Dis.* 1863, 3117–3127. doi: 10.1016/j.bbadis.2017.09.014

Valenti, D., Stagni, F., Emili, M., Guidi, S., Bartesaghi, R., and Vacca, R. A. (2021). Impaired brain mitochondrial bioenergetics in the Ts65Dn mouse model of down syndrome is restored by neonatal treatment with the polyphenol 7,8-Dihydroxyflavone. *Antioxidants (Basel)* 11:62. doi: 10.3390/antiox11010062

Valenti, D., Tullo, A., Caratozzolo, M. F., Merafina, R. S., Scartezzini, P., Marra, E., et al. (2010). Impairment of F1F0-ATPase, adenine nucleotide translocator and adenylate kinase causes mitochondrial energy deficit in human skin fibroblasts with chromosome 21 trisomy. *Biochem. J.* 431, 299–310. doi: 10.1042/BJ20100581

Vizcaíno, J. A., Deutsch, E. W., Wang, R., Csordas, A., Reisinger, F., Ríos, D., et al. (2014). ProteomeXchange provides globally coordinated proteomics data submission and dissemination. *Nat. Biotechnol.* 32, 223–226. doi: 10.1038/nbt.2839

Walter, C., Marada, A., Suhm, T., Ernsberger, R., Muders, V., Kücükköse, C., et al. (2021). Global kinome profiling reveals DYRK1A as critical activator of the human mitochondrial import machinery. *Nat. Commun.* 12:4284. doi: 10.1038/s41467-021-24426-9

Wei, W., Keogh, M. J., Wilson, I., Coxhead, J., Ryan, S., Rollinson, S., et al. (2017). Mitochondrial DNA point mutations and relative copy number in 1363 disease and control human brains. *Acta Neuropathol.* 5, 13–18. doi: 10.1186/s40478-016-0404-6

Yu, G., Wang, L.-G., Han, Y., and He, Q.-Y. (2012). clusterProfiler: an R package for comparing biological themes among gene clusters. *OMICS* 16, 284–287. doi: 10.1089/omi.2011.0118

frontiers | Frontiers in Molecular Neuroscience

TYPE Original Research
PUBLISHED 24 March 2023
DOI 10.3389/fnmol.2023.1122308

OPEN ACCESS

EDITED BY
Vittorio Maglione,
Mediterranean Neurological Institute Neuromed (IRCCS), Italy

REVIEWED BY
Jose Felix Moruno-Manchon,
University of Texas Health Science Center at Houston, United States
Di Hu,
Case Western Reserve University, United States

*CORRESPONDENCE
Maciej Figiel
✉ mfigiel@ibch.poznan.pl

SPECIALTY SECTION
This article was submitted to Brain Disease Mechanisms, a section of the journal Frontiers in Molecular Neuroscience

RECEIVED 12 December 2022
ACCEPTED 01 February 2023
PUBLISHED 24 March 2023

CITATION
Piasecki P, Wiatr K, Ruszkowski M, Marczak Ł, Trottier Y and Figiel M (2023) Impaired interactions of ataxin-3 with protein complexes reveals their specific structure and functions in SCA3 Ki150 model.
Front. Mol. Neurosci. 16:1122308.
doi: 10.3389/fnmol.2023.1122308

Impaired interactions of ataxin-3 with protein complexes reveals their specific structure and functions in SCA3 Ki150 model

Piotr Piasecki[1], Kalina Wiatr[1], Milosz Ruszkowski[1], Łukasz Marczak[1], Yvon Trottier[2] and Maciej Figiel[1]*

[1]Institute of Bioorganic Chemistry, Polish Academy of Sciences, Poznań, Poland, [2]Institute of Genetics and Molecular and Cellular Biology, University of Strasbourg, Illkirch, France

Spinocerebellar ataxia type 3 (SCA3/MJD) is a neurodegenerative disease caused by CAG expansion in mutant *ATXN3* gene. The resulting PolyQ tract in mutant ataxin-3 protein is toxic to neurons and currently no effective treatment exists. Function of both normal and mutant ataxin-3 is pleiotropic by their interactions and the influence on protein level. Our new preclinical Ki150 model with over 150 CAG/Q in ataxin-3 has robust aggregates indicating the presence of a process that enhances the interaction between proteins. Interactions in large complexes may resemble the real-life inclusion interactions and was never examined before for mutant and normal ataxin-3 and in homozygous mouse model with long polyQ tract. We fractionated ataxin-3-positive large complexes and independently we pulled-down ataxin-3 from brain lysates, and both were followed by proteomics. Among others, mutant ataxin-3 abnormally interacted with subunits of large complexes such as Cct5 and 6, Tcp1, and Camk2a and Camk2b. Surprisingly, the complexes exhibit circular molecular structure which may be linked to the process of aggregates formation where annular aggregates are intermediate stage to fibrils which may indicate novel ataxin-3 mode of interactions. The protein complexes were involved in transport of mitochondria in axons which was confirmed by altered motility of mitochondria along SCA3 Ki150 neurites.

KEYWORDS

SCA3, ataxin-3, CAG, polyQ, neurodegeneration, mouse mitochondria, aggregates, interactions

1. Introduction

Spinocerebellar ataxia type 3, also known as Machado-Joseph disease (SCA3/MJD), is the most common type of dominantly inherited ataxias and belongs to a group of polyQ neurodegenerative disorders (McLoughlin et al., 2020). SCA3 is typically characterized by progressive motor incoordination and brain neuronal loss (Bettencourt and Lima, 2011; Koeppen, 2018) caused by the expansion of the CAG repeats in exon 10 of the *ATXN3* gene (>45) (Lima and Raposo, 2018). There is a substantial correlation between the number of CAG repeats, the age of onset of symptoms, and the severity of the disease course (Maciel et al., 1995; Leotti et al., 2021). The mutation results in an expanded polyQ tract in the ataxin-3 protein, which forms aggregates (Orr and Zoghbi, 2007). Ataxin-3 is a multifunctional protein and protease with a pleiotropic effect on many cellular

pathways (Riess et al., 2008; Winborn et al., 2008; Grasty et al., 2019; Wiatr et al., 2019, 2021; Herzog et al., 2020). The pleiotropic influence results from interactions of both ataxin-3 and its aggregates with a plethora of other proteins, and these interactions may drive the disease. By interacting with K48-and non-canonical K63-linked ubiquitin chains, ataxin-3 plays diverse roles in ubiquitin signaling and protein quality control (Winborn et al., 2008; Todi et al., 2009, p. 3; Todi and Paulson, 2011; Carvalho et al., 2018). Furthermore, ataxin-3 regulates cytoskeleton function by interacting with dynein, an essential protein in retrograde axonal transport (Burnett and Pittman, 2005; Toulis et al., 2020). Ataxin-3 polyQ expansion results in either gain of function or loss of function of cellular processes and protein interactions (Paulson et al., 1997; Nascimento-Ferreira et al., 2011; Simões et al., 2012; Nóbrega et al., 2015). The pleiotropic function of the mutant protein (Wiatr et al., 2019, 2021) makes it difficult to untangle the molecular mechanisms of SCA3 and develop a treatment to prevent, cure, or stop the disease progression. Moreover, addressing the pathogenesis and the investigation of drug candidates requires a preclinical mouse model, which shows quick and intensive phenotype, and represents molecular, cellular, and motor changes mimicking SCA3. Phenotype acceleration in polyQ mouse models is always associated with a significantly greater number of CAGs in gene and glutamines in protein which results in an increasing number of aggregates.

We have previously shown a Ki91 model with 110–120 CAGs in the humanized *ATXN3* gene (Wiatr et al., 2019, 2021) with early inclusions and profound early proteome changes that play a crucial role in SCA3 pathogenesis. To demonstrate intensive SCA3 alterations and facilitate preclinical testing, we now generated a Ki150 knock-in mouse model containing 150–170 CAGs and obtained intensive SCA3-like symptoms. The Ki150 demonstrated dense and large aggregates, indicating intensive processes of protein aggregation and interactions. Protein interactions in SCA3 were previously investigated in isolated systems, in environments lacking large brain complexes or aggregates. To understand the SCA3 neuropathomechanism in our model, we determined the ataxin-3 interactions by identifying large complexes and proteins responsible for neuronal transport, mitochondria, and translation. We discovered that mutant ataxin-3 ultimately losses interaction with the complexes and that the marked feature of these complexes was their circular 3D structure. Guided by specific sets of interacting complexes and proteins, we assayed the physiological consequence in mouse neurons. We intensely investigated the functions of neurites in SCA3 by assesing live mitochondrial motility and mitochondrial transport in Ki150 neurites.

Abbreviations: ANOVA, Analysis of variance; CCT, Chaperon Containing TCP1-complex; DIV, Days *in vitro*; MJD, Machado-Joseph disease; MS, Mass spectrometry; mo, Month-old; polyQ, Polyglutamine; SCA3, Spinocerebellar ataxia type 3; SEM, Standard error of mean; IEC, Ion exchange chromatography; SEC, Size using size exclusion chromatography; WT, Wildtype.

2. Results

2.1. Ki150 SCA3 mouse model contains mutant ataxin-3 with a large polyQ tract

Expansion of the CAG repeats number in *ATXN3*, which occurs between generations (intergenerational expansion), usually correlates with the accelerated disease progression in SCA3 patients (Maciel et al., 1995; Leotti et al., 2021). Also, our Ki91 mouse showed intergenerational expansion (Switonski et al., 2015), resulting in a spontaneous increase in the number of CAG repeats in our mouse colonies, yielding mice containing between 110 and 130 CAG repeats. Therefore, our goal was to boost the phenotype further, to enhance the mouse model suitability for preclinical therapy testing. We used selective breeding of pairs with the highest number of CAGs repeats, reaching 150 units and above after multiple generations. Western blot analysis of the cerebral cortex of Ki150 mice showed differences in PAGE gel mobility of the ataxin-3 protein of various sizes (90–100 kDa) resulting from the number of glutamins between 153 and 174 (Figure 1A). Lamin B protein was used as a loading control. Figure 1B demonstrates capillary electroforesis detection of the DNA containing various numbers of CAGs in a PCR fragment resulting from Ki91 and Ki150 genome. The capillary electrophoresis demonstrates a dominant allele of 96 (Ki91), 153 and 163 (Ki150) and number of additional PCR products with lower or higher number of CAGs. Figure 1C demonstrates plots with examples of the CAG length of the longest and shortest allele in parents vs. offspring alleles (Figures 1B,C). The increase of variation in repeat numbers increase with generations, resulting in the identification of single expansions of 200 CAGs; however, the breeding of such animals was difficult.

2.2. The Ki150 mice produce robust inclusions across the brain

We have previously shown inclusions in the SCA3 Ki91 mouse occurring in all brain regions (Switonski et al., 2015; Wiatr et al., 2019, 2021). In the Ki150 mouse model, we observed the formation of larger inclusions in all brain regions and also in higher numbers than observed in Ki91 and at a younger Ki150 age. We quantified the number and density of aggregates in brain regions by Aggrecount Master macro (Klickstein et al., 2020) for Image J/Fiji (Figure 2). In Ki150 mice, we identified very large inclusions particularly apparent in brain regions with high cell density such as the hippocampus (Figure 2C). We also identified highest number of inclusions per mm^2 (n = 4) in the hippocampus (mean = 3,243; SEM = 460.7) as compared to cortex (mean = 838.7; SEM = 87.6), cerebellum (mean = 393.1; SEM = 88.8), and striatum (mean = 766.1; SEM = 109.3) (Figure 2E). Additionally, we measured the fluorescent signal intensity of each inclusion from the sample (n = 4 and 3 replicates/slices per brain), which was equivalent to the median density of an inclusion (Figure 2F). The density of a single inclusion was also highest in the hippocampus (median = 2,298) as compared to the cerebral cortex (median = 1969), cerebellum (median = 1727) and striatum (median = 382.2). In summary, in the Ki150 mouse model, inclusions are visibly larger than in Ki91 and denser. In addition, a picture of entire slice of the Ki150 brain immunostained with anti-ataxin-3 antibodies demonstrate the overview of inclusion pathology throughout the entire brain and visible regions

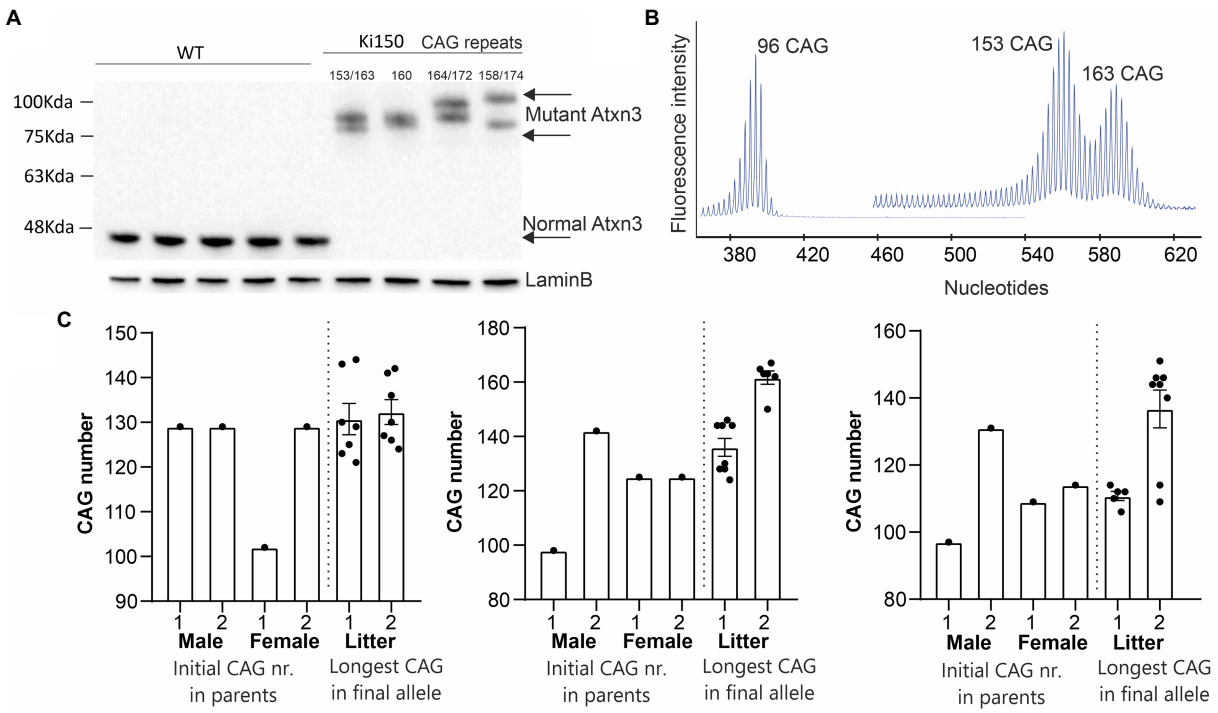

FIGURE 1
A new Ki150 mouse model expressing ataxin-3 with a large polyQ domain. Generation of the preclinical-type Ki150 mouse model with enhanced phenotype. **(A)** Homozygous Ki150 brain contains the polyQ-expanded ataxin-3 which reaches approximately 100kDa in weight on immunoblot. The number of glutamines in ataxin-3 proteins is indicated in Ki150. LaminB was used as a loading control. **(B)** Representative examples of increasing CAG number in alleles of parents vs. offspring in humanized *ATXN3* gene between Ki91 and Ki150 mouse models. **(C)** Analysis of the CAG number (96 and 153–163 CAGs) in alleles visible on peeks representing the capillary electrophoresis of the DNA PCR products. Male and female denote parent animals containing the indicated CAG number in ATXN3 of parents' allele. The "litter" denote the individual offspring mice with the CAG number of the final longest allele.

(Supplementary Figure 1A). Moreover, in Supplementary Figure 1B we included higher magnification images of ataxin-3 positive inclusion bodies in cerebellum, cerebral cortex, striatum, hippocampus, pons, and olfactory bulb.

2.3. Ki150 mice demonstrate a fast presentation and progression of a motor preclinical phenotype

In order to determine behavioral phenotypes characteristic of SCA3 in Ki150 mice, we performed several tests measuring motor performance. We discovered that first motor symptoms occur already in 1-month-old Ki150 animals ($n = 8$ per genotype). Already at this young age, Ki150 mice performed worse than WT in the elevated beam walk and Rotarod test, presenting loss of balance and incoordination (Figures 3A–C). Ki150 mice needed more time to turn on a rod (diameter: 9 mm) (Figure 3A) and took more time to traverse rods (diameter: 35 and 9 mm) in the elevated beam walk test ($p < 0.05$; two-way ANOVA, Bonferroni) (Figure 3B). With the progression of SCA3, the time needed for turning on a rod and traverse was significantly longer ultimately on all tested rods (diameter: 35, 28, 21, 17, 10, and 9 mm) ($p < 0.05$; two-way ANOVA, Bonferroni; Figures 3A,B). Moreover, Ki150 commit more foot slips while traversing rods. In addition, the incoordination observed in the Rotarod was observed starting from the age of 1-month and progressed with age ($p < 0.001$; two-way ANOVA, Bonferroni; Figure 3C). 5-month-old Ki150 mice showed deterioration of motor phenotype in the scoring test, which evaluated gait, motor coordination, balance, hindlimb clasping, and kyphosis ($p < 0.0001$; two-way ANOVA, Bonferroni) (Figure 3D). At the age of 8-months, Ki150 also demonstrated reduced body weight ($p < 0.0001$; two-way ANOVA, Bonferroni) (Figure 3E). There was no correlation between body weight and behavioral tests at any age ($p < 0.05$, correlation test).

2.4. Ki150 brain reveals the presence of mutant ataxin-3 in fractions containing subunits of large protein complexes

We have previously demonstrated that humanized mutant ataxin-3 from Ki91 model influenced very broad changes in protein levels and their phosphorylation. Since the protein from Ki150 contains an even more expanded polyQ tract and produces very dense brain inclusions, we decided to characterize the protein and the complexes to a greater extent. We asked how the protein interacts with other proteins and how large and stable are the complexes interacting with ataxin-3 containing a large polyQ domain. To separately analyze the influence of mutant or normal ataxin-3 on the complex formation, we took advantage of the fact that our models contain homozygous alleles (Ki150/150 or Ki21/Ki21).

10.3389/fnmol.2023.1122308

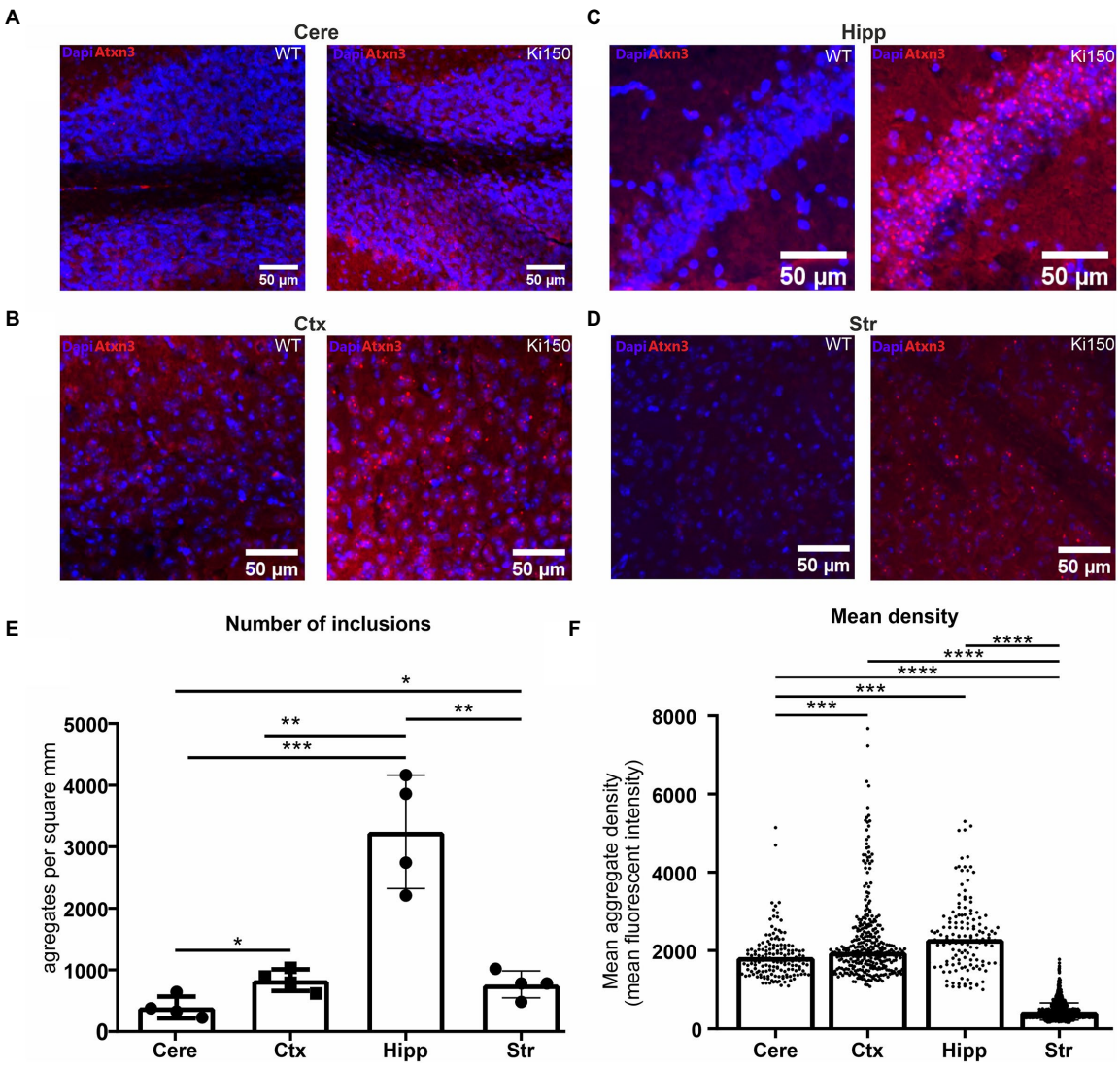

FIGURE 2
Ataxin-3-positive inclusions appear across the whole brain in SCA3 mouse model. **(A)** cerebellum (cere), **(B)** cerebral cortex (ctx), **(C)** hippocampus (hipp) **(D)** striatum (str). **(E)** Aggrecount imageJ macro identified about 400 inclusions per square millimeter in cerebellum, 800 inclusions per square millimeter in cerebral cortex, 3,000 inclusions per square millimeter in hippocampus and 760 inclusions per square millimeter in striatum (n =4). **(F)** The density of a single inclusion was also the highest in the hippocampus (median=2,298) as compared to cortex (median=1969), cerebellum (median=1727), and striatum (median=0.382). Two-sample t-test (*p<0.05, **p<0.01, ***p<0.001, ****p <0.0001), error bars: SEM (n=4 indicates 4 brains/4 mice. Per brain, 3 slices as technical replicates were used. Total number of 12 images were used for estimation of each brain region).

Therapeutic protein characterization often involves two or more or more orthagonal chromatographic methods. In our setup, we used orthogonal chromatographic methods in native conditions to resolve the protein brain lysates from Ki150 containing human mutant ataxin-3 with around 150Q and Ki21 containing human normal ataxin-3 21Q. First, we separated the proteins by charge using ion exchange chromatography (IEC) and then by size using size exclusion chromatography (SEC). We aimed to (i) investigate the distribution of ataxin-3 protein in SEC fractions, (ii) identify coeluting ataxin-3 partners, and (iii) assess the physical properties of putative mutant and normal ataxin-3 complexes In IEC, ataxin-3 was present in the flowthrough, likely due to the relatively high ionic strength of the PBS buffer (Supplementary Figure 2A). Nonetheless, IEC removed fat and nucleic acids, which was a necessary step prior to SEC. The SEC fractions contained native soluble proteins and preserved their interactions thanks to using PBS-EDTA buffer for SEC. The total protein concentration in the selected fraction (A280) was different for both genotypes. The protein concentration in ≥600-kDa fractions was higher in Ki150 samples, while protein concentration in 115–89 kDa fractions was higher in Ki21 samples (Supplementary Figure 1B). A vacuum dot-blot was performed and immunostained with anti-ataxin-3 antibodies to determine the ataxin-3 distribution in protein fractions from Ki150 and Ki21 brains (Figure 4A). The integrated optical density (IOD) of the ataxin-3 signal from dot blots was plotted against the SEC-calculated molecular weight within fractions. Additionally, after vacuum dot-blot Ponceau S staining was performed for loading control (Figure 4B). The plot demonstrated three peaks of the highest signal indicating a prominent presence of ataxin-3 in (i)

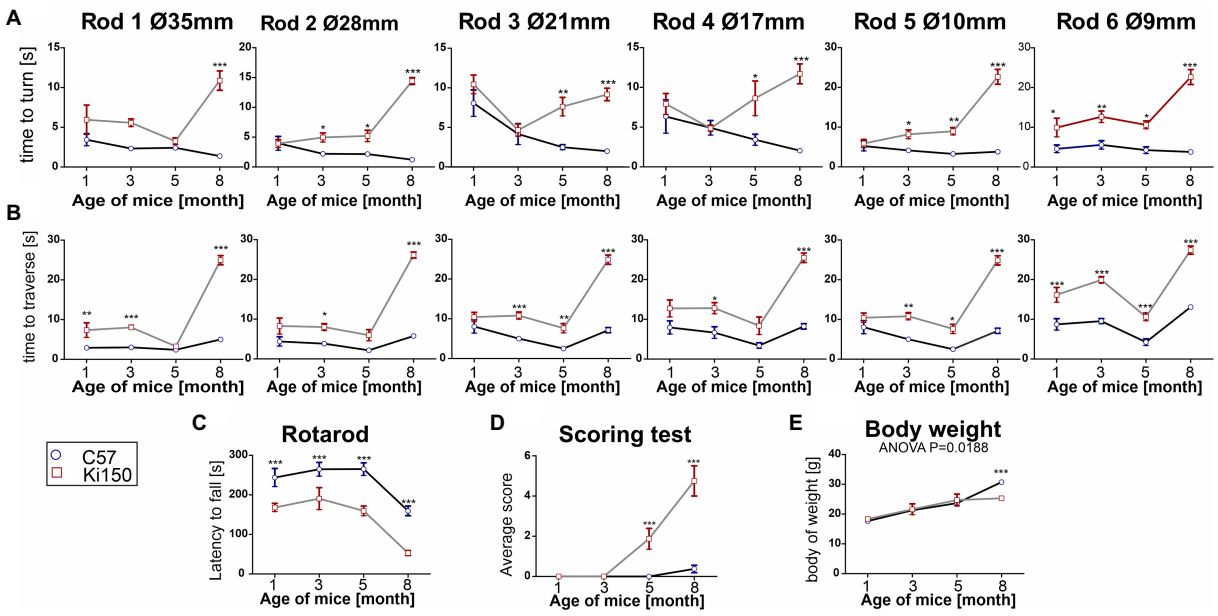

FIGURE 3
A progressive motor decline in Ki50 SCA3 knock-in model presents fast and severe phenotype. In the elevated beam walk test **(A,B)** "time to turn" and "traverse time" were measured on six rods with decreasing diameter (diameter of rods are indicated by Ø in mm). **(A)** One-month-old animals needed more time to turn on the rod 6 representing the highest level of difficulty and with disease progression more rods presented a challenge to Ki150 mice; Ultimately, at the age of 8months Ki150 mice needed more time to traverse on all rods. **(B)** Similarly to the "time to turn" 1-month-old Ki91 mice needed significantly more time to traverse on rod 6, but also 1, whereas older 8-month-old mice needed more time on all rods. **(C)** Motor incoordination in accelerated rotarod (4–40rpm in 5min) was presented by Ki150 already at the age of 1month. **(D)** In the scoring test, 5-month-old Ki150 mice presented SCA3 phenotype: incoordination, gait disturbances, kyphosis, and hind limb clasping. **(E)** The reduction of body weight gain in Ki150 was observed at the age of 8-month. Two-way ANOVA for every test besides body weight was $p<0.001$. Two-way ANOVA with Bonferroni *post hoc* test ($p\leq0.05$; total number of biological replicates: $n=16$, $n=8$ per genotype), error bars: SEM. Asterisks denotes a two-way ANOVA (*$p<0.05$, **$p<0.01$, ***$p<0.001$).

≥600 kDa, (ii) 282–218 kDa protein fractions in both genotypes, and markedly higher level of normal ataxin-3 in (iii) 115–89 kDa fraction (Figure 4C). The predicted sizes of fractions are not equivalent to the molecular weight for monomeric normal (48 kDa for Ki21) and mutant ataxin-3 (95 kDa for Ki150), suggesting that ataxin-3 forms extensive complexes with other proteins or forms homooligomers.

2.5. Fractions with mutant ataxin-3 show depletion or enrichment of proteins involved in large molecular complexes regulating aggregation, transport and CamK proteins

We traced the interaction of proteome in the presence of mutant or normal ataxin-3 to reveal the potential partners in the brain of homozygous Ki21 and Ki150. The collected fractions (ii) 282–192 kDa, and (iii) 115–89 kDa positive for ataxin-3 protein (by dot blot) were subjected to protein identification and quantitation by MS. The fraction (i) ≥600 kDa turned out to be unsuitable for MS analysis since it may contain aggregates inaccessible for trypsin and high content of peptide fragments that constitute background on MS spectrum. However, by comparing Ki21 and Ki150 samples from fractions (ii) and (iii), we identified the depletion or enrichment of proteins ($p<0.05$; two-sample *t*-test; Figure 5) that are part of specific cellular families of proteins and complexes. In fractions 282–218 kDa we found that proteins CCT5 and 6, and Tcp1 involved in Chaperon Containing TCP1-complex (CCT complex; T-complex), responsible for the regulation of protein folding, aggregation, and transport along neurites, were highly depleted in Ki150 brain fractions vs. Ki21 fractions (Table 1; Figure 5A). Also, the Ap2a1 and Aak1 (AP2-associated protein kinase 1), which are part of adaptor protein 2 complexes and together with Synj1 are responsible for vesicular transport, were depleted in Ki150 fractions (Table 1; Figure 5A). The most depleted proteins in Ki150 brain fractions were Camk2a and Camk2b kinases responsible for calcium homeostasis (Table 1; Figure 5A). The proteins highly enriched in 115–89 kDa Ki150 brain fractions were Hnrnpk and Eif4a2 involved in the translation initiation process (Table 2; Figure 5B). We also identified highly depleted Gad2, the GABA synthesizing enzyme, Calb2, a calcium-binding protein, and PCP2 proteins (Table 2; Figure 5B), all characteristic of GABAergic neurons such as Purkinje neurons in the cerebellum.

2.6. Mutant ataxin-3 interactors form sets of proteins that are functionally associated with mitochondria and translation

Molecular complexes identified in fractions 282–218 kDa such as CCT complex, AP2 and the family of Ca++ kinases usually bind a variety of other cellular proteins that tune their physiological function. Therefore, we used a co-immunoprecipitation assay with

10.3389/fnmol.2023.1122308

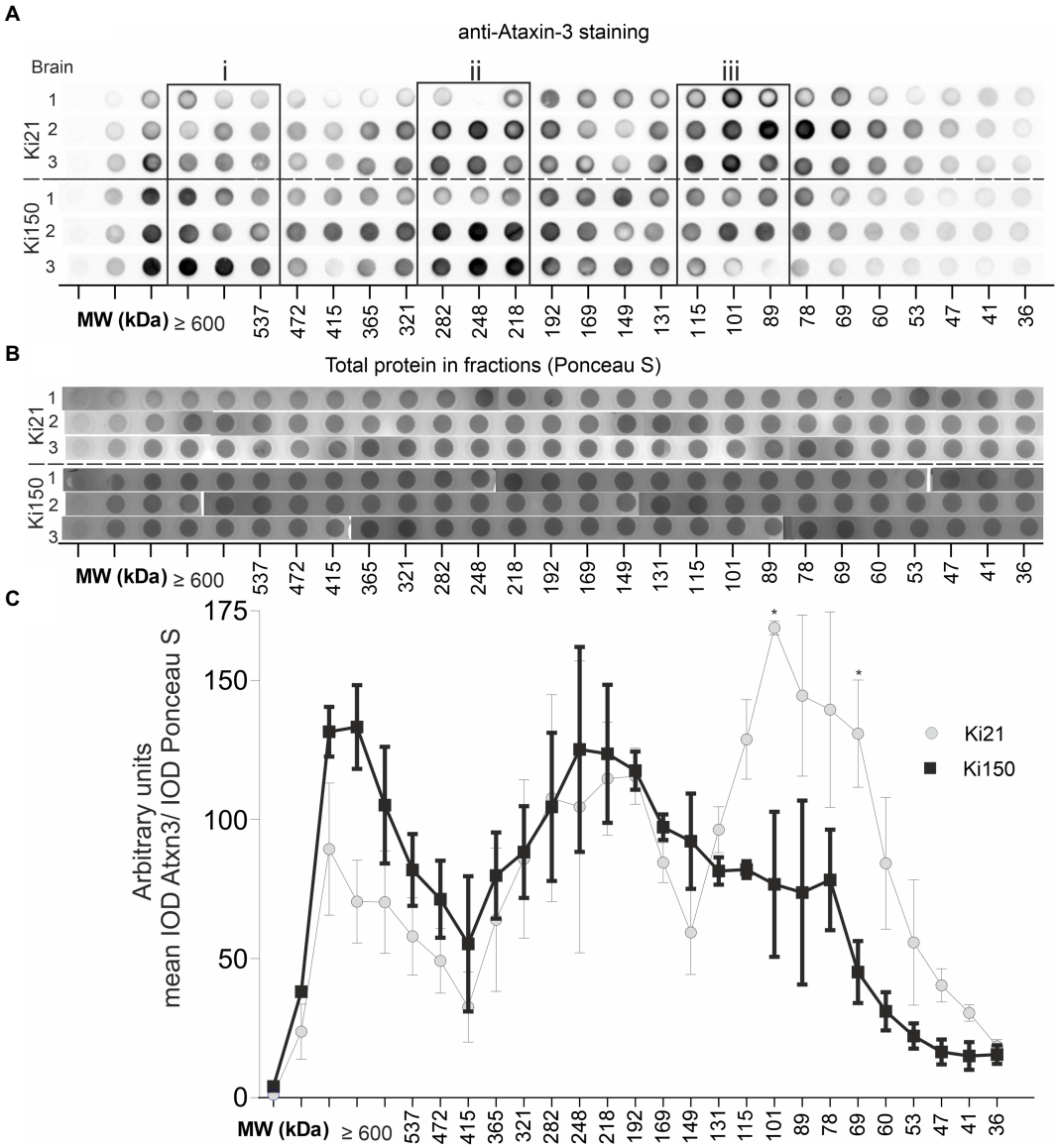

FIGURE 4
Ataxin-3 is distributied in large protein complexes after chromatographic fractionation. **(A)** Whole brain lysates after fractionation using size exclusion chromatography (SEC). Protein complexes were separated on the basis of their size (in the range of 600–22kDa) and divided into 31 fractions. Dot blots were probed with an anti-ataxin-3 antibody. The signal indicates the distribution of ataxin-3 among the fractions of the protein complexes in Ki21 and Ki150 protein complexes. **(B)** Ponceau-stained vacuum dot blot of protein fractions corresponding to the size range >600–22kDa. **(C)** Based on the dot blot results, we can distinguish 3 peaks; the first (>600kDa), the second (248–192kDa), and the third (115-89kDa). In the third peak (115–89kDa) the level of mutant ataxin-3 in Ki150 brains is significantly lower than in the control Ki21 brain lysates. Two-sample *t*-test (*p <0.05, **p <0.01, ***p <0.001), error bars: SEM total number of biological replicates: n =6, n =3 per genotype.

specific anti-ataxin-3 antibody on magnetic beads to identify the interacting proteins. We aimed to cross-correlate our findings of large molecular complexes and to further characterize the physiological and pathogenic mechanisms behind complex interactions of mutant and normal ataxin-3 in brain tissue. The immunoprecipitation and subsequent proteomic identification and quantitation involved brains from Ki21 knock-in mouse model, and the Ki150 knock-in previously used for SEC and IEC experiment. Artefactual interactors that may bind to dynabeads or antibodies were identified and excluded from the analysis by using immunoprecipitation on brain lysates with dynabeads coupled with mouse control IgG (Supplementary Tables 1, 2).

We identified 394 and 47 ataxin-3 interactors in cerebral cortex and cerebellum, respectively, that were significantly dysregulated in 2-month-old Ki150 vs. Ki21 (p <0.05; two-sample t-test; Supplementary Tables 3, 4). The network of functionally interconnected protein interactors of ataxin-3 was demonstrated by STRING (Figures 6A,C,E; PPI p <10e-16). The diagrams demonstrate relative levels of proteins after their pull-down and subsequent quantification by proteomics in Ki150 vs. Ki21, reflecting the change in protein–protein interactions between mutant vs. normal ataxin-3 (Figures 6B,D,F; p <0.05; two-sample t-test). The identified proteins belong to 3 functional clusters, and they showed considerably weakened or even lack of interaction with mutant ataxin-3 in Ki150

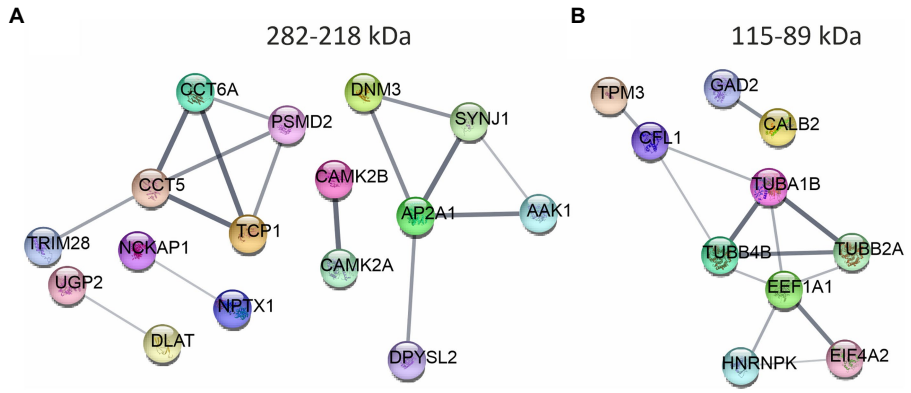

FIGURE 5
The networks of proteins composing complexes with ataxin-3 identified by ion exchange chromatography (IEC) and size using size exclusion chromatography (SEC) followed by LC–MS/MS. The networks were generated using String database and clustering (STRING Network p<10e-16) (https://string-db.org/). **(A)** The fraction 282–218kDa contains highly downregulated Camk2a, CamK2b, proteins belonging to Chaperon Containing TCP1-complex, and proteins being part of the adaptor protein 2 complexes. **(B)** In the fraction 115–89kDa proteins responsible for the translation initiation process: Hnrnpk and Eif4a2 were highly enriched in the Ki150 brains. Proteins characteristic for the GABAergic neurons Gad2, Calb2 and Pcp2 were also altered. N=3.

vs. Ki21 after pull-down. The first protein cluster contained proteins related to translation both in cerebellum (Rbm8a, Rpl39, Eef1a1, Rpl18a, Tpr, Rpl35a, Rps2, Hnrnpd, Rpl19, Eif5a;) and cortex (Eef1a2, Eef1d, Eif4g3, Tsr2, Rpl24, Rps5) (quantification: proteins pull-down and proteomics, $p < 0.05$; two-sample t-test; STRING Network $p <$10e-16; Figures 6A,B). Another two functional clusters were related to mitochondria and their transport in neurons. The mutant ataxin-3 from Ki150 demonstrated very week interactions vs. normal ataxin-3 from Ki21 with mitochondrial proteins in the cerebellum (Cyc1, Ndufa5, and Ndufa8, Figure 6C) and the cerebral cortex (Atp5k, Acly, Cox7c, Cox6b1, mt-Co2, Ndufa10, Ndufa12, Ndufb10, Ndufb4, Ndufs4, Ndufs7, Pdhb, Slc25a11, Hadhb, Vdac3) (quantification: proteins pull-down and proteomics, $p < 0.05$; two-sample t-test; STRING Network $p <$10e-16; Figures 6C,D). The third group are proteins with altered interactions with mutant ataxin-3 vs. normal ataxin-3 which belong to functional set related to transport of mitochondria (Letm1, Sfxn3, Vdac2, Slc25a12, Gdap1, Ywhaq, Ndufa13, Ywhab, Atp5mf, Atp5me, Camk2a, Slc25a4, Slc25a22, Opa1, Csnk2a2, Vps35, Atp5k, Atp5pd, Atp5f1a, Atp5pb, Atp5f1c, Hsp90aa1, Aifm1) (quantification: proteins pull-down and proteomics $p < 0.05$; two-sample t-test; STRING Network $p <$10e-16; Figures 6E,F).

2.7. Transport of mitochondria is slowed in neurites of Ki91 and Ki150 SCA3 cerebellar neurons

Our experiments on the Ki150 and Ki21 demonstrated that using brain tissue selectively expressing human mutant or normal ataxin-3 identifies loss of binding by specific functional sets of protein to the mutant protein. We demonstrated that the presence of mutant ataxin-3 protein results in weakened or loss of interaction with CCT chaperone complexes responsible for transport along neurits, several calcium binding proteins and kinases which were strongly downregulated. The largest group of proteins with affected interaction were mitochondrial proteins and proteins involved in their transport along axons. Therefore, after identification of such a consistent set of proteins, we determined whether the loss of protein interactions in Ki150 mice results in functional impairment of mitochondrial transport in SCA3 neurites. We have selected granule neurons as a neuronal model since our previous finding demonstrated aberrant energy metabolism in these cells (Wiatr et al., 2021). Granule cell culture provides the homogenous population of neurons in culture, equal timeline, length, and way of outgrowth of neurites which prevents variability in the precise tracing of live mitochondria. We quantified the mitochondrial motility in cerebellar neurons containing only mutant ataxin-3 (Figure 7). Primary cerebellar neurons were obtained from either control (C57BL6) mice or SCA3 mice, including Ki91 knock-in with 91 CAGs in the ataxin-3 gene and Ki150 (around 150 CAG repeats). The experiment was conducted using neuronal cultures isolated from brain of three different sets of P2 pups, $N = 3$ per genotype and the neurons were cultured for 7 days prior the experiment. We identified mitochondria in neurons by specific staining with the fluorescent dye MitoTracker® Deep Red (ThermoFisher) and examined their dynamics using live imaging. For the analysis, we included only long, distinct neurites that were clearly extended from a soma and excluded neurites that were discontinued or for which we were not able to identify the soma of origin. Neurons were incubated with MitoTracker® dye (ThermoFisher) for 25 min and imaged every second over 120 s on the heated microscopic stage (37°C).

We found that trafficking of mitochondria was impaired in primary cerebellar neurons from SCA3 mice (Ki91 and Ki150) compared to control. The velocity of mitochondria was calculated by dividing the total distance by the total time of mitochondrial movement during the observation period (Figure 7).

In SCA3 neurites, we observed significantly decreased average velocity of mitochondrial movement in the retrograde direction ($1.17 \pm 0.09\,\mu m\,s^{-1}$, mean ± SEM in Ki91 and $0.89 \pm 0.06\,\mu m\,s^{-1}$, mean ± SEM in Ki150) vs. the WT neurites ($2.06 \pm 0.13\,\mu m\,s^{-1}$, mean ± SEM, $p < 0.0001$) (Figure 7C). Notably, we found that the average velocity of mitochondria in the retrograde direction decreased when the CAG repeat length increased ($1.17 \pm 0.09\,\mu m\,s^{-1}$ – in Ki91

TABLE 1 Proteins depleted in Ki150 fractions 282–218kDa positive for ataxin-3 protein compared to Ki21 control.

Proteins by gene acronim fraction: 282–218kDa	Name	Student's *T*-test *p*-value	Student's *T*-test difference
Camk2b	Calcium/calmodulin-dependent protein kinase type II subunit beta	7.56E-05	−18.724
Camk2a	Calcium/calmodulin-dependent protein kinase type II subunit alpha	0.00030	−18.082
Nckap1	Nck-associated protein 1	0.00605	−11.789
Cct6a	T-complex protein 1 subunit zeta	0.00605	−12.009
Aak1	AP2-associated protein kinase 1	0.01448	−12.912
Nptx1	Neuronal pentraxin-1	0.02229	−9.112
Ap2a1	AP-2 complex subunit alpha-1	0.02229	−9.295
Psmd2	26S proteasome non-ATPase regulatory subunit 2	0.02230	−9.293
Dlat	Dihydrolipoyllysine-residue acetyltransferase component of pyruvate dehydrogenase complex. Mitochondrial	0.02231	−9.755
Tcp1	T-complex protein 1 subunit alpha	0.02233	−9.830
Synj1	Synaptojanin-1	0.02540	−10.568
Ugp2	UTP–glucose-1-phosphate uridylyltransferase	0.04267	−10.681
Cct5	T-complex protein 1 subunit epsilon	0.04395	−9.894
Dnm3	Dynamin-3	0.04742	−10.011
Trim28	Transcription intermediary factor 1-beta	0.04984	−9.135

TABLE 2 Proteins with altered levels in Ki150 fractions 115–89kDa positive for ataxin-3 protein compared to Ki21 control.

Proteins by gene acronim fraction: 115–89kDa	Gene name	Student's *T*-test *p*-value	Student's *T*-test difference
Hnrnpk	Heterogeneous nuclear ribonucleoprotein K	0.03204	9.168
Aldh6a1	Methylmalonate-semialdehyde dehydrogenase [acylating]. mitochondrial	0.0332	−8.259
Gad2	Glutamate decarboxylase 2	0.03325	−7.953
Tpm3	Tropomyosin 3	0.03333	8.944
Pcp2	Purkinje cell protein 2	0.03588	10.322
Calb2	Calbindin 2. isoform CRA_a	0.04949	6.770
Eif4a2	Eukaryotic initiation factor 4A-II	0.04951	6.907
Hp	Haptoglobin	0.04982	7.772

vs. $0.89 \pm 0.06\,\mu m\,s^{-1}$ in Ki150) (Figure 7C). Thus, the retrograde mitochondrial transport along neurites is slowed down in the presence of mutad ataxin-3 and the degree of diminished motility is dependent on the CAG repeat length.

A decrease in the average velocity of anterograde-moving mitochondria was also observed in Ki150 neurites ($0.69 \pm 0.06\,\mu m\,s^{-1}$, mean ± SEM) vs the WT neurons ($1.62 \pm 0.12\,\mu m\,s^{-1}$, mean ± SEM, $p < 0.0001$), but not in Ki91 ($1.38 \pm 0.12\,\mu m\,s^{-1}$, mean ± SEM, $p = 0.16$) (Figure 7B). Consistent with those results, the ratio of the mitochondria moving retrogradely vs. the mitochondria moving anterogradely was significantly decreased only in Ki91 neurites (0.5 ± 0.05, mean ± SEM) as compered to WT neurites (0.66 ± 0.04, mean ± SEM, $p < 0.015$, Figure 7D). Mitochondria not only moved slower in SCA3 neurites, they also were slightly more static as demonstrated by ratio of moving vs. unmoving entities (0.41 ± 0.02, mean ± SEM in Ki91 and $0.41 \pm 0.02\,\mu m\,s^{-1}$, mean ± SEM in Ki150 compared to 0.47 ± 0.02, mean ± SEM in WT $p < 0.05$, Figure 7E).

The impairment of mitochondrial trafficking in SCA3 neurites was not accompanied by any significant changes regarding the number, shape, or size of the mitochondria in primary cerebellar SCA3 neurons (Figures 7F–I). We did not detect any differences in the number of mitochondria normalized to the length of the measured neurite (*t*-test, $p < 0.05$; Figure 7G). There was also no change in the mitochondrial shape, which is related to fusion/fission events and which was calculated by dividing the width and height of each mitochondrion (*t*-test, $p < 0.05$; Figure 7H). Distribution of the mitochondria size was similar across all tested groups (*t*-test, $p < 0.05$; Figure 7I).

3. Discussion

The proteins containing long polyQ tracts are often pleiotropic and may either acquire new or lose the functions of the original protein. Ataxin-3 and its mutant counterpart is a particularly

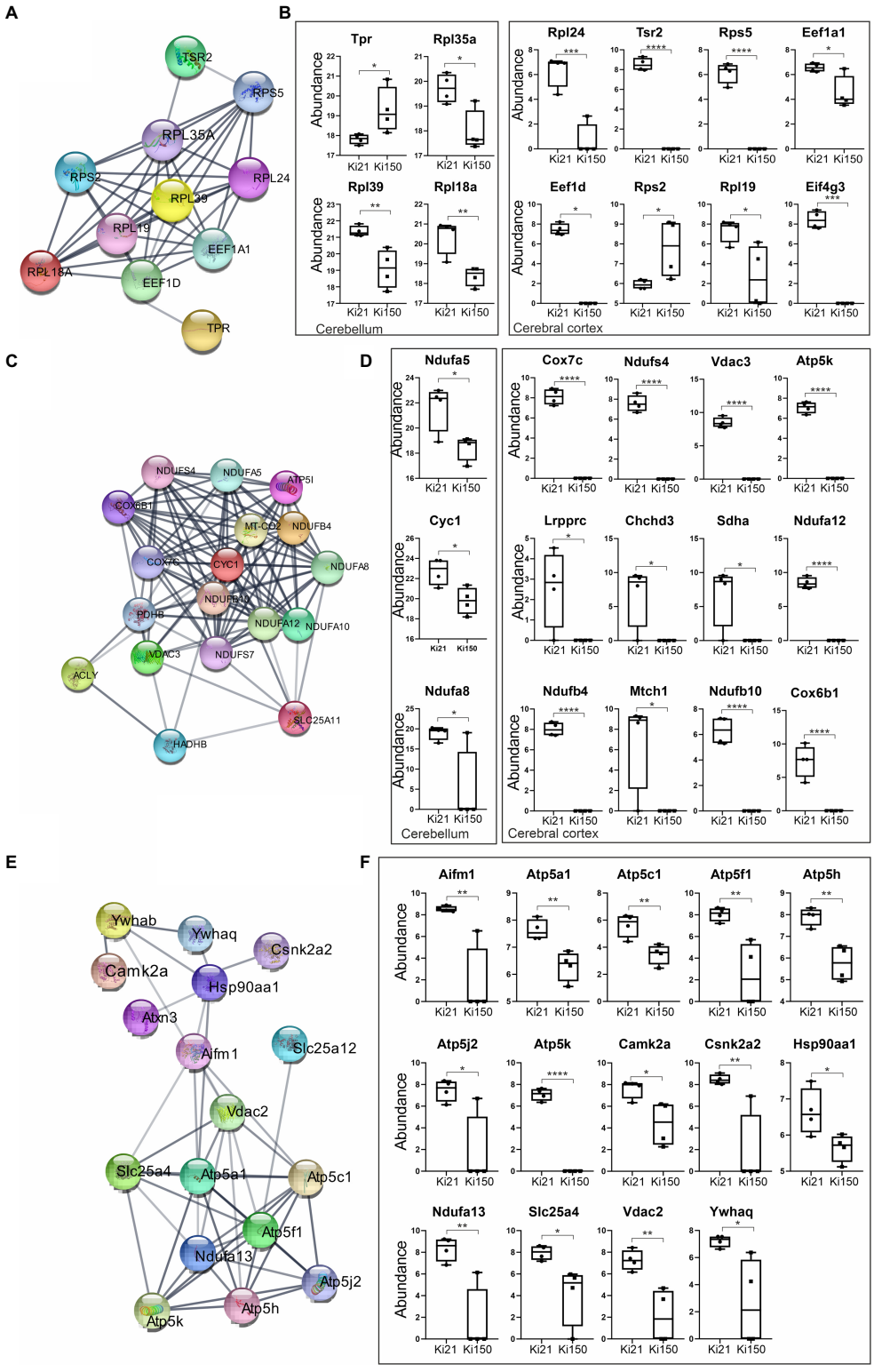

FIGURE 6
IP-LC–MS/MS proteomic analysis of ataxin-3 partners reveals 3 sets of proteins with significantly weakened interaction with the mutant ataxin-3 in the Ki150 SCA3/MJD cerebellum and cortex. The network of proteins displaying weakened interaction with the ataxin-3 containing expanded polyQ tract in the cerebellum **(A,C)** and cerebral cortex **(A,C,E)** of Ki50 mice were generated using String database and clustering (STRING Network p<10e-16) (https://string-db.org/). Diagrams demonstrate relative levels of proteins after their pull-down and proteomic analysis (Ki150 vs. Ki21) reflecting the change or even complete loss of protein interaction with mutant vs. normal ataxin-3 in the cerebellum and cerebral cortex (**B,D,F**; p<0.05; two-sample t-test). **(A,B)** The first cluster contained proteins related to the translation in the cerebellum and cerebral cortex. **(C,D)** The mutant ataxin-3 demonstrated very weak interactions with mitochondrial proteins (second cluster) in the Ki150 cerebellum and Ki150 cerebral cortex. **(E,F)** The third set of proteins with diminished interaction with mutant ataxin-3 (150 CAG repeats) in the cerebral cortex is involved in mitochondrial transport. Two-sample t-test ($p \leq 0.05$; *p<0.05, **p<0.01, ***p<0.001); total number of biological replicates: n=8, n=4 per genotype; error bars: SEM.

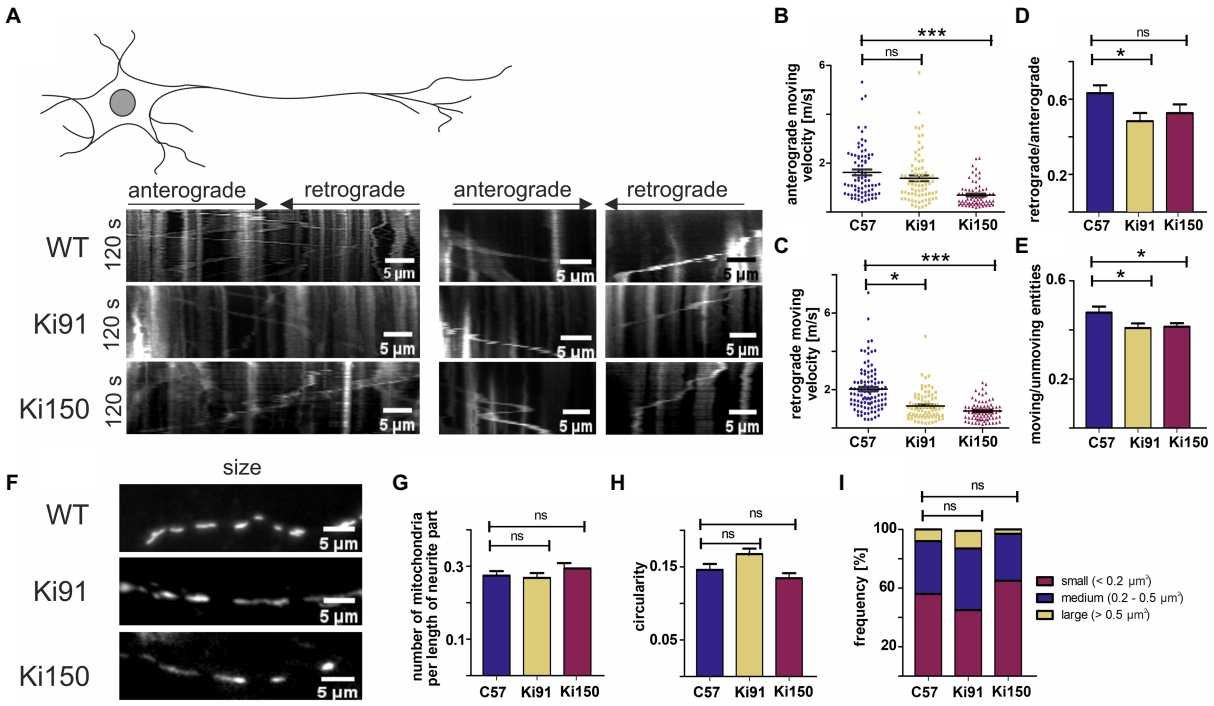

FIGURE 7
Transport of mitochondria is slower in neurites of SCA3 cerebellar neurons *in vitro*. **(A)** Representative kymographs of mitochondrial transport in primary cerebellar neurons and pictures of mitochondria size. **(B)** The average velocity (calculated as travelling distance/time) in the anterograde direction (from soma) was significantly lower in Ki150 neurites in comparison to WT. **(C)** The average velocity (calculated as travelling distance/time) in the retrograde direction (toward soma) was significantly lower in both Ki91 and Ki150 neurites in comparison to WT. **(D)** The ratio of mitochondria moving retrogradely to mitochondria moving anterogradely is lower in Ki91 neurites compared to WT. **(E)** The number of moving mitochondria is significantly lower in both Ki91 and Ki150 neurites as compared to WT. **(F)** The number of mitochondria per neurite length was not changed. **(G)** The circularity of mitochondria indicating fusion/fission events is not altered. **(H)** The average area of mitochondria is approximately the same in all tested groups. **(I)** The size distribution of mitochondria in Ki91 and Ki 150 cerebellar neurons is comparable to WT. All parameters were quantified using ImageJ. The measurements were from 3 independent experiments, with 15–25 cells analyzed each time. Two-sample *t*-test (**p*<0.05, ***p*<0.01, ****p*<0.001), error bars: SEM.

explicit example of a protease and deubiquitinase involved in nearly all cellular processes associated with protein degradation. Such pleiotropy is reflected by broad influence of mutant ataxin-3 on proteome and phosphoproteome (Wiatr et al., 2019, 2021). Therefore, it is very difficult to pinpoint a network of key pathogenic mechanism and to find the cure. Moreover the mouse models offered in the polyQ research are always compromised in their features such as lack of robust combination of preclinical, motor, molecular and neuropathological properties. For instance, the mild or moderate motor and molecular phenotype, accuracy of genetic constructs, full length human allele, and the concomitant presence of mouse allele are always compromised (Cemal et al., 2002; Switonski et al., 2015; Haas et al., 2022). The ideal model would have a quick phenotype for preclinical tests, have an entire human protein, uninterrupted CAG tract in mRNA and expansion phenotype. We previously generated Ki91 SCA3 mouse model (Wiatr et al., 2019, 2021), and slightly increased the CAG repeat count (110–120) resulting in the model that has demonstrated many prominent SCA3 alterations. However, for conducting swift preclinical testing, an additional and more severe SCA3 model with aggravated phenotype is in demand. Therefore using the Ki91 model, its expansion feature and the selective breeding, we obtained the Ki150 SCA3 model displaying a long CAG (150–170) tract in the humanized *ATXN3* gene and more severe phenotype. The Ki150 mice present deteriorated motor phenotype already at the age of 4 weeks and formation of early ataxin-3 inclusions in various brain tissues, which are large and dense. The neuropathology in Ki150 and the solid inclusions are compatible to investigate the mutant ataxin-3 pleiotropy, and the extensive presence of various protein complexes and aggregates. Considering that the binding of mutant ataxin-3 with long polyQ tract to different proteins may be intensified we aimed at identifying protein–protein interactions of normal and mutant ataxin-3. This would provide valuable information on proteome changes in the brain and the resulting pathogenic protein network of SCA3 which could later be connected to affected neuronal function. The protein partners of ataxin-3 identified so far came from several studies performed mostly in artificial overexpression system *in vitro* or non-mammalian animal models (Mazzucchelli et al., 2009; Sowa et al., 2009; Kristensen et al., 2018; Weishäupl et al., 2019; Antonicka et al., 2020). We determined ataxin-3 protein interactions in an *in vivo* pathogenic system consisting of Ki150/150 (mutant human ataxin-3) and Ki21/21 (normal human ataxin-3).

In order to find proteome differences in the Ki21 vs. Ki150 models, we performed orthogonal IEC/SEC fractionation of Ki21 and Ki150 brain lysates. Protein complexes associated with mutant ataxin-3 were generally identified in heavier fractions compared to

ataxin-3 with normal polyglutamine tract suggesting an intensive impact of mutant protein on the increased formation of protein–protein complexes. We subjected the samples to mass-spec analysis to identify the protein composition of fractions enriched in ataxin-3. We discovered highly deregulated proteins in protein fractions belonging to molecular chaperone CCT/TRiC complex which is the key regulator of protein aggregation of polyQ proteins (Darrow et al., 2015; Grantham, 2020). Downregulation of the TCP1 complex is linked to be common in neurodegenerative disorders such as Alzheimer's, and Huntington disease. The autophagic flux is reduced by compromise of individual CCT subunits, effect of loss-of-CCT activity on aggregation is primarily a consequence of autophagy inhibition (Pavel et al., 2016). Moreover, our results suggest that ataxin-3 shows a tendency to interact with subunits of protein complexes of a circular structure, such as CCT, proteasome and Camk2 subunits (Supplementary Figure 3). A disrupted interaction of mutant ataxin-3 with subunits of complexes of circular structure might lead to increase in formation of self ataxin-3 annular aggregates, which enables the transition to more toxic fibrillar aggregates and their precipitation in the form of inclusions. It must be noted that, e.g., Camk2a *in vivo* forms homo-12-mers of >600 kDa. This suggests that the extension of the polyQ tract in ataxin-3 affects protein oligomerization resulting from either incomplete folding or degradation. The same applies to the aforementioned chaperones and proteasome, whose fully-functional oligomers cannot appear in the 282–218 kDa fractions.

As a complementary and more direct approach, we aimed to identify any loss or gain of protein interaction of mutant ataxin-3 (150 CAG repeats) by performing co-immunoprecipitation in two representative brain regions: the cerebellum and cerebellar cortex which we previously demonstrated to be relevant for SCA3 (Wiatr et al., 2019, 2021). We found that many protein interactions are lost due to the presence of extended polyQ tract in the ataxin-3. The top result identified by two different strategies both in cerebellum and cerebral cortex was Calcium/Calmodulin Dependent Protein Kinase II alpha and beta (Camk2a and b), which plays a pivotal role in mitochondrial transport in axons (Woolums et al., 2020). Moreover, we identified impaired interactions of proteins involved in mitochondrial function, mitochondrial transport, translation, proteasome, and cytoskeleton.

We focused on the functional consequences of the altered protein interactions with ataxin-3 for the mitochondrial transport in neurons. The impairment of mitochondrial transport would correspond well with our previous findings, including impaired energy metabolism and mitochondrial parameters in SCA3 mouse primary cerebellar neurons, a number of dysregulated mitochondrial proteins in SCA3 cerebellum, and mislocalization of mitochondrial proteins in SCA3 axon (Wiatr et al., 2021). Moreover, an enhanced interaction of several mitochondrial proteins with mutant ataxin-3 have been demonstrated in an overexpression cellular model (Kristensen et al., 2018).

To clarify whether motility of mitochondria is disturbed in SCA3 cerebellar neurites, we conducted a quantitative analysis of the mitochondrial transport in cultured primary cerebellar neurons established from Ki91 and Ki150 knock-in mouse models. For the first time, we demonstrate in a direct manner that the transport of mitochondria is disturbed in SCA3 cerebellar neurites. Due to the complex and elongated structure of a neuron, perpetual delivery of cellular components between cell body and neuronal projections pose a unique challenge. Mitochondria are one of the crucial organelles for neuronal function that need to be replenish efficiently, since they are exposed to damaging influence of reactive oxygen species and age over time (Nicholls, 2004; Balaban et al., 2005; Tao et al., 2014). Mitochondria are produced primarily in the cell body and are delivered *via* microtubule-based transport to the neuronal projections (Davis and Clayton, 1996; Schwarz, 2013; Misgeld and Schwarz, 2017). Impairment of axonal mitochondrial transport ultimately results in the insufficient local energy demand and axon degeneration (Sheng and Cai, 2012). Indeed, defects in mitochondrial transport are associated with a number of neurodegenerative diseases, including Alzheimer's, Huntington's, and Parkinson's disease, ALS, Charcot–Marie-Tooth (Piccioni et al., 2002; Sheng and Cai, 2012, p. 2; Shirendeb et al., 2012; Itoh et al., 2013; Kalmar et al., 2017; Stykel et al., 2018; Otomo et al., 2022). Moreover, mitochondrial impairment likely plays a role in SCA3 pathogenesis (Da Silva et al., 2019).

Here, we hypothesize that the loss of interaction of ataxin-3 with two protein complexes of a circular structure, namely CaMKII and CCT (chaperonin containing TCP-1)/TCP-1/TRiC is disturbing mitochondrial transport in SCA3 neurites. CaMKII is a key regulator of calcium signaling which is pivotal in the regulation of axonal transport of mitochondria (Breuer and Atkinson, 1988; Saotome et al., 2008; Wang and Schwarz, 2009, p. 2; Brault et al., 2019). CaMKII controls mitochondrial translocation in smooth muscle and imbalance of CaMKII-dependent Ca^{2+} entry lead to disruption of mitochondrial axon transport and ultimately axonal degeneration (Woolums et al., 2020, p. 4) (Nguyen et al., 2018). In line with our hypothesis, the activity of the CaMKII is likely affected by the presence of mutant ataxin-3, as we have previously shown decreased phosphorylation of its many protein target sites and the CaMKII protein level dysregulation in SCA3 mouse brain (Wiatr et al., 2019). Of note, intracellular Ca^{2+} levels are also modulated by the presence of mutant ataxin-3 (Pellistri et al., 2013).

In addition, CCT (chaperonin containing TCP-1)/TCP-1/TRiC subunits enhance retrograde axonal transport by modulating tau phosphorylation of the AT8 phospho-epitope (Ser199, Ser202, Thr205) (Zhao et al., 2016). The AT8 epitope is crucial in regulating mitochondrial movement as its replacement with phosphomimetic aspartates lead to inhibition of mitochondria transport in the neurites of PC12 cells (Shahpasand et al., 2012). Tau hyperphosphorylation was also shown to be linked with reduced number of mitochondria in cortical axons (Rodríguez-Martín et al., 2016). Therefore, dysregulation of CCT/TCP-1/TRiC complex subunits resulting from compromised interaction with mutant ataxin-3 might have a direct impact on mitochondrial transport in axons. In addition to disrupted interaction of mutant ataxin-3 with CaMKII and CCT/TCP-1/TRiC, the presence of ataxin-3 inclusions which we previously shown in cereberal axons could also perturb mechanisms of axonal transport (Wiatr et al., 2021, p. 21).

In conclusion, to understand the SCA3 neuropathomechanism in our model we investigated the functional consequences of the expansion of CAG tract to over 150 repeats by discovering ataxin-3 mutant protein interactions and their influence on cellular structures. Guided by specific sets of identified protein interactors we investigated live mitochondrial motility in Ki150 neurites. Based on our study

we demonstrate a preclinical grade SCA3 knock-in model with intense neuropathology, leading to altered interactions and live organelle transport impairment in neurites.

4. Materials and methods

4.1. Animals

Maintaining and breeding were performed at standard conditions with an 18/6-h light/dark cycle and water and food *ad libitum*. The animals were marked using numerical ear tags (National Band & Tag Company, Newport, USA). The stress level of the animals was minimized throughout all procedures and animal handling. The animal experimentation and handling were approved and monitored by the Local Ethical Commission for Animal Experiments in Poznan. The animals were sacrificed according to AVMA Guidelines for the Euthanasia of Animals by placing them in the programmable CO2 chamber (Rothacher Medical, Heitenried, Switzerland). SCA3 Ki91 and Ki150 mice (C57BL/6 background) and age-matched C57 and Ki21 controls were used for co-immunoprecipitations. The cerebellum and cerebral cortex for proteomic analysis were collected from 2 month-old animals.

4.2. Western blot analysis

Samples were harvested from mouse brain regions and homogenized in the buffer containing 60 mM TRIS-base, 2% SDS, 10% sucrose, and 2 mM PMSF, followed by bath sonication. The protein concentration was estimated using a Pierce BCA protein assay kit (Thermo Scientific, Rockford, IL, USA). For each analysis, 25 µg of total protein was diluted in a loading buffer containing 2-mercaptoethanol and boiled for 5 min. The proteins were separated by SDS–polyacrylamide gel electrophoresis (5% stacking/ 10% resolving gel), transferred to nitrocellulose, and stained with Ponceau S solution. The blots were blocked with 5% non-fat milk in PBS/0.05% Tween 20 for 1 h at RT and, subsequently, incubated for 24 h at 4°C with the following primary antibodies: anti-ataxin-3 (1:2000; ProteinTech, Rosemont, IL, USA) and LaminB (1:2000; ProteinTech, Rosemont, IL, USA). The blots were probed with the respective HRP-conjugated secondary antibody (anti-rabbit or anti-mouse, 1:2000; Jackson ImmunoResearch, Suffolk, UK). The immunoreaction was detected using the ECL substrate (ThermoFisher Scientific, Waltham, MA, USA).

4.3. Immunofluorescence staining

The animals were deeply anesthetized and transcardially perfused using saline, followed by 4% PFA. The brains were removed, post-fixed in 4% PFA for 48 h, and cryopreserved with graded sucrose (10–20–30%) over 72 h. The 20-µm parasagittal mouse brain sections were cut using a cryostat at −20°C and collected on SuperFrost Plus slides (Thermo Fisher Scientific, Waltham, MA, United States). The sections were processed immediately. The HIER procedure was applied by incubation of the sections in citrate buffer (pH 9.0) for 30 min at 60°C. The sections were blocked *via* incubation in 4% normal goat serum in TBS for 1 h. For immunofluorescent staining, the sections were incubated overnight at 4°C, rabbit anti-ataxin-3 (1:200; ProteinTech, Rosemont, IL, United States), and subsequently with the anti-rabbit antibody labeled by AlexaFluor488, or AlexaFluor647 (1:400; Jackson ImmunoResearch; Suffolk, United Kingdom). The sections were end-stained with Hoechst 33342 (Sigma) nuclear stain at 1:1,000 and embedded in Fluoroshield (Sigma) mounting medium. For aggregates quantification Aggrecount v1.3 software was used and the applied parameters are available in Supplementary File 1. As an input file, we used 3 individual images of the same size per biological replicate $n = 4$. In the setup file, the parameter "Mean" (Mean fluorescent intensity from a cell ROI) was used for aggregate intensity and "aggregates" value denoted a total number of aggregates.

4.4. Co-immunoprecipitation

Sacrificed animals were decapitated, afterward, the cerebral cortex and cerebellum were dissected from the brain and snap freeze in liquid nitrogen and then stored at-80 ° C. A direct immunoprecipitation approach was performed with the primary mouse anti-ataxin-3 antibody 1H9, or negative control IgG (AC011; Santa Cruz Biotechnology, sc2025) and Dynabeads™ Co-Immunoprecipitation Kit (14321D, Thermo Fisher Scientific). To antibody coupling used 6 µg/mg beads, antibody coupling was performed according to the manufacturer's protocol. Briefly, Dynabeads were washed in C1 buffer then incubated overnight in C1, C2, and antibodies at 37 ° C. On the next day, antibodies coupled to the beads were washed in HB, LB, and SB buffers. After washing beads were stored until use in the SB buffer in the fridge. The lysis buffer from the kit was modified with 100 mM NaCl, 2 mM MgCl2, 1 mM DTT, and 40 µM PMSF. The rest procedure was performed according to the manufacturer's instructions, beads were incubated with the lysates for 30 min. at 4°C, to elute the protein complexes HPH EB (0.5 M NH4OH, 0.5 mM EDTA) was used. After elution samples were lyophilized in a speed vac overnight. Then the samples were directly digested for the mass spectrometry.

4.5. Protein purification

Whole brains from Ki21 and Ki150 mice were collected and snap froze in liquid nitrogen. Afterward, brains were homogenized using stainless steel beads in Allshend Bioprep-6 homogenizer in PBS EDTA 5 mM buffer supplemented with Halt™ Protease Inhibitor Cocktail (Thermo Fisher Scientific). Samples were homogenized 2× 30s 3,5 k RPM, between homogenization rounds samples, were placed on ice. After homogenization samples were centrifuged to collect supernatants. The clear supernatants were applied onto an ion-change CM-cellulose resin (negatively charged), next the flowthrough was applied onto DEAE-cellulose resin (positively charged) and the flowthrough was collected. The collected flow-through was concentrated to ∼2.5 ml and applied on size exclusion HiLoad Superdex 200 16/60 column (GE Healthcare) connected to the AKTA FPLC system (Amersham Biosciences). The size exclusion chromatography was run as the final step of purification in a buffer composed of PBS EDTA 50 uM, to yield 2 ml in each protein fraction.

4.6. Vacuum dot immunoblot

The nitrocellulose membrane and Whatman filters (all GE Healthcare, Chicago, Il, USA) were washed 2X with Milli-Q H20 and 2X with Tris-Buffered Saline (TBS) by vacuum filtration. 450uL of each fraction sample was spotted on nitrocellulose membrane and washed 2X with TBS by vacuum filtration, and then allowed to air-dry. The blots were stained with Ponceau S solution and blocked with 5% nonfat milk in PBS/0.05% Tween 20 for 1 h at RT and subsequently incubated at 4°C overnight with the following primary antibodies: anti-ataxin-3 (1:2000; ProteinTech, Rosemont, IL, USA) and LaminB (1:2000; ProteinTech, Rosemont, IL, USA). The blots were probed with the respective HRP-conjugated secondary antibody (anti-rabbit or anti-mouse, 1:2000; Jackson Immuno Research, Suffolk, UK). The immunoreaction was detected using the ECL substrate (Thermo Fisher Scientific, Waltham, MA, USA). Data was collected using ChemiDoc XRS+ System with Image Lab v5.2 Software (Bio-Rad). To avoid overexposure of any band or dots, image acquisition times were set based on image histograms. Images were not processed before quantitation. Data within a membrane were normalized to total protein (Ki21 vs. Ki150).

4.7. Mass spectrometry

The lyophilized samples were dissolved in 100 mM sodium bicarbonate, and then 5ug protein from each sample was taken to further processing. Volume containing 5ug protein was reduced in DTT for 5 min at 95°, then placed on ice, and then acylated in IAA for 20 min in dark at room temperature, afterward samples were digested by trypsin overnight at 37°C in a water bath. The analysis of the proteome was performed with the use of the Dionex UltiMate 3,000 RSLC nanoLC system connected to the Q Exactive Orbitrap mass spectrometer (Thermo Fisher Scientific, Waltham, MA, USA). Peptides derived from in-solution digestion were separated on a reverse-phase Acclaim PepMap RSLC nanoViper C18 column (75 µm × 25 cm, 2 µm granulation) using acetonitrile gradient (from 4 to 60%, in 0.1% formic acid) at 30°C and a flow rate of 300 nL/min (for 230 min). The spectrometer was operated in data-dependent MS/MS mode with survey scans acquired at a resolution of 70,000 at m/z 200 in MS mode, and 17,500 at m/z 200 in MS2 mode. Spectra were recorded in the scanning range of 300–2000 m/z in the positive ion mode. Higher energy collisional dissociation (HCD) ion fragmentation was performed with normalized collision energies set to 25. Swiss-Prot mouse database was used for protein identification with a precision tolerance set to 10 ppm for peptide masses and 0.08 Da for fragment ion masses. Raw data obtained for each dataset were processed by MaxQuant 1.5.3.30 version for protein identification and quantification. Protein was considered as successfully identified if the Andromeda search engine found at least two peptides per protein, and a peptide score reached the significance threshold FDR = 0.01.

4.8. Live imaging of mitochondrial transport

Primary neurons were obtained from P2 pups and cultured as previously described (Wiatr et al., 2021). Briefly, primary neuron cultures were derived from Ki150, Ki91 and C57 mice according to AVMA Guidelines for the Euthanasia of Animals. Followed by trypsin digestion, cells were washed in HBSS (Thermo Fisher Scientific, Waltham, MA, United States) with 1× penicillin–streptomycin (Thermo Fisher Scientific, Waltham, MA, United States), and then in a plating medium (Dulbecco's modified Eagle medium, 1× CTS GlutaMAX-I supplement, 1× penicillin–streptomycin (all Thermo Fisher Scientific, Waltham, MA, United States)). Clumps of tissue debris were allowed to settle down in a tube, and the supernatant containing dissociated cells was centrifuged for 3 min at 1,300 rpm. Cells were seeded onto poly-D-lysine (Thermo Fisher Scientific, Waltham, MA, United States) covered plates. Neurons were maintained in conditioned Neurobasal medium (Thermo Fisher Scientific, Waltham, MA, United States) supplemented with 2% B27 supplement, 1× CTS GlutaMAX-I supplement, 1× penicillin–streptomycin (all Thermo Fisher Scientific, Waltham, MA, United States), 1× apo-transferrin (Sigma-Aldrich, St. Louis, MO, United States), and N2 (0.005 mg/ml insulin, 0.0161 mg/ml putrescin, 30 nM Na-Selenite, 51 nM T3, 20 nM progesterone) in a humidified incubator with 5% O2 and 5% CO2 in air at 37°C. The maintenance medium was replenished with half-feed changes every 2–3 days.

To track mitochondria movement cerebellar neurons at DIV7 were incubated with 30 nM of MitoTracker® Deep Red (ThermoFisher) at 37°C for 25 min before imaging. Cells were then quickly rinsed with PBS and imaged to track mitochondrial trafficking. The series of time-lapsed images were captured at 1.0 frame/2 s for 2 min. The images were taken under a 63X objective using Opera LX (PerkinElmer) spinning disc microscope with a heated (37°C), 5% CO2-controlled stage. To analyze and quantify the movement of the mitochondria kymographs were generated with the open-source image-processing package Fiji/ImageJ. First, the "rectangular selection" function was used to choose the neurite region to be analyzed. Next, the "reslice" function was used to compress each cropped image to one line. Then, the "z-projection" function was used to compile all time-lapse image converted lines into one single picture. In each kymograph, the x-axis represents mitochondrial displacement, and the y-axis represents time. Vertical lines indicate stationary mitochondria while diagonal lines are moving mitochondria (Course et al., 2017). To asses if there were any alterations in mitochondria morphology, the area, width and height of individual organelles were measured. Lastly, the number of mitochondria normalized to the length of the measured neurite was calculated. The analysis was performed in 3 independent experiments, N = 3 per genotype. All statistical analyses were performed using the Student's *t*-test and are presented as mean ± SEM.

4.9. Statistical analysis

The data obtained in behavioral tests were subjected to a two-way ANOVA, followed by Bonferroni post-tests. value of *p*s of less than 0.05 were considered significant. Identification of proteins on raw proteomic data was performed by the Andromeda search engine in Mascot using the following inclusion criteria: at least two different peptides per protein were identified per sample, and a total peptide score reached the significance threshold FDR = 0.01. Identified proteins matching the inclusion criteria were subjected to further

statistical analysis with a two-sample *t*-test, and dysregulation of protein level reaching value of $p < 0.05$ was considered as significant.

Author's note

Imaging was performed using the facilities of the High-throughput Screening Laboratory (IBCh, PAS, Poland). Proteomic mass spectrometry analyses were performed in the Laboratory of Mass Spectrometry and the library synthesis was performed in the Laboratory of Genomics (European Centre for Bioinformatics and Genomics; ECBiG; IBCH, PAS, Poznań, Poland). Primary neuron cultures were maintained in the Cell and Tissue Culture Laboratory (IBCh, PAS, Poland).

Data availability statement

The original contributions presented in the study are included in the article/Supplementary material, further inquiries can be directed to the corresponding author.

Ethics statement

The animal study was reviewed and approved by Local Ethical Commission for Animal Experiments in Poznań.

Author contributions

PP and KW performed live animal behavioral experiments. KW performed live-imaging experiments in neurons and data analysis. PP and ŁM performed all proteomic experiments and analysis of proteomic data. PP and MR performed chromatography experiments. YT provided anti-Ataxin-3 1H9 antibody and revised the manuscript. MF, PP, KW, and MR wrote the manuscript. MF conceived, supervised all experiments, analyzed the data and was responsible for research concept and obtaining funding. All authors contributed to the article and approved the submitted version.

Funding

This work was supported by European Research Projects on Rare Diseases (JTC 2017), National Center for Research and Development, Poland [Grant Numbers: ERA-NET-E-RARE-3/III/TreatPolyQ/08/2018 (to MF and YT)], National Science Centre, Poland (OPUS grant: 2021/41/B/NZ2/03881 to MF; ETIUDA grant: 2019/32/T/NZ3/00504 to KW), and a Grant of National Ataxia Foundation: Pioneer SCA3/MJD Translational Research Award #688790 (to MF and YT).

Acknowledgments

We thank Adam Plewinski for his help in maintaining the colonies of mice. We also thank Chengbiao Wu for live-imaging training during KW scholarship at UCSD.

Conflict of interest

The authors declare that the research was conducted in the absence of any commercial or financial relationships that could be construed as a potential conflict of interest.

Publisher's note

Supplementary material

The Supplementary material for this article can be found online at: https://www.frontiersin.org/articles/10.3389/fnmol.2023.1122308/full#supplementary-material

References

Antonicka, H., Lin, Z.-Y., Janer, A., Aaltonen, M. J., Weraarpachai, W., Gingras, A.-C., et al. (2020). A high-density human mitochondrial proximity interaction network. *Cell Metab.* 32, 479–497.e9. doi: 10.1016/j.cmet.2020.07.017

Balaban, R. S., Nemoto, S., and Finkel, T. (2005). Mitochondria, oxidants, and aging. *Cells* 120, 483–495. doi: 10.1016/j.cell.2005.02.001

Bettencourt, C., and Lima, M. (2011). Machado-Joseph disease: from first descriptions to new perspectives. *Orphanet J. Rare Dis.* 6:35. doi: 10.1186/1750-1172-6-35

Brault, M. L., Petit, J. D., Immel, F., Nicolas, W. J., Glavier, M., Brocard, L., et al. (2019). Multiple C2 domains and transmembrane region proteins (MCTPs) tether membranes at plasmodesmata. *EMBO Rep.* 20:e47182. doi: 10.15252/embr.201847182

Breuer, A. C., and Atkinson, M. B. (1988). Calcium dependent modulation of fast axonal transport. *Cell Calcium* 9, 293–301. doi: 10.1016/0143-4160(88)90010-3

Burnett, B. G., and Pittman, R. N. (2005). The polyglutamine neurodegenerative protein ataxin 3 regulates aggresome formation. *Proc. Natl. Acad. Sci. U. S. A.* 102, 4330–4335. doi: 10.1073/pnas.0407252102

Carvalho, A. L., Silva, A., and Macedo-Ribeiro, S. (2018). "Polyglutamine-independent features in Ataxin-3 aggregation and pathogenesis of Machado-Joseph disease," in *Polyglutamine Disorders Advances in Experimental Medicine And Biology*., eds. C. Nóbrega and L. Pereira de Almeida Cham: Springer International Publishing, 275–288.

Cemal, C. K., Carroll, C. J., Lawrence, L., Lowrie, M. B., Ruddle, P., Al-Mahdawi, S., et al. (2002). YAC transgenic mice carrying pathological alleles of the MJD1 locus exhibit a mild and slowly progressive cerebellar deficit. *Hum. Mol. Genet.* 11, 1075–1094. doi: 10.1093/hmg/11.9.1075

Course, M. M., Hsieh, C.-H., Tsai, P.-I., Codding-Bui, J. A., Shaltouki, A., and Wang, X. (2017). "Live imaging mitochondrial transport in neurons," in *Techniques to Investigate Mitochondrial Function in Neurons Neuromethods*., eds. S. Strack and Y. M. Usachev New York, NY: Springer, 49–66.

Da Silva, J. D., Teixeira-Castro, A., and Maciel, P. (2019). From pathogenesis to novel therapeutics for Spinocerebellar ataxia type 3: evading potholes on the way to translation. *Neurotherapeutics* 16, 1009–1031. doi: 10.1007/s13311-019-00798-1

Darrow, M. C., Sergeeva, O. A., Isas, J. M., Galaz-Montoya, J. G., King, J. A., Langen, R., et al. (2015). Structural mechanisms of mutant Huntingtin aggregation suppression by the synthetic Chaperonin-like CCT5 complex explained by Cryoelectron tomography*. *J. Biol. Chem.* 290, 17451–17461. doi: 10.1074/jbc.M115.655373

Davis, A. F., and Clayton, D. A. (1996). In situ localization of mitochondrial DNA replication in intact mammalian cells. *J. Cell Biol.* 135, 883–893. doi: 10.1083/jcb.135.4.883

Grantham, J. (2020). The molecular chaperone CCT/TRiC: an essential component of proteostasis and a potential modulator of protein aggregation. *Front. Genet.* 11:172. doi: 10.3389/fgene.2020.00172

Grasty, K. C., Weeks, S. D., and Loll, P. J. (2019). Structural insights into the activity and regulation of human Josephin-2. *J. Struct. Biol.* 3:100011. doi: 10.1016/j.yjsbx.2019.100011

Haas, E., Incebacak, R. D., Hentrich, T., Huridou, C., Schmidt, T., Casadei, N., et al. (2022). A novel SCA3 Knock-in mouse model mimics the human SCA3 disease phenotype including neuropathological, behavioral, and transcriptional abnormalities especially in oligodendrocytes. *Mol. Neurobiol.* 59, 495–522. doi: 10.1007/s12035-021-02610-8

Herzog, L. K., Kevei, É., Marchante, R., Böttcher, C., Bindesbøll, C., Lystad, A. H., et al. (2020). The Machado-Joseph disease deubiquitylase ataxin-3 interacts with LC3C/GABARAP and promotes autophagy. *Aging Cell* 19:e13051. doi: 10.1111/acel.13051

Itoh, K., Nakamura, K., Iijima, M., and Sesaki, H. (2013). Mitochondrial dynamics in neurodegeneration. *Trends Cell Biol.* 23, 64–71. doi: 10.1016/j.tcb.2012.10.006

Kalmar, B., Innes, A., Wanisch, K., Kolaszynska, A. K., Pandraud, A., Kelly, G., et al. (2017). Mitochondrial deficits and abnormal mitochondrial retrograde axonal transport play a role in the pathogenesis of mutant Hsp27-induced Charcot Marie Tooth Disease. *Hum. Mol. Genet.* 26, 3313–3326. doi: 10.1093/hmg/ddx216

Klickstein, J. A., Mukkavalli, S., and Raman, M. (2020). AggreCount: an unbiased image analysis tool for identifying and quantifying cellular aggregates in a spatially defined manner. *J. Biol. Chem.* 295, 17672–17683. doi: 10.1074/jbc.RA120.015398

Koeppen, A. H. (2018). "The neuropathology of spinocerebellar ataxia type 3/Machado-Joseph disease," in *Polyglutamine Disorders Advances in Experimental Medicine and Biology*., eds. C. Nóbrega and L. Pereira de Almeida Cham: Springer International Publishing, 233–241.

Kristensen, L. V., Oppermann, F. S., Rauen, M. J., Fog, K., Schmidt, T., Schmidt, J., et al. (2018). Mass spectrometry analyses of normal and polyglutamine expanded ataxin-3 reveal novel interaction partners involved in mitochondrial function. *Neurochem. Int.* 112, 5–17. doi: 10.1016/j.neuint.2017.10.013

Leotti, V. B., de Vries, J. J., Oliveira, C. M., de Mattos, E. P., Te Meerman, G. J., Brunt, E. R., et al. (2021). CAG repeat size influences the progression rate of Spinocerebellar ataxia type 3. *Ann. Neurol.* 89, 66–73. doi: 10.1002/ana.25919

Lima, M., and Raposo, M. (2018). "Towards the identification of molecular biomarkers of spinocerebellar ataxia type 3 (SCA3)/Machado-Joseph disease (MJD)," in *Polyglutamine Disorders Advances in Experimental Medicine and Biology*., eds. C. Nóbrega and L. Pereira de Almeida Cham: Springer International Publishing, 309–319.

Maciel, P., Gaspar, C., DeStefano, A. L., Silveira, I., Coutinho, P., Radvany, J., et al. (1995). Correlation between CAG repeat length and clinical features in Machado-Joseph disease. *Am. J. Hum. Genet.* 57, 54–61.

Mazzucchelli, S., De Palma, A., Riva, M., D'Urzo, A., Pozzi, C., Pastori, V., et al. (2009). Proteomic and biochemical analyses unveil tight interaction of ataxin-3 with tubulin. *Int. J. Biochem. Cell Biol.* 41, 2485–2492. doi: 10.1016/j.biocel.2009.08.003

McLoughlin, H. S., Moore, L. R., and Paulson, H. L. (2020). Pathogenesis of SCA3 and implications for other polyglutamine diseases. *Neurobiology of Disease* 134:104635. doi: 10.1016/j.nbd.2019.104635

Misgeld, T., and Schwarz, T. L. (2017). Mitostasis in neurons: maintaining mitochondria in an extended cellular architecture. *Neuron* 96, 651–666. doi: 10.1016/j.neuron.2017.09.055

Nascimento-Ferreira, I., Santos-Ferreira, T., Sousa-Ferreira, L., Auregan, G., Onofre, I., Alves, S., et al. (2011). Overexpression of the autophagic beclin-1 protein clears mutant ataxin-3 and alleviates Machado-Joseph disease. *Brain* 134, 1400–1415. doi: 10.1093/brain/awr047

Nguyen, E. K., Koval, O. M., Noble, P., Broadhurst, K., Allamargot, C., Wu, M., et al. (2018). CaMKII (Ca2+/Calmodulin-dependent kinase II) in mitochondria of smooth muscle cells controls mitochondrial mobility, migration, and neointima formation. *Arterioscler. Thromb. Vasc. Biol.* 38, 1333–1345. doi: 10.1161/ATVBAHA.118.310951

Nicholls, D. G. (2004). Mitochondrial membrane potential and aging. *Aging Cell* 3, 35–40. doi: 10.1111/j.1474-9728.2003.00079.x

Nóbrega, C., Carmo-Silva, S., Albuquerque, D., Vasconcelos-Ferreira, A., Vijayakumar, U.-G., Mendonça, L., et al. (2015). Re-establishing ataxin-2 downregulates translation of mutant ataxin-3 and alleviates Machado-Joseph disease. *Brain* 138, 3537–3554. doi: 10.1093/brain/awv298

Orr, H. T., and Zoghbi, H. Y. (2007). Trinucleotide repeat disorders. *Annu. Rev. Neurosci.* 30, 575–621. doi: 10.1146/annurev.neuro.29.051605.113042

Otomo, A., Ono, S., Sato, K., Mitsui, S., Shimakura, K., Kimura, H., et al. (2022). High-throughput quantitative analysis of axonal transport in cultured neurons from SOD1H46R ALS mice by using a microfluidic device. *Neurosci. Res.* 174, 46–52. doi: 10.1016/j.neures.2021.07.005

Paulson, H. L., Perez, M. K., Trottier, Y., Trojanowski, J. Q., Subramony, S. H., Das, S. S., et al. (1997). Intranuclear inclusions of expanded polyglutamine protein in spinocerebellar ataxia type 3. *Neuron* 19, 333–344. doi: 10.1016/S0896-6273(00)80943-5

Pavel, M., Imarisio, S., Menzies, F. M., Jimenez-Sanchez, M., Siddiqi, F. H., Wu, X., et al. (2016). CCT complex restricts neuropathogenic protein aggregation via autophagy. *Nat. Commun.* 7:13821. doi: 10.1038/ncomms13821

Pellistri, F., Bucciantini, M., Invernizzi, G., Gatta, E., Penco, A., Frana, A. M., et al. (2013). Different ataxin-3 amyloid aggregates induce intracellular Ca2+ deregulation by different mechanisms in cerebellar granule cells. *Biochim. Biophys. Acta* 1833, 3155–3165. doi: 10.1016/j.bbamcr.2013.08.019

Piccioni, F., Pinton, P., Simeoni, S., Pozzi, P., Fascio, U., Vismara, G., et al. (2002). Androgen receptor with elongated polyglutamine tract forms aggregates that alter axonal trafficking and mitochondrial distribution in motor neuronal processes. *FASEB J.* 16, 1418–1420. doi: 10.1096/fj.01-1035fje

Riess, O., Rüb, U., Pastore, A., Bauer, P., and Schöls, L. (2008). SCA3: neurological features, pathogenesis and animal models. *Cerebellum* 7, 125–137. doi: 10.1007/s12311-008-0013-4

Rodríguez-Martín, T., Pooler, A. M., Lau, D. H. W., Mórotz, G. M., De Vos, K. J., Gilley, J., et al. (2016). Reduced number of axonal mitochondria and tau hypophosphorylation in mouse P301L tau knockin neurons. *Neurobiol. Dis.* 85, 1–10. doi: 10.1016/j.nbd.2015.10.007

Saotome, M., Safiulina, D., Szabadkai, G., Das, S., Fransson, Å., Aspenstrom, P., et al. (2008). Bidirectional Ca2+−dependent control of mitochondrial dynamics by the Miro GTPase. *Proc. Natl. Acad. Sci. U. S. A.* 105, 20728–20733. doi: 10.1073/pnas.0808953105

Schwarz, T. L. (2013). Mitochondrial trafficking in neurons. *Cold Spring Harb. Perspect. Biol.* 5:a011304. doi: 10.1101/cshperspect.a011304

Shahpasand, K., Uemura, I., Saito, T., Asano, T., Hata, K., Shibata, K., et al. (2012). Regulation of mitochondrial transport and inter-microtubule spacing by tau phosphorylation at the sites hyperphosphorylated in Alzheimer's disease. *J. Neurosci.* 32, 2430–2441. doi: 10.1523/JNEUROSCI.5927-11.2012

Sheng, Z.-H., and Cai, Q. (2012). Mitochondrial transport in neurons: impact on synaptic homeostasis and neurodegeneration. *Nat. Rev. Neurosci.* 13, 77–93. doi: 10.1038/nrn3156

Shirendeb, U. P., Calkins, M. J., Manczak, M., Anekonda, V., Dufour, B., McBride, J. L., et al. (2012). Mutant huntingtin's interaction with mitochondrial protein Drp1 impairs mitochondrial biogenesis and causes defective axonal transport and synaptic degeneration in Huntington's disease. *Hum. Mol. Genet.* 21, 406–420. doi: 10.1093/hmg/ddr475

Simões, A. T., Gonçalves, N., Koeppen, A., Déglon, N., Kügler, S., Duarte, C. B., et al. (2012). Calpastatin-mediated inhibition of calpains in the mouse brain prevents mutant ataxin 3 proteolysis, nuclear localization and aggregation, relieving Machado-Joseph disease. *Brain* 135, 2428–2439. doi: 10.1093/brain/aws177

Sowa, M. E., Bennett, E. J., Gygi, S. P., and Harper, J. W. (2009). Defining the human deubiquitinating enzyme interaction landscape. *Cells* 138, 389–403. doi: 10.1016/j.cell.2009.04.042

Stykel, M. G., Humphries, K., Kirby, M. P., Czaniecki, C., Wang, T., Ryan, T., et al. (2018). Nitration of microtubules blocks axonal mitochondrial transport in a human pluripotent stem cell model of Parkinson's disease. *FASEB J.* 32, 5350–5364. doi: 10.1096/fj.201700759RR

Switonski, P. M., Szlachcic, W. J., Krzyzosiak, W. J., and Figiel, M. (2015). A new humanized ataxin-3 knock-in mouse model combines the genetic features, pathogenesis of neurons and glia and late disease onset of SCA3/MJD. *Neurobiol. Dis.* 73, 174–188. doi: 10.1016/j.nbd.2014.09.020

Tao, K., Matsuki, N., and Koyama, R. (2014). AMP-activated protein kinase mediates activity-dependent axon branching by recruiting mitochondria to axon. *Dev. Neurobiol.* 74, 557–573. doi: 10.1002/dneu.22149

Todi, S. V., and Paulson, H. L. (2011). Balancing act: deubiquitinating enzymes in the nervous system. *Trends Neurosci.* 34, 370–382. doi: 10.1016/j.tins.2011.05.004

Todi, S. V., Winborn, B. J., Scaglione, K. M., Blount, J. R., Travis, S. M., and Paulson, H. L. (2009). Ubiquitination directly enhances activity of the deubiquitinating enzyme ataxin-3. *EMBO J.* 28, 372–382. doi: 10.1038/emboj.2008.289

Toulis, V., García-Monclús, S., Peña-Ramírez, C. D. L., Arenas-Galnares, R., Abril, J. F., Todi, S. V., et al. (2020). The deubiquitinating enzyme ataxin-3 regulates ciliogenesis and phagocytosis in the retina. *Cell Rep.* 33:108360. doi: 10.1016/j.celrep.2020.108360

Wang, X., and Schwarz, T. L. (2009). The mechanism of Ca2+-dependent regulation of kinesin-mediated mitochondrial motility. *Cells* 136, 163–174. doi: 10.1016/j.cell.2008.11.046

Weishäupl, D., Schneider, J., Peixoto Pinheiro, B., Ruess, C., Dold, S. M., von Zweydorf, F., et al. (2019). Physiological and pathophysiological characteristics of ataxin-3 isoforms. *J. Biol. Chem.* 294, 644–661. doi: 10.1074/jbc.RA118.005801

Wiatr, K., Marczak, Ł., Pérot, J.-B., Brouillet, E., Flament, J., and Figiel, M. (2021). Broad influence of mutant ataxin-3 on the proteome of the adult brain, young neurons, and axons reveals central molecular processes and biomarkers in SCA3/MJD using knock-in mouse model. *Front. Mol. Neurosci.* 14:74. doi: 10.3389/fnmol.2021.658339

Wiatr, K., Piasecki, P., Marczak, Ł., Wojciechowski, P., Kurkowiak, M., Płoski, R., et al. (2019). Altered levels of proteins and phosphoproteins, in the absence of early causative transcriptional changes, shape the molecular pathogenesis in the brain of young presymptomatic Ki91 SCA3/MJD mouse. *Mol. Neurobiol.* 56, 8168–8202. doi: 10.1007/s12035-019-01643-4

Winborn, B. J., Travis, S. M., Todi, S. V., Scaglione, K. M., Xu, P., Williams, A. J., et al. (2008). The deubiquitinating enzyme ataxin-3, a polyglutamine disease protein, edits Lys 63 linkages in mixed linkage ubiquitin chains. *J. Biol. Chem.* 283, 26436–26443. doi: 10.1074/jbc.M803692200

Woolums, B. M., McCray, B. A., Sung, H., Tabuchi, M., Sullivan, J. M., Ruppell, K. T., et al. (2020). TRPV4 disrupts mitochondrial transport and causes axonal degeneration via a CaMKII-dependent elevation of intracellular Ca2+. *Nat. Commun.* 11:2679. doi: 10.1038/s41467-020-16411-5

Zhao, X., Chen, X.-Q., Han, E., Hu, Y., Paik, P., Ding, Z., et al. (2016). TRiC subunits enhance BDNF axonal transport and rescue striatal atrophy in Huntington's disease. *Proc. Natl. Acad. Sci.* 113, E5655–E5664. doi: 10.1073/pnas.1603020113

frontiers | Frontiers in Molecular Neuroscience

TYPE Original Research
PUBLISHED 27 April 2023
DOI 10.3389/fnmol.2023.1166900

OPEN ACCESS

EDITED BY
Mitsuhiro Hashimoto,
Fukushima Medical University, Japan

REVIEWED BY
Naofumi Uesaka,
The University of Tokyo, Japan
Matthew B. Veldman,
Medical College of Wisconsin, United States

*CORRESPONDENCE
Kazuhiko Namikawa
✉ k.namikawa@tu-bs.de
Reinhard W. Köster
✉ r.koester@tu-bs.de

RECEIVED 15 February 2023
ACCEPTED 11 April 2023
PUBLISHED 27 April 2023

CITATION
Dorigo A, Valishetti K, Hetsch F, Matsui H, Meier JC, Namikawa K and Köster RW (2023) Functional regionalization of the differentiating cerebellar Purkinje cell population occurs in an activity-dependent manner.
Front. Mol. Neurosci. 16:1166900.
doi: 10.3389/fnmol.2023.1166900

Functional regionalization of the differentiating cerebellar Purkinje cell population occurs in an activity-dependent manner

Alessandro Dorigo[1], Komali Valishetti[1], Florian Hetsch[2,3], Hideaki Matsui [1,4], Jochen C. Meier [2], Kazuhiko Namikawa [1]* and Reinhard W. Köster [1]*

[1]Cellular and Molecular Neurobiology, Technische Universität Braunschweig, Braunschweig, Germany, [2]Cell Physiology, Zoological Institute, Technische Universität Braunschweig, Braunschweig, Germany, [3]Institute of Pathophysiology, University Medical Center, Johannes Gutenberg University, Mainz, Germany, [4]Department of Neuroscience of Disease, Brain Research Institute, Niigata University, Niigata, Japan

Introduction: The cerebellum is organized into functional regions each dedicated to process different motor or sensory inputs for controlling different locomotor behaviors. This functional regionalization is prominent in the evolutionary conserved single-cell layered Purkinje cell (PC) population. Fragmented gene expression domains suggest a genetic organization of PC layer regionalization during cerebellum development. However, the establishment of such functionally specific domains during PC differentiation remained elusive.

Methods and results: We show the progressive emergence of functional regionalization of PCs from broad responses to spatially restricted regions in zebrafish by means of in vivo Ca2+-imaging during stereotypic locomotive behavior. Moreover, we reveal that formation of new dendritic spines during cerebellar development using in vivo imaging parallels the time course of functional domain development. Pharmacological as well as cell-type specific optogenetic inhibition of PC neuronal activity results in reduced PC dendritic spine density and an altered stagnant pattern of functional domain formation in the PC layer.

Discussion: Hence, our study suggests that functional regionalization of the PC layer is driven by physiological activity of maturing PCs themselves.

KEYWORDS

zebrafish, cerebellum, Purkinje cell, functional regionalization, calcium imaging, optogenetics, spine density

Significance statement

Purkinje cells, (PC), the sole output neurons of the vertebrate cerebellum are organized into functional regions mediating different behaviors. By stimulating reflexive stereotypic behavior and high-resolution imaging of individual PCs during embryogenesis, we reveal that functional regionalization in the PC layer occurs concomitant with dendritic spine formation. Pharmacological as well as PC autonomous long-term optogenetic silencing of PC activity impairs dendritic spine density as well as functional regionalization of the PC layer. This demonstrates that functional regionalization and thus fine-tuning of PC connectivity is driven by neuronal activity of PCs themselves.

Introduction

The vertebrate cerebellum is dedicated to control body posture, balance, locomotor control and motor learning among other less well-clarified functions such as processing of sensory and emotional information and predicting dynamic events requiring motor activity (Timmann et al., 2010; Brooks et al., 2015; Khilkevich et al., 2018). Also, cerebellar development and its anatomy is highly conserved among vertebrates, which has been shown in particular for zebrafish and mammals (Wullimann et al., 2011; Hibi and Shimizu, 2012; Matsui et al., 2014). In contrast, the maturation of cerebellar neurons and the refinement of their physiological organization is understudied.

Purkinje cells (PCs) are arranged in a single cell layer and they represent the sole output neurons of the cerebellar cortex. In mammals, PCs are organized into functional domains dedicated to process and control different sensory and locomotive tasks. These functional domains can be clearly outlined and represented in form of a sensory and motor somatotopic map–albeit this map is fractured with topographically discontinuous patches of PCs representing non-adjacent areas of the body (Gibson et al., 1987; Gonzalez et al., 1993; Provini et al., 1998; Schlerf et al., 2010). In zebrafish, a similar regionalization of the PC layer has been shown by efferent connectivity mapping, Ca^{2+}-imaging during reflexive behavior and regionalized optogenetic interference with PC physiology (Matsui et al., 2014; Harmon et al., 2017; Knogler et al., 2019). Regionalization in the PC layer appears to be organized predominantly along the rostrocaudal axis with symmetric clusters in the caudal area being responsible for eye and body coordination corresponding to the vermis in the human cerebellum, while PCs in the rostro- and rostra-medial area are dedicated to swimming and turning corresponding to the human cerebellar paravermis (Matsui et al., 2014; Knogler et al., 2019).

Regionalized expression of signal transduction factors during PC differentiation in spatial correspondence to afferent projections and efferent circuitry appear to assemble PCs into coherent groups of roughly defined zones in mammals (Gravel and Hawkes, 1990; Rogers et al., 1999; Sillitoe et al., 2010; Ebner et al., 2012; Vibulyaseck et al., 2015; Takeuchi et al., 2017). In addition, elegant studies in mice have implicated electrophysiological activity of PCs to organize them into PC functional regions with zonal circuitry (White et al., 2014). Yet, until now, a zonal expression of genes in the zebrafish PC population either regionalized or fragmented has not been identified so far.

While, functional regionalization of the PC layer is evident in vertebrates, the developmental appearance of regionalized functional domains is far less understood. The small and nearly transparent zebrafish larvae with the unfolded PC layer are ideal for non-invasive *in vivo* imaging approaches (Weber and Köster, 2013). Hence, we combined triggering of stereotypic swimming movements with measurement of Ca^{2+} transients on the population level in zebrafish larvae on consecutive days to examine the development of functional domains. We also revealed that the formation of dendritic spines correlates with the temporal period of functional regionalization. Moreover, acute inhibition of PC activity interfered with dendritic spine formation and altered functional regionalization of the PC layer. Therefore, activity of PCs seems to be required for their own maturation and functional fine tuning within the PC layer.

Materials and methods

Animal husbandry

All experiments were performed with zebrafish (*Danio rerio*). Zebrafish were maintained, bred and raised at 28°C in a light–dark cycle of 14:10 h, respectively according to standard procedures (Westerfield, 2007) and legal regulations (EU Directive 2010_63). Experimental protocols for animal research were approved by governmental authorities of Lower Saxony, LAVES, (AZ33.19-42502-04-22/00208). No selection criteria were used to discriminate between sexes of zebrafish larvae. Embryos were incubated at 28°C in 30% Danieau [0.12 mM $MgSO_4$, 0.21 mM KCl, 0.18 mM $Ca(NO_3)_2$, 17.4 mM NaCl, 1.5 mM HEPES, pH 7.2]. To prevent pigmentation, at 10–12 h post fertilization (hpf) the medium was exchanged with 30% Danieau medium supplemented with 20 0μM 1-phenyl-2-thiourea (PTU, Sigma Aldrich, St. Louis, MO, USA). For *in vivo* Ca^{2+} imaging, PTU concentration was reduced to 75 μM. Following stable transgenic lines were used that have been described previously: Tg(ca8:FMAtagRFP)^{bz4} (Matsui et al., 2014), Tg(ca8-E1B:Hso.Arch3-TagRFPT,GCaMP5G)^{bz5}, Tg(ca8-E1B:FMATagRFP,GCaMP5G)^{bz6}, Tg(-7.5ca8:GFP)^{bz12} (Namikawa et al., 2019), and Tg(ca8-E1B:Hso.Arch3-TagRFPT,Hso.Arch3-TagRFPT)^{bz15} (Matsui et al., 2014).

Optovin induced swimming

For Optovin-induced swimming, larvae were embedded in 1.5% low melting agarose (Laboratorios CONDA, Madrid, Spain). After solidification of agarose, the matrix surrounding the trunk was removed to allow free trunk movements. Subsequently, the larvae were immersed in freshly diluted 10 μM Optovin (MedChem Express LLC, Monmouth Junction, NJ, USA) in 30%Danieau (stock solution: 100 μM Optovin dissolved in DMSO) (**Supplementary Figure 1**). Three UV light emitting diode (LED) diodes (405–412 nm) were positioned in a row on a microcontroller board (Arduino UNO). The open-source Arduino software was used to program the board that runs on a loop, with an ON-OFF cycle of 5 s of UV light followed by 15 s of darkness (**Supplementary Figure 1**), at the same time swimming related Ca^{2+} transients were recorded using a confocal microscope. All larvae used were naïve to the Optovin-stimulus and were not use on consecutive days repeatedly.

CNQX treatment

6-cyano-7-nitroquinoxaline-2,3-dione (CNQX) (Sigma-Aldrich Biochemie GmbH, Hamburg, Germany) was prepared as stock solution (10 mM in water) and kept as aliquots at −20°C. Freshly thawed CNQX was diluted to 20 μM in 30% Danieau directly before use.

Microinjection

For labeling individual PCs, zebrafish larvae were injected at the one-cell stage with 2 nl of a pTol2-2xcpce-EGFP construct (Namikawa et al., 2019) at a concentration of 5–10 ng/µl together with Tol2-encoding mRNA (25 ng/µl) and 0.05% Phenol Red into the yolk. At 3 dpf injected embryos were inspected under a fluorescence stereomicroscope for sparse EGFP fluorescence in the PC layer. Larvae suitable for single cell imaging were collected for further analysis.

Image acquisition and analysis

Anesthetized larvae (0.02% Tricaine/30% Danieau) were embedded in 1.5% low-melting agarose in imaging chambers with dorsal side facing the coverslip overlaid with 30% Danieau/0.02% Tricaine, whereas for recording Ca^{2+}-dynamics Tricaine was omitted. All image recordings were performed using a confocal laser scanning microscope (TCS SP8, Leica Microsystems, Wetzlar, Germany) at 28°C and rendered using the Las-X software (Leica Microsystems, Wetzlar, Germany).

For *in vivo* Ca^{2+} imaging combined with Optovin triggered swimming, short confocal movies about 2 min each were acquired with a frame interval of 500 ms. GCaMP5G fluorescence was recorded across the PC layer at a scan rate of two frames/s with optical sections of 10.92 µm using a 20x water immersion objective (NA: 0.75).

Raw data of Ca^{2+} transient recordings were processed with the help of ImageJ (NIH, Bethesda, MD, USA) plugin descriptor-based series registration (2d/3d+t). Within the Purkinje cell layer three regions of interests (ROIs) as described by Matsui et al. (2014) were defined. To measure ?F/F0, the first 10 frames, during which larvae were not stimulated with UV-light, were used to determine the average intensity (F0), which corresponds to the resting state that was used for processing the remaining frames. Ratiometric analysis of GCaMP5G fluorescence in relation to tagRFP-T intensities revealed (?F). These mean fluorescence intensities of GCaMP5G within ROIs at each time point were subtracted and divided by the average fluorescence intensity of frames (?F/F0). Only increases in signal intensity above 1.5 were included in the analysis to discriminate Ca^{2+}-signals from background activity.

Purkinje cell morphology was recorded using a 63x water immersion objective (NA1.4) and optical sectioning of 1.07 µm slices at increments of 0.36 µm. For spine density analysis dendritic protrusions through the z-planes of individual PC 3D reconstructions were counted using the Fiji Plugin Multi Point. Linear membrane protrusions longer than 1.9 µm were considered filopodia according to Peters and Kaiserman-Abramof (1970) and excluded from spine counts. Spine density was quantified as number of spines per length of the dendritic branch in µm.

Graphs and tables were generated using Microsoft Excel (Microsoft Corporation, Redmond, WA, USA) or Prism 6 (GraphPad Software Inc, San Diego, CA, USA).

Electrophysiology

Purkinje cells were recorded from zebrafish larvae at 5 dpf. Larvae were immobilized in 30% Danieau with 10 µM D-Tubocurarine and embedded in 2% low-melting agarose (Carl Roth, Karlsruhe, Germany) in extracellular solution. Tissue covering the cerebellum was removed with a fine glass capillary under stereo microscopic control (Schramm et al., 2021). Agarose blocks with fish inside were glued to 15 mm coverslips and transferred into a recording chamber perfused with standard extracellular solution constantly bubbled with carbogen gas. Viability of the animals was regularly monitored for by visual inspection of blood circulation. Cells were visualized with a 40x LUMPlanFL N water immersion objective (NA: 0.80, Olympus, Germany) on a SliceScope (Scientifica, Uckfield, United Kingdom) equipped with infrared optics and filters for the detection of FITC (visualization of cells) and tagRFPT (without excitation filter for detection of Alexa 594 and optogenetic stimulation, Chroma Technology GmbH, Olching, Germany). A Polychrome V monochromator (FEI Munich GmbH, Gräfelfing, Germany) was used for illumination and optogenetic stimulation. An ELC-03XS amplifier (NPI Electronic GmbH, Tamm, Germany), an ITC-18 interface and Patchmaster software (both HEKA Elektronik GmbH, Lambrecht, Germany) were used for whole-cell and cell-attached voltage clamp recordings and data acquisition. Electrophysiological recordings were acquired at a sampling rate of 20 kHz after current filtering at 1.3 kHz. Patch pipettes, made from borosilicate glass (Kwik-FIL glass capillaries, OD: 1.5 mm, #1B150F-4, World Precision Instruments GmbH, Friedberg, Germany), had resistances of 7–14 MΩ when filled with the intracellular solution containing (in mM): K-gluconate (115), KCl (15), $MgCl_2$ (2), EGTA (10), Mg-ATP (4), and HEPES (10), pH 7.2 (KOH) supplemented with 100 µM Alexa594 hydrazide (Molecular Probes, Eugene, OR, USA) to confirm cell morphology. The standard extracellular solution contained (in mM): NaCl (134), KCl (2.9), $MgCl_2$ (1.2), $CaCl_2$ (2.1), HEPES (10), and glucose (10), pH 7.8 (NaOH). Purkinje cells were identified by their EGFP or GCaMP5G fluorescence using an excitation wavelength of 480 nm. Pictures were recorded using Live Acquisition Software (FEI Munich GmbH, Gräfelfing, Germany) and a digital Orca R2 camera (Hamamatsu Photonics, Hamamatsu, Japan).

For the approach with the recording pipette a digital zoom factor of 2x was used. PCs were clamped at a holding potential of –60 mV. All voltage clamp data were recorded in standard extracellular solution. This solution was supplemented with CNQX (20 µM, Sigma-Aldrich Biochemie GmbH, Hamburg, Germany), where indicated. For optogenetic stimulation of Arch3 a wavelength of 517 nm was set using Live Acquisition software (FEI Munich GmbH, Gräfelfing, Germany) and light was applied for 30–60 s during voltage clamp recordings. Using a digital power meter (PM100D, Thorlabs GmbH, Bergkirchen, Germany) the power of the illuminating light was measured and lay at around 0.3 mW (0.45 mW/cm^2). Action potential quantification was performed before (control) and during phases of photostimulation.

Statistical analysis

For plotting the graphs and performing the appropriate statistical tests, the data sets were imported into Prism 6 (GraphPad Software Inc, San Diego, CA, USA). Unless otherwise mentioned, all data in the graphs are presented as mean + SD.

For statistical analysis the obtained data were subjected to normality test using D'Agostino-Pearson Omnibus (K2). For

comparing more than two groups, a one-way ANOVA followed by Tukey's multiple comparisons test for normally distributed data was applied, else ANOVA Kruskal-Wallis test followed by Dunn's multiple comparisons test was used.

For comparing only two groups, the data were tested for normality using D'Agostino-Pearson Omnibus (K2), F-test was used for comparing variances. A two-tailed unpaired *t*-test was applied for normally distributed data with equal variances, whereas for normally distributed data with unequal variances two-tailed unpaired *t*-test with Welch's correction was used for comparing two different groups. Additionally, for the data that did not pass the normality test two-tailed Mann-Whitney test was applied.

For statistical analysis of obtained electrophysiological results data were subjected to Shapiro-Wilk test for normality. If normality could be assumed, a one-way ANOVA with post-hoc Tukey test was performed, otherwise data were subjected to a non-parametric Mann-Whitney rank sum test.

Results

Establishment of functional domains in the zebrafish cerebellar PC population

To investigate the development of a functional regionalization in the zebrafish cerebellum a behavioral assay is needed that triggers PC activity prior to the regionalization process. Previous studies had demonstrated that UV-illumination triggers an early escape behavior in zebrafish larvae (Guggiana-Nilo and Engert, 2016). But induction of swimming by UV-illumination alone was only partly reliable and not predictable at 4 days post fertilization (dpf) due to feeble movements during these developmental stages. It has been shown that the photosensitive compound Optovin activates upon UV illumination early differentiating sensory neurons expressing the receptor A1 of the transient receptor potential A1 (TrpA1) receptor family including those neurons in the trunk (**Figure 1A**). This triggers a motor reflex, enabling light-controlled trunk movements for the duration of UV-illumination in larvae as young as 30 h post fertilization (hpf) (Kokel et al., 2013; Lam et al., 2017). Indeed, UV-illumination in the presence of 10 μM Optovin triggered swimming-related trunk movements paired with the UV-stimulus in a predictable and controlled pattern already at 4 dpf (**Figures 1B, C**).

To test whether Optovin-induced swimming results in increased Ca^{2+} transients in PCs, we recorded swimming-correlated Ca^{2+} transients of larvae of the stable transgenic strain Tg(ca8-E1B:FMATagRFP,GCaMP5G)^{bz6}. Zebrafish larvae of this strain express the genetically encoded Ca^{2+}-indicator (GECI) GCaMP5G specifically in PCs (Matsui et al., 2014). Such GECIs do not resolve individual events of neuronal activity, but report a long-lasting cumulative activity of neurons, which is well-suited to identify groups of neurons at the population level that are responsive to a certain stimulus. Optovin-triggered swimming movements resulted in an upregulation of GCaMP5G-fluorescence in a temporally restricted manner reflecting periods of trunk and tail deflections associated with swimming (**Figure 1D**).

To next address the development of functional domains in the PC layer, we overlaid images of GCaMP5G fluorescence recorded during Optovin-induced swimming with the same grid described by Matsui et al. (2014) to define rostral, rostromedial and caudal regions (**Figure 1E**). The analysis of recorded Ca^{2+}-transients in the PC layer associated with swimming movements at 4 dpf showed that the total percentage of swimming-correlated Ca^{2+}-transients were nearly equally distributed among all PC regions (**Figure 1F**, rostral: 32%, rostromedial: 38%, caudal: 30%). These findings suggest that PCs from all regions of the PC layer are physiologically involved in this behavior with similar probability, indicating that the PC layer at 4 dpf is not regionalized in its Ca^{2+}-activity with respect to this behavior.

When these measurements were repeated on consecutive days the maximum percentage of Ca^{2+} transients were progressively confined to the rostromedial region increasing from 30% at 4 dpf to 70% at 7 dpf, with a decline in responsiveness in rostral and caudal regions (**Figure 1F**). These observations indicate that by 6 dpf the PC layer displays a clear regionalized response to Optovin-stimulated trunk movements.

Changes in dendritic spine density correlate with progressive functional regionalization

The density of spines along dendritic branches can be used to evaluate the maturity of differentiating neurons. At 4 dpf, PC primary dendrite specification is completed and major dendritic branches are established (Tanabe et al., 2010). We therefore wondered, if formation of PC dendritic spines shows a developmental pattern similar to the progressive specification of functional PC domains. Mosaic labeling of single PCs was achieved by microinjecting a plasmid expressing membrane targeted EGFP under control of the PC specific enhancer cpce (Namikawa et al., 2019) into Tg(ca8:FMAtagRFP)^{bz4} embryos (Matsui et al., 2014) at the one cell stage. At 3 dpf zebrafish larvae with individual fluorescent PCs labeled by EGFP expression were selected. During the consecutive days from 4 to 6 dpf high resolution confocal microscopy was used to visualize spines along different dendritic branches from the same PCs (**Figures 2A–C**). The primary, secondary and tertiary dendritic structures of these PCs were manually traced and spine density was quantified along the dendritic branches of individual PCs from 4 to 6 dpf (**Figure 2D**).

At 4 dpf a large number of spines could be observed along all dendritic branches with exception of the primary branch. Quantification revealed that primary PC dendrites contained only few spines, and dendritic spine density remained constant from 4 to 6 dpf (**Figure 2D**, ordinary one-way ANOVA, $F_{2,\ 15} = 0.3638$, $p = 0.7010$, 4 dpf: $n = 7$, 0.30 ± 0.057; 5 dpf: $n = 4$, 0.28 ± 0.053; 6 dpf: $n = 7$, 0.28 ± 0.040; n indicates number of analyzed dendritic branches). In contrast, spine density along secondary and tertiary branches increased with developmental age of larvae, with tertiary dendrites displaying a higher spine density compared to secondary dendrites from 4 to 6 dpf (**Figure 2D**, secondary dendrites: ANOVA, $p = 0.0004$, 4 dpf: $n = 9$, 1 ± 0.053; 5 dpf: $n = 7$, 1.6 ± 0.13; 6 dpf: $n = 7$, 1.6 ± 0.29, tertiary dendrites: ANOVA, $p < 0.0001$, 4 dpf: $n = 18$, 1.1 ± 0.19; 5 dpf: $n = 30$ 2.0 ± 0.24; 6 dpf: $n = 33$, 2.0 ± 0.32). Interestingly, spine density along secondary and tertiary dendrites increased immensely from 4 to 5 dpf (**Figure 2D**, secondary dendrites: ANOVA, adjusted p-value = 0.0100, 4 dpf:

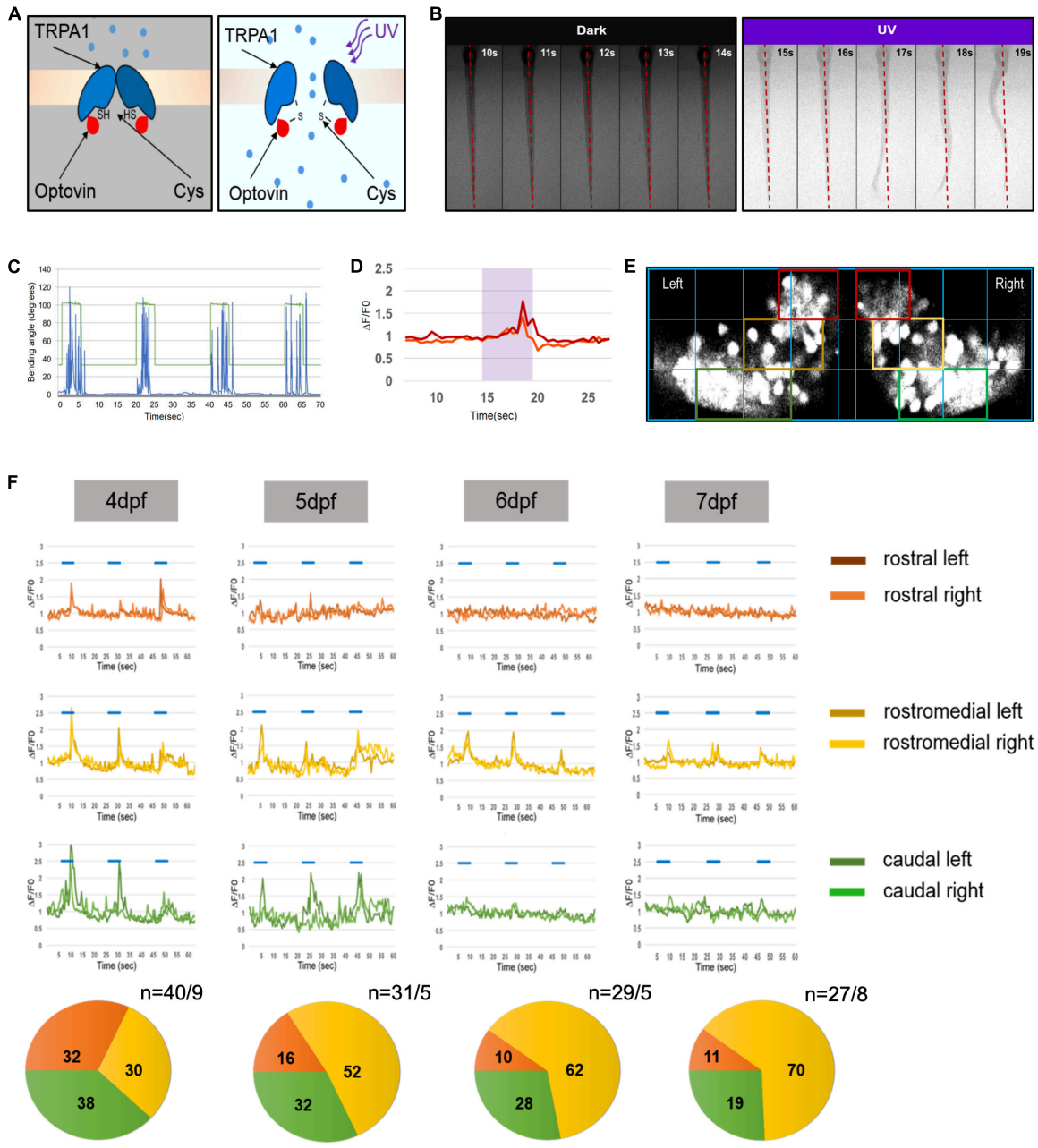

FIGURE 1
Progressive development of functional domains in the zebrafish Purkinje cell (PC) population during cerebellar development. **(A)** Graphic illustration of transient receptor potential A1 (TrpA1) channel activation in sensory neurons of the trunk by UV illumination of Optovin. **(B)** Montage of consecutive frames of 1 s intervals showing deflection of trunk in the presence of Optovin with and without UV light (red dashed line marks dorsal midline during resting state). **(C)** Graph illustrating angle of bending of trunk (blue peaks) during the time UV light was on (peaks in green) and off (green line). **(D)** Examples of Ca^{2+} transient amplitudes (red and orange) during Optovin induced swimming upon UV illumination (period marked in turquoise). **(E)** The grid used to define rostral (red boxes), rostromedial (yellow boxes) and caudal territories (green boxes) in the zebrafish PC layer expressing the calcium indicator GCaMP5G. **(F)** Illustration of measured swimming correlated Ca^{2+} transients (?F/F0) of different regions of PC layer from 4 to 7 dpf (blue lines indicate periods of UV-illumination). Pie charts below display the percentage of swimming-correlated Ca^{2+}-transients within the different PC regions with respect to days of analysis. To the right of pie charts *n* indicates number of recorded transients/number of larvae.

n = 9, 1.0 ± 0.0.053; 5 dpf: n = 7, 1.6 ± 0.1; tertiary dendrites: ANOVA, adjusted p-value < 0.0001, 4 dpf: n = 18, 1.1 ± 0.19; 5 dpf: n = 30, 2 ± 0.24), but remained constant from 5 to 6 dpf (Figure 2D, secondary dendrites: ANOVA, adjusted p-value > 0.9999, 5 dpf: n = 7, 1.6 ± 0.13; 6 dpf: n = 7, 1.6 ± 0.29, tertiary dendrites: ANOVA, adjusted p-value > 0.9999, 5 dpf: n = 30, 2 ± 0.24; 6 dpf: n = 33, 2.0 ± 0.32).

In summary, onset of PC differentiation at 3 dpf by initiation of dendritogenesis (Tanabe et al., 2010) followed by the appearance of a significant number of spines at 4 dpf suggests the initiation of synaptogenesis. This is consistent with the observation of first occurring Ca^{2+}-signals at 4 dpf in PCs during Optovin-stimulated trunk movements (Figure 1F). Subsequent maturation and refinement of dendrites lasts until 6dpf, when a plateau in

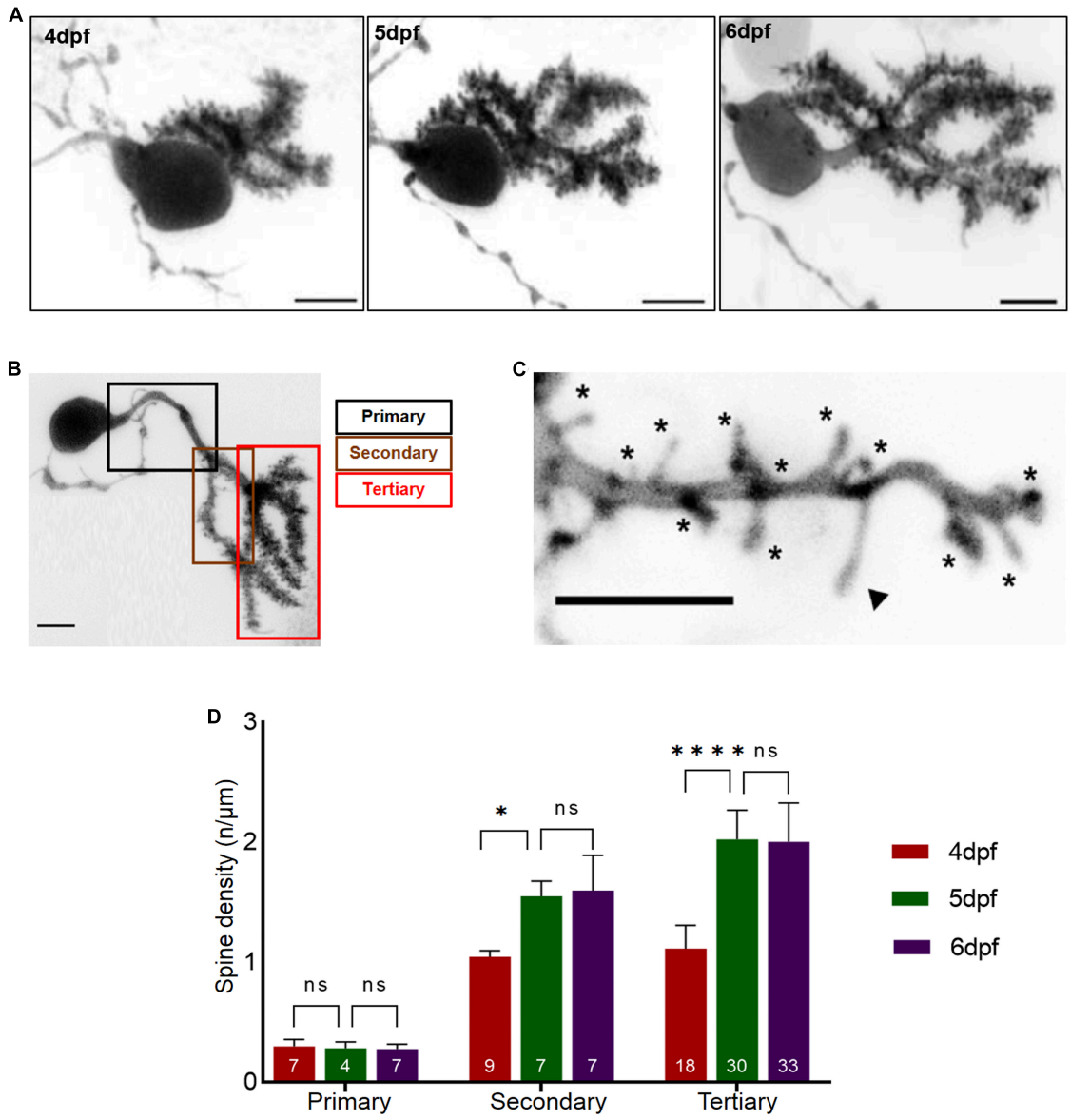

FIGURE 2
Dendritic spine density of individual Purkinje cell (PCs) with respect to developmental age of larvae. **(A)** Example of a 3D-reconstructed single PC from 4 to 6 dpf recorded by high-resolution confocal microscopy. Scale bar: 5 µm. **(B)** Single PC with demarcated dendritic branches. Scale bar: 5 µm. **(C)** Higher magnification of dendritic branch with visualized protrusions (asterisks indicate spines included for counting; arrowheads mark filopodia structures excluded from counting). Scale bar: 5 µm. **(D)**. The graph displays spine density along primary, secondary and tertiary dendritic branches from 4 to 6 dpf larvae. The data are represented as mean + SD. Numbers inside the bars include total number of dendritic branches analyzed of different individual PCs. Ordinary one-way ANNOVA followed by Tukey's multiple comparisons test was applied for normally distributed data, else Kruskal-Wallis test followed by Dunn's multiple comparisons test was used in **(D)**. Denotations for significance are non-significant (n s) $p > 0.1234$, *$p < 0.0332$, ****$p < 0.0001$.

spine density is reached. This developmental time window of PC maturation correlates well with the observed time course of progressive functional regionalization in the PC layer.

Silencing of PC activity reduces dendritic spine density

Since dendritic spine density is regulated by neuronal activity (McAllister, 2000; Segal, 2010), we wondered whether functional regionalization in the PC layer is influenced by PC activity itself. Purkinje cell excitability in zebrafish is mediated by AMPA-receptors (Sengupta and Thirumalai, 2015), hence we used 6-cyano-7-nitroquinoxaline-2,3-dione (CNQX) as AMPA-receptor antagonist in bath incubation experiments (Pietri et al., 2009; Theisen et al., 2018) and performed direct electrophysiological recordings from PCs (n = 9) *in vivo* at 5 dpf. Bath application of 20 µM CNQX significantly reduced spontaneous postsynaptic currents (sPSC) almost completely silencing PC activity (**Supplementary Figure 2**) and confirming that CNQX is able to suppress PC activity in zebrafish larvae.

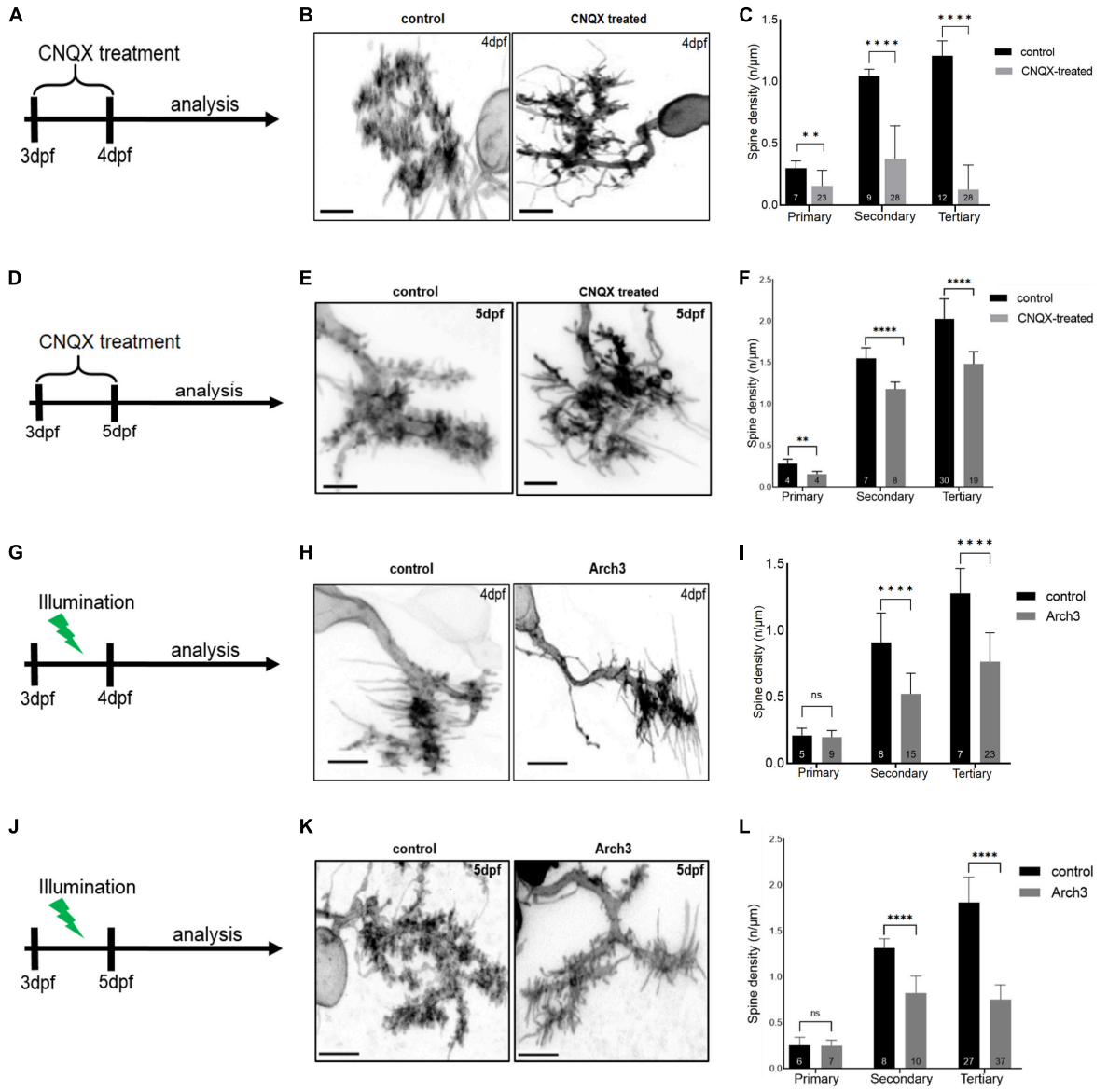

FIGURE 3
Inhibiting Purkinje cell (PC) neuronal activity reduces PC spine density. Schematic drawing illustrating the scheme of 6-cyano-7-nitroquinoxaline-2, 3-dione (CNQX) treatment from 3 dpf to analysis on 4 dpf **(A)** and on 5 dpf **(D)**. Maximum intensity projection of untreated and CNQX treated PC at 4 dpf **(B)** and 5 dpf **(E)**. Scale bar: 5 µm. Representation of spine density on primary, secondary and tertiary branches of CNQX treated PCs (gray) vs. controls (black) at 4 dpf **(C)** and at 5 dpf **(F)**. Schematic drawing illustrating the start of pulsed illumination of 517 nm monochromatic light until the confocal microscopy analysis of Arch3 and non-Arch3 expressing larvae at 4 dpf **(G)** and 5 dpf **(J)**. Maximum intensity projection of PC at 4 dpf **(H)** and 5 dpf **(K)** from Arch3 larvae and non-Arch3 expressing larvae, respectively. Scale bar: 5 µm. Graph showing PC spine density quantification in 4 dpf larvae **(I)** and 5 dpf larvae **(L)** on primary, secondary and tertiary dendritic branches of Arch3 larvae (gray) vs. controls (black). The data in graphs are presented as mean + SD. Numbers inside the bars include total number of dendritic branches analyzed of different individual PCs. For **(C)**, **(F)**, **(I)**, **(L)** two-tailed unpaired *t*-test for normally distributed data with equal variances was used, for normally distributed data with unequal variances two-tailed unpaired *t*-test with Welch's correction was applied. Additionally, for the data that did not pass the normality test, two tailed Mann-Whitney test was applied. Denotations for significance are non-significant (n s) $p > 0.1234$, $^{**}p < 0.0021$, $^{****}p < 0.0001$.

Next, we tested the role of neuronal activity in modulating dendritic spine density. For this purpose, larvae with PCs labeled by membrane targeted EGFP expression in a sparse, mosaic manner were selected at 3 dpf and treated with 20 µM CNQX for 24 or 48 h, respectively (Figures 3A, D). Untreated larvae were used as controls. Individual PCs of both groups were subjected to high resolution imaging at 4 dpf or 5 dpf by laser scanning confocal microscopy (Figures 3B, E). This analysis revealed that spine density of activity-silenced PCs treated with CNQX were significantly decreased after 24 h of CNQX-treatment compared to controls along primary (Figure 3C, control: $n = 7$, 0.30 ± 0.057; CNQX-treated: $n = 23$, 0.16 ± 0.13; two-tailed Mann Whitney test, $p = 0.0011$), secondary (Figure 3C, control: $n = 9$, 1.0 ± 0.053; CNQX-treated: $n = 28$, 0.38 ± 0.27; two-tailed unpaired *t*-test with Welch's correction, $p < 0.0001$) as well as tertiary dendrites (Figure 3C, control: $n = 12$, 1.2 ± 0.12, CNQX-treated: $n = 28$, 0.13 ± 0.20; two-tailed Mann Whitney test, $p < 0.0001$).

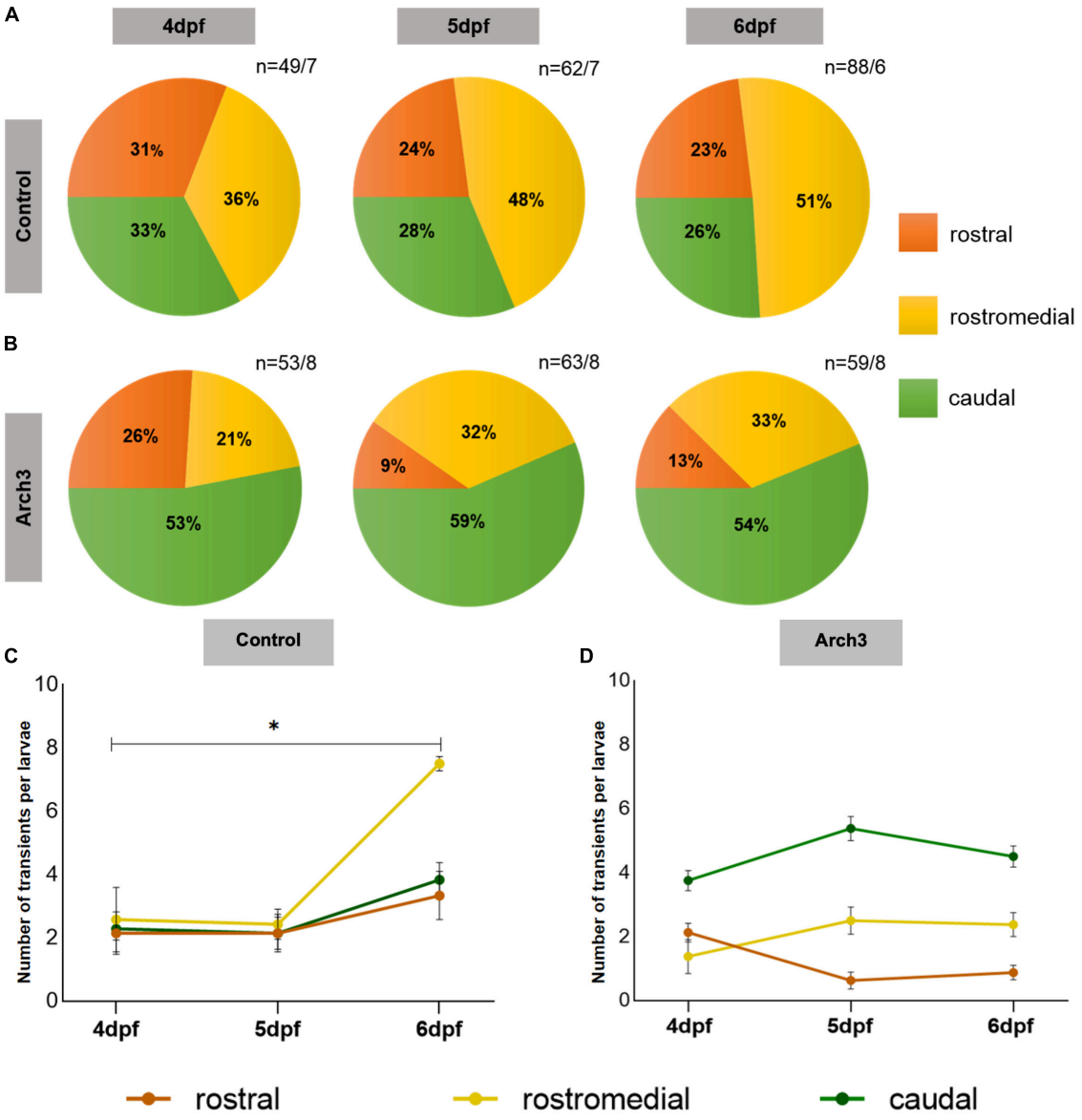

FIGURE 4
Formation of functional domains in the Purkinje cell (PC) population is impaired upon inhibiting PC neuronal activity. The pie charts represent the percentage of Optovin-induced swimming-correlated Ca^{2+} transients from 4 to 6 dpf localized in different regions of the PC layer. Ca^{2+} transients were recorded after continuous Arch3-stimulating illumination to suppress PC activity in **(A)** Tg(ca8-E1B:FMATagRFP,GCaMP5G)^{bz6} larvae as control and **(B)** Arch3-expressing Tg(ca8-E1B:Hso.Arch3-TagRFPT,GCaMP5G)^{bz5} larvae. *n* represents number of recorded Ca^{2+} transients/number of larvae. The number of transients per larvae in each PC subregion in **(C)** control and **(D)** Arch3-expressing larvae is displayed for consecutive days during which PC maturation occurs. The data are represented as mean ± SEM. Kruskal-Wallis test followed by Dunn's multiple comparisons test was used in **(C)**. Denotations for significance is $^*p < 0.0332$.

Similarly, a reduction in spine density was observed after 48 h of CNQX-mediated silencing of activity at 5 dpf compared to controls along primary (Figure 3F, control: $n = 4$, 0.28 ± 0.053; CNQX-treated: $n = 4$, 0.15 ± 0.035; two-tailed unpaired *t*-test, $p = 0.0069$), secondary (Figure 3F, control: $n = 7$, 1.55 ± 0.128; CNQX-treated: $n = 8$, 1.18 ± 0.088; two-tailed unpaired *t*-test, $p < 0.0001$) as well as tertiary dendrites (Figure 3F, control: $n = 30$, 2.02 ± 0.244, CNQX-treated: $n = 19$, 1.48 ± 0.149; two-tailed unpaired *t*-test with Welch's correction, $p < 0.0001$).

To corroborate these findings by cell type specific silencing of PC activity, we selected long-term optogenetics using Archaerhodopsin3 (Arch3) as light-gated hyperpolarizing outward-directed proton pump (Chow et al., 2010). We built a custom illumination chamber for petri dishes (diameter of 6 cm) equipped with an LED-panel that generates pulsed illumination of 517 nm monochromatic light (0.37, 0.52 mW/cm^2) at 1 Hz (duration of illumination 120 ms) to not exhaust light-gated Arch3 proton efflux (Supplementary Figures 3A, B). To confirm that this setup inhibits PC activity, we first performed direct electrophysiological recordings from individual PCs ($n = 5$) at 5 dpf of the Tg(ca8-E1B:Hso.Arch3-TagRFPT,GCaMP5G)^{bz5} transgenic line (Matsui et al., 2014), while Tg(ca8-E1B:FMATagRFP,GCaMP5G)^{bz6} were used as control. Equivalent illumination conditions (Supplementary Figure 3C)

using a monochromator during electrophysiological recordings eliminated spontaneous postsynaptic currents (sPSC) in PCs silencing their activity nearly completely and confirming that Arch3 is efficiently stimulated under this illumination paradigm (**Supplementary Figure 4**).

To ensure even more efficient Arch3-mediated PC silencing, we used a bidirectional Tg(ca8-E1B:Hso.Arch3-TagRFPT,Hso.Arch3-TagRFPT)^{bz15} transgenic line (Matsui et al., 2014) expressing two copies of the Arch3-TagRFP-T fusion protein in cerebellar Purkinje cells. Embryos were injected at the one cell stage with pTol2-2xcpce-EGFP. At 3 dpf heterozygous carriers of the Arch3-expressing transgene and sparse mosaic membrane targeted EGPF expression were selected and raised under continuous pulsed illumination for optogenetic PC inhibition for 24 (**Figure 3G**) or 48 h (**Figure 3J**), respectively, while Arch3 non-expressing siblings served as control. High resolution confocal microscopy of individual PCs at 4 and 5 dpf (**Figures 3H, K**) revealed that their spine density in Arch3 expressing larvae after 24 h of illumination along secondary [**Figure 3I**, control: n = 8, 0.91 ± 0.22; Arch3: n = 15, 0.52 ± 0.15; two-tailed unpaired t-test, $p < 0.0001$, t (5) = 21] and tertiary (**Figure 3I**, control: n = 7, 1.30 ± 0.19; Arch3: n = 23, 0.77 ± 0.22; two-tailed Mann-Whitney test, $p < 0.0001$) dendrites was significantly reduced compared to controls.

Similarly, confocal microscopy after 48 h of Arch3 stimulation by light revealed that at 5 dpf the spine density in individual PCs along secondary [**Figure 3L**, control: n = 8, 1.31 ± 0.101; Arch3: n = 10, 0.83 ± 0.184; two-tailed unpaired t-test, $p < 0.0001$, t (7) = 16] and tertiary [**Figure 3L**, control: n = 27, 1.09 ± 0.278; Arch3: n = 37, 0.88 ± 0.294; two-tailed unpaired t-test, $p < 0.0001$ t (13) = 62)] dendrites was significantly reduced compared to controls.

Taken together, pharmacological as well as cell-type specific optogenetic silencing of PC- neuronal activity consistently demonstrate that inhibition of neuronal activity in PCs leads to reduction in dendritic spine coverage. Hence the maturation of zebrafish cerebellar PCs is dependent on their proper electrophysiological activity.

Inhibition of neuronal activity impairs functional regionalization

Our results so far demonstrate that development of function specific domains of Ca^{2+} activity in the PC population correlates with formation of dendritic spines and also spine density is dependent on neuronal activity. Therefore, we asked if neuronal activity also modulates functional regionalization. To answer this, we combined optogenetics with Optovin-stimulated swimming assays. Here, larvae of stable transgenic lines Tg(ca8-E1B:Hso.Arch3-TagRFPT,GCaMP5G)^{bz5} and Tg(ca8-E1B:FMATagRFP,GCaMP5G)^{bz6} as controls, were raised under pulsed illumination from 3 dpf until swimming correlated Ca^{2+} transient recordings were performed. At 4 dpf Ca^{2+} transients were nearly equally distributed among PC regions (**Figure 4A**, 4 dpf: rostral 31%, rostromedial 37%, and caudal 33%) in control larvae. As observed previously, this pattern changed during the following 2 days and Ca^{2+} transients during Optovin stimulated swimming became progressively confined to the rostromedial region of the PC population (**Figure 4A**, 6 dpf: rostral 23%, rostromedial 51%, and caudal 26%). Thus, continuous exposure to pulsed illumination did not interfere with proper functional regionalization of PCs (compare **Figures 1F**, **4A**). This rostromedial region has been identified previously with the help of PC-specific Arch3 optogenetic inhibition to coordinate proper execution of oriented swimming (Matsui et al., 2014).

When Ca^{2+} transients per larvae were displayed for each PC region an overall increase of these transients was observed for each region from 4 to 6 dpf (**Figure 4C**) corresponding to the increase in spine density. Yet, Ca^{2+} transients in the rostromedial PC region were the only to show a statistically significant elevation from 4 to 6 dpf (**Figure 4C**, rostromedial: ANOVA, adjusted p-value = 0.0124, 4 dpf: 2.6 ± 1.02, n = 7; 6 dpf: 7.5 ± 0.23, n = 6; n indicates number of larvae) in comparison to the rostral and caudal PC regions suggesting that during the course of regionalization the rostromedial domain becomes more sensitive in responding to Optovin-induced trunk movements compared to the other subregions.

In Arch3-expressing larvae with optogenetic inhibition of neuronal activity, maximum percentage of measured Ca^{2+} transients were localized in the caudal region already at 4 dpf (**Figure 4B**, dpf: rostral 26%, rostromedial 21%, and caudal 53%). This pattern is different from larvae at 4 dpf with actively firing PCs (**Figure 1F**), and likely reflects altered initial PC circuitry formation under conditions of impaired spontaneous PC activity. Importantly, when Ca^{2+} measurements were performed on the following days after continuously silencing PC activity, the pattern of swimming-correlated Ca^{2+}-transients did not change dramatically, but was clearly different from controls. Optovin-stimulation mediated Ca^{2+}-transients appeared mostly in the caudal and not in the rostromedial region of the PC population and remained nearly stagnant in their percentage from 4 to 6 dpf (**Figure 4B**, caudal: 4 dfp: 53%, 6 dpf: 54%). In the rostromedial region some increase in the response to Optovin-stimulation from 21 to 33% could be observed from 4 to 6 dpf, suggesting that this region became more responsive and such slight increase in responsiveness could be observed when Ca^{2+} transients per larvae were displayed for each PC region (**Figure 4D**, rostromedial: 4 dpf: 1.38 ± 0.53, n = 8; 6 dpf: 2.38 ± 0.38, n = 8). Yet, this increase did not reach levels of controls, in which more than half of the Optovin-stimulation elicited Ca^{2+}-transients appeared in the rostromedial region. In the rostralmost region a decrease from 26 to 13% in responsiveness could be observed corresponding to the moderate increase in the rostromedial region. Of note, in none of the domains including the most responsive caudal one (6 dpf: 4.5 ± 0.31 transients per larva, n = 8 larvae) the number of Ca^{2+} transients per larvae in each subregion reached levels of responsiveness found in controls in the rostromedial domain (6 dpf: 7.5 ± 0.23 transient per larva, n = 6 larvae) (compare **Figures 4C, D**). Furthermore, in none of these regions the increase or decrease in Ca^{2+} transients per larvae reached statistical significance, supporting the suggestion that Arch3-mediated inhibition of PC-activity results in a lower responsiveness and stagnation of the regionalization pattern reached at 4 dpf.

In conclusion, these findings illustrate that silencing PC activity alters the progressive development of function specific domains in the PC population, initially rendering the caudal most instead

of the rostromedial region of PCs more responsive to Optovin-mediated stimuli. While a moderate increase in responsiveness of rostromedial PCs under conditions of constitutive PC silencing was observed during PC maturation, this increase did not enable rostromedial PCs to become the predominant domain in the PC layer responding to Optovin-mediated trunk movement. Furthermore, the process of regionalization in all subregions was interrupted and remained static. These findings suggest that the establishment of functional domains within the PC population is likely mediated by the electrophysiological activity of PCs themselves.

Discussion

Our results show that zebrafish PCs are not *a priori* confined to a distinct physiological response and functional output, but that they instead progressively refine their response within regional territories of the zebrafish PC layer. This spatially refined response within the PC population occurs during stages of PC maturation and development of new spines suggesting the involvement of neuronal activity in connectivity refinement. Indeed, silencing neuronal activity of PCs not only reduced spine formation, but was paralleled by an altered functional regionalization. This suggests that the segregated organization of the cerebellar PC population with subsets of PCs controlling different behaviors is subjected to a process of development based on physiological activity patterns of PCs.

Currently, we cannot distinguish whether Ca^{2+} signals in the PC layer upon Optovin-stimulated trunk movements represent either processing of sensory information, motor kinematics or motor intent. Nevertheless, our studies could reveal that Optovin-stimulation leads to a progressively regionalized Ca^{2+}-activity pattern in the cerebellar PC population, which seems to be mediated by an increase in responsiveness of PCs in the relevant (rostromedial) territory. In a recent elegant study such a regionalized organization of the PC layer in zebrafish was demonstrated for a number of visual and motor activities such as processing of visual sensory information or mediating locomotion. Here, responses of PCs to eye or tail motion were found to rather broadly activate the entire PC population (Knogler et al., 2019). Light-activated swimming behavior by Optovin is not visually mediated, but involves the spinal sensory-motor reflex (Kokel et al., 2013). Thus, PC activity following Optovin-activation likely represents either the processing of sensory information from the spinal cord or activating trunk locomotion. Unambiguous clarification will require in depth electrophysiological studies combined with functional analysis in order to identify the circuitry between activated Optovin-stimulated sensory neurons and cerebellar PCs. Nevertheless, because of the reliability in motor response already during early PC differentiation stages, Optovin-elicited Ca^{2+}-transients are well-suited to study the dynamics of the emerging segregation of PC activity in the PC layer associated with swimming.

While in control larvae the rostromedial PC region became more responsive to Optovin-stimulated trunk-movements during stages of PC differentiation, responsiveness to this stimulus remained static and declined in the rostral and caudal PC regions based on percentage. This does not mean that these PC regions are less active in general, but they likely respond to other stimuli as a consequence of functional segregation of the PC population. Further investigations will require the establishment of behavioral assays that elicit Ca^{2+}-signals in the PC layer in these areas already before this functional diversification is established. Imaging of Ca^{2+}-transients on the population level using genetically encoded Calcium indicators as reporters of cumulative neuronal activity is well-suited to address these questions of regionalization within the PC population. It would be interesting to perform single cell electrophysiology recordings from individual PCs of the different functional PC regions during Optovin-stimulated trunk movements. However, such measurements are invasive and may not allow proper recording during trunk motion due to the triggered movements of the larvae. The advent of voltage-sensitive fluorescent proteins with high temporal resolution and sufficient signal amplitude dynamics may allow for such single cell analytics in the future.

Interestingly, rostral and rostromedial PCs under constantly pulsed green light exposure showed a similar responsiveness to Optovin-stimulation at 4dpf as observed in PCs of control-larvae PCs of wildtype larvae. In contrast, the physiological inhibition of PCs by continuous pulsed light injection resulted in caudal PCs to become already more responsive to the Optovin-stimulus at this early phase of PC maturation compared to other PC regions. Currently, we have no mechanistic explanation for this observation. The data in wild type larvae suggest that PC regionalization is likely mediated by the activity of PCs themselves. One hypothesis could be that inhibition of this physiological activity may allow for a stronger impact of genetic factors regulating PC connectivity, thereby resulting in an altered cerebellar circuitry with caudal PCs contributing more extensively to circuits activated by Optovin-stimulation.

The activity-driven maturation of neuronal connectivity in the cerebellum resembles known mechanisms of neuronal learning and memory formation for example in the mammalian hippocampus (McGaugh, 2000). It will therefore be of interest whether similar cell biological mechanisms and molecular cues mediate the functional regionalization of zebrafish PCs downstream of altered membrane polarization. For example, functional regionalization could be mediated by Ca^{2+} regulated signal transduction factors such as Calmodulin, Ca^{2+}/Calmodulin-dependent protein (CaM) kinases, Calcineurin or Calmodulin-binding transcription activators (CAMTAs) (Colomer and Means, 2007). These in turn may drive cytoskeletal rearrangements to promote dendrite maturation and to remove or enhance synaptic contacts to modulate synaptic transmission (Borovac et al., 2018; Shimobayashi and Kapfhammer, 2018). Zebrafish with their accessibility for molecular genetics, *in vivo* imaging and behavioral modulation are well-suited to further expand our understanding about the crucial evolutionary conserved molecular, physiological and functional relationships of neuronal connectivity and plasticity in the central nervous system of vertebrates.

Data availability statement

The raw data supporting the conclusions of this article will be made available by the authors, without undue reservation.

Ethics statement

The animal study was reviewed and approved by Niedersächsisches Landesamt für Verbraucherschutz und Lebensmittelsicherheit Postfach 9262 26140 Oldenburg.

Author contributions

KN, HM, and RK conceived the study and designed experimental approaches. AD, KV, and FH generated and analyzed data. KN, JM, and RK supervised the project. All authors contributed to writing the manuscript and approved the submitted version.

Funding

The authors gratefully acknowledge funding of this project by the Deutsche Forschungsgemeinschaft (DFG, German Research Foundation–Projektnummer 241961032 to RK), the Volkswagenstiftung (project HOMEO-HIRN, ZN3673, to RK and JM), funds of Lower Saxony, Era Net Neuron II project CIPRESS (to JM), and an Alexander von Humboldt Fellowship (to HM).

Acknowledgments

We thank Alexandra Wolf-Asseburg and Iris Linde for excellent technical assistance as well as Timo Fritsch for outstanding animal care.

Conflict of interest

The authors declare that the research was conducted in the absence of any commercial or financial relationships that could be construed as a potential conflict of interest.

Publisher's note

Supplementary material

The Supplementary Material for this article can be found online at: https://www.frontiersin.org/articles/10.3389/fnmol.2023.1166900/full#supplementary-material

SUPPLEMENTARY FIGURE 1
Arrangement for triggering Optovin induced swimming upon UV illumination. **(A)** Arduino UNO board (left) connected to a power bank via Universal Serial Bus (USB) (not shown in image) and related circuits that are coupled to the breadboard with light emitting diode (LED) diodes of wavelength 405–412 nm (right). **(B)** Drawing showing the setup of Optovin-mediated swimming behavior in larvae. **(C)** Arduino script used to program the broad with ON-OFF time of UV illumination.

SUPPLEMENTARY FIGURE 2
Bath-application of CNQX inhibits PC activity in zebrafish larvae. **(A)** Schematic drawing of zebrafish head with green fluorescent PCs used for voltage-clamp recordings. **(B)** Tg(-7.5ca8:GFP)^{bz12} (Namikawa et al., 2019) expressing larvae with selective labeling of PCs by green fluorescence at 5 dpf were used for electrode positioning for whole cell-clamp recordings. **(C)** The correct morphology of the recorded cell was verified after electrophysiological recording by dye-filling of patched cells with the red fluorescence dye Alexa 594 followed by verification of colocalization of green and red fluorescence. **(D)** 20 μM CNQX suppressed PC spontaneous postsynaptic currents (sPSC) almost completely [compare example traces of wild type (black colored trace) PC to CNQX-exposed (gray colored trace) PC] in all recordings (n = 9, p < 0.005 Mann-Whitney rank sum test).

SUPPLEMENTARY FIGURE 3
Arrangement for optogenetic silencing of Purkinje cells (PCs). **(A)** Custom built illumination chamber with LED panel. **(B)** Set up illustrating generation of pulsed illumination of 517 nm monochromatic light (green color, 0.37, 0.52 mW/cm^2) that results in stimulating light-gated Arch3 proton efflux. **(C)** Equivalent illumination conditions (0.32, 0.45 mW/cm^2) were used for electrophysiological recordings to confirm that the delivered optical energy is sufficient to suppress PC activity (**Supplementary Figure 4**).

SUPPLEMENTARY FIGURE 4
Illumination of Arch3 expressing Purkinje cells (PCs) suppresses their neuronal activity. **(A)** Tg(Arch-tagRFP-T:PC:GCaMP5G)^{bz5} larvae were used for cell-attached recordings, while larvae were exposed to 517 nm green/yellow light (0.32 mW, continuous illumination for 30–60 s, **Supplementary Figure 3**) using a monochromator. **(B,C)** The correct morphology of the recorded cell was verified after electrophysiological recording by dye-filling of patched cells with the red fluorescence dye Alexa 594 followed by verification of colocalization of green and red fluorescence. **(D)** Upon 517 nm illumination (horizontal green bar indicates duration of illumination) action potential firing of PCs was transiently almost completely suppressed in Arch3 expressing PCs, (n = 5, p < 0.05 one way ANOVA with post-hoc Tukey test).

References

Borovac, J., Bosch, M., and Okamoto, K. (2018). Regulation of actin dynamics during structural plasticity of dendritic spines: Signaling messengers and actin-binding proteins. *Mol. Cell. Neurosci.* 91, 122–130. doi: 10.1016/j.mcn.2018.07.001

Brooks, J. X., Carriot, J., and Cullen, K. E. (2015). Learning to expect the unexpected: Rapid updating in primate cerebellum during voluntary self-motion. *Nat. Neurosci.* 18, 1310–1317. doi: 10.1038/nn.4077

Chow, B. Y., Han, X., Dobry, A. S., Qian, X., Chuong, A. S., Li, M., et al. (2010). High-performance genetically targetable optical neural silencing by light-driven proton pumps. *Nature* 463, 98–102. doi: 10.1038/nature08652

Colomer, J., and Means, A. R. (2007). Physiological roles of the Ca2+/CaM-dependent protein kinase cascade in health and disease. *Subcell. Biochem.* 45, 169–214. doi: 10.1007/978-1-4020-6191-2_7

Ebner, T. J., Wang, X., Gao, W., Cramer, S. W., and Chen, G. (2012). Parasagittal zones in the cerebellar cortex differ in excitability, information processing, and synaptic plasticity. *Cerebellum* 11, 418–419. doi: 10.1007/s12311-011-0347-1

Gibson, A. R., Robinson, F. R., Alam, J., and Houk, J. C. (1987). Somatotopic alignment between climbing fiber input and nuclear output of the cat intermediate cerebellum. *J. Comp. Neurol.* 260, 362–377. doi: 10.1002/cne.902600304

Gonzalez, L., Shumway, C., Morissette, J., and Bower, J. M. (1993). Developmental plasticity in cerebellar tactile maps: Fractured maps retain a fractured organization. *J. Comp. Neurol.* 332, 487–498. doi: 10.1002/cne.903320408

Gravel, C., and Hawkes, R. (1990). Parasagittal organization of the rat cerebellar cortex: Direct comparison of Purkinje cell compartments and the organization of the spinocerebellar projection. *J. Comp. Neurol.* 291, 79–102. doi: 10.1002/cne.902910107

Guggiana-Nilo, D. A., and Engert, F. (2016). Properties of the visible light phototaxis and UV avoidance behaviors in the larval zebrafish. *Front. Behav. Neurosci.* 10:160. doi: 10.3389/fnbeh.2016.00160

Harmon, T. C., Magaram, U., McLean, D. L., and Raman, I. M. (2017). Distinct responses of Purkinje neurons and roles of simple spikes during associative motor learning in larval zebrafish. *Elife* 6:e22537. doi: 10.7554/eLife.22537

Hibi, M., and Shimizu, T. (2012). Development of the cerebellum and cerebellar neural circuits. *Dev. Neurobiol.* 72, 282–301. doi: 10.1002/dneu.20875

Khilkevich, A., Zambrano, J., Richards, M.-M., and Mauk, M. D. (2018). Cerebellar implementation of movement sequences through feedback. *Elife* 7:e37443. doi: 10.7554/eLife.37443

Knogler, L. D., Kist, A. M., and Portugues, R. (2019). Motor context dominates output from Purkinje cell functional regions during reflexive visuomotor behaviours. *Elife* 8:e42138. doi: 10.7554/eLife.42138

Kokel, D., Cheung, C. Y. J., Mills, R., Coutinho-Budd, J., Huang, L., Setola, V., et al. (2013). Photochemical activation of TRPA1 channels in neurons and animals. *Nat. Chem. Biol.* 9, 257–263. doi: 10.1038/nchembio.1183

Lam, P.-Y., Mendu, S. K., Mills, R. W., Zheng, B., Padilla, H., Milan, D. J., et al. (2017). A high-conductance chemo-optogenetic system based on the vertebrate channel Trpa1b. *Sci. Rep.* 7:11839. doi: 10.1038/s41598-017-11791-z

Matsui, H., Namikawa, K., Babaryka, A., and Köster, R. W. (2014). Functional regionalization of the teleost cerebellum analyzed in vivo. *Proc. Natl. Acad. Sci. U.S.A.* 111, 11846–11851. doi: 10.1073/pnas.1403105111

McAllister, A. K. (2000). Cellular and molecular mechanisms of dendrite growth. *Cereb. Cortex* 10, 963–973. doi: 10.1093/cercor/10.10.963

McGaugh, J. L. (2000). Memory–a century of consolidation. *Science* 287, 248–251. doi: 10.1126/science.287.5451.248

Namikawa, K., Dorigo, A., Zagrebelsky, M., Russo, G., Kirmann, T., Fahr, W., et al. (2019). Modeling neurodegenerative spinocerebellar ataxia type 13 in zebrafish using a purkinje neuron specific tunable coexpression system. *J. Neurosci.* 39, 3948–3969. doi: 10.1523/JNEUROSCI.1862-18.2019

Peters, A., and Kaiserman-Abramof, I. (1970). The small pyramidal neuron of the rat cerebral cortex. The perikaryon, dendrites and spines. *Am. J. Anat.* 127, 321–355.

Pietri, T., Manalo, E., Ryan, J., Saint-Amant, L., and Washbourne, P. (2009). Glutamate drives the touch response through a rostral loop in the spinal cord of zebrafish embryos. *Dev. Neurobiol.* 69, 780–795. doi: 10.1002/dneu.20741

Provini, L., Marcotti, W., Morara, S., and Rosina, A. (1998). Somatotopic nucleocortical projections to the multiple somatosensory cerebellar maps. *Neuroscience* 83, 1085–1104. doi: 10.1016/S0306-4522(97)00477-6

Rogers, J. H., Ciossek, T., Menzel, P., and Pasquale, E. B. (1999). Eph receptors and ephrins demarcate cerebellar lobules before and during their formation. *Mech. Dev.* 87, 119–128. doi: 10.1016/S0925-4773(99)00154-9

Schlerf, J. E., Verstynen, T. D., Ivry, R. B., and Spencer, R. M. C. (2010). Evidence of a novel somatopic map in the human neocerebellum during complex actions. *J. Neurophysiol.* 103, 3330–3336. doi: 10.1152/jn.01117.2009

Schramm, P., Hetsch, F., Meier, J. C., and Köster, R. W. (2021). In vivo imaging of fully active brain tissue in awake zebrafish larvae and juveniles by skull and skin removal. *J. Vis. Exp.* e62166. doi: 10.3791/62166

Segal, M. (2010). Dendritic spines, synaptic plasticity and neuronal survival: Activity shapes dendritic spines to enhance neuronal viability. *Eur. J. Neurosci.* 31, 2178–2184. doi: 10.1111/j.1460-9568.2010.07270.x

Sengupta, M., and Thirumalai, V. (2015). AMPA receptor mediated synaptic excitation drives state-dependent bursting in Purkinje neurons of zebrafish larvae. *Elife* 4:e09158. doi: 10.7554/eLife.09158

Shimobayashi, E., and Kapfhammer, J. P. (2018). Calcium signaling, PKC gamma, IP3R1 and CAR8 link spinocerebellar ataxias and Purkinje cell dendritic development. *Curr. Neuropharmacol.* 16, 151–159. doi: 10.2174/1570159X15666170529104000

Sillitoe, R. V., Vogel, M. W., and Joyner, A. L. (2010). Engrailed homeobox genes regulate establishment of the cerebellar afferent circuit map. *J. Neurosci.* 30, 10015–10024. doi: 10.1523/JNEUROSCI.0653-10.2010

Takeuchi, M., Yamaguchi, S., Sakakibara, Y., Hayashi, T., Matsuda, K., Hara, Y., et al. (2017). Gene expression profiling of granule cells and Purkinje cells in the zebrafish cerebellum. *J. Comp. Neurol.* 525, 1558–1585. doi: 10.1002/cne.24114

Tanabe, K., Kani, S., Shimizu, T., Bae, Y.-K., Abe, T., and Hibi, M. (2010). Atypical protein kinase C regulates primary dendrite specification of cerebellar Purkinje cells by localizing Golgi apparatus. *J. Neurosci.* 30, 16983–16992. doi: 10.1523/JNEUROSCI.3352-10.2010

Theisen, U., Hennig, C., Ring, T., Schnabel, R., and Köster, R. W. (2018). Neurotransmitter-mediated activity spatially controls neuronal migration in the zebrafish cerebellum. *PLoS Biol.* 16:e2002226. doi: 10.1371/journal.pbio.2002226

Timmann, D., Drepper, J., Frings, M., Maschke, M., Richter, S., Gerwig, M., et al. (2010). The human cerebellum contributes to motor, emotional and cognitive associative learning. A review. *Cortex* 46, 845–857. doi: 10.1016/j.cortex.2009.06.009

Vibulyaseck, S., Luo, Y., Fujita, H., Oh-Nishi, A., Ohki-Hamazaki, H., and Sugihara, I. (2015). Compartmentalization of the chick cerebellar cortex based on the link between the striped expression pattern of aldolase C and the topographic olivocerebellar projection. *J. Comp. Neurol.* 523, 1886–1912. doi: 10.1002/cne.23769

Weber, T., and Köster, R. (2013). Genetic tools for multicolor imaging in zebrafish larvae. *Methods* 62, 279–291. doi: 10.1016/j.ymeth.2013.07.028

Westerfield, M. (2007). *The zebrafish book. A guide for the laboratory use of zebrafish (Danio rerio)*, 5th Edn. Eugene, OR: University of Orgeon.

White, J. J., Arancillo, M., Stay, T. L., George-Jones, N. A., Levy, S. L., Heck, D. H., et al. (2014). Cerebellar zonal patterning relies on Purkinje cell neurotransmission. *J. Neurosci.* 34, 8231–8245. doi: 10.1523/JNEUROSCI.0122-14.2014

Wullimann, M., Mueller, T., Distel, M., Babaryka, A., Grothe, B., and Köster, R. (2011). The long adventurous journey of rhombic lip cells in jawed vertebrates: A comparative developmental analysis. *Front. Neuroanat.* 5:27. doi: 10.3389/fnana.2011.00027

frontiers | Frontiers in Molecular Neuroscience

TYPE Brief Research Report
PUBLISHED 28 April 2023
DOI 10.3389/fnmol.2023.1161086

OPEN ACCESS

EDITED BY
Lilian Kisiswa,
Aarhus University, Denmark

REVIEWED BY
Luis R. Hernandez-Miranda,
Charité University Medicine Berlin, Germany
Antonio Gennaro Nicotera,
University of Messina, Italy

*CORRESPONDENCE
David F. Butler
✉ dfbutler@wustl.edu
Kathleen J. Millen
✉ kathleen.millen@seattlechildrens.org

†PRESENT ADDRESS
David F. Butler,
Division of Critical Care Medicine, Department of Pediatrics, Washington University School of Medicine, St. Louis, MO, United States

RECEIVED 07 February 2023
ACCEPTED 10 April 2023
PUBLISHED 28 April 2023

CITATION
Butler DF, Skibo J, Traudt CM and Millen KJ (2023) Neonatal subarachnoid hemorrhage disrupts multiple aspects of cerebellar development.
Front. Mol. Neurosci. 16:1161086.
doi: 10.3389/fnmol.2023.1161086

Neonatal subarachnoid hemorrhage disrupts multiple aspects of cerebellar development

David F. Butler[1*†], Jonathan Skibo[2], Christopher M. Traudt[3] and Kathleen J. Millen[2,4*]

[1]Division of Pediatric Critical Care, Seattle Children's Hospital, University of Washington, Seattle, WA, United States, [2]Center for Integrative Brain Research, Seattle Children's Research Institute, Seattle, WA, United States, [3]Salem Health Hospitals and Clinics, Salem, OR, United States, [4]Department of Pediatrics, University of Washington Medical School, Seattle, WA, United States

Over the past decade, survival rates for extremely low gestational age neonates (ELGANs; <28 weeks gestation) has markedly improved. Unfortunately, a significant proportion of ELGANs will suffer from neurodevelopmental dysfunction. Cerebellar hemorrhagic injury (CHI) has been increasingly recognized in the ELGANs population and may contribute to neurologic dysfunction; however, the underlying mechanisms are poorly understood. To address this gap in knowledge, we developed a novel model of early isolated posterior fossa subarachnoid hemorrhage (SAH) in neonatal mice and investigated both acute and long-term effects. Following SAH on postnatal day 6 (P6), we found significant decreased levels of proliferation with the external granular layer (EGL), thinning of the EGL, decreased Purkinje cell (PC) density, and increased Bergmann glial (BG) fiber crossings at P8. At P42, CHI resulted in decreased PC density, decreased molecular layer interneuron (MLI) density, and increased BG fiber crossings. Results from both Rotarod and inverted screen assays did not demonstrate significant effects on motor strength or learning at P35–38. Treatment with the anti-inflammatory drug Ketoprofen did not significantly alter our findings after CHI, suggesting that treatment of neuro-inflammation does not provide significant neuroprotection post CHI. Further studies are required to fully elucidate the mechanisms through which CHI disrupts cerebellar developmental programming in order to develop therapeutic strategies for neuroprotection in ELGANs.

KEYWORDS

cerebellar hemorrhage, cerebellar development, preterm brain injury, Purkinje cells, cerebellar granule cells

Introduction

Despite improvements in survival rates for extremely low gestational age neonates (ELGANs; <28 weeks gestation), ~50% of survivors go on to have significant neurodevelopmental dysfunction including cognitive, learning, and/or motor deficits. Many of these deficits do not seem to be explained by cerebral white matter injury and/or intraventricular hemorrhage, suggesting an alternate mechanism of injury (Nosarti et al., 2007; Limperopoulos et al., 2014). Recent data suggests that injury to the cerebellum contributes to neurodevelopmental deficits and that developmental disruption of the cerebellum has widespread effects on neurologic function (Haines et al., 2013; Dijkshoorn et al., 2020; Brossard-Racine and Limperopoulos, 2021; Spoto et al., 2021).

Between 20 and 40 weeks of gestation, cerebellar growth is vigorous, with the volume of the cerebellum increasing at least five-fold. This rapid growth is almost exclusively driven by massive proliferation of granule neuron progenitors in the external granule layer (EGL). These progenitors will then differentiate into cerebellar granule cells (GC) and migrate into to their final location beneath the developing Purkinje cells *via* fibers of Bergman Glial cells to form the internal granule cell layer (IGL) (Rakic, 1971; Abraham et al., 2001; Volpe, 2009; Consalez et al., 2020). As the cerebellum rapidly grows, the developing cerebellar circuitry is also undergoing rapid remodeling and maturation. Disruptions of this early circuitry alter long term cerebellar circuit maturity (Haldipur et al., 2011; Barron and Kim, 2020; van der Heijden and Sillitoe, 2021; van der Heijden et al., 2021) and deranged cerebro-cerebellar neuronal circuitry causing impaired cerebral development and profound neurologic dysfunction (Limperopoulos et al., 2010, 2014; Wang et al., 2014; D'Mello and Stoodley, 2015; Stoodley and Limperopoulos, 2016; Brossard-Racine and Limperopoulos, 2021).

Injury to the neonatal cerebellum has been increasingly recognized in the ELGANs population. Many factors, including nutritional deficits, infection, inflammation and glucocorticoid exposure can disrupt cerebellar development in preterm infants (Buddington et al., 2018; Iskusnykh et al., 2018, 2021; Gano and Barkovich, 2019; Chizhikov et al., 2020; Iskusnykh and Chizhikov, 2022). Cerebellar hemorrhagic injury (CHI) is a relatively frequent finding in preterm infants, and even more common in severely premature infants (Steggerda et al., 2009; Boswinkel et al., 2019; Villamor-Martinez et al., 2019). Radiologic evidence of cerebellar subarachnoid and parenchymal hemorrhages correlates with poor neurodevelopmental outcomes (Johnsen et al., 2005; Steggerda et al., 2009; Zayek et al., 2012; Matsufuji et al., 2017; Boswinkel et al., 2019; Brossard-Racine and Limperopoulos, 2021). Hemorrhage is also highly associated with cerebellar hypoplasia (Volpe, 2009; Aldinger et al., 2019; Gano and Barkovich, 2019; Scelsa et al., 2022). Additionally, documented fetal cerebellar hemorrhage has been associated with cerebellar hypoplasia and neurodevelopmental deficits in full term children (Poretti et al., 2008). Furthermore, cerebellar hypoplasia on MRI has been shown to be more predictive of neurodevelopmental deficits than supratentorial injuries such as intraventricular hemorrhage or white matter injury (Limperopoulos et al., 2007).

While hemorrhage has been associated with cerebellar hypoplasia, the underlying injury mechanism is not fully understood. Extravasated blood and/or blood components have been shown to be injurious to multiple cell populations in the developing cerebral cortex, including neurons, glia, and oligodendrocytes (Xue et al., 2003; Vinukonda et al., 2012). Lypophosphatidic acid (LPA), a component of serum, induces hydrocephalus when injected into the lateral ventricles of embryonic mice due to ependymal injury and progenitor delamination into the lateral ventricles (Yung et al., 2011). Additionally, hemosiderin deposition may contribute to increases in reactive oxygen species (Volpe, 2009). However, the cerebellar-specific literature is very limited. We previously reported that a rabbit model of cerebellar subarachnoid hemorrhage induced in neonatal rabbits *via* systemic glycerol administration is invalid since glycerol itself is toxic to cerebellar development even in the absence of hemorrhage (Traudt et al., 2014). One of the first mouse models of neonatal cerebellar hemorrhage involved intraventricular injection of bacterial collagenase into the fourth ventricle of early post-natal mice, when maximal EGL proliferation occurs in this species (Yoo et al., 2014). Subsequent hematomas in the fourth ventricle and on the cerebellar surface caused decreased granule cell density, decreased cerebellar volume and resulted abnormal open field testing behavior, and motor impairment on Rotarod testing in older mice (Yoo et al., 2014), which is exacerbated by inflammation (Tremblay et al., 2017). The effects of isolated posterior fossa blood exposure in the absence of intraventricular hemorrhage on cerebellar development have never been directly tested *in vivo*.

In this study, we developed a novel model of isolated posterior fossa subarachnoid hemorrhage in neonatal mice to directly examine the effects of blood exposure on cerebellar development. Our model avoids direct injury to the cerebellar parenchyma and isolates injury related to blood components. We examined acute and long-term effects on cerebellar biology, anatomy, and animal behavior following CHI. We hypothesized that exposure of the developing cerebellum to blood would result in disruption to multiple developmental programs leading to long-term cellular/anatomic abnormalities and motor deficits. Secondarily, we hypothesized that neuroinflammation may strongly contribute to the underlying injury mechanism and that treatment with an anti-inflammatory may be neuroprotective.

Materials and methods

Animals

This study was carried out in accordance with the recommendations in the Guide for the Care and Use of Laboratory Animals of the National Institutes of Health and was approved by the Institutional Animal Care and Use Committee (IACUC) at University of Washington (Protocol Number: IACUC00006). Mice from the CD1 strain were bred and housed in Optimice cages with aspen bedding at the Seattle Children's Research Institute specific pathogen-free (SPF) vivarium facility on a 14/10 hour light/dark cycle. All mice were monitored closely by both laboratory and veterinary staff. The day of birth was designated as postnatal day 0 (P0).

Posterior fossa injection procedure

On P6, mice underwent posterior fossa injections under anesthesia with isoflurane. Peak EGL proliferation occurs at P6. We chose this to model the timing of injury in ELGANs which also correlates with peak EGL proliferation. A single 8–10 mm vertical incision was made overlying the posterior calvaria (Figure 1A). Trunk blood from an adult CD1 mouse was obtained and anticoagulated with heparin at a ratio of 100 μl heparin to 900 μl of blood. For the CHI group, 20 μl of trunk blood was injected into the posterior fossa with a 28-gauge insulin needle at the midline position, 2.5 mm rostral from Lambda under direct visualization. Control group animals underwent posterior fossa injection with

20 μl of heparin containing artificial cerebrospinal fluid (aCSF) (Wei and Ramirez, 2019) as outlined above. Following injection, the needle was gently removed, and the skull defect was covered with Vetbond™ tissue adhesive (3M). Skin closure was performed with 7.0 Ethilon® nylon suture (Ethicon). Animals received either buprenorphine (opioid: 2 μg/g of body weight) or ketoprofen (non-steroidal anti-inflammatory: 5 μg/g of body weight) for analgesia, to assess the role of inflammation in injury. Mice were warmed and monitored closely during the entire procedure and recovered under a heat lamp until they were noted to have consistent spontaneous movements prior to return to their home cages.

Sample preparation

On P8 or P42, mice were pulsed with 5-bromo-2'-deoxyuridine (BrdU) *via* intraperitoneal injections (10 μg/g of body weight) 2 h prior to sacrifice. P8 was chosen to assess the immediate impact of injury, while P42 was chosen to assess the outcome, when cerebellar maturation is complete. On P8, mice were sacrificed *via* rapid decapitation, tissue was harvested and then fixed in 4% paraformaldehyde (PFA) overnight. On P42, mice underwent both cardiac fixation with 4% PFA infusion and drop fixation in 4% PFA overnight. At both timepoints, tissue was then equilibrated in 30% sucrose made in phosphate-buffered saline (PBS). Cerebellar tissue was isolated, placed in Tissue-Tek® O.C.T compound and stored at−80°C. Sections were performed at 18–20 μm on a freezing microtome.

Immunohistochemistry

Sections were dried at room temperature for 60 min, baked at 45°C for 30 min, and washed in PBS. Sections undergoing BrdU staining for were bathed in 2N HCl for 30 min. All sections underwent antigen retrieval by boiling sections in 10 mM sodium citrate for 10–15 min. Sections were then washed three times with PBS with 0.125% Triton X-100 (PBX) and blocked in 5% donkey serum in PBX in a humidified chamber for 90 min at room temperature. Sections were incubated at 4°C with primary antibodies in a humidified chamber overnight. The following day, sections were washed in PBX and then incubated with species-specific secondary antibodies conjugated with Alexa 488, 568 or 594 fluorophores (Invitrogen) for 90 min at room temperature. Sections were counterstained with DAPI (4',6-Diamidino-2-Phenylindole, Dihydrochloride; Invitrogen; D1306) and cover-slipped with Fluoromount-G (Southern Biotech, Cat. No. 0100-01). Primary antibodies used included: rat anti-BrdU (1:100, Abcam), mouse anti-Calbindin (1:20, Abcam), rabbit anti-GFAP (1:1,500, Dako), rabbit anti-Ki67 (1:150, Novus), mouse anti-Parvalbumin (1:5,000, Swant), rabbit anti-BLBP (1:400, Abcam).

Rotarod assay

At P35, all mice underwent motor learning and coordination testing using the Rota-Rod 2 (Med Associates Inc.). On day 1 of testing, each mouse underwent three trials, and on days 2 and 3, each mouse underwent two trials. Each trial consisted of programmed acceleration from 4 to 40 RPM over a period of 3 min and were separated by 120 min. The time spent on the rotarod was recorded for each trial. Statistical significance was defined as $p < 0.05$ by two-way ANOVA with Tukey's post-test and performed in GraphPad Prism v8.4.1(460) (GraphPad Software LLC., San Diego, USA).

Inverted screen test assay

At P38, all mice underwent strength and coordination testing using the inverted screen test (Kondziella, 1964). Mice were placed in the center of a wire mesh, which was then rotated into the inverted position (mouse headfirst) and held approximately 30 cm above a padded surface for a maximum of 120 s. The time spent in the inverted position was recorded for each mouse. Statistical significance was defined as $p < 0.05$ by one-way ANOVA with Tukey's post-test and performed in GraphPad Prism v8.4.1(460) (GraphPad Software LLC., San Diego, USA).

Quantitative analysis

All image and quantitative analysis were performed with Olympus VS-Desktop software and ImageJ 1.52p (NIH, Bethesda, Maryland, USA) software. Sections underwent extended focal imaging (EFI) at 10X and 20X with the Olympus VS-120 slide-scanner microscope and confocal imaging at 20X and 40X. To evaluate the local effect of hemorrhage at P8, areas of red blood cell (RBC) aggregation were identified, and neighboring lobules were selected for analysis. Quantitative data was collected from comparable sections from each treatment group. At P8, measurements of EGL thickness ($n = 2$ sections/animal, 4 animals/treatment group), Calbindin$^+$ PC density ($n = 4$ sections/animal, three animals/treatment group), GFAP$^+$ Bergmann glial (BG) fiber crossings ($n = 3$ sections/animal, three animals/treatment group), and BrDU/Ki67$^+$ labeling index (BrDU/Ki67$^+$ cells/DAPI$^+$ cells) were obtained ($n = 3$ sections/animal, three animals/treatment group). At P42, measurements of PC density, BG fiber crossings, and Parvalbumin$^+$ molecular layer interneuron (MLI) density ($n = 3$ sections/animal, three animals/treatment group) were obtained from lobules VI-X. Statistical significance was defined as $p < 0.05$ by one-way ANOVA with Tukey's post-test and performed in GraphPad Prism v8.4.1(460) (GraphPad Software LLC., San Diego, USA).

Results

Blood exposure at P6, during peak EGL proliferation, caused significant abnormalities in adjacent regions by P8

As shown in Figure 1B, regions of blood exposure were readily identified and we limited our analyses to these regions

10.3389/fnmol.2023.1161086

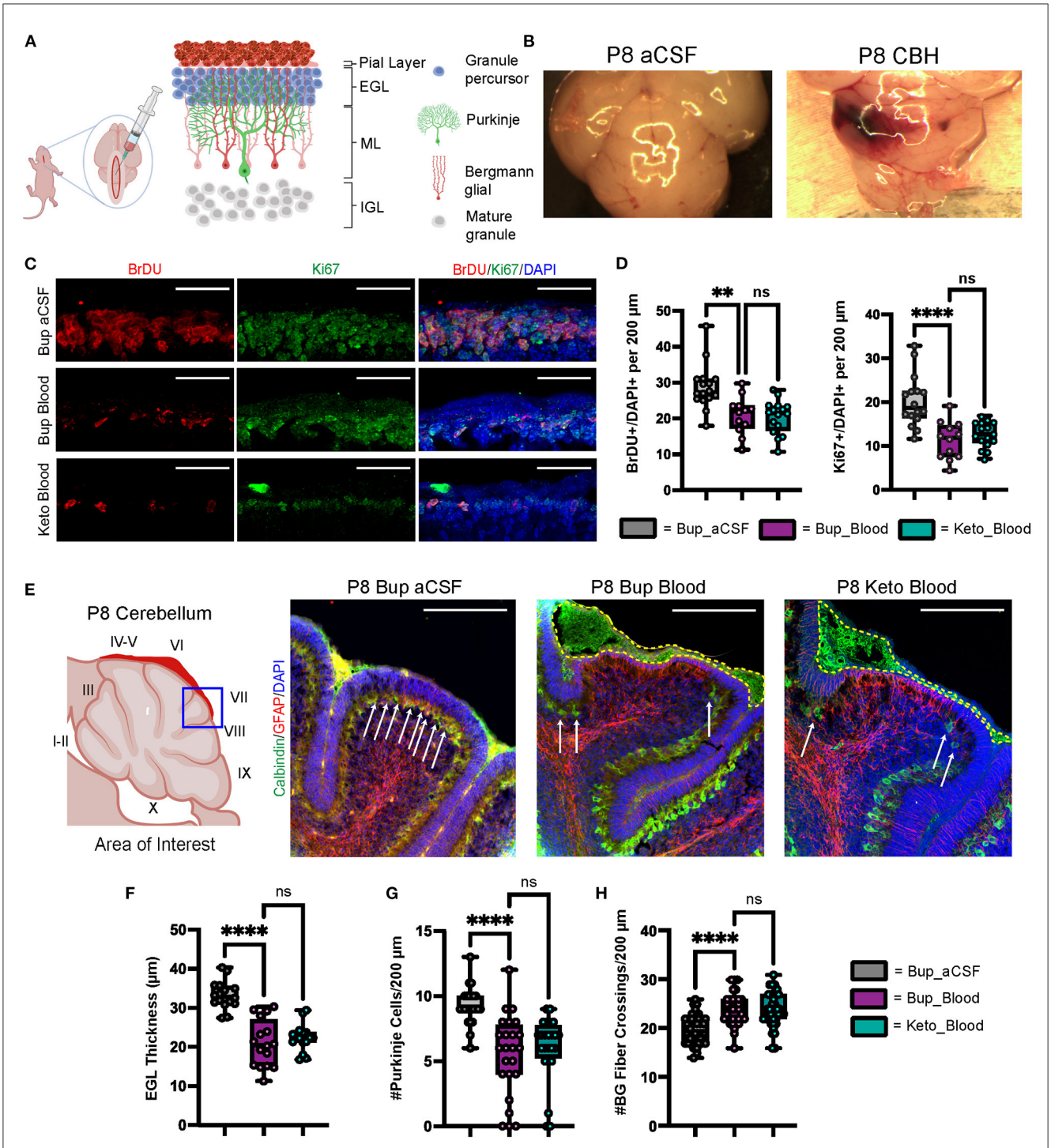

FIGURE 1
CHI results in decreased BrDU and Ki67 labeling indices, thinning of the EGL, decreased PC density, and increased BG fiber crossings at P8. **(A)** Schematic illustrating isolated posterior fossa hemorrhage model with typical P6 cerebellar architecture. **(B)** Representative comparative images of gross findings between aCSF and CHI groups; note large hematoma formation overlying left cerebellar hemisphere in the CHI specimen. **(C)** Representative confocal images at 40X of BrDU and Ki67 staining within the EGL. Only cells within the EGL were included in analysis. Scale bars are 25 µm. **(D)** Quantification of labeling indices for BrDU (left) and Ki67 (right); data obtained from 200 µm segment from lobule VI and VII ($N = 2$, $n = 12$ for Bup_Blood; $N = 3$, $n = 16$ for Bup_aCSF and Keto_Blood). **(E)** Representative confocal images at 20X magnification of lobule VII demonstrating differences in local findings including presence of large RBC collections (yellow dashed outline), PC density (white arrows), thickness of EGL, and architecture of BG fibers. Scale bars are 100 µm. **(F)** Quantification of EGL thickness for all treatment groups ($N = 4$, $n = 16$). **(G)** Quantification of PC density in lobule VI and VII for all treatment groups ($N = 3$, $n = 24$). **(H)** Quantification of BG fiber crossings in lobule I, VII-IX for all treatment groups ($N = 3$, $n = 27$). Significance defined as $p < 0.05$ by one-way ANOVA with Tukey post-test. Data are presented as SEM with minimum and maximum values. N = number of animals per group included for analysis; n = number of section segments per group included for analysis. **p-value ≤ 0.01; ****p-value ≤ 0.0001.

10.3389/fnmol.2023.1161086

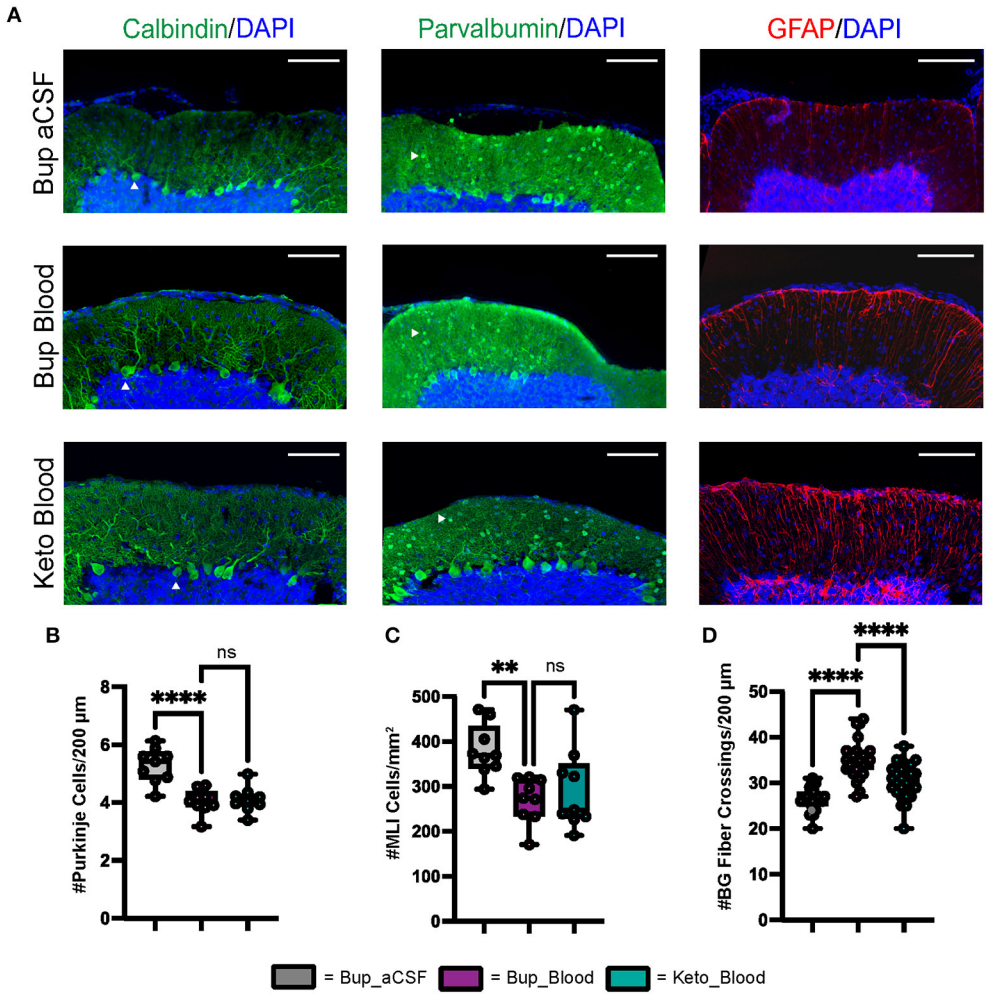

FIGURE 2
CHI results in decreased PC density, decreased MLI density, and increased BG fiber crossings within the ML at P42. **(A)** Representative confocal images at 20X demonstrating difference in PC (white arrowhead) density (left), MLI (white arrowhead) density (middle), and BG fiber density and morphology (right). Scale bars are 100 μm. **(B)** Quantification of PC density in lobule VI-X for all treatment groups ($N = 3$, $n = 9$). **(C)** Quantification of MLI density in lobule VI-X for all treatment groups ($N = 3$, $n = 9$). **(D)** Quantification of BG fiber crossings within the ML for all treatment groups ($N = 3$, $n = 27$). Significance defined as $p < 0.05$ by one-way ANOVA with Tukey's post-test. Data are presented as SEM with minimum and maximum values. N = number of animals per group included for analysis, n = number of section segments per group included for analysis.

in vermis and paravermis cerebellar lobules V-VII. Compared with aCSF at P8, blood exposure resulted in a significantly decreased EGL proliferation as measured by BrdU and Ki67 labeling ($p = 0.0015$ and $p < 0.0001$, respectively) (Figures 1C, D). Blood exposure also significantly decreased EGL thickness compared to aCSF ($p < 0.0001$) (Figures 1C, E, F). We also saw significant loss of (Calbindin +) Purkinje cells in regions of blood exposure (Figures 1E, G). GFAP+ Bergman glial fiber crossings were significantly increased following blood exposure compared to aCSF-buprenorphine ($p < 0.0001$) (Figures 1E, H) with erratic Bergman glial fiber branching and altered fiber architecture, compared to the typical ordered fiber structure seen in the aCSF groups. Additionally, breaks in Bergman glial fibers and endplate detachment were noted (Figure 1E and not shown). There were no differences between blood exposed animals that received buprenorphine vs. ketoprofen for BrdU labeling, Ki67 labeling, EGL thickness, Purkinje cell density, and Bergman glial crossings ($p = 0.9729$, $p = 0.7645$, $p = 0.63$, $p = 0.6873$, and $p = 0.9531$, respectively).

Regional morphological changes were persistant at P42, in the mature cerebellum

Similar to findings at P8, blood exposure was associated with decreased Purkinje cell density at P42 ($p < 0.0001$) (Figures 2A, B). Blood exposure was also associated with decreased MLI density compared to aCSF ($p = 0.0058$) (Figures 2A, C). There was no significant difference between blood exposed animals that received ketoprofen vs. buprenorphine for PC density and MLI density ($p = 0.9665$ and $p = 0.7783$, respectively) (Figures 2A–C).

Similar to findings at P8, blood exposure was associated with abnormal Bergman glial fiber branching and increased fiber crossings in animals that received buprenorphine at P42

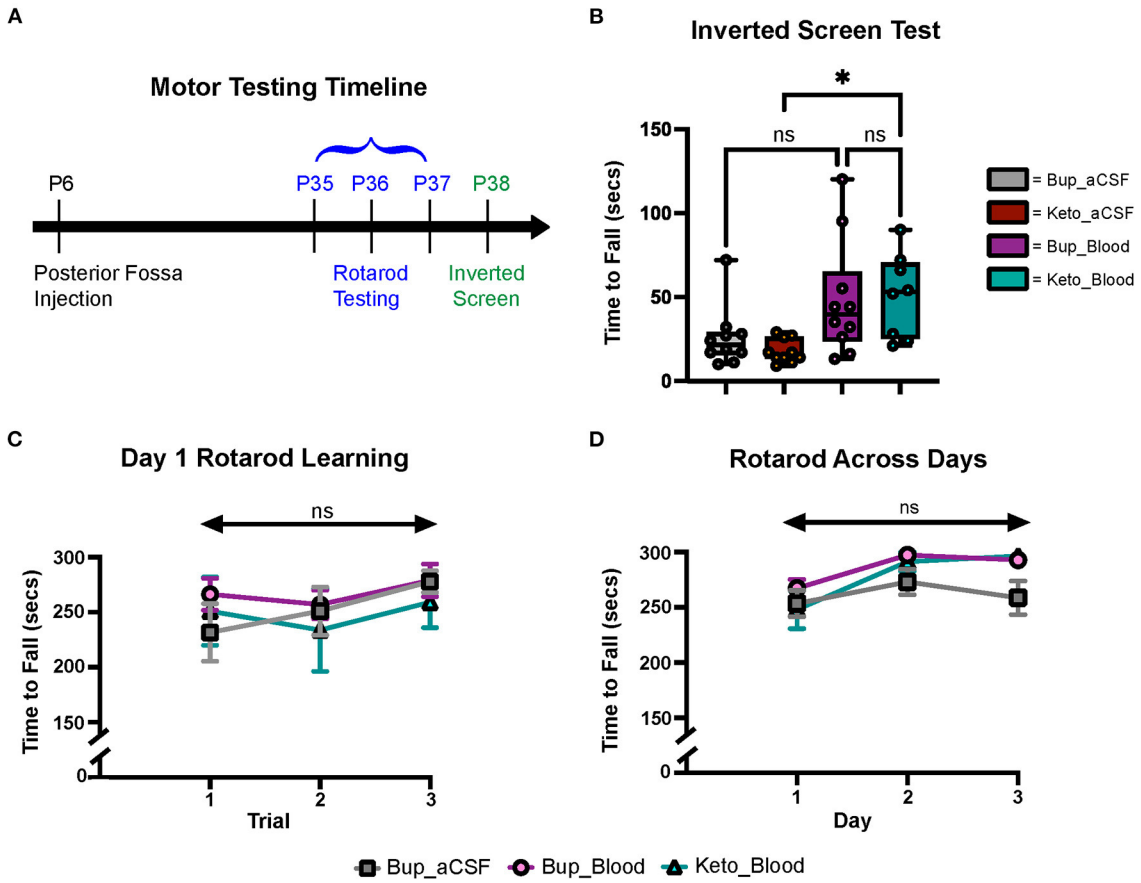

FIGURE 3
CHI did not result in significant motor learning/coordination deficits. **(A)** Schematic of motor testing assays and timeline. **(B)** Quantification of time to fall for the inverted screen test for all groups ($N = 10$*)†. **(C)** Quantification of the time to fall for Day 1 of Rotarod training for all groups ($N = 10$*)‡. **(D)** Quantification of the time to fall for Days 1-3 of Rotarod training for all groups ($N = 10$*)‡. Data are presented as mean ± SEM **(B)** or SEM with minimum and maximum values **(C, D)**. N = number of animals per group included for analysis. *Keto_Blood group with $N = 8$. †Significance defined as $p < 0.05$ by one-way ANOVA with Tukey's post-test. ‡Significance defined as $p < 0.05$ by two-way ANOVA with Tukey's post-test.

($p < 0.0001$) (Figures 2A, D). Blood exposed animals that received ketoprofen had significantly fewer Bergman glial fiber crossings compared to those receiving buprenorphine ($p < 0.0001$) (Figure 2D). Blood exposure did not result in significant difference in Bergman glial soma density, either in typical position or ectopic position within the molecular layer (Supplementary Figure 1).

Neonatal blood exposure did not result in significant gross motor learning/coordination deficits in older animals

Gross motor learning and coordination were assessed in mature animals at P35–38 (Figure 3A). Results from the inverted screen test demonstrated no significant differences between the blood and aCSF animals receiving buprenorphine ($p = 0.1580$); however, animals in the blood-ketoprofen group were noted to remain suspended for significantly longer than animals in the aCSF-ketoprofen group ($p = 0.024$) (Figure 3B). There were no significant differences noted between groups on Rotarod testing (Figures 3C, D).

Discussion

To examine how preterm and neonatal cerebellar bleeds during maximal EGL proliferation in humans alters cerebellar development, we developed a novel murine model of isolated posterior fossa subarachnoid hemorrhage at P6, when maximal EGL proliferation occurs in mice. Subarachnoid blood exposure resulted in immediate and sustained morphological abnormalities to multiple cell populations immediately adjacent to the blood, especially granule and Purkinje cells, BG, and MLIs.

Multiple studies have demonstrated that PCs are exquisitely sensitive to injury, with hypoxic and ischemic insults resulting in damage to PCs in both animal models and human studies (Barenberg et al., 2001; Hausmann et al., 2007; Kántor et al., 2007; Bartschat et al., 2012; Sathyanesan et al., 2018). Importantly, PCs are essential to the normal development of the cerebellum, as PC-derived Sonic hedgehog (Shh) protein is a key driver of granule cell precursor proliferation within the overlying EGL (Smeyne et al., 1995; Dahmane and Ruiz i Altaba, 1999; Wechsler-Reya and Scott, 1999; Lewis et al., 2004; Fleming and Chiang, 2015; De Luca et al., 2016). In the present study, subarachnoid hemorrhage was modeled

at P6, a key time point in cerebellar development characterized by rapid expansion of granule neuron progenitorss in the EGL and active Shh expression by PCs. Following CHI, we found localized thinning of the EGL and decreased EGL BrDU/Ki67 labeling at P8 (Figure 1). No changes to TUNEL/Caspase 3 staining were evident at P8 (data not shown) and we did not conduct immediate pulse chase experiments to determine if early differentiation contributed to this phenotype. However, it is likely that EGL thinning was result of a combination of immediate cell death, increased differentiation, and proliferative loss of EGL progenitors at these early timepoints immediately after injury. We also saw immediate localized loss of PCs, with significant decreased density at P8 that was sustained at P42 (Figures 1, 2). This result is in contrast to Yoo et al. (2014), who reported no significant change in PC count in adult mice after induction of neonatal cerebellar hemorrhage with a bacterial collagenase injection model. One caveat to our study is that we injected adult vs. age matched blood. We cannot distinguish if loss is due to a direct effect on each population independently, however, loss of PC derived Shh mitotic most certainly contributed to diminished granule cell precursor proliferation.

Recently, Bayin et al. (2018) demonstrated that the developing mouse cerebellum has intrinsic capacity for PC regeneration/replenishment by immature PC precursors. The regeneration capacity of these cells decreases during the first postnatal week at ∼P5 (Bayin et al., 2018). In this study, blood exposure at P6 resulted in persistent decreases in PC density at P42, demonstrating significant long-term effect of CHI occurring at this developmental timepoint on the PC population (Figure 2B). This is important, as PC loss has been associated with multiple neurodevelopmental disorders in children, including autism spectrum disorder (ASD), many of which are present in ELGANs post cerebellar hemorrhage (Fatemi et al., 2002; Jeong et al., 2014; Skefos et al., 2014). Additionally, this finding is supportive of the limited replenishment capacity of the mouse cerebellum after the first postnatal week.

In addition to significant PC loss, our results demonstrate CHI has long-term effects on MLIs, with significantly decreased MLI density noted at P42 (Figure 2C). Interneuron precursor cells undergo significant proliferation and migration during development of the cerebellum, a process which is supported by PC (Fahrion et al., 2013; Galas et al., 2017). Specifically, PC-derived Shh has been demonstrated to regulate neural stem-cell like primary progenitors within the WM which give rise to inhibitory interneurons (Fleming et al., 2013). Later in development, two subtypes (Stellate cells and Basket cells) will migrate into the cortex, a process which is active in mice until P16 and may be disrupted by early postnatal insults (Zhang and Goldman, 1996). Recently, data from Sergaki et al. (2017) demonstrated that neurotrophic factors expressed by PCs help regulate MLI survival, suggesting that damage to PCs in the postnatal cerebellum may also result in decreased MLI survival. We postulate that CHI induced PC loss may result in impaired interactions between PCs and MLIs, resulting in diminished development of the MLI population.

BG are specialized unipolar astrocytes which have been found to guide GC precursor migration from the EGL to the IGL and may contribute to PC dendrite maturation (Rakic, 1971; Yamada et al., 2000; Lippman et al., 2008; Cheng et al., 2018). We found that CHI was associated with increased BG fiber crossings and abnormal fiber architecture at both P8 and P42 (Figures 1E, H, D), but no difference in BG soma density (Supplementary Figure 1A). These data suggest that CHI primarily affects the branching of BG fibers rather than proliferation or maintenance of the BG population. The increase in fiber crossings likely represents reactive gliosis in response to CHI, as immature BG have previously been shown to be capable of increasing GFAP expression in response to injury (Lafarga et al., 1998).

Despite effects on multiple cell types within the developing cerebellum, we did not see statistically significant motor deficits on Rotarod or inverted screen test assays following CHI (Figures 3B–D). Subjectively, mice in the CHI treatment groups were noted to spend more time clinging to the rotating rod and less time demonstrating coordinated walking during the Rotarod trials compared to the aCSF mice. Additionally, mice in the aCSF groups exhibited increased exploratory behavior during the inverted screen test, while CHI mice tended to remain in a small area with less movement. It is possible that this increase in exploratory behavior resulted in increased likelihood of grip loss and falling from the wire mesh, explaining why mice in the Keto-aCSF group fell off of the mesh more quickly than mice in the Keto-CHI group (Figure 3B). Moreover, it is possible that subtle motor deficits may have been found utilizing different behavior assays, such as eyeblink conditioning or vestibulo-ocular reflex analysis. This is a limitation of our current study and requires further investigation to understand the relationship between CHI and motor deficits. There is ample evidence from human cerebellar bleed patients that severity of functional deficits is dependent on injury size and topography (Brossard-Racine and Limperopoulos, 2021).

Secondarily, we compared the use of the opiate buprenorphine and the non-steroidal anti-inflammatory drug (NSAID) ketoprofen in order to investigate the possible role of neuroinflammation in injury. The use of ketoprofen in our model was associated with variable results, but did not demonstrate a significant neuroprotective effect. In the acute injury phase (P6-8), we found no significant difference post CHI in EGL thickness, PC density, BrDU/Ki67 labeling indices, and BG crossings (Figure 1) between buprenorphine and ketoprofen cohorts. Similarly, we saw no significant difference in PC density, MLI density, oligodendrocyte density, or BG soma density at P42 (Figure 2; Supplementary Figure 1). We did see a significant decrease in BG fiber crossings at P42 in CHI mice treated with ketoprofen compared to those treated with buprenorphine (Figure 2D). Taken together, these data suggest that anti-inflammatory treatment does not have a profound protective effect on cerebellar development in our model of CHI; however, additional studies are required to further elucidate the role of neuroinflammation, particularly with regards to reactive Bergmann gliosis.

In summary, we developed a novel neonatal mouse model of isolated posterior fossa SAH to model neonatal CHI, directly examining the effects of blood exposure on cerebellar development.

Our data demonstrates that exposure of the developing cerebellum to blood results in immediate disruptions to multiple aspects of cellular development and most strongly suggests the involvement of PC loss in the pathophysiology.

Data availability statement

The raw data supporting the conclusions of this article will be made available by the authors, without undue reservation.

Ethics statement

The animal study was reviewed and approved by Institutional Animal Care and Use Committee University of Washington.

Author contributions

This study was conceived by KM, DB, JS, and CT. All experiments were designed and performed by DB, CT, and JS. KM and DB wrote the manuscript with input from all authors. All authors contributed to the article and approved the submitted version.

Funding

This work was funded by NIH R37NS095733 to KM.

Conflict of interest

The authors declare that the research was conducted in the absence of any commercial or financial relationships that could be construed as a potential conflict of interest.

Publisher's note

Supplementary material

The Supplementary Material for this article can be found online at: https://www.frontiersin.org/articles/10.3389/fnmol.2023.1161086/full#supplementary-material

SUPPLEMENTARY FIGURE 1
CHI did not result in significant differences in BG soma density or ectopic positioning of BG soma at P42. **(A)** Quantification of BG soma density for all treatment groups ($N = 1$, $n = 9$). **(B)** Quantification of BG soma density noted in ectopic positioning for all treatment groups ($N = 1$, $n = 9$). Significance defined as $p < 0.05$ by one-way ANOVA with Tukey's post-test. Data are presented as SEM with minimum and maximum values. N = number of animals per group included for analysis, n = number of sections per group included for analysis.

References

Abraham, H., Tornoczky, T., Kosztolanyi, G., and Seress, L. (2001). Cell formation in the cortical layers of the developing human cerebellum. *Int. J. Dev. Neurosci.* 19, 53–62. doi: 10.1016/S0736-5748(00)00065-4

Aldinger, K. A., Timms, A. E., Thomson, Z., Mirzaa, G. M., Bennett, J. T., Rosenberg, A. B., et al. (2019). Redefining the etiologic landscape of cerebellar malformations. *Am. J. Hum. Genet.* 105, 606–615. doi: 10.1016/j.ajhg.2019.07.019

Barenberg, P., Strahlendorf, H., and Strahlendorf, J. (2001). Hypoxia induces an excitotoxic-type of dark cell degeneration in cerebellar Purkinje neurons. *Neurosci. Res.* 40, 245–254. doi: 10.1016/S0168-0102(01)00234-6

Barron, T., and Kim, J. H. (2020). Preterm birth impedes structural and functional development of cerebellar purkinje cells in the developing baboon cerebellum. *Brain Sci.* 10:897. doi: 10.3390/brainsci10120897

Bartschat, S., Fieguth, A., Könemann, J., Schmidt, A., and Bode-Jänisch, S. (2012). Indicators for acute hypoxia–an immunohistochemical investigation in cerebellar Purkinje-cells. *Forensic Sci. Int.* 223, 165–170. doi: 10.1016/j.forsciint.2012.08.023

Bayin, N. S., Wojcinski, A., Mourton, A., Saito, H., Suzuki, N., and Joyner, A. L. (2018). Age-dependent dormant resident progenitors are stimulated by injury to regenerate Purkinje neurons. *Elife* 7. doi: 10.7554/eLife.39879.034

Boswinkel, V., Steggerda, S. J., Fumagalli, M., Parodi, A., Ramenghi, L. A., Groenendaal, F., et al. (2019). The CHOPIn study: a multicenter study on cerebellar hemorrhage and outcome in preterm infants. *Cerebellum* 18, 989–998. doi: 10.1007/s12311-019-01053-1

Brossard-Racine, M., and Limperopoulos, C. (2021). Cerebellar injury in premature neonates: Imaging findings and relationship with outcome. *Semin. Perinatol.* 45, 151470. doi: 10.1016/j.semperi.2021.151470

Buddington, R. K., Chizhikov, V. V., Iskusnykh, I. Y., Sable, H. J., Sable, J. J., Holloway, Z. R., et al. (2018). A phosphatidylserine source of docosahexanoic acid improves neurodevelopment and survival of preterm pigs. *Nutrients* 10:637. doi: 10.3390/nu10050637

Cheng, F. Y., Fleming, J. T., and Chiang, C. (2018). Bergmann glial Sonic hedgehog signaling activity is required for proper cerebellar cortical expansion and architecture. *Dev. Biol.* 440, 152–166. doi: 10.1016/j.ydbio.2018.05.015

Chizhikov, D., Buddington, R. K., and Iskusnykh, I. Y. (2020). Effects of phosphatidylserine source of docosahexaenoic acid on cerebellar development in preterm pigs. *Brain Sci.* 10:475. doi: 10.3390/brainsci10080475

Consalez, G. G., Goldowitz, D., Casoni, F., and Hawkes, R. (2020). Origins, development, and compartmentation of the granule cells of the cerebellum. *Front. Neural Circuits* 14:611841. doi: 10.3389/fncir.2020.611841

Dahmane, N., and Ruiz i Altaba, A. (1999). Sonic hedgehog regulates the growth and patterning of the cerebellum. *Development* 126, 3089–3100. doi: 10.1242/dev.126.14.3089

De Luca, A., Cerrato, V., Fuc,à, E., Parmigiani, E., Buffo, A., and Leto, K. (2016). Sonic hedgehog patterning during cerebellar development. *Cell. Mol. Life Sci.* 73, 291–303. doi: 10.1007/s00018-015-2065-1

Dijkshoorn, A. B. C., Turk, E., Hortensius, L. M., van der Aa, N. E., Hoebeek, F. E., Groenendaal, F., et al. (2020). Preterm infants with isolated cerebellar hemorrhage show bilateral cortical alterations at term equivalent age. *Sci. Rep.* 10, 5283. doi: 10.1038/s41598-020-62078-9

D'Mello, A. M., and Stoodley, C. J. (2015). Cerebro-cerebellar circuits in autism spectrum disorder. *Front. Neurosci.* 9, 408. doi: 10.3389/fnins.2015.00408

Fahrion, J., Komuro, Y., Ohno, N., Littner, Y., Nelson, C., Kumada, T., et al. (2013). Cerebellar patterning. *Comprehensive Developmental Neuroscience: Patterning and Cell Type Specification in the Developing CNS and PNS*, 211–225. doi: 10.1016/B978-0-12-397265-1.00042-3

Fatemi, S. H., Halt, A. R., Realmuto, G., Earle, J., Kist, D. A., Thuras, P., et al. (2002). Purkinje cell size is reduced in cerebellum of patients with autism. *Cell. Mol. Neurobiol.* 22, 171–175. doi: 10.1023/A:1019861721160

Fleming, J., and Chiang, C. (2015). The Purkinje neuron: A central orchestrator of cerebellar neurogenesis. *Neurogenesis* 2:e1025940. doi: 10.1080/23262133.2015.1025940

Fleming, J. T., He, W., Hao, C., Ketova, T., Pan, F. C., Wright, C. C., et al. (2013). The Purkinje neuron acts as a central regulator of spatially and functionally distinct cerebellar precursors. *Dev. Cell* 27, 278–292. doi: 10.1016/j.devcel.2013.10.008

Galas, L., Bénard, M., Lebon, A., Komuro, Y., Schapman, D., Vaudry, H., et al. (2017). Postnatal migration of cerebellar interneurons. *Brain Sci.* 7:62. doi: 10.3390/brainsci7060062

Gano, D., and Barkovich, A. J. (2019). Cerebellar hypoplasia of prematurity: causes and consequences. *Handb. Clin. Neurol.* 162, 201–216. doi: 10.1016/B978-0-444-64029-1.00009-6

Haines, K. M., Wang, W., and Pierson, C. R. (2013). Cerebellar hemorrhagic injury in premature infants occurs during a vulnerable developmental period and is associated with wider neuropathology. *Acta. Neuropathol. Commun.* 1, 69. doi: 10.1186/2051-5960-1-69

Haldipur, P., Bharti, U., Alberti, C., Sarkar, C., Gulati, G., Iyengar, S., et al. (2011). Preterm delivery disrupts the developmental program of the cerebellum. *PLoS ONE* 6:e23449. doi: 10.1371/journal.pone.0023449

Hausmann, R., Seidl, S., and Betz, P. (2007). Hypoxic changes in Purkinje cells of the human cerebellum. *Int. J. Legal Med.* 121, 175–183. doi: 10.1007/s00414-006-0122-x

Iskusnykh, I. Y., Buddington, R. K., and Chizhikov, V. V. (2018). Preterm birth disrupts cerebellar development by affecting granule cell proliferation program and Bergmann glia. *Exp. Neurol.* 306, 209–221. doi: 10.1016/j.expneurol.2018.05.015

Iskusnykh, I. Y., and Chizhikov, V. V. (2022). Cerebellar development after preterm birth. *Front. Cell Dev. Biol.* 10:1068288. doi: 10.3389/fcell.2022.1068288

Iskusnykh, I. Y., Fattakhov, N., Buddington, R. K., and Chizhikov, V. V. (2021). Intrauterine growth restriction compromises cerebellar development by affecting radial migration of granule cells via the JamC/Pard3a molecular pathway. *Exp. Neurol.* 336, 113537. doi: 10.1016/j.expneurol.2020.113537

Jeong, J. W., Tiwari, V. N., Behen, M. E., Chugani, H. T., and Chugani, D. C. (2014). In vivo detection of reduced Purkinje cell fibers with diffusion MRI tractography in children with autistic spectrum disorders. *Front. Hum. Neurosci.* 8, 110. doi: 10.3389/fnhum.2014.00110

Johnsen, S. D., Bodensteiner, J. B., and Lotze, T. E. (2005). Frequency and nature of cerebellar injury in the extremely premature survivor with cerebral palsy. *J. Child Neurol.* 20, 60–64. doi: 10.1177/08830738050200011001

Kántor, O., Schmitz, C., Feiser, J., Brasnjevic, I., Korr, H., Busto, R., et al. (2007). Moderate loss of cerebellar Purkinje cells after chronic bilateral common carotid artery occlusion in rats. *Acta Neuropathol.* 113, 549–558. doi: 10.1007/s00401-007-0204-y

Kondziella, W. (1964). [A new method for the measurement of muscle relaxation in white mice]. *Arch. Int. Pharmacodyn. Ther.* 152, 277–284.

Lafarga, M., Andres, M. A., Calle, E., and Berciano, M. T. (1998). Reactive gliosis of immature Bergmann glia and microglial cell activation in response to cell death of granule cell precursors induced by methylazoxymethanol treatment in developing rat cerebellum. *Anat. Embryol.* 198, 111–122. doi: 10.1007/s004290050169

Lewis, P. M., Gritli-Linde, A., Smeyne, R., Kottmann, A., and McMahon, A. P. (2004). Sonic hedgehog signaling is required for expansion of granule neuron precursors and patterning of the mouse cerebellum. *Dev. Biol.* 270, 393–410. doi: 10.1016/j.ydbio.2004.03.007

Limperopoulos, C., Bassan, H., Gauvreau, K., Robertson, R. L. Jr., Sullivan, N. R., Benson, C. B., et al. (2007). Does cerebellar injury in premature infants contribute to the high prevalence of long-term cognitive, learning, and behavioral disability in survivors? *Pediatrics* 120, 584–593. doi: 10.1542/peds.2007-1041

Limperopoulos, C., Chilingaryan, G., Guizard, N., Robertson, R. L., and Du Plessis, A. J. (2010). Cerebellar injury in the premature infant is associated with impaired growth of specific cerebral regions. *Pediatr. Res.* 68, 145–150. doi: 10.1203/PDR.0b013e3181e1d032

Limperopoulos, C., Chilingaryan, G., Sullivan, N., Guizard, N., Robertson, R. L., and du Plessis, A. J. (2014). Injury to the premature cerebellum: outcome is related to remote cortical development. *Cereb. Cortex* 24, 728–736. doi: 10.1093/cercor/bhs354

Lippman, J. J., Lordkipanidze, T., Buell, M. E., Yoon, S. O., and Dunaevsky, A. (2008). Morphogenesis and regulation of Bergmann glial processes during Purkinje cell dendritic spine ensheathment and synaptogenesis. *Glia* 56, 1463–1477. doi: 10.1002/glia.20712

Matsufuji, M., Sano, N., Tsuru, H., and Takashima, S. (2017). Neuroimaging and neuropathological characteristics of cerebellar injury in extremely low birth weight infants. *Brain Dev.* 39, 735–742. doi: 10.1016/j.braindev.2017.04.011

Nosarti, C., Giouroukou, E., Micali, N., Rifkin, L., Morris, R. G., and Murray, R. M. (2007). Impaired executive functioning in young adults born very preterm. *J. Int. Neuropsychol. Soc.* 13, 571–581. doi: 10.1017/S1355617707070725

Poretti, A., Leventer, R. J., Cowan, F. M., Rutherford, M. A., Steinlin, M., Klein, A., et al. (2008). Cerebellar cleft: a form of prenatal cerebellar disruption. *Neuropediatrics* 39, 106–112. doi: 10.1055/s-2008-1081460

Rakic, P. (1971). Neuron-glia relationship during granule cell migration in developing cerebellar cortex. a golgi and electronmicroscopic study in macacus rhesus. *J. Comp. Neurol.* 141, 283–312. doi: 10.1002/cne.901410303

Sathyanesan, A., Kundu, S., Abbah, J., and Gallo, V. (2018). Neonatal brain injury causes cerebellar learning deficits and Purkinje cell dysfunction. *Nat. Commun.* 9, 3235. doi: 10.1038/s41467-018-05656-w

Scelsa, B., Cutillo, G., Lanna, M. M., Righini, A., Balestriero, M. A., Brazzoduro, V., et al. (2022). Prenatal diagnosis and neurodevelopmental outcome in isolated cerebellar hypoplasia of suspected hemorrhagic etiology: a retrospective cohort study. *Cerebellum* 21, 944–953. doi: 10.1007/s12311-021-01341-9

Sergaki, M. C., López-Ramos, J. C., Stagkourakis, S., Gruart, A., Broberger, C., Delgado-García, J. M., et al. (2017). Compromised survival of cerebellar molecular layer interneurons lacking gdnf receptors GFRα1 or RET impairs normal cerebellar motor learning. *Cell Rep.* 19, 1977–1986. doi: 10.1016/j.celrep.2017.05.030

Skefos, J., Cummings, C., Enzer, K., Holiday, J., Weed, K., Levy, E., et al. (2014). Regional alterations in purkinje cell density in patients with autism. *PLoS ONE* 9:e81255. doi: 10.1371/journal.pone.0081255

Smeyne, R. J., Chu, T., Lewin, A., Bian, F., Sanlioglu, S., Kunsch, C., et al. (1995). Local control of granule cell generation by cerebellar Purkinje cells. *Mol. Cell. Neurosci.* 6, 230–251. doi: 10.1006/mcne.1995.1019

Spoto, G., Amore, G., Vetri, L., Quatrosi, G., Cafeo, A., Gitto, E., et al. (2021). Cerebellum and prematurity: a complex interplay between disruptive and dysmaturational events. *Front. Syst. Neurosci.* 15, 655164. doi: 10.3389/fnsys.2021.655164

Steggerda, S. J., Leijser, L. M., Wiggers-de Bruine, F. T., van der Grond, J., Walther, F. J., and van Wezel-Meijler, G. (2009). Cerebellar injury in preterm infants: incidence and findings on US and MR images. *Radiology* 252, 190–199. doi: 10.1148/radiol.2521081525

Stoodley, C. J., and Limperopoulos, C. (2016). Structure-function relationships in the developing cerebellum: evidence from early-life cerebellar injury and neurodevelopmental disorders. *Semin. Fetal Neonatal Med.* 21, 356–364. doi: 10.1016/j.siny.2016.04.010

Traudt, C. M., McPherson, R. J., Studholme, C., Millen, K. J., and Juul, S. E. (2014). Systemic glycerol decreases neonatal rabbit brain and cerebellar growth independent of intraventricular hemorrhage. *Pediatr. Res.* 75, 389–394. doi: 10.1038/pr.2013.236

Tremblay, S., Pai, A., Richter, L., Vafaei, R., Potluri, P., Ellegood, J., et al. (2017). Systemic inflammation combined with neonatal cerebellar haemorrhage aggravates long-term structural and functional outcomes in a mouse model. *Brain Behav. Immun.* 66, 257–276. doi: 10.1016/j.bbi.2017.07.013

van der Heijden, M. E., Gill, J. S., and Sillitoe, R. V. (2021). Abnormal cerebellar development in autism spectrum disorders. *Dev. Neurosci.* 43, 181–190. doi: 10.1159/000515189

van der Heijden, M. E., and Sillitoe, R. V. (2021). Interactions between purkinje cells and granule cells coordinate the development of functional cerebellar circuits. *Neuroscience* 462, 4–21. doi: 10.1016/j.neuroscience.2020.06.010

Villamor-Martinez, E., Fumagalli, M., Alomar, Y. I., Passera, S., Cavallaro, G., Mosca, F., et al. (2019). Cerebellar hemorrhage in preterm infants: a meta-analysis on risk factors and neurodevelopmental outcome. *Front. Physiol.* 10:800. doi: 10.3389/fphys.2019.00800

Vinukonda, G., Hu, F., Upreti, C., Ungvari, Z., Zia, M. T., Stanton, P. K., et al. (2012). Novel organotypic in vitro slice culture model for intraventricular hemorrhage of premature infants. *J. Neurosci. Res.* 90, 2173–2182. doi: 10.1002/jnr.23102

Volpe, J. J. (2009). Cerebellum of the premature infant: rapidly developing, vulnerable, clinically important. *J. Child Neurol.* 24, 1085–1104. doi: 10.1177/0883073809338067

Wang, S. S., Kloth, A. D., and Badura, A. (2014). The cerebellum, sensitive periods, and autism. *Neuron* 83, 518–532. doi: 10.1016/j.neuron.2014.07.016

Wechsler-Reya, R. J., and Scott, M. P. (1999). Control of neuronal precursor proliferation in the cerebellum by Sonic Hedgehog. *Neuron* 22, 103–114. doi: 10.1016/S0896-6273(00)80682-0

Wei, A. D., and Ramirez, J. M. (2019). Presynaptic mechanisms and KCNQ potassium channels modulate opioid depression of respiratory drive. *Front. Physiol.* 10:1407. doi: 10.3389/fphys.2019.01407

Xue, M., Balasubramaniam, J., Buist, R. J., Peeling, J., and Del Bigio, M. R. (2003). Periventricular/intraventricular hemorrhage in neonatal mouse cerebrum. *J. Neuropathol. Exp. Neurol.* 62, 1154–1165. doi: 10.1093/jnen/62.11.1154

Yamada, K., Fukaya, M., Shibata, T., Kurihara, H., Tanaka, K., Inoue, Y., et al. (2000). Dynamic transformation of Bergmann glial fibers proceeds in correlation with dendritic outgrowth and synapse formation of cerebellar Purkinje cells. *J. Comp. Neurol.* 418, 106–120.

Yoo, J. Y., Mak, G. K., and Goldowitz, D. (2014). The effect of hemorrhage on the development of the postnatal mouse cerebellum. *Exp. Neurol.* 252, 85–94. doi: 10.1016/j.expneurol.2013.11.010

Yung, Y. C., Mutoh, T., Lin, M. E., Noguchi, K., Rivera, R. R., Choi, J. W., et al. (2011). Lysophosphatidic acid signaling may initiate fetal hydrocephalus. *Sci. Transl. Med.* 3, 99ra87. doi: 10.1126/scitranslmed.3002095

Zayek, M. M., Benjamin, J. T., Maertens, P., Trimm, R. F., Lal, C. V., and Eyal, F. G. (2012). Cerebellar hemorrhage: a major morbidity in extremely preterm infants. *J. Perinatol.* 32, 699–704. doi: 10.1038/jp.2011.185

Zhang, L., and Goldman, J. E. (1996). Developmental fates and migratory pathways of dividing progenitors in the postnatal rat cerebellum. *J. Comp. Neurol.* 370, 536–550. doi: 10.1002/(SICI)1096-9861(19960708)370:4<536::AID-CNE9>3.0.CO;2-5

frontiers | Frontiers in Molecular Neuroscience

TYPE Review
PUBLISHED 12 May 2023
DOI 10.3389/fnmol.2023.1181397

OPEN ACCESS

EDITED BY
Tetsushi Sadakata,
Gunma University, Japan

REVIEWED BY
Ruben Deogracias,
University of Salamanca, Spain
Sonia Canterini,
Sapienza University of Rome, Italy

*CORRESPONDENCE
Lilian Kisiswa
✉ liki@biomed.au.dk

RECEIVED 07 March 2023
ACCEPTED 26 April 2023
PUBLISHED 12 May 2023

CITATION
Boxy P, Nykjær A and Kisiswa L (2023) Building better brains: the pleiotropic function of neurotrophic factors in postnatal cerebellar development.
Front. Mol. Neurosci. 16:1181397.
doi: 10.3389/fnmol.2023.1181397

Building better brains: the pleiotropic function of neurotrophic factors in postnatal cerebellar development

Pia Boxy[1,2,3], Anders Nykjær[1,2,3] and Lilian Kisiswa[1,2,3]*

[1]Department of Biomedicine, Aarhus University, Aarhus, Denmark, [2]Danish Research Institute of Translational Neuroscience (DANDRITE)–Nordic EMBL Partnership for Molecular Medicine, Aarhus University, Aarhus, Denmark, [3]The Danish National Research Foundation Center, PROMEMO, Aarhus University, Aarhus, Denmark

The cerebellum is a multifunctional brain region that controls diverse motor and non-motor behaviors. As a result, impairments in the cerebellar architecture and circuitry lead to a vast array of neuropsychiatric and neurodevelopmental disorders. Neurotrophins and neurotrophic growth factors play essential roles in the development as well as maintenance of the central and peripheral nervous system which is crucial for normal brain function. Their timely expression throughout embryonic and postnatal stages is important for promoting growth and survival of both neurons and glial cells. During postnatal development, the cerebellum undergoes changes in its cellular organization, which is regulated by a variety of molecular factors, including neurotrophic factors. Studies have shown that these factors and their receptors promote proper formation of the cerebellar cytoarchitecture as well as maintenance of the cerebellar circuits. In this review, we will summarize what is known on the neurotrophic factors' role in cerebellar postnatal development and how their dysregulation assists in developing various neurological disorders. Understanding the expression patterns and signaling mechanisms of these factors and their receptors is crucial for elucidating their function within the cerebellum and for developing therapeutic strategies for cerebellar-related disorders.

KEYWORDS

cerebellum, neurotrophic factors, signaling/signaling pathways, development, developmental disorder

Introduction

The cerebellum, or ¨little brain¨, is well-known for its sensorimotor function and its role in movement coordination (Gao et al., 1996; Strick et al., 2009). Nevertheless, growing evidence indicates that the little brain is also involved in higher-order cognitive processing, including spatial learning, attention, language, reward, emotion, social behavior and memory (Ito, 2006; Schmahmann and Caplan, 2006; Ito, 2008; Stoodley, 2012; Koziol et al., 2014; Adamaszek et al., 2017; Wagner et al., 2017; Carta et al., 2019; Kostadinov et al., 2019). Several neuroimaging and lesion studies have shown cerebellar aberrations to account for changes in affective and cognitive behavior, collectively termed the "cerebellar cognitive affective syndrome" with deficits in executive function, emotion regulation, and working memory (Schmahmann and Sherman, 1998). Aberrant cerebellar functionality and cerebellar-only genetic alterations have been

implicated in numerous neuropsychiatric disorders, such as schizophrenia and bipolar disorder, and neurodevelopmental disorders, including attention deficit hyperactivity disorder (ADHD) and autism spectrum disorder (ASD) (Allen et al., 2004; Peter et al., 2016; Stoodley, 2016; Sathyanesan et al., 2019). This is mainly because cerebellar learning, complementing its role in motor control, also has a bottom-up influence on cognitive functions through extensive interconnections between the deep cerebellar nuclei and limbic brain structures (Snider et al., 1976; Carta et al., 2019; Frontera et al., 2020). Hence, if genetically predisposed, environmental perturbations throughout most of the cerebellar development may impair neuronal maturation and synapse formation, and lead to incorrect circuit wiring.

The cerebellum is a highly conserved brain structure that has an extensive and elaborate development, which starts in humans at gestational week 7 (E13 in rodents) and ends around 12 months postnatal (P21 in rodents) (Larramendi and Victor, 1967; Altman, 1972; Sathyanesan et al., 2019). For this review we will focus on the postnatal development of the cerebellum since the embryonic development has been covered in plenum by other reviews (Leto et al., 2016; Sathyanesan et al., 2019; Amore et al., 2021). During early postnatal stages, the dendritic complexity of Purkinje cells (PCs) develops extensively in terms of both branching and arbor length, resulting in the thickening of the molecular layer (Leto et al., 2016). Granule cell progenitors (GCPs), on the one hand, form the temporary external granule layer (EGL) in which they actively proliferate and expand. Consequently, the immature GCPs exit the cell cycle, commence differentiation, after which they migrate radially until they reach their destination within the internal granule layer (IGL) and become mature cerebellar granule neurons (CGNs). During this process, there is both extension of the CGN axons, namely the parallel fibers, and growth of the CGN dendrites (Consalez et al., 2021). The inhibitory interneurons (IN), on the other hand, originate from a pool of progenitors located in the cerebellar white matter (WM) that give rise to a variety of glial cells, including astrocytes, oligodendrocytes, and Bergmann glia (BG), as well as several types of interneurons. These progenitors migrate through the WM into the cerebellar cortex and subsequently differentiate into mature glia and INs (Zhang and Goldman, 1996). Lastly, synaptogenesis and target innervation of the PC axons occurs followed by synaptic and dendritic pruning (Leto et al., 2016).

Cerebellar development is a complex process that is regulated by a variety of signaling molecules and growth factors, both in a cell-autonomous and non-cell-autonomous manner. One category of growth factors that play a crucial role in cerebellar development and circuit formation is the neurotrophic factors (Figure 1). This includes the classical neurotrophins brain-derived neurotrophic factor (BNDF), nerve growth factor (NGF), neurotrophin-3 (NT-3) and neurotrophin-4 (NT-4), that are widely and timely expressed in different regions of the central and peripheral nervous system. Neurotrophins are key players during nervous system development where they regulate neurogenesis, morphogenesis, synaptogenesis, and cell maintenance, as well as during adulthood, in processes of cellular survival or death and, synaptic plasticity (Huang and Reichardt, 2001). The neurotrophins occur as both their secreted precursor state and their cleaved mature form (Lee et al., 2001). Mature neurotrophins bind preferentially to the high-affinity Trk receptors, a family of transmembrane tyrosine kinases, to regulate neuronal survival and differentiation (Lu et al., 2005). Activation of Trks initiates several signaling cascades, including the mitogen-activated protein kinase (MAPK) cascade, the phosphatidylinositol-3-kinase (PI3K) cascade, and the protein kinase C (PKC)-phospholipase-Cγ (PLC-γ) cascade (Klesse and Parada, 1999; Reichardt, 2006). Proneurotrophins, however, preferentially interact with the low-affinity and nonselective p75 neurotrophin receptor ($p75^{NTR}$) of the tumor necrosis factor (TNF) receptor superfamily in a complex with members of the sortilin receptor family to regulate cell death via the c-Jun N-terminal kinase (JNK) or caspase-3 pathway (Yoon et al., 1998; Friedman, 2000; Hempstead and Salzer, 2002; Nykjaer et al., 2004). NGF binds TrkA, BDNF and NT-4 bind TrkB, and NT-3 binds primarily TrkC (Chao and Hempstead, 1995). In addition to the prototypical neurotrophins, there are numerous growth factors that also play a major role in proper brain development (Figure 1). These include ciliary neurotrophic factor (CNTF), ephrins, epidermal growth factor (EGF), glial cell line-derived neurotrophic factor (GDNF), neuregulins, progranulin (PGRN) and transforming growth factor (TGF-β). By binding to their respective receptors, they provide survival, differentiation, migration, maturation, and circuit formation signals to the developing nervous system (Abe et al., 1991; Lärkfors et al., 1994; Mount et al., 1995; Ozaki et al., 2000; Rodger et al., 2012; Araujo et al., 2016; Uesaka et al., 2018). CNTF binds the CNTF receptor (CNTFR), ephrins bind to the Eph tyrosine kinase receptors, EGF binds to the EGF receptor (EGFR) or receptor homologs, GDNF binds predominantly GFRα1 in complex with the RET receptor, neuregulins bind the ErbB family of receptors, PGRN binds TNF receptors as well as the sortilin receptor, and lastly, TGF-β isoforms binds to the TGF-β type I, II, and III receptors (TβRI, TβRII, and TβRIII) (Cheifetz et al., 1988; Treanor et al., 1996; Chang et al., 1997; Doré et al., 1998; Wieduwilt and Moasser, 2008; Hu et al., 2010; Tang et al., 2011; Fantone et al., 2020). Binding of these growth factors to their respective receptors activates various signaling pathways including the p38 and JNK-MAPK, Jak–STAT, Ras-MAPK, and PI3K-Akt signaling pathways (Bonni et al., 1993; Oh et al., 1998; Wong and Guillaud, 2004; Murphy and Bielby-Clarke, 2008; Paratcha and Ledda, 2008; Wee and Wang, 2017; Fantone et al., 2020; Wang et al., 2022).

In this review, we will summarize what is currently known about the spatiotemporal expression of the different neurotrophic factors and their receptors within the cerebellar system during postnatal development (Figure 2; Table 1). Additionally, we will outline the neurotrophic factors' diverse cellular functionalities and some of the downstream signaling mechanisms that require neurotrophic expression and activity. Lastly, we will highlight how aberrations in both neurotrophic expression and function affect the cerebellar cytoarchitecture and what it implicates for several neurodevelopmental disorders (Table 2).

BDNF

BDNF is abundantly expressed within the developing cerebellum, both embryonically and postnatally in humans and rodents (Menshanov et al., 2015; Camuso et al., 2022). While produced in both CGNs and PCs, BDNF is mostly expressed in the axons of mature CGNs of the IGL, mossy fibers (MFs), and the deep cerebellar nuclei (DCN) (Schwartz et al., 1997; Rico et al., 2002). The release of BDNF from CGN axonal terminals is facilitated by calcium-dependent

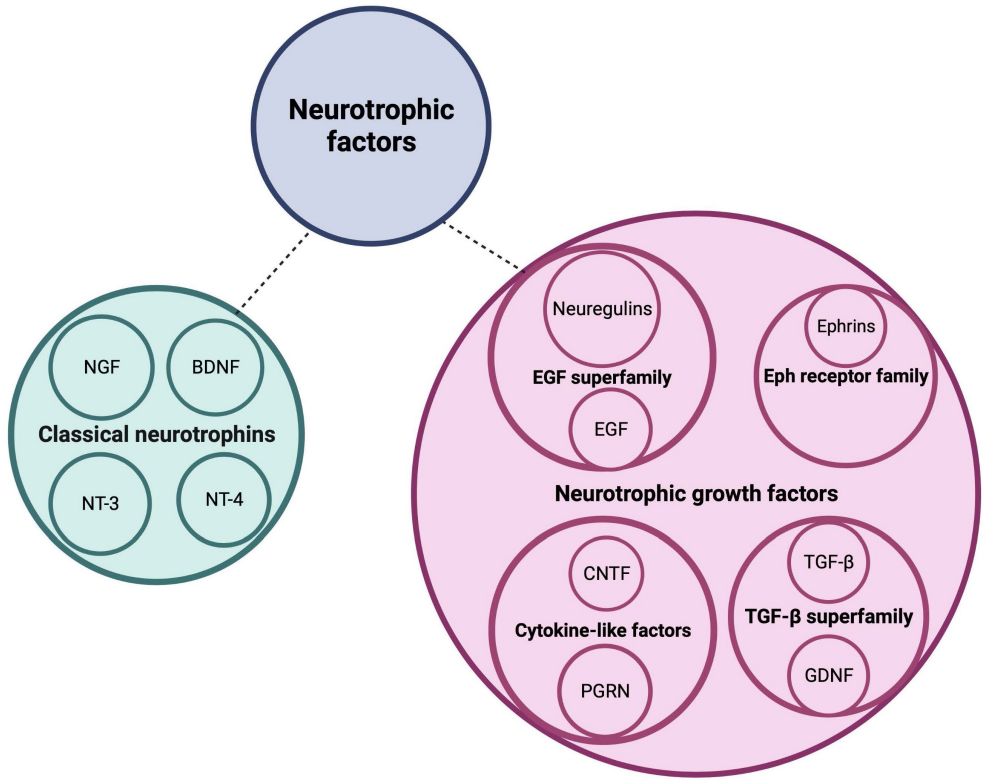

FIGURE 1
Neurotrophic factors regulate postnatal cerebellar development. This schematic diagram depicts the families of neurotrophic factors that regulate survival, differentiation, and migration of cerebellar neurons as well as neurite circuit formation and maintenance. BDNF, brain-derived neurotrophic factor; CNTF, ciliary neurotrophic factor; EGF, epidermal growth factor; GDNF, glial-derived neurotrophic factor; NGF, nerve growth factor; NT-3, neurotrophin-3; NT-4, neurotrophin-4; PGRN, progranulin; TGF-b, transforming growth factor beta. Figure produced in BioRender.

activator protein for secretion 2 (CAPS2), which is a granule-associated protein (Sadakata et al., 2007; Kokubo et al., 2009; Shinoda et al., 2019). BDNF binds TrkB on both postsynaptic PCs and presynaptic CGNs, thereby leading to Trk signaling in both a paracrine and autocrine manner, respectively (Lindholm et al., 1997). Both BDNF and its immature form, proBDNF can act as a mitogenic and chemotactic factor in cerebellar development. While BDNF exerts cell survival effects through TrkB activation, proBDNF is known to be a proapoptotic mediator through activation of $p75^{NTR}$, resulting in axon pruning and cell death (Glass et al., 1991; Ghosh et al., 1994; Singh et al., 2008).

As BDNF and TrkB are expressed in cerebellar PCs, they play a role in PC dendritogenesis and spine formation both *in vitro* and *in vivo* (Schwartz et al., 1997; Shimada et al., 1998; Yamashita et al., 2011). Lärkfors et al. (1996) found that survival of PCs increases after *in vitro* treatment with BDNF. Additionally, Morrison and Mason (1998) found that BDNF improves PC survival in isolated cultures, but decreases when co-cultured with CGNs, indicating that the neurotrophic action is context- and activity-dependent. However, recent findings suggest that BDNF does not exert a survival effect on naïve PCs *in vivo* but promotes survival in damaged PCs (Rakotomamonjy and Goumari, 2019). These data are supported by several other findings which show that BDNF does not affect survival in other neuronal populations such as cortical, hippocampal, and striatal neurons (Gorski et al., 2003; Baquet et al., 2004; Rauskolb et al., 2010).

In murine CGN cultures, BDNF–TrkB signaling promotes neurite extension and survival of differentiated mature CGNs (Gao et al., 1995; Nonomura et al., 1996; Tanaka et al., 2000). Accordingly, BDNF not only has pro-survival but also anti-apoptotic capacities in CGNs that are cultured in either serum-free media, low K^+ media, or media with high glutamate concentrations (Lindholm et al., 1993; Kubo et al., 1995; Zirrgiebel et al., 1995; Nonomura et al., 1996; Shimoke et al., 1997; Skaper et al., 1998; Tong and Perez-Polo, 1998; Bulleit and Hsieh, 2000; Leeds et al., 2005; Sanchez-Perez et al., 2005; Ortega et al., 2010). ProBDNF, on the other hand, does not exert a pro-survival effect on CGNs. Instead, proBDNF binds to $p75^{NTR}$, which in turn leads to the activation of the JNK signaling pathway and cell death (Koshimizu et al., 2010). Both the pro and mature form of BDNF affect the migration of CGNs *in vivo*. While endogenous BDNF promotes GCPs to exit the cell cycle and initiate migration in an autocrine manner, proBDNF acts as a negative regulator, an effect which is mediated by binding $p75^{NTR}$ and its co-receptor sortilin (Borghesani et al., 2002; Zhou et al., 2007; Kokubo et al., 2009).

Synaptogenesis is a crucial developmental step that promotes normal brain function. Improper synapse formation is, therefore, associated with neuronal dysfunction. BDNF–TrkB signaling is involved in correct circuit wiring, synaptogenesis, and establishing a balance between inhibitory and excitatory synapses within the cerebellar system (Minichiello, 1996; Schwartz et al., 1997; Carter et al., 2002; Rico et al., 2002; Bosman et al., 2006; Shinoda et al., 2019). For instance, BDNF secreted by both excitatory MFs and

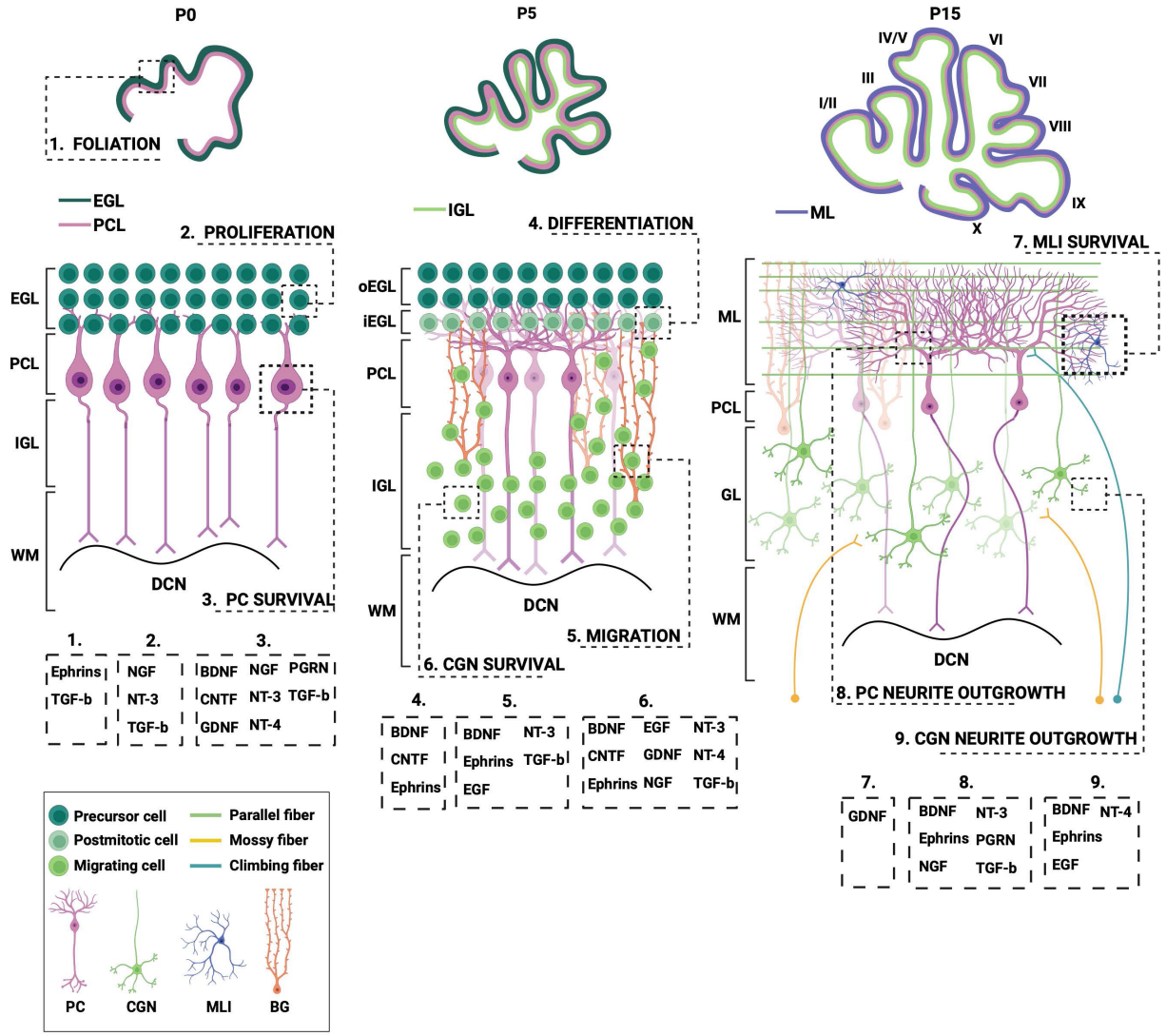

FIGURE 2
Different processes during postnatal cerebellar development require neurotrophic action. This schematic illustration depicts several stages of postnatal cerebellar development that involve the neurotrophic factors. EGL, external granule layer; oEGL, outer EGL; iEGL, inner EGL; PCL, Purkinje cell layer; ML, molecular layer; (I)GL, (internal) granule layer; WM, white matter; DCN, deep cerebellar nuclei; PC, Purkinje cell; CGN, cerebellar granule cell; MLI, molecular layer interneuron; BG, Bergmann glia; BDNF, brain-derived neurotrophic factor; CNTF, ciliary neurotrophic factor; EGF, epidermal growth factor; GDNF, glial-derived neurotrophic factor; NGF, nerve growth factor; NT-3, neurotrophin-3; NT-4, neurotrophin-4; PGRN, progranulin; TGF-b, transforming growth factor beta. Figure produced in BioRender.

CGNs aids in inhibitory synaptogenesis by regulating gephyrin, a postsynaptic scaffolding protein, clustering on CGN and PC dendrites, respectively, via the PLCy calcium-dependent and the PI3K-Akt signaling pathway (Chen et al., 2016). This is consistent with reports that BDNF–TrkB signaling promote gamma amino butyric acid (GABA)ergic synaptogenesis (Bao et al., 1999; Seil, 1999; Seil and Drake-Baumann, 2000). Moreover, BDNF contributes to the development of the two major afferent systems in the cerebellar cortex. Rabacchi et al. (1999) found that CGN-derived BDNF acts in a retrograde manner to promote the growth and maturation of innervating basilar pontine MFs. In addition, BDNF from PCs acts retrogradely on TrkB located within climbing fibers (CF) in facilitating late-phase CF synapse elimination from PC soma (Bosman et al., 2006; Choo et al., 2017). Secretion of BDNF from PCs is most likely triggered following metabotropic glutamate receptor (mGluR1) activation by parallel fiber (PF) signal transduction, the latter being a key player in CF synapse elimination (Kano et al., 1997; Ichise et al., 2000). The maturation of the cerebellar circuitry requires *de novo* synthesis of BDNF followed by activation of the TrkB-MAPK signaling pathway and phosphorylation of transcription factor ETS translocation variant 1 (Etv1) which upregulates the expression of several maturation genes with a role in dendritic development and functional synaptic assembly of the cerebellar circuit (Abe et al., 2012). Activation of Etv1 is also necessary for CaMKK2/CaMKIV-dependent phosphorylation of cAMP response element-binding protein (CREB) which drives BDNF autoregulation (Kokubo et al., 2009; Ding et al., 2018). Together, these findings demonstrate the importance of BDNF in cerebellar postnatal development as an imbalance in BDNF expression or signaling results in altered cerebellar architecture and functionality, leading to several

TABLE 1 Function of neurotrophic factors during postnatal cerebellar development.

Neurotrophic factors	Cerebellar function	References
BDNF	CGN survival	Bulleit and Hsieh (2000), Kubo et al. (1995), Leeds et al. (2005), Lindholm et al. (1993), Nonomura et al. (1996), Ortega et al. (2010), Sanchez-Perez et al. (2005), Shimoke et al. (1997), Skaper et al. (1998), Tong and Perez-Polo (1998), Zirrgiebel et al. (1995), and Koshimizu et al. (2010)
	CGN migration	Borghesani et al. (2002), Kokubo et al. (2009), and Zhou et al. (2007)
	CGN neurite outgrowth	Gao et al. (1995), Nonomura et al. (1996), and Tanaka et al. (2000)
	PC survival	Lärkfors et al. (1996), Rakotomamonjy and Goumari (2019), and Morrison and Mason (1998)
	PC neurite outgrowth	Schwartz et al. (1997), Shimada et al. (1998), and Yamashita et al. (2011)
	Circuit wiring	Bosman et al. (2006), Carter et al. (2002), Minichiello (1996), Rico et al. (2002), Schwartz et al. (1997), Shinoda et al. (2019), Chen et al. (2016), Bao et al. (1999), Seil (1999), Seil and Drake-Baumann (2000), Rabacchi et al. (1999), Choo et al. (2017), Ichise et al. (2000), Kano et al. (1997), and Abe et al. (2012)
CNTF	CGN survival	de Luca et al. (1996a)
	PC survival	Lärkfors et al. (1994)
	Astrocyte differentiation	Okano-Uchida et al. (2013)
Ephrins	CGN survival	Karam et al. (2000) and Sentürk et al. (2011)
	CGN migration	Yacubova and Komuro (2002)
	CGN neurite outgrowth	Karam et al. (2000), Sentürk et al. (2011), Moreno-Flores et al. (2002), and Wang et al. (2007)
	PC neurite outgrowth	Karam et al. (2000), Heintz et al. (2016), and Saywell et al. (2014)
	Circuit wiring	Lackey and Sillitoe (2020)
	Cerebellar foliation	Karam et al. (2000) and Rogers et al. (1999)
EGF	CGN survival	Abe et al. (1991, 1992), Morrison et al. (1988), Yamada et al. (1997), Gunn-Moore and Tavaré (1998) and Leutz and Schachner (1981)
	CGN migration	Carrasco et al. (2003), and Martinez et al. (2011)
	CGN neurite development	Abe et al. (1991, 1992), Morrison et al. (1988), and Yamada et al. (1997)
	NSC proliferation	Okano-Uchida et al. (2013) and Leutz and Schachner (1981)
GDNF	CGN survival	Subramaniam et al. (2008)
	PC survival	Mount et al. (1995)
	PC neurite outgrowth	Mount et al. (1995)
	MLI survival	Sergaki and Ibáñez (2017)
NGF	CGN survival	Legrand and Clos (1991), Muller et al. (1994), Khursigara et al. (2001), Kisiswa et al. (2018), and Vicario et al. (2015)
	PC survival	Cohen-Cory et al. (1991), Florez-McClure et al. (2004), Legrand and Clos (1991), and Mount et al. (1998)
	PC neurite outgrowth	Cohen-Cory et al. (1991), Legrand and Clos (1991), and Mount et al. (1998)
	Circuit wiring	Numakawa et al. (2003)
Neuregulins	Circuit wiring	Rieff and Corfas (2006), Ozaki (2001), Ozaki et al. (2000), Xie et al. (2004), Xie et al. (2007), Rieff et al. (1999), Ozaki et al. (2004), Gajendran et al. (2009), and Fenster et al. (2012)
NT-3	CGN survival	Katoh-Semba et al. (2000), Bates et al. (1999), Joo et al. (2014), Bates et al. (1999), Joo et al. (2014), Katoh-Semba et al. (2000), Kubo et al. (1995), and Shimoke et al. (1997)
	CGN differentiation	Doughty et al. (1998), Neveu and Arenas (1996), Takumi et al. (2005), Minichiello (1996), Zanin et al. (2016), Zanin and Friedman (2022), Zanin et al. (2019), and Segal et al. (1992)
	CGN migration	Neveu and Arenas (1996)
	PC survival	Lärkfors et al. (1996) and Mount et al. (1998)
	PC neurite outgrowth	Joo et al. (2014), Neveu and Arenas (1996), and Tepper et al. (2020)
	Circuit wiring	Sadakata et al. (2014), Shinoda et al. (2019), and Sherrard and Bower (2002)

(Continued)

TABLE 1 (Continued)

Neurotrophic factors	Cerebellar function	References
NT-4	CGN survival	Proenca et al. (2016), Gao et al. (1995), Kubo et al. (1995), Shimoke et al. (1997), and Skaper et al. (1998)
	CGN neurite outgrowth	Gao et al. (1995)
	PC survival	Proenca et al. (2016), Lärkfors et al. (1996), and Morrison et al. (1988)
	Circuit wiring	Sadakata et al. (2014), Shinoda et al. (2019), and Sherrard and Bower (2002)
PGRN	PC survival	Wang et al. (2022)
	PC neurite outgrowth	Matsuwaki et al. (2015)
	Circuit wiring	Uesaka et al. (2018)
TGF-b	CGN survival	Wang et al. (2011), Elvers et al. (2005), de Luca et al. (1996b), Brown (1999), Constam et al. (1994), and Kane et al. (1996)
	CGN migration	Wang et al. (2011)
	PC survival	Zhou et al. (2003) and Wang et al. (2011)
	PC neurite outgrowth	Wang et al. (2011)
	Circuit wiring	Araujo et al. (2016), Ondáčová et al. (2017)
	Cerebellar foliation	Wang et al. (2011)

CGN, cerebellar granule neuron; PC, Purkinje cell; MLI, molecular layer interneuron; NSC, neuronal stem cell; BDNF, brain-derived neurotrophic factor; CNTF, ciliary neurotrophic factor; EGF, epidermal growth factor; GDNF, glial cell line-derived neurotrophic factor; NGF, nerve growth factor; NT-3, neurotrophin-3; NT-4, neurotrophin-4; PGRN, progranulin; TGF-β, transforming growth factor beta.

cerebellar-related neurodevelopmental disorders which are discussed in the paragraph below.

BDNF in cerebellar-related neurodevelopmental disorders

Impairment in BDNF signaling within the cerebellum has been implicated in several cerebellar-related disorders. Ataxia is a group of neurological disorders mainly characterized by a lack of voluntary movement coordination (Schmahmann, 2004). Post-mortem studies of patients with spinocerebellar ataxia type 6 (SCA6) show reduced expression of BDNF which was also revealed in a SCA6 mouse model, as well as a spinocerebellar ataxia type 1 (SCA1) mouse model. Both mice models display PC pathology, abnormal firing rates and changes in motor behavior. Extrinsic BDNF delivery and subsequent activation of the TrkB-Akt signaling pathway improves the PC firing rate and delays the onset of the observed motor deficits (Mellesmoen et al., 2019; Cook et al., 2022).

Friedreich's ataxia (FA) is a predominantly neurodegenerative disease caused by recessive mutations that produce a deficiency of frataxin (FXN). FXN triggers apoptosis in CGNs, pathological changes in PCs as well as loss of motor coordination. In primary granule cultures of FXN-deficient mice, it was evidenced that BDNF can be used as a therapeutic agent that effectively prevents CGN apoptosis and PC pathogenesis (Katsu-Jiménez et al., 2016). However, this remains to be tested *in vivo*.

Furthermore, expression levels of BDNF, proBDNF, and its intrinsic receptor, TrkB, are reduced in the cerebella of patients with neuropsychiatric disorders, including schizophrenia, bipolar disorder (BPD), and major depressive disorder (MDD) as well as in a rodent model for ASD (Soontornniyomkij et al., 2011; Yang et al., 2017; Alò et al., 2021). Additionally, CAPS2-deficient mice that show reduced secretion of BDNF from CGNs exhibit developmental deficits around the cerebellar vermis, such as increased CGN apoptosis and impaired PC dendritogenesis. This leads to poor circuit connectivity and failed paired-pulse facilitation at PF-PC synapses. This is in line with changes observed in ASD patients who display cellular disturbances, as well as hypoplasia around the vermis (Sadakata and Furuichi, 2009; Sadakata et al., 2014).

CNTF

CNTF is a cytokine that has a multifunctional role in CNS development, for instance in neurite outgrowth and neuronal survival, as well as after injury (Oyesiku and Wigston, 1996). The expression of CNTF in cerebellum is relatively low during early postnatal weeks, however, it increases significantly during adulthood (Ohta et al., 1996). Due to this low expression of CNTF in the developing cerebellum, there are limited studies on the effects of CNTF on cerebellar cells and only reports on the role of CNTF in cultured cerebellar cells. Although the expression is low, it is not absent, suggesting that CNTF might play a role during development and, therefore, warrant further studies.

One report showed that CNTF improves PC and other cerebellar GABAergic neuron survival *in vitro* as showcased in rat primary PC cultures (Lärkfors et al., 1994). Furthermore, CNTF exercises a neuroprotective effect in immature cerebellar granule cultures that are maintained in physiological low concentrations of potassium *in vitro*, which under normal circumstances, leads to apoptosis. CNTF can also prolong their survival in such non-depolarizing conditions (de Luca et al., 1996b). However, the physiological relevance of CNTF in immature CGNs remains unclear. On the other hand, CNTF might act as a differentiation factor during development. The postnatal cerebellum contains neuronal stem cells (NSCs) which derive from the white matter and CNTF has been shown to facilitate NSCs differentiation into astrocytes (Okano-Uchida et al., 2013). However, it remains unclear whether CNTF is responsible for their differentiation *in vivo*.

TABLE 2 Involvement of neurotrophic factors in cerebellar-related neurodevelopmental disorders.

Neurotrophic factors	Cerebellar-associated neurodevelopmental disorder	References
BDNF	ASD	Sadakata and Furuichi (2009), Sadakata et al. (2014), and Alò et al. (2021)
	MDD	Yang et al. (2017)
	BPD	Soontornniyomkij et al. (2011) and Yang et al. (2017)
	Schizophrenia	Yang et al. (2017)
	FA	Katsu-Jiménez et al. (2016)
	SCA	Cook et al. (2022) and Mellesmoen et al. (2019)
CNTF	GLD	Lin et al. (2015)
Eprins	MB	Bhatia et al. (2015)
EGF	MB	Schönholzer et al. (2020) and Neve et al. (2017)
GDNF	ADHD	Bilgiç et al. (2017) and Shim et al. (2015)
	Schizophrenia	Tunca et al. (2015)
	CMD	Sakuma et al. (2002)
NGF	ADHD	Bilgiç et al. (2017), Clemow et al. (2000), Guney et al. (2014), Syed et al. (2007), and Tiveron et al. (2013)
	MS	Damarjian et al. (2004)
Neuregulins	MB	Di Marcotullio et al. (2006) and Gilbertson et al. (1998)
	Schizophrenia	Kircher et al. (2009), Nickl-Jockschat et al. (2014), Schmitt et al. (2010), Yeganeh-Doost et al. (2011), and Barros et al. (2009)
NT-3	ASD	Sajdel-Sulkowska et al. (2009), Sajdel-Sulkowska et al. (2011), and Sadakata et al. (2014)
NT-4	CMD	Sakuma et al. (2002)
PGRN	ASD	Matsuwaki et al. (2015), Uesaka et al. (2018), and Wang et al. (2022)
TGF-b	MB	Marino (2005), Roussel and Hatten (2011), Santhana Kumar et al. (2018), and Aref et al. (2013)
	ASD	Ferretti and Hollander (2015) and Xu et al. (2017)
	CA	Cook et al. (2022) and Mellesmoen et al. (2019)

MB, medulloblastoma; ASD, autism spectrum disorder; ADHD, attention deficit hyperactivity disorder; MDD, major depressive disorder; BPD, bipolar disorder; MS, multiple sclerosis; EAE, experimental autoimmune encephalomyelitis; CMD, congenital muscular dystrophy; FA, Friedreich's ataxia; CA, cerebellar ataxia; SCA, spinocerebellar ataxia; GLD, globoid cell leukodystrophy; BDNF, brain-derived neurotrophic factor; CNTF, ciliary neurotrophic factor; EGF, epidermal growth factor; GDNF, glial cell line-derived neurotrophic factor; NGF, nerve growth factor; NT-3, neurotrophin-3; NT-4, neurotrophin-4; PGRN, progranulin; TGF-β, transforming growth factor beta.

CNTF in cerebellar-related neurodevelopmental disorders

Globoid cell leukodystrophy (GLD) is a lysosomal storage disease that is characterized by demyelination and astrogliosis. Such neuropathy leads to neurobehavioral changes, including cerebellar ataxia. In a murine model of GLD, cerebellar neurons as well as Bergmann glia undergo degeneration, an effect which is accompanied by the altered expression of several neurotrophic factors. For example, CNTF expression is markedly increased in GLD cerebella, which could possibly mitigate remyelination of demyelinated neurons (Lin et al., 2015).

Ephrins

Ephrins are membrane-bound proteins that are expressed in many regions of the developing brain. They consist of two subclasses, the A-type (ephrin-A1-5) and the B-type (ephrin-B1-3) and bind to their respective tyrosine kinase receptors, namely the Eph receptors which are mainly type-specific and consist of two subfamilies, EphA and EphB (Chang et al., 1997). Their signaling is bidirectional, meaning it occurs via both phosphorylation of intracellular proteins via the Eph receptors or by intracellular signal transmission via the ephrin ligands itself upon receptor binding, a process known as reverse signaling (Rodger et al., 2012). In the chicken cerebellum, ephrin-A4 and ephrin-A5 are expressed at the earliest during embryonic stages, followed by expression of ephrin-A2 and ephrin-A3. Expression of ephrin-B1 and ephrin-B2, however, is mostly found during postnatal stages in migrating CGNs (Karam et al., 2000). Ephrin-B1 is expressed in both CGNs and PCs, while expression of its receptor, EphB, is mainly constricted to CGNs during postnatal development (Moreno-Flores et al., 2002).

The family of ephrins is involved in the formation and maintenance of PC compartments (Karam et al., 2000). For example, ephrin/Eph signaling regulates both the type and density of spines on PCs, a process which is required for defining either CFs or PFs that innervate different parts of PC dendrites. As a result, dendritogenesis on PCs is subject to competition between these fibers; CFs occupy the more proximal dendrites of PCs by suppressing the formation of

smaller spines that are typically associated with PFs. Instead, CFs make room for a few larger spines to form contact with PCs. In an *in vitro* cerebellar model, it was shown that the ephrin/Eph signaling pathway affects the more proximal dendrites on PCs by inactivating integrin downstream signaling (Heintz et al., 2016). Additionally, ephrins and their receptors effectively function as PC axon guidance and growth molecules in a spatiotemporal manner (Saywell et al., 2014). One study found that both ephrin-A2 and ephrin-A5 by binding to their respective receptor control PC-MF communication during circuit formation. This is necessary for the proper patterning of mossy fiber afferents into discrete zones located within the granule layer (Lackey and Sillitoe, 2020).

While the different types of ephrin-A are crucial for PC development, ephrin-Bs regulate CGN development. For example, ephrin-B1 facilitates CGN survival, migration, dendritogenesis, as well as axonal extension (Karam et al., 2000; Sentürk et al., 2011). It also mitigates the expression of certain cell adhesion and microtubule-associated proteins which are necessary for axonal extension and guidance, as well as dendritogenesis of CGNs (Moreno-Flores et al., 2002; Wang et al., 2007). Both ephrin-B2 and its receptor EphB2 are strongly expressed in the EGL at postnatal day 3 in mice, a timepoint prior to the initiation of postmitotic CGN migration. Their concerted action is thought to inhibit the effect of certain chemokines which control the migration GCPs, consequently leading to the initiation of migration (Yacubova and Komuro, 2002). On a macroscopic scale, the ephrins and Eph receptors are thought to play an important role in cerebellar foliation as they have the ability to demarcate the cerebellar anlage (Rogers et al., 1999; Karam et al., 2000).

Ephrins in cerebellar-related neurodevelopmental disorders

Ephrins have also been implicated in developmental disorders, in particular schizophrenia and medulloblastoma. The drug olanzapine is effective in treating schizophrenia, but its precise mechanism remains unclear. One study found that olanzapine treatment may regulate the DNA methylation of certain genes in the cerebellum, including the ephrin/Eph receptor family. This family plays a crucial role in axon guidance during development and synaptic plasticity in adulthood, including long-term potentiation, which has been linked to psychosis. Therefore, the epigenetic changes in these genes may account for the therapeutic effects of olanzapine observed in a rat model of schizophrenia (Melka et al., 2014).

Medulloblastoma (MB) is an aggressive tumor that arises from GCPs in the cerebellum. Proper formation and migration of these precursors require ephrin-A5 and its receptors. In a mouse model of MB, it was found that deletion of ephrin-A5 inhibits tumor growth, providing a platform for development of ephrin-based pharmacological interventions of medulloblastoma (Bhatia et al., 2015).

EGF

EGF is part of the large EGF superfamily which also contains the transforming growth factor alpha (TGF-α) and the neuregulins (Wieduwilt and Moasser, 2008). It binds the epidermal growth factor receptor (EGFR, also called ErbB1) or receptor homologs ErbB2, ErbB3, or ErbB4 (Wieduwilt and Moasser, 2008). EGF and its receptor, EGFR, are expressed during all stages of life depending on the cell type, however, during postnatal development, they can be found within the CGNs, PCs and astrocytes of the cerebellar cortex as well as the DCN (Gómez-Pinilla et al., 1988; Seroogy et al., 1995; Scalabrino, 2022). EGF binding to EGFR results in activation of several signaling pathways including the PLC, PI3-K, and the Ras-MAPK signaling pathway (Wong and Guillaud, 2004).

EGF has the ability to support neuronal growth and survival in cultured rodent CGNs (Morrison et al., 1988; Abe et al., 1991, 1992; Yamada et al., 1997). This indicates that EGF can act as a neurotrophic factor that promotes the elongation and maintenance of neurites in cerebellar neurons which is most likely achieved through the activation of protein kinases (Morrison et al., 1988; Abe et al., 1991, 1992; Yamada et al., 1997). Moreover, EGF effectively reduces glutamate-associated apoptosis in primary CGN cultures and has thus a neuroprotective effect against glutamate-induced neurotoxicity (Abe and Saito, 1992; Gunn-Moore and Tavaré, 1998). In addition, it also enhances survival of serum-deprived cerebellar cultures (Leutz and Schachner, 1981). Concomitant to its function in CGN survival and maturation, EGF has been suggested to be involved in CGN migration, largely due to expression of EGFR found in premigratory post-mitotic CGNs and its function in facilitating Bergmann glia elongation (Carrasco et al., 2003; Martinez et al., 2011). NSCs which derive from the cerebellar white matter require EGF to keep their proliferative ability (Okano-Uchida et al., 2013). Once these NSCs differentiate into astrocytes they express EGFR. It has been reported that EGF-EGFR signaling in these astrocytes stimulates DNA synthesis increasing their proliferation (Leutz and Schachner, 1981).

EGF cerebellar-related neurodevelopmental disorders

Similar to ephrins, EGF signaling is involved in MB as it rapidly increases nuclear activation of the ERK1/2-MAPK pathway in MB cells which speeds the invasion of these cells (Schönholzer et al., 2020). Neve et al. (2017) found that in organotypic cerebellar slices, EGF effectively enhances tumor growth and infiltration, indicating its tumor progressing capabilities.

GDNF

GDNF is expressed in several different types of neurons, including PCs, and plays a crucial role in regulating various processes in the developing nervous system, such as neuron survival, cell migration, axon growth, and synapse formation (Mount et al., 1995; McAlhany et al., 1997, 1999; Paratcha and Ledda, 2008). It acts in a paracrine manner by pairing with the GDNF family receptor α1 (GFRα1) (Treanor et al., 1996). The GDNF/GFRa1 complex subsequently binds with the "rearranged during transfection" (RET) tyrosine kinase receptor or the neural cell adhesion molecule (NCAM), though with lower affinity to activate either the MAPK or P13K–Akt pathway (Treanor et al., 1996; Trupp et al., 1996; Paratcha and Ledda, 2008; Sergaki and Ibáñez, 2017).

GDNF, expressed by PCs, has been shown to be crucial for the survival of molecular layer interneurons (MLIs) during postnatal cerebellar development (Sergaki and Ibáñez, 2017). It binds the GFRa1-RET receptor complex on MLIs in a cell-autonomous manner to stimulate IN survival. The absence of either receptor leads to the loss of MLIs, decreased GABAergic inputs to PC dendrites, and an increase in PC firing rate, subsequently resulting in compromised motor learning as well as eyeblink conditioning (Sergaki and Ibáñez, 2017). Additionally, GDNF has neurotrophic capacities in cultured PCs as it aids spine formation and thickening of the dendritic tree as well as in CGNs as it increases survival of these neurons (Mount et al., 1995; Subramaniam et al., 2008).

GDNF in cerebellar-related neurodevelopmental disorders

GDNF has been implicated in several cerebellar-related neurodevelopmental disorders including schizophrenia and ADHD. For example, serum of schizophrenia patients shows reduced levels of GDNF compared to healthy controls (Tunca et al., 2015). Conversely to schizophrenia, plasma levels of GDNF in children with ADHD are markedly increased (Shim et al., 2015; Bilgiç et al., 2017). Although the levels of GDNF are altered in both schizophrenia and ADHD children, both studies measured circulation levels of GDNF suggesting that this alteration might not be restricted to the cerebellum but a global nervous system impairment.

Furthermore, GDNF might also play a role in congenital muscular dystrophy (CMD). CMD encompasses a group of genetic muscle diseases, characterized by muscle weakness, hypotonia, and muscle atrophy and often accompanied by respiratory complications as well as intellectual disability (Bertini et al., 2011). In a mouse model of CMD, it was found that GDNF expression was markedly enhanced in both PCs and CGNs (Sakuma et al., 2002). Since GDNF is a potent PC survival agent, such elevated expression levels may be the result of a compensatory mechanism due to PC degeneration. Conversely, exuberant levels of GDNF may be neurotoxic to the PCs and contribute to cerebellar degeneration.

NGF

NGF expression has been shown in many brain regions, most prominently in the cerebellum (Shelton and Reichardt, 1986). Studies from our and other groups have reported expression of NGF in CGNs (Matsui et al., 1990; Cohen-Cory et al., 1993; Kisiswa et al., 2018). NGF can bind two distinct receptors, TrkA and $p75^{NTR}$, where activation of TrkA induces multiple signaling pathways such as PI3K-Akt and MAPK that regulate cellular survival, differentiation, and neurite outgrowth (Crowder and Freeman, 1998; Kaplan and Miller, 2000). The proform of NGF, proNGF is thought to induce apoptosis when bound to $p75^{NTR}$ in the presence of sortilin, but also acts as a growth factor and induces neurite outgrowth when bound to TrkA in the absence of $p75^{NTR}$ (Nykjaer et al., 2004; Buttigieg et al., 2007). In the cerebellum, $p75^{NTR}$ is expressed in PCs and CGNs (Pioro and Claudio Cuello, 1988; Kisiswa et al., 2018). TrkA, on the other hand, is not expressed in the healthy cerebellum, indicating that NGF signals through $p75^{NTR}$ to exert its neurotrophic capacities.

NGF has been implicated as a differentiation and a survival factor for PCs *in vitro* in the presence of BDNF/TrkB signaling support (Cohen-Cory et al., 1991; Legrand and Clos, 1991; Mount et al., 1998; Florez-McClure et al., 2004). Not only in PCs, NGF also promotes the proliferation of immature granule cells and the postmitotic survival of newly differentiated CGNs (Legrand and Clos, 1991; Muller et al., 1994). The *in vitro* and *in vivo* survival effect of NGF on CGNs is RIP2-dependent and leads to an increase in NF-κB activity (Khursigara et al., 2001). In the absence of RIP2, however, NGF can induce JNK-dependent apoptosis (Kisiswa et al., 2018). The ability of the NGF-$p75^{NTR}$ complex to induce cell death in CGNs is normally suppressed or masked by concurrent activation of NF-kB signaling (Vicario et al., 2015). proNGF, on the other hand, displays proapoptotic activity through the increase of c-Jun phosphorylation via the JNK-dependent pathway. Therefore, NGF and proNGF function in an antagonistic manner, and their balance is key deterministic in CGN survival during postnatal cerebellar development. It is worth noting that immature granule neuron-derived NGF can induce an increase in intracellular calcium through the ryanodine receptor, which is followed by a rapid release of glutamate via the $p75^{NTR}$-dependent pathway. Such release of glutamate from PF terminals is important for the strengthening of PF-PC synapses (Numakawa et al., 2003).

NGF in cerebellar-related neurodevelopmental disorders

ADHD has recently been associated with the cerebellum, although the degree of cerebellar contribution to ADHD pathophysiology requires further studies (Mackie et al., 2007; Sathyanesan et al., 2019). Nevertheless, the levels of NGF in ADHD animal models and in children with ADHD is significantly increased in blood samples (Clemow et al., 2000; Syed et al., 2007; Tiveron et al., 2013; Guney et al., 2014; Bilgiç et al., 2017). However, like GDNF, the current data indicate that the alteration of NGF in these patients is a global effect and not cerebellar-specific. Considering the beneficial effect of NGF on cerebellar neurons, we speculate that the increase of NGF could be a compensatory mechanism to protect the cerebellum from impairment caused by ADHD.

Patients with multiple sclerosis (MS) and animal models of experimental autoimmune encephalomyelitis (EAE) often display cerebellar ataxia. This pathophysiological phenomenon is partly caused by abnormal PC firing as a result of an imbalance in sodium channel expression. NGF acting via $p75^{NTR}$ has the ability to modulate the expression of sodium channel Nav1.8 in PCs and, therefore, contribute to the regular PC firing rate. In a murine EAE model, it was revealed that levels of NGF and $p75^{NTR}$ are increased which leads to the upregulation of Nav1.8 channels (Damarjian et al., 2004).

Neuregulins

Neuregulins are a group of trophic factors that are part of the large EGF superfamily and have an essential role in both the developing brain and during synaptic plasticity in the adult brain (Wong and Guillaud, 2004). The neuregulins which are composed of neuregulin-1 (or heregulin), neuregulin-2, neuregulin-3, and neuregulin-4 interact with the ErbB family of receptors (Chang et al., 1997). Both the

neuregulins and their receptors are expressed in a spatiotemporal manner within the developing cerebellum. Neuregulins and ErbB2, ErbB3 and ErbB4 are all expressed in CGNs while ErbB4 is also expressed in radial glial cells such as the Bergmann glia (Rio et al., 1997; Ozaki et al., 1998; Rahman et al., 2019). In the maturing cerebellum, neuregulins are concentrated in glutamatergic MFs that innervate CGNs located in the IGL (Ozaki et al., 1997). Several studies found that in murine primary cultures of CGN, neuregulin-1 signals through the ErbB4 receptor to regulate its interaction with PSD95 which is crucial for CGN differentiation. The C-terminal part of the ErbB4 receptor associates with PSD95 leading to the assembly of the nitric oxide synthase (NOS)-1 complex, a process which is thought to be mediated via the MAPK pathway (Krainock and Murphy, 2001a,b; Murphy and Bielby-Clarke, 2008). Neuregulin-1 also promotes differentiation and morphogenesis of Bergmann glia which in turn, enhances migration of CGNs (Rio et al., 1997; Yacubova and Komuro, 2002; Buffo and Rossi, 2013).

One *in vivo* study found that neuregulin–ErbB signaling initiates dendritogenesis and maturation of postsynaptic compartments in the developing murine cerebellum (Rieff and Corfas, 2006). Neuregulins have the ability to serve as cell adhesion molecules on CGNs for synaptic recognition of MFs, leading to the formation of the cerebellar MF system (Ozaki et al., 2000; Ozaki, 2001). These growth factors are not only essential for glutamatergic circuit wiring as they have also been ascribed a role in the GABA system as well. More specifically, neuregulin-1 through activation of the ErbB4 receptor tyrosine kinase effectively induces expression of the $GABA_A$ receptor β2 subunit via the MAPK, PI3K, and the cyclin-dependent kinase-5 (cdk5) pathway in primary CGN cultures (Xie et al., 2004). Activation of cdk5 leads to recruitment of PSD95 which in turn facilitates the effects of neuregulin through its interaction with ErbB4. As a result, this mechanism functions as a positive feedback system to neuregulin signaling and consequent expression of the $GABA_A$ β2 subunit (Xie et al., 2007). Extrinsic delivery of neuregulin causes an increase in the $GABA_A$ receptor β2 subunit expression of CGN cultures *in vitro* which is paralleled by an increase in functional $GABA_A$ receptors (Rieff et al., 1999).

It has been reported that neuregulin can mediate synaptogenesis via two distinctive mechanisms. First, the soluble form of neuregulin can be proteolytically cleaved from the membrane-associated form as a result of protein kinase activation. This soluble form is then able to transsynaptically and in a paracrine manner act as a neurotrophic factor and regulate the expression of the NMDA receptor subunit NR2C (Ozaki et al., 2000). The soluble form of neuregulin-1 can be shedded in a frequency-dependent manner due to electrical stimulation in both CGN and pontine nucleus neurons that form MF afferents and synapse onto CGN. Such cleaved neuregulin-1 is thus important for synaptic transmission across MF-CGN synapses (Ozaki et al., 2004). Second, the membrane-anchored form in both CGNs and MF terminals can serve as a cell-recognition molecule to stimulate MF-CGN synapse formation (Ozaki et al., 2000). However, there is some debate on neuregulins' role in synaptogenesis as one study found that neuregulin/ErbB signaling to CGNs is dispensable for the normal development of their synaptic inputs as compared to previous *in vitro* experiments (Gajendran et al., 2009). Nevertheless, expression of NR2C is specifically induced during synaptogenesis of CGNs within the IGL, leading to dramatic changes in the NMDA receptor composition during development. As neuregulins are expressed in the MFs that innervate CGNs located in the IGL, one study found that cultured cerebellar slices stimulated with a neuregulin isoform dramatically increase the expression of NR2C messenger RNAs. This mechanism is mediated by the binding of neuregulins onto its receptors ErbB2 and ErbB4 located on CGNs. In conclusion, cell-autonomous signaling of NRG1/ErbB can modulate both glutamatergic and GABAergic neurotransmitter receptor composition during development and regulate synaptic plasticity (Ozaki et al., 1997; Fenster et al., 2012).

Neuregulins in cerebellar-related neurodevelopmental disorders

Multiple studies have suggested that the neuregulin-1 gene (NRG1) serves as an important risk gene for schizophrenia that is thought to be characterized by deficits in glutamatergic neurotransmission (Kircher et al., 2009; Nickl-Jockschat et al., 2014). In patients with schizophrenia, it was found that gene expression of the NMDA receptor subunit 2D (NMDAR2D) was significantly increased in the cerebellum, which results in a hyperexcitability of the NMDA receptor, and which may be a secondary upregulation due to a dysfunctional receptor. In patients with the NRG1 risk variant, they found that expression of the NMDAR2C subunit was significantly reduced which could lead to hypofunctionality of the NMDA receptor, that in turn may lead to dysfunction of the GABA system (Schmitt et al., 2010). Accordingly, from post-mortem studies, there is accumulating evidence that GABAergic signaling is decreased in the cerebellum of schizophrenia patients (Yeganeh-Doost et al., 2011). Not only NRG1, but also its receptors, ErbB2 and ErbB4 are candidate susceptibility genes for schizophrenia. While deletion of ErbB2 and ErbB4 does not affect brain anatomy on a macroscopic scale, it can lead to impaired spine maturation as well impaired interactions with postsynaptic scaffold proteins, such as PSD95, with glutamate receptors which in turn leads to behavioral abnormalities (Barros et al., 2009).

MB is associated with decreased activity of the mitogen sonic hedghehog (shh). Under normal conditions, shh downregulates the expression of ErbB4, while in MB subsets, there is accumulation of both ErbB2 and ErbB4. This leads to both anti-apoptotic and loss of cell growth arrest signaling in neuronal progenitors of the cerebellum (Gilbertson et al., 1998; Di Marcotullio et al., 2006).

NT-3

In the developing cerebellum, NT-3 and its high-affinity tyrosine kinase receptor TrkC are expressed by both the differentiated CGNs of the IGL and their precursors in the EGL as well as in PCs (Neveu and Arenas, 1996; Doughty et al., 1998). In the rodent cerebellum, levels of NT-3 markedly decrease after the first 10 postnatal days (Katoh-Semba et al., 2000).

Formation of the PC arbor and competitive dendritogenesis in the mouse cerebellum is regulated by NT-3, expressed in CGNs, a process which is TrkC-dependent (Neveu and Arenas, 1996; Joo et al., 2014; Tepper et al., 2020). In cultured PCs, NT-3 effectively increases cell numbers via the PKC-dependent pathway while enhancing their survival and phenotypic differentiation (Lärkfors et al., 1996; Mount

et al., 1998). Concomitant to BDNF, CAPS2-mediated NT-3 release is known to be involved in the development and maturation of synapses and the balance between inhibitory and excitatory synapses (Sadakata et al., 2014; Shinoda et al., 2019). In addition, NT-3 promotes initial olivary axonal outgrowth to the cerebellar cortex and early CF synaptogenesis onto PCs (Sherrard and Bower, 2002).

NT-3 also has an important role in CGN development. In the murine cerebellum, NT-3 promotes the differentiation of premigratory granule cells, accelerating the cell cycle exit (Neveu and Arenas, 1996; Doughty et al., 1998; Takumi et al., 2005). It does this via either direct autocrine signaling, indirect via PCs, or by a combination of both and synergistically to BDNF (Minichiello, 1996). More recently, it was found that proNT-3, and not mature NT-3, affects GCP proliferation and differentiation. ProNT-3 binds to $p75^{NTR}$ and the co-receptor SorCS2, which is a member of the sortilin receptor family, to antagonize the shh-induced proliferation of GCPs and initiate cell cycle exit (Zanin et al., 2016, 2019; Zanin and Friedman, 2022). NT-3, on the other hand, aids the migration of newly differentiated GCPs from the EGL *in vivo*, an effect which is antagonized by $p75^{NTR}$ (Neveu and Arenas, 1996). Since GCPs express $p75^{NTR}$ during their proliferative but not their migratory state, $p75^{NTR}$ effectively prevents GCPs from migrating by maintaining elevated levels of active RhoA, a member of the Rho-GTPase family that plays a role in neuronal migration (Zanin and Friedman, 2022). Once CGPs have differentiated to CGNs and completed proliferation, NT-3 provides maturation support to these neurons (Segal et al., 1992). *In vitro*, NT-3 is known to support the survival of mature CGNs via TrkC (Bates et al., 1999; Katoh-Semba et al., 2000; Joo et al., 2014) and provide neuroprotective capacities in low K^+ cultured CGNs (Kubo et al., 1995; Shimoke et al., 1997; Bates et al., 1999; Katoh-Semba et al., 2000; Joo et al., 2014).

NT-3 in cerebellar-related neurodevelopmental disorders

Abnormalities in the expression of NT-3 have been associated with autism spectrum disorders. Exorbitant levels of NT-3 affect normal axonal targeting and synapse formation, and result in a decrease in PC numbers, all of which are effects seen in ASD pathology (Sajdel-Sulkowska et al., 2009, 2011). CAPS2 is essential for the release of NT-3 from CGNs, however, in patients with ASD, an alternative splice variant of CAPS2 that lacks exon 3, namely dex3, alters the release of NT-3. In a representative mouse model, NT-3 is markedly reduced in the axons of CGNs, an effect that results in reduced PC arborization and GCP proliferation. This leads to both a smaller vermal volume, as well as impaired paired-pulse facilitation at PF-PC synapses which is in line with autistic phenotypes (Sadakata et al., 2014).

NT-4

NT-4 has similar properties to BDNF within the developing cerebellum, although its expression levels peak higher during the first postnatal week (Proenca et al., 2016). NT-4 signals predominantly through the TrkB receptor and has a functional role in both CGN and PC maturation as well as survival and inhibitory synaptogenesis (Proenca et al., 2016). On the one hand, NT-4 improves the survival of isolated PCs (Morrison et al., 1988) as well as their phenotypic differentiation *in vitro* (Morrison et al., 1988; Lärkfors et al., 1996). In CGNs, on the other hand, NT-4 promotes survival as well as neurite extension and dendritic arborization in a similar manner to BDNF, via the TrkB-dependent pathway (Gao et al., 1995). In murine CGN cultures, NT-4 has a cytoprotective capacity and can circumvent glutamate-induced oxidative death via activation of the PI3K or MAPK pathway (Kubo et al., 1995; Shimoke et al., 1997; Skaper et al., 1998). NT-4 has similar capacities to BDNF and NT-3 in promoting correct circuit wiring of the cerebellar cortex and, concomitant to BDNF, NT-4 aids inhibitory synaptogenesis (Seil, 1999). Additionally, NT-4 promotes initial olivary axonal growth to the cerebellar plate and CF synaptogenesis as well as axonal outgrowth and survival of pontocerebellar MF neurons (Rabacchi et al., 1999; Sherrard and Bower, 2002).

NT-4 in cerebellar-related neurodevelopmental disorders

In a murine model for CMD, expression of NT-4 is markedly reduced in the cerebellum, in the spinal cord, and hindlimb muscles. Such a marked decrease may contribute to the progressive degeneration of muscle fibers and, due to its role in CGN and PC survival, cerebellar hypoplasia (Sakuma et al., 2002).

PGRN

PGRN is the precursor protein for granulin, expressed in both the periphery and central nervous system (Townley et al., 2018). The propeptide is mainly delivered into lysosomes as it plays a role in regulating protein homeostasis via the lysosomal pathway (Paushter et al., 2018). It has also been hypothesized to have neurotrophic capacities and function as an autocrine neuronal growth factor (Van Damme et al., 2008; Paushter et al., 2018). The expression levels of PGRN are thought to be regulated by the sortilin receptor which mediates its lysosomal endocytosis (Kao et al., 2017). However, PGRN can also exert its neurotrophic properties in a sortilin-independent manner, via prosaposin which carries PGRN into the lysosomes and regulates its expression (Zhou et al., 2015). PGRN is highly expressed in the cerebellar PCs during the late stages of postnatal development (Matsuwaki et al., 2015).

Matsuwaki et al. (2015) found that in PGRN-deficient mice, the PC dendritic density is significantly increased, possibly due to a lack of synaptic pruning, while no changes occur in the number of PCs. Taken together, this suggests that PGRN affects PC dendritogenesis but not neurogenesis and/or survival. However, in a study by Wang et al. (2022), it was found that PGRN aids neuronal survival and synaptic development via activation of the PI3K-Akt signaling pathway. In accordance with its role in synapse formation, PGRN also plays a role in defining CFs as a PC-derived regulator, by both counteracting redundant CFs and reinforcing the strongest CF inputs via the sortilin-dependent pathway. This retrograde mechanism is driven by voltage-gated calcium channels and the mGLuR1 signaling cascade (Uesaka et al., 2018).

PGRN in cerebellar-related neurodevelopmental disorders

PGRN has previously been implicated in cerebellar-associated degenerative but also in neurodevelopmental disorders (Matsuwaki et al., 2015; Simonati and Williams, 2022). It has been shown that PGRN is essential for PC dendritogenesis and CF-PC synaptogenesis and that abnormalities in PGRN expression may lead to synaptic disturbances as well as behavioral deficits, such as impaired motor function and coordination, reduced social preference, and increased repetitive behaviors (Matsuwaki et al., 2015; Uesaka et al., 2018; Wang et al., 2022). These behavioral phenotypes are all characteristic of those seen in ASD patients. Wang et al. (2022) found that abnormal spatiotemporal expression of PGRN is related to neurodevelopmental impairments in an ASD murine model.

TGF-β

TGF-β is a multipotent cytokine which is generally induced by acute or chronic brain injury, however, it also has cell differentiation, proliferation and apoptotic capacities during development (Dobolyi and Palkovits, 2008). Nonetheless, TGF- β does not only exert a neuroprotective function, as it can also induce neuronal and glial degeneration after injury (Wang et al., 1995; Yamashita et al., 1999). TGF-β exists as three isoforms in mammals, namely TGF-β1, TGF-β2, and TGF-β3 (Voisin et al., 2020). Under normal conditions, TGF-β is scarcely expressed within the cerebellum, however, TGF-β2 expression can be found in GCPs of the EGL and post-mitotic CGNs located in the IGL of the developing cerebellar cortex until postnatal day 10. It does remain expressed in PCs during both development and adulthood (Constam et al., 1994; Kane et al., 1996). TGF-β1 expression, on the other hand, is low during early postnatal stages but increases after postnatal day 12 and remains high until postnatal day 30 (Araujo et al., 2016). TGF- β signaling is initiated by the binding of extracellular TGF-β ligands to their respective receptors forming a complex. This complex formation allows phosphorylation of Smad proteins which then translocate to the cell nucleus to regulate the expression of multiple early target genes, including those that have a role in cell proliferation and differentiation, for example ID1-3, CDKN1A, OVOL1 and JUNB (Kowanetz et al., 2004; Zhang et al., 2016). However, their effects on cerebellar neurons are yet to be unraveled. We, therefore, propose that more studies are warranted for delineating cellular mechanisms regarding cerebellar-related neurodevelopmental disorders.

Deletion of Smad4, a critical mediator of TGF-β, results in Purkinje and GABAergic interneuron cell loss which leads to neurobehavioral deficits, including motor dysfunction (Zhou et al., 2003). Another study found that Smad2, another mediator of TGF-β signaling and highly expressed in the mouse brain during early postnatal development, is necessary for proper cerebellar foliation. Absence of Smad2 results in aberrant PC dendritic arborization and cell loss as well as other cerebellar deficits such as increased apoptosis and defect migration of CGNs which leads to motor dyscoordination (Wang et al., 2011).

TGF-β has a pro-survival and pro-growth effect on GCPs (Elvers et al., 2005). TGF-β1 effectively increases the number of glutamatergic synapses in CGN cultures, an effect which is dependent on binding to its receptor, TβRII. TGF-β1 thus mediates excitatory synapse formation in CGNs (Araujo et al., 2016). Moreover, TGF-β1 has the capacity to change the electrophysiological properties and voltage-dependent ion currents of CGNs after injury which leads to functional changes in the CNS (Ondáčová et al., 2017). However, TGF-β can also serve as a pro-apoptotic agent in low K^+ cultured CGNs (de Luca et al., 1996a). More specifically, TGF-β1 has a neurotoxic effect on mixed neuronal and astrocytic cultures as the CGNs become dependent on astrocytes for survival. TGF-β1 acts as a cytokine and inhibits the ability of astrocytes to clear glutamate, which leads to an increase in the glutamate concentration within the media that is toxic to the CGNs and eventually decreases their survival (Brown, 1999). TGF-β2, on the other hand, differently regulates proliferation and survival of CGNs, depending on the media conditions. TGF-β2 functions as a proliferative agent in serum-treated media, while it inhibits proliferation in serum-free media, indicating that as it requires exogenous regulatory factors (Constam et al., 1994; Kane et al., 1996).

TGF-β in cerebellar-related neurodevelopmental disorders

MB is thought to arise from disruptions in cerebellar development and growth factors, such as TGF-β, are thought to play a role in its progression (Marino, 2005; Roussel and Hatten, 2011; Santhana Kumar et al., 2018). The canonical TGF-β signaling pathway involves activation of Smad3 in a subset of GCPs that possibly represents the putative cells of origin for MB (Aref et al., 2013).

In a murine model of autism, TGF-β1 expression is significantly decreased within the cortex, hippocampus, and cerebellum. This is in line with a previous study which found reduced levels in patients with ASD (Ferretti and Hollander, 2015; Xu et al., 2017).

Cerebellar ataxia (CA) is usually accompanied by microglia-mediated neuroinflammation, yet how it contributes to cerebellar pathogenesis remains unsolved. In one study of CA model rats, it was found that exogenous administration of anti-inflammatory TGF-β1 reduces neuronal loss and microglial activation in both brain stem and cerebellum, and consequently ameliorates motor deficits as seen in CA (Cao et al., 2020). In another study of cerebellar ataxia, it was found that TGF-β1 is significantly upregulated, likely as a result of increased neuroinflammation (Jiang et al., 2015).

Conclusion

Neurotrophic factors and their receptors exert different cellular functions, and their spatiotemporal expression is crucial for the normal development of the cerebellar cytoarchitecture. In this review, we mainly focused on the purpose of these factors during the postnatal development of cells within the cerebellar cortex. However, several are also expressed during adulthood and play a role in both short-term and long-term synaptic plasticity. Because of their multifaceted features in neuronal differentiation, survival, synaptogenesis, and circuit wiring, it is inferred that the ablation of these factors can lead to serious defects on the tissue, cellular and molecular levels. A range of neurological disorders with a cerebellar component and abnormalities in either neurotrophic factor expression and/or activity have been discussed. It is important to note that this is not restricted to motor disorders, which are known to involve the cerebellar system, but also non-motor disorders. This indicates that the cerebellum, supplementing its role in motor performance, also plays a crucial role in cognitive and emotional

development. Further studies regarding neurotrophic factors and the effector downstream signaling mechanisms within the cerebellar system could illuminate whether they might serve as pharmacological agents to moderate certain disease models.

Author contributions

All authors listed have made a substantial, direct, and intellectual contribution to the work and approved it for publication.

Funding

This work was supported by Lundbeck Foundation grant no. R248-2017-431 and PROMEMO grant DNRF133.

Conflict of interest

The authors declare that the research was conducted in the absence of any commercial or financial relationships that could be construed as a potential conflict of interest.

Publisher's note

All claims expressed in this article are solely those of the authors and do not necessarily represent those of their affiliated organizations, or those of the publisher, the editors and the reviewers. Any product that may be evaluated in this article, or claim that may be made by its manufacturer, is not guaranteed or endorsed by the publisher.

References

Abe, H., Okazawa, M., and Nakanishi, S. (2012). Gene regulation via excitation and Bdnf is mediated by induction and phosphorylation of the Etv1 transcription factor in cerebellar granule cells. *Proc. Natl. Acad. Sci.* 109, 8734–8739. doi: 10.1073/pnas.1206418109

Abe, K., and Saito, H. (1992). Protective effect of epidermal growth factor on glutamate neurotoxicity in cultured cerebellar neurons. *Neurosci. Res.* 14, 117–123. doi: 10.1016/0168-0102(92)90087-S

Abe, K., Takayanagi, M., and Saito, H. (1991). Basic fibroblast growth factor and epidermal growth factor promote survival of primary cultured cerebellar neurons from neonatal rats. *Jpn. J. Pharmacol.* 56, 113–116. doi: 10.1016/S0021-5198(19)39906-8

Abe, K., Takayanagi, M., and Saito, H. (1992). Neurotrophic effects of epidermal growth factor on cultured brain neurons are blocked by protein kinase inhibitors. *Japan. J. Pharmacol.* 59, 259–261. doi: 10.1254/jjp.59.259

Adamaszek, M., D'agata, F., Ferrucci, R., Habas, C., Keulen, S., Kirkby, K. C., et al. (2017). Consensus paper: cerebellum and emotion. *Cerebellum* 16, 552–576. doi: 10.1007/s12311-016-0815-8

Allen, G., Müller, R.-A., and Courchesne, E. (2004). Cerebellar function in autism: functional magnetic resonance image activation during a simple motor task. *Biol. Psychiatry* 56, 269–278. doi: 10.1016/j.biopsych.2004.06.005

Alò, R., Olivito, I., Fazzari, G., Zizza, M., Di Vito, A., Avolio, E., et al. (2021). Correlation of distinct behaviors to the modified expression of cerebral Shank1,3 and Bdnf in two autistic animal models. *Behav. Brain Res.* 404:113165. doi: 10.1016/j.bbr.2021.113165

Altman, J. (1972). Postnatal development of the cerebellar cortex in the rat. Ii. Phases in the maturation of Purkinje cells and of the molecular layer. *J. Comp. Neurol.* 145, 399–463. doi: 10.1002/cne.901450402

Amore, G., Spoto, G., Ieni, A., Vetri, L., Quatrosi, G., Di Rosa, G., et al. (2021). A focus on the cerebellum: from embryogenesis to an age-related clinical perspective. *Front. Syst. Neurosci.* 15:646052. doi: 10.3389/fnsys.2021.646052

Araujo, A. P. B., Diniz, L. P., Eller, C. M., De Matos, B. G., Martinez, R., and Gomes, F. C. A. (2016). Effects of transforming growth factor Beta 1 in cerebellar development: role in synapse formation. *Front. Cell. Neurosci.* 10:104. doi: 10.3389/fncel.2016.00104

Aref, D., Moffatt, C. J., Agnihotri, S., Ramaswamy, V., Dubuc, A. M., Northcott, P. A., et al. (2013). Canonical Tgf-β pathway activity is a predictor of Shh-driven medulloblastoma survival and delineates putative precursors in cerebellar development. *Brain Pathol.* 23, 178–191. doi: 10.1111/j.1750-3639.2012.00631.x

Bao, S., Chen, L., Qiao, X., and Thompson, R. F. (1999). Transgenic brain-derived neurotrophic factor modulates a developing cerebellar inhibitory synapse. *Learn. Memory* 6, 276–283. doi: 10.1101/lm.6.3.276

Baquet, Z. C., Gorski, J. A., and Jones, K. R. (2004). Early striatal dendrite deficits followed by neuron loss with advanced age in the absence of anterograde cortical brain-derived neurotrophic factor. *J. Neurosci.* 24, 4250–4258. doi: 10.1523/JNEUROSCI.3920-03.2004

Barros, C. S., Calabrese, B., Chamero, P., Roberts, A. J., Korzus, E., Lloyd, K., et al. (2009). Impaired maturation of dendritic spines without disorganization of cortical cell layers in mice lacking Nrg1/ErbB signaling in the central nervous system. *Proc. Natl. Acad. Sci.* 106, 4507–4512. doi: 10.1073/pnas.0900355106

Bates, B., Rios, M., Trumpp, A., Chen, C., Fan, G., Bishop, J. M., et al. (1999). Neurotrophin–3 is required for proper cerebellar development. *Nat. Neurosci.* 2, 115–117. doi: 10.1038/5669

Bertini, E., D'amico, A., Gualandi, F., and Petrini, S. (2011). Congenital muscular dystrophies: a brief review. *Semin. Pediatr. Neurol.* 18, 277–288. doi: 10.1016/j.spen.2011.10.010

Bhatia, S., Hirsch, K., Baig, N. A., Rodriguez, O., Timofeeva, O., Kavanagh, K., et al. (2015). Effects of altered ephrin-A5 and EphA4/EphA7 expression on tumor growth in a medulloblastoma mouse model. *J. Hematol. Oncol.* 8:105. doi: 10.1186/s13045-015-0202-9

Bilgiç, A., Toker, A., Işık, Ü., and Kılınç, İ. (2017). Serum brain-derived neurotrophic factor, glial-derived neurotrophic factor, nerve growth factor, and neurotrophin-3 levels in children with attention-deficit/hyperactivity disorder. *Eur. Child Adolesc. Psychiatry* 26, 355–363. doi: 10.1007/s00787-016-0898-2

Bonni, A., Frank, D. A., Schindler, C., and Greenberg, M. E. (1993). Characterization of a pathway for ciliary neurotrophic factor signaling to the nucleus. *Science* 262, 1575–1579.

Borghesani, P. R., Peyrin, J. M., Klein, R., Rubin, J., Carter, A. R., Schwartz, P. M., et al. (2002). Bdnf stimulates migration of cerebellar granule cells. *Development* 129, 1435–1442. doi: 10.1242/dev.129.6.1435

Bosman, L. W. J., Hartmann, J., Barski, J. J., Lepier, A., Noll-Hussong, M., Reichardt, L. F., et al. (2006). Requirement of TrkB for synapse elimination in developing cerebellar Purkinje cells. *Brain Cell Biol.* 35, 87–101. doi: 10.1007/s11068-006-9002-z

Brown, D. R. (1999). Dependence of Neurones on astrocytes in a Coculture system renders Neurones sensitive to transforming growth factor \gb\1-induced glutamate toxicity. *J. Neurochem.* 72, 943–953. doi: 10.1046/j.1471-4159.1999.0720943.x

Buffo, A., and Rossi, F. (2013). Origin, lineage and function of cerebellar glia. *Prog. Neurobiol.* 109, 42–63. doi: 10.1016/j.pneurobio.2013.08.001

Bulleit, R. F., and Hsieh, T. (2000). Mek inhibitors block Bdnf-dependent and -independent expression of Gabaa receptor subunit mrnas in cultured mouse cerebellar granule neurons. *Dev. Brain Res.* 119, 1–10. doi: 10.1016/S0165-3806(99)00119-4

Buttigieg, H., Kawaja, M. D., and Fahnestock, M. (2007). Neurotrophic activity of prongf in vivo. *Exp. Neurol.* 204, 832–835. doi: 10.1016/j.expneurol.2006.12.011

Camuso, S., La Rosa, P., Fiorenza, M. T., and Canterini, S. (2022). Pleiotropic effects of Bdnf on the cerebellum and hippocampus: implications for neurodevelopmental disorders. *Neurobiol. Dis.* 163:105606. doi: 10.1016/j.nbd.2021.105606

Cao, B.-B., Zhang, X.-X., Du, C.-Y., Liu, Z., Qiu, Y.-H., and Peng, Y.-P. (2020). Tgf-β1 provides neuroprotection via inhibition of microglial activation in 3-Acetylpyridine-induced cerebellar Ataxia model rats. *Front. Neurosci.* 14:187. doi: 10.3389/fnins.2020.00187

Carrasco, E., Blum, M., Weickert, C. S., and Casper, D. (2003). Epidermal growth factor receptor expression is related to post-mitotic events in cerebellar development: regulation by thyroid hormone. *Dev. Brain Res.* 140, 1–13. doi: 10.1016/S0165-3806(02)00539-4

Carta, I., Chen, C. H., Schott, A. L., Dorizan, S., and Khodakhah, K. (2019). Cerebellar modulation of the reward circuitry and social behavior. *Science* 363:eaav0581. doi: 10.1126/science.aav0581

Carter, A. R., Chen, C., Schwartz, P. M., and Segal, R. A. (2002). Brain-derived neurotrophic factor modulates cerebellar plasticity and synaptic ultrastructure. *J. Neurosci.* 22:1316. doi: 10.1523/JNEUROSCI.22-04-01316.2002

Chang, H., Riese Ii, D. J., Gilbert, W., Stern, D. F., and Mcmahan, U. J. (1997). Ligands for ErbB-family receptors encoded by a neuregulin-like gene. *Nature* 387, 509–512. doi: 10.1038/387509a0

Chao, M. V., and Hempstead, B. L. (1995). p75 and Trk: a two-receptor system. *Trends Neurosci.* 18, 321–326. doi: 10.1016/0166-2236(95)93922-K

Cheifetz, S., Andres, J. L., and Massagué, J. (1988). The transforming growth factor-beta receptor type iii is a membrane proteoglycan. Domain structure of the receptor. *J. Biol. Chem.* 263, 16984–16991. doi: 10.1016/S0021-9258(18)37487-8

Chen, A. I., Zang, K., Masliah, E., and Reichardt, L. F. (2016). Glutamatergic axon-derived Bdnf controls Gabaergic synaptic differentiation in the cerebellum. *Sci. Rep.* 6:20201. doi: 10.1038/srep20201

Choo, M., Miyazaki, T., Yamazaki, M., Kawamura, M., Nakazawa, T., Zhang, J., et al. (2017). Retrograde Bdnf to TrkB signaling promotes synapse elimination in the developing cerebellum. *Nat. Commun.* 8:195. doi: 10.1038/s41467-017-00260-w

Clemow, D. B., Steers, W. D., and Tuttle, J. B. (2000). Stretch-activated signaling of nerve growth factor secretion in bladder and vascular smooth muscle cells from hypertensive and hyperactive rats. *J. Cell. Physiol.* 183, 289–300. doi: 10.1002/(SICI)1097-4652(200006)183:3<289::AID-JCP1>3.0.CO;2-6

Cohen-Cory, S., Dreyfus, C. F., and Black, I. B. (1991). Ngf and excitatory neurotransmitters regulate survival and morphogenesis of cultured cerebellar Purkinje cells. *J. Neurosci.* 11:462. doi: 10.1523/JNEUROSCI.11-02-00462.1991

Cohen-Cory, S., Elliott, R. C., Dreyfus, C. F., and Black, I. B. (1993). Depolarizing influences increase low-affinity Ngf receptor gene expression in cultured Purkinje neurons. *Exp. Neurol.* 119, 165–175. doi: 10.1006/exnr.1993.1018

Consalez, G. G., Goldowitz, D., Casoni, F., and Hawkes, R. (2021). Origins, development, and compartmentation of the granule cells of the cerebellum. *Front. Neural Circuits* 14:611841. doi: 10.3389/fncir.2020.611841

Constam, D. B., Schmid, P., Aguzzi, A., Schachner, M., and Fontana, A. (1994). Transient production of Tgf-β2 by postnatal cerebellar neurons and its effect on neuroblast proliferation. *Eur. J. Neurosci.* 6, 766–778. doi: 10.1111/j.1460-9568.1994.tb00988.x

Cook, A. A., Jayabal, S., Sheng, J., Fields, E., Leung, T. C. S., Quilez, S., et al. (2022). Activation of TrkB-Akt signaling rescues deficits in a mouse model of Sca6. *Sci. Adv.* 8:eabh3260. doi: 10.1126/sciadv.abh3260

Crowder, R. J., and Freeman, R. S. (1998). Phosphatidylinositol 3-kinase and Akt protein kinase are necessary and sufficient for the survival of nerve growth factor-dependent sympathetic neurons. *J. Neurosci.* 18:2933. doi: 10.1523/JNEUROSCI.18-08-02933.1998

Damarjian, T. G., Craner, M. J., Black, J. A., and Waxman, S. G. (2004). Upregulation and colocalization of p75 and Nav1.8 in Purkinje neurons in experimental autoimmune encephalomyelitis. *Neurosci. Lett.* 369, 186–190. doi: 10.1016/j.neulet.2004.07.023

de Luca, A., Weller, M., and Fontana, A. (1996a). Tgf-beta-induced apoptosis of cerebellar granule neurons is prevented by depolarization. *J. Neurosci.* 16, 4174–4185.

de Luca, A., Weller, M., Frei, K., and Fontana, A. (1996b). Maturation-dependent modulation of apoptosis in cultured cerebellar granule neurons by cytokines and Neurotrophins. *Eur. J. Neurosci.* 8, 1994–2005.

Di Marcotullio, L., Ferretti, E., De Smaele, E., Screpanti, I., and Gulino, A. (2006). Suppressors of hedgehog signaling. *Mol. Neurobiol.* 34, 193–204. doi: 10.1385/MN:34:3:193

Ding, B., Dobner, P. R., Mullikin-Kilpatrick, D., Wang, W., Zhu, H., Chow, C.-W., et al. (2018). Bdnf activates an Nfi-dependent neurodevelopmental timing program by sequestering Nfatc4. *Mol. Biol. Cell* 29, 975–987. doi: 10.1091/mbc.E16-08-0595

Dobolyi, A., and Palkovits, M. (2008). Expression of latent transforming growth factor beta binding proteins in the rat brain. *J. Comp. Neurol.* 507, 1393–1408. doi: 10.1002/cne.21621

Doré, J. J. E., Edens, M., Garamszegi, N., and Leof, E. B. (1998). Heteromeric and Homomeric transforming growth factor-β receptors show distinct signaling and endocytic responses in epithelial cells*. *J. Biol. Chem.* 273, 31770–31777. doi: 10.1074/jbc.273.48.31770

Doughty, M. L., Lohof, A., Campana, A., Delhaye-Bouchaud, N., and Mariani, J. (1998). Neurotrophin-3 promotes cerebellar granule cell exit from the Egl. *Eur. J. Neurosci.* 10, 3007–3011. doi: 10.1111/j.1460-9568.1998.00333.x

Elvers, M., Pfeiffer, J., Kaltschmidt, C., and Kaltschmidt, B. (2005). Tgf-β2 neutralization inhibits proliferation and activates apoptosis of cerebellar granule cell precurors in the developing cerebellum. *Mech. Dev.* 122, 587–602. doi: 10.1016/j.mod.2004.10.012

Fantone, S., Tossetta, G., Montironi, R., Senzacqua, M., Marzioni, D., and Mazzucchelli, R. (2020). Ciliary neurotrophic factor (Cntf) and its receptor (Cntfrα) signal through Mapk/Erk pathway in human prostate tissues: a morphological and biomolecular study. *Europ. J. Histochem.* 64:3147. doi: 10.4081/ejh.2020.3147

Fenster, C., Vullhorst, D., and Buonanno, A. (2012). Acute neuregulin-1 signaling influences Ampa receptor mediated responses in cultured cerebellar granule neurons. *Brain Res. Bull.* 87, 21–29. doi: 10.1016/j.brainresbull.2011.10.011

Ferretti, C. J., and Hollander, E. (2015). "The role of inflammation in autism Spectrum disorder" in *Immunology and psychiatry: from basic research to therapeutic interventions*. eds. N. Müller, A.-M. Myint and M. J. Schwarz (Cham: Springer International Publishing)

Florez-Mcclure, M. L., Linseman, D. A., Chu, C. T., Barker, P. A., Bouchard, R. J., Le, S. S., et al. (2004). The p75 Neurotrophin receptor can induce autophagy and death of cerebellar Purkinje neurons. *J. Neurosci.* 24:4498. doi: 10.1523/JNEUROSCI.5744-03.2004

Friedman, W. J. (2000). Neurotrophins induce death of hippocampal neurons via the p75 receptor. *J. Neurosci.* 20:6340. doi: 10.1523/JNEUROSCI.20-17-06340.2000

Frontera, J. L., Baba Aissa, H., Sala, R. W., Mailhes-Hamon, C., Georgescu, I. A., Léna, C., et al. (2020). Bidirectional control of fear memories by cerebellar neurons projecting to the ventrolateral periaqueductal grey. *Nat. Commun.* 11:5207. doi: 10.1038/s41467-020-18953-0

Gajendran, N., Kapfhammer, J. P., Lain, E., Canepari, M., Vogt, K., Wisden, W., et al. (2009). Neuregulin signaling is dispensable for Nmda- and Gaba(a)-receptor expression in the cerebellum in vivo. *J. Neurosci.* 29, 2404–2413. doi: 10.1523/JNEUROSCI.4303-08.2009

Gao, J.-H., Parsons, L. M., Bower, J. M., Xiong, J., Li, J., and Fox, P. T. (1996). Cerebellum implicated in sensory acquisition and discrimination rather than Motor control. *Science* 272, 545–547. doi: 10.1126/science.272.5261.545

Gao, W. Q., Zheng, J. L., and Karihaloo, M. (1995). Neurotrophin-4/5 (Nt-4/5) and brain-derived neurotrophic factor (Bdnf) act at later stages of cerebellar granule cell differentiation. *J. Neurosci.* 15:2656. doi: 10.1523/JNEUROSCI.15-04-02656.1995

Ghosh, A., Carnahan, J., and Greenberg, M. E. (1994). Requirement for Bdnf in activity-dependent survival of cortical neurons. *Science* 263, 1618–1623. doi: 10.1126/science.7907431

Gilbertson, R. J., Clifford, S. C., Macmeekin, W., Wright, C., Perry, R. H., Kelly, P., et al. (1998). Expression of the ErbB-Neuregulin signaling network during human cerebellar development: implications for the biology of Medulloblastoma1. *Cancer Res.* 58, 3932–3941.

Glass, D. J., Nye, S. H., Hantzopoulos, P., Macchi, M. J., Squinto, S. P., Goldfarb, M., et al. (1991). Trkl3 mediates Bdnf/Nt-3-dependent survival and proliferation in fibroblasts lacking the low affinity Ngf receptor. *Cells* 66, 405–413. doi: 10.1016/0092-8674(91)90629-D

Gómez-Pinilla, F., Knauer, D. J., and Nieto-Sampedro, M. (1988). Epidermal growth factor receptor immunoreactivity in rat brain development and cellular localization. *Brain Res.* 438, 385–390. doi: 10.1016/0006-8993(88)91369-8

Gorski, J. A., Zeiler, S. R., Tamowski, S., and Jones, K. R. (2003). Brain-derived neurotrophic factor is required for the maintenance of cortical dendrites. *J. Neurosci.* 23, 6856–6865. doi: 10.1523/JNEUROSCI.23-17-06856.2003

Guney, E., Ceylan, M. F., Kara, M., Tekin, N., Goker, Z., Senses Dinc, G., et al. (2014). Serum nerve growth factor (Ngf) levels in children with attention deficit/hyperactivity disorder (Adhd). *Neurosci. Lett.* 560, 107–111. doi: 10.1016/j.neulet.2013.12.026

Gunn-Moore, F. J., and Tavaré, J. M. (1998). Apoptosis of cerebellar granule cells induced by serum withdrawal, glutamate or β-amyloid, is independent of Jun kinase or p38 mitogen activated protein kinase activation. *Neurosci. Lett.* 250, 53–56. doi: 10.1016/S0304-3940(98)00438-8

Heintz, T. G., Eva, R., and Fawcett, J. W. (2016). Regional regulation of Purkinje cell dendritic spines by Integrins and Eph/Ephrins. *PLoS One* 11:e0158558. doi: 10.1371/journal.pone.0158558

Hempstead, B. L., and Salzer, J. L. (2002). A Glial Spin on Neurotrophins. *Science* 298, 1184–1186. doi: 10.1126/science.1078709

Hu, F., Padukkavidana, T., Vægter, C. B., Brady, O. A., Zheng, Y., Mackenzie, I. R., et al. (2010). Sortilin-mediated endocytosis determines levels of the frontotemporal dementia protein, progranulin. *Neuron* 68, 654–667. doi: 10.1016/j.neuron.2010.09.034

Huang, E. J., and Reichardt, L. F. (2001). Neurotrophins: roles in neuronal development and function. *Annu. Rev. Neurosci.* 24, 677–736. doi: 10.1146/annurev.neuro.24.1.677

Ichise, T., Kano, M., Hashimoto, K., Yanagihara, D., Nakao, K., Shigemoto, R., et al. (2000). mGluR1 in cerebellar Purkinje cells essential for long-term depression, synapse elimination, and motor coordination. *Science* 288, 1832–1835. doi: 10.1126/science.288.5472.1832

Ito, M. (2006). Cerebellar circuitry as a neuronal machine. *Prog. Neurobiol.* 78, 272–303. doi: 10.1016/j.pneurobio.2006.02.006

Ito, M. (2008). Control of mental activities by internal models in the cerebellum. *Nat. Rev. Neurosci.* 9, 304–313. doi: 10.1038/nrn2332

Jiang, Y.-Y., Cao, B.-B., Wang, X.-Q., Peng, Y.-P., and Qiu, Y.-H. (2015). Cerebellar ataxia induced by 3-Ap affects immunological function. *Neuro Endocrinol. Lett.* 36, 246–256.

Joo, W., Hippenmeyer, S., and Luo, L. (2014). Dendrite morphogenesis depends on relative levels of Nt-3/TrkC signaling. *Science* 346, 626–629. doi: 10.1126/science.1258996

Kane, C. J. M., Brown, G. J., and Phelan, K. D. (1996). Transforming growth factor-β2 both stimulates and inhibits neurogenesis of rat cerebellar granule cells in culture. *Dev. Brain Res.* 96, 46–51. doi: 10.1016/0165-3806(96)00092-2

Kano, M., Hashimoto, K., Kurihara, H., Watanabe, M., Inoue, Y., Aiba, A., et al. (1997). Persistent multiple climbing Fiber Innervationof cerebellar Purkinje Cellsin mice lacking mGluR1. *Neuron* 18, 71–79. doi: 10.1016/S0896-6273(01)80047-7

Kao, A. W., Mckay, A., Singh, P. P., Brunet, A., and Huang, E. J. (2017). Progranulin, lysosomal regulation and neurodegenerative disease. *Nat. Rev. Neurosci.* 18, 325–333. doi: 10.1038/nrn.2017.36

Kaplan, D. R., and Miller, F. D. (2000). Neurotrophin signal transduction in the nervous system. *Curr. Opin. Neurobiol.* 10, 381–391. doi: 10.1016/s0959-4388(00)00092-1

Karam, S. D., Burrows, R. C., Logan, C., Koblar, S., Pasquale, E. B., and Bothwell, M. (2000). Eph receptors and ephrins in the developing chick cerebellum: relationship to sagittal patterning and granule cell migration. *J. Neurosci.* 20, 6488–6500. doi: 10.1523/JNEUROSCI.20-17-06488.2000

Katoh-Semba, R., Takeuchi, I. K., Semba, R., and Kato, K. (2000). Neurotrophin-3 controls proliferation of granular precursors as well as survival of mature granule neurons in the developing rat Cerbellum. *J. Neurochem.* 74, 1923–1930. doi: 10.1046/j.1471-4159.2000.0741923.x

Katsu-Jiménez, Y., Loría, F., Corona, J. C., and Díaz-Nido, J. (2016). Gene transfer of brain-derived neurotrophic factor (Bdnf) prevents neurodegeneration triggered by Fxn deficiency. *Mol. Ther.* 24, 877–889. doi: 10.1038/mt.2016.32

Khursigara, G., Bertin, J., Yano, H., Moffett, H., Distefano, P. S., and Chao, M. V. (2001). A Prosurvival function for the p75 receptor death domain mediated via the caspase recruitment domain receptor-interacting protein 2. *J. Neurosci.* 21:5854. doi: 10.1523/JNEUROSCI.21-16-05854.2001

Kircher, T., Thienel, R., Wagner, M., Reske, M., Habel, U., Kellermann, T., et al. (2009). Neuregulin 1 ice-single nucleotide polymorphism in first episode schizophrenia correlates with cerebral activation in fronto-temporal areas. *Eur. Arch. Psychiatry Clin. Neurosci.* 259, 72–79. doi: 10.1007/s00406-008-0837-4

Kisiswa, L., Fernández-Suárez, D., Sergaki, M. C., and Ibáñez, C. F. (2018). Rip2 gates Traf6 interaction with death receptor p75ntr to regulate cerebellar granule neuron survival. *Cell Rep.* 24, 1013–1024. doi: 10.1016/j.celrep.2018.06.098

Klesse, L. J., and Parada, L. F. (1999). Trks: signal transduction and intracellular pathways. *Microsc. Res. Tech.* 45, 210–216. doi: 10.1002/(SICI)1097-0029(19990515/01)45:4/5<210::AID-JEMT4>3.0.CO;2-F

Kokubo, M., Nishio, M., Ribar, T. J., Anderson, K. A., West, A. E., and Means, A. R. (2009). Bdnf-mediated cerebellar granule cell development is impaired in mice null for Camkk2 or Camkiv. *J. Neurosci.* 29:8901. doi: 10.1523/JNEUROSCI.0040-09.2009

Koshimizu, H., Hazama, S., Hara, T., Ogura, A., and Kojima, M. (2010). Distinct signaling pathways of precursor Bdnf and mature Bdnf in cultured cerebellar granule neurons. *Neurosci. Lett.* 473, 229–232. doi: 10.1016/j.neulet.2010.02.055

Kostadinov, D., Beau, M., Blanco-Pozo, M., and Häusser, M. (2019). Predictive and reactive reward signals conveyed by climbing fiber inputs to cerebellar Purkinje cells. *Nat. Neurosci.* 22, 950–962. doi: 10.1038/s41593-019-0381-8

Kowanetz, M., Valcourt, U., Bergström, R., Heldin, C.-H., and Moustakas, A. (2004). Id2 and Id3 define the potency of cell proliferation and differentiation responses to transforming growth factor β and bone morphogenetic protein. *Mol. Cell. Biol.* 24, 4241–4254. doi: 10.1128/MCB.24.10.4241-4254.2004

Koziol, L. F., Budding, D., Andreasen, N., D'arrigo, S., Bulgheroni, S., Imamizu, H., et al. (2014). Consensus paper: the Cerebellum's role in movement and cognition. *Cerebellum* 13, 151–177. doi: 10.1007/s12311-013-0511-x

Krainock, R., and Murphy, S. (2001a). Heregulin upregulates the expression of nitric oxide synthase (Nos)-1 in rat cerebellar granule neurons via the ErbB4 receptor. *J. Neurochem.* 76, 312–315. doi: 10.1046/j.1471-4159.2001.00089.x

Krainock, R., and Murphy, S. (2001b). Regulation of functional nitric oxide synthase-1 expression in cerebellar granule neurons by heregulin is post-transcriptional, and involves mitogen-activated protein kinase. *J. Neurochem.* 78, 552–559. doi: 10.1046/j.1471-4159.2001.00420.x

Kubo, T., Nonomura, T., Enokido, Y., and Hatanaka, H. (1995). Brain-derived neurotrophic factor (bdnf) can prevent apoptosis of rat cerebellar granule neurons in culture. *Dev. Brain Res.* 85, 249–258. doi: 10.1016/0165-3806(94)00220-T

Lackey, E. P., and Sillitoe, R. V. (2020). Eph/ephrin function contributes to the patterning of spinocerebellar mossy fibers into parasagittal zones. *Front. Syst. Neurosci.* 14:7. doi: 10.3389/fnsys.2020.00007

Lärkfors, L., Lindsay, R. M., and Alderson, R. F. (1994). Ciliary neurotrophic factor enhances the survival of Purkinje cells in vitro. *Eur. J. Neurosci.* 6, 1015–1025. doi: 10.1111/j.1460-9568.1994.tb00596.x

Lärkfors, L., Lindsay, R. M., and Alderson, R. F. (1996). Characterization of the responses of Purkinje cells to Neurotrophin treatment. *J. Neurochem.* 66, 1362–1373. doi: 10.1046/j.1471-4159.1996.66041362.x

Larramendi, L. M. H., and Victor, T. (1967). Synapses on the purkinje cell spines in the mouse an electronmicroscopic study. *Brain Res.* 5, 15–30. doi: 10.1016/0006-8993(67)90216-8

Lee, R., Kermani, P., Teng, K. K., and Hempstead, B. L. (2001). Regulation of cell survival by secreted Proneurotrophins. *Science* 294, 1945–1948. doi: 10.1126/science.1065057

Leeds, P., Leng, Y., Chalecka-Franaszek, E., and Chuang, D. M. (2005). Neurotrophins protect against cytosine arabinoside-induced apoptosis of immature rat cerebellar neurons. *Neurochem. Int.* 46, 61–72. doi: 10.1016/j.neuint.2004.07.001

Legrand, C., and Clos, J. (1991). Biochemical, Immunocytochemical and morphological evidence for an interaction between thyroid hormone and nerve growth factor in the developing cerebellum of Normal and hypothyroid rats. *Dev. Neurosci.* 13, 382–396. doi: 10.1159/000112189

Leto, K., Arancillo, M., Becker, E. B. E., Buffo, A., Chiang, C., Ding, B., et al. (2016). Consensus Paper: Cerebellar Development. *Cerebellum* 15, 789–828. doi: 10.1007/s12311-015-0724-2

Leutz, A., and Schachner, M. (1981). Epidermal growth factor stimulates Dna-synthesis of astrocytes in primary cerebellar cultures. *Cell Tissue Res.* 220, 393–404. doi: 10.1007/BF00210517

Lin, D.-S., Hsiao, C.-D., Lee, A. Y.-L., Ho, C.-S., Liu, H.-L., Wang, T.-J., et al. (2015). Mitigation of cerebellar neuropathy in globoid cell leukodystrophy mice by Aav-mediated gene therapy. *Gene* 571, 81–90. doi: 10.1016/j.gene.2015.06.049

Lindholm, D., Dechant, G., Heisenberg, C.-P., and Thoenen, H. (1993). Brain-derived neurotrophic factor is a survival factor for cultured rat cerebellar granule neurons and protects them against glutamate-induced neurotoxicity. *Eur. J. Neurosci.* 5, 1455–1464. doi: 10.1111/j.1460-9568.1993.tb00213.x

Lindholm, D., Hamnér, S., and Zirrgiebel, U. (1997). Neurotrophins and cerebellar development. *Perspect. Dev. Neurobiol.* 5, 83–94.

Lu, B., Pang, P. T., and Woo, N. H. (2005). The yin and yang of neurotrophin action. *Nat. Rev. Neurosci.* 6, 603–614. doi: 10.1038/nrn1726

Mackie, S., Shaw, P., Lenroot, R., Pierson, R., Greenstein, D. K., Nugent, T. F., et al. (2007). Cerebellar development and clinical outcome in attention deficit hyperactivity disorder. *Am. J. Psychiatr.* 164, 647–655. doi: 10.1176/ajp.2007.164.4.647

Marino, S. (2005). Medulloblastoma: developmental mechanisms out of control. *Trends Mol. Med.* 11, 17–22. doi: 10.1016/j.molmed.2004.11.008

Martinez, R., Eller, C., Viana, N. B., and Gomes, F. C. A. (2011). Thyroid hormone induces cerebellar neuronal migration and Bergmann glia differentiation through epidermal growth factor/mitogen-activated protein kinase pathway. *Eur. J. Neurosci.* 33, 26–35. doi: 10.1111/j.1460-9568.2010.07490.x

Matsui, K., Furukawa, S., Shibasaki, H., and Kikuchi, T. (1990). Reduction of nerve growth factor level in the brain of genetically ataxic mice (weaver, reeler). *FEBS Lett.* 276, 78–80. doi: 10.1016/0014-5793(90)80511-G

Matsuwaki, T., Kobayashi, A., Mase, K., Nakamura, K., Nakano, S.-I., Miyoshi, T., et al. (2015). Possible involvement of the cerebellum in motor-function impairment in progranulin-deficient mice. *Neuroreport* 26:442. doi: 10.1097/WNR.0000000000000442

Mcalhany, R. E. Jr., Miranda, R. C., Finnell, R. H., and West, J. R. (1999). Ethanol decreases glial derived neurotrophic factor (Gdnf) protein release but not mrna expression and increases Gdnf-stimulated Shc phosphorylation in the developing cerebellum. *Alcohol Clin. Exp. Res.* 23, 1691–1697. doi: 10.1111/j.1530-0277.1999.tb04062.x

Mcalhany, R. E. Jr., West, J. R., and Miranda, R. C. (1997). Glial-derived neurotrophic factor rescues calbindin-D28k-immunoreactive neurons in alcohol-treated cerebellar explant cultures. *J. Neurobiol.* 33, 835–847. doi: 10.1002/(SICI)1097-4695(19971120)33:6<835::AID-NEU10>3.0.CO;2-3

Mellesmoen, A., Sheeler, C., Ferro, A., Rainwater, O., and Cvetanovic, M. (2019). Brain derived neurotrophic factor (Bdnf) delays onset of pathogenesis in transgenic mouse model of spinocerebellar Ataxia type 1 (Sca1). *Front. Cell. Neurosci.* 12:509. doi: 10.3389/fncel.2018.00509

Melka, M. G., Laufer, B. I., Mcdonald, P., Castellani, C. A., Rajakumar, N., O'reilly, R., et al. (2014). The effects of olanzapine on genome-wide DNA methylation in the hippocampus and cerebellum. *Clinical Epigenetics* 6:1.

Menshanov, P., Lanshakov, D., and Dygalo, N. (2015). Probdnf is a major product of bdnf gene expressed in the perinatal rat cortex. *Physiol. Res.* 64:996. doi: 10.33549/physiolres.932996

Minichiello, L. (1996). TrkB and TrkC neurotrophin receptors cooperate in promoting survival of hippocampal and cerebellar granule neurons. *Genes Dev.* 10, 2849–2858. doi: 10.1101/gad.10.22.2849

Moreno-Flores, M. T., MartíN-Aparicio, E., Ávila, J., Díaz-Nido, J., and Wandosell, F. (2002). Ephrin-B1 promotes dendrite outgrowth on cerebellar granule neurons. *Mol. Cell. Neurosci.* 20, 429–446. doi: 10.1006/mcne.2002.1128

Morrison, R. S., Keating, R. F., and Moskal, J. R. (1988). Basic fibroblast growth factor and epidermal growth factor exert differential trophic effects on Cns neurons. *J. Neurosci. Res.* 21, 71–79. doi: 10.1002/jnr.490210111

Morrison, M. E., and Mason, C. A. (1998). Granule neuron regulation of Purkinje cell development: striking a balance between Neurotrophin and glutamate signaling. *J. Neurosci.* 18:3563. doi: 10.1523/JNEUROSCI.18-10-03563.1998

Mount, H. T., Dean, D. O., Alberch, J., Dreyfus, C. F., and Black, I. B. (1995). Glial cell line-derived neurotrophic factor promotes the survival and morphologic differentiation of Purkinje cells. *Proc. Natl. Acad. Sci.* 92, 9092–9096. doi: 10.1073/pnas.92.20.9092

Mount, H. T. J., Elkabes, S., Dreyfus, C. F., and Black, I. B. (1998). Differential involvement of metabotropic and p75 Neurotrophin receptors in effects of nerve growth factor and Neurotrophin-3 on cultured Purkinje cell survival. *J. Neurochem.* 70, 1045–1053. doi: 10.1046/j.1471-4159.1998.70031045.x

Muller, Y., Duperray, C., Caruso, F., and Clos, J. (1994). Autocrine regulation of proliferation of cerebellar granule neurons by nerve growth factor. *J. Neurosci. Res.* 38, 41–55. doi: 10.1002/jnr.490380107

Murphy, S. P., and Bielby-Clarke, K. (2008). Neuregulin signaling in neurons depends on ErbB4 interaction with Psd-95. *Brain Res.* 1207, 32–35. doi: 10.1016/j.brainres.2008.02.063

Neve, A., Santhana Kumar, K., Tripolitsioti, D., Grotzer, M. A., and Baumgartner, M. (2017). Investigation of brain tissue infiltration by medulloblastoma cells in an ex vivo model. *Sci. Rep.* 7:5297. doi: 10.1038/s41598-018-28051-3

Neveu, I., and Arenas, E. (1996). Neurotrophins promote the survival and development of neurons in the cerebellum of hypothyroid rats in vivo. *J. Cell Biol.* 133, 631–646. doi: 10.1083/jcb.133.3.631

Nickl-Jockschat, T., Stöcker, T., Krug, A., Markov, V., Huang, R., Schneider, F., et al. (2014). A Neuregulin-1 schizophrenia susceptibility variant causes perihippocampal fiber tract anomalies in healthy young subjects. *Brain Behavior* 4, 215–226. doi: 10.1002/brb3.203

Nonomura, T., Kubo, T., Oka, T., Shimoke, K., Yamada, M., Enokido, Y., et al. (1996). Signaling pathways and survival effects of Bdnf and Nt-3 on cultured cerebellar granule cells. *Dev. Brain Res.* 97, 42–50. doi: 10.1016/S0165-3806(96)00130-7

Numakawa, T., Nakayama, H., Suzuki, S., Kubo, T., Nara, F., Numakawa, Y., et al. (2003). Nerve growth factor-induced glutamate release is via p75 receptor, ceramide, and Ca2+ from ryanodine receptor in developing cerebellar neurons*. *J. Biol. Chem.* 278, 41259–41269. doi: 10.1074/jbc.M304409200

Nykjaer, A., Lee, R., Teng, K. K., Jansen, P., Madsen, P., Nielsen, M. S., et al. (2004). Sortilin is essential for prongf-induced neuronal cell death. *Nature* 427, 843–848. doi: 10.1038/nature02319

Oh, H., Fujio, Y., Kunisada, K., Hirota, H., Matsui, H., Kishimoto, T., et al. (1998). Activation of phosphatidylinositol 3-kinase through glycoprotein 130 induces protein kinase B and p70 S6 kinase phosphorylation in cardiac myocytes*. *J. Biol. Chem.* 273, 9703–9710.

Ohta, M., Ohi, T., Nishimura, M., Itoh, N., Hayashi, K., and Ohta, K. (1996). Distribution of and age-related changes in ciliary neurotrophic factor protein in rat tissues. *IUBMB Life* 40:1273. doi: 10.1080/15216549600201273

Okano-Uchida, T., Naruse, M., Ikezawa, T., Shibasaki, K., and Ishizaki, Y. (2013). Cerebellar neural stem cells differentiate into two distinct types of astrocytes in response to Cntf and Bmp2. *Neurosci. Lett.* 552, 15–20. doi: 10.1016/j.neulet.2013.07.021

Ondáčová, K., Jurkovičová, D., and Lacinová, Ľ. (2017). Altered sodium and potassium, but not calcium currents in cerebellar granule cells in an in vitro model of neuronal injury. *Cell. Mol. Neurobiol.* 37, 771–782. doi: 10.1007/s10571-016-0416-6

Ortega, F., Pérez-Sen, R., Morente, V., Delicado, E. G., and Miras-Portugal, M. T. (2010). P2X7, Nmda and Bdnf receptors converge on Gsk3 phosphorylation and cooperate to promote survival in cerebellar granule neurons. *Cell. Mol. Life Sci.* 67, 1723–1733. doi: 10.1007/s00018-010-0278-x

Oyesiku, N. M., and Wigston, D. J. (1996). Ciliary neurotrophic factor stimulates neurite outgrowth from spinal cord neurons. *J. Comp. Neurol.* 364, 68–77. doi: 10.1002/(SICI)1096-9861(19960101)364:1<68::AID-CNE6>3.0.CO;2-Q

Ozaki, M. (2001). Neuregulins and the shaping of synapses. *Neuroscientist* 7, 146–154. doi: 10.1177/107385840100700209

Ozaki, M., Itoh, K., Miyakawa, Y., Kishida, H., and Hashikawa, T. (2004). Protein processing and releases of neuregulin-1 are regulated in an activity-dependent manner. *J. Neurochem.* 91, 176–188. doi: 10.1111/j.1471-4159.2004.02719.x

Ozaki, M., Kishigami, S., and Yano, R. (1998). Expression of receptors for neuregulins, ErbB2, ErbB3 and ErbB4, in developing mouse cerebellum. *Neurosci. Res.* 30, 351–354.

Ozaki, M., Sasner, M., Yano, R., Lu, H. S., and Buonanno, A. (1997). Neuregulin-β induces expression of an Nmda-receptor subunit. *Nature* 390, 691–694. doi: 10.1038/37795

Ozaki, M., Tohyama, K., Kishida, H., Buonanno, A., Yano, R., and Hashikawa, T. (2000). Roles of neuregulin in synaptogenesis between mossy fibers and cerebellar granule cells. *J. Neurosci. Res.* 59, 612–623. doi: 10.1002/(SICI)1097-4547(20000301)59:5<612::AID-JNR4>3.0.CO;2-V

Paratcha, G., and Ledda, F. (2008). Gdnf and Gfrα: a versatile molecular complex for developing neurons. *Trends Neurosci.* 31, 384–391. doi: 10.1016/j.tins.2008.05.003

Paushter, D. H., Du, H., Feng, T., and Hu, F. (2018). The lysosomal function of progranulin, a guardian against neurodegeneration. *Acta Neuropathol.* 136, 1–17. doi: 10.1007/s00401-018-1861-8

Peter, S., Ten Brinke, M. M., Stedehouder, J., Reinelt, C. M., Wu, B., Zhou, H., et al. (2016). Dysfunctional cerebellar Purkinje cells contribute to autism-like behaviour in Shank2-deficient mice. *Nat. Commun.* 7:12627. doi: 10.1038/ncomms12627

Pioro, E. P., and Claudio Cuello, A. (1988). Purkinje cells of adult rat cerebellum express nerve growth factor receptor immunoreactivity: light microscopic observations. *Brain Res.* 455, 182–186. doi: 10.1016/0006-8993(88)90131-X

Proenca, C. C., Song, M., and Lee, F. S. (2016). Differential effects of Bdnf and neurotrophin 4 (Nt4) on endocytic sorting of TrkB receptors. *J. Neurochem.* 138, 397–406. doi: 10.1111/jnc.13676

Rabacchi, S. A., Kruk, B., Hamilton, J., Carney, C., Hoffman, J. R., Meyer, S. L., et al. (1999). Bdnf and Nt4/5 promote survival and neurite outgrowth of pontocerebellar mossy fiber neurons. *J. Neurobiol.* 40, 254–269. doi: 10.1002/(SICI)1097-4695(199908)40:2<254::AID-NEU11>3.0.CO;2-4

Rahman, A., Weber, J., Labin, E., Lai, C., and Prieto, A. L. (2019). Developmental expression of Neuregulin-3 in the rat central nervous system. *J. Comp. Neurol.* 527, 797–817. doi: 10.1002/cne.24559

Rakotomamonjy, J., and Ghoumari, A. M. (2019). Brain-Derived Neurotrophic Factor Is Required for the Neuroprotective Effect of Mifepristone on Immature Purkinje Cells in Cerebellar Slice Culture. *Int. J. Mol. Sci.* Online, 20.

Rauskolb, S., Zagrebelsky, M., Dreznjak, A., Deogracias, R., Matsumoto, T., Wiese, S., et al. (2010). Global deprivation of brain-derived neurotrophic factor in the Cns reveals an area-specific requirement for dendritic growth. *J. Neurosci.* 30, 1739–1749. doi: 10.1523/JNEUROSCI.5100-09.2010

Reichardt, L. F. (2006). Neurotrophin-regulated signalling pathways. *Philos. Trans. Royal Soc. B Biol. Sci.* 361, 1545–1564. doi: 10.1098/rstb.2006.1894

Rico, B., Xu, B., and Reichardt, L. F. (2002). TrkB receptor signaling is required for establishment of Gabaergic synapses in the cerebellum. *Nat. Neurosci.* 5, 225–233. doi: 10.1038/nn808

Rieff, H. I., and Corfas, G. (2006). ErbB receptor signalling regulates dendrite formation in mouse cerebellar granule cells in vivo. *Eur. J. Neurosci.* 23, 2225–2229. doi: 10.1111/j.1460-9568.2006.04727.x

Rieff, H. I., Raetzman, L. T., Sapp, D. W., Yeh, H. H., Siegel, R. E., and Corfas, G. (1999). Neuregulin induces Gaba(a) receptor subunit expression and neurite outgrowth in cerebellar granule cells. *J. Neurosci.* 19, 10757–10766. doi: 10.1523/JNEUROSCI.19-24-10757.1999

Rio, C., Rieff, H. I., Qi, P., and Corfas, G. (1997). Neuregulin and erbB receptors play a critical role in neuronal migration. *Neuron* 19, 39–50.

Rodger, J., Salvatore, L., and Migani, P. (2012). Should I stay or should I go? Ephs and Ephrins in neuronal migration. *Neurosignals* 20, 190–201. doi: 10.1159/000333784

Rogers, J. H., Ciossek, T., Menzel, P., and Pasquale, E. B. (1999). Eph receptors and ephrins demarcate cerebellar lobules before and during their formation. *Mech. Dev.* 87, 119–128. doi: 10.1016/S0925-4773(99)00154-9

Roussel, M. F., and Hatten, M. E. (2011). Cerebellum development and medulloblastoma. *Curr. Top. Dev. Biol.* 94, 235–282. doi: 10.1016/B978-0-12-380916-2.00008-5

Sadakata, T., and Furuichi, T. (2009). Developmentally regulated Ca2+-dependent activator protein for secretion 2 (Caps2) is involved in Bdnf secretion and is associated with autism susceptibility. *Cerebellum* 8, 312–322. doi: 10.1007/s12311-009-0097-5

Sadakata, T., Kakegawa, W., Mizoguchi, A., Washida, M., Katoh-Semba, R., Shutoh, F., et al. (2007). Impaired cerebellar development and function in mice lacking Caps2, a protein involved in Neurotrophin release. *J. Neurosci.* 27:2472. doi: 10.1523/JNEUROSCI.2279-06.2007

Sadakata, T., Kakegawa, W., Shinoda, Y., Hosono, M., Katoh-Semba, R., Sekine, Y., et al. (2014). Axonal localization of Ca2+-dependent activator protein for secretion 2 is critical for subcellular locality of brain-derived neurotrophic factor and Neurotrophin-3 release affecting proper development of postnatal mouse cerebellum. *PLoS One* 9:e99524. doi: 10.1371/journal.pone.0099524

Sajdel-Sulkowska, E. M., Xu, M., and Koibuchi, N. (2009). Increase in cerebellar Neurotrophin-3 and oxidative stress markers in autism. *Cerebellum* 8, 366–372. doi: 10.1007/s12311-009-0105-9

Sajdel-Sulkowska, E. M., Xu, M., Mcginnis, W., and Koibuchi, N. (2011). Brain region-specific changes in oxidative stress and Neurotrophin levels in autism Spectrum disorders (Asd). *Cerebellum* 10, 43–48. doi: 10.1007/s12311-010-0223-4

Sakuma, K., Watanabe, K., Totsuka, T., Sano, M., Nakano, H., Nakao, R., et al. (2002). The reciprocal change of neurotrophin-4 and glial cell line-derived neurotrophic factor protein in the muscles, spinal cord and cerebellum of the dy mouse. *Acta Neuropathol.* 104, 482–492. doi: 10.1007/s00401-002-0576-y

Sanchez-Perez, A., Llansola, M., Cauli, O., and Felipo, V. (2005). Modulation of Nmda receptors in the cerebellum. Ii. Signaling pathways and physiological modulators regulating Nmda receptor function. *Cerebellum* 4, 162–170. doi: 10.1080/14734220510008003

Santhana Kumar, K., Neve, A., Guerreiro Stucklin, A. S., Kuzan-Fischer, C. M., Rushing, E. J., Taylor, M. D., et al. (2018). Tgf-β determines the pro-migratory potential of bfgf signaling in Medulloblastoma. *Cell Rep.* 23, 3798–3812.e8. doi: 10.1016/j.celrep.2018.05.083

Sathyanesan, A., Zhou, J., Scafidi, J., Heck, D. H., Sillitoe, R. V., and Gallo, V. (2019). Emerging connections between cerebellar development, behaviour and complex brain disorders. *Nat. Rev. Neurosci.* 20, 298–313. doi: 10.1038/s41583-019-0152-2

Saywell, V., Cioni, J.-M., and Ango, F. (2014). Developmental gene expression profile of axon guidance cues in Purkinje cells during cerebellar circuit formation. *Cerebellum* 13, 307–317. doi: 10.1007/s12311-014-0548-5

Scalabrino, G. (2022). Epidermal growth factor in the Cns: a beguiling journey from integrated cell biology to multiple sclerosis. An extensive translational overview. *Cell. Mol. Neurobiol.* 42, 891–916. doi: 10.1007/s10571-020-00989-x

Schmahmann, J. D. (2004). Disorders of the cerebellum: Ataxia, Dysmetria of thought, and the cerebellar cognitive affective syndrome. *J. Neuropsychiatry Clin. Neurosci.* 16, 367–378. doi: 10.1176/jnp.16.3.367

Schmahmann, J. D., and Caplan, D. (2006). Cognition, emotion and the cerebellum. *Brain* 129, 290–292. doi: 10.1093/brain/awh729

Schmahmann, J. D., and Sherman, J. C. (1998). The cerebellar cognitive affective syndrome. *Brain* 121, 561–579. doi: 10.1093/brain/121.4.561

Schmitt, A., Koschel, J., Zink, M., Bauer, M., Sommer, C., Frank, J., et al. (2010). Gene expression of Nmda receptor subunits in the cerebellum of elderly patients with schizophrenia. *Eur. Arch. Psychiatry Clin. Neurosci.* 260, 101–111. doi: 10.1007/s00406-009-0017-1

Schönholzer, M. T., Migliavacca, J., Alvarez, E., Santhana Kumar, K., Neve, A., Gries, A., et al. (2020). Real-time sensing of Mapk signaling in medulloblastoma cells reveals cellular evasion mechanism counteracting dasatinib blockade of Erk activation during invasion. *Neoplasia* 22, 470–483. doi: 10.1016/j.neo.2020.07.006

Schwartz, P. M., Borghesani, P. R., Levy, R. L., Pomeroy, S. L., and Segal, R. A. (1997). Abnormal cerebellar development and foliation in Bdnf−/− mice reveals a role for Neurotrophins in Cns patterning. *Neuron* 19, 269–281. doi: 10.1016/S0896-6273(00)80938-1

Segal, R. A., Takahashi, H., and Mckay, R. D. G. (1992). Changes in neurotrophin responsiveness during the development of cerebellar granule neurons. *Neuron* 9, 1041–1052. doi: 10.1016/0896-6273(92)90064-K

Seil, F. J. (1999). Bdnf and Nt-4, but not Nt-3, promote development of inhibitory synapses in the absence of neuronal activity. *Brain Res.* 818, 561–564. doi: 10.1016/S0006-8993(98)01304-3

Seil, F. J., and Drake-Baumann, R. (2000). TrkB receptor ligands promote activity-dependent inhibitory synaptogenesis. *J. Neurosci.* 20:5367. doi: 10.1523/JNEUROSCI.20-14-05367.2000

Sentürk, A., Pfennig, S., Weiss, A., Burk, K., and Acker-Palmer, A. (2011). Ephrin Bs are essential components of the Reelin pathway to regulate neuronal migration. *Nature* 472, 356–360. doi: 10.1038/nature09874

Sergaki, M. C., and Ibáñez, C. F. (2017). Gfrα1 regulates Purkinje cell migration by counteracting Ncam function. *Cell Rep.* 18, 367–379. doi: 10.1016/j.celrep.2016.12.039

Seroogy, K. B., Gall, C. M., Lee, D. C., and Kornblum, H. I. (1995). Proliferative zones of postnatal rat brain express epidermal growth factor receptor mrna. *Brain Res.* 670, 157–164. doi: 10.1016/0006-8993(94)01300-7

Shelton, D. L., and Reichardt, L. F. (1986). Studies on the expression of the beta nerve growth factor (Ngf) gene in the central nervous system: level and regional distribution of Ngf mrna suggest that Ngf functions as a trophic factor for several distinct populations of neurons. *Proc. Natl. Acad. Sci.* 83, 2714–2718. doi: 10.1073/pnas.83.8.2714

Sherrard, R. M., and Bower, A. J. (2002). Climbing fiber development: do neurotrophins have a part to play? *Cerebellum* 1, 265–275. doi: 10.1080/147342202320883579

Shim, S.-H., Hwangbo, Y., Yoon, H.-J., Kwon, Y.-J., Lee, H.-Y., Hwang, J.-A., et al. (2015). Increased levels of plasma glial-derived neurotrophic factor in children with attention deficit hyperactivity disorder. *Nord. J. Psychiatry* 69, 546–551. doi: 10.3109/08039488.2015.1014834

Shimada, A., Mason, C. A., and Morrison, M. E. (1998). TrkB signaling modulates spine density and morphology independent of dendrite structure in cultured neonatal Purkinje cells. *J. Neurosci.* 18:8559. doi: 10.1523/JNEUROSCI.18-21-08559.1998

Shimoke, K., Kubo, T., Numakawa, T., Abiru, Y., Enokido, Y., Takei, N., et al. (1997). Involvement of phosphatidylinositol-3 kinase in prevention of low K+-induced apoptosis of cerebellar granule neurons. *Dev. Brain Res.* 101, 197–206. doi: 10.1016/S0165-3806(97)00065-5

Shinoda, Y., Sadakata, T., Yagishita, K., Kinameri, E., Katoh-Semba, R., Sano, Y., et al. (2019). Aspects of excitatory/inhibitory synapses in multiple brain regions are correlated with levels of brain-derived neurotrophic factor/neurotrophin-3. *Biochem. Biophys. Res. Commun.* 509, 429–434. doi: 10.1016/j.bbrc.2018.12.100

Simonati, A., and Williams, R. E. (2022). Neuronal ceroid Lipofuscinosis: the multifaceted approach to the clinical issues, an overview. *Front. Neurol.* 13:811686. doi: 10.3389/fneur.2022.811686

Singh, K. K., Park, K. J., Hong, E. J., Kramer, B. M., Greenberg, M. E., Kaplan, D. R., et al. (2008). Developmental axon pruning mediated by Bdnf-p75ntr–dependent axon degeneration. *Nat. Neurosci.* 11, 649–658. doi: 10.1038/nn.2114

Skaper, S. D., Floreani, M., Negro, A., Facci, L., and Giusti, P. (1998). Neurotrophins rescue cerebellar granule neurons from oxidative stress-mediated apoptotic death: selective involvement of phosphatidylinositol 3-kinase and the mitogen-activated protein kinase pathway. *J. Neurochem.* 70, 1859–1868. doi: 10.1046/j.1471-4159.1998.70051859.x

Snider, R. S., Maiti, A., and Snider, S. R. (1976). Cerebellar pathways to ventral midbrain and nigra. *Exp. Neurol.* 53, 714–728. doi: 10.1016/0014-4886(76)90150-3

Soontornniyomkij, B., Everall, I. P., Chana, G., Tsuang, M. T., Achim, C. L., and Soontornniyomkij, V. (2011). Tyrosine kinase B protein expression is reduced in the cerebellum of patients with bipolar disorder. *J. Affect. Disord.* 133, 646–654. doi: 10.1016/j.jad.2011.04.044

Stoodley, C. J. (2012). The cerebellum and cognition: evidence from functional imaging studies. *Cerebellum* 11, 352–365. doi: 10.1007/s12311-011-0260-7

Stoodley, C. J. (2016). The cerebellum and neurodevelopmental disorders. *Cerebellum* 15, 34–37. doi: 10.1007/s12311-015-0715-3

Strick, P. L., Dum, R. P., and Fiez, J. A. (2009). Cerebellum and nonmotor function. *Annu. Rev. Neurosci.* 32, 413–434. doi: 10.1146/annurev.neuro.31.060407.125606

Subramaniam, S., Strelau, J., and Unsicker, K. (2008). Gdnf prevents Tgf-β-induced damage of the plasma membrane in cerebellar granule neurons by suppressing activation of p38-Mapk via the phosphatidylinositol 3-kinase pathway. *Cell Tissue Res.* 331, 373–383. doi: 10.1007/s00441-007-0538-8

Syed, Z., Dudbridge, F., and Kent, L. (2007). An investigation of the neurotrophic factor genes Gdnf, Ngf, and Nt3 in susceptibility to Adhd. *Am. J. Med. Genet. B Neuropsychiatr. Genet.* 144B, 375–378. doi: 10.1002/ajmg.b.30459

Takumi, K., Mori, T., Shimizu, K., and Hayashi, M. (2005). Developmental changes in concentrations and distributions of neurotrophins in the monkey cerebellar cortex. *J. Chem. Neuroanat.* 30, 212–220. doi: 10.1016/j.jchemneu.2005.08.004

Tanaka, S., Sekino, Y., and Shirao, T. (2000). The effects of neurotrophin-3 and brain-derived neurotrophic factor on cerebellar granule cell movement and neurite extension in vitro. *Neuroscience* 97, 727–734. doi: 10.1016/S0306-4522(00)00049-X

Tang, W., Lu, Y., Tian, Q.-Y., Zhang, Y., Guo, F.-J., Liu, G.-Y., et al. (2011). The growth factor progranulin binds to Tnf receptors and is therapeutic against inflammatory arthritis in mice. *Science* 332, 478–484. doi: 10.1126/science.1199214

Tepper, B., Bartkowska, K., Okrasa, M., Ngati, S., Braszak, M., Turlejski, K., et al. (2020). Downregulation of TrkC receptors increases dendritic Arborization of Purkinje cells in the developing cerebellum of the opossum, *Monodelphis domestica*. *Front. Neuroanat.* 14:614617. doi: 10.3389/fnana.2020.614617

Tiveron, C., Fasulo, L., Capsoni, S., Malerba, F., Marinelli, S., Paoletti, F., et al. (2013). Prongf\Ngf imbalance triggers learning and memory deficits, neurodegeneration and spontaneous epileptic-like discharges in transgenic mice. *Cell Death Differ.* 20, 1017–1030. doi: 10.1038/cdd.2013.22

Tong, L., and Perez-Polo, R. (1998). Brain-derived neurotrophic factor (Bdnf) protects cultured rat cerebellar granule neurons against glucose deprivation-induced apoptosis. *J. Neural Transm.* 105, 905–914. doi: 10.1007/s007020050101

Townley, R. A., Boeve, B. F., and Benarroch, E. E. (2018). Progranulin: functions and neurologic correlations. *Neurology* 90, 118–125. doi: 10.1212/WNL.0000000000004840

Treanor, J. J. S., Goodman, L., De Sauvage, F., Stone, D. M., Poulsen, K. T., Beck, C. D., et al. (1996). Characterization of a multicomponent receptor for Gdnf. *Nature* 382, 80–83. doi: 10.1038/382080a0

Trupp, M., Arenas, E., Fainzilber, M., Nilsson, A.-S., Sieber, B.-A., Grigoriou, M., et al. (1996). Functional receptor for Gdnf encoded by the c-ret proto-oncogene. *Nature* 381, 785–789. doi: 10.1038/381785a0

Tunca, Z., Kıvırcık Akdede, B., Özerdem, A., Alkın, T., Polat, S., Ceylan, D., et al. (2015). Diverse glial cell line-derived neurotrophic factor (Gdnf) support between mania and schizophrenia: a comparative study in four major psychiatric disorders. *Eur. Psychiatry* 30, 198–204. doi: 10.1016/j.eurpsy.2014.11.003

Uesaka, N., Abe, M., Konno, K., Yamazaki, M., Sakoori, K., Watanabe, T., et al. (2018). Retrograde signaling from Progranulin to Sort1 counteracts synapse elimination in the developing cerebellum. *Neuron* 97, 796–805.e5. doi: 10.1016/j.neuron.2018.01.018

Van Damme, P., Van Hoecke, A., Lambrechts, D., Vanacker, P., Bogaert, E., Van Swieten, J., et al. (2008). Progranulin functions as a neurotrophic factor to regulate neurite outgrowth and enhance neuronal survival. *J. Cell Biol.* 181, 37–41. doi: 10.1083/jcb.200712039

Vicario, A., Kisiswa, L., Tann, J. Y., Kelly, C. E., and Ibáñez, C. F. (2015). Neuron-type-specific signaling by the p75ntr death receptor is regulated by differential proteolytic cleavage. *J. Cell Sci.* 128, 1507–1517. doi: 10.1242/jcs.161745

Voisin, A., Damon-Soubeyrand, C., Bravard, S., Saez, F., Drevet, J. R., and Guiton, R. (2020). Differential expression and localisation of Tgf-β isoforms and receptors in the murine epididymis. *Sci. Rep.* 10:995. doi: 10.1038/s41598-020-57839-5

Wagner, M. J., Kim, T. H., Savall, J., Schnitzer, M. J., and Luo, L. (2017). Cerebellar granule cells encode the expectation of reward. *Nature* 544, 96–100. doi: 10.1038/nature21726

Wang, L., Chen, J., Hu, Y., Liao, A., Zheng, W., Wang, X., et al. (2022). Progranulin improves neural development via the Pi3K/Akt/Gsk-3β pathway in the cerebellum of a Vpa-induced rat model of Asd. *Transl. Psychiatry* 12:114. doi: 10.1038/s41398-022-01875-4

Wang, W., Mullikin-Kilpatrick, D., Crandall, J. E., Gronostajski, R. M., Litwack, E. D., and Kilpatrick, D. L. (2007). Nuclear factor I coordinates multiple phases of cerebellar granule cell development via regulation of cell adhesion molecules. *J. Neurosci.* 27, 6115–6127. doi: 10.1523/JNEUROSCI.0180-07.2007

Wang, L., Nomura, M., Goto, Y., Tanaka, K., Sakamoto, R., Abe, I., et al. (2011). Smad2 protein disruption in the central nervous system leads to aberrant cerebellar development and early postnatal Ataxia in mice*. *J. Biol. Chem.* 286, 18766–18774. doi: 10.1074/jbc.M111.223271

Wang, X., Yue, T.-L., White, R. F., Barone, F. C., and Feuerstein, G. Z. (1995). Transforming growth factor-β1 exhibits delayed gene expression following focal cerebral ischemia. *Brain Res. Bull.* 36, 607–609. doi: 10.1016/0361-9230(94)00243-T

Wee, P., and Wang, Z. (2017). Epidermal growth factor receptor cell proliferation signaling pathways. *Cancers* 9:52. doi: 10.3390/cancers9050052

Wieduwilt, M. J., and Moasser, M. M. (2008). The epidermal growth factor receptor family: biology driving targeted therapeutics. *Cell. Mol. Life Sci.* 65, 1566–1584. doi: 10.1007/s00018-008-7440-8

Wong, R. W. C., and Guillaud, L. (2004). The role of epidermal growth factor and its receptors in mammalian Cns. *Cytokine Growth Factor Rev.* 15, 147–156. doi: 10.1016/j.cytogfr.2004.01.004

Xie, F., Padival, M., and Siegel, R. E. (2007). Association of Psd-95 with ErbB4 facilitates neuregulin signaling in cerebellar granule neurons in culture. *J. Neurochem.* 100, 62–72. doi: 10.1111/j.1471-4159.2006.04182.x

Xie, F., Raetzman, L. T., and Siegel, R. E. (2004). Neuregulin induces Gabaa receptor β2 subunit expression in cultured rat cerebellar granule neurons by activating multiple signaling pathways. *J. Neurochem.* 90, 1521–1529. doi: 10.1111/j.1471-4159.2004.02685.x

Xu, X., Wu, D., Hou, S., Zhu, J., Li, J., and Tang, J. (2017). Prenatal exposure to Tak242 affects the childhood autism in offspring in animal models of autism spectrum disorder. *Iran. J. Basic Med. Sci.* 20, 1016–1020. doi: 10.22038/IJBMS.2017.9270

Yacubova, E., and Komuro, H. (2002). Cellular and molecular mechanisms of cerebellar granule cell migration. *Cell Biochem. Biophys.* 37, 213–234. doi: 10.1385/cbb:37:3:213

Yamada, M., Ikeuchi, T., and Hatanaka, H. (1997). The neurotrophic action and signalling of epidermal growth factor. *Prog. Neurobiol.* 51, 19–37. doi: 10.1016/S0301-0082(96)00046-9

Yamashita, K., Gerken, U., Vogel, P., Hossmann, K. A., and Wiessner, C. (1999). Biphasic expression of Tgf-β1 mrna in the rat brain following permanent occlusion of the middle cerebral artery. *Brain Res.* 836, 139–145. doi: 10.1016/S0006-8993(99)01626-1

Yamashita, N., Mosinger, B., Roy, A., Miyazaki, M., Ugajin, K., Nakamura, F., et al. (2011). Crmp5 (Collapsin response mediator protein 5) regulates dendritic development and synaptic plasticity in the cerebellar Purkinje cells. *J. Neurosci.* 31:1773. doi: 10.1523/JNEUROSCI.5337-10.2011

Yang, B., Ren, Q., Zhang, J. C., Chen, Q. X., and Hashimoto, K. (2017). Altered expression of Bdnf, Bdnf pro-peptide and their precursor probdnf in brain and liver tissues from psychiatric disorders: rethinking the brain–liver axis. *Transl. Psychiatry* 7:e1128. doi: 10.1038/tp.2017.95

Yeganeh-Doost, P., Gruber, O., Falkai, P., and Schmitt, A. (2011). The role of the cerebellum in schizophrenia: from cognition to molecular pathways. *Clinics* 66, 71–77. doi: 10.1590/S1807-59322011001300009

Yoon, S. O., Casaccia-Bonnefil, P., Carter, B., and Chao, M. V. (1998). Competitive signaling between TrkA and p75 nerve growth factor receptors determines cell survival. *J. Neurosci.* 18:3273. doi: 10.1523/JNEUROSCI.18-09-03273.1998

Zanin, J. P., Abercrombie, E., and Friedman, W. J. (2016). Proneurotrophin-3 promotes cell cycle withdrawal of developing cerebellar granule cell progenitors via the p75 neurotrophin receptor. *elife* 5:e16654. doi: 10.7554/eLife.16654

Zanin, J. P., and Friedman, W. J. (2022). p75ntr prevents the onset of cerebellar granule cell migration via RhoA activation. *elife* 11:e79934. doi: 10.7554/eLife.79934

Zanin, J. P., Verpeut, J. L., Li, Y., Shiflett, M. W., Wang, S. S. H., Santhakumar, V., et al. (2019). The p75ntr influences cerebellar circuit development and adult behavior via regulation of cell cycle duration of granule cell progenitors. *J. Neurosci.* 39:9119. doi: 10.1523/JNEUROSCI.0990-19.2019

Zhang, Y., Alexander, P., and Wang, X.-F. (2016). Tgf-β family signaling in the control of cell proliferation and survival. *Cold Spring Harb. Perspect. Biol.* 9:a022145. doi: 10.1101/cshperspect.a022145

Zhang, L., and Goldman, J. E. (1996). Generation of cerebellar interneurons from dividing progenitors in White matter. *Neuron* 16, 47–54. doi: 10.1016/S0896-6273(00)80022-7

Zhou, P., Porcionatto, M., Pilapil, M., Chen, Y., Choi, Y., Tolias, K. F., et al. (2007). Polarized signaling endosomes coordinate Bdnf-induced chemotaxis of cerebellar precursors. *Neuron* 55, 53–68. doi: 10.1016/j.neuron.2007.05.030

Zhou, X., Sun, L., Bastos De Oliveira, F., Qi, X., Brown, W. J., Smolka, M. B., et al. (2015). Prosaposin facilitates sortilin-independent lysosomal trafficking of progranulin. *J. Cell Biol.* 210, 991–1002. doi: 10.1083/jcb.201502029

Zhou, Y.-X., Zhao, M., Li, D., Shimazu, K., Sakata, K., Deng, C.-X., et al. (2003). Cerebellar deficits and hyperactivity in mice lacking Smad4*. *J. Biol. Chem.* 278, 42313–42320. doi: 10.1074/jbc.M308287200

Zirrgiebel, U., Ohga, Y., Carter, B., Berninger, B., Inagaki, N., Thoenen, H., et al. (1995). Characterization of TrkB receptor-mediated signaling pathways in rat cerebellar granule neurons: involvement of protein kinase C in neuronal survival. *J. Neurochem.* 65, 2241–2250. doi: 10.1046/j.1471-4159.1995.65052241.x

frontiers | Frontiers in Molecular Neuroscience

TYPE Original Research
PUBLISHED 12 May 2023
DOI 10.3389/fnmol.2023.1175851

OPEN ACCESS

EDITED BY
Eva Zerovnik,
Institut Jožef Stefan (IJS), Slovenia

REVIEWED BY
Natasha Kopitar-Jerala,
Institut Jožef Stefan (IJS), Slovenia
Manikandan Samidurai,
SENS Research Foundation, United States

*CORRESPONDENCE
Anna-Elina Lehesjoki
✉ anna-elina.lehesjoki@helsinki.fi

RECEIVED 28 February 2023
ACCEPTED 25 April 2023
PUBLISHED 12 May 2023

CITATION
Gorski K, Jackson CB, Nyman TA, Rezov V, Battersby BJ and Lehesjoki A-E (2023) Progressive mitochondrial dysfunction in cerebellar synaptosomes of cystatin B-deficient mice.
Front. Mol. Neurosci. 16:1175851.
doi: 10.3389/fnmol.2023.1175851

Progressive mitochondrial dysfunction in cerebellar synaptosomes of cystatin B-deficient mice

Katarin Gorski[1,2], Christopher B. Jackson[3], Tuula A. Nyman[4], Veronika Rezov[1,2], Brendan J. Battersby[5] and Anna-Elina Lehesjoki[1,2]*

[1]Folkhälsan Research Center, Helsinki, Finland, [2]Medicum, Faculty of Medicine, University of Helsinki, Helsinki, Finland, [3]Department of Biochemistry and Developmental Biology, Medicum, Faculty of Medicine, University of Helsinki, Helsinki, Finland, [4]Department of Immunology, Oslo University Hospital, University of Oslo, Oslo, Norway, [5]Institute of Biotechnology, University of Helsinki, Helsinki, Finland

The involvement of mitochondrial dysfunction in cystatin B (CSTB) deficiency has been suggested, but its role in the onset of neurodegeneration, myoclonus, and ataxia in the CSTB-deficient mouse model (*Cstb*$^{-/-}$) is yet unknown. CSTB is an inhibitor of lysosomal and nuclear cysteine cathepsins. In humans, partial loss-of-function mutations cause the progressive myoclonus epilepsy neurodegenerative disorder, EPM1. Here we applied proteome analysis and respirometry on cerebellar synaptosomes from early symptomatic (*Cstb*$^{-/-}$) mice to identify the molecular mechanisms involved in the onset of CSTB-deficiency associated neural pathogenesis. Proteome analysis showed that CSTB deficiency is associated with differential expression of mitochondrial and synaptic proteins, and respirometry revealed a progressive impairment in mitochondrial function coinciding with the onset of myoclonus and neurodegeneration in (*Cstb*$^{-/-}$) mice. This mitochondrial dysfunction was not associated with alterations in mitochondrial DNA copy number or membrane ultrastructure. Collectively, our results show that CSTB deficiency generates a defect in synaptic mitochondrial bioenergetics that coincides with the onset and progression of the clinical phenotypes, and thus is likely a contributor to the pathogenesis of EPM1.

KEYWORDS

mitochondria, myoclonus, neurodegeneration, OXPHOS, synaptosome, respiration, proteomics

1. Introduction

Progressive myoclonus epilepsy EPM1 (Unverricht-Lundborg disease; OMIM 254800), caused by biallelic partial loss-of-function mutations in the cystatin B (*CSTB*) gene (Pennacchio et al., 1996; Joensuu et al., 2008), is a neurodegenerative disorder manifesting with minor or no cognitive decline (Koskiniemi et al., 1974; Kälviäinen et al., 2008). Patients develop severely disabling and treatment-resistant myoclonus and tonic–clonic epileptic seizures between 6 and 16 years of age, followed by ataxia, incoordination and dysarthria (Koskiniemi et al., 1974; Kälviäinen et al., 2008). Magnetic resonance imaging of EPM1 patient brains show widespread degenerative changes in both white and grey matter (Koskenkorva et al., 2009, 2012; Manninen

et al., 2013), and MRI-navigated transcranial magnetic stimulation analyses altered cortical responses (Danner et al., 2009; Julkunen et al., 2013). Postmortem analyses have shown widespread atrophy, neuronal loss, and gliosis in both cerebrum and cerebellum (Haltia et al., 1969; Koskiniemi et al., 1974; Eldridge et al., 1983; Cohen et al., 2011).

Most EPM1 patients are homozygous for a 12-nucleotide repeat expansion mutation in the promoter region of *CSTB*, reducing *CSTB* mRNA and protein expression to less than 10% of that in controls (Joensuu et al., 2007). Patients that are compound heterozygous for the repeat expansion and a truncating null mutation have a more severe phenotype with an earlier onset and poorer cognitive performance (Koskenkorva et al., 2011; Canafoglia et al., 2012). In contrast, patients homozygous for two null mutations manifest a severe neonatal-onset progressive encephalopathy that is clinically distinct from EPM1 (Mancini et al., 2016; O'Brien et al., 2017). These genotype–phenotype correlations suggest that CSTB is essential for normal brain development and for maintaining neuronal integrity in mature brain. The CSTB deficient knockout mouse (*Cstb*$^{-/-}$) is a model for EPM1. It recapitulates the key clinical features and pathological changes of the disorder: myoclonus, progressive ataxia, and grey and white matter degeneration (Pennacchio et al., 1998; Tegelberg et al., 2012; Manninen et al., 2013, 2014).

Cystatin B is a ubiquitously expressed inhibitor of cysteine proteases of the cathepsin family (Green et al., 1984; Čeru et al., 2010) showing both cytoplasmic and nuclear localization. In the cytoplasm, CSTB partially co-localizes with lysosomal markers (Alakurtti et al., 2005) and is thought to prevent inappropriate proteolytic activity and redistribution of cysteine cathepsins in the cytosol (Boya and Kroemer, 2008). In line with its lysosomal association, CSTB function has been linked to protecting neurons from oxidative damage through an oxidative stress-responsive cystatin B-cathepsin B signaling pathway (Lehtinen et al., 2009). In the nucleus, CSTB interacts with histones and cathepsin L, which affects cell cycle regulation and proteolytic cleavage of the histone H3 tail (Čeru et al., 2010; Daura et al., 2021). Downstream effects of CSTB function are implicated in several cellular and biological processes, including inflammation (Tegelberg et al., 2012; Maher et al., 2014; Okuneva et al., 2016), apoptosis (Pennacchio et al., 1998), neurogenesis (Di Matteo et al., 2020; Daura et al., 2021), and synapse physiology (Joensuu et al., 2014; Penna et al., 2019; Gorski et al., 2020). CSTB deficiency induces widespread physiological and pathological changes in the mouse brain, which are most pronounced in the cerebellum. This includes progressive loss of cerebellar granule cells from 1 month of age onwards (Pennacchio et al., 1998) and a decrease in the cerebellar volume by 50% at 6 months of age (Tegelberg et al., 2012). Other changes include altered GABAergic signaling (Joensuu et al., 2014), glial activation (Tegelberg et al., 2012) and inflammation (Okuneva et al., 2016). All of these events precede neuronal death.

To gain insight into the molecular defects associated with synaptic function in *Cstb*$^{-/-}$ mice, we previously performed a quantitative proteomics study of cerebellar synaptosomes isolated from presymptomatic two-week old mice (Gorski et al., 2020). We found that one third of the cerebellar synaptosomal proteins that differed in abundance belong to the mitochondrial proteome, primarily those involved with oxidative phosphorylation (OXPHOS). These data imply that mitochondrial dysfunction is associated with the early pathogenesis of altered synaptic function in CSTB deficiency. In line with these findings, neural progenitor cells from *Cstb*$^{-/-}$ mice had altered mRNA expression levels of nuclear-encoded OXPHOS genes and impaired mitochondrial respiration upon neural stem cell differentiation (Daura et al., 2021).

In the present study, we investigated cerebellar synaptosomes from symptomatic *Cstb*$^{-/-}$ mice early in the phenotype onset. Our results show that changes in the mitochondrial proteome and respiration are linked to the early onset of myoclonus and neurodegeneration. Collectively, our study expands the current understanding of mitochondrial involvement in the early neuronal pathology in CSTB deficiency.

2. Materials and methods

2.1. Ethics statement

The Animal Ethics Committee of the State Provincial Office of Southern Finland approved all animal research protocols (decisions ESAVI/10765/2015 and ESAVI/471/2019).

2.2. Mice

Cstb$^{-/-}$ mice were derived from The Jackson Laboratory (Bar Harbor, ME; 129-Cstb^{tm1Rm}/SvJ; stock #003486) (Pennacchio et al., 1998). Wild type mice of same age and background were used as controls. Heterozygous *Cstb*$^{+/-}$ males were backcrossed with inbred wild type females to expand the colony from heterozygous littermates and to maintain the *Cstb*$^{-/-}$ mouse line. The genetic background of the mouse colony was refreshed annually with wild type females, and F1-F3 generations were used for experimental procedures. Mice were sacrificed by carbon dioxide euthanasia, followed by cervical dislocation.

2.3. Synaptosome isolation

For proteomics analysis, cerebellar synaptosomes from P30 *Cstb*$^{-/-}$ and wild type mice were isolated using a sucrose-based separation protocol, as previously described (Gorski et al., 2020). For analyses of high-resolution respirometry, mitochondrial DNA (mtDNA) copy number, immunoblot, and electron microscopy, cerebellar synaptosomes from P30 and P45 *Cstb*$^{-/-}$ and wild type mice were isolated using a Percoll-based separation protocol, modified from protocols by Dunkley et al. (2008) and Tenreiro et al. (2017). Briefly, cerebella were dissected and rinsed three times in ice-cold homogenization buffer (H1; 0.32 M sucrose, 1 mM EDTA, 5 mM Tris, pH 7.4), followed by homogenization with 10 even strokes in ice-cold H1 using a glass-Teflon homogenizer. The homogenizer was rinsed with an equal volume of H1, and the combined homogenate was centrifuged at 1000 × *g* for 10 min at +4°C. The resulting supernatant was further centrifuged at 14000 × *g* for 20 min at +4°C. The resulting pellet was resuspended in 45% Percoll (Cytiva, MA, United States) (v/v; Percoll:H1), and centrifuged at 14000 × *g* for 2 min at +4°C. The synaptosomal-enriched fraction on the top layer was washed with four volumes H1 and pelleted twice at 14000 × *g* for 2 min at +4°C with an

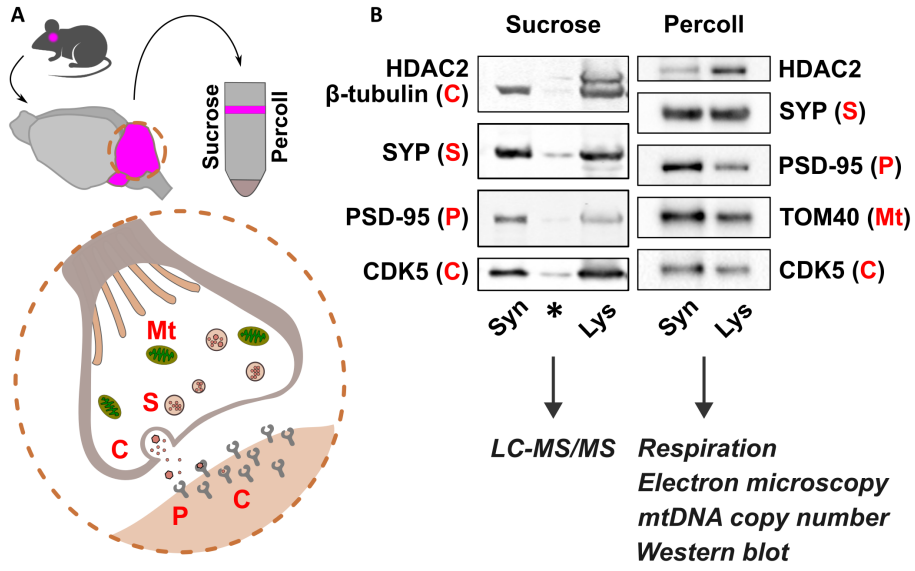

FIGURE 1
Synaptosomal fractionation and characterization. **(A)** Schematic presentation of synaptosome isolation from mouse cerebella (pink) using sucrose and Percoll. Synaptosome preparations consist of functional pre- and postsynaptic terminals containing organelles, synaptic vesicles, and receptors for neurotransmitters. **(B)** Immunoblot detection of pre- and postsynaptic proteins Synaptophysin (SYP) and Post-synaptic density 95 (PSD-95), respectively, and depletion of Histone deacetylase 2 (HDAC2) show synaptic protein enrichment in synaptosome preparations (Syn) compared to cerebellar lysate (Lys). Mitochondrial abundance is shown in Percoll-fractions by detection of Mitochondrial import receptor subunit TOM40. Cytosolic proteins are represented by β-tubulin and cyclin dependent kinase 5 (CDK5). Sucrose and Percoll-isolated fractions were used for mass spectrometry, and analyses of synaptic mitochondria, respectively. Mt., mitochondria; S, SYP; C, cytoplasm; P, PSD-95. Asterisk indicates carry-over signal.

additional H1 wash in between. Synaptosomal purity and protein enrichment were analyzed by immunoblotting (Figure 1).

2.4. Proteomics

2.4.1. Sample preparation and LC–MS/MS analysis

Lipids were removed from synaptosome samples ($n = 5 + 5$ mice/genotype) as previously described (Gorski et al., 2020). Briefly, samples were incubated overnight at −20°C in five volumes ice-cold (−20°C) acetone and centrifuged twice at 1000 × *g* for 10 min at +4°C with an additional acetone wash in between. Pellets were air dried for 5 min and resuspended in freshly prepared 6.0 M urea/25 mM ammonium bicarbonate. Protein concentrations (µg/µl) were determined spectrophotometrically using the BCA protein assay kit (Pierce, Thermo Fisher Scientific) according to the manufacturer's instructions.

For proteome analysis, 5 µg of each sample was reduced and alkylated using dithiothreitol (DTT) and iodoacetamide (IAA), and the urea concentration was diluted to 1 M, followed by overnight digestion with trypsin (Promega Corporation, WI, USA) at +37°C. Peptides were desalted and concentrated by the STAGE-TIP method using a C18 resin disk (3 M Empore). Samples were eluted with 0.1% formic acid/60% acetonitrile, dried, and solubilized in 7 µl 0.1% formic acid prior to mass spectrometry analysis. Each peptide mixture was analyzed using an EASY-nLC system coupled to the QExactive Plus mass spectrometer (ThermoElectron, Bremen, Germany) equipped with the EASY Spray PepMap®RSLC column (C18, 2 µl, 100 Å, 75 µm x 25 cm) using a 120 min LC separation gradient.

2.4.2. Protein identification, label-free quantification and bioinformatic analyses

The resulting MS raw files were submitted to the MaxQuant software (Cox and Mann, 2008) version 1.6.2.10 for protein identification and label-free quantification. Carbamidomethyl (C) was set as a fixed modification, and acetyl (protein N-term), carbamyl (N-term) and oxidation (M) were set as variable modifications. First search peptide tolerance of 20 ppm and main search error 4.5 ppm were used. Trypsin without proline restriction enzyme option was used with two allowed miscleavages. The minimal unique + razor peptides number was set to 1, and the allowed false discovery rate (FDR) was 0.01 (1%) for peptide and protein identification. Label-free quantitation (LFQ) was employed with default settings. The Uniprot database with 'mouse' entries (January 2019) was used for the database searches.

The mass spectrometry proteomics data have been deposited to the ProteomeXchange Consortium[1] *via* the PRIDE partner repository (Vizcaíno et al., 2013) with the dataset identifier PXD040382.

2.4.3. Data processing and analysis

The LFQ values were log10 -transformed, filtered to include only proteins identified and quantified in at least three out of five replicates in at least one experimental group, and missing values were imputed with default settings. Based on Principal component analysis, one wild type sample was removed as an outlier before statistical testing. To find statistically significant differences between the two groups

1 http://proteomecentral.proteomexchange.org

(*Cstb*$^{-/-}$ vs. wild type), *t*-test was performed using permutation-based FDR ≤ 0.05 as cut-off.

Downstream analyses were conducted to proteins with a q-value <0.05 using the following softwares and statistical tests: PANTHER (version 17.0, released 2022-22-02) Overrepresentation Test (Released 20,220,712) (Mi et al., 2013) using the Gene Ontology (GO) enrichment analysis tool (Ashburner et al., 2000; Gene Ontology Consortium, 2021) and Reactome pathway analysis (Wu and Haw, 2017) version 65 (released 2021-10-01), using Fisher's exact test followed by Benjamini–Hochberg correction (FDR) for multiple testing, considering FDR <0.01 statistically significant; DAVID functional annotation clustering version 2021 (Huang et al., 2009a,b), using medium classification stringency, and EASE scoring followed by Benjamini–Hochberg correction (FDR) for multiple testing, considering FDR <0.05 statistically significant, and Heatmapper (Babicki et al., 2016), using average linkage clustering. Mitochondrial proteins and their functions were retrieved using MitoCarta3.0 (Rath et al., 2021). The software Inkscape[2] was used for visualization of the data.

2.5. High-resolution respirometry

Mitochondrial oxygen consumption rates were measured from freshly isolated synaptosome fractions of P30 and P45 *Cstb*$^{-/-}$ and wild type mice ($n = 7 + 7$/age group, males and females) using a high-resolution oxygraph (Oroboros Instruments GmbH, Innsbruck, Austria). Samples were resuspended in respiration buffer (0.5 mM EGTA, 3 mM $MgCl_2$, 60 mM Lactobionic acid, 20 mM Taurine, 10 mM KH_2PO_4, 20 mM HEPES, 110 mM D-Sucrose, 1% fat-free BSA), and oxygen consumption rates [pmol/(s*mg synaptosomal proteins)] were measured at 37°C according to a substrate-uncoupler-inhibitor-titration (SUIT) protocol as previously described (Awadhpersad and Jackson, 2021).

Briefly, measurements were performed in the presence of 1 mM malate, 5 mM pyruvate and 5 mM glutamate, and additional substrates and inhibitors were injected to oxygraph chambers in the following order: (i) 1.25 mM ADP; (ii) 10 mM succinate; (iii) 1 µg/ml oligomycin A; (iv) titration of carbonyl cyanide 4-(trifluoromethoxy) phenylhydrazone (FCCP); (v) 0.5 µM rotenone; (vi) 1 µg/ml antimycin A; (vii) 2 mM ascorbate; (viii) 0.5 mM *N,N,N′,N′*-tetramethyl-*p*-phenylenediamine (TMPD); and (ix) 10 mM sodium azide. All substrates and inhibitors were purchased from Sigma Aldrich (Saint Louis, MO, United States). Polarographic oxygen sensors monitored changes in oxygen concentration as substrates and inhibitors were applied, and changes in oxygen concentration and consumption were plotted over time.

The DatLab software (Oroboros Instruments GmbH, Innsbruck, Austria) was used for calculating oxygen consumption rates (OCR). Rates were normalized to sample protein concentration, determined using the BCA protein assay kit (Pierce, Thermo Fisher Scientific) according to the manufacturer's instructions.

CI and CII-linked coupled respiration was achieved after addition of succinate (ii), leak-respiration after uncoupling the ATP-synthase (CV) from the electron transport system using oligomycin, and maximal uncoupled respiration by titrating FCCP until no further increase in respiration was detected. Complex IV (CIV) -dependent respiration was achieved by addition of ascorbate (vii), TMPD (viii), and sodium azide (ix). The difference between oxygen consumption before and after addition of sodium azide was considered as CIV-dependent respiration. Residual oxygen consumption (ROX) values were achieved after addition of rotenone (v) and antimycin A (vi), and subtracted from all oxygen consumption rates to correct for non-mitochondrial oxygen consumption. The coupling control ratio (CCR) was calculated according to the protocol by the MitoEAGLE Task Group (Gnaiger et al., 2020).

2.6. Immunoblot analysis

2.6.1. Sample preparation

For immunoblot analysis, synaptosome samples were diluted in lysis buffer (50 mM This-HCl pH 7.5, 100 mM NaCl, 1 mM DTT) with 1% n-Dodecyl-beta-Maltoside (DDM) (Thermo Fisher Scientific, Waltham, MA, United States), and protease and phosphatase inhibitors (Pierce Protease and Phosphatase Inhibitor Mini Tablets, Thermo Fisher Scientific), and incubated on ice for 15 min. Protein concentrations (µg/µl) were determined spectrophotometrically using the BCA protein assay kit (Pierce, Thermo Fisher Scientific) according to the manufacturer's instructions.

2.6.2. SDS-PAGE, electroblotting, and antibodies

Protein samples were mixed with Laemmli buffer containing β-mercaptoethanol, and proteins were separated in stain-free 4–20, 7.5%, or all kD pre-cast gels (TGX Stain-Free, BioRad, CA, United States) and electroblotted to PVDF membranes (Trans-blot Turbo Transfer pack, BioRad). Membranes were blocked in 5% milk/PBST for 60 min at r/t and incubated with primary antibodies against SYP (M0776, Dako; 1:500), HDAC2 (05–814, Millipore, 1:500), PSD-95 (610,495, BD Transduction Laboratories, 1:500), CDK-5 (05–364, Upstate, 1:2000), VDAC-1 (ab14734, Abcam; 1:4000), Vinculin (ab129002, Abcam; 1:4000), SDHA (ab14715, Abcam; 1:10000), mtCO1 (ab14705, Abcam; 1:3000), Atp5b (17247-1-AP, Proteintech, 1:5000), TOM40 (sc-11,414, Santa Cruz; 1:2000), TOM20 (11802-1-AP, Proteintech, 1:4000), OPA1 (612,606, BD Biosciences, 1,1,000), and β-tubulin (T4026, Sigma Aldrich; 1:5000) o/n at +8°C. Secondary antibodies against mouse (P0447, DAKO) and rabbit (P0399, DAKO), diluted 1:5000 in 1% milk/PBST +0.01% SDS, were incubated for 60 min at r/t. Antibody detection and signal intensity quantification was performed using the ChemiDoc XRS+ imaging system (BioRad, CA, United States) utilizing stain-free technology for total protein normalization, or the Odyssey Infrared Imaging system (LI-COR Biosciences).

2.7. Mitochondrial DNA copy number analysis

2.7.1. Standard curve preparation

Mitochondrial DNA (mtDNA) copy number (cn) was quantified from cerebellar synaptosomes of P30 and P45

2 https://inkscape.org

Cstb$^{-/-}$ and wild type mice using a standard curve-based method, as previously described (Rooney et al., 2015). Briefly, a standard curve of template copies using a plasmid [501–1 mtDNA in the pBR325 backbone (Blanc et al., 1981)] was amplified in a 2-fold dilution series ranging from 4,000 to 256,000 copies. The standard line was plotted as log (plasmid copy number) versus real-time quantitative PCR (RT-qPCR) cycle threshold (Ct). Ct values were obtained from the RT-qPCR amplification plots.

2.7.2. DNA isolation from synaptosomes

Total DNA was isolated from synaptosomes ($n = 10–13$/genotype/age group, males and females) using the DNeasy Blood & Tissue Kit (Qiagen, Venlo, Netherlands) according to the manufacturer's instructions. Prior to lysis, samples were resuspended in ice-cold 1xPBS, and 50% of the sample volume was removed and used for determination of protein concentration using the BCA protein assay kit (Pierce, Thermo Fisher Scientific) according to the manufacturer's instructions. Stock DNA (sDNA) elution volume was set to 20 µl and samples of working concentration DNA (wDNA) of approximately 0.1 ng/µl were diluted of these. The concentrations of sDNA and wDNA were assessed using the Qubit dsDNA HS Assay Kit (Thermo Fisher Scientific).

2.7.3. Real-time quantitative PCR

For each reaction, 1 µl of DNA template (standard or wDNA) was mixed with iQ SYBR Green Supermix (BioRad) and 10 uM of forward (5′-AGGAGCCTGTTCTATAATCGATAAA-3′) and reverse (5′-GATGGCGGTATATAGGCTGAA-3′) primers. RT-qPCR reactions were run once in triplicate using the CFX96 Real-time PCR detection system (BioRad) and the CFX Maestro software under the following program: 7 min at 95°C, 10 s at 95°C, and 40 cycles of 30 s at 60°C, followed by a melt curve protocol of 0.5 s + plate read at 65°C, and then 0.5 s + plate read at each 0.5°C increments between 65°C and 95°C. MtDNA copy number per µl wDNA was determined using Ct-values of the unknown samples in relation to the standard curve, and further calculated to mtDNA copy number/mg protein. RT-qPCR assays were performed in accordance with MIQE guidelines (Bustin et al., 2009).

2.8. Electron microscopy

Cerebellar tissue pieces ($n = 1–3$; P30, P45) from *Cstb*$^{-/-}$ and wild type mice were fixed in 2% glutaraldehyde in phosphate buffer, post-fixed in 1% osmium tetroxide and dehydrated through ascending concentrations of alcohol and embedded in Epon 812 resin. 60 nm ultrathin sections were obtained on a Reichert-Jung Ultracut ultramicrotome (Leica Microsystems, Wetzlar, Germany) equipped with a Diatome diamond knife (Diatome Ltd., Nidau, Switzerland), transferred to copper grids, stained with uranyl acetate and lead citrate, and observed in a CM12 transmission electron microscope (Philips Healthcare, Amsterdam, the Netherlands) at 80 kV. Images were recorded with a Morada digital camera and analyzed using the iTEM software (ResAlta Research Technologies, Golden, CO, United States).

2.9. Statistical analyses

Statistical analyses were carried out using GraphPad Prism version 9.4 for Windows (GraphPad Software, La Jolla, CA, United States[3]). Data was tested for normal distribution and comparisons between experimental conditions were evaluated using the two-tailed unpaired *t*-test, the nonparametric Mann–Whitney *U* test, and the one-way ANOVA with the Šídák correction. Statistical significance was defined as $p < 0.05$.

3. Results

3.1. Differential abundance of mitochondrial and synaptic proteins in *Cstb*$^{-/-}$ synaptosomes

To investigate synaptic alterations associated with the early symptomatic phase of CSTB deficiency, we used label-free quantitative proteomics to analyze cerebellar synaptosomes from P30 *Cstb*$^{-/-}$ and wild type mice. Principal component analysis (PCA) showed that the first component, PC1, explained 34.3% of the total variation, and segregated the samples into two genotype-specific clusters (Supplementary Figure 1A). We identified more than 2,500 and reliably quantified 1,555 proteins (Supplementary Table 1_sheet1). Of these, 349 proteins differed significantly between *Cstb*$^{-/-}$ and wild type mice (Supplementary Figure 1B and Supplementary Table 1_sheet2). In addition, we identified 34 proteins in one genotype only (Supplementary Table 1_sheet3).

To investigate the biological relationships between the 349 differentially abundant proteins, we performed Gene Ontology (GO) classification (Ashburner et al., 2000; Gene Ontology Consortium, 2021), DAVID functional annotation clustering (Huang et al., 2009a,b), Reactome pathway analysis (Wu and Haw, 2017), and PANTHER enrichment analysis (Mi et al., 2013). Analysis of statistically significant (FDR <0.01) overrepresented GO terms revealed that Synapse and Mitochondria were the most overrepresented cellular components in the dataset (Supplementary Figure 1B and Supplementary Table 2_sheet1). Correspondingly, the top 15 GO terms of biological processes were associated with energy metabolism and nucleotide biosynthesis and they grouped into several overlapping GO-terms (Supplementary Figure 2 and Supplementary Table 2_sheet2). The DAVID functional annotation clustering tool annotated proteins with increased abundance ($n = 188$) to mitochondrial function and energy metabolism, whereas proteins with decreased abundance ($n = 161$) were annotated to synaptic structure and function (Figures 2A,B, Supplementary Table 2_sheet3, and Supplementary Table 2_sheet4). The Reactome pathway database annotated the differentially abundant proteins to pathways related to immunological functions, mitochondrial energy metabolism, and intracellular trafficking (Supplementary Figure 3 and Supplementary Table 2_sheet5).

3 www.graphpad.com

10.3389/fnmol.2023.1175851

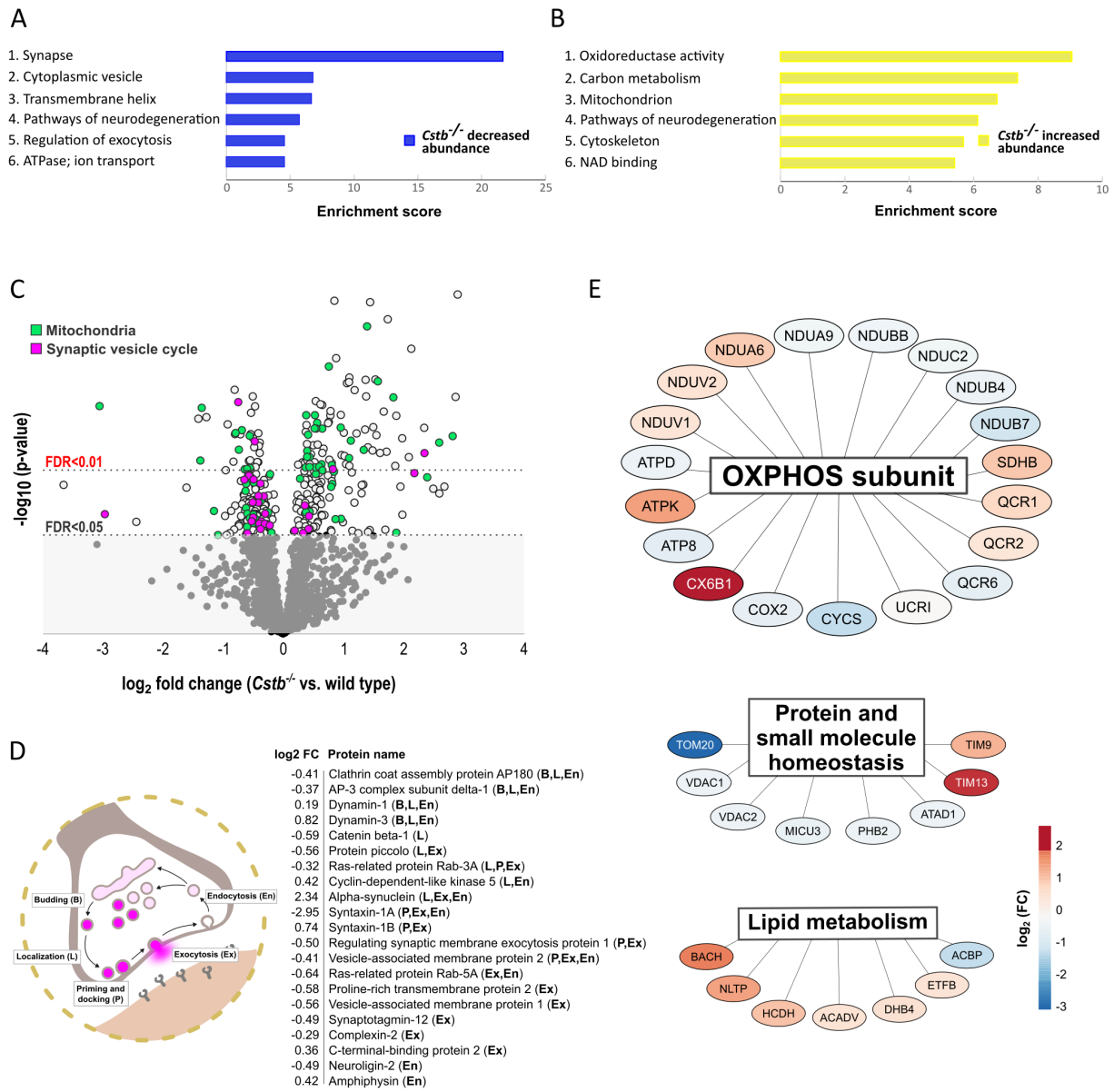

FIGURE 2
Differentially abundant proteins between wild type and *Cstb*$^{-/-}$ mice synaptosomes at P30. **(A,B)** Bar charts of enriched (enrichment score>4.0) DAVID functional annotation clusters of proteins with decreased **(A)** and increased **(B)** abundance in *Cstb*$^{-/-}$ synaptosomes. **(C)** Volcano plot of differentially abundant proteins plotted as −log10-transformed value of *p* [derived from the *t*-test (*Cstb*$^{-/-}$/wild type; *n*=5+4)] vs. log2 fold change protein abundance. The 349 DAPs significantly differing in abundance (*q*-value ≤0.05) are plotted above the threshold limit of −log10 (value of *p*) 1.62. Mitochondrial proteins (*n*=66) are plotted in green and proteins of the synaptic vesicle cycle (*n*=30) in purple. The remaining quantified proteins (1206) with non-significant *q*-values are plotted in the gray area below the threshold limit. **(D)** Schematic figure of the synaptic vesicle cycle and the differentially abundant synaptic vesicle cycle proteins (*n*=21) with fold changes (*Cstb*$^{-/-}$/wt), labeled according to function (B, budding; L, localization; P, priming and docking; Ex, exocytosis; En, endocytosis). **(E)** A subset of the differentially abundant mitochondrial proteins grouped by biological function. Most proteins (*n*=19) are subunits of the oxidative phosphorylation (OXPHOS), followed by proteins involved in homeostasis of proteins and small molecules (*n*=8) and lipid metabolism (*n*=7). Red and blue color indicate increased and decreased protein abundance (*Cstb*$^{-/-}$/wild type), respectively.

3.2. Alterations in proteins of the synaptic vesicle cycle and mitochondrial metabolism in *Cstb*$^{-/-}$ synaptosomes

Grouping of the differentially abundant proteins by their biological mechanisms revealed that a substantial number were members of the synaptic vesicle cycle or functioned within the mitochondria (Figure 2C). Of the synaptic vesicle cycle proteins, 21 were direct members and an additional 9 were regulators of this pathway (Supplementary Table 3_sheet1). A majority of these were decreased in *Cstb*$^{-/-}$ synaptosomes. Most of these altered proteins function in localizing synaptic vesicles to the active zone, the fusion and release of neurotransmitters, and the retrieval of synaptic vesicle proteins by endocytosis (Figure 2D).

Of all significantly different proteins, 66 were mitochondrial (Figure 2C and Supplementary Table 3_sheet2). Of these, 28 were

10.3389/fnmol.2023.1175851

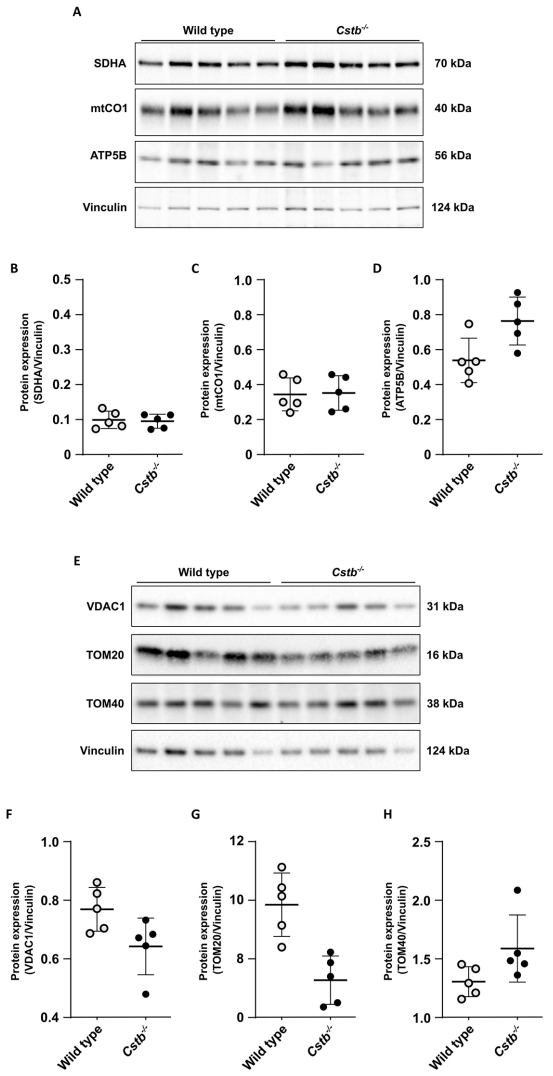

FIGURE 3
Immunoblot detection of mitochondrial proteins in wild type and *Cstb*$^{-/-}$ cerebellar synaptosomes at P30. Representative immunoblot detection **(A,E)** and relative expression of SDHA **(B)**, mtCO1 **(C)**, ATP5B **(D)**, VDAC1 **(F)**, TOM20 **(G)**, and TOM40 **(H)** in synaptosomes of wild type (white) and *Cstb*$^{-/-}$ (black) mice (n=5+5). Antibody intensity values were normalized to that of Vinculin. Bars represent mean, and error bars standard deviation (SD).

decreased and 38 increased in abundance. The single largest group was oxidative phosphorylation (OXPHOS) subunits, which were distributed across complexes I–V (Figure 2E). The highest fold changes were observed for complex I, complex IV and complex V subunits, with abundance of complex I subunits being decreased and complex IV and complex V subunits increased in *Cstb*$^{-/-}$ synaptosomes. Altered abundance was also observed for components of the TOM and TIM mitochondrial import translocon complexes and several other proteins involved in protein and small molecule homeostasis (Figure 2E). In addition, the proteome analysis showed changes in proteins involved in lipid metabolism, including acyl-coenzyme A hydrolysis and lipid transport (Figure 2E).

We further examined differences in the mitochondrial proteins by immunoblot analysis of individual OXPHOS complexes and mitochondrial outer membrane proteins (Figures 3A,E). We did not detect clear genotype-specific changes in the expression of marker proteins for OXPHOS complexes II (succinate dehydrogenase flavoprotein subunit; SDHA), IV (cytochrome c oxidase subunit 1; mtCO1), and V (ATP synthase subunit beta; ATP5B) (Figures 3B–D), neither in the expression of Voltage-dependent anion-selective channel protein 1 (VDAC1), Mitochondrial import receptor subunit TOM20 homolog (Tom20), nor Mitochondrial import receptor subunit TOM40 homolog (Tom40), although variation was high within genotypes (Figures 3F–H).

3.3. Mitochondrial respiration declines progressively in *Cstb*$^{-/-}$ synaptosomes

To test whether alterations to the mitochondrial proteome in *Cstb*$^{-/-}$ synaptosomes affected organelle function, we performed high-resolution respirometry to investigate oxidative phosphorylation in synaptosomal preparations. We analyzed mice at the early-symptomatic stage (P30) and later once there are detectable myoclonus phenotypes and signs of neuronal loss (P45). These two time points allowed us to determine if any alterations in mitochondrial oxidative phosphorylation function preceded the onset of the clinical symptoms in *Cstb*$^{-/-}$ mice.

Following synaptosome isolation, samples were immediately recorded for mitochondrial respiration. Associated with CSTB deficiency we observed a progressive decline in oxidative phosphorylation capacity. At P30, we found no differences between genotypes in any of the examined respiration states, but at P45 the overall respiration declined significantly in *Cstb*$^{-/-}$ mice (Figure 4A). ADP-linked complex I and combined succinate-induced complex I and complex II oxygen-consumption rates were all reduced in *Cstb*$^{-/-}$ mice, implying for decreased utilization of complex I and complex II substrates. Both coupled (Figure 4A) and uncoupled (Figure 4C) respiration was reduced in *Cstb*$^{-/-}$ mice, implying that the respiratory dysfunction is not dependent on complex V. Oligomycin-induced leak respiration, indicative of damaged mitochondrial inner membrane, was lower in *Cstb*$^{-/-}$ samples, but the difference was caused by increased leak respiration in wild type mice (Supplementary Figure 4). Such increase was not observed in *Cstb*$^{-/-}$ mice. The coupling control ratio showed no differences in synaptosome samples between genotypes at either time point (Supplementary Figure 5). Independent complex IV activity was also reduced in *Cstb*$^{-/-}$ mice (Figure 4D), further pointing toward an oxidative phosphorylation complex impairment and general respiratory dysfunction. Immunoblot analysis for nuclear and mitochondrial encoded subunits of the OXPHOS complexes showed no difference in electron transport system proteins, complex II and complex IV subunits SDHA and mtCO1, or in the complex V subunit, ATP5B at P45 (Figures 4E–H).

3.4. No change in mitochondrial DNA copy number and membrane ultrastructure in *Cstb*$^{-/-}$ cerebella

Next, we investigated whether other mitochondrial phenotypes were affected in *Cstb*$^{-/-}$ cerebella. No significant differences in mitochondrial DNA (mtDNA) copy number were detected in synaptosomal preparations between *Cstb*$^{-/-}$ and wild type mice at P30 and P45 (Figure 5A). Further, no gross alterations in the mitochondrial

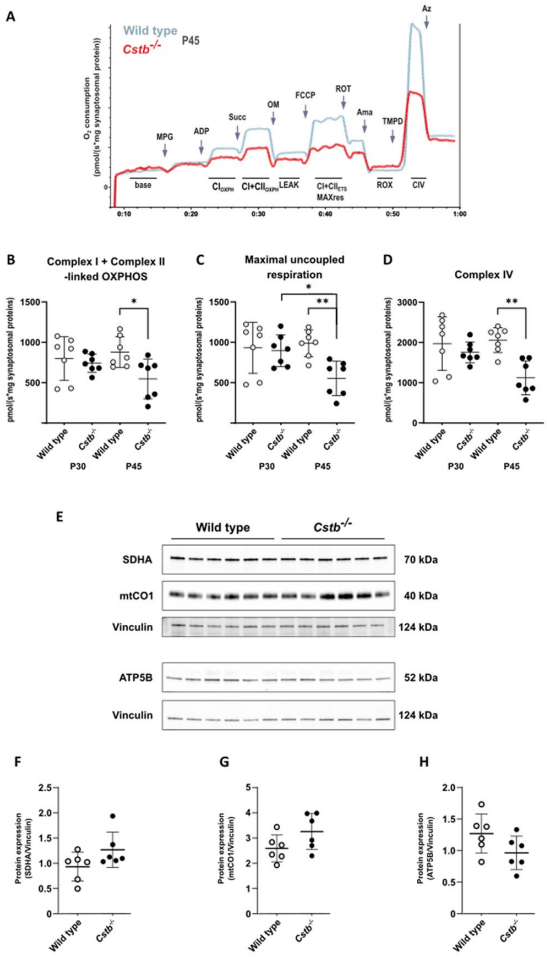

FIGURE 4
Mitochondrial respiration in wild type and *Cstb*$^{-/-}$ synaptosomes. **(A)** Representative traces of the SUIT-protocol from wild type and *Cstb*$^{-/-}$ samples at P45 showing oxygen consumption consumption (pmol/(s*mg synaptosomal protein); y-axis) during substrate and coupling states (x-axis). MPG, malate/pyruvate/glutamate; ADP, adenosine diphosphate; Succ, succinate; OM, oligomycin; FCCP, carbonyl cyanide-*p*-trifluoromethoxyphenylhydrazone; ROT, rotenone; Ama, antimycin A; TMPD, *N,N,N,N*-tetramethyl-*p*-phenylenediamine; Az, azide; CI_{OXPH}, phosphorylating respiration (OXPHOS) in presence of CI substrates; $CI+CII_{OXPH}$, OXPHOS respiration in presence of CI and CII substrates; LEAK, oligomycin-inhibited non-phosphorylating basal respiration; $CI+CII_{ETS}$ MAX_{res}, maximal capacity of the electron transport system; ROX, residual oxygen consumption; CIV, complex IV activity. **(B–D)** Complex I+Complex II-linked OXPHOS **(B)**, Maximal uncoupled respiration **(C)**, and Complex IV activity **(D)** in wild type (gray) and *Cstb*$^{-/-}$ (black) synaptosomes at P30 and P45 (n=7+7+7+7). Statistical significance was determined by one-way ANOVA with correction for multiple comparisons using the Šídák method; *p<0.05; **p<0.01; bars represent mean and error bars standard deviation of oxygen consumption [pmol/(second*mg synaptosomal protein)]. **(E)** Representative immunoblot detection and relative expression of SDHA **(F)**, mtCO1 **(G)**, and ATP5B **(H)** in synaptosomes of wild type (white) and *Cstb*$^{-/-}$ (black) mice (n=6+6) at P45. Antibody intensity values were normalized to that of Vinculin. Bars represent mean, and error bars standard deviation (SD).

membrane ultrastructure were observed in cerebellar tissue preparations using transmission electron microscopy (TEM) (Figures 5B,C). We also investigated early indicators of cellular stress affecting mitochondrial dynamics by analyzing the (OPA1) isoforms in synaptosomal preparations. The proteolytic cleavage of the long isoforms (L-OPA1) was estimated as a percentage of short isoforms (S-OPA1) of total OPA1. No differences were observed between *Cstb*$^{-/-}$ and wild type mice (Figures 5D,E).

4. Discussion

Identifying the mechanisms underlying the synaptic pathophysiology associated with CSTB deficiency is important for understanding EPM1 disease onset and progression. In mice, CSTB deficiency causes progressive neuron loss, which is most striking in the cerebellum, the emergence of which coincides with the onset of myoclonus (Pennacchio et al., 1998) and is preceded by prevalent rearrangements of synaptic proteins in the cerebellum (Gorski et al., 2020) and altered GABAergic signaling in cerebellar Purkinje cells (Joensuu et al., 2014). Following our previous study from presymptomatic *Cstb*$^{-/-}$ mice (Gorski et al., 2020), we here extended the analysis of cerebellar synaptosomes to the early symptomatic phase. We identified an impairment in mitochondrial respiration, which was preceded by widespread changes in the mitochondrial proteome. Our data reveal that mitochondrial dysfunction contributes to the early pathogenesis of CSTB deficiency.

Neurons are metabolically active and have a high energy demand, most of which is used for neurotransmission (Harris et al., 2012). Synaptic energy in the form of adenosine triphosphate is synthetized locally through glycolysis and mitochondrial oxidative phosphorylation (OXPHOS) (Harris et al., 2012). Presynaptic mitochondrial dysfunction and bioenergetic failure have been associated with several, both common and rare neurodegenerative diseases and their models (reviewed in Li and Sheng, 2022), and our findings presented here establish the presence of EPM1 among these disorders. However, the question remains how deficiency of a protein with a cytosolic and nuclear localization can cause failure of synaptic mitochondria without evident alterations in the mitochondrial phenotype.

Cystatin B is a soluble cytoplasmic protein that associates with cytoplasmic granular structures representing lysosomes (Alakurtti et al., 2005). It has previously been reported to have synaptic localization with an implied crucial role in synaptic physiology (Penna et al., 2019; Gorski et al., 2020). CSTB belongs to the cystatin superfamily of endogenous inhibitors of lysosomal cysteine proteases of the cathepsin family that are thought to protect cells from cathepsin-mediated proteolysis in the cytoplasm in the case of lysosomal membrane damage (Boya and Kroemer, 2008). Leakage of lysosomal cathepsins has been reported in several pathological conditions and neurodegenerative disorders (Nagai et al., 2000; Sundelöf et al., 2010; Morena et al., 2017), and mutations in mitochondrial genes are often associated with impairment of the lysosomal system and *vice versa* (Deus et al., 2020). Increased activity of cathepsin B, one of the cysteine proteases inhibited by CSTB, has been described in lymphoblastoid cells from EPM1 patients (Rinne et al., 2002), in cultured cerebellar granule neurons from *Cstb*$^{-/-}$ mice (Lehtinen et al., 2009), and in neural progenitor cells from *Cstb*$^{-/-}$ mice (Daura et al., 2021). Cathepsin B maintains proteolytic activity in the cytoplasm and initiates mitochondrial apoptosis though activation of Bcl-2 family members (Droga-Mazovec et al., 2008; de Castro et al., 2016). Indeed, apoptotic cell death of cerebellar granule neurons is one of the

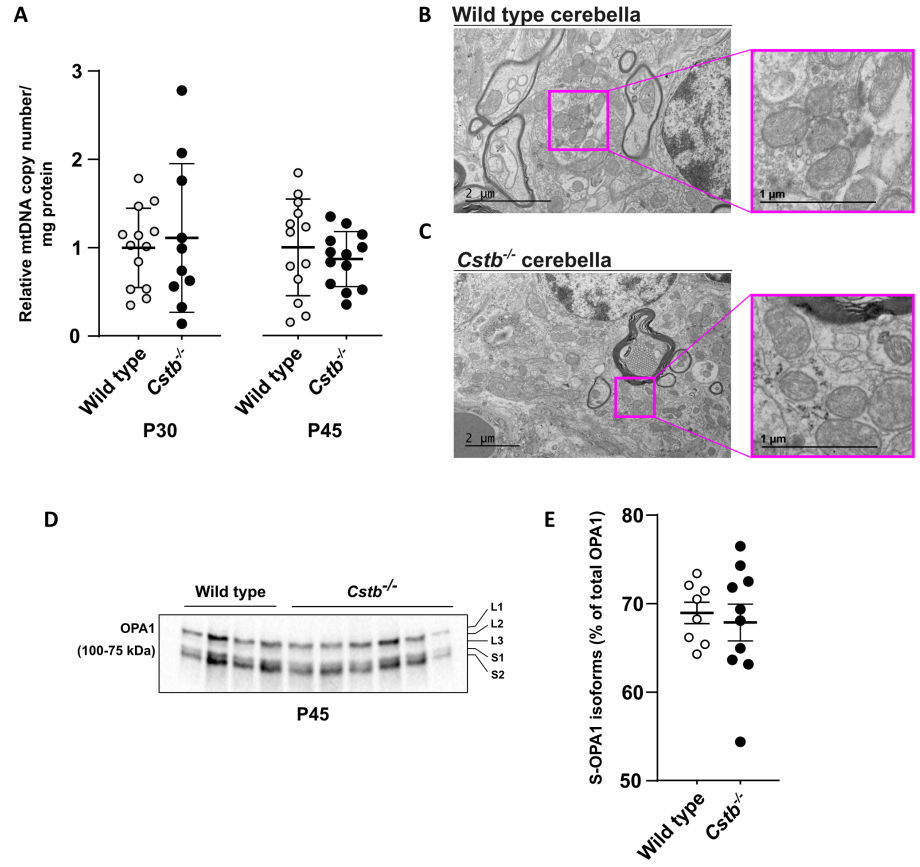

FIGURE 5
Mitochondrial DNA copy number and membrane ultrastructure is not altered in *Cstb*$^{-/-}$ cerebella. **(A)** The relative ratio between mtDNA copy number and protein amount in synaptosomes of wild type (white) and *Cstb*$^{-/-}$ (black) mice cerebella at P30 (n=10–13) and P45 (n=13). Bars represent mean, and error bars standard deviation (SD) of relative mtDNA copy number/mg synaptosomal protein. **(B,C)** Transmission electron microscopy images showing mitochondrial ultrastructure in wild type **(B)** and *Cstb*$^{-/-}$ **(C)** cerebellar tissue at P45. **(D)** Representative immunoblot detection using an antibody against OPA1 in synaptosomes of wild type and *Cstb*$^{-/-}$ mice (n=4+6) at P45. The long and short OPA1 isoforms are marked L1-L3 and S1-S2, respectively. **(E)** The short isoforms of OPA1 (S-OPA1) in relation to total OPA1 in synaptosomes of wild type (white) and *Cstb*$^{-/-}$ (black) mice at P45 (n=8–10). Bars represent mean, and error bars standard deviation (SD).

hallmarks of brain pathology in *Cstb*$^{-/-}$ mice (Pennacchio et al., 1998) with cystatin B-cathepsin B double knockout mice showing a reduction in the amount of cerebellar granule neuron apoptosis compared to *Cstb*$^{-/-}$ mice (Houseweart et al., 2003). Recently, lysosomal leakage and consequent increased proteolytic activity of cathepsins B and L were reported to initiate a metabolic remodeling of the mitochondrial proteome in a human iPSC-derived macrophage model (Bussi et al., 2022). This lysosome-mitochondria crosstalk was implied to modulate macrophage immunometabolism *via* cathepsin-mediated degradation of mitochondrial proteins leading to impaired OXPHOS activity (Bussi et al., 2022). It remains to be investigated whether similar mechanisms contribute to compromised mitochondrial function in neurons. Interestingly, a more than twofold increase in cathepsin B abundance was observed in our proteomics data of cerebellar synaptosomes from *Cstb*$^{-/-}$ mice. Considering that cathepsin B also regulates lysosome and autophagosome dynamics (Man and Kanneganti, 2016; Qi et al., 2016), and activates the NLRP3 neuroinflammasome (Chevriaux et al., 2020) and subsequent production of interleukin (IL) 1β (Bai et al., 2018), all of which are implicated in experimental models of CSTB deficiency (Maher et al., 2014; Polajnar et al., 2014), it is possible that many of the pathological consequences of CSTB deficiency, including mitochondrial dysfunction, are mediated through increased cathepsin B activity.

The polarized structure and compartmentalized functions of neurons require long-distance transport of a variety of cargoes, including organelles and synaptic vesicle precursors (Maday et al., 2014). In addition to housing metabolic pathways, mitochondria form contact sites with other organelles to modulate the exchange of lipids, ions, and proteins (Vance, 2014). Cellular stress has been shown to increase contact sites between the endoplasmic reticulum (ER) and mitochondria *in vitro* (Bravo et al., 2011), and for several neurodegenerative disorders, including Alzheimer's disease, Parkinson's disease, and Charcot–Marie–Tooth disease, many dysregulated cellular functions have been associated with these (Wilson and Metzakopian, 2021). Impaired mitochondrial respiration in *Cstb*$^{-/-}$ synaptosomes could result from reduced or dysregulated mitochondria-ER signaling, causing destabilization of OXPHOS supercomplexes. This has been reported in a neuronal model of Alzheimer's disease, where loss of mitochondria-ER contact sites leads to dysfunctions in mitochondrial bioenergetics due to reduced levels of cardiolipin, a phospholipid that stabilizes OXPHOS

supercomplexes in the mitochondrial inner membrane (Martino Adami et al., 2019).

Impaired redox homeostasis has previously been implicated as a key mechanism by which CSTB deficiency causes neuronal death and oxidative damage in the cerebellum of *Cstb*$^{-/-}$ mice (Lehtinen et al., 2009). In addition, mitochondrial dysfunction has been demonstrated in several *in vitro* models derived from *Cstb*$^{-/-}$ mice, leading to propositions of both direct and indirect mechanisms linking CSTB function to mitochondria. Maher et al. (2014) investigated inflammatory responses in lipopolysaccharide (LPS)-stimulated bone marrow-derived macrophages from *Cstb*$^{-/-}$ mice and showed that mitochondrial membrane potential stability is impaired upon LPS stimulation and leads to increased ROS generation (Maher et al., 2014). The authors suggested that CSTB translocates to mitochondria where it physically protects the mitochondrial membrane integrity (Maher et al., 2014). More recently, in a cell culture model of murine neural stem cell renewal and differentiation, activation of nuclear-encoded mitochondrial genes was shown to be delayed in CSTB-deficient cells leading to impairment of the enhanced mitochondrial respiration that is induced upon induction of differentiation (Daura et al., 2021). We previously reported proteomic alterations in cerebellar synaptosomes of presymptomatic *Cstb*$^{-/-}$ mice and showed extensive rearrangements of the mitochondrial proteome, especially in proteins involved in mitochondrial energy metabolism, ROS production, and antioxidant-mediated maintenance of redox homeostasis (Gorski et al., 2020). Since the data also showed changes in several key structural transport proteins, previously reported on gene expression level (Joensuu et al., 2014), we suggested that defects in axonal transport could contribute to synaptic mitochondrial dysfunction (Gorski et al., 2020). None of these studies reported alterations in mitochondrial morphology. Alterations in mitochondrial membrane morphology are often associated with organelle dysfunction (Bertholet et al., 2016). In the present study, we did not identify alterations in the abundance of key factors that coordinate mitochondrial membrane fission and fusion. Furthermore, cleavage of the long isoform of OPA1, which regulates mitochondrial cristae integrity, mtDNA maintenance, and mitochondrial inner membrane fusion, was not altered in the synaptic mitochondria from *Cstb*$^{-/-}$ mice. Taken together, these data suggest that mitochondrial dysfunction in CSTB deficiency is due to a secondary event rather than primary defect to organelle function.

It is likely that the consequences of reduced mitochondrial respiration affect the energy-demanding downstream functions of the synapse, including neurotransmission. Synaptic vesicle refilling and recycling are processes sensitive for energy depletion (Pathak et al., 2015). Indeed, in the present proteomics data, we observed differential abundance of several members involved in the synaptic vesicle cycle, predicted to affect synaptic vesicle mobilization, docking and fusion (John et al., 2021). The previously implicated alterations in GABAergic inhibition in brains of *Cstb*$^{-/-}$ mice (Joensuu et al., 2014) may thus be, at least partially, a consequence of impaired synaptic mitochondrial function. Whether the mitochondrial dysfunction is exclusive to cerebellar synaptosomes or applies also to other cell compartments or cell types, needs to be clarified in future studies.

In conclusion, our study shows that significant alterations in the synaptic proteome and consequent mitochondrial dysfunction are early changes in cerebellar synaptosomes of *Cstb*$^{-/-}$ mice, coinciding with the onset and progression of clinical symptoms. Understanding the underlying mechanisms is a prerequisite for designing new therapeutic strategies for EPM1.

Data availability statement

The mass spectrometry proteomics data have been deposited to the ProteomeXchange Consortium *via* the PRIDE partner repository with the dataset identifier PXD040382.

Ethics statement

The animal study was reviewed and approved by The Animal Ethics Committee of the State Provincial Office of Southern Finland (decisions ESAVI/10765/2015 and ESAVI/471/2019).

Author contributions

KG, CJ, BB, and A-EL contributed to the study design. KG, CJ, TN, and VR performed the experiments. KG, CJ, TN, and BB analyzed the data. KG, BB, and A-EL wrote the manuscript. All authors discussed and commented on the manuscript.

Funding

This work was supported by Folkhälsan Research Foundation (A-EL), the Sigrid Jusélius Foundation (A-EL), Medicinska Understödsföreningen Liv och Hälsa r.f. (A-EL), the Sigrid Juselius Foundation Senior Investigator Award (BB), Academy of Finland Research Fellowship (CJ), and the Magnus Ehrnroot Foundation (CJ). Mass spectrometry-based proteomic analyses were performed by the Proteomics Core Facility, Department of Immunology, University of Oslo/Oslo University Hospital, which is supported by the Core Facilities program of the South-Eastern Norway Regional Health Authority. This core facility is also a member of the National Network of Advanced Proteomics Infrastructure (NAPI), which is funded by the Research Council of Norway INFRASTRUKTUR-program (project number: 295910).

Acknowledgments

We acknowledge Paula Hakala, Carina Lund, Pauliina Repo, Mira Aronen, and Sonja Jansson for technical assistance; animal caretakers at the Laboratory Animal Center (University of Helsinki) for flexible cooperation and professional care of animals; the Electron microscopy (EMBI) unit at the University of Helsinki for preparation of TEM samples; Eduard Daura, Janne Purhonen, and Saara Tegelberg for scientific advice.

Conflict of interest

The authors declare that the research was conducted in the absence of any commercial or financial relationships that could be construed as a potential conflict of interest.

Publisher's note

All claims expressed in this article are solely those of the authors and do not necessarily represent those of their affiliated organizations, or those of the publisher, the editors and the reviewers. Any product that may be evaluated in this article, or claim that may be made by its manufacturer, is not guaranteed or endorsed by the publisher.

Supplementary material

The Supplementary material for this article can be found online at: https://www.frontiersin.org/articles/10.3389/fnmol.2023.1175851/full#supplementary-material

References

Alakurtti, K., Weber, E., Rinne, R., Theil, G., Haan, G.-J.De, Lindhout, D., et al. (2005). Loss of lysosomal association of cystatin B proteins representing progressive myoclonus epilepsy, EPM1, mutations. *Eur. J. Hum. Genet.* 13, 208–215. doi: 10.1038/sj.ejhg.5201300

Ashburner, M., Ball, C. A., Blake, J. A., Botstein, D., Butler, H., Cherry, J. M., et al. (2000). Gene ontology: tool for the unification of biology. *Gene Ontol. Consort. Nat. Genet.* 25, 25–29. doi: 10.1038/75556

Awadhpersad, R., and Jackson, C. B. (2021). High-resolution respirometry to assess bioenergetics in cells and tissues using chamber- and plate-based respirometers. *J. Vis. Exp.* 63000. doi: 10.3791/63000

Babicki, S., Arndt, D., Marcu, A., Liang, Y., Grant, J. R., Maciejewski, A., et al. (2016). Heatmapper: web-enabled heat mapping for all. *Nucleic Acids Res.* 44, W147–W153. doi: 10.1093/nar/gkw419

Bai, H., Yang, B., Yu, W., Xiao, Y., Yu, D., and Zhang, Q. (2018). Cathepsin B links oxidative stress to the activation of NLRP3 inflammasome. *Exp. Cell Res.* 362, 180–187. doi: 10.1016/j.yexcr.2017.11.015

Bertholet, A. M., Delerue, T., Millet, A. M., Moulis, M. F., David, C., Daloyau, M., et al. (2016). Mitochondrial fusion/fission dynamics in neurodegeneration and neuronal plasticity. *Neurobiol. Dis.* 90, 3–19. doi: 10.1016/j.nbd.2015.10.011

Blanc, H., Wright, C. T., Bibb, M. J., Wallace, D. C., and Clayton, D. A. (1981). Mitochondrial DNA of chloramphenicol-resistant mouse cells contains a single nucleotide change in the region encoding the 3′ end of the large ribosomal RNA. *Proc. Natl. Acad. Sci.* 78, 3789–3793. doi: 10.1073/pnas.78.6.3789

Boya, P., and Kroemer, G. (2008). Lysosomal membrane permeabilization in cell death. *Oncogene* 27, 6434–6451. doi: 10.1038/onc.2008.310

Bravo, R., Vicencio, J. M., Parra, V., Troncoso, R., Munoz, J. P., Bui, M., et al. (2011). Increased ER-mitochondrial coupling promotes mitochondrial respiration and bioenergetics during early phases of ER stress. *J. Cell Sci.* 124, 2143–2152. doi: 10.1242/jcs.080762

Bussi, C., Heunis, T., Pellegrino, E., Bernard, E. M., Bah, N., dos Santos, M. S., et al. (2022). Lysosomal damage drives mitochondrial proteome remodelling and reprograms macrophage immunometabolism. *Nat. Commun.* 13:7338. doi: 10.1038/s41467-022-34632-8

Bustin, S. A., Benes, V., Garson, J. A., Hellemans, J., Huggett, J., Kubista, M., et al. (2009). The MIQE guidelines: minimum information for publication of quantitative real-time PCR experiments. *Clin. Chem.* 55, 611–622. doi: 10.1373/clinchem.2008.112797

Canafoglia, L., Gennaro, E., Capovilla, G., Gobbi, G., Boni, A., Beccaria, F., et al. (2012). Electroclinical presentation and genotype-phenotype relationships in patients with Unverricht-Lundborg disease carrying compound heterozygous CSTB point and indel mutations. *Epilepsia* 53, 2120–2127. doi: 10.1111/j.1528-1167.2012.03718.x

Čeru, S., Konjar, S., Maher, K., Repnik, U., Križaj, I., Benčina, M., et al. (2010). Stefin B interacts with histones and cathepsin L in the nucleus. *J. Biol. Chem.* 285, 10078–10086. doi: 10.1074/jbc.M109.034793

Chevriaux, A., Pilot, T., Derangère, V., Simonin, H., Martine, P., Chalmin, F., et al. (2020). Cathepsin B is required for NLRP3 Inflammasome activation in macrophages, through NLRP3 interaction. *Front. Cell Dev. Biol.* 8:167. doi: 10.3389/fcell.2020.00167

Cohen, N. R., Hammans, S. R., Macpherson, J., and Nicoll, J. A. R. (2011). New neuropathological findings in Unverricht-Lundborg disease: neuronal intranuclear and cytoplasmic inclusions. *Acta Neuropathol. (Berl.)* 121, 421–427. doi: 10.1007/s00401-010-0738-2

Cox, J., and Mann, M. (2008). MaxQuant enables high peptide identification rates, individualized p.p.b.-range mass accuracies and proteome-wide protein quantification. *Nat. Biotechnol.* 26, 1367–1372. doi: 10.1038/nbt.1511

Danner, N., Julkunen, P., Khyuppenen, J., Hukkanen, T., Könönen, M., Säisänen, L., et al. (2009). Altered cortical inhibition in Unverricht-Lundborg type progressive myoclonus epilepsy (EPM1). *Epilepsy Res.* 85, 81–88. doi: 10.1016/j.eplepsyres.2009.02.015

Daura, E., Tegelberg, S., Yoshihara, M., Jackson, C., Simonetti, F., Aksentjeff, K., et al. (2021). Cystatin B-deficiency triggers ectopic histone H3 tail cleavage during neurogenesis. *Neurobiol. Dis.* 156:105418. doi: 10.1016/j.nbd.2021.105418

de Castro, M., Bunt, G., and Wouters, F. S. (2016). Cathepsin B launches an apoptotic exit effort upon cell death-associated disruption of lysosomes. *Cell Death Discov.* 2:16012. doi: 10.1038/cddiscovery.2016.12

Deus, C. M., Yambire, K. F., Oliveira, P. J., and Raimundo, N. (2020). Mitochondria-lysosome crosstalk: from physiology to neurodegeneration. *Trends Mol. Med.* 26, 71–88. doi: 10.1016/j.molmed.2019.10.009

Di Matteo, F., Pipicelli, F., Kyrousi, C., Tovecci, I., Penna, E., Crispino, M., et al. (2020). Cystatin B is essential for proliferation and interneuron migration in individuals with EPM 1 epilepsy. *EMBO Mol. Med.* 12:e11419. doi: 10.15252/emmm.201911419

Droga-Mazovec, G., Bojic, L., Petelin, A., Ivanova, S., Romih, R., Repnik, U., et al. (2008). Cysteine cathepsins trigger caspase-dependent cell death through cleavage of bid and antiapoptotic Bcl-2 homologues. *J. Biol. Chem.* 283, 19140–19150. doi: 10.1074/jbc.M802513200

Dunkley, P. R., Jarvie, P. E., and Robinson, P. J. (2008). A rapid Percoll gradient procedure for preparation of synaptosomes. *Nat. Protoc.* 3, 1718–1728. doi: 10.1038/nprot.2008.171

Eldridge, R., Iivanainen, M., Stern, R., Koerber, T., and Wilder, B. J. (1983). "Baltic" myoclonus epilepsy: hereditary disorder of childhood made worse by phenytoin. *Lancet Lond. Engl.* 2, 838–842. doi: 10.1016/s0140-6736(83)90749-3

Gene Ontology Consortium (2021). The gene ontology resource: enriching a GOld mine. *Nucleic Acids Res.* 49, D325–D334. doi: 10.1093/nar/gkaa1113

Gnaiger, E., Aasander Frostner, E., Abdul Karim, N., Abdel-Rahman, E. A., Abumrad, N. A., Acuna-Castroviejo, D., et al. (2020). Mitochondrial physiology. *Bioenerg. Commun.* doi: 10.26124/BEC:2020-0001.V1

Gorski, K., Spoljaric, A., Nyman, T. A., Kaila, K., Battersby, B. J., and Lehesjoki, A.-E. (2020). Quantitative changes in the mitochondrial proteome of cerebellar synaptosomes from preclinical cystatin B-deficient mice. *Front. Mol. Neurosci.* 13:570640. doi: 10.3389/fnmol.2020.570640

Green, G. D., Kembhavi, A. A., Davies, M. E., and Barrett, A. J. (1984). Cystatin-like cysteine proteinase inhibitors from human liver. *Biochem. J.* 218, 939–946. doi: 10.1042/bj2180939

Haltia, M., Kristensson, K., and Sourander, P. (1969). Neuropathological studies in three Scandinavian cases of progressive myoclonus epilepsy. *Acta Neurol. Scand.* 45, 63–77. doi: 10.1111/j.1600-0404.1969.tb01220.x

Harris, J. J., Jolivet, R., and Attwell, D. (2012). Synaptic energy use and supply. *Neuron* 75, 762–777. doi: 10.1016/j.neuron.2012.08.019

Houseweart, M. K., Pennacchio, L. A., Vilaythong, A., Peters, C., Noebels, J. L., and Myers, R. M. (2003). Cathepsin B but not cathepsins L or S contributes to the pathogenesis of Unverricht-Lundborg progressive myoclonus epilepsy (EPM1). *J. Neurobiol.* 56, 315–327. doi: 10.1002/neu.10253

Huang, D. W., Sherman, B. T., and Lempicki, R. A. (2009a). Bioinformatics enrichment tools: paths toward the comprehensive functional analysis of large gene lists. *Nucleic Acids Res.* 37, 1–13. doi: 10.1093/nar/gkn923

Huang, D. W., Sherman, B. T., and Lempicki, R. A. (2009b). Systematic and integrative analysis of large gene lists using DAVID bioinformatics resources. *Nat. Protoc.* 4, 44–57. doi: 10.1038/nprot.2008.211

Joensuu, T., Kuronen, M., Alakurtti, K., Tegelberg, S., Hakala, P., Aalto, A., et al. (2007). Cystatin B: mutation detection, alternative splicing and expression in progressive myclonus epilepsy of Unverricht-Lundborg type (EPM1) patients. *Eur. J. Hum. Genet* 15, 185–193. doi: 10.1038/sj.ejhg.5201723

Joensuu, T., Lehesjoki, A. E., and Kopra, O. (2008). Molecular background of EPM1-Unverricht-Lundborg disease. *Epilepsia* 49, 557–563. doi: 10.1111/j.1528-1167.2007.01422.x

Joensuu, T., Tegelberg, S., Reinmaa, E., Segerstrale, M., Hakala, P., Pehkonen, H., et al. (2014). Gene expression alterations in the cerebellum and granule neurons of Cstb(−/−) mouse are associated with early synaptic changes and inflammation. *PLoS One* 9:e89321. doi: 10.1371/journal.pone.0089321

John, A., Ng-Cordell, E., Hanna, N., Brkic, D., and Baker, K. (2021). The neurodevelopmental spectrum of synaptic vesicle cycling disorders. *J. Neurochem.* 157, 208–228. doi: 10.1111/jnc.15135

Julkunen, P., Säisänen, L., Könönen, M., Vanninen, R., Kälviäinen, R., and Mervaala, E. (2013). TMS-EEG reveals impaired intracortical interactions and coherence in Unverricht-Lundborg type progressive myoclonus epilepsy (EPM1). *Epilepsy Res.* 106, 103–112. doi: 10.1016/j.eplepsyres.2013.04.001

Kälviäinen, R., Khyuppenen, J., Koskenkorva, P., Eriksson, K., Vanninen, R., and Mervaala, E. (2008). Clinical picture of EPM1-Unverricht-Lundborg disease. *Epilepsia* 49, 549–556. doi: 10.1111/j.1528-1167.2008.01546.x

Koskenkorva, P., Hyppönen, J., Aikiä, M., Mervaala, E., Kiviranta, T., Eriksson, K., et al. (2011). Severer phenotype in Unverricht-Lundborg disease (EPM1) patients compound heterozygous for the dodecamer repeat expansion and the c.202C>T mutation in the CSTB gene. *Neurodegener Dis* 8, 515–522. doi: 10.1159/000323470

Koskenkorva, P., Khyuppenen, J., Niskanen, E., Könönen, M., Bendel, P., Mervaala, E., et al. (2009). Motor cortex and thalamic atrophy in Unverricht-Lundborg disease: voxel-based morphometric study. *Neurology* 73, 606–611. doi: 10.1212/WNL.0b013e3181b3888b

Koskenkorva, P., Niskanen, E., Hyppönen, J., Könönen, M., Mervaala, E., Soininen, H., et al. (2012). Sensorimotor, visual, and auditory cortical atrophy in Unverricht-Lundborg disease mapped with cortical thickness analysis. *AJNR Am. J. Neuroradiol.* 33, 878–883. doi: 10.3174/ajnr.A2882

Koskiniemi, M., Donner, M., Majuri, H., Haltia, M., and Norio, R. (1974). Progressive myoclonus epilepsy. A clinical and histopathological study. *Acta Neurol. Scand.* 50, 307–332.

Lehtinen, M. K., Tegelberg, S., Schipper, H., Su, H., Zukor, H., Manninen, O., et al. (2009). Cystatin B deficiency sensitizes neurons to oxidative stress in progressive myoclonus epilepsy, EPM1. *J. Neurosci.* 29, 5910–5915. doi: 10.1523/JNEUROSCI.0682-09.2009

Li, S., and Sheng, Z.-H. (2022). Energy matters: presynaptic metabolism and the maintenance of synaptic transmission. *Nat. Rev. Neurosci.* 23, 4–22. doi: 10.1038/s41583-021-00535-8

Maday, S., Twelvetrees, A. E., Moughamian, A. J., and Holzbaur, E. L. F. (2014). Axonal transport: cargo-specific mechanisms of motility and regulation. *Neuron* 84, 292–309. doi: 10.1016/j.neuron.2014.10.019

Maher, K., Kokelj, B. J., Butinar, M., Mikhaylov, G., Manček-Keber, M., Stoka, V., et al. (2014). A role for stefin B (cystatin B) in inflammation and endotoxemia. *J. Biol. Chem.* 289, 31736–31750. doi: 10.1074/jbc.M114.609396

Man, S. M., and Kanneganti, T.-D. (2016). Regulation of lysosomal dynamics and autophagy by CTSB/cathepsin B. *Autophagy* 12, 2504–2505. doi: 10.1080/15548627.2016.1239679

Mancini, G. M. S., Schot, R., de Wit, M. C. Y., De Coo, R. F., Oostenbrink, R., Heus, K. B., et al. (2016). CSTB null mutation associated with microcephaly, early developmental delay, and severe dyskinesia. *Neurology* 86, 877–878. doi: 10.1212/WNL.0000000000002422

Manninen, O., Koskenkorva, P., Lehtimaki, K. K., Hypponen, J., Kononen, M., Laitinen, T., et al. (2013). White matter degeneration with Unverricht-Lundborg progressive myoclonus epilepsy: a translational diffusion-tensor imaging study in patients and cystatin B-deficient mice. *Radiology* 269, 232–239. doi: 10.1148/radiol.13122458 [doi]

Manninen, O., Laitinen, T., Lehtimaki, K. K., Tegelberg, S., Lehesjoki, A. E., Grohn, O., et al. (2014). Progressive volume loss and white matter degeneration in cstb-deficient mice: a diffusion tensor and longitudinal volumetry MRI study. *PLoS One* 9:e90709. doi: 10.1371/journal.pone.0090709

Martino Adami, P. V., Nichtová, Z., Weaver, D. B., Bartok, A., Wisniewski, T., Jones, D. R., et al. (2019). Perturbed mitochondria-ER contacts in live neurons that model the amyloid pathology of Alzheimer's disease. *J. Cell Sci.* 132:jcs229906. doi: 10.1242/jcs.229906

Mi, H., Muruganujan, A., Casagrande, J. T., and Thomas, P. D. (2013). Large-scale gene function analysis with the PANTHER classification system. *Nat. Protoc.* 8, 1551–1566. doi: 10.1038/nprot.2013.092

Morena, F., Argentati, C., Trotta, R., Crispoltoni, L., Stabile, A., Pistilli, A., et al. (2017). A comparison of lysosomal enzymes expression levels in peripheral blood of mild- and severe-Alzheimer's disease and MCI patients: implications for regenerative medicine approaches. *Int. J. Mol. Sci.* 18:1806. doi: 10.3390/ijms18081806

Nagai, A., Murakawa, Y., Terashima, M., Shimode, K., Umegae, N., Takeuchi, H., et al. (2000). Cystatin C and cathepsin B in CSF from patients with inflammatory neurologic diseases. *Neurology* 55, 1828–1832. doi: 10.1212/wnl.55.12.1828

O'Brien, A., Marshall, C. R., Blaser, S., Ray, P. N., and Yoon, G. (2017). Severe neurodegeneration, progressive cerebral volume loss and diffuse hypomyelination associated with a homozygous frameshift mutation in CSTB. *Eur. J. Hum. Genet.* 25, 775–778. doi: 10.1038/ejhg.2017.39

Okuneva, O., Li, Z., Korber, I., Tegelberg, S., Joensuu, T., Tian, L., et al. (2016). Brain inflammation is accompanied by peripheral inflammation in Cstb (−/−) mice, a model for progressive myoclonus epilepsy. *J. Neuroinflammation* 13, 298–297. doi: 10.1186/s12974-016-0764-7

Pathak, D., Shields, L. Y., Mendelsohn, B. A., Haddad, D., Lin, W., Gerencser, A. A., et al. (2015). The role of mitochondrially derived ATP in synaptic vesicle recycling. *J. Biol. Chem.* 290, 22325–22336. doi: 10.1074/jbc.M115.656405

Penna, E., Cerciello, A., Chambery, A., Russo, R., Cernilogar, F. M., Pedone, E. M., et al. (2019). Cystatin B involvement in synapse physiology of rodent brains and human cerebral Organoids. *Front. Mol. Neurosci.* 12:195. doi: 10.3389/fnmol.2019.00195

Pennacchio, L. A., Bouley, D. M., Higgins, K. M., Scott, M. P., Noebels, J. L., and Myers, R. M. (1998). Progressive ataxia, myoclonic epilepsy and cerebellar apoptosis in cystatin B-deficient mice. *Nat. Genet.* 20, 251–258. doi: 10.1038/3059

Pennacchio, L. A., Lehesjoki, A. E., Stone, N. E., Willour, V. L., Virtaneva, K., Miao, J., et al. (1996). Mutations in the gene encoding cystatin B in progressive myoclonus epilepsy (EPM1). *Science* 271, 1731–1734. doi: 10.1126/science.271.5256.1731

Polajnar, M., Zavašnik-Bergant, T., Škerget, K., Vizovišek, M., Vidmar, R., Fonović, M., et al. (2014). Human Stefin B role in Cell's response to Misfolded proteins and autophagy. *PLoS One* 9:e102500. doi: 10.1371/journal.pone.0102500

Qi, X., Man, S. M., Malireddi, R. K. S., Karki, R., Lupfer, C., Gurung, P., et al. (2016). Cathepsin B modulates lysosomal biogenesis and host defense against *Francisella novicida* infection. *J. Exp. Med.* 213, 2081–2097. doi: 10.1084/jem.20151938

Rath, S., Sharma, R., Gupta, R., Ast, T., Chan, C., Durham, T. J., et al. (2021). MitoCarta3.0: an updated mitochondrial proteome now with sub-organelle localization and pathway annotations. *Nucleic Acids Res.* 49, D1541–D1547. doi: 10.1093/nar/gkaa1011

Rinne, R., Saukko, P., Järvinen, M., and Lehesjoki, A.-E. (2002). Reduced cystatin B activity correlates with enhanced cathepsin activity in progressive myoclonus epilepsy. *Ann. Med.* 34, 380–385. doi: 10.1080/078538902320772124

Rooney, J. P., Ryde, I. T., Sanders, L. H., Howlett, E. H., Colton, M. D., Germ, K. E., et al. (2015). PCR based determination of mitochondrial DNA copy number in multiple species. *Methods Mol. Biol. Clifton NJ* 1241, 23–38. doi: 10.1007/978-1-4939-1875-1_3

Sundelöf, J., Sundström, J., Hansson, O., Eriksdotter-Jönhagen, M., Giedraitis, V., Larsson, A., et al. (2010). Higher cathepsin B levels in plasma in Alzheimer's disease compared to healthy controls. *J. Alzheimers Dis. JAD* 22, 1223–1230. doi: 10.3233/JAD-2010-101023

Tegelberg, S., Kopra, O., Joensuu, T., Cooper, J. D., and Lehesjoki, A. E. (2012). Early microglial activation precedes neuronal loss in the brain of the Cstb−/− mouse model of progressive myoclonus epilepsy, EPM1. *J. Neuropathol. Exp. Neurol.* 71, 40–53. doi: 10.1097/NEN.0b013e31823e68e1

Tenreiro, P., Rebelo, S., Martins, F., Santos, M., Coelho, E. D., Almeida, M., et al. (2017). Comparison of simple sucrose and percoll based methodologies for synaptosome enrichment. *Anal. Biochem.* 517, 1–8. doi: 10.1016/j.ab.2016.10.015

Vance, J. E. (2014). MAM (mitochondria-associated membranes) in mammalian cells: lipids and beyond. *Biochim. Biophys. Acta* 1841, 595–609. doi: 10.1016/j.bbalip.2013.11.014

Vizcaíno, J. A., Côté, R. G., Csordas, A., Dianes, J. A., Fabregat, A., Foster, J. M., et al. (2013). The proteomics identifications (PRIDE) database and associated tools: status in 2013. *Nucleic Acids Res.* 41, D1063–D1069. doi: 10.1093/nar/gks1262

Wilson, E. L., and Metzakopian, E. (2021). ER-mitochondria contact sites in neurodegeneration: genetic screening approaches to investigate novel disease mechanisms. *Cell Death Differ.* 28, 1804–1821. doi: 10.1038/s41418-020-00705-8

Wu, G., and Haw, R. (2017). "Functional interaction network construction and analysis for disease discovery" in *Protein bioinformatics methods in molecular biology*. eds. C. H. Wu, C. N. Arighi and K. E. Ross (New York, NY: Springer New York), 235–253.

frontiers | Frontiers in Molecular Neuroscience

TYPE Brief Research Report
PUBLISHED 24 May 2023
DOI 10.3389/fnmol.2023.1185665

OPEN ACCESS

EDITED BY
Lilian Kisiswa,
Aarhus University, Denmark

REVIEWED BY
Keeley Brookes,
Nottingham Trent University, United Kingdom
Ram Madabhushi,
University of Texas Southwestern Medical Center, United States

*CORRESPONDENCE
Wilbert P. Vermeij
✉ W.P.Vermeij@prinsesmaximacentrum.nl
Dick Jaarsma
✉ D.Jaarsma@erasmusmc.nl

RECEIVED 13 March 2023
ACCEPTED 03 May 2023
PUBLISHED 24 May 2023

CITATION
van't Sant LJ, Birkisdóttir MB, Ozinga RA, Gyenis Á, Hoeijmakers JHJ, Vermeij WP and Jaarsma D (2023) Gene expression changes in cerebellum induced by dietary restriction. *Front. Mol. Neurosci.* 16:1185665. doi: 10.3389/fnmol.2023.1185665

Gene expression changes in cerebellum induced by dietary restriction

Lisanne J. van't Sant[1], María B. Birkisdóttir[1,2,3], Rutger A. Ozinga[2,3], Ákos Gyenis[4], Jan H.J. Hoeijmakers[2,3,4,5], Wilbert P. Vermeij[2,3]* and Dick Jaarsma[1]*

[1]Department of Neuroscience, Erasmus MC, Rotterdam, Netherlands, [2]Princess Máxima Center for Pediatric Oncology, Utrecht, Netherlands, [3]Oncode Institute, Utrecht, Netherlands, [4]Cologne Excellence Cluster for Cellular Stress Responses in Aging-Associated Diseases (CECAD), Faculty of Medicine, Institute for Genome Stability in Ageing and Disease, University of Cologne, Cologne, Germany, [5]Department of Molecular Genetics, Erasmus MC Cancer Institute, Erasmus University Medical Center, Rotterdam, Netherlands

Background: Dietary restriction (DR) is a well-established universal anti-aging intervention, and is neuroprotective in multiple models of nervous system disease, including models with cerebellar pathology. The beneficial effects of DR are associated with a rearrangement of gene expression that modulate metabolic and cytoprotective pathways. However, the effect of DR on the cerebellar transcriptome remained to be fully defined.

Results: Here we analyzed the effect of a classical 30% DR protocol on the transcriptome of cerebellar cortex of young-adult male mice using RNAseq. We found that about 5% of expressed genes were differentially expressed in DR cerebellum, the far majority of whom showing subtle expression changes. A large proportion of down-regulated genes are implicated in signaling pathways, in particular pathways associated with neuronal signaling. DR up regulated pathways in large part were associated with cytoprotection and DNA repair. Analysis of the expression of cell-specific gene sets, indicated a strong enrichment of DR down genes in Purkinje cells, while genes specifically associated with granule cells did not show such a preferential down-regulation.

Conclusion: Our data show that DR may have a clear effect on the cerebellar transcriptome inducing a mild shift from physiology towards maintenance and repair, and having cell-type specific effects.

KEYWORDS

Purkinje neurons, aging, neurodegeneration, neuroprotective mechanisms, neuronal signaling, DNA repair

Introduction

Dietary restriction (DR, also known as caloric restriction) is a well-established anti-aging intervention that consists of reduced food intake without malnutrition (Speakman and Mitchell, 2011; Lee et al., 2021; Acosta-Rodriguez et al., 2022). DR increases health- and lifespan in organisms ranging from yeast to primates with benefits throughout the body (Lee et al., 2021; Green et al., 2022). In rodents and primates, DR has been shown to reduce age-related decline in motor and cognitive function and age-related nervous system pathologies,

and to increase resistance to oxidative, metabolic, and excitotoxic insults (Valdez et al., 2010; Wahl et al., 2016; Mattison et al., 2017; van den Boogaard et al., 2021). Furthermore, DR has been shown to reduce neurological deficits and nervous system pathologies in a subset of mouse models for age-related neurodegenerative diseases (Xie et al., 2020; Green et al., 2022; Mitchell and Mitchell, 2022). The anti-aging and neuroprotective effects of DR are thought to be primarily mediated by a network of evolutionary conserved nutrient and energy-sensing pathways that include mTOR, FGF21, insulin/IGF1, AMPK, and sirtuin signaling, and that modulate a variety of intra- and intercellular processes (Mattson and Arumugam, 2018; Komatsu et al., 2019; Lee et al., 2021; Green et al., 2022). Cell-intrinsic neuroprotective mechanisms associated with DR include reduced oxidative stress, improved glucose metabolism, improved proteostasis, increased organelle recycling and enhanced DNA repair (Speakman and Mitchell, 2011; Mattson and Arumugam, 2018; Xie et al., 2020), while cell-extrinsic mechanisms include local factors such as altered glial function and increased neurotrophic signaling, as well as systemic factors such as improved cardiovascular health or immune function (Mattson and Arumugam, 2018; Pluvinage and Wyss-Coray, 2020; Xie et al., 2020; Green et al., 2022). Transcriptome analyses have demonstrated that DR rearranges gene expression in cytoprotective and metabolic pathways, and has differential effects in different tissues and cell types, with relatively limited changes in gene expression in central nervous system as compared to other tissues (Xu et al., 2007; Swindell, 2009; Plank et al., 2012; Barger et al., 2017; Ma et al., 2020). The relatively small effects of DR on gene expression in brain, may reflect the limited bandwidth of brain tissue to adapt its metabolic pathways, because of the continuous high energy demands associated with neuronal function (Harris et al., 2012; Dienel, 2019; Padamsey and Rochefort, 2023).

The cerebellum is affected by a large number of acquired and inherited diseases usually leading to motor and balance abnormalities (Cerminara et al., 2015; Beaudin et al., 2022), and is vulnerably to aging (Andersen et al., 2003). The cerebellum displays different age-related transcriptome and epigenetic changes, and differential vulnerabilities to age-related disorders as compared to forebrain areas (Fraser et al., 2005; Horvath et al., 2015; Liang and Carlson, 2020). Only, a few studies have reported on the effects of DR in the cerebellum. DR has been shown to be beneficial in at least two disease models with cerebellar pathology: In a transgenic mouse model carrying the Atxn3 gene with expanded CAG-repeat region DR reduced cerebellar pathology, potentially mediated by sirtuin signaling (Cunha-Santos et al., 2016). We recently showed that DR strongly delayed Purkinje cell degeneration in progeroid DNA repair-deficient mice (Birkisdottir et al., 2021; Birkisdóttir et al., 2023). The mechanisms underlying the neuroprotective effects of DR in our progeroid mice remain to be defined, although we found that mTOR inhibition seemed not causally involved (Birkisdottir et al., 2021).

To our knowledge there is only a single transcriptome study in the literature that comprehensively examined the effect of DR on gene expression in the cerebellum (Xu et al., 2007). This study suggests that the effect of DR on cerebellar gene expression is minimal, and, in fact, it was concluded that the cerebellar transcriptome was insensitive to DR, yielding no differentially expressed genes (Xu et al., 2007; Swindell, 2009). The study of Xu et al. was performed using microarray's (Xu et al., 2007), and, hence, the lack of differentially expressed genes in DR cerebellum might be explained by the relative insensitivity of this approach compared to RNAseq (Wang et al., 2014; Zhao et al., 2014). Therefore, to further explore the effect of DR on cerebellum, and to map subtle changes in gene expression, here we analyzed the transcriptome of cerebellar cortex from Ad Libitum (AL) and DR wild-type mice using deep (>50 M reads/sample) sequencing. We found that about 5% of expressed genes were differentially expressed, the far majority of whom showing subtle expression changes in the range of 10%–40% altered expression. The changes in gene expression profiles indicated that DR down-regulated expression of neuronal signaling genes, while upregulated pathways in large part were linked to cytoprotection.

Methods

Ethic statements

Animal experiments were performed according to institutional guidelines as overseen by the Animal Welfare Board of the Erasmus MC, following Dutch and EU legislation. Prior to the start of the experiments, a project license for the animal experiments performed for this study was obtained from the Dutch national authority and filed under no. AVD101002015273 (DEC no. 139-12-13, 139-12-18).

Housing conditions and dietary regimens

Dietary restriction (DR) experiments were performed with wild-type (WT) C57BL6J/FVB F1 hybrid young adult male mice, housed in individual ventilated cages under specific pathogen-free conditions. The environment was controlled with a temperature of 20–22°C and 12 h light:12 h dark cycles. Animals were bred and maintained on AIN93G synthetic pellets (Research Diet Services B.V., Wijk bij Duurstede, Netherlands; gross energy content 4.9 kcal/g dry mass, digestible energy 3.97 kcal/g). Mice were weighed, visually inspected weekly, and scored blindly for gross morphological and motor abnormalities weekly. *Ad libitum*-fed mice (AL, $n = 6$) had unlimited access to food. Animals from the 30% DR group ($n = 6$) received food once a day just before the start of the dark (active) period, Zeitgeber Time (ZT) 12:00. The size of food portions was determined in a prior pilot study where food intake of the AL-fed mice was continuously monitored. Mice on average ate 3.0 g food per day, resulting in 2.1 g/day for 30% DR. Water was freely available to all animals throughout the study. DR was initiated at 7 weeks of age with 10% food reduction, and food was gradually reduced to 30% DR from 9 weeks of age onward as previously published (Vermeij et al., 2016).

RNA sequencing and analysis

At 12 weeks of age, DR and AL animals were sacrificed at the beginning of the dark period (between ZT13 and ZT16), the DR animals without receiving their last meal at ZT12. For RNA isolation a part cerebellar cortex containing multiple folia from the hemisphere, paravermis and vermis, but no cerebellar nuclei (Figure 1A) was rapidly dissected, immediately flash frozen in liquid nitrogen and stored at −80°C.

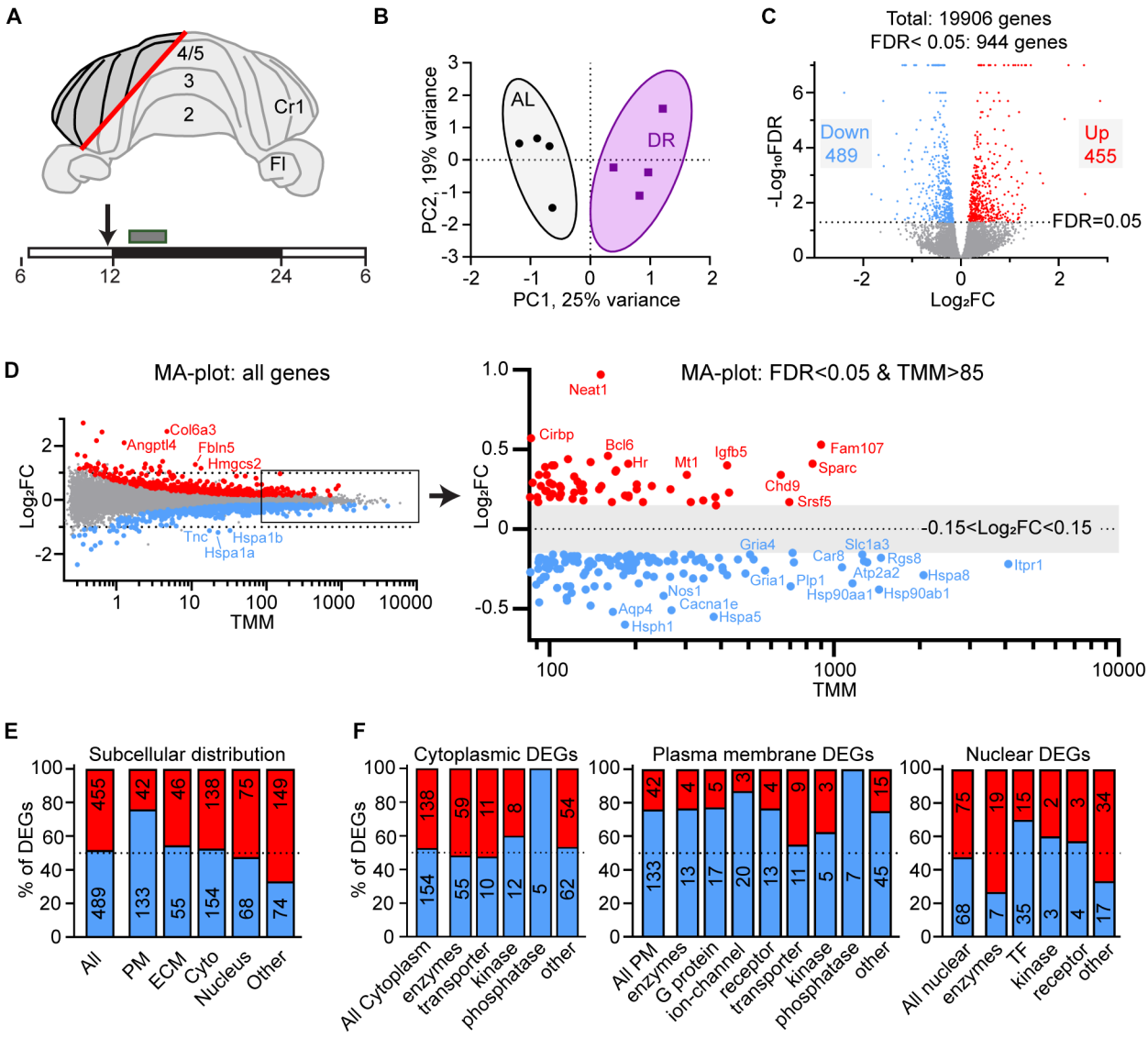

FIGURE 1
Differential gene expression in DR cerebellum. **(A)** Layout of dissected area of cerebellar cortex from DR and AL wild-type mice used for RNAseq analysis. The box above the time bar indicates the time interval of dissection at the beginning of the dark period (ZT13–ZT16). The arrow indicates the normal time of food delivery, just before the onset of dark period (ZT12) to DR animals. Note that the DR animals did not receive food on the day of dissection. **(B)** Principal component analysis plot showing separation of AL and DR animals. **(C)** Volcano plot showing the distribution of differently expressed genes (DEGs) between AL and DR mice with fold change in expression (log_2FC) on the x-axis, and false discovery rate ($-Log_{10}$FDR) on the y-axis; DEGs are defined as all genes with FDR<0.05 ($-Log_{10}$FDR=1.3, above the dotted line; DR-down genes in blue and DR-up genes in red). **(D)** MA plot illustrating relatively low Log_2FC values of DEGs of DR versus AL cerebellar cortex. TMM values on the x-axis are means of AL and DR values. The right panel shows a higher magnification of abundantly expressed DEGs (mean TMM≥85) with only DEGs (blue and red dots are down and up in DR DEGs, respectively). Note that the abundantly expressed DR-down DEGs are dominated by heat shock proteins (Hspa5, Hspa8, Hsp90aa1, and Hsp90ab1) and genes linked to glutamatergic signaling (Rgs8, Slc1a3, Gria1, and Gria4) and calcium signaling (Itpr1, Atp2a2, and Car8). **(E,F)** Gene Ontology (GO) annotated subcellular localization **(E)** and functional classes **(F)** of DEGs. PM, plasma membrane; ECM, extra cellular matrix; Cyto, cytolplasm; TF, transcription factors.

Total RNA was extracted using QIAzol lysis reagent and TissueLyser LT (Qiagen). For increased purity, miRNeasy Mini Kits (Qiagen) with additional on-column DNase treatment were used. Concentration and quality of RNA was measured by Nanodrop One (Thermo Fisher Scientific, United States) and BioAnalyser 2,100 (Agilent, United States). RNA sequencing was performed with 4 of 6 AL and DR RNA samples selected on the basis of RNA quality (RIN values between 8.9 and 9.3). The TruSeq RNA Library prep kit V2 (Illumina) was used to capture poly(A) RNA from 500 ng total RNA. Subsequently cDNA was made to which single indexed adapters were ligated. To obtain enough material for sequencing a PCR of 13 cycles was performed. Product size was checked on the Labchip GX (Perkin Elmer) and concentrations were measured with picogreen (Invitrogen).

Paired-end sequencing of 2 × 150 bp was performed using the Illumina Hiseq 4,000 platform to obtain at least 15 GB per sample. Removal of sequence adaptors from sequence reads was performed using Trimmomatic (version 0.39). Trimmed reads were aligned to

mouse reference genome (annotation: gencode.vM20.annotation.gtf; genome: GRCm38.p6.genome.fa) using STAR (version 2.7.0f). Read counts for each gene were obtained using FeatureCounts (as part of SubRead version 1.6.4). Next, *filterbyExpr* function of EdgeR (version 3.32.1) was used to filter out genes with very low count (average CPM value of 10 or less in both AL and DR groups). This is a common step used to decrease noise in the dataset, as genes with very low counts in deep sequencing are unlikely to be translated into proteins. At the same time, a small difference of counts between groups in lowly expressed genes, can result in large, but often misleading log-fold changes (Chen et al., 2016). Following this step, the genes with sufficiently large counts were TMM-normalized using EdgeR. Normalized genes were used for principal component analysis (PCA), which was performed using the *prcomp* function in R. Lastly, normalized gene counts were quantified, and log2-fold change (logFC) and false discovery rate (FDR) were calculated using EdgeR. All genes with FDR < 0.05 were designated differentially expressed genes (DEGs; Supplementary Table S1). We performed linear correlation analysis between individual sample values of DEGs and selected genes using R and GraphPad Prism software. Heatmaps showing z-scores of gene expression of individual samples were generated in R. All data files have been submitted to the NCBI gene expression omnibus (GEO number: GSE228418).

Ingenuity pathway analysis (IPA) analysis, subcellular location annotation, and GSEA

Significantly changed pathways associated with differentially expressed genes (DEGs, Supplementary Table S1) were identified using Ingenuity Pathway Analysis (IPA, QIAgen; Supplementary Tables S2). The same program was used to annotate subcellular localizations of the DEGs (Supplementary Table S2).

Gene set enrichment analysis (GSEA) was performed with all expressed genes (19,006 genes, TMM > 0.02) using MSigDB software (GSEA version 3.0; Subramanian et al., 2005), and multiple gene set collections. We first tested gene sets from Hallmark (50 gene sets), KEGG (186 sets) and Reactome (1,654 sets) subsets human curated pathways, and all gene sets from the GO collections (10,532 sets, https://www.gsea-msigdb.org/gsea/msigdb/human/collections.jsp). We only report significant gene sets ($p < 0.05$) whose false discovery rate (FDR) was <0.25 (Supplementary Table S3). Additional gene sets investigated were selected from published datasets with cerebellar cell-specific genes (Rosenberg et al., 2018; Kozareva et al., 2021), neuronal activity-induced genes (Tyssowski et al., 2018), and circadian genes (Zhang et al., 2014). To define cerebellar cortex cell-specific gene sets based on the study of Kozareva et al. (2021), in which each cerebellar cell type is differentiated into multiple subtypes (e.g., 9 subclasses of Purkinje cells), we used different criteria for different cell types as outlined in Supplementary Table S4. For instance, for Purkinje cells we included genes that were found in at least 5 of 9 Purkinje cell subclasses, but were not expressed in other cells.

Statistical analyses

Statistical analyses were performed using GraphPad Prism Software (San Diego, CA, United States, version 9.5.1). Aggregated *p*-values, where the Fischer method is used to combine statistical values from individual GSEA tests were calculated using the *fisher* function in Rstudio (Version 1.3.1056).

Results

We applied a 30% DR regimen that we previously have used in progeroid DNA repair-deficient mice starting with 10% restriction at the age of 7 weeks, 20% at 8 weeks, and 30% thereafter (Vermeij et al., 2016). We collected cerebellar tissue at 12 weeks, i.e., 4 weeks after DR onset when the effects of DR on body temperature and metabolic parameters are known to reach stability (Mitchell et al., 2015a). DR animals showed strongly reduced glucose and insulin blood concentrations, increased blood ketones, as well as reduced HDL, LDL and triglyceride blood levels compared to AL animals (Supplementary Figure S1). Body weight was reduced by approximately 30%, while brain weight was relatively preserved, consistent with previous studies (Mitchell et al., 2015b). RNA-seq was performed using an Illumina platform and mapped to the mouse reference genome, yielding 19,906 transcripts. Principal component analysis showed a separation of DR and AL transcriptomes by a single component explaining 25% of the variance (Figure 1B). 5% (944 of 19,006) of expressed genes displayed differential expression (FDR < 0.05), 48% and 52% showing increased (DR-up) versus reduced (DR-down) expression, respectively (Figure 1C, Supplementary Table S1). Large fold changes ($\log_2$FC > 1) were rare and primarily occurred in DEGs with low mean expression values (TMM < 1; Figure 1D), while the majority of DEGs showed subtle expression changes in the range of 10%–40% (0.15 < Log_2FC < 0.5, Figure 1D, Supplementary Table S1).

Gene ontology (GO) assessment of the DEGs revealed specific changes according to subcellular distribution with an increased relative abundance of DR-down DEGs in plasma membrane genes (76% down; Figure 1E), including ion channels, receptors and G-proteins (Figure 1F). Accordingly, Ingenuity pathway analysis (IPA) of DEGs identified neuronal signaling pathways, including calcium signaling and glutamate receptor signaling, and synaptic plasticity, among the top enriched pathways of down regulated genes by DR (Figure 2A; Supplementary Table S2). Down-regulated processes, further consisted of additional signaling pathways, including integrin signaling, nutrient-sensing, and inflammatory signaling, as well as protein folding and ER stress (Figure 2A; Supplementary Table S2). Upregulated pathways included NAD signaling and DNA repair pathways (Figure 2A; Supplementary Table S2).

To further define down- and upregulated processes in DR cerebellum we compared DR vs. AL gene expression of all genes using gene set enrichment analysis (GSEA; Subramanian et al., 2005) with all gene sets from Hallmark, KEGG and Reactome curated pathways, and GO collections (Figure 2B; Supplementary Table S3). Consistent with IPA pathway analysis of DEGs, gene sets showing overall reduced expression in DR were predominantly associated with nutrient-sensing, inflammatory, extracellular matrix, and neuronal signaling (Figures 2B–E and Supplementary Figures S2A–D; Supplementary Table S3). Since the global down-regulation of neuronal signaling pathways may be associated with reduced neuronal activity, we also performed GSEA with gene sets activated by neuronal activity (Tyssowski et al., 2018). This analysis showed reduced expression of neuronal-activity regulated genes in DR

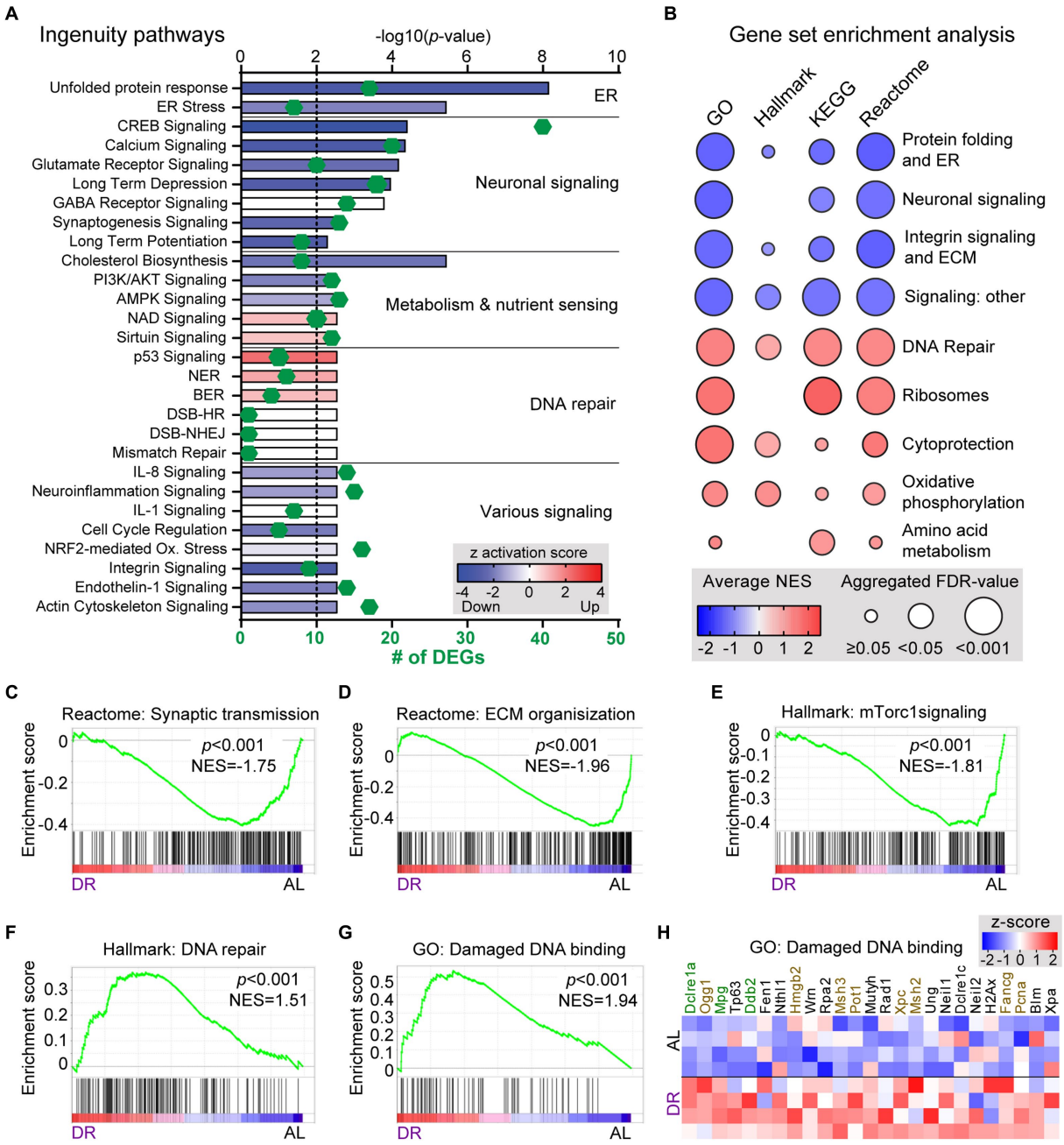

FIGURE 2
Pathway and GSEA analysis of the effect of DR on cerebellar transcriptome. **(A)** Selection of significantly altered pathways of DEGs as identified with Ingenuity Pathway Analysis. Length of bars indicate the $-\log_{10}(p\text{-value})$ with the dashed line at p =0.01. Color of bars (z-score) indicates whether and to which degree pathways are up- (red) or down-regulated (blue). Green diamonds show the number of DEGs associated with the pathway. **(B)** Graph showing summary of results of gene set enrichment analysis (GSEA) with all gene sets from Hallmark, KEGG and Reactome canonical pathways, and Gene Ontology (GO) collections. The graph is based on gene sets with p <0.05 and FDR<0.25 categorized as outlined in Supplementary Table S3. **(C–E)** Exemplary GSEA graphs illustrating enrichment of down-regulated genes in gene sets associated with synaptic transmission **(C)**, extra cellular matrix **(D)**, and mTorc1 signaling **(E)** in DR cerebellar cortex. **(F–H)** GSEA graphs **(F,G)** and heat map [**(H)** with z-scores of genes of **(G)**] illustrating enrichment of up-regulated genes in gene sets associated with DNA repair pathways in DR cerebellum. In **(H)** genes in green and brown have FDR and p values <0.05, respectively.

cerebellum, consistent with attenuated neuronal activity (Supplementary Figure S2F). Gene sets with increased expression in DR predominantly consisted of ribosomal genes, DNA repair genes, and gene sets associated with cytoprotective pathways (Figures 2B,F–H, Supplementary Figure S2G,H; Supplementary Table S3). Top enriched DNA repair gene sets included base excision repair, interstrand crosslink repair and mismatch repair pathways, as well as processes like DNA damage recognition and binding (Figures 2F–H, Supplementary Figure S2G; Supplementary Table S3). Finally, GSEA analysis indicated that gene sets of metabolic pathways were relatively unaffected by DR, except for mild upregulation of some gene sets associated with oxidative phosphorylation and amino acid metabolism (Figure 2B; Supplementary Figure S2; Supplementary Table S3).

Many DR-down DEGs associated with neuronal signaling, including Abdh2, Atp2a3, Baiap2, Car8, Grid2, Itpr1, Prkg1, Ryr1, Shank2, Shisha6, and Trpc3, are preferentially expressed in Purkinje cells. Further analysis of changes in Purkinje cells using GSEA analysis with Purkinje cell-specific gene lists (Rosenberg et al., 2018; Kozareva et al., 2021) indicated a preferential down-regulation of Purkinje cell genes by DR (Figures 3A–D; Supplementary Table S4). Instead, no enrichment of up or down genes were observed in granule cells, representing another major class of neurons in the cerebellar cortex (Figures 3E–G), while variable changes were observed with gene sets associated with glia cells (Figures 3H,I; Supplementary Figure S4). Thus GSEA analysis with cell-specific gene sets indicates that DR differentially impacts on Purkinje cells as compared to granule cells causing a preferential down-regulation of Purkinje cell-specific genes. Analysis of cell-specific gene sets further enabled to identify cell-specific pathways in glia cells altered by DR, including altered myelin regulation (Hhip, Plp1, Gpr37, Prox1, Hcn2, and Fth1) in oligodendrocytes (Figures 3H,I), and altered Shh signaling (Gli1, Ptch1, Ptch2, Trib2, and Bcl6) in Bergman glia cells (Supplementary Figure S4).

Since DR may affect circadian physiology and metabolism, and have tissue-specific effects on circadian gene expression (Speakman and Mitchell, 2011; Greco and Sassone-Corsi, 2019; Acosta-Rodriguez et al., 2022), we looked at the effect of DR on a list of 220 cerebellar circadian genes from the CircaDB database (http://circadb.hogeneschlab.org/; Zhang et al., 2014). A subset of these (26 of 220) were DEGs, most of which (17 of 26) were DR-down DEGs with peak phases both in the dark and the light period (Figures 4A,B). Instead, the DR-up circadian DEGs (9 of 26) predominantly have a peak phase in the dark (Figure 4B). Also,

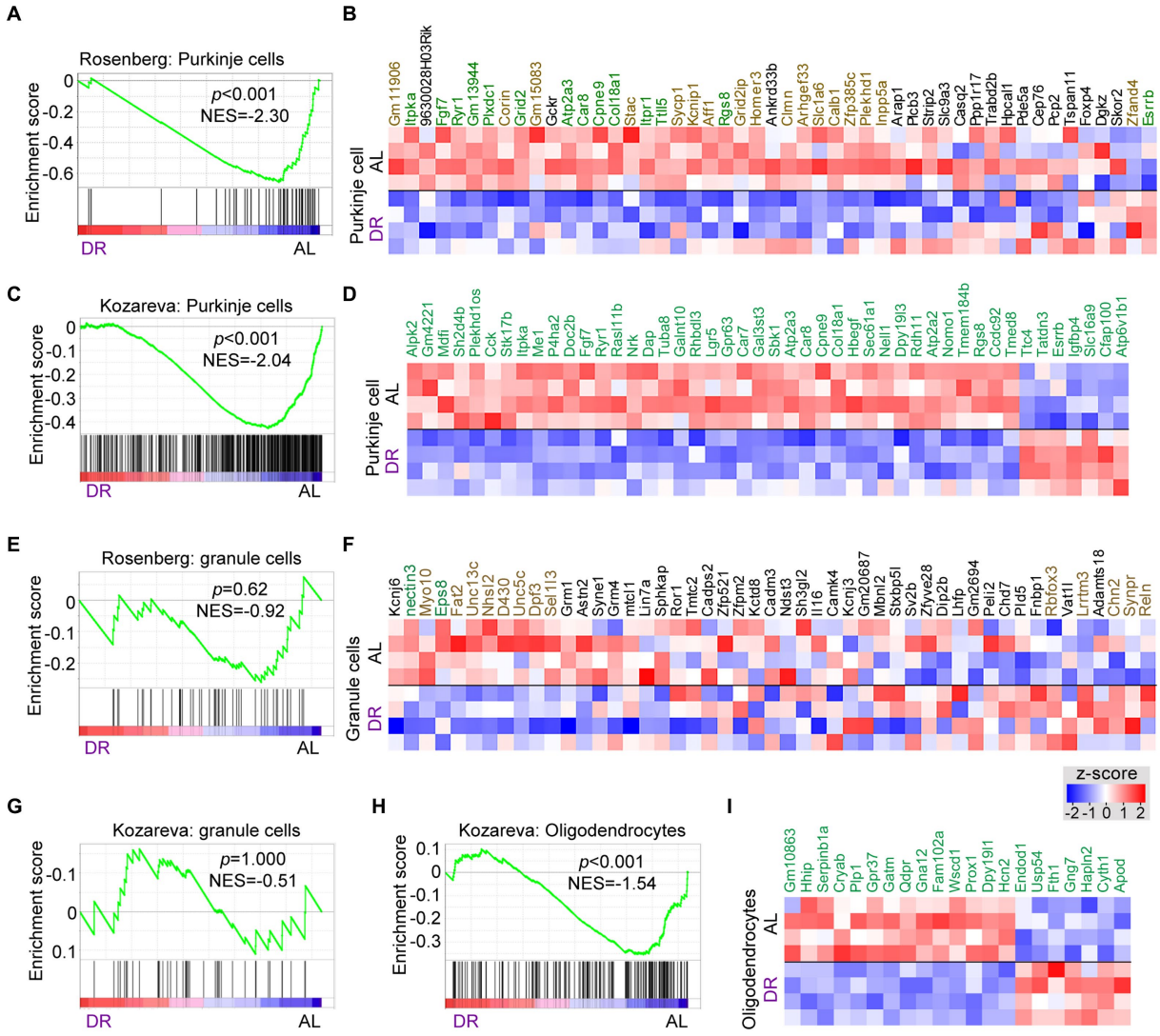

FIGURE 3
Cell specific effects of DR in cerebellum. GSEA graphs and heat maps gene sets specifically expressed in Purkinje cells **(A–D)**, granule cells **(E–G)** and oligodendrocytes **(H–I)**, based on gene lists from Rosenberg et al. (2018) and Kozareva et al. (2021) (see Supplementary Table S4 for gene sets). Heat maps in **(D)** and **(I)** only show differentially expressed genes (DEGs, in green), while the heat maps in **(B)** and **(F)** shows all genes of the Rosenberg Purkinje and granule cell lists, with genes in green and brown showing FDR<0.05 and p <0.05, respectively, in DR versus AL comparison. Note, enrichment of down-regulated genes (p <0.01) in gene sets associated with Purkinje cells **(A,C)** and oligodendrocytes **(H)**, while no specific enrichments occur in granule cell gene sets.

10.3389/fnmol.2023.1185665

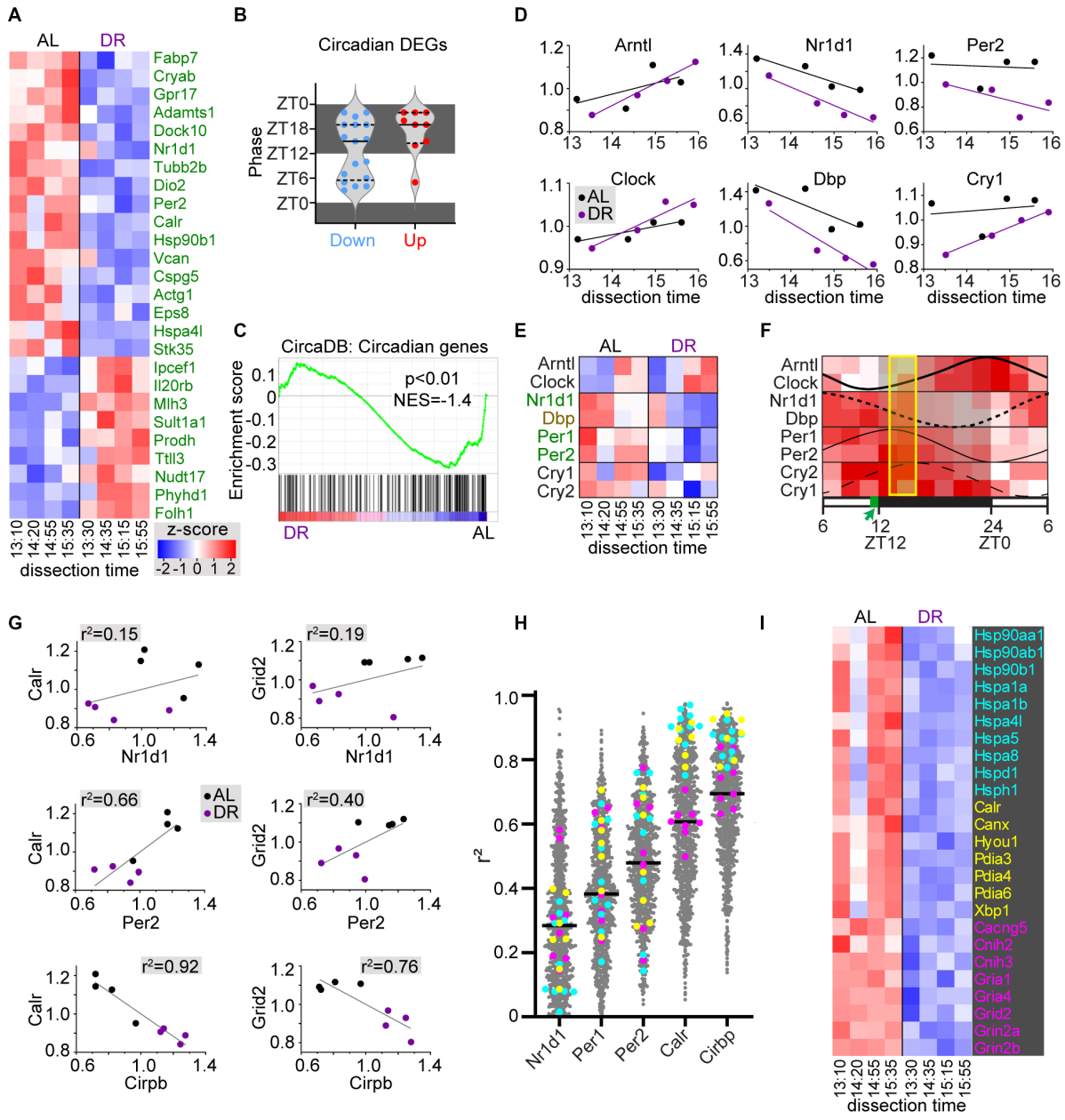

FIGURE 4
DR induces changes in circadian cerebellar genes and heat shock chaperones. **(A,B)** Heatmap **(A)** and bar graph with peak phases **(B)** of differentially expressed circadian genes in DR versus AL cerebellar cortex. Dissection time [x-axis in **(A)**] is indicated as zeitgeber time (ZT). **(C)** GSEA plot of cerebellar circadian genes (i.e., genes from CircaDB mouse cerebellar database with JTK q-value<0.05) in DR versus AL cerebellar cortex. **(D–F)** x-y plots **(D)** and heat map **(E)** of core clock genes expression related to time of dissection show that changes in core clock gene expression throughout the dissection period in both AL and DR cerebellum are consistent with oscillation phases of core clock gene expression in cerebellum as illustrated in panel **(F)** that is based on Supplementary Figure S5 of Zhang et al. (2014). Genes in green and brown have FDR<0.05 and p <0.05, respectively in DR versus AL comparison. The yellow box in **(F)** indicate the period of dissection (ZT13–ZT16), and the green box in the time bar indicates the time of daily food delivery to DR animals. **(G)** x-y plots with linear correlation lines **(G)** illustrate a poor correlation between sample values of 2 exemplary DEGs (Calr and Grid2) and differentially expressed core clock genes Nr1d1 and Per2. Instead, Calr values show a strong negative correlation with the hypothermia-induced factor Cirbp that shows increased expression in DR cerebellum. Further linear correlation analysis of all DEGs [grey dots in **(H)**] versus differentially expressed core clock genes and Cirbp, indicates stronger correlations with Cirbp compared than with Nr1d1, Per1, and Per2, in particular for all differentially expressed heat shock proteins [cyan in **(H,I)**], and ER chaperones [yellow in **(H,I)**]. Genes in pink in **(H,I)** are glutamate receptor subunits and adaptors.

GSEA analysis indicated a trend of reduced expression of circadian genes in DR cerebellum (Figure 4C). DR down DEGs included negative feedback loop factors (Nr1d1, Per1, and Per2) of the core clock genes, while the key positive regulators Arntl (Bmal1) and Clock showed no differential expression in DR cerebellum. Interestingly, plotting of core clock gene expression values of individual samples against dissection time, revealed gene-dependent upward (Arntl, Clock, and Cry1) or downward (Nr1d1, Dbp, and Per2) changes in expression throughout the dissection time window (Figures 4D,E). These changes in time were consistent

with expected directionality based on documented oscillation phases of cerebellar core clock genes (Figure 4F; Zhang et al., 2014), and support the notion that our DR procedure does not have a major effect on the phase of core clock genes as previously documented (Mendoza et al., 2010; Acosta-Rodriguez et al., 2022), and unlike other feeding schemes such as food delivery halfway the light period (Mendoza et al., 2010; Acosta-Rodriguez et al., 2022). Importantly, the analysis of core clock gene expression of individual samples also indicates that the variability between samples from the same treatment groups embodies biological meaningful information. Linear correlation analysis of individual sample values suggested relatively poor correlations between expression of differentially expressed core clock genes (Nr1d, Per1, Per2) and other DEGs (Figures 4G,H). Instead, expression of many DEGs showed a better linear correlation with Cirbp mRNA, a hypothermia-induced factor that showed increased expression in DR cerebellum (Figures 4G,H). For instance, DR-down heat shock proteins and ER chaperones showed a strong negative correlation with Cirbp mRNA levels (Figures 4G–I), indicating that these changes in molecular chaperone expression may reflect changes in body temperature triggered by DR (Mitchell et al., 2015a; Guijas et al., 2020), and further illustrating that the variability between samples in our RNAseq dataset may embody biological meaningful information.

Discussion

In this study we show that a classical 30% DR protocol with strong anti-aging effects and neuroprotection in multiple neurodegenerative models, including models with cerebellar pathology (Speakman and Mitchell, 2011; Cunha-Santos et al., 2016; Vermeij et al., 2016; Xie et al., 2020; Acosta-Rodriguez et al., 2022; Birkisdóttir et al., 2023), does have a distinct and important effect on gene expression in cerebellar cortex, with about 5% of the expressed genes showing differential expression compared to AL-fed control mice. The far majority of DEGs showed relatively small expression changes in the range of 10–40% increased or reduced expression, which may explain why no consistent gene expression changes have been observed in DR cerebellum in previous microarray experiments (Xu et al., 2007; Swindell, 2009) with reduced sensitivity compared to the deep sequencing approach of our study. The overall picture that emerges from the DR-induced gene expression changes is a mild shift from physiology towards maintenance and repair (Finkel, 2015; Vermeij et al., 2016). Thus, a considerable proportion of down-regulated genes are involved in neuronal signaling, while many upregulated genes are linked to cytoprotective mechanisms, including DNA repair. Upregulation of cytoprotective and DNA repair pathways is consistent with data from other brain areas and tissues (Xu et al., 2007; Swindell, 2009; Plank et al., 2012; Barger et al., 2017; Ma et al., 2020; Wahl and LaRocca, 2021), and can be mechanistically linked to the neuroprotective effect of DR in cerebellar neurodegeneration mouse models (Cunha-Santos et al., 2016; Birkisdottir et al., 2021; Birkisdóttir et al., 2023). Upregulation of DNA repair pathways, for instance, may reduce the accumulation DNA damage in aging (Heydari et al., 2007; Van Houten et al., 2018), and contribute to the strong beneficial effect of DR in DNA-repair-deficient accelerated aging mouse models (Vermeij et al., 2016; Birkisdottir et al., 2021; Birkisdóttir et al., 2023).

The nervous system requires continuous supply of glucose and oxygen, and has limited opportunities to save energy, which results in reallocation of energy from other tissues to the brain in condition of scarcity (Harris et al., 2012; Dienel, 2019; Padamsey and Rochefort, 2023). Brain energy consumption may be reducing by reducing body temperature and physical activity, by modulating sleep, and, in mice, by inducing torpor, a state in which whole-body metabolism and neuronal activity is substantially reduced (Speakman and Mitchell, 2011; Sonntag and Arendt, 2019; Padamsey and Rochefort, 2023). Interestingly, recently it has been found that circuitries in neocortex in conditions of food restriction can adapt their properties, and reduce their energy demand via a leptin-dependent mechanism and involving adaptation of AMPA-receptor signaling (Padamsey et al., 2022). The reduced expression in synaptic and neuron signaling genes as we observed in DR cerebellum may reflect a similar adaptation to reduce energy consumption. Interestingly, reduced synaptic gene expression predicts a longer lifespan among healthy aging individuals (Zullo et al., 2019), raising the possibility that adapting neuronal excitation and synaptic function may be one of the mechanisms by which DR exerts its anti-aging and neuroprotective effects (Aron et al., 2022). Our data indicate that a large proportion of down-regulated neuronal signaling genes is expressed by Purkinje cells, representing large continuously firing neurons. Interestingly, Purkinje cells can be grouped in different subtypes with distinct firing properties coupled to differences in metabolic and signaling gene expression, and differences in disease vulnerabilities (Cerminara et al., 2015). The precise impact, of DR on firing properties and gene expression of these Purkinje cell subtypes remains to be determined in future studies.

Our demonstration that DR indeed significantly alters the cerebellar transcriptome, provides a starting point for further analyses of cerebellar changes triggered by DR. In this study we examined young adult male C57BL6J/FVB F1 hybrid mice at a single time window of the diurnal cycle. Thus, our findings remain to be examined in cohorts with female mice, with mice with different genetic background, and with old mice (Acosta-Rodriguez et al., 2022; Mitchell and Mitchell, 2022). Furthermore, analysis of gene expression at multiple diurnal time points, may provide a dynamic picture of DR induced transcriptome changes throughout the day, and could expose how transcriptome changes relate to DR-induced diurnal changes in metabolism, body temperature, as well as sleeping and physical activity patterns (Nelson and Halberg, 1986; Speakman and Mitchell, 2011; Greco and Sassone-Corsi, 2019; Guijas et al., 2020; Acosta-Rodriguez et al., 2022). Finally, cell specific approaches, for instance *via* cell specific isolation of ribosomes or nuclei (Doyle et al., 2008; Chen et al., 2022) may further expose cell specific pathways induced by DR in the cerebellum.

Data availability statement

The original contributions presented in the study are publicly available. This data can be found here: https://www.ncbi.nlm.nih.gov/, GSE228418.

Ethics statement

The animal study was reviewed and approved by Animal Welfare Board of the Erasmus MC. Written informed consent was obtained from the owners for the participation of their animals in this study.

Author contributions

WV and DJ conceptualized and designed the experiments. MB, LvS, ÁG, RO, WV, and DJ performed transcriptomics analysis. MB, LvS, WV, and DJ wrote the manuscript. JH contributed to editing the manuscript. All authors contributed to the article and approved the submitted version.

Funding

We acknowledge financial support of the National Institute of Health (NIH)/National Institute of Aging (NIA) (AG17242), European Research Council Advanced Grants Dam2Age (to JH), ONCODE supported by the Dutch Cancer Society, ADPS Longevity Research Award (to WV), Memorabel (ZonMW 733050810), BBoL (NWO-ENW 737.016.015), Deutsche Forschungsgemeinschaft (DFG, German Research Foundation—Project-ID 73111208—SFB 829), Regiodeal Foodvalley (162135) and the European Joint Programme Rare Diseases (TC-NER RD20-113).

Conflict of interest

The authors declare that the research was conducted in the absence of any commercial or financial relationships that could be construed as a potential conflict of interest.

Publisher's note

All claims expressed in this article are solely those of the authors and do not necessarily represent those of their affiliated organizations, or those of the publisher, the editors and the reviewers. Any product that may be evaluated in this article, or claim that may be made by its manufacturer, is not guaranteed or endorsed by the publisher.

Supplementary material

The Supplementary material for this article can be found online at: https://www.frontiersin.org/articles/10.3389/fnmol.2023.1185665/full#supplementary-material

References

Acosta-Rodriguez, V., Rijo-Ferreira, F., Izumo, M., Xu, P., Wight-Carter, M., Green, C. B., et al. (2022). Circadian alignment of early onset caloric restriction promotes longevity in male C57BL/6J mice. *Science* 376, 1192–1202. doi: 10.1126/science.abk0297

Andersen, B. B., Gundersen, H. J., and Pakkenberg, B. (2003). Aging of the human cerebellum: a stereological study. *J. Comp. Neurol.* 466, 356–365. doi: 10.1002/cne.10884

Aron, L., Zullo, J., and Yankner, B. A. (2022). The adaptive aging brain. *Curr. Opin. Neurobiol.* 72, 91–100. doi: 10.1016/j.conb.2021.09.009

Barger, J. L., Vann, J. M., Cray, N. L., Pugh, T. D., Mastaloudis, A., Hester, S. N., et al. (2017). Identification of tissue-specific transcriptional markers of caloric restriction in the mouse and their use to evaluate caloric restriction mimetics. *Aging Cell* 16, 750–760. doi: 10.1111/acel.12608

Beaudin, M., Manto, M., Schmahmann, J. D., Pandolfo, M., and Dupre, N. (2022). Recessive cerebellar and afferent ataxias—clinical challenges and future directions. *Nat. Rev. Neurol.* 18, 257–272. doi: 10.1038/s41582-022-00634-9

Birkisdottir, M. B., Jaarsma, D., Brandt, R. M. C., Barnhoorn, S., van Vliet, N., Imholz, S., et al. (2021). Unlike dietary restriction, rapamycin fails to extend lifespan and reduce transcription stress in progeroid DNA repair-deficient mice. *Aging Cell* 20:e13302. doi: 10.1111/acel.13302

Birkisdóttir, M. B., van't Sant, L. J., Brandt, R. M. C., Barnhoorn, S., Hoeijmakers, J. H. J., Vermeij, W. P., et al. (2023). Purkinje-cell-specific DNA repair-deficient mice reveal that dietary restriction protects neurons by cell-intrinsic preservation of genomic health. *Front. Aging Neurosci.* 14:1498. doi: 10.3389/fnagi.2022.1095801

Cerminara, N. L., Lang, E. J., Sillitoe, R. V., and Apps, R. (2015). Redefining the cerebellar cortex as an assembly of non-uniform Purkinje cell microcircuits. *Nat. Rev. Neurosci.* 16, 79–93. doi: 10.1038/nrn3886

Chen, X., Du, Y., Broussard, G. J., Kislin, M., Yuede, C. M., Zhang, S., et al. (2022). Transcriptomic mapping uncovers Purkinje neuron plasticity driving learning. *Nature* 605, 722–727. doi: 10.1038/s41586-022-04711-3

Chen, Y., Lun, A. T., and Smyth, G. K. (2016). From reads to genes to pathways: differential expression analysis of RNA-Seq experiments using Rsubread and the edgeR quasi-likelihood pipeline. *F1000Res* 5:1438. doi: 10.12688/f1000research.8987.2

Cunha-Santos, J., Duarte-Neves, J., Carmona, V., Guarente, L., Pereira de Almeida, L., and Cavadas, C. (2016). Caloric restriction blocks neuropathology and motor deficits in Machado-Joseph disease mouse models through SIRT1 pathway. *Nat. Commun.* 7:11445. doi: 10.1038/ncomms11445

Dienel, G. A. (2019). Brain glucose metabolism: integration of energetics with function. *Physiol. Rev.* 99, 949–1045. doi: 10.1152/physrev.00062.2017

Doyle, J. P., Dougherty, J. D., Heiman, M., Schmidt, E. F., Stevens, T. R., Ma, G., et al. (2008). Application of a translational profiling approach for the comparative analysis of CNS cell types. *Cells* 135, 749–762. doi: 10.1016/j.cell.2008.10.029

Finkel, T. (2015). The metabolic regulation of aging. *Nat. Med.* 21, 1416–1423. doi: 10.1038/nm.3998

Fraser, H. B., Khaitovich, P., Plotkin, J. B., Paabo, S., and Eisen, M. B. (2005). Aging and gene expression in the primate brain. *PLoS Biol.* 3:e274. doi: 10.1371/journal.pbio.0030274

Greco, C. M., and Sassone-Corsi, P. (2019). Circadian blueprint of metabolic pathways in the brain. *Nat. Rev. Neurosci.* 20, 71–82. doi: 10.1038/s41583-018-0096-y

Green, C. L., Lamming, D. W., and Fontana, L. (2022). Molecular mechanisms of dietary restriction promoting health and longevity. *Nat. Rev. Mol. Cell Biol.* 23, 56–73. doi: 10.1038/s41580-021-00411-410.1038/s41580-021-00411-4

Guijas, C., Montenegro-Burke, J. R., Cintron-Colon, R., Domingo-Almenara, X., Sanchez-Alavez, M., Aguirre, C. A., et al. (2020). Metabolic adaptation to calorie restriction. *Sci. Signal.* 13:eabb2490. doi: 10.1126/scisignal.abb2490

Harris, J. J., Jolivet, R., and Attwell, D. (2012). Synaptic energy use and supply. *Neuron* 75, 762–777. doi: 10.1016/j.neuron.2012.08.019

Heydari, A. R., Unnikrishnan, A., Lucente, L. V., and Richardson, A. (2007). Caloric restriction and genomic stability. *Nucleic Acids Res.* 35, 7485–7496. doi: 10.1093/nar/gkm860

Horvath, S., Mah, V., Lu, A. T., Woo, J. S., Choi, O. W., Jasinska, A. J., et al. (2015). The cerebellum ages slowly according to the epigenetic clock. *Aging (Albany NY)* 7, 294–306. doi: 10.18632/aging.100742

Komatsu, T., Park, S., Hayashi, H., Mori, R., Yamaza, H., and Shimokawa, I. (2019). Mechanisms of calorie restriction: a review of genes required for the life-extending and tumor-inhibiting effects of calorie restriction. *Nutrients* 11:3068. doi: 10.3390/nu11123068

Kozareva, V., Martin, C., Osorno, T., Rudolph, S., Guo, C., Vanderburg, C., et al. (2021). A transcriptomic atlas of mouse cerebellar cortex comprehensively defines cell types. *Nature* 598, 214–219. doi: 10.1038/s41586-021-03220-z

Lee, M. B., Hill, C. M., Bitto, A., and Kaeberlein, M. (2021). Antiaging diets: separating fact from fiction. *Science* 374:eabe7365. doi: 10.1126/science.abe7365

Liang, K. J., and Carlson, E. S. (2020). Resistance, vulnerability and resilience: a review of the cognitive cerebellum in aging and neurodegenerative diseases. *Neurobiol. Learn. Mem.* 170:106981. doi: 10.1016/j.nlm.2019.01.004

Ma, S., Sun, S., Geng, L., Song, M., Wang, W., Ye, Y., et al. (2020). Caloric restriction reprograms the single-cell transcriptional landscape of *Rattus Norvegicus* aging. *Cells* 180, 984–1001.e22. doi: 10.1016/j.cell.2020.02.008

Mattison, J. A., Colman, R. J., Beasley, T. M., Allison, D. B., Kemnitz, J. W., Roth, G. S., et al. (2017). Caloric restriction improves health and survival of rhesus monkeys. *Nat. Commun.* 8:14063. doi: 10.1038/ncomms14063

Mattson, M. P., and Arumugam, T. V. (2018). Hallmarks of brain aging: adaptive and pathological modification by metabolic states. *Cell Metab.* 27, 1176–1199. doi: 10.1016/j.cmet.2018.05.011

Mendoza, J., Pevet, P., Felder-Schmittbuhl, M. P., Bailly, Y., and Challet, E. (2010). The cerebellum harbors a circadian oscillator involved in food anticipation. *J. Neurosci.* 30, 1894–1904. doi: 10.1523/JNEUROSCI.5855-09.2010

Mitchell, S. E., Delville, C., Konstantopedos, P., Derous, D., Green, C. L., Chen, L., et al. (2015a). The effects of graded levels of calorie restriction: III. Impact of short term calorie and protein restriction on mean daily body temperature and torpor use in the C57BL/6 mouse. *Oncotarget* 6, 18314–18337. doi: 10.18632/oncotarget.4506

Mitchell, S. E., and Mitchell, J. R. (2022). Sexual dimorphism in the response to dietary restriction in mice: a systematic review of the literature. *Nutr. Healthy Aging* 7, 87–120. doi: 10.3233/NHA-220162

Mitchell, S. E., Tang, Z., Kerbois, C., Delville, C., Konstantopedos, P., Bruel, A., et al. (2015b). The effects of graded levels of calorie restriction: I. impact of short term calorie and protein restriction on body composition in the C57BL/6 mouse. *Oncotarget* 6, 15902–15930. doi: 10.18632/oncotarget.4142

Nelson, W., and Halberg, F. (1986). Meal-timing, circadian rhythms and life span of mice. *J. Nutr.* 116, 2244–2253. doi: 10.1093/jn/116.11.2244

Padamsey, Z., Katsanevaki, D., Dupuy, N., and Rochefort, N. L. (2022). Neocortex saves energy by reducing coding precision during food scarcity. *Neuron* 110, 280–296.e10. doi: 10.1016/j.neuron.2021.10.024

Padamsey, Z., and Rochefort, N. L. (2023). Paying the brain's energy bill. *Curr. Opin. Neurobiol.* 78:102668. doi: 10.1016/j.conb.2022.102668

Plank, M., Wuttke, D., van Dam, S., Clarke, S. A., and de Magalhaes, J. P. (2012). A meta-analysis of caloric restriction gene expression profiles to infer common signatures and regulatory mechanisms. *Mol. BioSyst.* 8, 1339–1349. doi: 10.1039/c2mb05255e

Pluvinage, J. V., and Wyss-Coray, T. (2020). Systemic factors as mediators of brain homeostasis, ageing and neurodegeneration. *Nat. Rev. Neurosci.* 21, 93–102. doi: 10.1038/s41583-019-0255-9

Rosenberg, A. B., Roco, C. M., Muscat, R. A., Kuchina, A., Sample, P., Yao, Z., et al. (2018). Single-cell profiling of the developing mouse brain and spinal cord with split-pool barcoding. *Science* 360, 176–182. doi: 10.1126/science.aam8999

Sonntag, M., and Arendt, T. (2019). Neuronal activity in the hibernating brain. *Front. Neuroanat.* 13:71. doi: 10.3389/fnana.2019.00071

Speakman, J. R., and Mitchell, S. E. (2011). Caloric restriction. *Mol. Asp. Med.* 32, 159–221. doi: 10.1016/j.mam.2011.07.001

Subramanian, A., Tamayo, P., Mootha, V. K., Mukherjee, S., Ebert, B. L., Gillette, M. A., et al. (2005). Gene set enrichment analysis: a knowledge-based approach for interpreting genome-wide expression profiles. *Proc. Natl. Acad. Sci. U. S. A.* 102, 15545–15550. doi: 10.1073/pnas.0506580102

Swindell, W. R. (2009). Genes and gene expression modules associated with caloric restriction and aging in the laboratory mouse. *BMC Genomics* 10:585. doi: 10.1186/1471-2164-10-585

Tyssowski, K. M., DeStefino, N. R., Cho, J. H., Dunn, C. J., Poston, R. G., Carty, C. E., et al. (2018). Different neuronal activity patterns induce different gene expression programs. *Neuron* 98, 530–546.e11. doi: 10.1016/j.neuron.2018.04.001

Valdez, G., Tapia, J. C., Kang, H., Clemenson, G. D. Jr., Gage, F. H., Lichtman, J. W., et al. (2010). Attenuation of age-related changes in mouse neuromuscular synapses by caloric restriction and exercise. *Proc. Natl. Acad. Sci. U. S. A.* 107, 14863–14868. doi: 10.1073/pnas.1002220107

van den Boogaard, W. M. C., van den Heuvel-Eibrink, M. M., Hoeijmakers, J. H. J., and Vermeij, W. P. (2021). Nutritional preconditioning in Cancer treatment in relation to DNA damage and aging. *Annu. Rev. Cancer Biol.* 5, 161–179. doi: 10.1146/annurev-cancerbio-060820-090737

Van Houten, B., Santa-Gonzalez, G. A., and Camargo, M. (2018). DNA repair after oxidative stress: current challenges. *Curr. Opin. Toxicol.* 7, 9–16. doi: 10.1016/j.cotox.2017.10.009

Vermeij, W. P., Dolle, M. E., Reiling, E., Jaarsma, D., Payan-Gomez, C., Bombardieri, C. R., et al. (2016). Restricted diet delays accelerated ageing and genomic stress in DNA-repair-deficient mice. *Nature* 537, 427–431. doi: 10.1038/nature19329

Wahl, D., Cogger, V. C., Solon-Biet, S. M., Waern, R. V., Gokarn, R., Pulpitel, T., et al. (2016). Nutritional strategies to optimise cognitive function in the aging brain. *Ageing Res. Rev.* 31, 80–92. doi: 10.1016/j.arr.2016.06.006

Wahl, D., and LaRocca, T. J. (2021). Transcriptomic effects of Healthspan-promoting dietary interventions: current evidence and future directions. *Front. Nutr.* 8:712129. doi: 10.3389/fnut.2021.712129

Wang, C., Gong, B., Bushel, P. R., Thierry-Mieg, J., Thierry-Mieg, D., Xu, J., et al. (2014). The concordance between RNA-seq and microarray data depends on chemical treatment and transcript abundance. *Nat. Biotechnol.* 32, 926–932. doi: 10.1038/nbt.3001

Xie, K., Kapetanou, M., Sidiropoulou, K., Bano, D., Gonos, E. S., Djordjevic, A. M., et al. (2020). Signaling pathways of dietary energy restriction and metabolism on brain physiology and in age-related neurodegenerative diseases. *Mech. Ageing Dev.* 192:111364. doi: 10.1016/j.mad.2020.111364

Xu, X., Zhan, M., Duan, W., Prabhu, V., Brenneman, R., Wood, W., et al. (2007). Gene expression atlas of the mouse central nervous system: impact and interactions of age, energy intake and gender. *Genome Biol.* 8:R234. doi: 10.1186/gb-2007-8-11-r234

Zhang, R., Lahens, N. F., Ballance, H. I., Hughes, M. E., and Hogenesch, J. B. (2014). A circadian gene expression atlas in mammals: implications for biology and medicine. *Proc. Natl. Acad. Sci. U. S. A.* 111, 16219–16224. doi: 10.1073/pnas.1408886111

Zhao, S., Fung-Leung, W. P., Bittner, A., Ngo, K., and Liu, X. (2014). Comparison of RNA-Seq and microarray in transcriptome profiling of activated T cells. *PLoS One* 9:e78644. doi: 10.1371/journal.pone.0078644

Zullo, J. M., Drake, D., Aron, L., O'Hern, P., Dhamne, S. C., Davidsohn, N., et al. (2019). Regulation of lifespan by neural excitation and REST. *Nature* 574, 359–364. doi: 10.1038/s41586-019-1647-8

frontiers | Frontiers in Molecular Neuroscience

TYPE Original Research
PUBLISHED 25 May 2023
DOI 10.3389/fnmol.2023.1147597

OPEN ACCESS

EDITED BY
Lilian Kisiswa,
Aarhus University, Denmark

REVIEWED BY
Paul J. Mathews,
Lundquist Institute for Biomedical Innovation, United States
Mónica Santos,
University of Coimbra, Portugal

*CORRESPONDENCE
Michael W. Shiflett
✉ shiflett@psychology.rutgers.edu

RECEIVED 18 January 2023
ACCEPTED 24 April 2023
PUBLISHED 25 May 2023

CITATION
Zanin JP, Pandya MA, Espinoza D, Friedman WJ and Shiflett MW (2023) Excess cerebellar granule neurons induced by the absence of p75NTR during development elicit social behavior deficits in mice. *Front. Mol. Neurosci.* 16:1147597. doi: 10.3389/fnmol.2023.1147597

Excess cerebellar granule neurons induced by the absence of p75NTR during development elicit social behavior deficits in mice

Juan Pablo Zanin[1], Mansi A. Pandya[1], Diego Espinoza[2], Wilma J. Friedman[1] and Michael W. Shiflett[2]*

[1]Department of Biological Sciences, Rutgers, The State University of New Jersey, Newark, NJ, United States, [2]Department of Psychology, Rutgers, The State University of New Jersey, Newark, NJ, United States

Introduction: Recently, the cerebellum has been implicated with non-motor functions, including cognitive and emotional behavior. Anatomical and functional studies demonstrate bidirectional cerebellar connections with brain regions involved in social cognition. Cerebellar developmental abnormalities and injury are often associated with several psychiatric and mental disorders including autism spectrum disorders and anxiety. The cerebellar granule neurons (CGN) are essential for cerebellar function since they provide sensorimotor, proprioceptive, and contextual information to Purkinje cells to modify behavior in different contexts. Therefore, alterations to the CGN population are likely to compromise cerebellar processing and function. Previously we demonstrated that the p75 neurotrophin receptor (p75NTR) was fundamental for the development of the CGN. In the absence of p75NTR, we observed increased proliferation of the granule cell precursors (GCPs), followed by increased GCP migration toward the internal granule layer. The excess granule cells were incorporated into the cerebellar network, inducing alterations in cerebellar circuit processing.

Methods: In the present study, we used two conditional mouse lines to specifically delete the expression of p75NTR in CGN. In both mouse lines, deletion of the target gene was under the control of the transcription factor Atoh-1 promotor, however, one of the lines was also tamoxifen-inducible.

Results: We observed a loss of p75NTR expression from the GCPs in all cerebellar lobes. Compared to control animals, both mouse lines exhibited a reduced preference for social interactions when presented with a choice to interact with a mouse or an object. Open-field locomotor behavior and operant reward learning were unaffected in both lines. Lack of preference for social novelty and increased anxiety-related behavior was present in mice with constitutive p75NTR deletion; however, these effects were not present in the tamoxifen-inducible mice with p75NTR deletion that more specifically targeted the GCPs.

Discussion: Our findings demonstrate that alterations to CGN development by loss of p75NTR alter social behavior, and contribute to the increasing evidence that the cerebellum plays a role in non-motor-related behaviors, including social behavior.

KEYWORDS

p75NTR, granule cell precursor (GCPs), neurotrophins, cerebellum, social behavior

Introduction

Traditionally, the cerebellum has been associated with motor balance and coordination, yet it is also involved in cognitive and emotional behavior. *In vivo* experimental data demonstrated the importance of the cerebellum in non-motor responses such as reward expectation (Wagner et al., 2017), decision-making (Blackwood et al., 2004; Deverett et al., 2018), and social interaction (Van Overwalle et al., 2014, 2020; Carta et al., 2019). Functional MRI in humans demonstrated that activation of the cerebellum is associated with addiction (Miquel et al., 2009; Moulton et al., 2014) and social cognition (Van Overwalle et al., 2014). Consistent with these findings, cerebellar developmental abnormalities and injury are often associated with several psychiatric and mental disorders including autism spectrum disorders (ASD) (Bauman and Kemper, 1985; Bailey et al., 1998; Fatemi et al., 2002; Whitney et al., 2008; Limperopoulos et al., 2009; Wang et al., 2014), schizophrenia (Andreasen and Pierson, 2008; Yeganeh-Doost, 2011; Parker et al., 2014), and anxiety (Hilber et al., 2004; Phillips, 2015; Moreno-Rius, 2018).

The cerebellum is well placed to influence non-motor behavior since it receives and sends information to many non-motor areas in the brain. For instance, a monosynaptic pathway between the cerebellum and the ventral tegmental area (VTA) was recently identified, suggesting the cerebellum can modulate reward circuitry with implications for social behavior (Carta et al., 2019). Sensory and motor information flow through the cerebellum via two pathways: (1) contextual sensory/motor information is provided to the CGN by the mossy fibers (MF); and (2) event inputs coming from the inferior olive transit via a single climbing fiber (CF). Both pathways converge in the Purkinje cells (PC), and this is likely one of the main reasons why this is the most studied cell population in the cerebellum; however, less attention has been paid to the other cell populations that feed information to PC, such as the CGN population.

The neurotrophin receptor p75 (p75NTR) is expressed throughout development as early as the blastocyst stage and continues to be expressed throughout development in different cell populations (Moscatelli et al., 2009; Vandamme and Berx, 2019). The function in each cell population depends on the cellular context, including the nature of the ligand, the receptor complex formed, and the intracellular pathway involved. p75NTR is abundantly expressed in the granule cell precursors (GCPs) in the developing cerebellum. Previously, we demonstrated that the absence of p75NTR specifically from cerebellar GCPs was sufficient to accelerate the cell cycle of the GCP, increasing the level of proliferation in this cell population compared to WT mice (Zanin et al., 2016, 2019). Moreover, the absence of p75NTR was also sufficient to allow an increase in GCP migration to the internal granule layer (IGL) (Zanin and Friedman, 2022). The excess neurons are incorporated into the cerebellar circuitry, affecting cerebellar network activity, characterized by the increased firing activity of the Purkinje cells (Zanin et al., 2019). These mice showed deficits in eyeblink conditioning, an associative learning task highly dependent on the cerebellum (Zanin et al., 2019). P75NTR is expressed in the proliferating GCPs in the external granule layer (EGL) of every lobe during cerebellar development, and, similarly, the increased proliferation mentioned above is observed in the entire cerebellum. Since the cerebellum has recently been associated with cognitive and emotional behavior, the cerebellar defects observed in the p75NTR conditional KO mouse suggest that other behaviors might be compromised in these animals. In the present work, using two different p75NTR conditional mouse lines, we evaluated the behavioral consequences of the specific deletion of p75NTR from the GCPs. Our analysis suggests that the deletion of p75NTR from GCPs during cerebellar development induces alterations in the social behavior of these animals.

Materials and methods

Subjects

Three- to four-month-old mice, both male and female, were used in all experiments. No sex difference was observed for any of the tests used. The same animals were used for the different behavioral tests, except the instrumental learning tasks, which were run on a separate cohort of animals. The order of the tests was as follows: 1. Open Field; 2. Elevated Zero Maze; 3. Light Avoidance Test; 4. Grooming Behavior; 5. Novel Object Recognition; 6. Social Novelty Test.

Conditional deletion of p75NTR

To remove the expression of p75NTR from GCPs in the cerebellum, we mated floxed p75NTR mice ($p75^{FL/FL}$) (Bogenmann et al., 2011) with $Atoh1^{Cre}$ mice (Jackson Labs. B6.Cg-Tg(P75Atoh1-Cre)1Bfri/J. RRID:IMSR_JAX:011104) (Matei et al., 2005). The genotype of each mouse was confirmed by PCR. The absence of p75NTR specifically from the EGL was confirmed by immunohistochemistry. For all behavioral analysis we used

littermate mice, control mice were p75 with both floxed alleles (p75FL), conditional KO mice were also p75FL/FL with the expression of the Cre enzyme under the control of the Atoh1 promotor (p75Atoh1-Cre).

Tamoxifen inducible p75NTR deletion

To remove expression of p75NTR from GCPs in the cerebellum at specific developmental stages, we mated floxed p75NTR mice ($p75^{FL/FL}$) (Bogenmann et al., 2011) with p75Atoh1-CreERTM mice (RRID:MMRRC_029581-UNC) (Chow et al., 2006). The *p75Atoh1-CreERTM* generated was crossed with a Td-Tomato reporter mouse [Jackson Lab Gt(ROSA)26Sortm9(CAG-tdTomato)Hze; RRID:IMSR_JAX:007905] (Song et al., 2010) to allow assessment of the recombination efficiency following tamoxifen treatment. Tamoxifen was delivered via oral gavage to pregnant females at E17/18. Each female received one dose of tamoxifen (300 mg/kg of tamoxifen). Tamoxifen was dissolved in Corn oil (Sigma Cat # C8267). For all behavioral analysis we used mice with the same genotype (p75Atoh1-CreERTM) with or without tamoxifen exposure.

Open field assessment

The open field apparatus (Stoelting Co., Wood Dale, IL, USA) is 40 cm x 40 cm (w/d) and constructed of gray plastic walls and a gray metal base. Mice were placed in the center of the open field and removed after 30 min. A video camera mounted above the open field captured video footage, which was processed to extract movement data using Noldus Ethovision XT v.11.5 (Noldus Information Technology, Leesburg VA, USA).

Elevated zero maze

An elevated zero maze (Stoelting) measuring 50 cm in diameter and raised 50 cm from the floor was used. Mice were placed in one of the closed arms of the maze and removed after 5 min. A video camera mounted above the maze recorded mouse movement. Analysis of mouse movement in the elevated zero maze and time spent in the open arms of the arena was carried out using Noldus Ethovision v 11.5.

Light-dark transition test

Mice were placed in a two-chambered arena (Med Associates, Fairfax, VT, USA). Each chamber measured 20.46 × 16.5 × 21.3 cm (L × W × H) with clear plastic walls and a stainless-steel floor. An automatic door separated each chamber. One chamber was covered with black material and was designated the dark chamber. The light chamber had a light source over the arena, which was lit to approximately 200 lumens on the floor. Mice were placed in the dark chamber for 2 min before the door was opened. The latency to enter the light chamber, and the amount of time spent in that chamber were recorded with a photobeam array installed in the chamber.

Self-grooming assessment

Mice were placed in a standard polycarbonate mouse container identical to their home cage. The container was filled with approximately 1 cm of wood chip bedding. A video camera recorded mouse activity. Two observers blind to the subject genotype viewed mouse videos and scored them for self-grooming behavior using Noldus Ethovision 11.5.

Novel object recognition test

Novel object recognition testing was based on previously described procedures (Shiflett, 2017). Mice were tested in an open field arena, as described above. During the sample phase, two identical objects (plastic bath toys) were placed in opposite corners of the arena 10 cm from the nearest walls. Mice were placed in the center of the arena and allowed to freely investigate both objects for 10 min after which they were returned to their home cage for 60 min. During the 5-min test phase, mice encountered one "familiar" object from the sample phase and a novel object. The number of sniffs on the familiar and novel objects was quantified from video footage.

Social novelty test

Preference for social novelty was tested in a three-chambered arena, modified from that previously described (Shiflett, 2017). Each of the three chambers of the arena was equally sized and separated from each other by a plexiglass barrier. A small hole allowed passage between the chambers. Mice were first habituated to the empty arena for 30 min. During the 10-min sample phase, an unfamiliar male mouse was confined to one of the chambers by a small wire cage placed over it and the test mouse was allowed to freely roam the apparatus for 10 min. The opposite chamber contained a wire cage with no mouse. During the test phase, the mouse from the sample phase was returned to the apparatus and confined to one chamber. This mouse was designated the "familiar" mouse. An unfamiliar mouse was confined to the opposite chamber. The chamber where the familiar and novel mice were localized was randomized across subjects. The test mouse was placed in the center of the arena and allowed to freely roam the apparatus for 10 min. The amount of time spent in each chamber was quantified using Noldus Ethovision. The number of sniffs directed at the familiar and novel mouse was also quantified from video footage.

Instrumental peak procedure

Mice were placed on a restricted food diet of approximately 2 g of standard chow each day. The chow (Purina, St. Louis, MO, USA) was given in their home cage after behavioral procedures were complete. Animals were weighed daily, and their body weights were maintained at 85−90% of their non-restricted body weight. Mice were trained in 8 standard mouse operant chambers (Med Associates, Fairfax, VT, United States) to lever press for a chocolate

pellet (Bio-serv, Frenchtown, NJ, USA). In the first and second training sessions, each response the mouse made immediately delivered a single 20-mg food pellet into a food magazine. Mice were then trained on a fixed interval (FI) 15 s schedule for 7 sessions followed by a FI 25 s schedule for 7 sessions. Under these schedules, a response delivered a pellet only after an elapsed interval from the previous reward delivery. Responses before the interval elapsing produced no pellets. The session terminated after mice earned 20 pellets or 20 min elapsed.

Instrumental reversal learning

A separate set of mice was tested under instrumental reversal learning. Mice were placed on a restricted food diet of approximately 2 g of standard chow each day. The chow was given in their home cage after behavioral procedures were complete. Animals were weighed daily, and their body weights were maintained at 85−90% of their non-restricted body weight. While placed on food restriction, mice were simultaneously habituated to the operant conditioning chamber for one 15-min session. The next day, mice were conditioned to find pellets in the food cup in a 20-min session in which food pellets were dispensed on a random-time 60-s schedule. Levers were retracted during this phase. The next day mice were trained to use levers. During each session, a single lever was inserted into the operant conditioning chamber. Each lever press resulted in the delivery of a single 20-mg grain-based chocolate-flavored food pellet into the food cup. The session terminated after either 20 lever presses or 20 min elapsed from the start of the session. The mice completed two training sessions per day, one session with the left lever and one session with the right lever.

After acquiring a lever press response mice were placed on a reversal-learning task as previously described (Eisenberg et al., 2021). In this phase, both levers were extended simultaneously. One lever was designated as the rewarded lever and the other lever as the non-rewarded lever. For each trial, responses on the rewarded lever always produced a food pellet, and responses on the non-rewarded lever never delivered a pellet. When no pellet was attained, both levers were retracted for 3 s and reinserted. After the mouse earned between 10 and 14 food pellets, the contingencies assigned to each lever were reversed; responses on the previously rewarded lever produced no pellets, whereas responses on the non-rewarded lever produced pellets. Mice remained in the operant chamber until 80 trials were completed/day or 1 h had passed since the start of the session. Mice underwent 13 reversal-learning sessions, one session per day. The training and testing regimen was completed in approximately 5 weeks, with 1 week of food restriction and habituation to the chambers, 1 week of instrumental training, and 3 weeks of reversal learning.

Immunohistochemistry

Animals were deeply anesthetized with ketamine/xylazine and perfused with 4% paraformaldehyde (PFA) in phosphate buffered saline (PBS). Brains were removed and post-fixed in 4% PFA/PBS overnight at 4°C, then cryopreserved with 30% sucrose. Sections (12 μm) were cut using a Leica cryostat and mounted onto charged slides. Sections were permeabilized with 0.5% triton in PBS for 20 min and blocked with 1% bovine serum albumin (BSA) and 5% donkey serum in PBS for 1 h at room temperature (RT). Primary and secondary antibodies were prepared in 1% BSA. Sections were incubated with primary antibodies overnight at 4°C in a humidified chamber. Sections were then washed 3 times with PBS for 15 min each. All secondary antibodies were diluted at 1:1000 and incubated for 1 h at RT and washed three times with PBS for 15 min each. Sections were mounted using 4',6-diamidino-2-phenylindole (DAPI) Fluoromount-G (Southern Biotech #0100−20). Controls for immunostaining included incubation with secondary antibodies in the absence of primary antibodies. Antibodies used: goat anti-p75 (R&D AF367, RRID:AB_2152638, 1:500), rabbit anti-Calbindin (ab49899 RRID:AB_1267903, 1:1000), donkey anti-goat Alexa Fluor 488 (Fisher Scientific #A-11055), donkey anti-goat Alexa Fluor 555 (Fisher Scientific # A-21432), donkey anti-rabbit Alexa Fluor 647 (Fisher Scientific # A-31573).

For the Td-Tomato detection, no antibody was used, since the fluorescence intensity of the marker was strong enough to be detected without immunostaining. Horizontal sections (12 μm) were cut using a Leica cryostat and mounted onto charged slides. Sections were mounted using DAPI Fluoromount-G (Southern Biotech #0100−20). Pictures of the entire cerebellum were taken using a Zeiss LSM 510 Meta confocal microscope, objectives EC Plan-Neo 10X/0.30 M27 and Plan Apo 20X/0.8. Filter configuration for imaging: For the blue channel we used a 405 excitation laser with an HFT 405/488/543/633, emission was detected using BP 420−480. For the green channel, we used a 488 excitation laser with an HFT 405/488/543/633, emission was detected using LP 560. For the red channel, we used a 543 excitation laser with an HFT 405/488/543/633, emission was detected using LP 560. For the far red channel, we used a 633 excitation laser with an HFT 405/488/543/633, emission was detected using LP 560.

Statistical analysis

For behavioral experiments involving a single measurement (e.g., distance traveled in the open field) we compared genotypes using independent samples *t*-tests. For behavioral experiments with multiple within-subject measurements (e.g., sniffs directed at different objects), we used 2-Way ANOVA's with within and between-subject factors. If no interaction was detected between the two factors (e.g., genotype and novel/familiar), we proceeded to analyze the single factor (e.g., novel/familiar) within the results of the two-way ANOVA. When a significant interaction was detected between the factors, we proceeded with a simple effect analysis. Within-subject planned comparisons were made using paired *t*-tests, and comparisons between genotypes were made using independent samples *t*-tests with Bonferroni correction.

To correlate recombination levels with a behavioral response, we calculated a recombination index. Using FIJI (Image J), the area of the IGL was measured based on Dapi staining. An ROI was obtained from the Dapi signal and established as the total area.

Using this ROI as a mask, we calculated the area positive for Td-Tomato (recombined area). The index was obtained by dividing the recombined area over the total area. Only the cerebellum from animals injected with tamoxifen was used to calculate the correlation index, since no expression of TD-Tomato was detected in the animals without tamoxifen. The recombination index was regressed against different behavioral measurements (e.g., time spent in closed arms of the zero maze), and R-squared was calculated along with estimates of goodness-of-fit.

Results

Deletion of *p75NTR* from granule cell precursors

P75NTR is widely expressed during embryonic development; its expression starts as early as the blastocyst stage (Vandamme and Berx, 2019). In the nervous system, *p75NTR* is expressed in multiple populations in the developing brain including the cerebellum and the hippocampus. During cerebellar development, p75NTR is expressed in the proliferating GCPs and is downregulated upon cell cycle exit. P75NTR is also expressed in postmitotic Purkinje cells, suggesting a different role for the receptor in this cell population. In adult animals, however, p75NTR expression is restricted to a small number of brain areas, such as the basal forebrain (Lee et al., 1998) and the Purkinje cells in the cerebellum (Carter et al., 2003). To specifically evaluate the role of p75NTR in GCPs and the effects on cerebellar behavior, we used two conditional mouse lines. In both mice lines deletion of p75NTR was under the control of the *Atoh1* promoter, with the difference that in one of the mouse lines deletion of p75NTR was regulated by the normal expression of Atoh1 [p75Atoh1-Cre] while the other mouse line, *Atoh1* expression was tamoxifen-inducible [p75Atoh1-CreERTM] (see methods), which allows better temporal regulation of p75NTR deletion. Additionally, the p75Atoh1-CreERTM mice also have a Td-Tomato reporter, to track the cells that underwent recombination.

The p75Atoh1-Cre mice have a deletion of p75NTR from GCPs in all lobes in the cerebellum but maintain wildtype expression in Purkinje cells (**Figure 1A**). In the cerebellum, *Atoh-1* is expressed in all the rhombic lip derivatives, which include the GCPs and the excitatory neurons of the cerebellar nuclei (MacHold and Fishell, 2005; Wang et al., 2005). Therefore, to target more specifically the GCPs in the cerebellum, we took advantage of the late development of this cell population in comparison with the rest of the rhombic lip derivatives. We exposed the mice to tamoxifen by oral gavage of pregnant females at E17/18. With this tamoxifen exposure paradigm, we specifically targeted the deletion of p75NTR in the cerebellar granule cells, indicated by the robust expression of Td-Tomato (**Figures 1B, C**), without affecting the cerebellar nuclei (**Figure 1D**). We used these two mouse models to evaluate the role of the cerebellar granule cells in cerebellar function. *Atoh1* is also expressed in the hippocampus; however, injecting tamoxifen at the late stages of embryonic development (E17/18) induced the recombination of only a small number of neurons, leaving the great majority of cells unaffected (**Figure 1E**).

Social behavior deficits induced by loss of cerebellar CGN *p75NTR*

We evaluated social behavior in the p75Atoh1-Cre and p75Atoh1-CreERTM mice using tests of sociality and social novelty (**Figures 2A–H**). In the sociality test, we presented mice with a novel mouse in one chamber and an inanimate object in the other, and quantified the number of nose pokes directed at the mouse or object as well as time spent in each chamber. Analysis of nose pokes revealed that loss of p75NTR significantly altered performance in the sociality test. p75Atoh1-Cre mice showed no preference for the mouse over the object, unlike control mice who directed significantly more nose pokes at the mouse compared to the object [ANOVA interaction $F(1,32) = 20.19$, $p = 0.0001$; paired t-test object versus mouse: p75FL $p = 0.0001$; p75Atoh1-Cre $p = 0.4295$] (**Figure 2A**). We observed similar results when analyzing the tamoxifen (TM) inducible mice (**Figure 2E**). Adult p75Atoh1-CreERTM mice with tamoxifen exposure during embryonic stage E17/18 showed no preference for the mouse over the object, unlike control mice [ANOVA interaction $F(1,48) = 21.99$ $p = 0.0001$; paired t-test object vs. mouse: no TM $p = 0.0001$; with TM $p = 0.0924$] (**Figure 2E**). In contrast to the nose-poke results, time spent in the chamber containing the mouse or object showed no significant interaction with genotype for p75Atoh1-Cre ($p = 0.0854$) or for p75Atoh1-CreERTM mice ($p = 0.5954$) (**Figure 2B**). p75Atoh1-CreERTM mice with or without TM spent significantly more time with the mouse over the object (ANOVA main effect of object/mouse factor $F(1,48) = 7.851$, $p < 0.0073$) (**Figure 2F**). Overall, the results from nose-poke behavior suggest that loss of p75NTR from cerebellar GCN's alters preference for social interactions.

During the social novelty test, we confined a novel mouse to one chamber of the arena, and evaluated nose pokes and the time spent with either the novel or the familiar mouse. Among p75Atoh1-Cre mice, analysis of nose pokes revealed that loss of p75NTR significantly modulated preference for social novelty. p75Atoh1-Cre mice showed a modest preference for the novel mouse compared to the familiar mouse, unlike control mice, which directed significantly more nose pokes at the novel mouse [ANOVA: interaction $F(1,34) = 15.10$, $p = 0.0004$: paired t-test familiar vs. novel: p75FL $p = 0.0001$; p75Atoh1-Cre ($p = 0.0573$) (**Figure 2C**)]. Similarly, p75FL mice spent significantly more time in the chamber housing the novel mouse, whereas p75Atoh1-Cre mice spent a similar amount of time in each chamber [ANOVA: interaction $F(1,34) = 10.96$, $p = 0.0022$; paired t-test familiar vs. novel: p75FL $p = 0.0011$; p75Atoh1-Cre $p = 0.2202$] (**Figure 2D**).

In contrast, we found no significant effects of genotype on social novelty among p75Atoh1-CreERTM mice. We found no significant interaction involving genotype and novelty for nose pokes or chamber time (p's > 0.6) (**Figure 2G**). We observed a main effect of novelty on nose-pokes [$F(1,48) = 4.101$ $p = 0.0484$] and on chamber time that approached significance [$F(1,48) = 3.9$ $p = 0.0541$] (**Figure 2H**), suggesting that, independent of genotype, mice showed a preference for novel social interactions.

Taken together, the results from the sociality test suggest that loss of p75NTR, either in constitutive or inducible-Cre mice, reduces social-directed nose-poke behavior in the sociality test. Constitutive loss of p75NTR also reduces novelty-directed

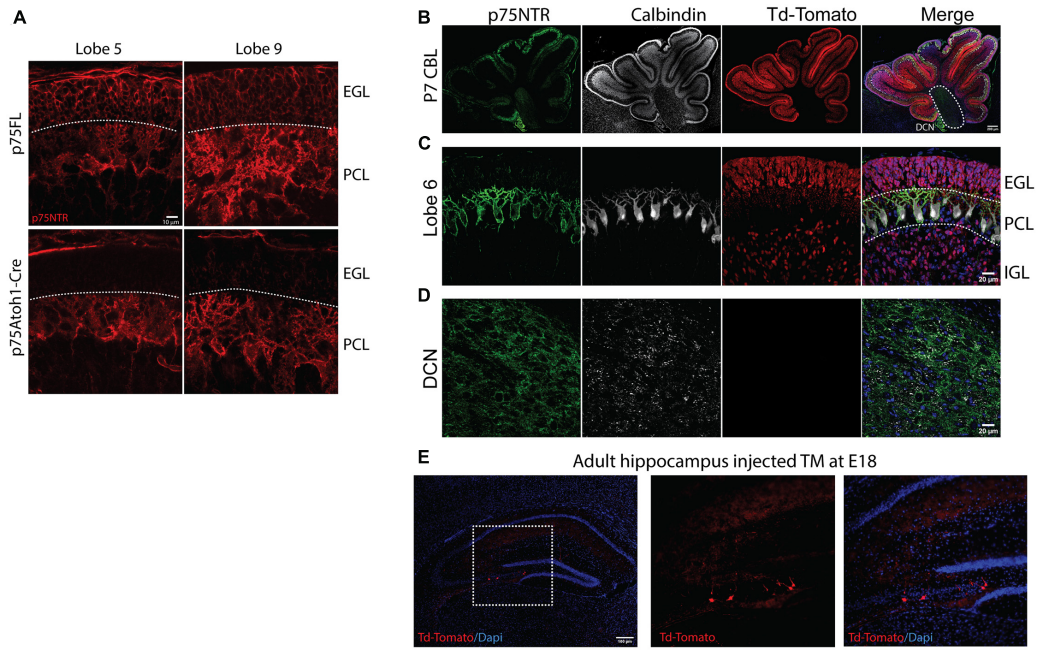

FIGURE 1
Loss of cerebellar p75NTR. Immunostaining of cerebellar sections. **(A)** Immunostaining for p75NTR in control (p75FL) and p75Atoh1-Cre P7 mouse pups. Note the deletion of p75NTR specifically from the GCPs located in the external granule layer in two different cerebellar lobes. **(B–D)** Immunostaining for p75NTR (green), Calbindin, a Purkinje cell marker (white), and Td-Tomato (red) for p75Atoh1-CreERTM P7 mouse pups injected with tamoxifen. Note the expression of the reporter Td-Tomato only in the GCPs in the EGL and the differentiated granule cells in the internal granule layer **(C)**, no expression of the reporter was observed in the deep cerebellar nuclei **(D)**. **(E)** Expression of Td-Tomato in the hippocampus. With the late delivery of tamoxifen (E17/18), only a reduced number of cells were labeled with tamoxifen. (EGL) external granule layer, (PCL) Purkinje cell layer, (IGL) internal granule layer.

investigatory behavior in the social novelty test, although this effect was not observed in the inducible-Cre mice.

Novel object recognition

Object identity memory was assessed in the novel object recognition test. We found that constitutive loss of p75NTR disrupted performance in the task. p75Atoh1-Cre mice showed no preference for the novel object, while control mice preferred to explore the novel object over the familiar one [ANOVA: genotype x object interaction $F(1,24) = 23.20$; $p = 0.0001$]. In the single factor analysis, control p75FL mice nose-poked the novel object significantly more frequently ($p = 0.0004$); p75Atoh1-Cre, in contrast, showed no significant difference in nose-pokes toward the novel and familiar objects ($p = 0.3962$) (Figure 2J). Interestingly, we found no genotype effect on social novelty in p75Atoh1-CreERTM mice. Mice with or without TM showed a significant preference to explore the novel object over the familiar object. No significant genotype x object interaction was observed ($p = 0.5623$). A significant main effect of novelty was observed [$F(1,44) = 75.14$ $p = 0.0001$], indicating that these mice investigated the novel over familiar object independent of genotype (Figure 2L). During the training session, there was no biased exploratory preference for either of the two identical objects in p75Atoh1-Cre ($p = 0.2276$) (Figure 2I) or p75Atoh1-CreERTM mice ($p = 0.7253$) (Figure 2K).

These results indicate that p75Atoh1-Cre mice were impaired in the novel object recognition task. The lack of effect in p75Atoh1-CreERTM might be due to the defects induced by the absence of p75NTR in other areas outside the cerebellum, perhaps the hippocampus.

Increased anxiety in p75Atoh1-Cre but not p75Atoh1-CreERTM mice

We observed anxiety-related behavior in p75Atoh1-Cre but not p75Atoh1-CreERTM mice in multiple tests. In the open field test, p75Atoh1-Cre mice spent significantly less time in the center of the arena compared to controls ($p = 0.0001$) (Figure 3A). Similarly, in the elevated zero maze, p75Atoh1-Cre mice spent significantly less time in the zero maze's open arms compared to control mice ($p = 0.0048$) (Figure 3B). Likewise, in the light-dark transition test, p75Atoh1-Cre mice were slower to enter the lit chamber compared to control mice ($p = 0.0105$) (Figure 3C), although we did not observe any significant difference in the time spent exploring the lit chamber between the two groups ($p = 0.136$) (Figure 3D). We additionally observed that p75Atoh1-Cre engaged in longer self-grooming bouts compared to control mice ($p = 0.0001$) (Figure 3E), and more frequent grooming ($p = 0.0059$) (Figure 3F). Taken together, the performance of p75Atoh1-Cre mice on these tests is consistent with an elevated anxiety phenotype.

In contrast, p75Atoh1-CreERTM mice with or without tamoxifen showed no differences in anxiety behavior. There was no significant difference in the cumulative time spent in the center of the arena between groups ($p = 0.1679$) (Figure 3G). Similarly,

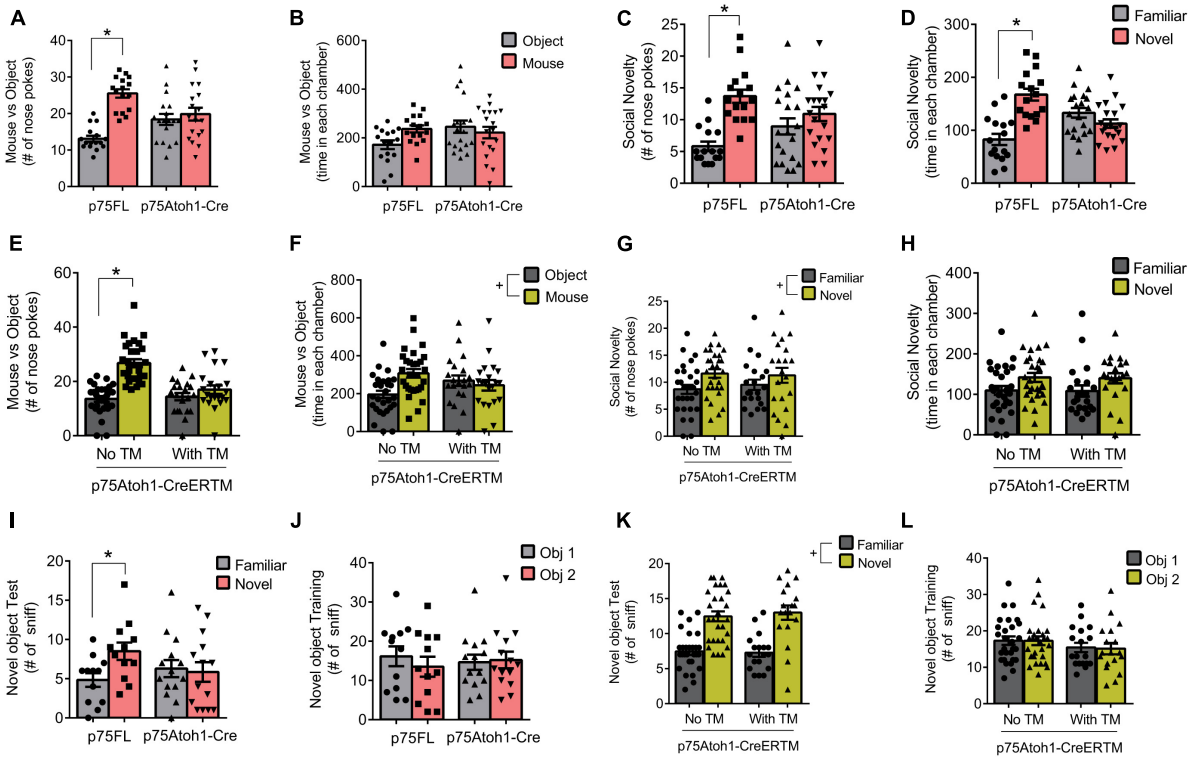

FIGURE 2
Loss of p75NTR alters social behavior. **(A)** p75Atoh1-Cre mice show no difference in nose pokes directed at a mouse versus non-social object, unlike control mice which show significantly more mouse-directed nose pokes. **(B)** This genotype effect was not observed when examining time spent in the chambers housing the mouse or object. **(C,D)** p75Atoh1-Cre mice show no difference in nose pokes **(C)** and time in chamber **(D)** between novel and familiar mice, unlike control mice which show significantly more nose pokes and chamber time directed at the novel mouse. **(E)** p75Atoh1-CreERTM with TM show no difference in nose pokes directed at a mouse versus non-social object, unlike control mice. **(F)** This treatment effect was not observed when examining time spent in the different chambers. No effect of TM was observed on nose pokes **(G)** and time spent in chamber **(H)** between novel and familiar mice. **(I–L)** Novel object recognition test. **(I)** p75Atoh1-Cre mice show no difference in nose pokes directed at a novel versus familiar object, unlike control mice, which show a significant preference for the novel object. **(J)** This effect was not due to biased object exploration in the training phase. **(K,L)** No effect of TM was observed in novel object exploration in p75Atoh1-CreERTM mice. All data are expressed as the mean ± S.E.M. *Significantly different at $p < 0.05$. $^{+}$Significant main effect of object or novelty factor.

in the elevated zero maze, both groups of mice spent similar time in the zero maze's open arms ($p = 0.6208$) (Figure 3H). In the light-dark transition test, there was no difference in the latency to first cross into the illuminated chamber between the two groups ($p = 0.2513$) (Figure 3I); however, p75Atoh1-CreERTM spent less time exploring the lit chamber compared to controls ($p = 0.0108$) (Figure 3J). In the grooming test, no difference was observed in the total time of self-grooming bouts between the two groups longer self-grooming bouts compared to control mice ($p = 0.4504$) (Figure 3K), or the frequency of grooming longer self-grooming bouts compared to control mice ($p = 0.8931$) (Figure 3L). Taken together, these data suggest that loss of p75NTR specifically in early-developing granule cells of the cerebellum may not produce the anxiety phenotype seen with the p75Atoh1-Cre mice.

Loss of p75NTR does not affect basic locomotor parameters

Loss of p75NTR did not affect basic locomotor parameters in the open field. P75Atoh1-Cre were no different from controls in velocity ($p = 0.7331$) and total distance traveled ($p = 0.9465$). Similarly, we observed no difference between p75Atoh-CreERTM and controls in velocity ($p = 0.6331$) and distance traveled in the open field test ($p = 0.4432$) (Supplementary Figure 1). Therefore, the effects observed in the different behavioral tests are not due to an inability to move about the arena.

The recombination induced by tamoxifen was highly variable

The p75Atoh1-CreERTM expresses a Td-Tomato reporter allowing assessment of the recombination efficiency following tamoxifen treatment. After finishing the battery of behavioral tests on the mice injected with tamoxifen, we collected the brains and confirmed the recombination efficiency in these animals. Surprisingly, even though the animals received the same dose of tamoxifen (pregnant female received the tamoxifen treatment), we observed a high degree of variability in the level of recombination induced by the exposure to tamoxifen (Figure 4A). To examine the possibility that lower transfection levels may explain the discrepancy between p75Atoh1-Cre and p75Atoh1-CreERTM mice, we correlated behavior with the level

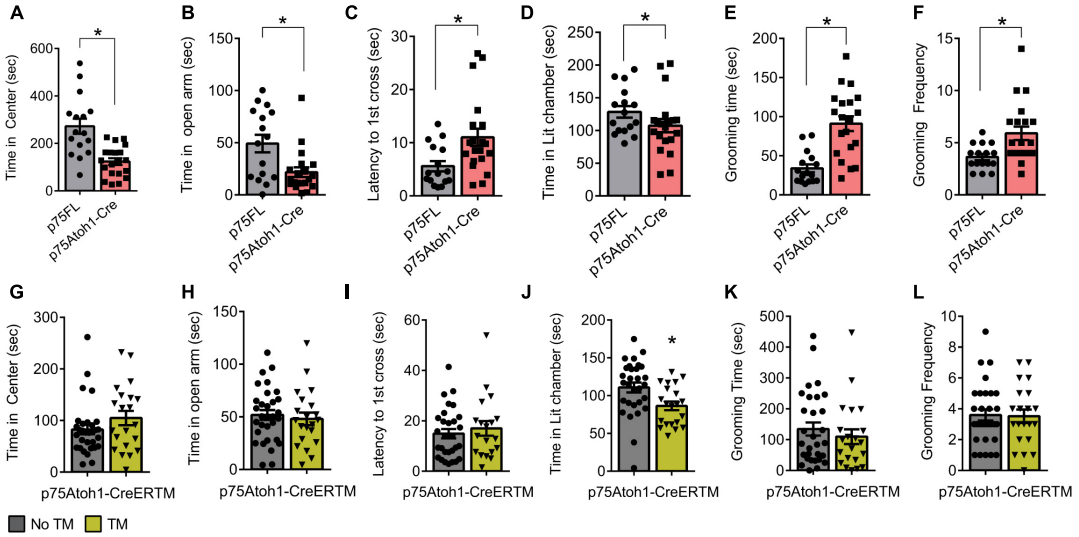

FIGURE 3
p75Atoh1-Cre mice show increased anxiety-related behavior. **(A–F)** p75Atoh1-Cre show differences in: **(A)** time spent in the center of the open-field arena; **(B)** time spent in the open arms of the elevated zero maze; **(C)** latency to cross to the illuminated chamber in the light-dark transition test and **(D)** time spent in the illuminated chamber; **(E)** time self-grooming, and **(F)** frequency of grooming bouts. In contrast p75Atoh1-CreERTM mice treated with TM did not differ from controls on any measure **(G–L)**. *$p < 0.05$ Student *t*-test; mean ± S.E.M.

of recombination in the cerebellum. If a strong correlation between the recombination level and the behavioral response is observed, this might indicate that the granule cells might be involved in anxiety-like behavior, but in the animals with low recombination efficiency, we may not have reached a threshold of recombined cells to affect the behavior. When comparing behavioral measures against recombination density (see methods), we observed no significant correlation with any of the anxiety-like behavior measures analyzed (open field $R^2 = 0.0074$; elevated zero maze $R^2 = 0.0003$; light transition test time in lit chamber $R^2 = 0.0815$; light transition test latency to 1st cross $R^2 = 0.088$; grooming test time $R^2 = 0.005$, grooming test frequency $R^2 = 0.007$) (**Figures 4B–G**). These findings confirm that even in the animals with high-recombination level, removing p75NTR from granule cells does not affect anxiety-related behaviors, supporting our previous conclusion that loss of p75NTR expression in granule cells progenitors, with the developmental consequences for proliferation and circuit development previously described (Zanin et al., 2016, 2019), may not produce an anxiety phenotype.

Loss of *p75NTR* using the Atoh1 promoter has no observable effect on reward learning

We examined the behavior of p75Atoh1-Cre mice in two reward-learning tasks that have recently been linked to cerebellar function. In the instrumental peak procedure mice learned over multiple sessions to time their response toward the end of the fixed interval. We trained mice on two intervals, an FI-15 s interval, followed by an FI-25 s interval. Mice showed significantly greater allocation of responses near the end of the interval compared to the beginning (**Figures 5A, B**). Responses were significantly greater 15- or 25-s after the trial start compared to 5 s after the trial start (ANOVA: main effect of trial time $p's < 0.001$). We found no effect of genotype or interaction for either interval ($p's > 0.9$), indicating that all mice learned to time their responses to the interval schedule and that loss of p75NTR in cerebellar GCPs did not influence learning in this task.

In the reversal learning task, mice chose between two levers-one lever delivered a reward and the opposite lever had no effect. The lever-reward contingencies were reversed every 10−14 rewarded trials. Mice had to adapt their responses to the changing reward contingencies. We classified responses in each trial into one of four categories, depending on the choice and outcome of the previous trial: win-stay responses occurred when animals repeated a previously rewarded action; win-shift responses occurred when animals shifted to a new action following a reward; lose-stay responses occurred when animals repeated an action following no reward; lose-shift responses occurred when animals shifted actions following no reward. As shown in **Figure 5C**, mice predominately engaged in win-stay responses. Following loss trials, mice engaged in equal numbers of lose-shift and lose-stay responses. Loss of p75NTR did not affect behavior in this task. We found no effect of genotype on the allocation of responses in the task ($p's > 0.8$), indicating that loss of p75NTR in GCPs does not impact behavioral flexibility in a reversal-learning task.

Discussion

Our previous studies have demonstrated that the absence of p75NTR from developing GCPs alters their cell cycle regulation, resulting in excess production of CGNs. The excess number of CGNs, in turn, alters the excitatory-inhibitory balance of inputs to Purkinje cells. In our present work, we find that mice with an excess number of CGNs show deficits in tests of sociality. These results

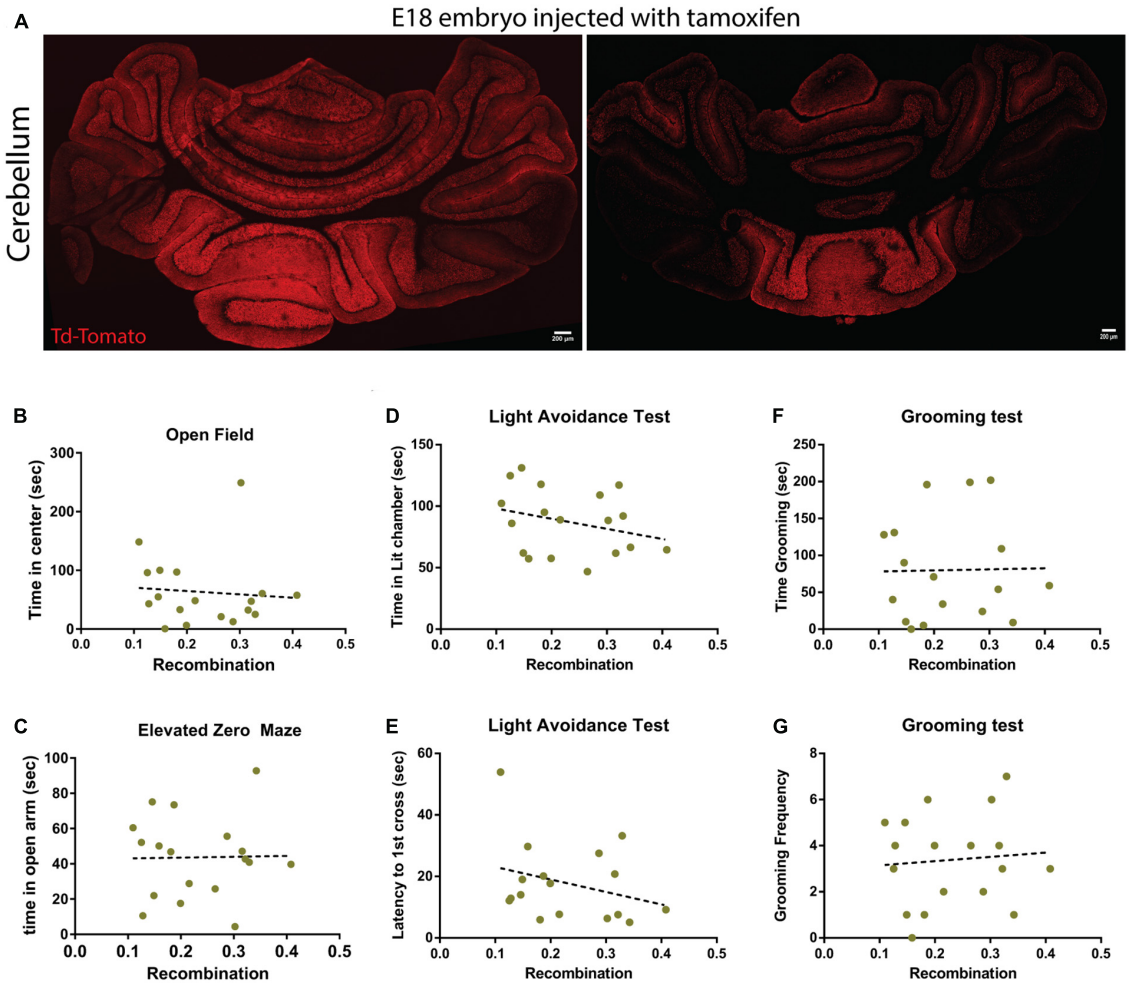

FIGURE 4
Recombination levels do not correlate with behavior in p75Atoh1-CreERTM mice. Analysis of the recombination level of p75Atoh1-CreERTM adult mice after tamoxifen injection during development. **(A,B)** Immunostaining for Td-Tomato (red) and Dapi (blue) in p75Atoh1-CreERTM adult mouse injected with tamoxifen at embryonic day 17/18. **(A)** Expression of Td-Tomato in the cerebellum of two sibling mice that received the same tamoxifen doses. Note the high variability in the recombination levels. **(B–G)** Correlation analysis between the level of recombination and the behavioral results shown in this figure. The brains of all the mice injected with tamoxifen used in this figure were obtained, sectioned, and stained for Td-Tomato as a proxy of recombination level. **(B)** Correlation between the level of recombination and the time spent in the center of the open field arena. **(C)** Correlation between the level of recombination and the time spent in the open arm of the elevated zero maze. **(D,E)** Light-dark transition test: correlation between the level of recombination and **(E)** the time spent in the lit chamber or **(D)** the delay time to first cross to the illuminated chamber. **(F,G)** Correlation with the grooming test: correlation between the level of recombination and **(F)** the time the mice spent grooming or **(G)** the frequency of grooming.

suggest that perturbations of CGN development by loss of p75NTR disrupt social engagement in mice, which has implications for understanding the etiology of neurodevelopmental disorders that feature social behavior deficits, such as Autism Spectrum Disorder.

The granule cells receive a large variety of signals from the mossy fibers; this includes sensory, motor, and contextual information. Sensory-motor stimulus (joint angle, visual and whisker cues, head position, body velocity, etc.) is encoded in a group of CGN, allowing the system to combine multiple stimuli to generate an accurate representation of the behavioral context necessary to control behavior. The granule cells will re-code this information in a way that can be recognized and learned by their targets, the Purkinje cells. Hence, a quantitative imbalance between the different neuronal populations of the cerebellum (mossy fibers, CGN, and PC) is likely to affect the encoding of information leading to suboptimal responses. For instance, one of the most consistent findings in postmortem analysis of autistic patients is a loss of Purkinje cells (Kern, 2003; Skefos et al., 2014), with no apparent loss of the other neuronal types. Therefore, the disabilities observed in these patients might be explained, at least in part, by the disruption of the information flow caused by the quantitative imbalance between the CGN and PC populations. An excess of granule cells, such as the one observed in the p75Atoh1-Cre mice could potentially "dilute" the information received from the mossy fibers. In our previous publications, we have confirmed that Purkinje cells in these mice have an increased firing frequency (Zanin et al., 2019), consistent with an excess of excitatory input, likely from the excess CGN. Although we did not measure the activity in the deep cerebellar nuclei (DCN), the alteration in PC activity most likely will compromise the

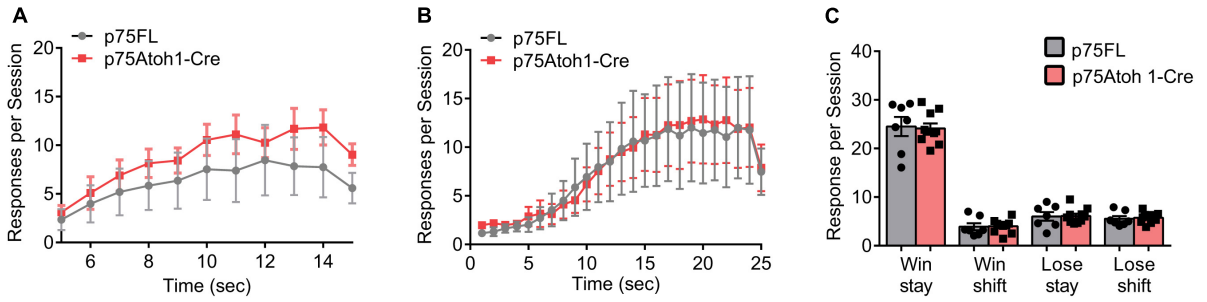

FIGURE 5
Loss of p75NTR spares performance in the reward-based operant tasks. **(A,B)** Responses during the fixed instrumental peak procedure. The trial interval was divided into 1-s bins, and lever presses were binned according to the time point they occurred during the trial interval. Responses per session were averaged for each mouse, and the group means, and SEM is illustrated in the plot for mice trained under an FI-15 schedule **(A)** and FI-25 schedule **(B)**. **(C)** Responses during the reversal learning task. Responses were classified as win stay, win shift, lose stay or lose shift, depending on the current trial's response and the preceding trial's outcome and response (see methods for additional description). Responses per session were averaged for each mouse, and the group means, and SEM is illustrated in the plot in panel **(C)**.

output information of the DCN to the rest of the brain. Moreover, substantial evidence suggests that learning occurs in the Purkinje cells, however, new experimental data predicts that learning would also take place at the cerebellar input stage — the granular layer (Giovannucci et al., 2017). Therefore, an excess number of CGNs can compromise the contextual information transfer to the PC, as well as the information processing at the CGN level.

How does the absence of *p75NTR* induce social behavior deficits?

Several studies have established the role of the cerebellum in the social domain, including emotion and intentions (Schmahmann and Sherman, 1998; Baumann et al., 2015; Guell et al., 2018). Thus, it has been hypothesized that the cerebellum may modulate non-motor behavior, such as social behavior, in the same way it modulates motor control (Andreasen and Pierson, 2008; Stoodley and Schmahmann, 2010). Recently it was shown that the cerebellum can carry information about reward expectation (Wagner et al., 2017; Carta et al., 2019), and its known that crus I projects to somatosensory and anterior cingulate cortex, areas highly involved in social interactions, therefore encoding information that is necessary for the expression of some forms of behavior. The excess of CGN observed in the *p75P75Atoh1-Cre* could generate a suboptimal context representation in these mice, affecting their social interaction responses. Previously, we demonstrated that mice lacking p75NTR expression in the cerebellar GCP (p75Atoh1-Cre) have motor (Zanin et al., 2016) and associative learning deficits (Zanin et al., 2019). In the present work, we extended our findings and demonstrated that these mice also present social interaction deficits. In the mouse vs. object test, both sets of conditional mice (p75Atoh1-Cre and p75Atoh1-CreERTM with tamoxifen) made similar numbers of investigatory nose pokes toward the object and the mouse, in contrast to control mice (p75FL or p75Atoh1-CreERTM without tamoxifen, respectively), which prefer the mouse over the object. In the social novelty test, p75Atoh1-Cre showed no preference for the familiar over the novel mouse, in contrast to control mice, which show a significant preference for the novel mouse, represented as the number of sniffs toward the novel mouse. In contrast, we found no effects on social novelty of p75NTR deletion in the TM-inducible Cre mice. This may indicate that social novelty preference, as opposed to choices between social and non-social encounters, is less sensitive to p75NTR deletion. Although we observed some Td-Tomato recombination in the hippocampus of p75Atoh1-CreERTM injected with tamoxifen, the actual number appears extremely low to have had an impact on social behavior, further supporting our hypothesis that sociality (mouse versus object) deficits in these animals is driven by the excess of CGN generated during development. Taken together, the results obtained from both mouse lines strongly suggest that removing p75NTR from GCP during development is sufficient to induce sociality alterations in adult animals. These findings highlight the role of p75NTR as a potential susceptibility gene in neurological disorders with ontogeny in developmental deficits.

Interestingly, we observed some differences between the conditional (p75Atoh1-Cre) and the tamoxifen-inducible mice (p75Atoh1-CreERTM). In the anxiety-related behaviors, e.g., open field, grooming, elevated zero maze, and light transition test, p75Atoh1-Cre mice performed significantly different than control mice (p75FL) suggesting elevated anxiety in these animals. However, no difference was observed between the p75Atoh1-CreERTM with and without tamoxifen. One possible explanation for these differences is that another neuronal population that expresses Atoh1 and p75NTR is responsible for the behavioral difference only observed in the p75Atoh1-Cre. In mice, Atoh1 is first detected at E9 and continues throughout development, but it is absent from adult brains, although, the specific location of Atoh1 expression is controversial. Using *in situ* hybridization and immunostaining, Atoh1 expression was detected in the cranial ganglia, the dorsal wall of the neural tube, and the hindbrain, there is also a strong expression of Atoh1 in the rhombic lip, which contains the GCPs of the cerebellum as well as the excitatory cells of the deep cerebellar nuclei (Akazawa et al., 1995; Ben-Arie et al., 1996, 1997). Using a Cre reporter line, besides the above-mentioned places, Atoh1 was also found in the dentate gyrus in the hippocampus (Lumpkin et al., 2003); consistently, we identified a small number of Td-Tomato positive cells in the p75Atoh1-CreERTM injected with tamoxifen,

suggesting that Atoh1 is present during hippocampal development. P75NTR is expressed in the developing hippocampus (Koh et al., 1989; Zuccaro et al., 2014). The hippocampus and the cerebellum are both involved in anxiety behaviors (Bannerman et al., 2004; McHugh et al., 2004; Engin and Treit, 2007; Phillips, 2015; Moreno-Rius, 2018), therefore the elevated anxiety observed only in the conditional p75Atoh1-Cre might be due to developmental defects in the hippocampus induced by the deletion of p75NTR after Atoh1 is expressed. This is supported by the findings of a small proportion of recombined neurons in the p75Atoh1-CreERTM mice after tamoxifen injection. The late tamoxifen injection seems to impact a reduced number of cells, therefore the great majority of cells in the hippocampus would still maintain wild-type expression of p75NTR; thus, no impact on anxiety levels (as well as performance on the novel object recognition test) was observed in these animals.

An alternative explanation is that the p75Atoh1-CreERTM might not reach the threshold of excess CGN to affect anxiety-related behavior. The absence of p75NTR accelerates the GCP cell cycle, generating an excess of granule cell neurons (Zanin et al., 2016, 2019). In the p75Atoh1-Cre mouse, the entire GCP population lacks p75NTR expression, and a full penetrance of recombination was expected, generating the highest excess of CGN number; however, even in the highest level of recombination in the p75Atoh1-CreERTM we did not observe a 100% penetrance, suggesting that only a fraction of the GCP lack p75NTR, and thus fewer excess CGN are generated in these animals. Further experiments that allowed more broad deletion of the expression of p75NTR specifically from the GCP are required to completely rule out whether an excess of granule cells would also affect anxiety-related behaviors. It is worth mentioning that both mice models used in our study affect CGN development; however, our findings do not directly address how an excess number of neurons alter the activity of the CGN. Further studies that evaluate neuronal activity are required to answer these questions.

The extensive range of behaviors affected by the absence of p75NTR might be explained by the expression pattern of this receptor and the multiple behaviors in which the cerebellum is involved. P75NTR is expressed in every proliferating GCP. In our previous work, we demonstrated that the absence of the receptor induced defects in proliferation and migration, and these cellular defects were observed in both the anterior and posterior lobes in the cerebellum. Each area of the cerebellum is involved in different aspects of cerebellar function; therefore, it is possible that the defects induced by p75NTR will affect every folium of the cerebellum impacting multiple behaviors in adult animals. Further behavioral tests would likely elucidate other behaviors impacted by the excess of CGN. Regardless, our research identifies p75NTR as a potential risk factor in cerebellar development that contributes to the growing evidence by which the cerebellum impacts non-motor as well as motor behaviors.

Data availability statement

The datasets presented in this study can be found in online repositories. The names of the repository/repositories and accession number(s) can be found below: https://figshare.com/articles/dataset/Excess_cerebellar_granule_neurons_induced_by_the_absence_of_p75NTR_during_development_elicit_social_behavior_deficits_in_mice/21919035.

Ethics statement

This animal study was reviewed and approved by Rutgers IACUC.

Author contributions

JZ, WF, and MS conceived the experiments and wrote the manuscript. JZ, MP, and DE performed the experiments. All authors contributed to the article and approved the submitted version.

Funding

This work was funded by Rutgers Busch Biomedical Grant AWD00009650 to JZ.

Acknowledgments

The authors thank Drs. K. Kwan and J. Kim from the Department of Cell Biology & Neuroscience at Rutgers University, New Brunswick, for providing us with the Atoh1Cre-ERTM R26R Td-Tomato mice.

Conflict of interest

The authors declare that the research was conducted in the absence of any commercial or financial relationships that could be construed as a potential conflict of interest.

Publisher's note

Supplementary material

The Supplementary Material for this article can be found online at: https://www.frontiersin.org/articles/10.3389/fnmol.2023.1147597/full#supplementary-material

References

Akazawa, C., Ishibashi, M., Shimizu, C., Nakanishi, S., and Kageyama, R. (1995). "A mammalian helix-loop-helix factor structurally related to the product of *Drosophila proneural* gene atonal is a positive transcriptional regulator expressed in the developing nervous system". *J. Biol. Chem.* 270, 8730–8738.

Andreasen, N. C., and Pierson, R. (2008). "The role of the cerebellum in schizophrenia". *Biol. Psychiatry* 64, 81–88. doi: 10.1016/j.biopsych.2008.01.003

Bailey, A., Luthert, P., Dean, A., Harding, B., Janota, I., Montgomery, M., et al. (1998). "A clinicopathological study of autism". *Brain* 121, 889–905.

Bannerman, D. M., Rawlins, J., McHugh, S., Deacon, R., Yee, B., Bast, T., et al. (2004). "Regional dissociations within the hippocampus - memory and anxiety". *Neurosci. Biobehav. Rev.* 28, 273–283. doi: 10.1016/j.neubiorev.2004.03.004

Bauman, M., and Kemper, T. (1985). "Histoanatomic observation of the brain in early infantile autism". *Neurology* 35, 866–874. doi: 10.1212/wnl.35.6.866

Baumann, O., Borra, R., Bower, J., Cullen, K., Habas, C., Ivry, R., et al. (2015). "Consensus paper: the role of the cerebellum in perceptual processes". *Cerebellum* 14, 197–220. doi: 10.1007/s12311-014-0627-7

Ben-Arie, N., Bellen, H., Armstrong, D., McCall, A., Gordadze, P., Guo, Q., et al. (1997). "Math1 is essential for genesis of cerebellar granule neurons". *Nature* 390, 169–172. doi: 10.1038/36579

Ben-Arie, N., McCall, A., Berkman, S., Eichele, G., Bellen, H., Zoghbi, H., et al. (1996). "Evolutionary conservation of sequence and expression of the bHLH protein atonal suggests a conserved role in neurogenesis". *Hum. Mol. Genet.* 5, 1207–1216. doi: 10.1093/hmg/5.9.1207

Blackwood, N., Ffytche, D., Simmons, A., Bentall, R., Murray, R., and Howard, R. (2004). "The cerebellum and decision making under uncertainty". *Brain Res. Cogn. Brain Res.* 20, 46–53. doi: 10.1016/j.cogbrainres.2003.12.009

Bogenmann, E., Thomas, P., Li, Q., Kim, J., Yang, L., Pierchala, B., et al. (2011). "Generation of mice with a conditional allele for the p75 NTR neurotrophin receptor gene". *Genesis* 49, 862–869. doi: 10.1002/dvg.20747

Carta, M., Chen, C., Schott, A., Dorizan, S., and Khodakhah, K. (2019). "Cerebellar modulation of the reward circuitry and social behavior". *Science* 248, 1–10. doi: 10.1126/science.aav0581

Carter, A. R., Berry, E. M., and Segal, R. A. (2003). Regional expression of p75NTR contributes to neurotrophin regulation of cerebellar patterning. *Mol. Cell. Neurosci.* 22, 1–13. doi: 10.1016/S1044-7431(02)00015-5

Chow, L. M. L., Tian, Y., Weber, T., Corbett, M., Zuo, J., and Baker, S. (2006). "Inducible cre recombinase activity in mouse cerebellar granule cell precursors and inner ear hair cells". *Dev. Dyn.* 235, 2991–2998. doi: 10.1002/dvdy.20948

Deverett, B., Koay, S., Oostland, M., and Wang, S. (2018). "Cerebellar involvement in an evidence- accumulation decision-making task". *eLife* 36781, 1–22. doi: 10.7554/eLife.36781

Eisenberg, C., Subramanian, D., Afrasiabi, M., Ziobro, P., DeLucia, J., Hirschberg, P., et al. (2021). "Reduced hippocampal inhibition and enhanced autism-epilepsy comorbidity in mice lacking neuropilin 2". *Trans. Psychiatry* 11, 1–12. doi: 10.1038/s41398-021-01655-6

Engin, E., and Treit, D. (2007). "The role of hippocampus in anxiety: intracerebral infusion studies". *Behav. Pharmacol.* 18, 365–374. doi: 10.1097/FBP.0b013e3282de7929

Fatemi, S. H., Halt, A., Realmuto, G., Earle, J., Kist, D., Thuras, P., et al. (2002). "Purkinje cell size is reduced in cerebellum of patients with autism". *Cell. Mol. Neurobiol.* 22, 171–175.

Giovannucci, A., Badura, A., Badura, A., Deverett, B., Najafi, F., Pereira, T., et al. (2017). "Cerebellar granule cells acquire a widespread predictive feedback signal during motor learning". *eLife* 20, 727–734. doi: 10.1038/nn.4531

Guell, X., Gabrieli, J. D. E., and Schmahmann, J. D. (2018). "Triple representation of language, working memory, social and emotion processing in the cerebellum: convergent evidence from task and seed-based resting-state fMRI analyses in a single large cohort". *NeuroImage* 172, 437–449. doi: 10.1016/j.neuroimage.2018.01.082

Hilber, P., Lorivel, T., Delarue, C., and Caston, J. (2004). "Stress and anxious-related behaviors in lurcher mutant mice". *Brain Res.* 1003, 108–112. doi: 10.1016/j.brainres.2004.01.008

Kern, J. K. (2003). "Purkinje cell vulnerability and autism: a possible etiological connection". *Brain Dev.* 25, 377–382. doi: 10.1016/S0387-7604(03)00056-1

Koh, S., Oyler, G. A., and Higgins, G. A. (1989). "Localization of nerve growth factor receptor messenger RNA and protein in the adult rat brain". *Exp. Neurol.* 106, 209–221. doi: 10.1016/0014-4886(89)90154-4

Lee, T. H., Kato, H., Pan, L., Ryu, J., Kogure, K., and Itoyama, Y. (1998). "Localization of nerve growth factor, trka and P75 immunoreactivity in the hippocampal formation and basal forebrain of adult rats". *Neuroscience* 83, 335–349. doi: 10.1016/S0306-4522(97)00346-1

Limperopoulos, C., Robertson, R., Sullivan, N., Bassan, H., and du Plessis, A. (2009). "Cerebellar injury in term infants : clinical characteristics, magnetic resonance imaging findings, and outcome". *Pediat. Neurol.* 41, 1–8. doi: 10.1016/j.pediatrneurol.2009.02.007

Lumpkin, E. A., Collisson, T., Omer-Abdalla, A., Haeberle, H., and Chen, P. (2003). "Math1-driven GFP expression in the developing nervous system of transgenic mice". *Gene Exp. Patt.* 3, 389–395. doi: 10.1016/S1567-133X(03)00089-9

MacHold, R., and Fishell, G. (2005). "Math1 is expressed in temporally discrete pools of cerebellar rhombic-lip neural progenitors". *Neuron* 48, 17–24. doi: 10.1016/j.neuron.2005.08.028

Matei, V., Pauley, S., Kaing, S., Rowitch, D., Beisel, K., Morris, K., et al. (2005). "Smaller inner ear sensory epithelia in Neurog1 null mice are related to earlier hair cell cycle exit". *Dev. Dyn.* 234, 633–650. doi: 10.1002/dvdy.20551

McHugh, S., Deacon, R., Rawlins, J., and Bannerman, D. (2004). "Amygdala and ventral hippocampus contribute differentially to mechanisms of fear and anxiety". *Behav. Neurosci.* 118, 63–78. doi: 10.1037/0735-7044.118.1.63

Miquel, M., Toledo, R., García, L., Coria-Avila, G., and Manzo, J. (2009). "Why should we keep the cerebellum in mind when thinking about addiction?" *Curr. Drug Abuse Rev.* 2, 26–40. doi: 10.2174/1874473710902010026

Moreno-Rius, J. (2018). "The cerebellum in fear and anxiety-related disorders". *Prog. Neuro Psychopharmacol. Biol. Psychiatry* 85, 23–32. doi: 10.1016/j.pnpbp.2018.04.002

Moscatelli, I., Pierantozzi, E., Camaioni, A., Siracusa, G., and Campagnolo, L. (2009). "P75 neurotrophin receptor is involved in proliferation of undifferentiated mouse embryonic stem cells". *Exp. Cell Res.* 315, 3220–3232. doi: 10.1016/j.yexcr.2009.08.014

Moulton, E. A., Elman, I., Becerra, L., Goldstein, R., and Borsook, D. (2014). "The cerebellum and addiction: insights gained from neuroimaging research". *Addict. Biol.* 19, 317–331. doi: 10.1111/adb.12101

Parker, K. L., Narayanan, N. S., and Andreasen, N. C. (2014). "The therapeutic potential of the cerebellum in schizophrenia". *Front. Syst. Neurosci.* 8:1–11. doi: 10.3389/fnsys.2014.00163

Phillips, J. R. (2015). "The cerebellum and psychiatric disorders". *Front. Public Health* 3:1–8. doi: 10.3389/fpubh.2015.00066

Schmahmann, J. D., and Sherman, J. C. (1998). "The cerebellar cognitive affective/schmahmann syndrome scale". *Brain* 141, 248–270.

Shiflett, M. W. (2017). "Functions of neuropilins in wiring the nervous system and their role in neurological disorders," in *The neuropilins: role and function in health and disease*, eds G. Neufeld and O. Kessler. doi: 10.1242/dev.119909

Skefos, J., Cummings, C., Enzer, K., Holiday, J., Weed, K., Levy, E., et al. (2014). "Regional alterations in purkinje cell density in patients with autism". *PLoS One* 9:1–12. doi: 10.1371/journal.pone.0081255

Song, J., Xu, Y., Hu, X., Choi, B., and Tong, Q. (2010). "Brain expression of cre recombinase driven by pancreas-specific promoters". *Genesis* 48, 628–634. doi: 10.1002/dvg.20672

Stoodley, C. J., and Schmahmann, J. D. (2010). "Evidence for topographic organization in the cerebellum of motor control versus cognitive and affective processing". *Cortex* 46, 831–844. doi: 10.1016/j.cortex.2009.11.008

Van Overwalle, F., Manto, M., Cattaneo, Z., Clausi, S., Ferrari, C., Gabrieli, J., et al. (2020). Consensus paper: cerebellum and social cognition. *Cerebellum* 19, 833–868. doi: 10.1007/s12311-020-01155-1

Van Overwalle, F., Mariën, P., and Vandekerckhove, M. (2014). "Social cognition and the cerebellum: a meta-analysis of over 350 fMRI studies". *NeuroImage* 86, 554–572. doi: 10.1016/j.neuroimage.2013.09.033

Vandamme, N., and Berx, G. (2019). "From neural crest cells to melanocytes: cellular plasticity during development and beyond". *Cell. Mol. Life Sci.* 76, 1919–1934. doi: 10.1007/s00018-019-03049-w

Wagner, M. J., Kim, T., Savall, J., Schnitzer, M., and Luo, L. (2017). "Cerebellar granule cells encode the expectation of reward". *Nature* 000, 1–18. doi: 10.1038/nature21726

Wang, S. S. H., Kloth, A. D., and Badura, A. (2014). "Perspective the cerebellum. Sensitive periods, and autism". *Neuron* 83, 518–532. doi: 10.1016/j.neuron.2014.07.016

Wang, V. Y., Rose, M. F., and Zoghbi, H. Y. (2005). "Math1 expression redefines the rhombic lip derivatives and reveals novel lineages within the brainstem and cerebellum". *Neuron* 48, 31–43. doi: 10.1016/j.neuron.2005.08.024

Whitney, E. R., Kemper, T., Bauman, M., Rosene, D., and Blatt, G. (2008). Cerebellar purkinje cells are reduced in a subpopulation of autistic brains : a stereological experiment using calbindin-D28k. *Cerebellum* 7, 406–416. doi: 10.1007/s12311-008-0043-y

Yeganeh-Doost, P. (2011). "The role of the cerebellum in schizophrenia: from cognition to molecular pathways". *Clinics* 66, 71–77. doi: 10.1590/S1807-59322011001300009

Zanin, J. P., and Friedman, W. J. (2022). p75NTR prevents the onset of cerebellar granule cell migration via RhoA activation. *eLife* 11, 1–23. doi: 10.7554/elife.79934

Zanin, J. P., Verpeut, J., Li, Y., Shiflett, M., Wang, S., Santhakumar, V., et al. (2019). "The p75NTR influences cerebellar circuit development and adult behavior via regulation of cell cycle duration of granule cell progenitors". *J. Neurosci.* 39, 9119–9129. doi: 10.1523/JNEUROSCI.0990-19.2019

Zanin, J., Abercrombie, E., and Friedman, W. (2016). "Proneurotrophin-3 promotes cell cycle withdrawal of developing cerebellar granule cell progenitors via the p75 neurotrophin receptor". *eLife* 5, 1–21. doi: 10.7554/eLife.16654

Zuccaro, E., Bergami, M., Vignoli, B., Bony, G., Pierchala, B., Santi, S., et al. (2014). "Polarized expression of p75NTR specifies axons during development and adult neurogenesis". *Cell Rep.* 7, 138–152. doi: 10.1016/j.celrep.2014.02.039

frontiers | Frontiers in Molecular Neuroscience

TYPE Original Research
PUBLISHED 22 June 2023
DOI 10.3389/fnmol.2023.1206245

OPEN ACCESS

EDITED BY
Catarina Osorio,
Erasmus Medical Center, Netherlands

REVIEWED BY
Aleksandra Badura,
Erasmus Medical Center, Netherlands
Martijn Schonewille,
Erasmus University Rotterdam, Netherlands

*CORRESPONDENCE
Masanobu Kano
✉ mkano-tky@m.u-tokyo.ac.jp
Takaki Watanabe
✉ wtakaki@m.u-tokyo.ac.jp

RECEIVED 15 April 2023
ACCEPTED 25 May 2023
PUBLISHED 22 June 2023

CITATION
Okuno Y, Sakoori K, Matsuyama K, Yamasaki M, Watanabe M, Hashimoto K, Watanabe T and Kano M (2023) PTPδ is a presynaptic organizer for the formation and maintenance of climbing fiber to Purkinje cell synapses in the developing cerebellum. *Front. Mol. Neurosci.* 16:1206245. doi: 10.3389/fnmol.2023.1206245

PTPδ is a presynaptic organizer for the formation and maintenance of climbing fiber to Purkinje cell synapses in the developing cerebellum

Yuto Okuno[1], Kazuto Sakoori[1], Kyoko Matsuyama[1], Miwako Yamasaki[2], Masahiko Watanabe[2], Kouichi Hashimoto[3], Takaki Watanabe[1,4]* and Masanobu Kano[1,4]*

[1]Department of Neurophysiology, Graduate School of Medicine, The University of Tokyo, Tokyo, Japan, [2]Department of Anatomy, Hokkaido University Graduate School of Medicine, Sapporo, Japan, [3]Department of Neurophysiology, Graduate School of Biomedical and Health Sciences, Hiroshima University, Hiroshima, Japan, [4]International Research Center for Neurointelligence (WPI-IRCN), The University of Tokyo Institutes for Advanced Study, The University of Tokyo, Tokyo, Japan

Functionally mature neural circuits are shaped during postnatal development by eliminating redundant synapses formed during the perinatal period. In the cerebellum of neonatal rodents, each Purkinje cell (PC) receives synaptic inputs from multiple (more than 4) climbing fibers (CFs). During the first 3 postnatal weeks, synaptic inputs from a single CF become markedly larger and those from the other CFs are eliminated in each PC, leading to mono-innervation of each PC by a strong CF in adulthood. While molecules involved in the strengthening and elimination of CF synapses during postnatal development are being elucidated, much less is known about the molecular mechanisms underlying CF synapse formation during the early postnatal period. Here, we show experimental evidence that suggests that a synapse organizer, PTPδ, is required for early postnatal CF synapse formation and the subsequent establishment of CF to PC synaptic wiring. We showed that PTPδ was localized at CF-PC synapses from postnatal day 0 (P0) irrespective of the expression of Aldolase C (Aldoc), a major marker of PC that distinguishes the cerebellar compartments. We found that the extension of a single strong CF along PC dendrites (CF translocation) was impaired in global PTPδ knockout (KO) mice from P12 to P29-31 predominantly in PCs that did not express Aldoc [Aldoc (−) PCs]. We also demonstrated via morphological and electrophysiological analyses that the number of CFs innervating individual PCs in PTPδ KO mice were fewer than in wild-type (WT) mice from P3 to P13 with a significant decrease in the strength of CF synaptic inputs in cerebellar anterior lobules where most PCs are Aldoc (−). Furthermore, CF-specific PTPδ-knockdown (KD) caused a reduction in the number of CFs innervating PCs with decreased CF synaptic inputs at P10-13 in anterior lobules. We found a mild impairment of motor performance in adult PTPδ KO mice. These results indicate that PTPδ acts as a presynaptic organizer for CF-PC formation and is required for normal CF-PC synaptic transmission, CF translocation, and presumably CF synapse maintenance predominantly in Aldoc (−) PCs. Furthermore, this study suggests that the impaired CF-PC synapse formation and development by the lack of PTPδ causes mild impairment of motor performance.

KEYWORDS

synapse elimination, synapse formation, synapse organizer, cerebellum, PTPδ, climbing fiber, Purkinje cell

Introduction

Neural circuits are known to be remodeled and become functionally mature during postnatal development. Extensive synapse formation (or synaptogenesis) occurs during the perinatal period, and excess synaptic connections are present in the nervous system of newborn animals compared to mature animals. During postnatal development, some synapses are strengthened functionally and/or morphologically, while other synapses are weakened and finally eliminated. This process is called "synapse elimination" and is thought widely to be a fundamental process for the developmental refinement of neural circuits (Kano and Hashimoto, 2009).

In newborn mice, Purkinje cells (PCs) receive excitatory inputs from multiple climbing fibers (CFs) (more than 4 CFs) with similar strength of synaptic inputs. Thereafter, synaptic inputs from a single CF become progressively stronger than those from the other CFs from postnatal day 3 (P3) to around P7 (Hashimoto and Kano, 2003). Then, only the strengthened CF extends its synaptic territory along the PC dendrites from around P9 (Hashimoto et al., 2009a). In parallel, synapses of the other weaker CFs are eliminated from PC soma from P7 to around P11. Finally, remaining somatic CF synapses are eliminated from P12 to P17 in a manner dependent on parallel fibers (PFs)-PC synapse formation (Hashimoto and Kano, 2013). Although many molecules involved in CF synapse elimination and strengthening/maintenance of CF synapses in postnatal life have been identified, much less is known about the molecular mechanism of CF synapse formation during the early postnatal period before the sequence of developmental CF synapse elimination is initiated.

Synapse formation is induced by *trans*-synaptic interactions between selective pairs of pre- and post-synaptic cell adhesion molecules, called "synapse organizer" (Shen and Scheiffele, 2010; Siddiqui and Craig, 2011; Takahashi and Craig, 2013; Um and Ko, 2013; de Wit and Ghosh, 2016; Südhof, 2017; Yuzaki, 2018). Among synapse organizers, Neurexins (NRXNs: Nrxn1-3) and leukocyte common antigen-related receptor tyrosine phosphatases (LAR-RPTPs) have been reported as presynaptic organizers. LAR-RPTPs consist of LAR (also known as Ptprf), PTPδ (Ptprd), and PTPσ (Ptprs) (Takahashi and Craig, 2013). NRXNs and LAR-RPTPs with their alternative splicing variants are known to interact with different postsynaptic ligands (Südhof, 2017). For example, Neuroligins (NLGNs: NLGN1-4), Cblns (Cbln1-4)-GluRδs (GluD1 and 2) and LRRTMs (LRRTM1-4) have been reported as postsynaptic ligands for NRXN variants (Südhof, 2017). On the other hand, interleukin-1 receptor accessory protein (IL1RAcP also known as IL1RAP), IL1RAcP-like1 (IL1RAPL1), TrkC, Slitrks (Slitrk1-5), synaptic adhesion-like molecule family (SALM3 and SALM5), TrkC, and NGL-3 have been reported as postsynaptic ligands for LAR-RPTPs variants (Takahashi and Craig, 2013; Fukai and Yoshida, 2021). However, a recent report identified NLGN3, known as the postsynaptic ligand for NRXNs, as a novel postsynaptic ligand of PTPδ (Yoshida et al., 2021). Moreover, Nrxns have been reported as not being required for presynaptic formation to bind directly to intracellular proteins (Gokce and Südhof, 2013), while LAR-RPTPs are shown to induce presynaptic differentiation via direct interaction with several synaptic proteins (Serra-Pagès et al., 1998; Wakita et al., 2020), suggesting that Nrxns and LAR-RPTPs mediate presynaptic assembly by distinct molecular mechanism. Several studies also reported that Nrxns and LAR-RPTPs are not essential for synapse formation but are involved in regulating synapse properties (Uetani et al., 2000; Horn et al., 2012; Anderson et al., 2015; Chen et al., 2017).

The roles of synapse organizers in the cerebellum have recently been revealed. For example, presynaptic NRXNs in PFs interact with postsynaptic GluD2 via Cbln1 to induce PF-PC synapse formation (Matsuda et al., 2010; Uemura et al., 2010). Knockout of all NRXNs (Nrxn1-3) in mouse CFs showed a reduction of CF territories along PC dendrites and a decrease in the amplitude of CF-EPSCs at P24. However, the contribution of NRXNs in the formation and elimination of CF to PC synapses during postnatal development remained unknown (Chen et al., 2017). NLGN3 knock-in mice harboring the ASD-related R451C mutation (R451C) reduced the expression of NLGN3 protein in the cerebellum, resulting in the impairment of CF synapse elimination transiently from P10 to P15, associated with the enhancements of inhibitory synaptic transmission on PCs (Lai et al., 2021). PTPδ, which also binds NLGN3, is expressed in various regions of the brain, including the cerebellum, inferior olivary nucleus, hippocampus, and cerebral cortex (Shishikura et al., 2016). PTPδ knockout (KO) mice exhibit impaired spatial learning, memory, and motor function. While a previous study has shown that PTPδ is involved in the regulation of synaptic activity in the hippocampus (Uetani et al., 2000), its role in the cerebellum has not been investigated.

This study aimed at investigating whether and how PTPδ is involved in the formation and development of CF-PC synapses in the cerebellum. The results to be presented collectively suggest that PTPδ functions as a presynaptic organizer for the formation of CF to PC synapses during the perinatal period, maintenance of CF to PC synapses and thereby antagonizing their elimination during postnatal development, and establishment of normal strength of CF to PC synaptic transmission predominantly in Aldolase C-negative PCs.

Materials and methods

Animal

C57BL/6NCr wild-type mice (male and female, SLC, Japan) were used for knockdown (KD) experiments. PTPδ knockout (KO) mice used by Uetani et al. (2000) had a mixed genetic background of C57BL/6J;129/SvJ, and they were subsequently crossed with the C57BL/6N mice during frozen embryo creation. Therefore, they had a mixed genetic background of C57BL/6J, C57BL/6N, and 129/SvJ. In this study, we used wild-type and PTPδ KO mice that were born by crossing PTPδ heterozygous mice with this genetic background. We used both male and female mice for morphological, electrophysiological, and behavioral analyses. All the experiments were performed in accordance with the guidelines of the animal welfare committees of the University of Tokyo and the Japan Neuroscience Society.

Preparation of viral vector constructs

We constructed virus vectors as previously described (Uesaka et al., 2012). Vesicular stomatitis virus G (VSVG) pseudotyped lentiviral vectors were used (Hanawa et al., 2002). The vectors were designed to express mOrange2, microRNA (miRNA) for PTPδ KD, and/or cDNA for PTPδ expression under the control of the murine embryonic stem cell virus (MSCV) (pCL20c-MSCV) for their expression in CFs.

The following engineered microRNAs were designed by the BLOCK-iT Pol II miR RNAi expression vector kit guidelines (Thermo Fisher Scientific, Japan):

5′-TGCTGTTTAGTGGCTGCCCTGGTACTGTTTTGGCCACTGACTGACAGTACCAGCAGCCACTAAAT−3′

for PTPδ-microRNA 1;

5′-TGCTGATTGGAGGATGGCTAGCCATAGTTTTGGCCACTGACTGACTATGGCTACATCCTCCAAT−3′

for PTPδ-microRNA 2

5′-TGCTGCAACTGCACCAAGGAAGCTGTTTTGGCCACTGACTGACAGCTTCCTTGTCGTGCAGTTG−3′

for PTPδ-scramble 1

5′-TGCTGGAGAAGCTCGATTGGAATGCTGTTTTGGCCACTGACTGAC AGCATTCCAATCGAGCTTCTC-3′

for PTPδ-scramble 2.

The cDNA for PTPδ expression was obtained using RT-PCR of a cDNA library from the cerebellum of P12 mice (Uesaka et al., 2018). RNAi-resistant forms of PTPδ (PTPδ RES) were generated using the QuikChange Lightning site-directed mutagenesis kit (#210518, Agilent Technologies, USA). The mutations of 5–6 nucleotides in the miRNA targeted sites of PTPδ were introduced without changing the amino acid sequence. PTPδ RES was linked in-frame to GFP interposed by a picornavirus "self-cleaving" P2A peptide sequence to enable efficient bicistronic expression, and the cDNA was subcloned into pCL20c-MSCV (Uesaka et al., 2018). All constructs were confirmed by DNA sequencing.

Preparation and injection of lentivirus into the inferior olive

We produced lentivirus as previously described (Uesaka et al., 2012). A lentivirus vector (pCL20c-MSCV of 10 μg) was mixed with an envelope vector (3.5 μg of pCAG-VSV-G) and a packaging vector (7 μg of psPAX2) and transfected into cultured human embryonic kidney (HEK) 293T cells. The lentivirus produced from the HEK293T cells was collected and mixed in phosphate buffer saline (PBS). The head of a C57BL/6 mouse at P0-2 was fixed under isoflurane (0.6–2.5%) anesthesia. The solution containing the lentivirus (1.5 μl) was injected into the inferior olive using a conventional Hamilton syringe at the speed of 80 nl/min.

Electrophysiological recordings from PCs

The electrophysiological recordings were performed as described previously (Hashimoto and Kano, 2003; Uesaka et al., 2012). Mice anesthetized by CO_2 inhalation were decapitated and their brains were removed. The acute parasagittal slices of 250 μm thickness were prepared from the cerebellar vermis of mice and were incubated in a reservoir chamber filled with artificial cerebrospinal fluid (ACSF) (125 mM NaCl, 2.5 mM KCl, 2 mM $CaCl_2$, 1 mM $MgSO_4$, 1.25 mM NaH_2PO_4, 26 mM $NaHCO_3$, and 20 mM glucose oxygenated with 95% O_2 and 5% CO_2) for at least 30 min at room temperature. For recording, the cerebellar slices were placed in a recording chamber at the stage of an Olympus BX51WI microscope (Olympus, Japan) perfused continuously with oxygenated ACSF at 32°C. Whole-cell patch clamp recordings were conducted from visually identified PCs or PCs associated with fluorescent protein-labeled CFs using an upright fluorescence microscope (Olympus BX51WI) (Hashimoto and Kano, 2003; Uesaka et al., 2014, 2018). For recording climbing fiber-induced excitatory postsynaptic currents (CF-EPSCs) and parallel fiber-induced EPSCs (PF-EPSCs), picrotoxin (100 μM, Nacalai, Japan) was added to the bath solution. For recording miniature inhibitory postsynaptic currents (mIPSCs), NBQX (10 μM, Tocris, UK), D-AP5 (50 μM, Tocris), and tetrodotoxin (1 μM, Nacalai, Japan) were added to the bath solution. Ionic currents were recorded with an EPC10 patch clamp amplifier (HEKA, USA) with the holding potential being −10 mV for CF-EPSCs and −70 mV for PF-EPSCs, asynchronous quantal CF-EPSCs, and mIPSCs. Liquid junction potential was corrected. The resistance of patch pipettes was 1.5–2.5 MΩ when filled with an intracellular solution composed of 60 mM CsCl, 10 mM D-gluconate, 20 mM TEA-Cl, 20 mM BAPTA, 4 mM $MgCl_2$, 4 mM Na_2-ATP, 0.4 mM Na_2-GTP, and 30 mM HEPES (pH 7.3), adjusted with CsOH.

CF-EPSCs were evoked by electrically stimulating CFs with pairs of pulses (duration, 0.1 ms; interval, 50 ms; current intensity, 0–100 μA) through a stimulating pipette placed in the granule cell layer (GCL). When a CF was stimulated, EPSCs with a clear amplitude step and showing depression to the second stimulus pairs were elicited (Konnerth et al., 1990; Aiba et al., 1994). To search all CFs innervating the recorded PC, the stimulus pipette was systematically moved in the GCL around the PC soma and the stimulus strength was gradually increased from 0 to 100 μA at each stimulation site (Hashimoto and Kano, 2003). The number of CFs innervating the recorded PC was estimated as the number of discrete CF-EPSC steps elicited in that PC (Hashimoto and Kano, 2003). PF-EPSCs were elicited by stimulating PFs in the middle of the molecular layer (ML) with pairs of pulses whose parameters were similar to those used for CF stimulation. PF-EPSCs exhibited facilitation to the second of stimulus pairs and their amplitudes were graded to the intensity of PF stimulation (Konnerth et al., 1990). The position of the PF stimulating pipette was adjusted so that the maximum response was elicited with the stimulus current of 10 μA (Uesaka et al., 2018). The stimulus intensity was gradually decreased from 10 to 1 μA to obtain input–output relations. For recording quantal CF-EPSCs, 2 mM Ca^{2+}/1 mM Mg^{2+} was replaced with 2 mM Sr^{2+}/1 mM Mg^{2+} (Hashimoto and Kano, 2003; Uesaka et al., 2018). For recording mIPSCs, the recording was started 3 min after the PC membrane was breached (Uesaka et al., 2018). Online data acquisition was performed using Patch Master (HEKA), and offline data analysis was performed using Fit Master (HEKA) and MATLAB (MathWorks, USA) software.

Quantification of disparity ratio and disparity index of multiple CF-EPSCs

To quantitatively evaluate the disparity among the amplitudes of multiple CF-EPSCs in individual PCs, we calculated the disparity ratio and the disparity index as shown previously (Hashimoto and Kano, 2003).

$$\circ\text{Disparity ratio} = \frac{\left(\frac{A1}{AN} + \frac{A2}{AN} + \cdots + \frac{AN-1}{AN}\right)}{(N-1)}$$

$$\circ\text{Disparity index} = \frac{\text{S.D.}}{\text{M}}$$

$$M = \sum \frac{Ai}{N}\ (i = 1, 2, 3, \ldots N;\ N > 2)$$

$$\text{S.D.} = \sqrt{\sum \frac{(Ai - M)\,2}{N-1}}$$

To calculate the disparity ratio and disparity index, the amplitudes of individual CF-EPSCs in a given PC with multiple CF innervations were measured at the same holding potential and numbered in the order of their amplitudes (A1, A2, ..., AN, N ≥ 2; N is the number of CFs innervating a given PC. AN represents the largest CF-EPSC) (Hashimoto and Kano, 2003). The smaller the difference in the amplitude between AN and other weak CF-EPSCs, the larger the value of the disparity ratio. If all CFs innervating a PC exhibit similar amplitude of CF-EPSCs, the disparity ratio approaches 1. The disparity index is the coefficient of variation for all CF-EPSC amplitudes recorded in a PC (Hashimoto and Kano, 2003). The larger the difference in the amplitude of CF-EPSCs, the larger the value of the disparity index.

Immunohistochemistry

Mice from P0 to P31 of age were deeply anesthetized with pentobarbital (100 μg/g of body weight) by intraperitoneal injection and perfused with 4% paraformaldehyde in 0.1 M phosphate buffer for immunostaining a CF terminal marker, vesicular glutamate transporter VGluT2, to evaluate CF translocation, with 3% glyoxal solution (3% glyoxal and 0.3% acetic acid, pH 4.0 with NaOH) for immunostaining PTPδ (Richter et al., 2018) or with 9% glyoxal solution (9% glyoxal and 8% acetic acid, pH 4.0) for immunostaining RIM1/2. Fixed brains were placed in the same fixative overnight, and then parasagittal sections (100 or 150 μm in thickness) were prepared with a microslicer. The sections were incubated in 1 or 0.1% TritonX-100/PBS for permeabilization and blockade of non-specific binding. Primary antibodies against the following molecules were added overnight at 4°C: Car8 (Car8-GP-Af500, diluted 1:300, Frontier Institute, Japan) and Calbindin (Calbindin-Go-Af1040, 1 μg/ml, Frontier Institute) for immunostaining PCs, VGluT2 (VGluT2-GO-Af310, 1:300 and VGluT2-GP-Af810, 1 μg/ml, Frontier Institute) for immunostaining CF terminals, VGluT1 (VGluT1-Rb-Af500, 1 μg/ml, Frontier Institute) for immunostaining PF terminals, PTPδ (Anti-PTPRD, clone F34a6,f 1:300, Merck, Germany), Aldolase C (Aldolase C-Rb-Af1390, Frontier Institute), and RIM1/2 (RIM1/2 Zn-finger domain, Cat. No. 140 203, 1 μg/ml, Synaptic systems, Germany). Then, the sections were incubated with species-specific secondary antibodies (an anti-guinea pig Alexa Fluor 405 antibody, an anti-rat Alexa Fluor 488 antibody, an anti-goat Alexa Fluor 647, and an anti-rabbit Cy3 antibody, 1:200, Jackson Immuno-Research, USA) at room temperature for 2 or 4 h. The immunolabeled cerebellar sections were observed under a confocal laser scanning microscope (FV1200, Olympus). For evaluation of CF translocation, the thickness of the molecular layer containing Car8-positive PC dendrites and the height of CF terminals visualized by VGluT2 immunostaining at P12 and P29-30 were measured. Images were captured from all cerebellar lobules at the same microscopic settings (field of view: 186.2 μm × 186.2 μm for P12, 317.2 μm × 317.2 μm for P29-31). The degree of CF translocation was quantified as the ratio of the height of CF terminals to the thickness of the molecular layer. Z stacks of 12.2 μm images were analyzed using ImageJ (NIH, USA) software. For the morphological analysis of CF synapses, images were taken from anterior lobules of WT and PTPδ KO mice at the same microscopic settings (field of view: 20 μm × 20 μm for P4 (Figure 2C), 10 μm × 30 μm for P11 (Figures 3C, D), 10 μm × 50 μm for P30 (Figures 3J, K) and were compared using a MetaMorph software (Molecular Devices, USA).

Fluorescence *in situ* hybridization

For the detection of mRNA, fluorescence *in situ* hybridization (FISH) was performed using Invitrogen ViewRNA ISH (Tokushima Molecular Pathology Institute, Inc., Japan). The ViewRNA™ probe set of PTPδ (2620-3556, GenBank: NM_011211, Probe ID: VB1-17688-06) and VGluT2 (1335-2403, GenBank: NM_080853, Probe ID: VB1-3201379-06) were used. Fast red and Fast blue were prepared for the simultaneous detection of multiple mRNAs using FISH. Paraffin sections containing the medulla oblongata from P7, P14, P21, and 2-month-old mice were hybridized using a Probe set and Fast blue and Fast red liquid substrates. Hoechst was used for fluorescent nuclear counterstaining.

Behavioral tests

Behavioral analyses were performed using 2–4-month-old male and female mice as described previously (Uesaka et al., 2018). In the open field test, mice were placed in an open field box [50 cm × 50 cm × 40 cm (W × D × H) size] for 10 min and their behaviors were recorded using the video camera attached to the ceiling of the experimental room to assess the activity of mice. The total distance traveled was automatically analyzed using the TimeOF4 software (O'Hara & Co., Japan). The beam walking test was performed to assess motor coordination. Mice were placed on the origin of a columnar beam (thin beam; 1 cm diameter, thick beam; 2.8 cm diameter, 80 cm long, placed 70 cm above the floor) and habituated to walk on the beam and to enter the black goal box placed at the end of the beam before the trial. During this habituation, mice were placed on the middle of the beam and allowed to walk to the goal box five times. The number of slips until the mice reached the black

TABLE 1 Experimental details: number of mice, normality assessment and statistics.

Figures	Number of mice	Normality (Shapiro-Wilk test)	Statistical methods
Figure 1B	WT: 6 male mice, 5 female mice. KO: 4 male mice, 6 female mice	Yes	Student's *t*-test
Figure 1L	WT and KO 3 mice, each	No	Steel-Dwass test
Figure 1N	WT and KO 2 mice, each	No	Steel-Dwass test
Figures 2D, E	WT and KO 2 mice, each	Yes	Student's *t*-test
Figures 3E, F, L–N	WT and KO 2 mice, each	Yes	Student's *t*-test
Figures 3P, Q	WT and KO 2 mice, each	Yes	Student's *t*-test
Figures 4A–E	WT: 2 (P3-5), 7 (P8-10), 7 (P11-12), 4 (P13-15), 4 (P19-29) mice KO: 2 (P3-5), 5 (P8-10), 7 (P11-12), 5 (P13-15), 4 (P19-29) mice	N.A.	Mann-Whitney U test
Figure 4F	Same as Figures 4A–E	No	Mann-Whitney U test
Figures 5A–D	WT: 2 (P3-5), 7 (P8-10), 7 (P11-12), 4 (P13-15), 4 (P19-29) mice KO: 2 (P3-5), 5 (P8-10), 7 (P11-12), 5 (P13-15), 4 (P19-29) mice	N.A.	Mann-Whitney U test
Figure 5E	Same as Figures 5A–D	No	Mann-Whitney U test
Figures 6B, C	WT and KO 3 mice, each	Yes	Student's *t*-test
Figure 6G	WT and KO 3 mice, each	Yes	Two-way repeated measures ANOVA
Figure 6E	WT: 4 mice, KO: 3 mice	Yes	Two-way repeated measures ANOVA
Figure 7D	Ctrl: 6 mice, KD: 4 mice, RES: 4 mice	N.A.	Mann-Whitney U test
Figure 7E	Same as Figure 7D	Yes	Student's *t*-test
Figures 8B, D, H	Same as Figure 1B	Yes	Student's *t*-test
Figure 8F	Same as Figure 1B	Yes	Two-way repeated measures ANOVA

goal box was counted. The rotarod test was carried out to assess motor coordination and motor learning. Mice were placed on a stationary rotarod (model LE8205, Panlab, Spain) for 3 consecutive days with five trials per day with a 30-min break in-between. The rotarod was accelerated linearly from 4 rpm to 40 rpm over 300 s in each trial. The time from the start of rotation until the mice fell was measured. The coat hanger test was performed to evaluate limb strength and coordination (Jang et al., 2019). Mice were hung on the middle of a coat hanger and allowed to climb toward the top. The score was determined by the position that the mice could reach within 60 s.

Quantification and statistical analysis

Data were represented as the mean ± SEM. Normality was checked for individual datasets by using the Shapiro–Wilk test. To compare two independent datasets, the Student's *t*-test was used when both datasets showed normal distribution, and the Mann–Whitney U-test was conducted when either of the two did not show normal distribution. For multiple comparisons, two-way repeated measures ANOVA was used for datasets with normal distributions, and the Steel–Dwass test was used for those without normal distributions. The statistics used for comparing datasets shown in individual figure panels are summarized in Table 1. A significant difference between the groups was determined when the *p*-value was <0.05. All statistical analyses were performed using EZR (Kanda, 2013).

Results

Impaired CF synapse formation and diminished CF synaptic territory during development in PTPδ KO mice

As reported previously (Uetani et al., 2000), PTPδ KO mice were significantly lower in their body weights than WT mice (Male WT: 26.7 ± 0.9 g, Male KO: 17.3 ± 1.7 g, Female WT: 17.4 ± 0.4 g, Female KO: 16.3 ± 1.6 g) due to insufficient food intake (Figures 1A, B). We first examined the gloss morphology of the cerebellum at P30. The organization and structure of cerebellar lobules appeared normal, but the degree of CF innervation was apparently reduced in PTPδ KO mice (Figures 1C–H). Since the cerebellum has a compartmental structure depending on expression patterns of several marker molecules of PCs such as Aldolase C (Aldoc) and PLCβ3/4 (Kano et al., 1998; Sugihara and Quy, 2007), we scrutinized CF innervation in PCs with Aldoc

10.3389/fnmol.2023.1206245

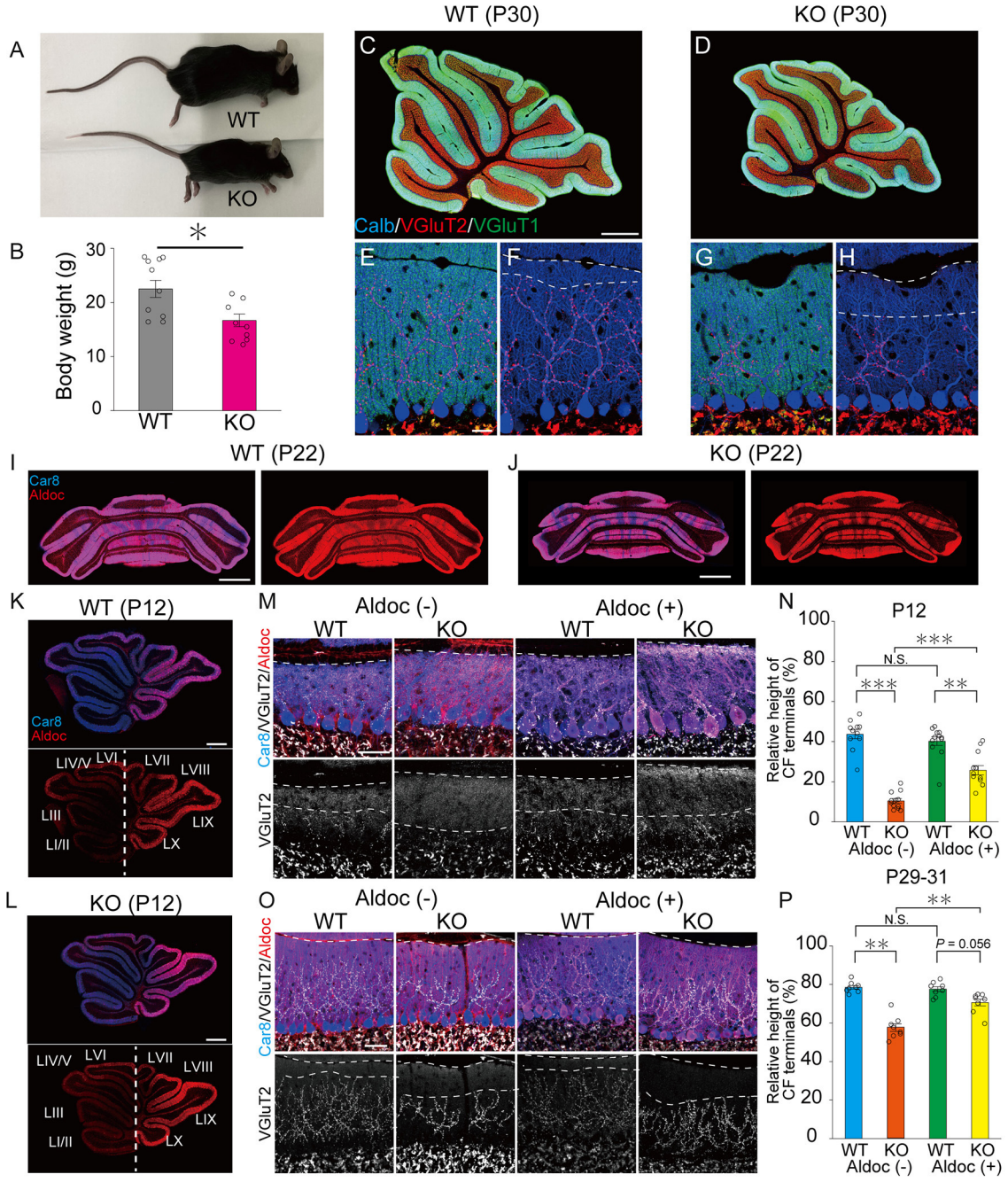

FIGURE 1
PTPδ promotes the extension of CF synaptic territory along PC dendrites predominantly in Aldoc (–) PCs. **(A)** Representative photos of a young adult WT and PTPδ KO mouse at P60. **(B)** Body weight of WT (gray) and PTPδ KO (purple) mice from 2 to 4 months of age. WT (male $n = 6$, female $n = 5$) and PTPδ KO (male $n = 4$ female $n = 6$) mice from 2 to 4 months of age. **(C–H)** Gross morphology of the cerebellar vermis with immunofluorescence for the PC marker Calbindin (Calb) (blue), the CF terminal marker VGluT2 (red), and the PF terminal marker VGluT1 (green) in a WT and a PTPδ KO mouse at P30. Scale bars, 200 μm **(C, D)** and 20 μm **(E–H)**. **(I–L)** Gross morphology of the coronal (P22) and sagittal (P12) sections of the cerebellum with immunofluorescence for Car8 (blue), a PC marker, and Aldoc (red) from a WT and a PTPδ KO mouse. Scale bars, 1,000 μm **(I, J)** and 500 μm **(K, L)**. **(M–P)** Confocal images of the cerebellum showing immunoreactivities of Car8 (blue), Aldoc (red), and VGluT2 (white) in WT and PTPδ KO mice at P12 **(M)** and at P29-31 **(O)**. Scale bar, 20 μm. The relative height of VGluT2-labeled CF terminals to the molecular layer thickness for WT [N; Aldoc (–) $n = 11$ regions, Aldoc (+) $n = 12$ regions, from 3 mice at P12 P; Aldoc (–) $n = 8$ regions, Aldoc (+) $n = 8$ regions from 2 mice at P29-31] and PTPδ KO [N; Aldoc (–) $n = 12$ regions, Aldoc (+) $n = 12$ regions, from 3 mice at P12. P; Aldoc (–) $n = 8$ regions, Aldoc (+) $n = 8$ regions from 2 mice at P29-31]. $^*P < 0.05$, $^{**}p < 0.01$, $^{***}P < 0.001$ by the Steel–Dwass test. Error bars in the graphs represent ± SEM.

expression [Aldoc (+) PCs] and those without [Aldoc (–) PCs] in WT and PTPδ KO mice at P12 and P29-31. We found that the Aldoc expression pattern was not altered in PTPδ KO mice at P12 and P22 (Figures 1I–L), indicating that the lack of PTPδ does not affect Aldoc expression in PCs. Then, we examined whether the effects of PTPδ deletion were different between Aldoc (+) and

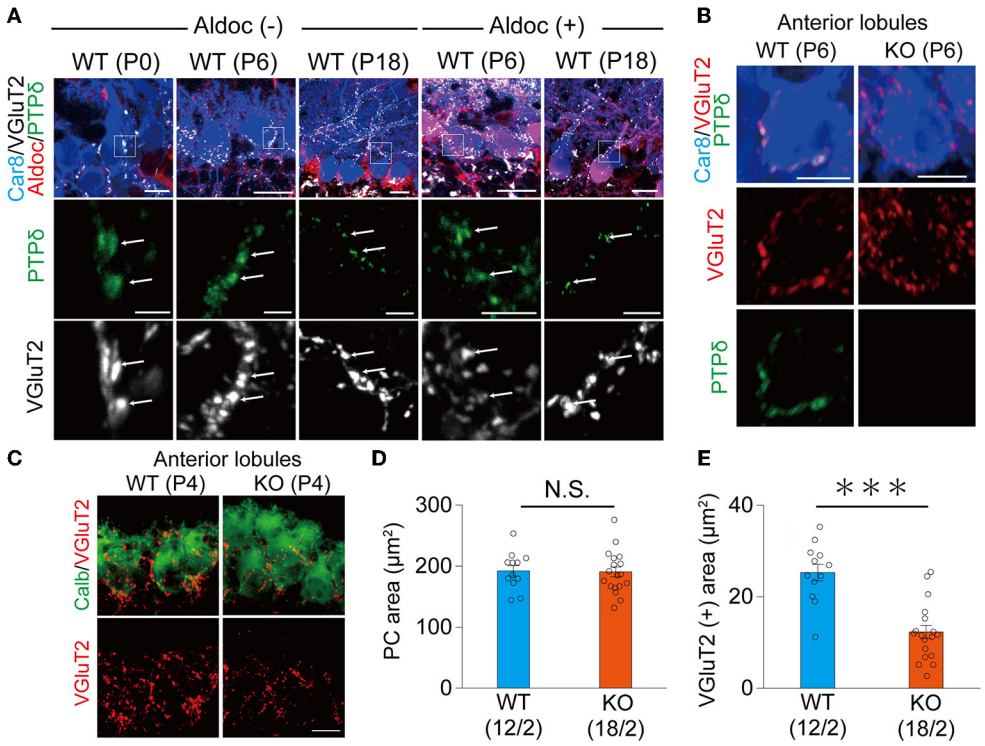

FIGURE 2
PTPδ protein is localized at the CF-PC synapse during perinatal and postnatal periods and is involved in CF synapse formation. **(A)** Confocal images of the cerebellum at P0, P6, and P18 showing immunoreactivities of Car8 (blue), Aldoc **(red)**, VGluT2 **(white)**, and PTPδ (green) in Aldoc (-) Purkinje cells **(left)** and Aldoc (+) Purkinje cells **(right)**. Scale bar (upper), 10 μm for P0, 20 μm for P6 and P18; Scale bar (lower), 5 μm. White arrows indicate the colocalization of PTPδ and VGluT2. **(B)** Confocal images of immunofluorescence for PTPδ (green), Car8 (blue), and VGluT2 (red) in a WT (upper) and a PTPδ KO (lower) mouse cerebellum at P6. Scale bars, 10 μm. **(C)** Confocal images of anterior lobules of a WT **(left)** and a PTPδ KO **(right)** mouse cerebellum at P4 showing immunoreactivities of Calbindin (green) (green) and VGluT2 (red). Scale bar, 10 μm. **(D, E)** Bar graphs for PC area (μm^2) **(D)** and VGluT2 positive area (μm^2) **(E)** in WT (blue columns) and PTPδ KO (orange columns) mice. Sample numbers of cells/mice are shown in parentheses. Error bars in the graphs represent ± SEM. ***$P < 0.001$ by Student's *t*-test.

Aldoc (–) PCs. We found that the territory of CF innervation over PC dendrites was significantly reduced in PTPδ KO mice in both Aldoc (+) and Aldoc (–) PCs at P12 and P29-31 when compared to WT mice (Figures 1M–P). We also found that the CF innervation territory in Aldoc (–) PCs was significantly reduced when compared to Aldoc (+) PCs in PTPδ KO mice, while the extent of CF innervation was similar between Aldoc (+) and Aldoc (–) PCs in WT mice (Figures 1M–P).

It is reported that the expression of Aldoc is seen between P5 and P8, and a characteristic zonal pattern of expression is observed between P12 and P17 (Fujita et al., 2014). Therefore, we examined the localization of PTPδ in WT mouse cerebellum at P0, at the beginning of (P6), and at a time of clear expression (P18) of Aldolase C. Our immunohistochemical (IHC) analysis revealed that PTPδ immunoreactivity is colocalized with VGluT2, on soma and dendrites of PCs from P0 to P18 in both of Aldoc (–) and (+) PCs (Figure 2A) and found no PTPδ immunoreactivity in PTPδ KO cerebellum (Figure 2B). These results suggest that the PTPδ protein is localized at CF-PC synapses during early postnatal development from P0. We then investigated whether PTPδ is involved in CF synapse formation during the perinatal period. We found that there was no difference in the area of the cell body of PC, but the area of VGluT2 in PTPδ KO mice was smaller than in WT mice in anterior lobules (1/2-3) (Figures 2C–E), indicating CF synapses in PTPδ KO mice is reduced or/and smaller than in WT mice. Taken together, these results indicate that PTPδ is involved in CF synapse formation during the perinatal period and extension of CF innervation territory along PC dendrites and the effect of PTPδ deletion for CF translocation is more prominent in Aldoc (–) PCs than in Aldoc (+) PCs during postnatal development.

The size of the CF synapse was smaller in PTPδ KO mice during postnatal development in the anterior cerebellum

LAR-RPTPs have been reported to contribute to the presynaptic formation by accumulating active zone proteins such as calcium/calmodulin-dependent serine kinase (CASK) and RIM1/2 via liprin-α (Serra-Pagès et al., 1998; Spangler et al., 2013). We investigated whether PTPδ is involved in presynaptic formation via the accumulation of synapse protein at CF-PC synapses. We performed immunostaining with VGluT2 and RIM1/2, an active zone marker, to determine the density of VGluT2, the area of VGluT2, and the area of overlap between

10.3389/fnmol.2023.1206245

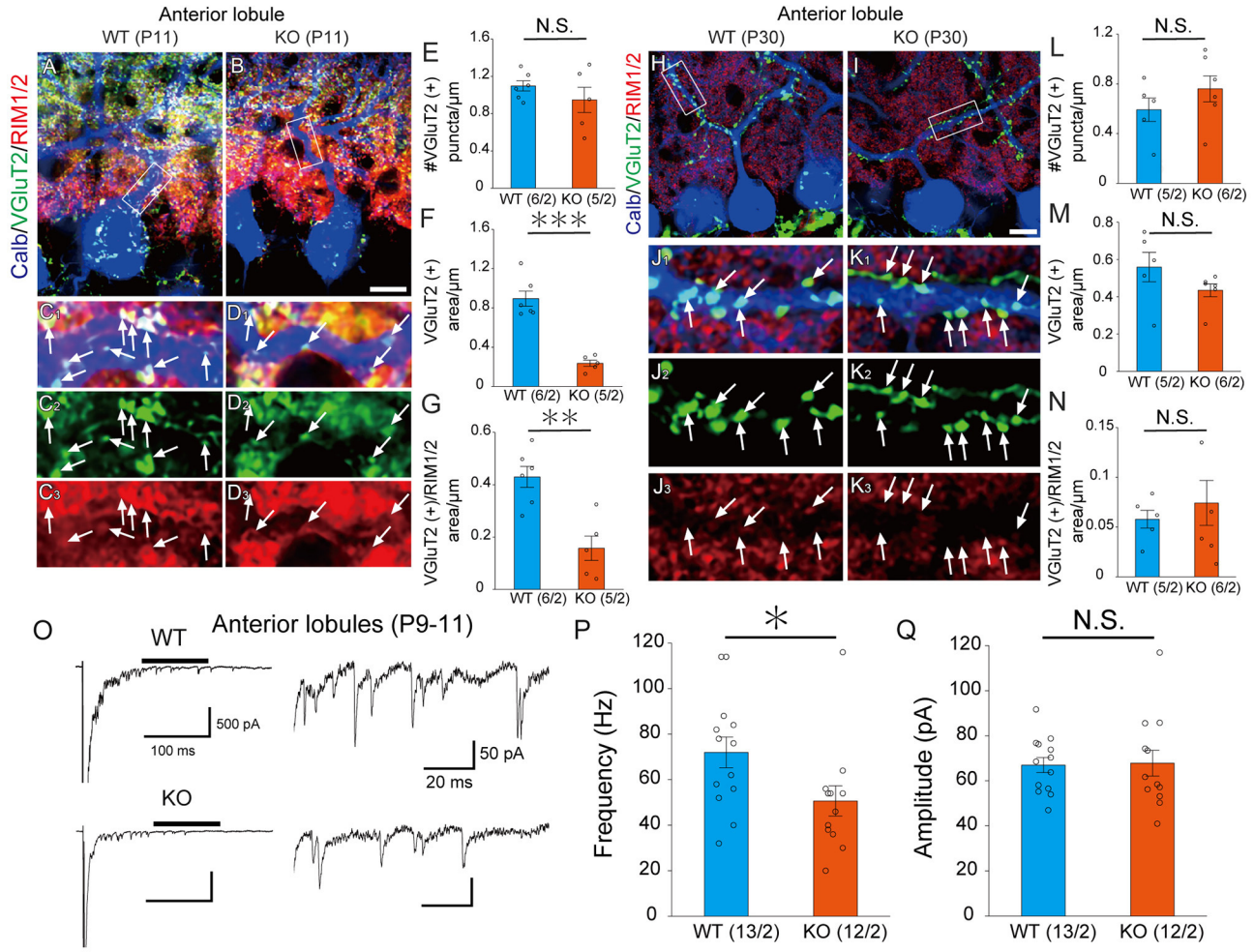

FIGURE 3
PTPδ KO is required for normal presynapse development. **(A–D)** Confocal images of an anterior lobule (Lobule III) of a WT **(left)** and a PTPδ KO **(right)** mouse cerebellum at P11 showing immunoreactivities of Calbindin (blue), VGluT2 (green), and RIM1/2 (red), a maker for the active zone. The rectangular areas demarked with white lines in **(A, B)** are enlarged in **(C_1–C_3, D_1–D_3)**, respectively. Scale bar, 20 μm. White arrows indicate overlapping areas of VGluT2 and RIM1/2. **(E–G)** Bar graphs showing **(E)** Number of VGluT2 puncta/μm, **(F)** VGluT2 positive area/μm, and **(G)** VGluT2 positive area/overlapping area of VGluT2 and RIM1/2 area/μm in WT (blue) and PTP KO (orange) mice. Sample numbers of regions/mice are shown in parentheses. $^{**}P < 0.01$, $^{***}P < 0.001$ by Student's *t*-test. Error bars in the graphs represent ± SEM. **(H–N)** Similar to **(A–G)** but for data at P30. **(O)** Representative traces of asynchronous quantal EPSCs were elicited by stimulating the strongest CF in an anterior lobule of a WT and a PTPδ KO mouse at P9-11 in the Sr^{2+}-containing extracellular solution. Holding potential was −70 mV. Scale bars, 100 ms and 500 pA **(left)** and 20 ms and 50 pA **(right)**. **(P, Q)** Histograms showing **(P)** the average frequency and **(Q)** amplitude of quantal EPSCs in WT (blue) and PTP KO (orange). Sample numbers of PCs/mice are shown in parentheses. $^{*}P < 0.05$ by Student's *t*-test. Error bars in the graphs represent ± SEM.

VGluT2 and RIM1/2 on PC dendrites at P11 and P30 (Figures 3A–D, H–K). In anterior lobules, there was no difference in the density of VGluT2 between WT and PTPδ KO mice (Figure 3E), but the size of VGluT2 and the area of overlap between VGluT2 and RIM1/2 in PTPδ KO mice were smaller than WT mice (Figures 3F, G). We also found no difference between WT and PTPδ KO mice at P30 in each parameter (Figures 3H–N). We analyzed quantum EPSCs (qEPSCs) elicited by stimulating the strongest CFs in Sr^{2+}-containing external solution (Hashimoto and Kano, 2003) (Figure 3O). The frequency of qEPSCs was lower in PTPδ KO mice than in WT mice at P9 to P11 (Figures 3O, P). However, there was no difference in the amplitude of qEPSCs (Figure 3Q). These results indicate that CF synapses are immature in PTPδ KO mice at P9 to P11 and the synaptic vesicle release sites may be small because of the low frequency of qEPSCs in the anterior cerebellum.

The number of CFs innervating individual PCs in PTPδ KO mice was decreased from the perinatal period to postnatal development

Our IHC analysis has revealed that PTPδ is localized at CF-PC synapses from P0 and is involved in CF synapse formation

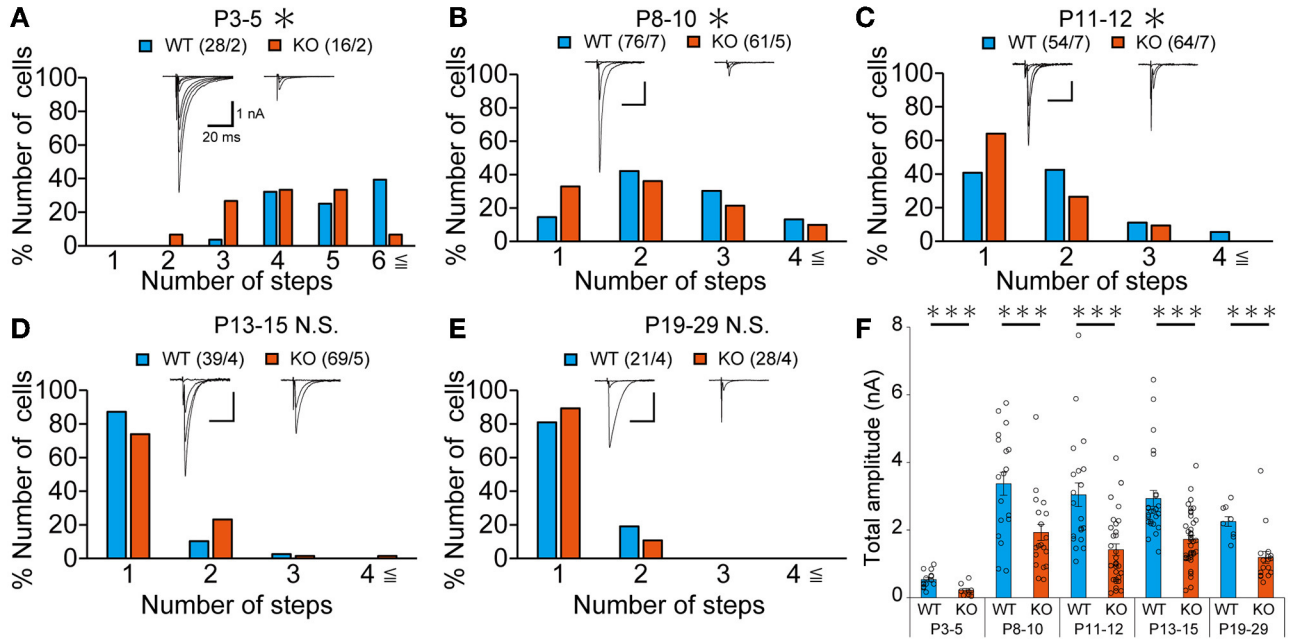

FIGURE 4
Transient acceleration of CF synapse elimination during P8 to P12 and persistent reduction of CF-EPSC amplitude in PCs of cerebellar anterior lobules of PTPδ KO mice. **(A–E)** Representative traces of CF-EPSC and summary histograms showing the number of discrete steps of CF-EPSCs in cerebellar anterior lobules of WT (blue) and PTPδ KO (orange) mice during postnatal development. Sample numbers of PCs/mice are shown in parentheses. The holding potential was −70 mV for P3-5 and −10 mV for P8-29. Scale bars, 20 ms and 1 nA. *$P < 0.05$ by the Mann–Whitney U-test. **(F)** Developmental changes in the total amplitude of CF-EPSCs in individual PCs of WT (blue) and PTPδ KO (orange) mice. The total amplitudes of CF-EPSCs including all CF-EPSC steps were averaged at each postnatal age. ***$P < 0.001$ by the Mann–Whitney U-test. Error bars represent ± SEM.

from P4 before Aldoc expression (Figure 2). We then analyzed CF synaptic inputs and CF innervation of PCs in anterior lobules of neonatal PTPδ KO mice electrophysiologically in acute cerebellar slices during the perinatal stage. We found that PCs in anterior lobules of PTPδ KO mice were innervated by significantly fewer CFs than those of WT mice at P3-5 (Figure 4A), implicating that CF innervation is reduced in PCs in anterior lobules of PTPδ KO mice. To investigate whether PTPδ is involved in CF synapse elimination, we next examined the number of CFs innervating individual PCs in WT and PTPδ KO mice during postnatal development (P8-29) after Aldoc expression. In addition, to examine the effect of PTPδ on CF synapse elimination in Aldoc (+) and (–) PCs, we analyzed CF innervation in anterior and posterior lobules (8-10) where Aldoc (–) and (+) PCs were predominant, respectively. PCs in anterior lobules of PTPδ KO mice had fewer CFs than those of WT mice from P8 to P12 (Figures 4B, C). In contrast, PCs in posterior lobules of PTPδ KO mice had fewer CFs than those of WT mice transiently at P13-15 (Figure 5C). There was no difference in the number of CFs innervating each PC in anterior lobules from P13 to P29 and in posterior lobules at P19-27 (Figures 4D, E, 5D). These results suggest that PTPδ is required for CF synapse elimination to proceed normally during limited developmental periods without causing persistent abnormality in the CF innervation pattern after P19.

The total amplitude of CF-EPSC in PTPδ KO mice was decreased during perinatal to postnatal development

To determine the role of PTPδ in CF to PC synaptic transmission during postnatal development, we evaluated the strengths of CF synaptic inputs in PTPδ KO mice. We found that the total amplitude of CF-EPSCs in anterior lobules was significantly smaller in PTPδ KO mice than in WT mice from P3 to P29 (Figure 4F; Table 2). In contrast, while the total amplitude in posterior lobules was smaller also in PTPδ KO mice than in WT during P8-15, it recovered at P19-27 (Figure 5E; Table 3). We then determined the disparity ratio, which has been utilized to assess the relative difference among the strengths of multiple CF inputs (Hashimoto and Kano, 2003). The disparity ratio was unchanged in PTPδ KO mice when compared to WT during P8-30 in both anterior and posterior lobules (Tables 2, 3), indicating that PTPδ may equally affect synaptic inputs from the strongest and weaker CFs. We next compared paired-pulse plasticity that reflects the probability of neurotransmitter release from presynaptic terminals unless postsynaptic AMPA-type glutamate receptors are not saturated (Wadiche and Jahr, 2001). We found that the paired-pulse ratio (PPR) in PTPδ KO mice was smaller than that in WT mice in anterior lobules at P8-15 and in posterior lobules at P8-10 (Tables 4, 5). This

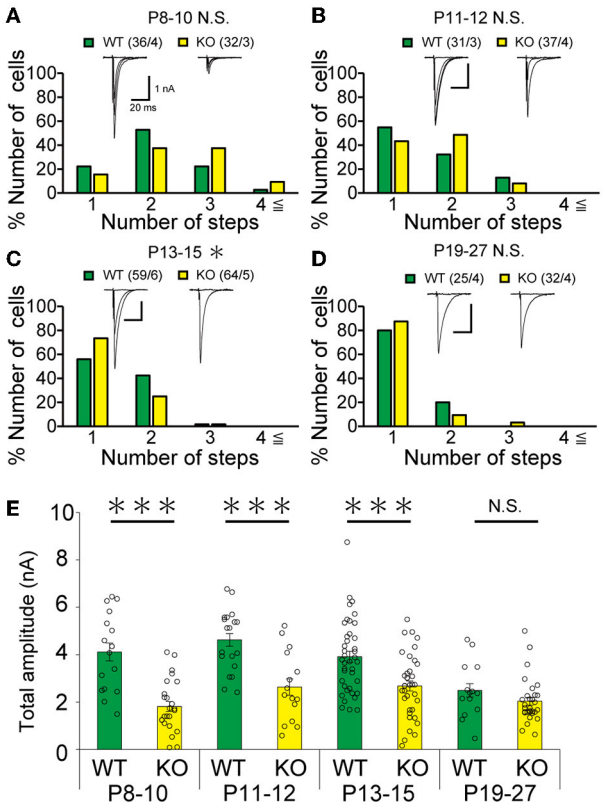

FIGURE 5
Transient acceleration of CF synapse elimination during P13 to P15 and reduction of CF-EPSC amplitude until P15 in PCs of cerebellar posterior lobules of PTPδ KO mice. **(A–D)** Similar to Figures 4B–E but for data from PCs in posterior lobules. Holding potential was −10 mV. Scale bars, 20 ms and 1 nA. *$p < 0.05$, ***$p < 0.001$ by the Mann–Whitney U-test. Error bars represent ± SEM. **(E)** Similar to Figure 4F but for data from PCs in posterior lobules. ***$P < 0.001$ by the Mann–Whitney U-test. Error bars represent ± SEM.

result may suggest that the release probability of CF synaptic terminals in PTPδ KO mice was higher than in WT mice. However, the degree of paired-pulse depression for the strongest CF input is usually underestimated with normal extracellular Ca^{2+} concentration. This is because the 1st pulse of CF stimulation induces multivesicular release of glutamate, causes saturation of postsynaptic AMPA receptors, and therefore the 1st EPSC is smaller than reality, whereas the 2nd pulse of CF stimulation does not induce postsynaptic AMPA receptor saturation (Hashimoto and Kano, 2003). Therefore, it is possible that the degree of paired-pulse depression of CF synaptic responses in PTPδ KO appears stronger than in WT mice presumably because the postsynaptic AMPA receptors may not be saturated in response to the 1st pulse of CF stimulation. In addition to the paired-pulse ratio, the decay time constant of CF-EPSC was shorter in PTPδ KO mice than in WT mice in both anterior and posterior lobules (Tables 4, 5), which may reflect the shorter electrotonic distance between the site of CF synapses in PC dendrites and the recording site in the soma presumably due to the impairment of CF translocation. Taken together, these results indicate that PTPδ is involved in multiple aspects of events required for normal CF to PC synaptic transmission.

Transient increase of PF-PC excitatory synaptic transmission at P12-13 in PTPδ KO mice

Previous studies have shown that inhibitory synaptic inputs to PCs (Nakayama et al., 2012) and abnormal PF-PC synapse formation have a significant influence on CF elimination (Hashimoto et al., 2001, 2009b, 2011; Ichikawa et al., 2002). We recorded the amplitude and frequency of miniature inhibitory postsynaptic currents (mIPSCs) in anterior lobules and found that the amplitude and frequency of mIPSCs were not different between WT and PTP KO mice during P9-12 (Figures 6A–C). We next recorded PF mediated-EPSCs (PF-EPSCs) in anterior lobules to investigate whether PTPδ is involved in normal PF synapse development. PF-EPSCs in PTPδ KO mice were increased in amplitude during P12-13 (Figures 6D, E), but they became normal during P28-30 (Figures 6F, G) when compared to WT mice. These results suggest that the lack of PTPδ transiently increases PF-PC excitatory transmission during the second postnatal week during which CF innervation was reduced.

Knockdown of PTPδ in CFs from P0-2 caused reduced CF innervation of PCs at P10-13

Since PTPδ is known to be a presynaptic organizer (Takahashi and Craig, 2013), we assume that PTPδ functions at CF synaptic terminals but not at postsynaptic PCs. Therefore, we investigated whether mRNA of PTPδ is expressed in the inferior olive, the origin of CFs, using FISH during postnatal to adult stages. We revealed that VGluT2-positive neurons in the inferior olive expressed PTPδ mRNA during early postnatal stages to adulthood (Figure 7A). Then, to examine whether PTPδ in CFs is involved in CF synaptic function and CF synapse development, we performed RNAi-mediated knockdown (KD) of PTPδ in CFs during postnatal development (Figure 7B). We found that PCs of PTPδ KD mice were innervated by fewer CFs than those of control (Ctrl) mice (Figures 7C, D), and the total amplitude of CF-EPSC in PTPδ KD mice tended to be decreased when compared to that in Ctrl mice (Figure 7E; Table 6) in anterior lobules at P10-13. These results are consistent with those of PTPδ KO mice (Figures 4B, C, F; Table 2). The effects of PTPδ KD in CFs on most parameters were rescued by co-expression of a miRNA-resistant PTPδ (PTPδ RES) (Figures 7C–E; Table 6), except the rise time and decay time constant of CF-EPSCs (Table 7). These results suggest that PTPδ in CFs is required for CF synapse formation, augmentation of CF synaptic strength, and possibly maintenance and strengthening of CF innervation during postnatal cerebellar development.

Young adult PTPδ KO mice showed motor dysfunction in several behavioral tests

Finally, we examined whether the lack of PTPδ resulted in any abnormality in cerebellum-related behaviors. In the open field

TABLE 2 Total amplitudes and disparity parameters for CF-EPSCs in cerebellar anterior lobules (1/2-3) of WT and PTPδ KO mice.

Anterior lobule (1-3)	Total amplitude (nA)	Disparity ratio	Disparity index
WT (P8-10)	3.37 ± 0.36 ($n = 18$)	0.56 ± 0.09 ($n = 12$)	0.52 ± 0.12 ($n = 12$)
PTPδ KO (P8-10)	1.93 ± 0.25 ($n = 20$)**	0.52 ± 0.08 ($n = 11$)	0.52 ± 0.11 ($n = 11$)
WT (P11-12)	3.04 ± 0.37 ($n = 20$)	0.5 ± 0.09 ($n = 4$)	0.5 ± 0.11 ($n = 4$)
PTPδ KO (P11-12)	1.42 ± 0.18 ($n = 33$)***	0.39 ± 0.1 ($n = 5$)	0.71 ± 0.17 ($n = 5$)
WT (P13-15)	2.63 ± 0.22 ($n = 19$)	0.44 ± 0 ($n = 1$)	0.71 ± 0 ($n = 1$)
PTPδ KO (P13-15)	1.72 ± 0.12 ($n = 41$)***	0.41 ± 0.08 ($n = 10$)	0.78 ± 0.12 ($n = 9$)
WT (P21-29)	2.25 ± 0.16 ($n = 8$)	0.07 ± 0.02 ($n = 2$)	1.22 ± 0.05 ($n = 2$)
PTPδ KO (P19-29)	1.26 ± 0.21 ($n = 14$)**	0.3 ± 0 ($n = 1$)	0.77 ± 0 ($n = 1$)

CF-EPSC amplitudes were measured at holding potential of −10 mV. Disparity parameters were calculated with the formulas described in Methods. *P*-value was determined by Mann-Whitney U-test. All data are expressed as mean ± SEM.
** $P < 0.01$; *** $P < 0.001$.

TABLE 3 Total amplitudes and disparity parameters for CF-EPSCs in cerebellar posterior lobules (1/2-3) of WT and PTPδ KO mice.

Posterior lobule (8-10)	Total amplitude (nA)	Disparity ratio	Disparity index
WT (P8-10)	4.11 ± 0.4 ($n = 16$)	0.54 ± 0.09 ($n = 11$)	0.49 ± 0.1 ($n = 11$)
PTPδ KO (P8-10)	1.81 ± 0.21 ($n = 25$)***	0.49 ± 0.05 ($n = 17$)	0.57 ± 0.07 ($n = 17$)
WT (P11-12)	4.77 ± 0.27 ($n = 22$)	0.34 ± 0.09 ($n = 4$)	0.73 ± 0.18 ($n = 4$)
PTPδ KO (P11-12)	2.45 ± 0.34 ($n = 14$)***	0.46 ± 0.07 ($n = 7$)	0.58 ± 0.11 ($n = 7$)
WT (P13-15)	3.91 ± 0.24 ($n = 40$)	0.42 ± 0.08 ($n = 15$)	0.67 ± 0.11 ($n = 15$)
PTPδ KO (P13-15)	2.68 ± 0.22 ($n = 36$)***	0.36 ± 0.1 ($n = 6$)	0.75 ± 0 ($n = 6$)
WT (P21-29)	2.49 ± 0.3 ($n = 14$)	0.03 ± 0 ($n = 1$)	1.34 ± 0 ($n = 1$)
PTPδ KO (P19-27)	2.04 ± 0.17 ($n = 30$)	0.25 ± 0 ($n = 1$)	0.84 ± 0 ($n = 1$)

Data are measured and described similarly to Table 1.
*** $P < 0.001$.

test, there was no difference in total distance traveled between WT and PTPδ KO mice (Figures 8A, B). In the beam walking test, the average number of slips on the thick beam was larger in PTPδ KO mice than in WT mice, whereas those on the thin beam were not significantly different between the genotypes (Figures 8C, D), indicating impaired motor coordination and balance in PTPδ KO mice. In the rotarod test, PTPδ KO mice exhibited reduced latency to fall compared with WT, suggesting impaired motor coordination and/or motor learning (Figures 8E, F). We performed the coat hanger test to evaluate motor coordination. For the coat hanger test, mice were hung in the middle of the coat hanger (score 0) and allowed to climb to the top (score 6) within 60 s. The score was determined by the position where mice could reach (Figure 8G). The average score of the hanger test for PTPδ KO mice was lower than that for WT mice (Figure 8H), suggesting impaired motor coordination and/or limb strength in PTPδ KO mice. Taken together, these results show that the lack of PTPδ causes deficits in motor coordination and motor learning.

Discussion

Presynaptic PTPδ functions as a synapse organizer for CF-PC synapse formation

We demonstrated that PTPδ mRNA was expressed in the inferior olive and PTPδ protein was localized at CF-PC synapses at least from P0 in WT mice. PCs of PTPδ KO mice were innervated by fewer CFs than those of WT mice during the perinatal period of P3-5, and CF-specific KD of PTPδ from P0-2 yielded the reduced CF innervation at P10-12. These results suggest that presynaptic PTPδ may act as a synapse organizer for CF-PC synapse formation during the perinatal period before CF synapse elimination.

A previous study reported that global deletion of all neurexins (NRXN1, 2, and 3), which are known as presynaptic organizers, from CFs caused a decrease in the CF-EPSC amplitude and reduction in the height of CF terminal along PC dendrites at P24 (Chen et al., 2017). While these phenotypes are similar to those induced by PTPδ deletion, contributions of neurexins in CF synapse formation and possible lobule differences in their effects were not investigated (Chen et al., 2017). It remains to be clarified whether neurexins and PTPδ influence the formation, development, elimination, and maintenance of CF to PC synapses independently from each other or by sharing common molecules and mechanisms.

Although several trans-synaptic adhesion molecules have been identified to contribute to CF-PC synapse maintenance or elimination including Sema3A-PlxnA4, Sema7A-PlxnC1/ItgB1, Sort1-progranulin, BDNF-TrkB, and C1q1-Bai3 (Uesaka et al., 2014, 2018; Kakegawa et al., 2015; Choo et al., 2017), specific synaptic molecules involved in the formation and/or maintenance of CF synapses during perinatal stages or synaptic molecules with differential functions in cerebellar lobules related to the

TABLE 4 Electrophysiological parameters of CF-EPSCs in cerebellar anterior lobules (1/2-3) of WT and PTPδ KO mice.

Anterior lobule (1-3)	CF group	Amplitude (nA)	Paired pulse ratio (interval, 50 ms)	10–90% rise time (ms)	Decay time constant (ms)	*n*
WT (P8-10)	CF-mono	3.13 ± 0.65	0.5 ± 0.03	0.74 ± 0.09	4.6 ± 0.81	6
	CF-multi-s	2.13 ± 0.18	0.47 ± 0.03	0.51 ± 0.04	4.76 ± 0.4	12
	CF-multi-w	1.03 ± 0.2	0.51 ± 0.03	0.64 ± 0.07	4.33 ± 0.5	18
PTPδ KO (P8-10)	CF-mono	1.48 ± 0.28	0.34 ± 0.03*	0.82 ± 0.14	4.58 ± 1.18	9
	CF-multi-s	1.52 ± 0.27*	0.38 ± 0.04	0.52 ± 0.04	3.89 ± 0.35	11
	CF-multi-w	0.57 ± 0.09	0.37 ± 0.06	0.48 ± 0.05	3.14 ± 0.24	14
WT (P11-12)	CF-mono	3.69 ± 0.72	0.58 ± 0.02	0.5 ± 0.03	5.11 ± 0.44	15
	CF-multi-s	2.55 ± 0.36	0.55 ± 0.07	0.54 ± 0.04	4.01 ± 0.48	4
	CF-multi-w	1.37 ± 0.37	0.55 ± 0.03	0.48 ± 0.03	3.28 ± 0.43	4
PTPδ KO (P11-12)	CF-mono	1.36 ± 0.21***	0.46 ± 0.02***	0.44 ± 0.02	2.11 ± 0.14***	28
	CF-multi-s	1.31 ± 0.44	0.39 ± 0.05	0.55 ± 0.02	2.35 ± 0.19*	5
	CF-multi-w	0.35 ± 0.08*	0.51 ± 0.05	0.48 ± 0.02	2.18 ± 0.17	7
WT (P13-15)	CF-mono	2.42 ± 0.08	0.69 ± 0.02	0.45 ± 0.03	6.27 ± 0.3	18
	CF-multi-s	3.41 ± 0	0.69 ± 0	0.56 ± 0	4.66 ± 0	1
	CF-multi-w	1.52 ± 0.29	0.64 ± 0.04	0.48 ± 0.01	4.59 ± 0.69	2
PTPδ KO (P13-15)	CF-mono	1.68 ± 0.14***	0.58 ± 0.02***	0.44 ± 0.02	3.45 ± 0.3***	31
	CF-multi-s	1.44 ± 0.21	0.49 ± 0.04	0.47 ± 0.02	3.06 ± 0.27	10
	CF-multi-w	0.39 ± 0.08*	0.44 ± 0.07	0.67 ± 0.11	2.34 ± 0.44	13
WT (P21-29)	CF-mono	2.12 ± 0.17	0.75 ± 0.02	0.46 ± 0.04	6.82 ± 0.6	6
	CF-multi-s	2.47 ± 0.26	0.76 ± 0.04	0.46 ± 0.02	6.9 ± 0.25	2
	CF-multi-w	0.17 ± 0.03	0.5 ± 0.08	0.51 ± 0.1	3.81 ± 1.08	2
PTPδ KO (P19-29)	CF-mono	1.19 ± 0.22***	0.72 ± 0.01	0.5 ± 0.05	5.94 ± 0.89	13
	CF-multi-s	1.69 ± 0	0.61 ± 0	0.47 ± 0	5 ± 0	1
	CF-multi-w	0.4 ± 0	0.7 ± 0	0.45 ± 0	2.21 ± 0	1

Amplitudes were measured at holding potential of −10 mV. Rise time was defined as the time required for the membrane current to change from 10 to 90% of the maximal CF-EPSC amplitude. PPR (Paired-pulse ratio) was defines as the relative portion of the second EPSC amplitude to the first one with the inter-stimulus interval of 50 ms. The decay time constant was obtained by fitting the EPSC decay with a single exponential. *P*-value was determined by Mann-Whitney U-test. All data are expressed as mean ± SEM.
*$P < 0.05$; ***$P < 0.001$.

Aldoc expression are yet to be identified. Even in mice with PC-selective deletion of P/Q type voltage-gated Ca^{2+} channels (PQ-VDCCs), which are known to cause the most severe impairments in CF synapse elimination processes including CF-PC synapse strengthening, CF translocation, and CF synapse elimination, the initial CF-PC synapse formation at P4-6 appears normal (Hashimoto et al., 2011). Therefore, PTPδ is thought to be the first identified presynaptic molecule involved in CF-PC synapse function and/or maintenance during the perinatal period before the sequential events of CF synapse elimination possibly in a manner independent of PQ-VDCCs in PCs and in predominantly Aldoc (–) PCs of anterior lobules.

PTPδ is required for proper CF-PC synaptic transmission and CF translocation

Synapse organizers induce synapse formation by promoting the accumulation of synaptic vesicles and the construction of active zones at presynaptic terminals and the formation of postsynaptic density at the postsynaptic membrane (Südhof, 2018). LAR-RPTPs have two tandem phosphatase domains in their intracellular domains to which several active zone proteins such as Liprin-α, Caskin, and Trio are known to bind directly (Debant et al., 1996; Serra-Pagès et al., 1998; Weng et al., 2011). Liprin-α plays a role in synaptic vesicle release and normal presynaptic output by regulating the dynamics of active zone proteins such as RIM and CASK (Spangler et al., 2013). We found that the synapse size was small and the RIM1/2 structure was obscured in PTPδ KO mice, suggesting that accumulation of active zone proteins by PTPδ is required for CF synaptic development during postnatal development.

Proper CF translocation and extension along PC dendrites are known to require PQ-VDCC-mediated Ca^{2+} flux into PCs (Hashimoto et al., 2011). Reduced CF translocation along PC dendrites is also seen in mice with PC-specific KO of TARPγ2 (Kawata et al., 2014), a major AMPA receptor auxiliary subunit in PCs. In this PC-specific TARPγ2 KO

TABLE 5 Electrophysiological parameters of CF-EPSCs in cerebellar posterior lobules (8-10) of WT and PTPδ KO mice.

Posterior lobule (8-10)	CF group	Amplitude (nA)	Paired pulse ratio (interval, 50 ms)	10–90% rise time (ms)	Decay time constant (ms)	*n*
WT (P8-10)	CF-mono	2.91 ± 0.57	0.44 ± 0.06	0.47 ± 0.06	4.76 ± 0.47	4
	CF-multi-s	2.63 ± 0.22	0.56 ± 0.02	0.43 ± 0.01	5.83 ± 0.4	12
	CF-multi-w	1.42 ± 0.22	0.56 ± 0.04	0.44 ± 0.04	4.96 ± 0.58	16
PTPδ KO (P8-10)	CF-mono	1.59 ± 0.47	0.51 ± 0.06	0.62 ± 0.06	3.12 ± 0.29***	8
	CF-multi-s	1.19 ± 0.15***	0.49 ± 0.02*	0.61 ± 0.03***	3.87 ± 0.26***	19
	CF-multi-w	0.47 ± 0.08***	0.57 ± 0.03	0.53 ± 0.03*	3.31 ± 0.19*	30
WT (P11-12)	CF-mono	4.44 ± 0.28	0.63 ± 0.02	0.45 ± 0.03	5.08 ± 0.29	18
	CF-multi-s	4.78 ± 0.51	0.63 ± 0.04	0.46 ± 0.04	5.88 ± 0.03	4
	CF-multi-w	1.46 ± 0.24	0.65 ± 0.03	0.44 ± 0.03	7.92 ± 1.99	4
PTPδ KO (P11-12)	CF-mono	2.6 ± 0.56*	0.55 ± 0.04	0.53 ± 0.03	5.32 ± 0.94	7
	CF-multi-s	1.56 ± 0.27*	0.44 ± 0.06	0.55 ± 0.03	5.63 ± 1.01	7
	CF-multi-w	0.65 ± 0.19*	0.49 ± 0.06	0.52 ± 0.04	4.12 ± 0.47	8
WT (P13-15)	CF-mono	3.97 ± 0.34	0.68 ± 0.01	0.44 ± 0.02	5.83 ± 0.34	25
	CF-multi-s	3.14 ± 0.26	0.6 ± 0.03	0.46 ± 0.03	6.82 ± 0.46	15
	CF-multi-w	1.17 ± 0.2	0.62 ± 0.03	0.41 ± 0.03	4.99 ± 1.11	15
PTPδ KO (P13-15)	CF-mono	2.39 ± 0.22***	0.64 ± 0.02	0.48 ± 0.02	5.22 ± 0.29	30
	CF-multi-s	3.03 ± 0.35	0.67 ± 0.04	0.42 ± 0.04	4.97 ± 0.6	6
	CF-multi-w	0.93 ± 0.23	0.54 ± 0.05	0.41 ± 0.03	3 ± 0.51	7
WT (P21-29)	CF-mono	2.33 ± 0.28	0.67 ± 0.03	0.51 ± 0.03	4.84 ± 0.32	13
	CF-multi-s	4.52 ± 0	0.7 ± 0	0.38 ± 0	4.22 ± 0	1
	CF-multi-w	0.12 ± 0	0.31 ± 0	0.35 ± 0	11.4 ± 0	1
PTPδ KO (P19-27)	CF-mono	2.05 ± 0.17	0.66 ± 0.01	0.47 ± 0.02	4.53 ± 0.29	29
	CF-multi-s	1.4 ± 0	0.65 ± 0	0.45 ± 0	4.06 ± 0	1
	CF-multi-w	0.35 ± 0	0.51 ± 0	0.44 ± 0	1.95 ± 0	1

Data are presented similarly to Table 3.
*$P < 0.05$; ***$P < 0.001$.

mouse, CF-EPSCs are small in amplitude due to the reduction of AMPAR-mediated currents leading to a decrease in PQ-VDCC-mediated Ca^{2+} flux into PCs during CF activity (Kawata et al., 2014). Hence, these results suggest that the reduction of CF synaptic inputs in PTPδ KO mice also causes diminished CF translocation and extension along PC dendrites due to the reduction of Ca^{2+} influx into PCs. In line with this notion, the impairment of CF translocation in Aldoc (+) PCs of PTPδ KO mice at P29-31 was relatively milder than in Aldoc (–) PCs, which may ascribe at least partially to the recovery of reduced CF-EPSC amplitude in Aldoc (+) PCs after P15 to P19-27. However, another possibility remains that PTPδ may directly regulate CF translocation and extension along PCs irrespective of the activity of PCs.

PTPδ is required for CF-PC synapse maintenance and is involved indirectly in PF synapse development

Our electrophysiological data showed reduced multiple CF innervation of PCs in PTPδ KO mice at P8-12 in anterior lobules and at P13-15 in posterior lobules, which corresponded to the early (P7-11) and late phases (P12-17) of CF elimination (Hashimoto et al., 2009b). In addition, the CF-specific PTPδ KD, which was caused by the injection of the lentivirus for PTPδ KD into the inferior olive after perinatal CF synapse formation, caused reductions in multiple CF innervations of PCs during P10-13. These results suggest that PTPδ contributes to the maintenance of CF-PC synapses and to antagonizing CF elimination, although the reduced multiple CF innervation in Aldoc (–) PCs during P8-12

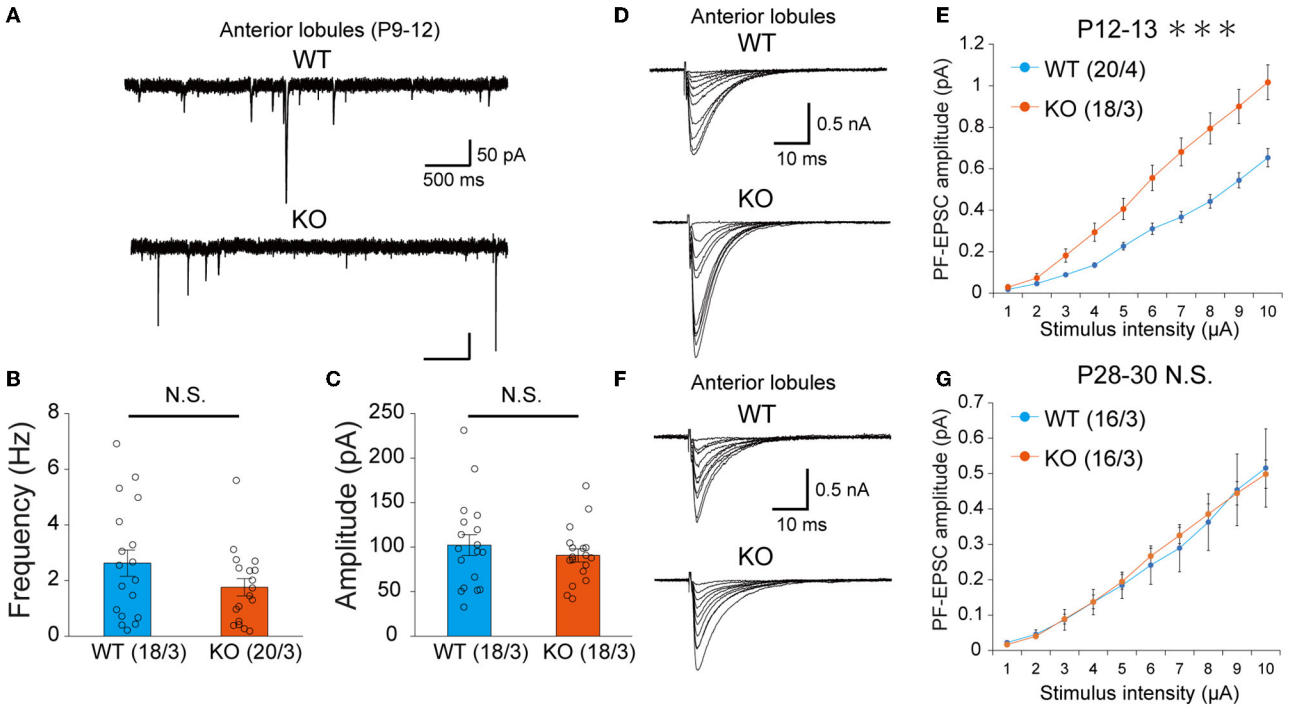

FIGURE 6
Transient increase of PF-PC excitatory synaptic transmission at P12-13 but normalization at P28-30 in PTPδ KO mice. **(A)** Representative traces of mIPSC recorded from a WT (top, P11) and a PTPδ KO (bottom, P12) mouse. Vh was −70 mV. Scale bars, 500 ms and 50 pA. **(B, C)** Bar graphs showing **(B)** the average mIPSC frequency and **(C)** the average mIPSC amplitude in WT (blue) and PTP KO (orange) mice at P9-12. Sample numbers of cells/mice are shown in parentheses. Error bars in the graphs represent ± SEM. **(D)** Representative traces of PF-EPSCs recorded from a WT (top, P12) and a PTPδ KO mouse (bottom, P12). Vh was −70 mV. Scale bars, 10 ms and 500 pA. **(E)** Input–output curve of PF-EPSCs in WT ($n = 12$) and PTPδ KO mice ($n = 12$) at P12-13 with stimulus intensities from 1 to 10 μA. Vh was −70 mV. A significant difference was observed between WT and PTPδ KO mice (Repeated-measures ANOVA: factor genotype, $P = 0.0003555$; factor stimulus intensity, $P < 2.2e\text{-}16$; interaction, genotype ×stimulus intensity, $P = 2.2e\text{-}16$). Sample numbers of cells/mice are shown in parentheses. ***$P < 0.001$. **(F)** Representative traces of PF-EPSCs recorded from a WT mouse (top, P28) and a PTPδ KO mouse (bottom, P28). Vh was −70 mV. Scale bars; 10 ms and 500 pA. **(G)** Input–output curve of PF-EPSCs in WT ($n = 12$) and PTPδ KO mice ($n = 11$) at P28-30 with stimulus intensities from 1 to 10 μA. Vh was −70 mV. No significant difference was observed between WT and PTPδ KO mice (Repeated-measures ANOVA: factor genotype, $P = 0.8857$; factor stimulus intensity, $P < 2.2e\text{-}16$; interaction, genotype × stimulus intensity, $P = 0.9885$). Sample numbers of cells/mice are shown in parentheses.

might be attributable at least partially to the impaired CF synapse formation during the perinatal period.

The acceleration of CF synapse elimination has been observed from P8 to P18 in mice with Sema3A KD in PCs (Uesaka et al., 2014) and from P11 to P16 in PC-specific Progranulin KO mice (Uesaka et al., 2018). The developmental stage of the CF synapse affected by PTPδ KO was partially overlapped with that dependent on Sema3A or Progranulin. One previous study reported that PTPδ mediated the Sema3A signaling in cerebral cortical neurons (Nakamura et al., 2017). Further study is needed to elucidate whether PTPδ interacts with Sema3A-PlxnA4 or Progranulin-Sort1 pathway for CF synapse development.

In both PTPδ KO mice and Sema3A-PlxnA4 KD mice, PF-PC synaptic transmission was enhanced at P12-13. The enhanced PF-PC synaptic transmission has been found also in PC-specific PQ-VDCC KO mice (Miyazaki et al., 2012), suggesting that the diminished CF territories in PQ-VDCC KO mice or Sema3A KD mice caused enlargement of PF synaptic territories. Considering the expression of PTPδ on CFs but not on PFs, it is likely that the enhanced PF synaptic inputs in PTPδ KO mice resulted indirectly from the reduced CF synaptic territory on PC dendrites.

Previous studies have shown that PTPδ is involved in excitatory synapse formation and maintenance *in vivo*. For example, in PTPδ KO mice, decreased excitatory synapse density and strength in distal dendrites of hippocampal CA1 neurons (Park et al., 2020) and impaired synaptic plasticity (Uetani et al., 2000) were found. Therefore, PTPδ is considered to have similar functions on excitatory synapses in the hippocampus and the cerebellum.

PTPδ KO mice show motor dysfunction in young adulthood

PTPδ has been reported to be associated with behavioral abnormalities due to impairment in the hippocampal and cerebral cortical neural circuits. For example, the first report showed that PTPδ KO mice have defects in learning and memory ability with the enhancement of hippocampus long-term potentiation (Uetani et al., 2000). One recent report by Yoshida et al. (2021) identified the NLGN3-PTPδ interaction that competes with the well-known NLGN3-NRXN1 interaction. Interruption of the NLGN3-PTPδ interaction in mice caused impairment of

10.3389/fnmol.2023.1206245

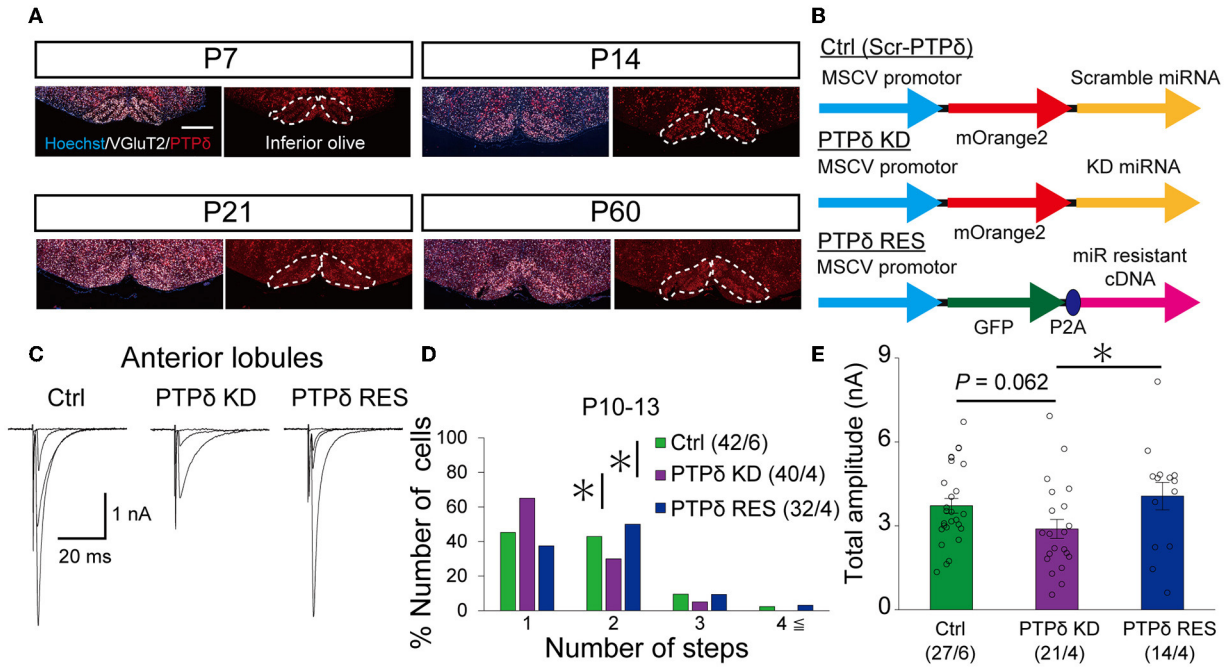

FIGURE 7
PTPδ KD in CFs reduced the CF-EPSC amplitude and the number of CFs innervating PCs from P10 to P13. **(A)** Expression of mRNAs for PTPδ in the inferior olive of P7, P14, P21, and 2-month-old mice. Images from double fluorescence *in situ* hybridization analyses to detect PTPδ (red) and VGluT2 (white) mRNAs expressed in inferior olivary neurons projecting CFs to the cerebellar cortex. Scale bars, 500 μm. **(B)** Vector constructs for Control (Ctrl; Scr-PTPδ), PTPδ knockdown (KD), and PTPδ rescue (RES). **(C)** Sample traces of CF-EPSCs from a Ctrl mouse, a mouse with PTPδ KD, and that with PTPδ RES recorded from PCs in anterior lobules during P10 to P13. Holding potential was −10 mV. Scale bars, 20 ms and 1 nA. **(right)**. **(D)** Summary histogram showing the number of CFs innervating individual PCs in anterior lobules of Ctrl (green column), PTPδ KD (purple column), and PTPδ RES (blue column) mice during P10–13. The numbers of PCs/mice are shown in parentheses. *$P < 0.05$ by the Mann–Whitney U-test. **(E)** Average total amplitudes of CF-EPSCs in anterior lobules of Ctrl (green column), PTPδ KD (purple column), and PTPδ RES (blue column) mice. Error bars in the graphs represent ± SEM. The numbers of PCs/mice are shown in parentheses. *$P < 0.05$ by Student's *t*-test.

TABLE 6 Total amplitudes and disparity parameters in cerebellar anterior lobules (1/2-3) of control, PTPδ KD and PTPδ RES mice.

	Total amplitude (nA)	Disparity ratio	Disparity index
Control (P10-13)	3.72 ± 0.26 ($n = 27$)	0.39 ± 0.1 ($n = 11$)	0.72 ± 0.14 ($n = 11$)
PTPδ KD (P10-13)	2.89 ± 0.34 ($n = 21$)*	0.17 ± 0.02 ($n = 4$)	1.04 ± 0.07 ($n = 4$)
PTPδ RES (P10-13)	4.07 ± 0.49 ($n = 14$)	0.27 ± 0.08 ($n = 6$)	0.89 ± 0.13 ($n = 6$)

Data are measured and described similarly to Tables 1, 2.
*$P < 0.05$.

TABLE 7 Electrophysiological parameters of CF-EPSCs in anterior lobules of control, PTPδ KD and PTPδ RES mice.

Anterior lobule (1-3)	CF group	Amplitude (nA)	Paired pulse ratio (interval, 50 ms)	10–90% rise time (ms)	Decay time constant (ms)	*n*
Control (P10-13)	CF-mono	3.44 ± 0.37	0.53 ± 0.03	0.59 ± 0.02	4.62 ± 0.31	16
	CF-multi-s	3.4 ± 0.31	0.5 ± 0.02	0.55 ± 0.02	3.72 ± 0.45	11
	CF-multi-w	1.17 ± 0.27	0.51 ± 0.03	0.44 ± 0.03	2.86 ± 0.31	10
PTPδ KD (P10-13)	CF-mono	2.87 ± 0.41	0.6 ± 0.03	0.54 ± 0.03	4.35 ± 0.33	17
	CF-multi-s	2.5 ± 0.28	0.63 ± 0.03*	0.49 ± 0.01	4.78 ± 0.66	4
	CF-multi-w	0.42 ± 0.06	0.52 ± 0.05	0.42 ± 0.02	2.44 ± 0.36	1
PTPδ RES (P10-13)	CF-mono	4.55 ± 0.68	0.53 ± 0.02	0.48 ± 0.02	4.0 ± 0.36	8
	CF-multi-s	2.71 ± 0.51	0.49 ± 0.04	0.47 ± 0.03	3.7 ± 0.61	6
	CF-multi-w	0.72 ± 0.21	0.52 ± 0.04	0.37 ± 0.03	2.64 ± 0.39	7

Data were measured and shown similarly to Tables 3, 4.
*$P < 0.05$.

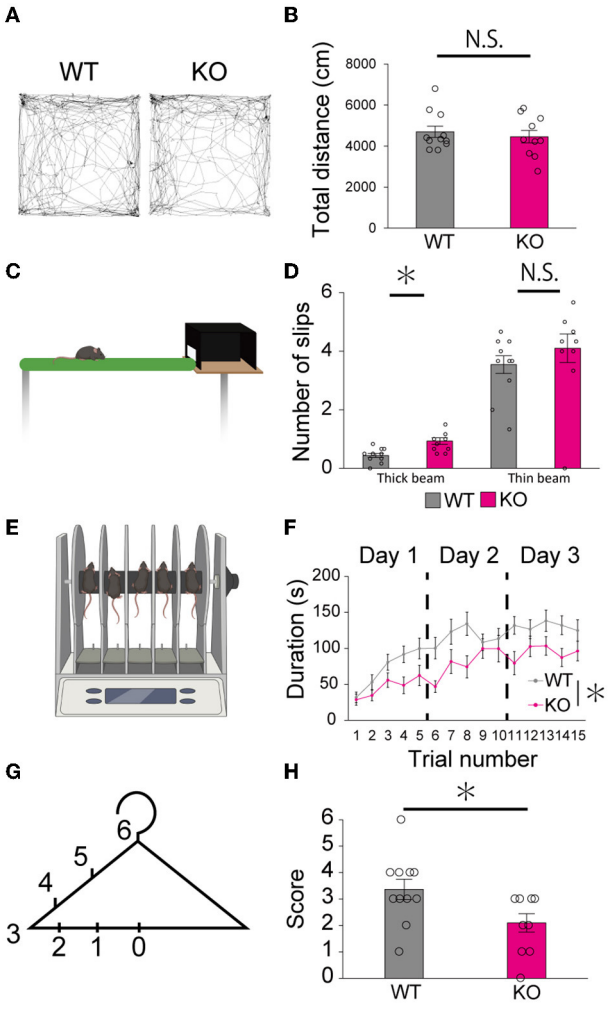

FIGURE 8
Motor dysfunction in young-adult PTPδ KO mice. **(A, B)** Open field test. Representative tracks for WT **(left)** and PTPδ KO **(right) (A)** and total distance traveled **(B)** in an open field arena over 10 min trial for WT (male $n = 6$, female $n = 5$) and PTPδ KO (male $n = 4$, female $n = 6$) mice from 2 to 4 months of age. *$P < 0.05$ (Student's t-test). **(C, D)** Beam walking test. Cartoon of balance walking test **(C)** and average number of slips on a thick beam and a thin beam **(D)** for WT (male $n = 6$, female $n = 5$) and PTPδ KO (male $n = 4$, female $n = 6$) mice from 2 to 4 months of age. *$P < 0.05$ (Student's t-test). **(E, F)** Rotarod test. Cartoon of rotarod test **(E)** and a summary graph showing durations for which mice stayed on the rod **(F)**. The rod was rotated at the speed of 40 rpm. The duration on the rod was measured **(F)** in five sessions of each of 3 consecutive days for WT (male $n = 6$, female $n = 5$) and PTPδ KO (male $n = 4$, female $n = 6$) mice from 2 to 4 months of age. A significant difference was observed between WT and PTPδ KO mice (repeated-measures ANOVA: factor genotype, $P = 0.02487$; factor stimulus intensity, $P < 2.2e\text{-}16$; interaction, genotype × stimulus intensity, $P = 0.09550$). *$P < 0.05$. **(F, G)** Hanger test. The score set at different positions of a coat-hanger **(G)** and average scores **(H)** for WT (male $n = 6$, female $n = 5$) and PTPδ KO (male $n = 4$, female $n = 6$) mice from 2 to 4 months of age. *$P < 0.05$ (Student's t-test).

sociability and enhancement of motor learning with an imbalance in excitatory/inhibitory synaptic protein expression in the forebrain (Yoshida et al., 2021). Moreover, PTPδ KO mice and meA (binding site for IL1RAPL1)-specific PTPδ mutant mice showed abnormal sleep behavior and non-REM rhythms with decreased excitatory synaptic transmission in the hippocampal CA1 neurons (Park et al., 2020).

In addition to these reported results, we found in the present study that young adult PTPδ KO mice showed impaired motor coordination in the beam test and reduced motor learning in the rotarod test, suggesting that PTPδ KO mice are impaired in cerebellum-related motor functions. Accumulating evidence from connectomics and functional imaging studies suggest that motor and non-motor functions of the cerebellum are likely attributable to Aldoc (–) and (+) PCs, respectively (Jan and Mitchell, 1998; Voogd, 2014; Lin et al., 2020). Because our data indicate that PTPδ predominantly functions in Aldoc (–) PCs of anterior lobules, impairment of CF synaptic function or CF innervation of Aldoc (–) PCs in anterior lobules of PTPδ KO mice is thought to contribute to the cerebellum-related motor dysfunction.

Possible postsynaptic ligands for PTPδ and phenotype of PTPδ KO mice

As mentioned above, NLGN3 is one of the postsynaptic ligands for PTPδ (Yoshida et al., 2021). However, in NLGN3 R451C mice, NLGN3 expression in the cerebellum was greatly reduced and CF synapse elimination was impaired transiently from P10 to P15 with increased amplitude of EPSCs by weaker CF stimulation (Lai et al., 2021). Since these phenotypes are clearly different from those of PTPδ KO mice, NLGN3 is not likely to be the postsynaptic ligand of PTPδ responsible for the cerebellar phenotypes of PTPδ KO mice.

PTPδ interacts with a variety of postsynaptic ligands, including NGL-3, IL-1RAP, IL1RAPL1, and SALM3,5 (Takahashi and Craig, 2013). In addition, LAR-RPTPs were identified as cellular receptors of proteoglycans (Aricescu et al., 2002; Shen et al., 2009). A previous study suggests that astrocyte-secreted glypican 4, a type of heparan sulfate proteoglycans, interacts with PTPδ and recruits AMPA receptors in postsynaptic sites via the release of neuronal pentraxin 1 from presynaptic terminals (Farhy-Tselnicker et al., 2017). Further study is needed to identify postsynaptic ligands for PTPδ on CF-PC synapses from these candidates. Multiple molecules have been reported to be complementarily expressed in PCs in accordance with the aldolase C expression patterns. For example, PLCβ3 and PLCβ4 are expressed in Aldoc (+) and Aldoc (–) PCs, respectively (Hawkes, 2014; Cerminara et al., 2015). Thus, it is likely that some postsynaptic ligands for PTPδ are differentially expressed in Aldoc (+) and Aldoc (–) PCs, which may underlie the differential phenotypes of PTPδ KO mice in these two populations of PCs.

Data availability statement

The raw data supporting the conclusions of this article will be made available by the authors, without undue reservation.

Ethics statement

The animal study was reviewed and approved by the animal welfare committees of The University of Tokyo.

Author contributions

YO, TW, and MK designed the experiment and wrote the manuscript. YO performed knockdown and rescue of PTPδ in CFs, morphological experiments and analyses, and electrophysiological experiments and analyses. KM and KH performed electrophysiological experiments and analyses. MY and MW performed immunohistochemical experiments and analyses. All authors contributed to the article and approved the submitted version.

Funding

This study was supported by Grants-in-Aid for Scientific Research (18H04012 and 21H04785 to MK) from the Japan Society for the Promotion of Science (JSPS) and by Grants-in-Aid for Transformative Research Areas (A) (20H05915 to MK) from the Ministry of Education, Culture, Sports, Science and Technology (MEXT) of Japan.

Acknowledgments

We thank N. Uesaka, Y. Sugaya, S. Fujino, and T. Noro for helpful advice and discussion. We also thank Y. Kato, M. Watanabe-Suzuki, T. Tanaka, K. Akasaka, and K. Aoyama for technical assistance and animal care. Cartoons were created using the software from BioRender.com.

Conflict of interest

The authors declare that the research was conducted in the absence of any commercial or financial relationships that could be construed as a potential conflict of interest.

Publisher's note

References

Aiba, A., Kano, M., Chen, C., Stanton, M. E., Fox, G. D., Herrup, K., et al. (1994). Deficient cerebellar long-term depression and impaired motor learning in mGluR1 mutant mice. *Cell* 79, 377–388. doi: 10.1016/0092-8674(94)90205-4

Anderson, G. R., Aoto, J., Tabuchi, K., Földy, C., Covy, J., Yee, A. X., et al. (2015). β-neurexins control neural circuits by regulating synaptic endocannabinoid signaling. *Cell* 162, 593–606. doi: 10.1016/j.cell.2015.06.056

Aricescu, A. R., McKinnell, I. W., Halfter, W., and Stoker, A. W. (2002). Heparan sulfate proteoglycans are ligands for receptor protein tyrosine phosphatase σ. *Mol. Cell. Biol.* 22, 1881–1892. doi: 10.1128/MCB.22.6.1881-1892.2002

Cerminara, N. L., Lang, E. J., Sillitoe, R. V., and Apps, R. (2015). Redefining the cerebellar cortex as an assembly of non-uniform Purkinje cell microcircuits. *Nat. Rev. Neurosci.* 16, 79–93. doi: 10.1038/nrn3886

Chen, L. Y., Jiang, M., Zhang, B., Gokce, O., and Südhof, T. C. (2017). Conditional deletion of all neurexins defines diversity of essential synaptic organizer functions for neurexins. *Neuron* 94, 611–625.e4. doi: 10.1016/j.neuron.2017.04.011

Choo, M., Miyazaki, T., Yamazaki, M., Kawamura, M., Nakazawa, T., Zhang, J., et al. (2017). Retrograde BDNF to TrkB signaling promotes synapse elimination in the developing cerebellum. *Nat. Commun.* 8, 195. doi: 10.1038/s41467-017-00260-w

de Wit, J., and Ghosh, A. (2016). Specification of synaptic connectivity by cell surface interactions. *Nat. Rev. Neurosci.* 17, 22–35. doi: 10.1038/nrn.2015.3

Debant, A., Serra-Pages, C., Seipel, K., O'brien, S., Tang, M., Parks, S. H., et al. (1996). The multidomain protein Trio binds the LAR transmembrane tyrosine phosphatase, contains a protein kinase domain, and has separate rac-specific and rho-specific guanine nucleotide exchange factor domains. *Proc. Natl. Acad. Sci. U. S. A.* 93, 5466–5471. doi: 10.1073/pnas.93.11.5466

Farhy-Tselnicker, I., van Casteren, A. C. M., Lee, A., Chang, V. T., Aricescu, A. R., and Allen, N. J. (2017). Astrocyte-secreted glypican 4 regulates release of neuronal pentraxin 1 from axons to induce functional synapse formation. *Neuron* 96, 428–445.e13. doi: 10.1016/j.neuron.2017.09.053

Fujita, H., Aoki, H., Ajioka, I., Yamazaki, M., Abe, M., Oh-Nishi, A., et al. (2014). Detailed expression pattern of aldolase C (Aldoc) in the cerebellum, retina and other areas of the CNS studied in Aldoc-Venus knock-in mice. *PLoS ONE* 9, e86679. doi: 10.1371/journal.pone.0086679

Fukai, S., and Yoshida, T. (2021). Roles of type IIa receptor protein tyrosine phosphatases as synaptic organizers. *FEBS J.* 288, 6913–6926. doi: 10.1111/febs.15666

Gokce, O., and Südhof, T. C. (2013). Membrane-tethered monomeric neurexin LNS-domain triggers synapse formation. *J. Neurosci.* 33, 14617–14628. doi: 10.1523/JNEUROSCI.1232-13.2013

Hanawa, H., Kelly, P. F., Nathwani, A. C., Persons, D. A., Vandergriff, J. A., Hargrove, P., et al. (2002). Comparison of various envelope proteins for their ability to pseudotype lentiviral vectors and transduce primitive hematopoietic cells from human blood. *Mole. Ther.* 5, 242–251. doi: 10.1006/mthe.2002.0549

Hashimoto, K., Ichikawa, R., Kitamura, K., Watanabe, M., and Kano, M. (2009a). Translocation of a "winner" climbing fiber to the Purkinje cell dendrite and subsequent elimination of "losers" from the soma in developing cerebellum. *Neuron* 63, 106–118. doi: 10.1016/j.neuron.2009.06.008

Hashimoto, K., and Kano, M. (2003). Functional differentiation of multiple climbing fiber inputs during synapse elimination in the developing cerebellum. *Neuron* 38, 785–796. doi: 10.1016/S0896-6273(03)00298-8

Hashimoto, K., and Kano, M. (2013). Synapse elimination in the developing cerebellum. *Cell. Mol. Life Sci.* 70, 4667–4680. doi: 10.1007/s00018-013-1405-2

Hashimoto, K., Miyata, M., Watanabe, M., and Kano, M. (2001). Roles of phospholipase Cβ4 in synapse elimination and plasticity in developing and mature cerebellum. *Mol. Neurobiol.* 23, 69–82. doi: 10.1385/MN:23:1:69

Hashimoto, K., Tsujita, M., Miyazaki, T., Kitamura, K., Yamazaki, M., Shin, H. S., et al. (2011). Postsynaptic P/Q-type Ca^{2+} channel in Purkinje cell mediates synaptic competition and elimination in developing cerebellum. *Proc. Natl. Acad. Sci. U. S. A.* 108, 9987–9992. doi: 10.1073/pnas.1101488108

Hashimoto, K., Yoshida, T., Sakimura, K., Mishina, M., Watanabe, M., and Kano, M. (2009b). Influence of parallel fiber-Purkinje cell synapse formation on postnatal development of climbing fiber-Purkinje cell synapses in the cerebellum. *Neuroscience* 162, 601–611. doi: 10.1016/j.neuroscience.2008.12.037

Hawkes, R. (2014). Purkinje cell stripes and long-term depression at the parallel fiber-Purkinje cell synapse. *Front. Syst. Neurosci.* 8, 41. doi: 10.3389/fnsys.2014.00041

Horn, K. E., Xu, B., Gobert, D., Hamam, B. N., Thompson, K. M., Wu, C. L., et al. (2012). Receptor protein tyrosine phosphatase sigma regulates synapse structure, function and plasticity. *J. Neurochem.* 122, 147–161. doi: 10.1111/j.1471-4159.2012.07762.x

Ichikawa, R., Miyazaki, T., Kano, M., Hashikawa, T., Tatsumi, H., Sakimura, K., et al. (2002). Distal extension of climbing fiber territory and multiple innervation caused by aberrant wiring to adjacent spiny branchlets in cerebellar Purkinje cells lacking glutamate receptor 2. *J. Neurosci.* 22, 8487–8503. doi: 10.1523/JNEUROSCI.22-19-08487.2002

Jan, V., and Mitchell, G. (1998). The anatomy of the cerebellum. *Trends Neurosci.* 12, 370–375. doi: 10.1016/S0166-2236(98)01318-6

Jang, H. C., Ryu, J. H., Shin, K. M., Seo, N., young, Kim, G. H., Huh, Y. H., et al. (2019). Gait ignition failure in JNPL3 human tau-mutant mice. *Exp. Neurobiol.* 28, 404–413. doi: 10.5607/en.2019.28.3.404

Kakegawa, W., Mitakidis, N., Miura, E., Abe, M., Matsuda, K., Takeo, Y. H., et al. (2015). Anterograde C1ql1 signaling is required in order to determine and maintain a single-winner climbing fiber in the mouse cerebellum. *Neuron* 85, 316–329. doi: 10.1016/j.neuron.2014.12.020

Kanda, Y. (2013). Investigation of the freely available easy-to-use software "EZR" for medical statistics. *Bone Marrow Transplant.* 48, 452–458. doi: 10.1038/bmt.2012.244

Kano, M., and Hashimoto, K. (2009). Synapse elimination in the central nervous system. *Curr. Opin. Neurobiol.* 19, 154–161. doi: 10.1016/j.conb.2009.05.002

Kano, M., Hashimoto, K., Watanabe, M., Kurihara, H., Offermanns, S., Jiang, H., et al. (1998). Phospholipase Cβ4 is specifically involved in climbing fiber synapse elimination in the developing cerebellum. *Proc. Nat. Acad. Sci.* 95, 15724–15729. doi: 10.1073/pnas.95.26.15724

Kawata, S., Miyazaki, T., Yamazaki, M., Mikuni, T., Yamasaki, M., Hashimoto, K., et al. (2014). Global scaling down of excitatory postsynaptic responses in cerebellar purkinje cells impairs developmental synapse elimination. *Cell Rep.* 8, 1119–1129. doi: 10.1016/j.celrep.2014.07.014

Konnerth, A., Llanot, I., and Armstrongt, C. M. (1990). Synaptic currents in cerebellar Purkinje cells. *Proc. Nat. Acad. Sci.* 87, 2662–2665. doi: 10.1073/pnas.87.7.2662

Lai, E. S. K., Nakayama, H., Miyazaki, T., Nakazawa, T., Tabuchi, K., Hashimoto, K., et al. (2021). An autism-associated neuroligin-3 mutation affects developmental synapse elimination in the cerebellum. *Front. Neural Circuits* 15, 676891. doi: 10.3389/fncir.2021.676891

Lin, Y. C., Hsu, C. C. H., Wang, P. N., Lin, C. P., and Chang, L. H. (2020). The relationship between zebrin expression and cerebellar functions: insights from neuroimaging studies. *Front. Neurol.* 11, 315. doi: 10.3389/fneur.2020.00315

Matsuda, K., Miura, E., Miyazaki, T., Kakegawa, W., Emi, K., Narumi, S., et al. (2010). Cbln1 is a ligand for an orphan glutamate receptor δ2, a bidirectional synapse organizer. *Science* 328, 363–368. doi: 10.1126/science.1185152

Miyazaki, T., Yamasaki, M., Hashimoto, K., Yamazaki, M., Abe, M., Usui, H., et al. (2012). $Ca_v2.1$ in cerebellar Purkinje cells regulates competitive excitatory synaptic wiring, cell survival, and cerebellar biochemical compartmentalization. *J. Neurosci.* 32, 1311–1328. doi: 10.1523/JNEUROSCI.2755-11.2012

Nakamura, F., Okada, T., Shishikura, M., Uetani, N., Taniguchi, M., Yagi, T., et al. (2017). Protein tyrosine phosphatase δ mediates the sema3a-induced cortical basal dendritic arborization through the activation of fyn tyrosine kinase. *J. Neurosci.* 37, 7125–7139. doi: 10.1523/JNEUROSCI.2519-16.2017

Nakayama, H., Miyazaki, T., Kitamura, K., Hashimoto, K., Yanagawa, Y., Obata, K., et al. (2012). GABAergic inhibition regulates developmental synapse elimination in the cerebellum. *Neuron* 74, 384–396. doi: 10.1016/j.neuron.2012.02.032

Park, H., Choi, Y., Jung, H., Kim, S., Lee, S., Han, H., et al. (2020). Splice-dependent trans-synaptic PTP δ- IL 1 RAPL 1 interaction regulates synapse formation and non-REM sleep. *EMBO J.* 39, e104150. doi: 10.15252/embj.2019104150

Richter, K. N., Revelo, N. H., Seitz, K. J., Helm, M. S., Sarkar, D., Saleeb, R. S., et al. (2018). Glyoxal as an alternative fixative to formaldehyde in immunostaining and super-resolution microscopy. *EMBO J.* 37, 139–159. doi: 10.15252/embj.201695709

Serra-Pagès, C., Medley, Q. G., Tang, M., Hart, A., and Streuli, M. (1998). Liptins, a family of LAR transmembrane protein-tyrosine phosphatase- interacting proteins. *J. Biol. Chem.* 273, 15611–15620. doi: 10.1074/jbc.273.25.15611

Shen, K., and Scheiffele, P. (2010). Genetics and cell biology of building specific synaptic connectivity. *Annu. Rev. Neurosci.* 33, 473–507. doi: 10.1146/annurev.neuro.051508.135302

Shen, Y., Tenney, A. P., Busch, S. A., Horn, K. P., Cuascut, F. X., Liu, K., et al. (2009). PTPσ Is a receptor for chondroitin sulfate proteoglycan, an inhibitor of neural regeneration. *Science* 326, 592–596. doi: 10.1126/science.1178310

Shishikura, M., Nakamura, F., Yamashita, N., Uetani, N., Iwakura, Y., and Goshima, Y. (2016). Expression of receptor protein tyrosine phosphatase δ, PTPδ, in mouse central nervous system. *Brain Res.* 1642, 244–254. doi: 10.1016/j.brainres.2016.03.030

Siddiqui, T. J., and Craig, A. M. (2011). Synaptic organizing complexes. *Curr. Opin. Neurobiol.* 21, 132–143. doi: 10.1016/j.conb.2010.08.016

Spangler, S. A., Schmitz, S. K., Kevenaar, J. T., de Graaff, E., de Wit, H., Demmers, J., et al. (2013). Liprin-α2 promotes the presynaptic recruitment and turnover of RIM1/CASK to facilitate synaptic transmission. *J. Cell Biol.* 201, 915–928. doi: 10.1083/jcb.201301011

Südhof, T. C. (2017). Synaptic neurexin complexes: a molecular code for the logic of neural circuits. *Cell* 171, 745–769. doi: 10.1016/j.cell.2017.10.024

Südhof, T. C. (2018). Towards an understanding of synapse formation. *Neuron.* 100, 276–293. doi: 10.1016/j.neuron.2018.09.040

Sugihara, I., and Quy, P. N. (2007). Identification of aldolase C compartments in the mouse cerebellar cortex by olivocerebellar labeling. *J. Compar. Neurol.* 500, 1076–1092. doi: 10.1002/cne.21219

Takahashi, H., and Craig, A. M. (2013). Protein tyrosine phosphatases PTPδ, PTPς, and LAR: presynaptic hubs for synapse organization. *Trends Neurosci.* 36, 522–534. doi: 10.1016/j.tins.2013.06.002

Uemura, T., Lee, S. J., Yasumura, M., Takeuchi, T., Yoshida, T., Ra, M., et al. (2010). Trans-synaptic interaction of GluRδ2 and neurexin through Cbln1 mediates synapse formation in the cerebellum. *Cell* 141, 1068–1079. doi: 10.1016/j.cell.2010.04.035

Uesaka, N., Abe, M., Konno, K., Yamazaki, M., Sakoori, K., Watanabe, T., et al. (2018). Retrograde signaling from progranulin to sort1 counteracts synapse elimination in the developing cerebellum. *Neuron* 97, 796–805.e5. doi: 10.1016/j.neuron.2018.01.018

Uesaka, N., Mikuni, T., Hashimoto, K., Hirai, H., Sakimura, K., and Kano, M. (2012). Organotypic coculture preparation for the study of developmental synapse elimination in mammalian brain. *J. Neurosci.* 32, 11657–11670. doi: 10.1523/JNEUROSCI.1097-12.2012

Uesaka, N., Uchigashima, M., Mikuni, T., Nakazawa, T., Nakao, H., Hirai, H., et al. (2014). Retrograde semaphorin signaling regulates synapse elimination in the developing mouse brain. *Science* 344, 1020–1023. doi: 10.1126/science.1252514

Uetani, N., Kato, K., Ogura, H., Mizuno, K., Kawano, K., Mikoshiba, K., et al. (2000). Impaired learning with enhanced hippocampal long-term potentiation in PTPδ deficient mice. *EMBO J.* 19, 2775–2785. doi: 10.1093/emboj/19.12.2775

Um, J. W., and Ko, J. (2013). LAR-RPTPs: synaptic adhesion molecules that shape synapse development. *Trends Cell Biol.* 23, 465–475. doi: 10.1016/j.tcb.2013.07.004

Voogd, J. (2014). What we do not know about cerebellar systems neuroscience. *Front. Syst. Neurosci.* 8, 227. doi: 10.3389/fnsys.2014.00227

Wadiche, J. I., and Jahr, C. E. (2001). Multivesicular release at climbing fiber-Purkinje cell synapses. *Neuron* 32, 301–313. doi: 10.1016/S0896-6273(01)00488-3

Wakita, M., Yamagata, A., Shiroshima, T., Izumi, H., Maeda, A., Sendo, M., et al. (2020). Structural insights into selective interaction between type IIa receptor protein tyrosine phosphatases and Liprin-α. *Nat. Commun.* 11, 649. doi: 10.1038/s41467-020-14516-5

Weng, Y. L., Liu, N., DiAntonio, A., and Broihier, H. T. (2011). The cytoplasmic adaptor protein caskin mediates Lar signal transduction during Drosophila motor axon guidance. *J. Neurosci.* 31, 4421–4433. doi: 10.1523/JNEUROSCI.5230-10.2011

Yoshida, T., Yamagata, A., Imai, A., Kim, J., Izumi, H., Nakashima, S., et al. (2021). Canonical versus non-canonical transsynaptic signaling of neuroligin 3 tunes development of sociality in mice. *Nat. Commun.* 12, 1848. doi: 10.1038/s41467-021-22059-6

Yuzaki, M. (2018). Two classes of secreted synaptic organizers in the central nervous system. *Annu. Rev. Physiol.* 80, 243–262. doi: 10.1146/annurev-physiol-021317-121322

frontiers | Frontiers in Molecular Neuroscience

TYPE Review
PUBLISHED 22 June 2023
DOI 10.3389/fnmol.2023.1182431

OPEN ACCESS

EDITED BY
Clevio Nobrega,
University of Algarve, Portugal

REVIEWED BY
Hirofumi Fujita,
University of Texas Southwestern Medical Center, United States
Tilmann Achsel,
Université de Lausanne, Switzerland

*CORRESPONDENCE
Josef P. Kapfhammer
✉ josef.kapfhammer@unibas.ch

RECEIVED 08 March 2023
ACCEPTED 22 May 2023
PUBLISHED 22 June 2023

CITATION
Kapfhammer JP and Shimobayashi E (2023) Viewpoint: spinocerebellar ataxias as diseases of Purkinje cell dysfunction rather than Purkinje cell loss.
Front. Mol. Neurosci. 16:1182431.
doi: 10.3389/fnmol.2023.1182431

Viewpoint: spinocerebellar ataxias as diseases of Purkinje cell dysfunction rather than Purkinje cell loss

Josef P. Kapfhammer* and Etsuko Shimobayashi

Institute of Anatomy, Department of Biomedicine, University of Basel, Basel, Switzerland

Spinocerebellar ataxias (SCAs) are a group of hereditary neurodegenerative diseases mostly affecting cerebellar Purkinje cells caused by a wide variety of different mutations. One subtype, SCA14, is caused by mutations of Protein Kinase C gamma (PKCγ), the dominant PKC isoform present in Purkinje cells. Mutations in the pathway in which PKCγ is active, i.e., in the regulation of calcium levels and calcium signaling in Purkinje cells, are the cause of several other variants of SCA. In SCA14, many of the observed mutations in the PKCγ gene were shown to increase the basal activity of PKCγ, raising the possibility that increased activity of PKCγ might be the cause of most forms of SCA14 and might also be involved in the pathogenesis of SCA in related subtypes. In this viewpoint and review article we will discuss the evidence for and against such a major role of PKCγ basal activity and will suggest a hypothesis of how PKCγ activity and the calcium signaling pathway may be involved in the pathogenesis of SCAs despite the different and sometimes opposing effects of mutations affecting these pathways. We will then widen the scope and propose a concept of SCA pathogenesis which is not primarily driven by cell death and loss of Purkinje cells but rather by dysfunction of Purkinje cells which are still present and alive in the cerebellum.

KEYWORDS

cerebellum, neurodegenerative diseases, spinocerebellar ataxia (SCA), Purkinje cell, Protein Kinase C gamma

Introduction

Spinocerebellar ataxias (SCAs) are neurodegenerative hereditary diseases affecting the cerebellum and presenting with typical symptoms and signs of cerebellar dysfunction, in particular a stance and gait ataxia often accompanied by nystagmus and varying additional problems (Klockgether et al., 2019; Muller, 2021). These diseases are rare with only 1–5 in 10.000 people affected (Bhandari et al., 2022) and these patients are then further stratified into more than 40 subtypes with different genes affected by the respective mutations. Nevertheless, there is remarkable interest into this disease from the scientific community (Soong and Morrison, 2018; Sullivan et al., 2019). Why are SCAs so interesting from a scientific point of view? One reason certainly is that the underlying mutations are by now well-defined and offer the chance to better understand the pathway from a defined genetic mutation to the disease manifestation. This is further helped by the finding that in most subtypes the cellular target are Purkinje cells, the major projection neuron of the cerebellar cortex. The connectivity pattern of the cerebellar neurons is very stereotyped and alterations can be identified relatively easy (Eccles, 1967). On the other hand, there is a remarkable heterogeneity of the affected genes, yet mutations in these

different genes produce a rather similar pathology and disease phenotype. In this viewpoint article we will initially focus on one particular subtype, spinocerebellar ataxia type 14 (SCA14) (Chen et al., 2012), which is caused by mutations in the gene of Protein Kinase C gamma (PKCγ) and we will discuss how the mutations might cause the disease. In a second part we will widen the scope and propose a concept of SCA pathogenesis which is not primarily driven by cell death and loss of Purkinje cells but rather by Purkinje cell dysfunction.

SCA14 mutations and possible pathogenic pathways

SCA14 (OMIM 605361) is a rather rare subtype of SCAs caused by mutations in PKCγ, a well characterized signaling protein kinase in Purkinje cells (Chen et al., 2012; Chelban et al., 2018). PKCγ is very strongly expressed in Purkinje cells and is involved in Purkinje cell neuronal plasticity, in particular in long term depression (LTD), the major form of adaptation of synaptic efficacy in cerebellar Purkinje cells (Ito, 2001; Watanave et al., 2022). While it was shown that PKCα can substitute for PKCγ for parallel fiber LTD expression (Leitges et al., 2004), there is good evidence that PKCγ is contributing to LTD induction (Shuvaev et al., 2011; Tsumagari et al., 2020). Furthermore, it is involved in developmental processes such as multiple climbing fibers (CFs) elimination (Saito and Shirai, 2002) and in Purkinje cell dendritic expansion (Kapfhammer, 2004).

The generation of PKCγ-deficient mice was reported in 1993 (Abeliovich et al., 1993). Studies with PKCγ deficient mice revealed that the innervation of CFs which are axonal projections from the inferior olivary nucleus to Purkinje cells was impaired, meaning that PKCγ is involved in multiple CFs elimination needed to establish a one-to-one innervation. Furthermore, PKCγ was shown to be involved in Purkinje cell dendritic expansion (Kano et al., 1995; Schrenk et al., 2002). However, PKCγ deficient mice showed no gross morphological changes in the cerebellum and in the Purkinje cells. Interestingly, PKCγ deficient mice show only a subtle phenotype and do not show typical signs of SCAs (Chen et al., 1995; Saito and Shirai, 2002) meaning that a mere loss of function of PKCγ is not sufficient for the development of SCA pathogenesis. The reason for this mild phenotype of loss of function mutations is probably found in the presence of other PKC isoforms which are also present in Purkinje cells, in particular PKCα, which is thought to compensate for the lack of PKCγ in Purkinje cells (Leitges et al., 2004).

As of today, more than 40 different mutations have been identified in the PKCγ gene from SCA14 patients. If one looks in which domains of PKCγ the mutations of human families affected by SCA14 are located, an intriguing pattern emerges. About 85–90% of the mutations cluster in the regulatory C1A and C1B domains of the protein which are binding diacylglycerol (DAG) and are required for relieving the inhibition of the kinase domain by the auto-inhibitory pseudosubstrate domain of the protein (Pilo et al., 2022). The remaining 10–15% of the mutations map to the kinase domain (Chelban et al., 2018; Schmitz-Hübsch et al., 2021). There is only little information about the neuropathology of human SCA14 cases, but Purkinje cell atrophy and loss have been found (Wong et al., 2018). Although the mutations are in the same protein, there is a huge range of phenotypes and a large variability in the degree of cerebellar atrophy (De Michele et al., 2022). These findings suggest that it is not a loss of function of PKCγ which is causative for the development of the SCA phenotype, but rather an altered regulation of the activity of PKCγ (Verbeek et al., 2005). This view is supported by studies looking at the kinase activity of mutated PKCγ. In a first systematic testing of the effects of the known mutations on PKCγ activity and function, it was shown that most of the SCA14 related mutants had an increased constitutive PKCγ activity in a cell-based assay (Adachi et al., 2008). These findings were confirmed in a recent study that found that basal activity was increased due to impaired kinase autoinhibition in all of the tested mutations causing SCA14 (Pilo et al., 2022).

These findings have raised the question whether an increased activity of PKCγ is causative for the development of an SCA14 phenotype. This question was addressed by two transgenic mouse models developed in our laboratory. In the first mouse model, the S361G mutation found in the human PKCγ kinase domain was transgenically expressed in Purkinje cells using a Purkinje cell-specific promotor construct (Ji et al., 2014). The mutated S361G-PKCγ was confirmed to have an increased constitutive activity in two studies using cell-based assays. In both studies, PKCγ activity was assessed by *in vitro* assays after transfection of the mutated PKCγ into COS7 cells, but not in Purkinje cells (Adachi et al., 2008; Pilo et al., 2022). The mouse model allowed the expression of the mutated S361G-PKCγ protein exclusively in Purkinje cells and offered the possibility to confirm the presence of increased biological PKCγ activity within Purkinje cells. From previous studies in our laboratory it is well known that increased PKC activity in Purkinje cells induced by treatment with phorbol esters during the phase of dendritic development compromises dendritic expansion and results in the development of a stunted dendritic tree of greatly reduced size in cerebellar slice cultures (Metzger and Kapfhammer, 2000; Schrenk et al., 2002; Gugger et al., 2012). Remarkably, the same stunted dendritic trees were found in Purkinje cells of cerebellar slice cultures derived from the S361G-PKCγ mice without pharmacological stimulation of PKC activity demonstrating the presence of increased PKCγ activity in the Purkinje cells and confirming the validity of the mouse model (Ji et al., 2014). Interestingly, these mice have a clear behavioral phenotype with deficits in motor coordination compatible with an SCA14-like pathology (Ji et al., 2014). The morphological changes found in these mice are subtler and there is no massive degeneration of Purkinje cells but a widespread reduction of Purkinje cell dendritic tree size and some localized loss of Purkinje cells in the cerebellum (Trzesniewski et al., 2019). Taken together, this mouse model shows that a constitutive activation of PKCγ in Purkinje cells results in an SCA14-like phenotype in the absence of widespread Purkinje cell loss.

There are two limitations of this mouse model: First, the phenotype is dependent on the activity of the Purkinje-cell specific L7 promoter and second the mutation is present in the kinase domain, not in the regulatory domains of the protein where the vast majority of SCA14 mutations were identified. We therefore investigated a second mouse model with a mutation in the pseudosubstrate domain (A24E) preventing the "closed" conformation of the PKCγ protein and forcing it permanently in the open active conformation (Pears et al., 1990).

The increased constitutive activity of PKCγ with such a mutation is known for a long time (Pears et al., 1990) but nothing was known about the consequences of the presence of such a mutation *in vivo*. A

knock-in mouse carrying this A24E mutation was created and studied in our laboratory. As expected, Purkinje cells from A24E-PKCγ mice studied in cell culture developed only stunted dendritic trees which could be rescued by pharmacological inhibitors of PKC activity demonstrating the presence of increased constitutive PKCγ activity within the Purkinje cells (Shimobayashi and Kapfhammer, 2021). The increase of PKCγ activity could also be confirmed by an increased phosphorylation of PKC target proteins. The SCA14-like phenotype of these mice was similar to that of the S361G-PKCγ mice with a marked deficit in motor coordination and a reduction of Purkinje cell dendritic tree size. The heterozygous A24E also shows a clear motor deficit indicating that the heterozygous A24E is a valid mouse model related to SCA14 (Shimobayashi and Kapfhammer, 2021). Despite these clear indications of increased PKC activity, PKCγ protein expression was greatly reduced in homozygous A24E-PKCγ mice. This is in line with the nature of the mutation which fixes the protein in the open active conformation. In this open conformation the protein is subject to dephosphorylation and degradation giving it a rather short half-life and it is remarkable that despite this rapid degradation there is still an increased constitutive activity of PKCγ present in Purkinje cells of the A24E-PKCγ mice.

These two mouse models clearly show that the presence of an increased constitutive PKCγ activity in Purkinje cells does cause an SCA14-like pathology in the mice. While it can be taken for granted that most mutations have an increased basal activity, it is not clear whether this will result in an increased PKCγ activity present in the Purkinje cells *in vivo* as found in the two mouse models discussed above. There are several aspects about the mutated PKCγ proteins which may limit the impact of the increased basal activity. First of all, most of the mutated PKCγ proteins show a strongly increased tendency for aggregation and PKCγ aggregates are present in cells transfected with Wild type or mutated proteins (Seki et al., 2005, 2007; Takahashi et al., 2015). These aggregates were suggested to be neurotoxic and may contribute to Purkinje cell degeneration (Nakazono et al., 2018). While the presence and significance of PKCγ protein aggregates is controversial (Seki et al., 2009) and may vary from mutation to mutation, it is clear that PKCγ aggregates of mutated proteins can contribute to SCA14 pathology (Seki et al., 2005; Jezierska et al., 2014; Wong et al., 2018). Another important aspect for considering the role of PKCγ activity is the ability of the mutated proteins to translocate to the membrane in order to be fully activated by phosphatidylserine and DAG released at the plasma membrane. There is evidence that the translocation to the plasma membrane of mutated PKCγ proteins can be enhanced or impaired (Verbeek et al., 2008; Wong et al., 2018). In a cell-based assay, Adachi et al. (2008) found that two mutant PKCγs failed to phosphorylate one of PKCγ natural substrates, the Transient Receptor Potential cation channel subfamily C member 3 (TRPC3) channel (Adachi et al., 2008). Similarly, C1B domain mutations were found to have altered membrane dynamics and failed to activate downstream targets (Verbeek et al., 2008). The V138E mutation was shown to have a reduced availability in the cytoplasm and was directed to the insoluble fraction reducing their activity and possibly giving rise to protein aggregates (Jezierska et al., 2014). Altogether, mutated PKCγs show altered kinetics for the translocation to the membrane upon activation resulting in improper PKCγ signal transduction.

We have tested the potential of several mutant PKCγs to induce an increased PKCγ activity strong enough for showing a dendritic phenotype in developing Purkinje cells in dissociated Purkinje cell cultures as we had observed for Purkinje cells from S361G-PKCγ mice. When we transfected Purkinje cells with mutations either in the catalytic domain or in the regulatory domains, only the mutations in the catalytic domain could induce a dendritic phenotype (Shimobayashi and Kapfhammer, 2017). In later experiments, a strong dendritic reduction was also found with mutations in the pseudosubstrate domain (A24E, A24T). The A24T mutation was identified in human SCA14 patients (Chelban et al., 2018). The finding that the mutations in the regulatory C1A nor C1B domain did not induce a dendritic reduction of the Purkinje cells means that despite the observed increase in basal activity these mutations do not induce a long-lived and substantial increase of PKCγ activity in developing Purkinje cells. This is compatible with the failure of these mutations to induce an increased phosphorylation of their substrates (see above). Another important aspect considering the role of PKCγ activity for the pathogenesis of SCA is the presence of a nonsense mutation giving rise to a truncated PKCγ protein (Shirafuji et al., 2019). For this mutation, a dominant negative mechanism suppressing PKC activity is possible but it is difficult to conceive a mechanism involving an increase in PKC activity. The results of these studies suggest that both an increase of PKCγ activity and a reduction or alteration of PKCγ activity might cause the SCA14 phenotype.

Other SCA mutations affecting Ca^{2+} homeostasis and synaptic function in Purkinje cells

The SCA14 mutation is affecting PKCγ which is part of a signaling cascade, the metabotropic glutamate receptor 1 (mGluR1)-PKCγ signaling pathway generating an intracellular calcium signal, which is crucial for changes in synaptic transmission and synaptic efficacy (Ito, 2001; Watanabe and Kano, 2011; Sugawara et al., 2017). The importance of this pathway with respect to SCA pathogenesis is underlined by the fact that molecules both upstream and downstream of PKCγ are also causative genes of SCAs. This is true for mutations in the mGluR1 receptor upstream of PKCγ (SCA44) (Watson et al., 2017), the Inositol 1,4,5-trisphosphate Receptor (IP3R1) upstream of PKCγ (SCA15, SCA29) (Tada et al., 2016), and the TRPC3 channel (SCA41) (Fogel et al., 2015) downstream of PKCγ. In all these cases the mGluR1-PKCγ signaling pathway will be affected and it will eventually be rendered dysfunctional by mutations in critical proteins (Shimobayashi and Kapfhammer, 2018).

Besides mutations which directly affect molecules in this signaling pathway, there is evidence that this pathway may also be altered in forms of SCAs caused by CAG repeats in the Ataxin genes. In SCA1 mutant mice, there is evidence that alterations of the mGluR1 signaling pathway contribute to pathogenesis (Power et al., 2016; Shuvaev et al., 2017). Similarly, there is evidence that altered activity of the mGluR1 signaling pathway is also contributing to pathogenesis in SCA2 (Meera et al., 2017) and SCA3 (Konno et al., 2014), indicating an important role of mGluR1 signaling for the pathogenesis of SCAs (Wu and Kapfhammer, 2021). Moreover, PKCγ expression and activity is altered in SCA1 and SCA2 suggesting the function of this signaling pathway is altered in these SCA subtypes (Chopra et al., 2018). In SCA5, mutations are present in β-III-spectrin resulting in abnormal formation and function of

Purkinje cell synapses (Ikeda et al., 2006). Mutant β-III-spectrin decreases mGluR1 localization at dendritic spines of Purkinje cells suggesting that β-III-spectrin is directly involved in the mGluR1 signaling pathway (Armbrust et al., 2014).

Apart from mutations directly affecting the mGluR1-PKCγ signaling pathway, there are a number of mutations present in different SCA subtypes which do affect either ion channels or other molecules related to Purkinje cell synaptic function. A mutation affecting the cytoskeleton is found in SCA11 where Tau tubulin kinase is affected which is critical for ciliogenesis (Houlden et al., 2007; Bowie et al., 2018). Due to the mutations, cilia are lost in neurons and the synaptic connectivity and function of Purkinje cells is altered including changes of mGluR1 signaling and calcium homeostasis (Bowie et al., 2018). In SCA27, mutations are found in FGF14 which is regulating synaptic transmission and Purkinje cell spiking activity (Shakkottai et al., 2009; Yan et al., 2013). SCA13 is caused by mutations in KCNC3 encoding a potassium channel (Kv3.3) (Waters and Pulst, 2008). Although it is not completely clear how these mutations cause the SCA phenotype there is evidence that the mutations will eventually affect synaptic transmission in Purkinje cells (Waters et al., 2006; Zhang and Kaczmarek, 2016). Similar considerations apply to SCA19 and SCA22 which are caused by mutations in the KCND3 gene encoding voltage-gated potassium channel Kv4.3. Again, the exact consequences of the mutations on Purkinje cell synaptic transmission are not known, but there is evidence that the mutations do affect spiking patterns in Purkinje cells (Duarri et al., 2012) and may interfere with mGluR1 signaling (Ishibashi et al., 2016).

It is striking that of the various mutations causing SCAs a large part of them affects synaptic function and spiking response characteristics of Purkinje cells (Shakkottai et al., 2011; Dell'Orco et al., 2017), mostly by altering Purkinje cell calcium homeostasis and modifying the mGluR1 signaling pathway (reviewed in Robinson et al., 2020). This evidence establishes functional changes and altered response characteristics of Purkinje cells as one major mechanism underlying the pathogenesis of SCAs. For example, in the SCA1 mouse model, neuronal atrophy was found to be an adaptive change restoring repetitive firing (Dell'Orco et al., 2015). In an SCA6 mouse model, firing precision of floccular Purkinje cells was reduced resulting in a deficit of the vestibulo-ocular reflex VOR (Chang et al., 2022). Watanave and colleagues showed that in PKCγ deficient Purkinje cells, climbing fiber LTD was impaired (Watanave et al., 2022).

It is remarkable that many functional deficits associated with SCA are independent of Purkinje cell degeneration and cell death and are rather the consequence of Purkinje cell dysfunction. It should be noted that this type of pathogenesis affected by signaling molecules from mGluR1 to PKCγ may not be applicable to all cases of SCAs. Some mutations also affect mitochondrial function as in SCA28. It is known that SCA28 is caused by mutations in the mitochondrial protease AFG3L2 which leads to mitochondrial dysfunction (Maltecca et al., 2015). The brain activity needs lots of energy and mitochondria are the organelles generating the energy for cell activities, thus mitochondrial dysfunction may cause SCA more by apoptosis and loss of Purkinje cells rather than by Purkinje cell dysfunction (Harmuth et al., 2018; Barbier et al., 2022). For the rather frequent SCA cases caused by enhanced CAG repeats in the Ataxin transcriptional regulators it is open which type of pathogenesis is more important.

A hypothesis for SCA pathogenesis with SCA14 as a starting point

While SCA14 is a rather rare subtype of SCA it falls into a group of SCA causing mutations which are affecting the calcium equilibrium in Purkinje cells. Calcium signaling in Purkinje cells is absolutely crucial for Purkinje cell functions (Kitamura and Kano, 2013). All of the known mechanisms modifying Purkinje cell functional activity do depend on calcium signaling, most notably LTD. Functional deficits of LTD may be an important contributor to cerebellar symptoms in SCAs (Tempia and Konnerth, 1994; Mitoma et al., 2022). A crucial aspect about calcium concentrations in Purkinje cells is that they can change rapidly upon external and internal signals (Kitamura and Hausser, 2011). For SCA14, there is some discussion of whether the mutations will cause a gain of function, loss of function or dominant negative phenotype (Wong et al., 2018). As discussed above, there is good evidence that all three types of phenotypes may be present with different SCA14 subtypes which may either cause an increased or a decreased level of PKCγ activity. This wide range of functional changes of PKCγ activity may look confusing first but becomes more meaningful when one considers the functional requirements for this signaling pathway of the Purkinje cells. For the proper function of these neurons it is essential that PKCγ activity can rise and fall fast, depending on external signals. What in the end matters for the cell is not whether the basic level of PKCγ activity is increased or decreased, what matters is the ability of the Purkinje cells to change its activity quickly and appropriately in order to produce a meaningful reaction to external signals. Any mutation which interferes with the dynamics of PKC activity or changes the magnitude and time frame of Purkinje cell responses will prevent Purkinje cells from functioning properly. In that sense, a constitutive activation of PKC activity as seen in the mouse models S361G-PKCγ mice and A24E-PKCγ mice may be "gain of function" with respect to PKC activity, but is a "loss of function" with respect to the dynamics and size of PKC activity changes upon external stimuli and it will interfere with the proper function of the cell. This broader concept could also explain the apparent discrepancy that a deletion of the PKCγ gene is not causing much functional deficits, but that a point mutation in the regulatory domain causes an SCA phenotype. In the case of the gene knockout, PKCγ function can be taken over by PKCα, and this will mostly preserve the dynamics and size of the response. But a mutation in the regulatory domain of PKCγ protein will change the dynamics and/or the amount of PKCγ activity in response to external signals, and because PKCγ is the dominant isoform in Purkinje cells and the PKCγ signal is dominant in Purkinje cells (Takahashi et al., 2017), an altered PKCγ activity will render the cell dysfunctional despite intact PKCα. Similar considerations apply for the mutations in pathways affecting the calcium equilibrium and synaptic function of the Purkinje cells (Hoxha et al., 2018). Because of the high spiking activity and of the strong stimulation by parallel and climbing fibers, Purkinje cells are strongly depending on an intact and efficient regulation of their intracellular calcium levels. Every mutation which is interfering with or modulating the calcium regulation will also alter the response characteristics of the Purkinje cells making them in many cases inappropriate. These mechanisms will make Purkinje cells dysfunctional, eventually producing an SCA pathology.

In our view, the labels "loss of function," "gain of function" or "toxic gain of function" are too simplistic to properly describe the

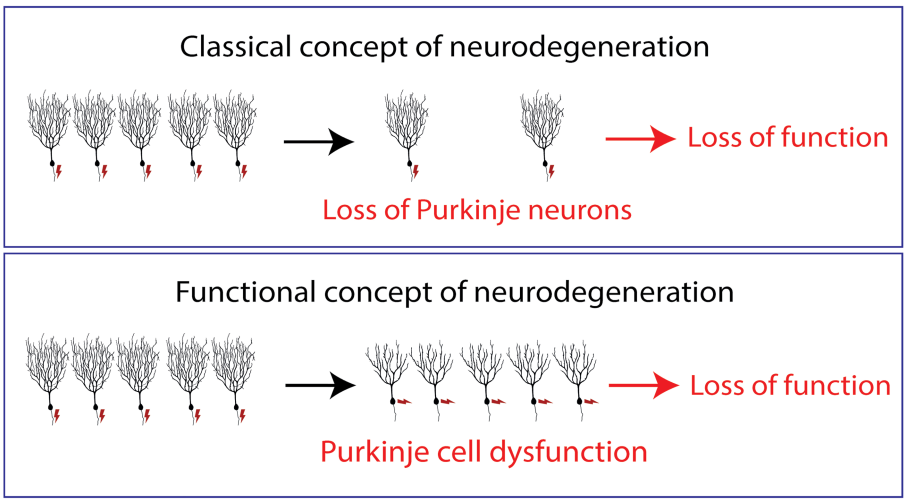

FIGURE 1
Normally neurodegenerative diseases are regarded as diseases caused by the death and loss of neurons. The symptoms of the patients in this view are caused by fact that not enough neurons are present to fulfill their tasks properly. In the concept of "Functional neurodegeneration" proposed in this article, the symptoms of the patients are caused by neurons which are alive but do not function properly, i.e., they may respond inappropriately to afferent stimuli ("dysfunctional neurons"). In this model, neuronal death is just a late event and not causally linked to the symptoms of the patients.

alterations caused by the mutations causing SCA which may affect Purkinje cell functional properties in multiple ways. The crucial aspect is a change in the response characteristics of Purkinje cells to external stimuli, eventually making the responses inappropriate and rendering Purkinje cells dysfunctional. The focus in SCA research in the past may have been too strongly on Purkinje cell loss and cerebellar atrophy (Durr, 2010; Reetz et al., 2013; Mascalchi et al., 2014). We think that in many cases Purkinje cell loss and cerebellar atrophy are just late manifestations of a Purkinje cell dysfunction going on for a much longer time period. In fact, there is considerable variability in the amount of cerebellar atrophy and Purkinje cell loss present in human SCA subtypes (Schulz et al., 2010; Goel et al., 2011) and the correlation of these findings with the clinical severity of the disease is poor (Robinson et al., 2020). Furthermore, from mouse studies, it is well known that a severe ataxia and motor impairment can be present in the absence of any or only little Purkinje cell loss (Clark et al., 1997; Shakkottai et al., 2004; Duvick et al., 2010; Hourez et al., 2011; Shakkottai et al., 2011) and that on the other side a substantial loss of Purkinje cells is compatible with near normal cerebellar function as long as there is a sufficient number (10–25%) of normal functioning Purkinje cells preserved (Martin et al., 2003, 2004).

In many cases of human SCAs, the presence of cerebellar atrophy and Purkinje cell loss might be considered simply late signs of a dysfunctional cerebellum, but many of the functional deficits found in SCA patients are likely to be caused not by the Purkinje cells lost in the course of the disease but rather by the Purkinje cells which are still alive and present in the cerebellum of these patients, but are dysfunctional (Jayabal et al., 2015; Brown et al., 2018; Chang et al., 2022). We are convinced that a more appropriate view of SCAs is to see at least several subtypes in this group of diseases less as neurodegenerative in the classical sense, i.e., caused by the loss of neurons, but rather as diseases of Purkinje cell dysfunction (see Figure 1). Such a functional view of neurodegeneration may also apply to many other neurodegenerative diseases and is certainly an important aspect of functional deficits found in neurodegenerative diseases. For the patients, this may be good and bad news. On the one hand it means that the cause and type of Purkinje cell dysfunction may be different from subtype to subtype and may require quite different treatment strategies. On the other hand, it may give also hope because it means that in many cases of SCA there are still enough Purkinje cells present to principally ensure better cerebellar function if it was possible to rectify Purkinje cell activity by appropriate treatments.

Author contributions

JK and ES developed the idea and wrote the manuscript. All authors were involved in discussions on the final manuscript.

Funding

The authors are funded by the Swiss National Science Foundation, grant number 310030_189083.

Acknowledgments

The authors thank Paula Torrents-Solé for discussions and Aleksandar Kovacevic for technical support.

Conflict of interest

The authors declare that the research was conducted in the absence of any commercial or financial relationships that could be construed as a potential conflict of interest.

Publisher's note

References

Abeliovich, A., Chen, C., Goda, Y., Silva, A. J., Stevens, C. F., and Tonegawa, S. (1993). Modified hippocampal long-term potentiation in PKC gamma-mutant mice. *Cells* 75, 1253–1262. doi: 10.1016/0092-8674(93)90613-u

Adachi, N., Kobayashi, T., Takahashi, H., Kawasaki, T., Shirai, Y., Ueyama, T., et al. (2008). Enzymological analysis of mutant protein kinase Cgamma causing spinocerebellar ataxia type 14 and dysfunction in Ca2+ homeostasis. *J. Biol. Chem.* 283, 19854–19863. doi: 10.1074/jbc.M801492200

Armbrust, K. R., Wang, X., Hathorn, T. J., Cramer, S. W., Chen, G., Zu, T., et al. (2014). Mutant beta-III spectrin causes mGluR1alpha mislocalization and functional deficits in a mouse model of spinocerebellar ataxia type 5. *J. Neurosci.* 34, 9891–9904. doi: 10.1523/JNEUROSCI.0876-14.2014

Barbier, M., Bahlo, M., Pennisi, A., Jacoupy, M., Tankard, R. M., Ewenczyk, C., et al. (2022). Heterozygous PNPT1 variants cause spinocerebellar ataxia type 25. *Ann. Neurol.* 92, 122–137. doi: 10.1002/ana.26366

Bhandari, J., Thada, P. K., and Samanta, D. (2022). *Spinocerebellar ataxia*. StatPearls: Treasure Island, FL.

Bowie, E., Norris, R., Anderson, K. V., and Goetz, S. C. (2018). Spinocerebellar ataxia type 11-associated alleles of Ttbk2 dominantly interfere with ciliogenesis and cilium stability. *PLoS Genet.* 14:e1007844. doi: 10.1371/journal.pgen.1007844

Brown, A. S., Meera, P., Altindag, B., Chopra, R., Perkins, E. M., Paul, S., et al. (2018). MTSS1/Src family kinase dysregulation underlies multiple inherited ataxias. *Proc. Natl. Acad. Sci. U. S. A.* 115, E12407–E12416. doi: 10.1073/pnas.1816177115

Chang, H. H. V., Cook, A. A., Watt, A. J., and Cullen, K. E. (2022). Loss of flocculus purkinje cell firing precision leads to impaired gaze stabilization in a mouse model of spinocerebellar ataxia type 6 (SCA6). *Cells* 11:2739. doi: 10.3390/cells11172739

Chelban, V., Wiethoff, S., Fabian-Jessing, B. K., Haridy, N. A., Khan, A., Efthymiou, S., et al. (2018). Genotype-phenotype correlations, dystonia and disease progression in spinocerebellar ataxia type 14. *Mov. Disord.* 33, 1119–1129. doi: 10.1002/mds.27334

Chen, C., Kano, M., Abeliovich, A., Chen, L., Bao, S., Kim, J. J., et al. (1995). Impaired motor coordination correlates with persistent multiple climbing fiber innervation in PKC gamma mutant mice. *Cells* 83, 1233–1242. doi: 10.1016/0092-8674(95)90148-5

Chen, D. H., Raskind, W. H., and Bird, T. D. (2012). Spinocerebellar ataxia type 14. *Handb. Clin. Neurol.* 103, 555–559. doi: 10.1016/B978-0-444-51892-7.00036-X

Clark, H. B., Burright, E. N., Yunis, W. S., Larson, S., Wilcox, C., and Hartman, B. (1997). Purkinje cell expression of a mutant allele of SCA1 in transgenic mice leads to disparate effects on motor behaviors, followed by a progressive cerebellar dysfunction and histological alterations. *J Neurosci.* 17, 7385–7395. doi: 10.1523/JNEUROSCI.17-19-07385.1997

Chopra, R., Wasserman, A. H., Pulst, S. M., De Zeeuw, C. I., and Shakkottai, V. G. (2018). Protein kinase C activity is a protective modifier of Purkinje neuron degeneration in cerebellar ataxia. *Hum. Mol. Genet.* 27, 1396–1410. doi: 10.1093/hmg/ddy050

de Michele, G., Galatolo, D., Galosi, S., Mignarri, A., Silvestri, G., Casali, C., et al. (2022). Episodic ataxia and severe infantile phenotype in spinocerebellar ataxia type 14: expansion of the phenotype and novel mutations. *J. Neurol.* 269, 1476–1484. doi: 10.1007/s00415-021-10712-5

Dell'Orco, J. M., Wasserman, A. H., Chopra, R., Ingram, M. A., Hu, Y. S., and Singh, V. (2015). Neuronal atrophy early in degenerative ataxia is a compensatory mechanism to regulate membrane excitability. *J Neurosci.* 35, 11292–11307. doi: 10.1523/JNEUROSCI.1357-15.2015

Dell'Orco, J. M., Pulst, S. M., and Shakkottai, V. G. (2017). Potassium channel dysfunction underlies Purkinje neuron spiking abnormalities in spinocerebellar ataxia type 2. *Hum. Mol. Genet.* 26, 3935–3945. doi: 10.1093/hmg/ddx281

Duarri, A., Jezierska, J., Fokkens, M., Meijer, M., Schelhaas, H. J., den Dunnen, W. F., et al. (2012). Mutations in potassium channel kcnd3 cause spinocerebellar ataxia type 19. *Ann. Neurol.* 72, 870–880. doi: 10.1002/ana.23700

Durr, A. (2010). Autosomal dominant cerebellar ataxias: polyglutamine expansions and beyond. *Lancet Neurol.* 9, 885–894. doi: 10.1016/S1474-4422(10)70183-6

Duvick, L., Barnes, J., Ebner, B., Agrawal, S., Andresen, M., Lim, J., et al. (2010). SCA1-like disease in mice expressing wild-type ataxin-1 with a serine to aspartic acid replacement at residue 776. *Neuron* 67, 929–935. doi: 10.1016/j.neuron.2010.08.022

Eccles, J. C. (1967). Circuits in the cerebellar control of movement. *Proc. Natl. Acad. Sci. U. S. A.* 58, 336–343. doi: 10.1073/pnas.58.1.336

Fogel, B. L., Hanson, S. M., and Becker, E. B. (2015). Do mutations in the murine ataxia gene TRPC3 cause cerebellar ataxia in humans? *Mov. Disord.* 30, 284–286. doi: 10.1002/mds.26096

Goel, G., Pal, P. K., Ravishankar, S., Venkatasubramanian, G., Jayakumar, P. N., Krishna, N., et al. (2011). Gray matter volume deficits in spinocerebellar ataxia: an optimized voxel based morphometric study. *Parkinsonism Relat. Disord.* 17, 521–527. doi: 10.1016/j.parkreldis.2011.04.008

Gugger, O. S., Hartmann, J., Birnbaumer, L., and Kapfhammer, J. P. (2012). P/Q-type and T-type calcium channels, but not type 3 transient receptor potential cation channels, are involved in inhibition of dendritic growth after chronic metabotropic glutamate receptor type 1 and protein kinase C activation in cerebellar Purkinje cells. *Eur. J. Neurosci.* 35, 20–33. doi: 10.1111/j.1460-9568.2011.07942.x

Harmuth, T., Prell-Schicker, C., Weber, J. J., Gellerich, F., Funke, C., Drießen, S., et al. (2018). Mitochondrial morphology, function and homeostasis are impaired by expression of an N-terminal calpain cleavage fragment of ataxin-3. *Front. Mol. Neurosci.* 11:368. doi: 10.3389/fnmol.2018.00368

Houlden, H., Johnson, J., Gardner-Thorpe, C., Lashley, T., Hernandez, D., Worth, P., et al. (2007). Mutations in TTBK2, encoding a kinase implicated in tau phosphorylation, segregate with spinocerebellar ataxia type 11. *Nat. Genet.* 39, 1434–1436. doi: 10.1038/ng.2007.43

Hourez, R., Servais, L., Orduz, D., Gall, D., Millard, I., de Kerchove d'Exaerde, A., et al. (2011). Aminopyridines correct early dysfunction and delay neurodegeneration in a mouse model of spinocerebellar ataxia type 1. *J. Neurosci.* 31, 11795–11807. doi: 10.1523/JNEUROSCI.0905-11.2011

Hoxha, E., Balbo, I., Miniaci, M. C., and Tempia, F. (2018). Purkinje cell signaling deficits in animal models of ataxia. *Front. Synaptic Neurosci.* 10:6. doi: 10.3389/fnsyn.2018.00006

Ikeda, Y., Dick, K. A., Weatherspoon, M. R., Gincel, D., Armbrust, K. R., Dalton, J. C., et al. (2006). Spectrin mutations cause spinocerebellar ataxia type 5. *Nat. Genet.* 38, 184–190. doi: 10.1038/ng1728

Ishibashi, K., Miura, Y., Ishikawa, K., Zhang, M. R., Toyohara, J., Ishiwata, K., et al. (2016). Relationship between type 1 metabotropic glutamate receptors and cerebellar ataxia. *J. Neurol.* 263, 2179–2187. doi: 10.1007/s00415-016-8248-3

Ito, M. (2001). Cerebellar long-term depression: characterization, signal transduction, and functional roles. *Physiol. Rev.* 81, 1143–1195. doi: 10.1152/physrev.2001.81.3.1143

Jayabal, S., Ljungberg, L., Erwes, T., Cormier, A., Quilez, S., el Jaouhari, S., et al. (2015). Rapid onset of motor deficits in a mouse model of spinocerebellar ataxia type 6 precedes late cerebellar degeneration. *eNeuro* 2:ENEURO.0094-15.2015. doi: 10.1523/ENEURO.0094-15.2015

Jezierska, J., Goedhart, J., Kampinga, H. H., Reits, E. A., and Verbeek, D. S. (2014). SCA14 mutation V138E leads to partly unfolded PKCgamma associated with an exposed C-terminus, altered kinetics, phosphorylation and enhanced insolubilization. *J. Neurochem.* 128, 741–751. doi: 10.1111/jnc.12491

Ji, J., Hassler, M. L., Shimobayashi, E., Paka, N., Streit, R., and Kapfhammer, J. P. (2014). Increased protein kinase C gamma activity induces Purkinje cell pathology in a mouse model of spinocerebellar ataxia 14. *Neurobiol. Dis.* 70, 1–11. doi: 10.1016/j.nbd.2014.06.002

Kano, M., Hashimoto, K., Chen, C., Abeliovich, A., Aiba, A., Kurihara, H., et al. (1995). Impaired synapse elimination during cerebellar development in PKC gamma mutant mice. *Cells* 83, 1223–1231. doi: 10.1016/0092-8674(95)90147-7

Kapfhammer, J. P. (2004). Cellular and molecular control of dendritic growth and development of cerebellar Purkinje cells. *Prog. Histochem. Cytochem.* 39, 131–182. doi: 10.1016/j.proghi.2004.07.002

Kitamura, K., and Hausser, M. (2011). Dendritic calcium signaling triggered by spontaneous and sensory-evoked climbing fiber input to cerebellar Purkinje cells in vivo. *J. Neurosci.* 31, 10847–10858. doi: 10.1523/JNEUROSCI.2525-10.2011

Kitamura, K., and Kano, M. (2013). Dendritic calcium signaling in cerebellar Purkinje cell. *Neural Netw.* 47, 11–17. doi: 10.1016/j.neunet.2012.08.001

Klockgether, T., Mariotti, C., and Paulson, H. L. (2019). Spinocerebellar ataxia. *Nat. Rev. Dis. Primers.* 5:24. doi: 10.1038/s41572-019-0074-3

Konno, A., Shuvaev, A. N., Miyake, N., Miyake, K., Iizuka, A., Matsuura, S., et al. (2014). Mutant ataxin-3 with an abnormally expanded polyglutamine chain disrupts dendritic development and metabotropic glutamate receptor signaling in mouse cerebellar Purkinje cells. *Cerebellum* 13, 29–41. doi: 10.1007/s12311-013-0516-5

Leitges, M., Kovac, J., Plomann, M., and Linden, D. J. (2004). A unique PDZ ligand in PKCalpha confers induction of cerebellar long-term synaptic depression. *Neuron* 44, 585–594. doi: 10.1016/j.neuron.2004.10.024

Maltecca, F., Baseggio, E., Consolato, F., Mazza, D., Podini, P., Young, S. M. Jr., et al. (2015). Purkinje neuron Ca2+ influx reduction rescues ataxia in SCA28 model. *J. Clin. Invest.* 125, 263–274. doi: 10.1172/JCI74770

Martin, L. A., Escher, T., Goldowitz, D., and Mittleman, G. (2004). A relationship between cerebellar Purkinje cells and spatial working memory demonstrated in a lurcher/chimera mouse model system. *Genes Brain Behav.* 3, 158–166. doi: 10.1111/j.1601-183x.2004.00067.x

Martin, L. A., Goldowitz, D., and Mittleman, G. (2003). The cerebellum and spatial ability: dissection of motor and cognitive components with a mouse model system. *Eur. J. Neurosci.* 18, 2002–2010. doi: 10.1046/j.1460-9568.2003.02921.x

Mascalchi, M., Diciotti, S., Giannelli, M., Ginestroni, A., Soricelli, A., Nicolai, E., et al. (2014). Progression of brain atrophy in spinocerebellar ataxia type 2: a longitudinal tensor-based morphometry study. *PLoS One* 9:e89410. doi: 10.1371/journal.pone.0089410

Meera, P., Pulst, S., and Otis, T. (2017). A positive feedback loop linking enhanced mGluR function and basal calcium in spinocerebellar ataxia type 2. *ELife* 6:e26377. doi: 10.7554/eLife.26377

Metzger, F., and Kapfhammer, J. P. (2000). Protein kinase C activity modulates dendritic differentiation of rat Purkinje cells in cerebellar slice cultures. *Eur. J. Neurosci.* 12, 1993–2005. doi: 10.1046/j.1460-9568.2000.00086.x

Mitoma, H., Kakei, S., and Manto, M. (2022). Development of cerebellar reserve. *Cells* 11:3013. doi: 10.3390/cells11193013

Muller, U. (2021). Spinocerebellar ataxias (SCAs) caused by common mutations. *Neurogenetics* 22, 235–250. doi: 10.1007/s10048-021-00662-5

Nakazono, A., Adachi, N., Takahashi, H., Seki, T., Hamada, D., Ueyama, T., et al. (2018). Pharmacological induction of heat shock proteins ameliorates toxicity of mutant PKCgamma in spinocerebellar ataxia type 14. *J. Biol. Chem.* 293, 14758–14774. doi: 10.1074/jbc.RA118.002913

Pears, C. J., Kour, G., House, C., Kemp, B. E., and Parker, P. J. (1990). Mutagenesis of the pseudosubstrate site of protein kinase C leads to activation. *Eur. J. Biochem.* 194, 89–94. doi: 10.1111/j.1432-1033.1990.tb19431.x

Pilo, C. A., Baffi, T. R., Kornev, A. P., Kunkel, M. T., Malfavon, M., Chen, D. H., et al. (2022). Mutations in protein kinase Cgamma promote spinocerebellar ataxia type 14 by impairing kinase autoinhibition. *Sci. Signal.* 15:eabk1147. doi: 10.1126/scisignal.abk1147

Power, E. M., Morales, A., and Empson, R. M. (2016). Prolonged type 1 metabotropic glutamate receptor dependent synaptic signaling contributes to spino-cerebellar ataxia type 1. *J. Neurosci.* 36, 4910–4916. doi: 10.1523/JNEUROSCI.3953-15.2016

Reetz, K., Costa, A. S., Mirzazade, S., Lehmann, A., Juzek, A., Rakowicz, M., et al. (2013). Genotype-specific patterns of atrophy progression are more sensitive than clinical decline in SCA1, SCA3 and SCA6. *Brain* 136, 905–917. doi: 10.1093/brain/aws369

Robinson, K. J., Watchon, M., and Laird, A. S. (2020). Aberrant cerebellar circuitry in the spinocerebellar ataxias. *Front. Neurosci.* 14:707. doi: 10.3389/fnins.2020.00707

Saito, N., and Shirai, Y. (2002). Protein kinase C gamma (PKC gamma): function of neuron specific isotype. *J. Biochem.* 132, 683–687. doi: 10.1093/oxfordjournals.jbchem.a003274

Schmitz-Hübsch, T., Lux, S., Bauer, P., Brandt, A. U., Schlapakow, E., Greschus, S., et al. (2021). Spinocerebellar ataxia type 14: refining clinicogenetic diagnosis in a rare adult-onset disorder. *Ann. Clin. Transl. Neurol.* 8, 774–789. doi: 10.1002/acn3.51315

Schrenk, K., Kapfhammer, J. P., and Metzger, F. (2002). Altered dendritic development of cerebellar Purkinje cells in slice cultures from protein kinase Cgamma-deficient mice. *Neuroscience* 110, 675–689. doi: 10.1016/s0306-4522(01)00559-0

Schulz, J. B., Borkert, J., Wolf, S., Schmitz-Hübsch, T., Rakowicz, M., Mariotti, C., et al. (2010). Visualization, quantification and correlation of brain atrophy with clinical symptoms in spinocerebellar ataxia types 1, 3 and 6. *Neuroimage* 49, 158–168. doi: 10.1016/j.neuroimage.2009.07.027

Seki, T., Matsubayashi, H., Amano, T., Shirai, Y., Saito, N., and Sakai, N. (2005). Phosphorylation of PKC activation loop plays an important role in receptor-mediated translocation of PKC. *Genes Cells* 10, 225–239. doi: 10.1111/j.1365-2443.2005.00830.x

Seki, T., Shimahara, T., Yamamoto, K., Abe, N., Amano, T., Adachi, N., et al. (2009). Mutant gammaPKC found in spinocerebellar ataxia type 14 induces aggregate-independent maldevelopment of dendrites in primary cultured Purkinje cells. *Neurobiol. Dis.* 33, 260–273. doi: 10.1016/j.nbd.2008.10.013

Seki, T., Takahashi, H., Adachi, N., Abe, N., Shimahara, T., Saito, N., et al. (2007). Aggregate formation of mutant protein kinase C gamma found in spinocerebellar ataxia type 14 impairs ubiquitin-proteasome system and induces endoplasmic reticulum stress. *Eur. J. Neurosci.* 26, 3126–3140. doi: 10.1111/j.1460-9568.2007.05933.x

Shakkottai, V. G., Chou, C. H., Oddo, S., Sailer, C. A., Knaus, H. G., Gutman, G. A., et al. (2004). Enhanced neuronal excitability in the absence of neurodegeneration induces cerebellar ataxia. *J. Clin. Invest.* 113, 582–590. doi: 10.1172/JCI20216

Shakkottai, V. G., Xiao, M., Xu, L., Wong, M., Nerbonne, J. M., Ornitz, D. M., et al. (2009). FGF14 regulates the intrinsic excitability of cerebellar Purkinje neurons. *Neurobiol. Dis.* 33, 81–88. doi: 10.1016/j.nbd.2008.09.019

Shakkottai, V. G., do Carmo Costa, M., Dell'Orco, J. M., Sankaranarayanan, A., Wulff, H., and Paulson, H. (2011). Early changes in cerebellar physiology accompany motor dysfunction in the polyglutamine disease spinocerebellar ataxia type 3. *J Neurosci.* 31, 13002–13014. doi: 10.1523/JNEUROSCI.2789-11.2011

Shimobayashi, E., and Kapfhammer, J. P. (2017). Increased biological activity of protein kinase C gamma is not required in spinocerebellar ataxia 14. *Mol. Brain* 10:34. doi: 10.1186/s13041-017-0313-z

Shimobayashi, E., and Kapfhammer, J. P. (2018). Calcium signaling, PKC gamma, IP3R1 and CAR8 link spinocerebellar ataxias and Purkinje cell dendritic development. *Curr. Neuropharmacol.* 16, 151–159. doi: 10.2174/1570159X15666170529104000

Shimobayashi, E., and Kapfhammer, J. P. (2021). A new mouse model related to SCA14 carrying a pseudosubstrate domain mutation in PKCgamma shows perturbed Purkinje cell maturation and ataxic motor behavior. *J. Neurosci.* 41, 2053–2068. doi: 10.1523/JNEUROSCI.1946-20.2021

Shirafuji, T., Shimazaki, H., Miyagi, T., Ueyama, T., Adachi, N., Tanaka, S., et al. (2019). Spinocerebellar ataxia type 14 caused by a nonsense mutation in the PRKCG gene. *Mol. Cell. Neurosci.* 98, 46–53. doi: 10.1016/j.mcn.2019.05.005

Shuvaev, A. N., Horiuchi, H., Seki, T., Goenawan, H., Irie, T., Iizuka, A., et al. (2011). Mutant PKCγ in spinocerebellar ataxia type 14 disrupts synapse elimination and long-term depression in Purkinje cells in vivo. *J. Neurosci.* 31, 14324–14334. doi: 10.1523/JNEUROSCI.5530-10.2011

Shuvaev, A. N., Hosoi, N., Sato, Y., Yanagihara, D., and Hirai, H. (2017). Progressive impairment of cerebellar mGluR signalling and its therapeutic potential for cerebellar ataxia in spinocerebellar ataxia type 1 model mice. *J. Physiol.* 595, 141–164. doi: 10.1113/JP272950

Soong, B.-W., and Morrison, P. J. (2018). "Chapter 10 – spinocerebellar ataxias" in *Handbook of clinical neurology*. eds. M. Manto and T. A. G. M. Huisman (Oxford: Elsevier), 143–174.

Sugawara, T., Hisatsune, C., Miyamoto, H., Ogawa, N., and Mikoshiba, K. (2017). Regulation of spinogenesis in mature Purkinje cells via mGluR/PKC-mediated phosphorylation of CaMKIIbeta. *Proc. Natl. Acad. Sci. U. S. A.* 114, E5256–E5265. doi: 10.1073/pnas.1617270114

Sullivan, R., Yau, W. Y., O'Connor, E., and Houlden, H. (2019). Spinocerebellar ataxia: an update. *J. Neurol.* 266, 533–544. doi: 10.1007/s00415-018-9076-4

Tada, M., Nishizawa, M., and Onodera, O. (2016). Roles of inositol 1,4,5-trisphosphate receptors in spinocerebellar ataxias. *Neurochem. Int.* 94, 1–8. doi: 10.1016/j.neuint.2016.01.007

Takahashi, H., Adachi, N., Shirafuji, T., Danno, S., Ueyama, T., Vendruscolo, M., et al. (2015). Identification and characterization of PKCgamma, a kinase associated with SCA14, as an amyloidogenic protein. *Hum. Mol. Genet.* 24, 525–539. doi: 10.1093/hmg/ddu472

Takahashi, N., Shuvaev, A. N., Konno, A., Matsuzaki, Y., Watanave, M., and Hirai, H. (2017). Regulatory connection between the expression level of classical protein kinase C and pruning of climbing fibers from cerebellar Purkinje cells. *J. Neurochem.* 143, 660–670. doi: 10.1111/jnc.14239

Tempia, F., and Konnerth, A. (1994). Calcium requirement of long-term depression and rebound potentiation in cerebellar Purkinje neurons. *Semin. Cell Biol.* 5, 243–250. doi: 10.1006/scel.1994.1030

Trzesniewski, J., Altmann, S., Jager, L., and Kapfhammer, J. P. (2019). Reduced Purkinje cell size is compatible with near normal morphology and function of the cerebellar cortex in a mouse model of spinocerebellar ataxia. *Exp. Neurol.* 311, 205–212. doi: 10.1016/j.expneurol.2018.10.004

Tsumagari, R., Kakizawa, S., Kikunaga, S., Fujihara, Y., Ueda, S., and Yamanoue, M. (2020). DGKγ knock-out mice show impairments in cerebellar motor coordination, LTD, and the dendritic development of purkinje cells through the activation of PKCγ. eneuro 7, ENEURO.0319-0319.2020. doi: 10.1523/eneuro.0319-19.2020

Verbeek, D. S., Goedhart, J., Bruinsma, L., Sinke, R. J., and Reits, E. A. (2008). PKC gamma mutations in spinocerebellar ataxia type 14 affect C1 domain accessibility and kinase activity leading to aberrant MAPK signaling. *J. Cell Sci.* 121, 2339–2349. doi: 10.1242/jcs.027698

Verbeek, D. S., Knight, M. A., Harmison, G. G., Fischbeck, K. H., and Howell, B. W. (2005). Protein kinase C gamma mutations in spinocerebellar ataxia 14 increase kinase activity and alter membrane targeting. *Brain* 128, 436–442. doi: 10.1093/brain/awh378

Watanabe, M., and Kano, M. (2011). Climbing fiber synapse elimination in cerebellar Purkinje cells. *Eur. J. Neurosci.* 34, 1697–1710. doi: 10.1111/j.1460-9568.2011.07894.x

Watanave, M., Takahashi, N., Hosoi, N., Konno, A., Yamamoto, H., and Yasui, H. (2022). Protein kinase Cgamma in cerebellar Purkinje cells regulates $Ca^{(2+)}$-activated large-conductance $K^{(+)}$ channels and motor coordination. *Proc Natl Acad Sci USA 119.* doi: 10.1073/pnas.2113336119

Waters, M. F., Minassian, N. A., Stevanin, G., Figueroa, K. P., Bannister, J. P., Nolte, D., et al. (2006). Mutations in voltage-gated potassium channel KCNC3 cause degenerative and developmental central nervous system phenotypes. *Nat. Genet.* 38, 447–451. doi: 10.1038/ng1758

Waters, M. F., and Pulst, S. M. (2008). Sca13. *Cerebellum* 7, 165–169. doi: 10.1007/s12311-008-0039-7

Watson, L. M., Bamber, E., Schnekenberg, R. P., Williams, J., Bettencourt, C., Lickiss, J., et al. (2017). Dominant mutations in GRM1 cause spinocerebellar ataxia type 44. *Am. J. Hum. Genet.* 101:866. doi: 10.1016/j.ajhg.2017.10.008

Wong, M. M. K., Hoekstra, S. D., Vowles, J., Watson, L. M., Fuller, G., Németh, A. H., et al. (2018). Neurodegeneration in SCA14 is associated with increased PKCγ kinase activity, mislocalization and aggregation. *Acta Neuropathol. Commun.* 6:99. doi: 10.1186/s40478-018-0600-7

Wu, Q. W., and Kapfhammer, J. P. (2021). Serine/threonine kinase 17b (STK17B) signalling regulates Purkinje cell dendritic development and is altered in multiple spinocerebellar ataxias. *Eur. J. Neurosci.* 54, 6673–6684. doi: 10.1111/ejn.15465

Yan, H., Pablo, J. L., and Pitt, G. S. (2013). FGF14 regulates presynaptic Ca2+ channels and synaptic transmission. *Cell Rep.* 4, 66–75. doi: 10.1016/j.celrep.2013.06.012

Zhang, Y., and Kaczmarek, L. K. (2016). Kv3.3 potassium channels and spinocerebellar ataxia. *J. Physiol.* 594, 4677–4684. doi: 10.1113/JP271343

frontiers | Frontiers in Molecular Neuroscience

TYPE Review
PUBLISHED 14 July 2023
DOI 10.3389/fnmol.2023.1236015

OPEN ACCESS

EDITED BY
Catarina Osorio,
Erasmus Medical Center, Netherlands

REVIEWED BY
Lilian Kisiswa,
Aarhus University, Denmark
Inês Serra,
Erasmus Medical Center, Netherlands

*CORRESPONDENCE
Yukio Yamamoto
✉ yukio.kist@gmail.com
Keiko Tanaka-Yamamoto
✉ keikoyamat@gmail.com

†These authors have contributed equally to this work

RECEIVED 07 June 2023
ACCEPTED 27 June 2023
PUBLISHED 14 July 2023

CITATION
Kim M, Jun S, Park H, Tanaka-Yamamoto K and Yamamoto Y (2023) Regulation of cerebellar network development by granule cells and their molecules.
Front. Mol. Neurosci. 16:1236015.
doi: 10.3389/fnmol.2023.1236015

Regulation of cerebellar network development by granule cells and their molecules

Muwoong Kim[1,2†], Soyoung Jun[1,2†], Heeyoun Park[1], Keiko Tanaka-Yamamoto[1,2*] and Yukio Yamamoto[1*]

[1]Brain Science Institute, Korea Institute of Science and Technology (KIST), Seoul, Republic of Korea, [2]Division of Bio-Medical Science and Technology, KIST School, University of Science and Technology (UST), Seoul, Republic of Korea

The well-organized cerebellar structures and neuronal networks are likely crucial for their functions in motor coordination, motor learning, cognition, and emotion. Such cerebellar structures and neuronal networks are formed during developmental periods through orchestrated mechanisms, which include not only cell-autonomous programs but also interactions between the same or different types of neurons. Cerebellar granule cells (GCs) are the most numerous neurons in the brain and are generated through intensive cell division of GC precursors (GCPs) during postnatal developmental periods. While GCs go through their own developmental processes of proliferation, differentiation, migration, and maturation, they also play a crucial role in cerebellar development. One of the best-characterized contributions is the enlargement and foliation of the cerebellum through massive proliferation of GCPs. In addition to this contribution, studies have shown that immature GCs and GCPs regulate multiple factors in the developing cerebellum, such as the development of other types of cerebellar neurons or the establishment of afferent innervations. These studies have often found impairments of cerebellar development in animals lacking expression of certain molecules in GCs, suggesting that the regulations are mediated by molecules that are secreted from or present in GCs. Given the growing recognition of GCs as regulators of cerebellar development, this review will summarize our current understanding of cerebellar development regulated by GCs and molecules in GCs, based on accumulated studies and recent findings, and will discuss their potential further contributions.

KEYWORDS

cerebellum, granule cell, parallel fiber, developmental regulation, gross structure, neuronal maturation, molecule secretion, cell–cell interaction

1. Introduction

Neuronal network structures in the brain are precisely formed during developmental periods through intrinsic programs in individual neurons and influence from neighboring neurons. Molecular expression patterns are dynamically altered in neurons during developmental periods, as revealed by transcriptome studies (Mody et al., 2001; Saito et al., 2002; Thompson et al., 2014; La Manno et al., 2021), and these molecules likely function not only in the development of own cells but also in the development of other cells or neuronal networks. The cerebellar cortex is one of the most regularly structured brain regions and consists of three layers: the internal granular layer (IGL), the Purkinje cell (PC) layer (PCL), and the molecular

layer (ML; Eccles et al., 1967). Although recent studies have discovered diversity of circuits and cell population in the cerebellum (De Zeeuw et al., 2021; Hull and Regehr, 2022), the basic structures are highly conserved throughout the cerebellum. As the sole output of the cerebellar cortex, PCs send inhibitory projections mostly to the deep cerebellar nuclei (DCN). The somas of PCs are aligned in the PCL, while their highly elaborate dendrites expand in the ML, where ML interneurons (MLIs) exist. Granule cells (GCs) are the only excitatory neurons among the major types of cerebellar neurons. Their small somas and short dendrites are located in the IGL, while their parallel fiber (PF) axons run parallel to the layer structures in the ML. In addition to the three major types of neurons, the cerebellar cortex contains several types of less abundant neurons, and their somas are located in the IGL or the PCL. The cerebellum receives two major excitatory inputs: climbing fibers (CFs) directly innervate PC dendrites in the ML, and mossy fibers (MFs) innervate GCs in the IGL. Thus, the somas, dendrites, and axons of individual types of cerebellar neurons and afferent projections from outside the cerebellum are present in the designated layers. Such organized cerebellar structures and synaptic connections are considered to be formed through well-orchestrated mechanisms during developmental periods (Park et al., 2021).

Granule cells convey information coming from MFs to PCs, making them a functionally important component in cerebellar networks. In addition to their role as components of neuronal networks, GCs have been shown to regulate the formation of cerebellar structures and networks during developmental periods (e.g., Hashimoto et al., 2009b; Legué et al., 2016; Park et al., 2019; Cadilhac et al., 2021; van der Heijden et al., 2021). The regulation is likely mediated through synaptic transmission, secreted molecules, molecular interactions, morphological constraints, or physical actions arising from the large number of GCs. Meanwhile, GCs themselves also go through dynamic events to mature (Vaudry et al., 2003; Iulianella et al., 2019; Wang and Liu, 2019; Consalez et al., 2021). In brief, GC precursors (GCPs) are originated in the rhombic lip (RL) and migrate to the external granular layer (EGL) in the cerebellum during mid-late embryonic days. GCPs then undergo intensive proliferation in the outer EGL during the first 2 weeks after birth in mice, while a portion of GCPs located in the inner EGL completes mitosis. The postmitotic GCs begin migration and simultaneously extend PFs. They first tangentially migrate at the border between the ML and the EGL, and then radially migrate along the processes of Bergmann glial cells toward the IGL. Once GCs reach the IGL, they remodel their dendrites through extension and retraction, form synapses with presynaptic MFs, and finally mature. Each GC matures through these events in turn, with all GCs reaching maturity within 3 weeks of the postnatal period in mice. Thus, GCs having PFs in the deep ML are born earlier than GCs having PFs in the superficial ML. Extensive research has been conducted on the developmental processes of GCs, leading to a comprehensive understanding of the molecules that regulate these processes, particularly in the early stages of development. These regulatory mechanisms have been thoroughly documented in various review articles (Vaudry et al., 2003; Leto et al., 2016; Lackey et al., 2018; Iulianella et al., 2019; Wang and Liu, 2019; Consalez et al., 2021). In contrast, our understanding of how GCs and their molecules regulate the structure and network formation of the cerebellum is gradually increasing. In this article, we discuss such regulation of cerebellar formation by GCs and molecules in GCs, which have been found in experimental studies using mice, unless otherwise stated. The regulation discussed here is summarized in Table 1.

2. Contributions of GCs and their molecules to the formation of cerebellar size and foliation

The cerebellum, which is Latin for the "little brain," accounts for more than 10% of the total brain volume in mice (Angenstein et al., 2007; Ma et al., 2008). The cerebellum has a complex 3D structure, with lobules divided by fissures along the anterior–posterior (a-p) axis. The lobules in the cerebellar vermis of rodents are grouped into four zones: the anterior zone (lobules I–V), the central zone (lobules VI–VII), the posterior zone (lobule VIII and anterior lobule IX), and the nodular zone (posterior lobule IX and lobule X), based on specific gene expression (Ozol et al., 1999). Despite varying sizes and shapes in individual lobules, the tri-layered cytoarchitecture with specific cell types present in designated layers is consistent throughout the cerebellum. These cerebellar gross structures begin to form in the late embryonic stage and continue to develop during the first 2 weeks after birth. This coincides with the massive proliferation of GCPs in the EGL (Lauder et al., 1974), suggesting a link between the two events. Indeed, numerous studies have demonstrated that the proliferation of GCPs is crucial not just for cerebellar enlargement but also for the formation of gross structures (Figure 1). Early studies used animals with severely reduced numbers of GCs (hypogranular or agranular cerebellum), including scrambler, weaver, reeler, and staggerer spontaneous mutation mice or x-irradiated rats, and found abnormal foliation and lamination in the cerebellum of these animals (Altman and Anderson, 1971; Rezai and Yoon, 1972; Rakic and Sidman, 1973; Mariani et al., 1977; Mikoshiba et al., 1980; Herrup, 1983; Herrup and Sunter, 1987; Smeyne and Goldowitz, 1989; Ferguson, 1996; Goldowitz et al., 1997). Based on the observation of both macroscopic and microscopic morphogenesis of the cerebellum, it was further demonstrated how GCP proliferation contributes to foliation. Foliation was initiated at the late embryonic day 17.5 (E17.5) by the increase in GCP proliferation and consequent inward thickening of the EGL in the anchoring centers, which are regions that will become the base of fissures in the future (Sudarov and Joyner, 2007). At later developmental stages, differentially regulated GCP proliferation in different lobules appears to be involved in determining the different shapes and lengths of cerebellar lobules (Legué et al., 2015, 2016). Thus, GCP proliferation and their locally differential control largely contribute to the formation of unique cerebellar gross structures, although the determinants of locally differential control remain uncertain.

Similar to other neurons (Hevner, 2006; Hevner et al., 2006; Stevanovic et al., 2021), early GC development is regulated by several types of transcription factors and their regulating molecules (see reviews in Wang and Liu, 2019; Consalez et al., 2021). Because cerebellar lobule and folium formation depend on the expansion of the GC population, these molecules in GCs have been shown to be essential not only for GC proliferation, survival, or neurogenesis, but also for the formation of the gross structure of the cerebellum (Figure 1i). One of the molecules for which such a link has been described is the atonal basic helix–loop–helix transcription factor 1

TABLE 1 Summary of GC involvement in the regulation of cerebellar development.

Cerebellar developmental events		Involvement of GCs		Reference
		Mechanical or biological contributions	Molecules involved	
Size and foliation	Enlargement foliation, and lamination	Coincidental massive proliferation		Lauder et al. (1974)
		Proliferation (observation in agranular cerebellum)		Altman and Anderson (1971); Rezai and Yoon (1972); Rakic and Sidman (1973); Mariani et al. (1977); Mikoshiba et al. (1980); Herrup (1983); Herrup and Sunter (1987); Smeyne and Goldowitz (1989); Ferguson (1996); Goldowitz et al. (1997)
		Proliferation	Atoh1	Ben-Arie et al. (1997); Jensen et al. (2004); van der Heijden et al. (2021)
		Proliferation and differentiation	Wnt/β-catenin	Lorenz et al. (2011); Pei et al. (2012); Wen et al. (2013)
	Enlargement and foliation	Shh-dependent proliferation	Gli1, Gli2	Corrales et al. (2004, 2006)
		Radial migration at appropriate speed	Lkb1	Ryan et al. (2017)
		Proliferation and differentiation	CHD8	Kawamura et al. (2021); Chen et al. (2022)
	Enlargement	Proliferation	En1, En2	Orvis et al. (2012)
	Foliation	Increase in proliferation in anchoring center		Sudarov and Joyner (2007)
		Anterior–posterior orientation of cell division	CHD7	Reddy et al. (2021)
	Regulation of folia length	Differentially regulated proliferation		Legué et al. (2015); Legué et al. (2016)
		(Theoretical study) Migration at experimentally observed speed		Takeda et al. (2021)
PCs	PC migration in primordial cerebellum	Providing molecular guidance	Reelin	Mariani et al. (1977); Mikoshiba et al. (1980)
	PC monolayer formation	Accumulation of GCs in the IGL and stacking of PFs in the ML		Altman et al. (1969)
		Providing a short-range signal		Carletti et al. (2008)
			Reelin*	Miyata et al. (1997); Magdaleno et al. (2002)
	PF-PC synapse formation	Providing synaptic organizers that interact with GluD2 in PCs	Cbln1, NRX	Kurihara et al. (1997); Hirai et al. (2005); Matsuda et al. (2010); Uemura et al. (2010); Hashizume et al. (2013); Elegheert et al. (2016)
		PF bouton maturation for synapse formation with PCs	Mea6	Wang et al. (2021)
			Chd4	Yamada et al. (2014)
	MLI-PC synapse formation	Competition of synapse formation by forming PF synapses	Cbln1	Ito-Ishida et al. (2014)
	PC dendrite development	Supplying competing substances that activate TrkC in PCs	NT-3	Joo et al. (2014)
		Supplying competing substances that interact with GluD2 in PCs	Cbln1	Takeo et al. (2021)
		Unbiased synaptic transmission		Park et al. (2019)
	Maturation of PC firing properties	(recording in agranular mice)		van der Heijden et al. (2021)
MLIs	MLI migration	Synaptic transmission		Park et al. (2019)
		Molecular scaffolding	TAG-1	Cadilhac et al. (2021)
	Maturation	Interacting in the EGL	TAG-1	Park et al. (2019); Cadilhac et al. (2021)
		Activation of TrkB in MLIs	BDNF*	Rico et al. (2002)
	PF-MLI synapse formation and MLI survival	Providing synaptic organizers that interact with GluD1 in MLIs	Cbln1, NRX*	Yasumura et al. (2012); Konno et al. (2014)

(Continued)

TABLE 1 (Continued)

Cerebellar developmental events		Involvement of GCs		Reference
		Mechanical or biological contributions	Molecules involved	
CF inputs	Elimination of surplus CF synapses	(observation in hypogranular rats)		Crepel et al. (1981)
		PF-PC synapse formation	Cbln1	Kurihara et al. (1997); Hirai et al. (2005); Hashizume et al. (2013)
		PF-PC synaptic transmission		Chen et al. (1995); Kano et al. (1997); Offermanns et al. (1997); Kano et al. (1998)
	CF territory elongation	PF-PC synaptic transmission		Ichikawa et al. (2002); Hirai et al. (2005)
		PF-PC synaptic transmission in the deep ML		Park et al. (2019)
	CF territory segregation	PF-PC synaptic formation	Cbln1	Ichikawa et al. (2002); Hirai et al. (2005)
MF inputs	MF terminal remodeling	Coincidental GC dendritogenesis		Hámori and Somogyi (1983)
		Providing substances that promote the maturation	WNT-7a	Hall et al. (2000)
			Neuroligin	Scheiffele et al. (2000)
			FGF22	Umemori et al. (2004)
	MF-GC synapse formation	Interactions through cell adhesion molecules	Cdh7	Kuwako et al. (2014)
	Structured MF-GC synaptic connections	Coincidental development		Shuster et al. (2021); Kim et al. (2023)
Other GCs	GC radial migration	A source of glutamate*		Komuro and Rakic (1993)
			BDNF*	Wetmore et al. (1990); Rocamora et al. (1993)
	GCP proliferation in the EGL	Microenvironment of mitogenic niche*		Choi et al. (2005)

Abbreviations are defined in the text. Note that asterisks (*) in this table indicate that the molecules or mechanisms described are likely to be involved but have not been clearly identified.

(Atoh1, Math1), which is expressed in the RL from E13. In mice lacking Atoh1, GCs were not produced, and the EGL was not formed, leading to severely altered cerebellar gross structures without foliation and lamination (Ben-Arie et al., 1997; Jensen et al., 2004; van der Heijden et al., 2021). Sonic hedgehog (Shh) produced in PCs has long been known as a potent inducer of GCP proliferation and as an important factor for appropriate folium formation in the cerebellum (Dahmane and Altaba, 1999; Lewis et al., 2004). Three Gli proteins (Gli1, Gli2, and Gli3), zinc-finger transcription factors participating in the Shh signaling pathway (Carballo et al., 2018), are expressed in the EGL (Corrales et al., 2004). Considering the reduced foliation in mice lacking Gli2 and the further reduction of foliation in mice lacking both Gli1 and Gli2 (Corrales et al., 2004, 2006), Gli1 and Gli2 are likely to cooperate as targets of Shh in GCPs to promote proliferation and consequent folium formation. Apart from its role in GCP production during embryonic days, Atoh1 promotes GCP proliferation during postnatal development by controlling cilia formation required for Shh signaling (Flora et al., 2009; Chang et al., 2019). Thus, Atoh1 and the Shh signaling pathways likely cooperate in cerebellar folium formation during postnatal development. In addition to the Shh signaling pathway, the Wnt/β-catenin signaling pathway has been shown to be involved in folium and layer formations through regulating GC development (Lorenz et al., 2011; Pei et al., 2012; Wen et al., 2013). Both the absence and enhancement of Wnt/β-catenin signaling in GCPs led to abnormal cerebellar gross structures and reduced cerebellar size, although they caused different changes at the cellular level: the absence of signaling facilitated GCP proliferation, leading to an accumulation of abnormally matured GCs near the pial surface, whereas increasing signaling inhibited GCP proliferation, leading to a reduction of GCs. Homeobox transcription factors, Engrailed 1 (En1) and 2 (En2), have also been implicated in cerebellar folium formation (Bilovocky et al., 2003; Sudarov and Joyner, 2007; Cheng et al., 2010). However, based on a study that used En1/2 conditional knockout mice either in the RL or the ventricular zone (VZ), the latter of which gives rise to cerebellar γ-aminobutyric acid (GABA)-ergic neurons, their expression in GCs appears to contribute more to cerebellar enlargement than to the regulation of foliation (Orvis et al., 2012).

The abovementioned example of the absence of Wnt/β-catenin signaling raises a possibility that the formation of cerebellar gross structures relies not only on the expansion of the GC population but also on the proper maturation of GCs. In line with this concept, multiple studies have demonstrated that cerebellar foliation is influenced by events in GC development beyond just proliferation (Figures 1ii–iv). The absence of liver kinase B1 (Lkb1), also known as serine/threonine kinase 11, in GCPs was shown to increase cerebellar size and foliation without affecting proliferation, but through delayed radial migration of GCs (Ryan et al., 2017). A theoretical study also predicted that GC migration at the experimentally observed speed (Yacubova and Komuro, 2002) resulted in non-uniform GC accumulation in the IGL and consequent folia lengthening (Takeda et al., 2021). Moreover, cerebellar gross structures are also regulated by two chromodomain helicase DNA-binding (CHD) proteins, CHD7 and CHD8, which are associated with cerebellum-related neurodevelopmental disorders. CHD7 is a major causative molecule of CHARGE syndrome, and CHD8 is a risk factor for autism spectrum disorder. Deletion of CHD8 in GCPs induced defects in foliation and hypoplasia through the attenuated proliferation and precocious

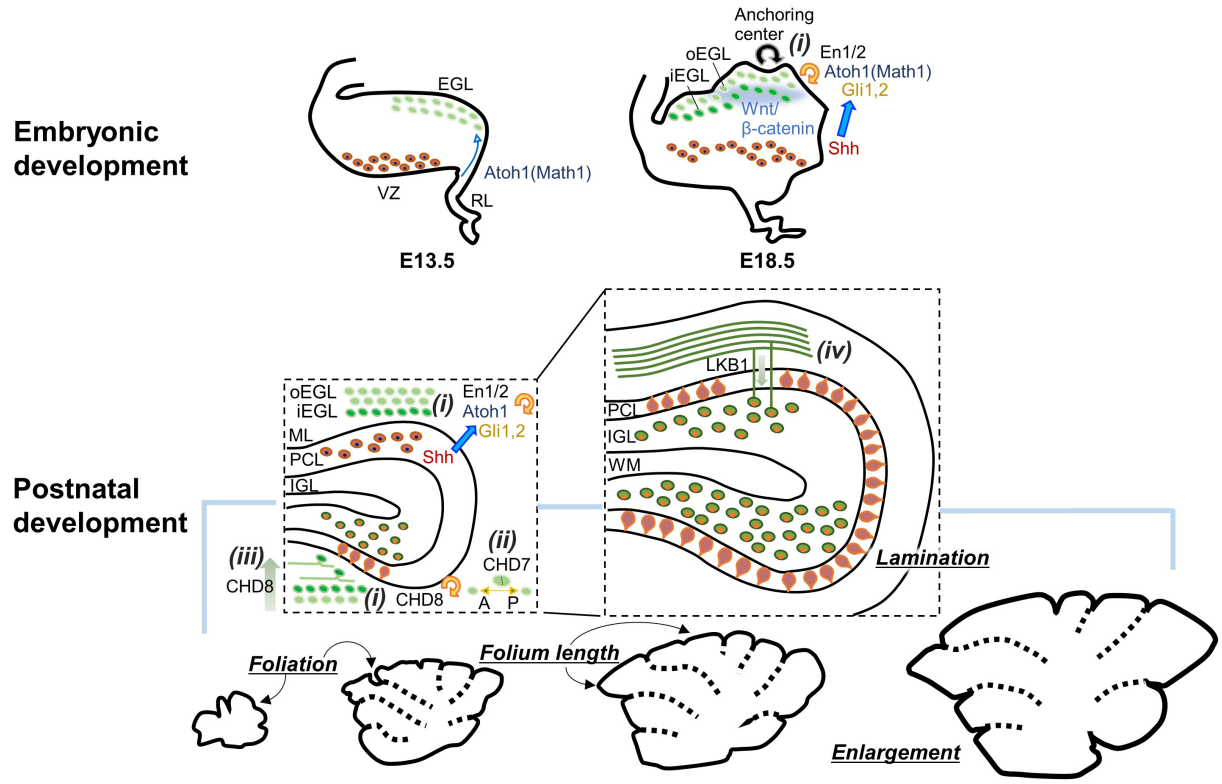

FIGURE 1
Diagram showing how GCs contribute to the formation of the cerebellar gross structures during embryonic and postnatal development. GCP proliferation **(i)**, axis of GCP division **(ii)**, GC differentiation **(iii)**, and GC migration **(iv)** affect the enlargement, foliation, and lamination of the cerebellum. Consequently, molecules involved in these GC developmental processes are also implicated. oEGL, outer EGL; iEGL, inner EGL. Other abbreviations are defined in the text.

differentiation of GCs (Kawamura et al., 2021; Chen et al., 2022). The conditional knockout of CHD7 in GCPs resulted in a unique cerebellar structure with polymicrogyria and reduced anterior–posterior foliation (Reddy et al., 2021). Interestingly, the CHD7 deletion did not alter GCP proliferation, GC migration, and neurite development, but altered the preferred axis of division of GCPs from anterior–posterior orientation to mediolateral orientation, supporting the idea that the axis of GCP division is important for the formation of cerebellar foliation (Legué et al., 2015; Lejeune et al., 2019).

3. Contributions of GCs and their molecules to cerebellar development at the cellular and synaptic levels

When the size and gross structures of the cerebellum are altered during postnatal development, the neuronal morphology also undergo changes through proliferation, differentiation, migration, dendritogenesis, and synaptogenesis. Consequently, the formation of the cerebellar network is typically completed by around 3–4 weeks of age. While GCs are a major factor of the macroscopic alterations in the developing cerebellum, as described above, they also serve as regulators of cerebellar network formation through their mechanical, morphological, functional, or molecular influences on neuronal development and synaptic formation. In this section, we aim to introduce the implications of GCs for the development of individual components and to further predict possible functions or relevance of GCs for their development based on recent studies. For clarification, we simply describe the developmental processes of individual components at the beginning of each subsection, and then describe the contributions of GCs to these processes.

3.1. PC development

Purkinje cells are generated from the VZ of the cerebellar anlage and undergo their final mitosis around E10–E13 in mice (Miale and Sidman, 1961; Hatten and Heintz, 1995; Sotelo and Rossi, 2013). The newborn PCs migrate toward the pial surface of the primordial cerebellum and form a multilayered structure called the PC plate (Hatten and Heintz, 1995; Miyata et al., 2010; Sotelo and Rossi, 2013). PC somas are then organized into a monolayer by the end of the first postnatal week (Sotelo and Rossi, 2013). While PC axonal projections to the DCN appear to be formed during embryonic periods, PC dendritic morphology is dynamically remodeled during postnatal development through growth, branching, and regression (Armengol and Sotelo, 1991; Kapfhammer, 2004; Sotelo and Rossi, 2013; Beekhof et al., 2021). Such dendritogenesis leads to the characteristic structure of highly arborized PC dendrites mostly with one or two primary dendrites (Cerminara et al., 2015). During the second and third postnatal weeks when dendritogenesis actively occurs, PCs also establish synaptic connections with two excitatory inputs, PFs and

CFs, and inhibitory inputs from MLIs (Sassoè-Pognetto and Patrizi, 2017).

Granule cells can influence PC development from the moment PCs migrate in the primordial cerebellum (Figure 2A). The PC migration toward the pial surface is mediated by an extracellular glycoprotein, Reelin, and as a consequence, PCs remained in the central area of the cerebellum in mice lacking *reelin* (Mariani et al., 1977; Mikoshiba et al., 1980). There are two sources of Reelin around E13 (Miyata et al., 1996; Schiffmann et al., 1997; Rice and Curran, 2001), the EGL and the nuclear transitory zone (NTZ), the latter of which presumably includes future DCN neurons (Fink et al., 2006; Elsen et al., 2013). In Atoh1-null mice that lack the EGL, a significant subpopulation of PCs failed to migrate from the central area to the pial surface (Ben-Arie et al., 1997; Jensen et al., 2002). In addition, abnormal PC positions in cultured slices obtained from mice lacking Reelin were restored by co-culturing with Reelin-positive GCs (Miyata et al., 1997). These data indicate that normal PC migration requires Reelin originating not only from the NTZ but also from GCPs in the EGL. The formation of the PC monolayer during the first postnatal week also relies on GCs (Figure 2B). A concept was proposed that monolayer formation is mediated by the mechanical pressure due to the accumulation of GCs in the IGL and simultaneous stacking of their PFs in the ML (Altman and Winfree, 1977), based on the observation of PC soma misalignment in hypogranular cerebella caused by X-ray irradiation (Altman et al., 1969). The positions of PCs transplanted into the developing cerebellum were affected by the locations of the EGL at the time of PC transplantation (Carletti et al., 2008), indicating that interactions with the EGL via short-range signals determine the positions of PC somas. The signals may include Reelin, because two studies suggested that Reelin secreted from GCs may play roles in the formation of the PC monolayer (Miyata et al., 1997; Magdaleno et al., 2002). This idea is reasonable, considering that Reelin is present in the EGL from the embryonic period to the first postnatal week (Miyata et al., 1996).

Among the events that take place later in PC development, synaptic formation between PFs and PCs largely relies on molecules released from PFs or expressed in GCs (Figure 3A). A C1q family protein, Cbln1, is released from PFs through a unique, activity-dependent mechanism, which is a release from lysosomes (Ibata et al., 2019). Cbln1 then forms a tripartite complex with neurexin (NRX) expressed in PFs and glutamate receptor δ2 (GluD2) expressed in PC dendrites, leading to the formation and maintenance of PF-PC synapses (Matsuda et al., 2010; Uemura et al., 2010; Elegheert et al., 2016). This NRX/Cbln1/GluD2 tripartite complex appears to regulate the clustering of postsynaptic molecules, such as AMPA-type glutamate receptors or Homer 3, in PCs (Matsuda et al., 2010). GC-specific deletion of meningioma expressed antigen 6 (Mea6), initially found in tumor cells (Heckel et al., 1997), resulted in a reduction of PF-PC synapse formation, presumably due to impaired intracellular transportation of molecules required for synapse formation, including vesicular glutamate transporter 1 (vGluT1) and brain-derived neurotrophic factor (BDNF; Wang et al., 2021). PF-PC synapse density was also found to be reduced in mice lacking Chd4, a subunit of the nucleosome remodeling and deacetylation (NuRD) complex, specifically in GCs (Yamada et al., 2014). These observations suggest the functions of Mea6, Chd4, the NuRD complex, or their downstream molecules in GCs for PF-PC synaptogenesis. In addition, the maturation of synapses between CFs and PCs is highly dependent on PFs, which will be elaborated in the subsequent section regarding major afferent pathways (section 3.3). Conversely, while GCs appear to be involved in the maturation of MLIs, as described below (section 3.2), and this, in a broader context, could be interpreted as their contribution to the formation of inhibitory synapses from MLIs to PCs, their specific role in the process of inhibitory synapse formation itself remains uncertain. A study demonstrated that the absence of Cbln1 led to an increase in MLI-PC synapses, and this increase was reversed by the addition of recombinant Cbln1 in a GluD2-dependent manner (Ito-Ishida et al., 2014). Because Cbln1 and GluD2 are critical for PF-PC synapse formation, this study raises the possibility that PF synapses may engage in competitive interactions with MLI inhibitory synapses for PC dendrites through the release of Cbln1, which binds to GluD2 (Figure 3B). However, a partial blockade of transmitter release from PFs located in the middle ML did not affect the distribution of MLI synapses (Park et al., 2019), indicating that the competitive interactions would not be mediated by PF synaptic transmission.

Even though studies in cultured cerebellar neurons demonstrated the role of GCs in PC dendrite outgrowth (Baptista et al., 1994; Morrison and Mason, 1998; Hirai and Launey, 2000), GCs were originally considered to be inessential for PC dendrite development *in vivo*. This is because PC dendrite morphology was not altered when PF-PC synapses were globally impaired in transgenic mice expressing tetanus toxin (TeTx) in GCs (Kim et al., 2009) or in knockout mice lacking GluD2 (Kashiwabuchi et al., 1995; Kurihara et al., 1997), type 1 metabotropic glutamate receptor (mGluR1; Kano et al., 1997), or Cbln1 (Hirai et al., 2005). In contrast, clearly abnormal PC dendrites have been observed with partial impairment of GC-PC interaction (Figure 2C). Sparse knockout of the neurotrophin receptor tropomyosin-related kinase C (TrkC) in PCs, but not global knockout of TrkC, reduced the complexity of PC dendritic arborization (Joo et al., 2014). The phenotype was rescued by additional removal of its ligand, neurotrophin-3 (NT-3), from GCs. Similarly, sparse but not global knockout of GluD2 resulted in abnormal PC dendrite morphology, with under-elaboration in the deep ML and overelaboration in the superficial ML, which was rescued by additional removal of the GluD2 interacting partner, Cbln1, secreted from GCs (Takeo et al., 2021). In simple terms, these studies demonstrated that a sparse reduction of TrkC or GluD2 in PCs resulted in abnormal PC dendrite morphology due to a lack of interaction with NT-3 or Cbln2 secreted by GCs, indicating that molecules secreted by GCs actually play a crucial role in PC dendrite morphogenesis. In particular, these specific molecules are not universally essential but rather exert their influence through competition-based mechanisms. In this process, neighboring PCs appear to compete for binding to these molecules, which ultimately affects the dendritic arborization of each PC. Supporting this idea that molecules secreted by GCs contribute to PC dendrite morphogenesis, blocking transmitter release by expressing TeTx specifically in PFs located in the middle ML led to the local reduction of PC dendritic branches (Park et al., 2019). Thus, GCs likely regulate PC dendrite development by providing molecules that promote normal dendritic branching and outgrowth.

Although Atoh1-null mice have often been used to test the importance of GCs in cerebellar embryonic development, they are neonatal lethal and cannot be used to test postnatal functional development. On the other hand, conditional knockout mice lacking Atoh1 in En1-expressing cells are useful, because they remain viable

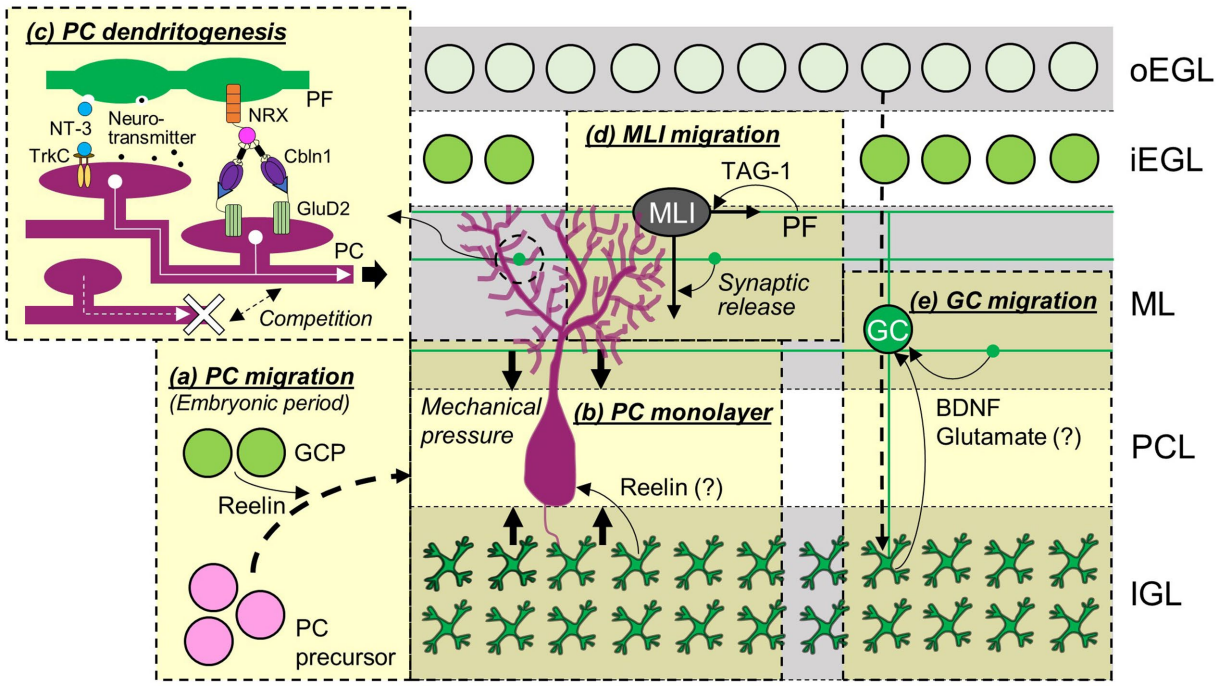

FIGURE 2
Contributions of GCs to the development of cerebellar neurons. The migration of PC precursors during embryonic periods **(A)**, formation of PC monolayers **(B)**, development of PC dendrites **(C)**, and migration of MLI **(D)** and other GCs **(E)** are regulated by GCs and molecules released from or expressed in GCs. Abbreviations are defined in the text.

during the second postnatal week and still have an agranular cerebellum. While PC firing patterns were dynamically altered during postnatal developmental periods in control mice (Beekhof et al., 2021; van der Heijden et al., 2021), conditional Atoh1 knockout mice maintained an immature state of firing patterns (van der Heijden et al., 2021). Thus, GCs are also critical for the maturation of PC firing properties. Overall GC-mediated regulation of structural and functional PC development during postnatal periods appears to be achieved through several mechanisms, including synaptic organizers, neurotrophin release, or synaptic transmission, as described above. It was previously shown that the presynaptic coupling between calcium channels and the sensor for vesicle fusion at PF boutons changes from a loose microdomain to a tight nanodomain around the second or third postnatal week (Baur et al., 2015; Kusch et al., 2018; Schmidt, 2019). Considering the temporal coincidence, it is possible to speculate that synaptic transmission via the loose microdomain at PF boutons is appropriate for the regulation of PC development.

3.2. MLI development

Molecular layer interneurons, consisting of two types of neurons, basket and stellate cells, provide a feedforward inhibition motif by receiving inputs from GCs and sending inhibitory signals to PCs. MLIs are part of the cerebellar GABAergic interneurons derived from specific progenitor populations in the VZ that differ from PC progenitor populations (Leto et al., 2012; Prestori et al., 2019). Progenitors of GABAergic interneurons continue to proliferate in the prospective white matter (pWM) from late embryonic days to the second postnatal week. According to the inside-out sequence of differentiation, MLIs are finally born in the first to second postnatal week (Leto et al., 2016). Immature postmitotic MLIs then travel toward their final destinations by taking a complex migratory route via radial and tangential migration in the ML (Simat et al., 2007; Cameron et al., 2009).

To the best of our knowledge, no studies have been reported regarding the question of whether GCs or molecules released from GCs are involved in the developmental process of MLIs in the VZ or pWM. It has been shown that GABAergic interneurons, including MLIs, differentiate into mature identities under the influence of local environmental cues existing in the pWM (Leto et al., 2006, 2009, 2012). Although the nature or source of such cues has not been identified, one possible involvement of GCs in MLI development in the pWM might be the provision of the cues, since many GCs already exist in the IGL, right next to the pWM, at the time when MLIs acquire their identities. In contrast to the early developmental process of MLIs, the complex migration of MLIs is at least partially regulated by GCs (Figure 2D). This was first suggested by a study showing that glutamatergic synaptic transmission was involved in MLI migration (Wefers et al., 2017). A specific blockade of synaptic transmission from PFs resulted in abnormal distributions of MLIs (Park et al., 2019), providing direct evidence of the involvement of GC-dependent synaptic transmission in the positioning of MLIs, likely through regulating their migrations. Furthermore, a recent study demonstrated an interesting interaction between immature GCs and migrating MLIs (Cadilhac et al., 2021). Once late-born MLIs migrate to the EGL, they stop radial migration and start tangential migration at the inner EGL. The study demonstrated that this tangential migration was supported by

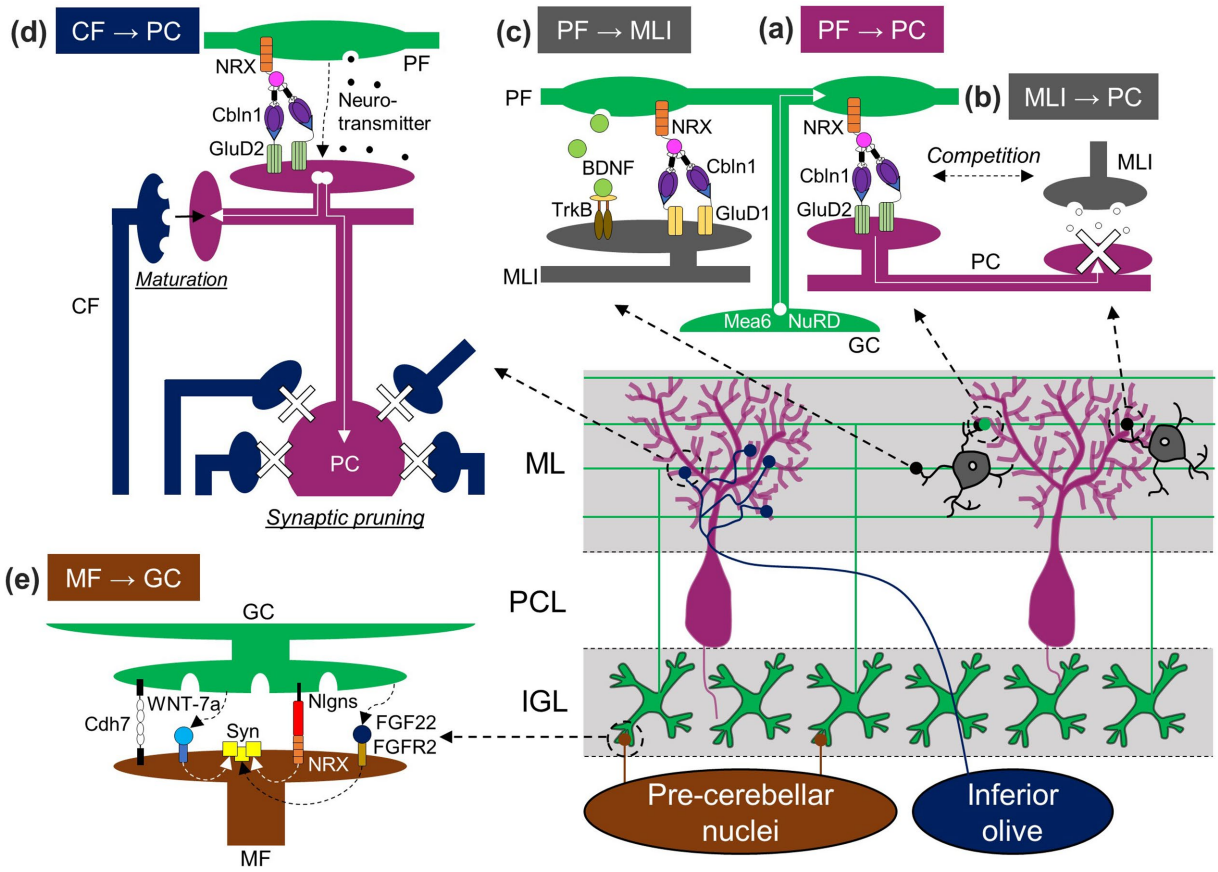

FIGURE 3
GC-dependent regulation of synaptic formation in the cerebellum. GCs influence the establishment not only of GC synapses [PF-PC **(A)**, PF-MLI **(C)**, and MF-GC **(E)** synapses], but also other synapses [MLI-PC **(B)** and CF-PC **(D)** synapses] through the release of molecules, presentation of membrane molecules, synaptic activation, or physical competition. Nlgns, Neuroligin. Other abbreviations are defined in the text.

PFs of premigratory GCs and TAG-1 expressed in such immature PFs.

In addition to MLI migration, GCs and molecules in GCs appear to promote the functional and structural maturation of MLIs. After deleting Atoh1 from GCPs in the first postnatal week, which resulted in the depletion of GCPs in the EGL, the expression of parvalbumin, a mature MLI marker, was absent in MLIs located in the outer ML, and the levels of glutamic acid decarboxylase (GAD) 65, a GABAergic presynaptic marker, were reduced in the ML (Cadilhac et al., 2021). The reduction of GAD65 in the ML was also observed when a neurotrophin receptor, TrkB, was depleted in the cerebellum (Rico et al., 2002). Although the source of neurotrophins regulating MLI synaptic differentiation is not completely clarified, BDNF released from GCs is likely involved in the regulation. BDNF is one of the two major neurotrophins activating TrkB (Huang and Reichardt, 2001), and its mRNA is specifically expressed in GCs within the rat cerebellar cortex during postnatal developmental periods (Rocamora et al., 1993), although immunohistochemical BDNF signals were detected in PCs of adult mice (Cook et al., 2022). Similar to PF-PC synapses, PF-MLI synapses are believed to be formed via a tripartite trans-synaptic bridge (Andrews and Dravid, 2021), because MLIs express GluD1, which can also form a tripartite trans-synaptic bridge with Cbln1 and NRX (Yasumura et al., 2012), and GluD1 knockout mice showed a reduction of PF-MLI synapses (Figure 3C, Konno et al., 2014). In the GluD1 knockout mice, the size and number of MLIs were reduced (Konno et al., 2014). Thus, GCs appear to play a role in the regulation of neuronal maturation and survival of MLIs through physical interaction in the EGL, neurotrophin release, or synaptic formation with MLIs.

3.3. Major afferent pathways

Climbing fibers originating from the inferior olivary nucleus arrive in the developing cerebellum around E14–E15 (Reeber et al., 2013; Rahimi-Balaei et al., 2015) and make immature synapses onto PCs by P3 (Hashimoto and Kano, 2013; Kano et al., 2018). During the early postnatal stages known as the creeper stage and pericellular nest stage (Chedotal and Sotelo, 1993), multiple CFs form contacts with immature PC dendrites and PC somas (Hashimoto et al., 2009a). The CF-PC synapses are then dynamically rearranged to create characteristic mono-innervation. To generate such mature CF-PC synapses, one CF is strengthened and forms a few hundred synapses on PC dendrites, while surplus CFs are gradually eliminated through two distinct steps, early and late elimination.

In the agranular cerebellar model, vGluT2 staining signals were present around PC somas, and complex spikes were detected from PCs, both of which are signs of the existence of CF synapses (van der

Heijden et al., 2021). This suggests that GCs are not required for early CF development, namely, the arrival to the cerebellum and the formation of immature synapses. In contrast, several stages of CF synapse maturation rely on GCs (Figure 3D). GCs are well known to be required for the elimination of surplus CFs. Multiple CF innervations remained in the mature cerebellum of hypogranular rats (Crepel et al., 1981; Bailly et al., 2018) or knockout mice lacking molecules required for the functional or structural formation of PF-PC synapses, such as mGluR1, protein kinase Cγ, phospholipase Cβ4, α-subunit of heterotrimeric Gq protein, or GluD2 in PCs, and Cbln1 in GCs (Chen et al., 1995; Kano et al., 1997, 1998; Kurihara et al., 1997; Offermanns et al., 1997; Hirai et al., 2005; Hashizume et al., 2013). In addition to the elimination of surplus CFs, GCs also contribute to the strengthening and maturation of the remaining CFs, known as winner CFs. The strengthening and maturation involve complex processes, such as the elongation of CF synapse territories along PC dendrites, the reorganization of CF synapses within the CF territories, and the segregation of CF territories from PF territories (Ichikawa et al., 2016). Consequently, the involvement of GCs appears to be complex. In mice lacking mGluR1, the CF territory was reduced, and CF and PF territories remained largely mixed (Ichikawa et al., 2016). Considering that mGluR1 mainly functions at PF synapses due to the glutamate transporters limiting mGluR1 responses at CF synapses (Dzubay and Otis, 2002), the results suggest the requirement of PF inputs for CF territory elongation and territory segregation. Despite reduced CF territories when PF inputs were functionally impaired, CF territories increased when PF synapses were structurally reduced in mice lacking GluD2 or Cbln1 (Ichikawa et al., 2002; Hirai et al., 2005). Furthermore, CF territories were reduced by inhibiting PF synaptic transmission in the deep ML, but not in the superficial ML (Park et al., 2019). Taken together, it is possible that the physical competition of CF synapses with PF synapses limits CF territories within appropriate regions, while functional PF inputs at the deeper ML promote CF territory elongation.

Another major input, MFs, originates from multiple nuclei in the brainstem and spinal cord. Their arrivals in the developing cerebellum vary according to their origins, yet all types of MFs arrive by P0 (Rahimi-Balaei et al., 2015). Although the EGL includes precursors of GCs, which MFs innervate in the mature cerebellum, MFs do not enter the EGL and wait for GCs to differentiate and migrate into the IGL. Meanwhile, MF terminals increase in size to form characteristic mature MF terminals (Hámori and Somogyi, 1983; Kim et al., 2023), called rosettes. On the other hand, some MFs originating from the pontine nucleus or spinal cord transiently contact PCs during this developmental period (Kuwako et al., 2014; Sillitoe, 2016). Around the third postnatal week, MF synaptic connections are finally established with the dendrites of GCs and Golgi cells in the glomeruli in the IGL.

The MFs originating from the spinal cord, labeled by an anterograde tracer dye, were present in the agranular cerebellum (van der Heijden et al., 2021), suggesting that GCs are not required for the arrival of MFs in the cerebellum. In contrast, GCs are easily expected to have a significant impact on MF development inside the cerebellum, because synaptogenesis often relies on the interplay between pre- and post-synaptic neurons (Akins and Biederer, 2006; Petzoldt and Sigrist, 2014). Indeed, studies have revealed the role of GCs and their molecules in MF development (Figure 3E). An early electron microscopy study first suggested the role of GCs by demonstrating the correlation between rapid MF enlargement and intense increase in GC dendrites (Hámori and Somogyi, 1983). The increase in size and presynaptic differentiation of MF terminals, the latter of which can be observed by clustering of synaptic vesicles or presynaptic molecules, have been shown to be mediated by secreted molecules from GCs, WNT-7a, and fibroblast growth factor 22 (FGF22), and by postsynaptically localized membrane protein in GCs, neuroligins (Hall et al., 2000; Scheiffele et al., 2000; Umemori et al., 2004). Furthermore, another study demonstrated the role of a cell adhesion molecule, cadherin-7 (Cdh7), expressed in MFs and GC dendrites: Cdh7 regulates MF axonal growth termination in the IGL and specific synapse formation between MFs and dendrites of GCs through homophilic binding (Kuwako et al., 2014). These molecules released from GCs or expressed in GC membranes are likely critical for synaptic formation and/or maturation not just between GCs and MF terminals originally located in the IGL but also between GCs and MF terminals that transiently make contact with PCs and are subsequently eliminated.

One of the characteristic anatomical features of GCs is that their PFs are stacked in the ML, and as a result, each of them is located in a specific sublayer of the ML. Early studies using Golgi staining suggested correlations between the locations of GC somas in the IGL and the locations of their PFs in the ML, as well as the projections of MFs originating from specific nuclei to specific sublayers of the IGL (Eccles et al., 1967; Altman, 1982), leading to the hypothesis that signals arising from MFs of different origins would be conveyed to different sublayers of the ML through activated PFs. However, later studies demonstrated no apparent correlations between GC soma locations and their PF locations (Zong et al., 2005; Wilms and Häusser, 2015; Markwalter et al., 2019; Rhee et al., 2021), which required a revisiting of this hypothesis. Recent studies using advanced labeling techniques have finally demonstrated the presence of structured synaptic connections between the specific origin of MFs and dendrites of GCs that have PFs at specific sublayers of the ML (Shuster et al., 2021; Kim et al., 2023). Furthermore, it has been suggested that such arrangement results from the synaptic formation between partners of MFs and GC dendrites that have matched developmental timing (Kim et al., 2023). Thus, the expression of the abovementioned molecules involved in synapse formation and maturation may be temporally controlled during postnatal development, contributing to the formation of a structured network.

3.4. GC–GC interaction

As described earlier in this article, GCs go through dynamic developmental processes, namely the proliferation of GCPs in the RL and the EGL, tangential migration in the EGL, radial migration through the ML and the PCL, and maturation in the IGL. The sequential expression of many molecules in developing GCs has been shown to be crucial for the development of GCs themselves (Vaudry et al., 2003; Leto et al., 2016; Lackey et al., 2018; Iulianella et al., 2019; Wang and Liu, 2019; Consalez et al., 2021). Since this article focuses on the GC-dependent regulation of cerebellar network formation, we discuss interactions of GCs that affect the development of other GCs. One likely interaction would occur during GC radial migration in the ML (Figure 2E). The N-methyl-D-aspartate (NMDA) type of glutamate receptor was shown to accelerate GC migration through

nonsynaptic activation (Komuro and Rakic, 1993). Although the sources of glutamate are not clarified, PFs may be one of them, considering that GCs migrate through previously developed PFs in the ML. GC migration is also promoted by BDNF, as mice lacking BDNF showed impaired migration (Borghesani et al., 2002). During postnatal development, *Bdnf* mRNA is expressed in GCs of the IGL (Rocamora et al., 1993). In addition, a study revealed the generation of a BDNF gradient, with increasing BDNF levels along the migration path from the EGL to the IGL, which plays a crucial role in guiding GC migration (Zhou et al., 2007). This suggests that BDNF released by previously developed GCs promotes the migration of other GCs. BDNF also appears to stimulate autocrine release of BDNF from migrating GCs, thereby further amplifying the BDNF gradient and enhancing migration (Zhou et al., 2007).

After an extensive series of cell divisions of GCPs in the outer EGL, GCPs in the inner EGL exit mitosis and commence their migration. The cell cycle exit of GCPs appears to be regulated by several kinds of molecules, such as transcriptional regulators, membrane proteins, growth factors, or signaling molecules (Penas et al., 2019; Kullmann et al., 2020; Adachi et al., 2021; Consalez et al., 2021; Miyashita et al., 2021; Van Battum et al., 2021; Zanin and Friedman, 2022; Watanabe et al., 2023). When GCPs exit the cell cycle, these molecules are presumably upregulated, while molecules involved in proliferation are downregulated. An important question arises regarding the initiation of such upregulation and downregulation. It was reported that increasing oxygen tension is a critical switch for cell cycle exit (Kullmann et al., 2020). During the early postnatal days, limited vascularization led to the expression of hypoxia-inducible factor 1α (Hif1α) in GCPs, subsequently inhibiting the differentiation of GCs. As vascularization advanced later on, these inhibitory mechanisms were downregulated. While this study offers valuable insight, the timing of vascularization alone may not fully explain the gradual GC differentiation during the initial two postnatal weeks. A study showed that GCPs proliferate in the microenvironment of the outer EGL, and migration away from such a mitogenic niche of the outer EGL promotes cell cycle exit (Choi et al., 2005), providing the possibility that signals in the outer EGL trigger the migration of GCPs toward the inner EGL and, in turn, facilitate cell cycle exit. These signals may function by reducing the expression of molecules that prevent GCP migration, such as the p75 neurotrophin receptor (Zanin and Friedman, 2022). Given the high density of proliferating GCPs in the outer EGL, such signals may be derived from the interactions between GCPs. A recent study using electron microscopy analysis revealed a unique way of interactions between developing GCs in the EGL through intercellularly connecting structures (Cordero Cervantes et al., 2023), although the functions of these structures remain to be elucidated.

4. Conclusion and perspectives

It is progressively being recognized that GCs play an important role not only as essential components for information processing in the mature cerebellum but also as critical regulators of cerebellar network construction during development. We discussed such GC-dependent regulation of cerebellar development, as summarized in Table 1. As seen in this article, the majority of the regulation is also related to, mediated by, or occurring concurrently with GCs' own development. The developmental processes of GCs are also supported by other developing components in the cerebellum, and consequently, they can reciprocally regulate each other. Thus, GCs are not only crucial regulators of cerebellar network formation. Nevertheless, it would be particularly interesting to understand how GCs contribute to the cerebellar network formation, considering three properties of GCs. First, GCs, including GCPs and PFs, occupy large areas of the cerebellar cortex throughout cerebellar development. Secondly, a substantial number of developing GCs travel dynamically from the surface to the inside of lobules. Third, GCs are the only major excitatory neurons in the cerebellar cortex. We would like to close this article by proposing four prospective research directions that could help us better understand the GC-dependent regulation of cerebellar development.

1. In our exploration of the GC-dependent regulation of cerebellar development, we have also raised remaining questions in this article. The questions include understanding the determinants of locally differential control of GCP proliferation, which in turn impact the cerebellar gross structures; elucidating the role of microdomain coupling in PF boutons for PC development; examining potential cues for MLI differentiation in the pWM; unraveling the temporal control of molecule expression that regulates MF-GC synaptic connections; and uncovering signals that dictate the cell cycle exit of GCPs. Addressing these questions would stand as a primary direction.
2. Granule cells may separately regulate the development of individual components, such as specific types of neurons or synapses, as we mostly discussed in this article. However, considering the abovementioned three properties of GCs, GCs might be appropriate regulators that systematically orchestrate the overall cerebellar network formation. Particularly, it is interesting to test whether there is coordinated network formation between the ML and IGL, and if so, whether GCs are involved in its regulation. An example of such coordination would be the structured synaptic connections between MFs originating from specific origins and dendrites of GCs having PFs in specific areas of the ML (Shuster et al., 2021; Kim et al., 2023).
3. In this article, we discussed several elements of cerebellar development, such as the development of PCs and MLIs, or the establishment of CF and MF inputs. However, there are other types of neurons and glial cells besides GCs, PCs, and MLIs (Schilling et al., 2008; Hull and Regehr, 2022), and neuromodulatory projections are also present in the cerebellum (Jaarsma et al., 1997; Li et al., 2014; Oostland and van Hooft, 2016; Zitnik et al., 2016). In addition, synaptic connections within the cerebellar cortex are more complex than previously understood (Hull and Regehr, 2022). While our understanding of the developmental regulation of other types of neurons, projections, and synaptic connections is limited at the moment, it is possible that GCs and their molecules coordinate the incorporation of these elements into cerebellar networks, taking into account the three properties of GCs stated above.
4. The involvement of GCs in certain aspects of cerebellar development could be elucidated using molecule deficits, as has been done frequently, and transcriptional analyses would

provide valuable insights into identifying prospective molecules. In general, spatiotemporal patterns of gene expression are precisely regulated during development, and such a coordinated gene expression program is critical for appropriate brain development. In other words, molecules exhibiting dynamic changes in expression during certain times are expected to function in developmental events occurring at that time. Indeed, it has been shown that the expression of many molecules required for specific GC developmental events is tightly regulated in GCs at specific developmental stages (Consalez et al., 2021). Thus, spatiotemporal expression patterns of molecules in developing GCs would provide predictions regarding the involvement of the molecules not only in GC developmental events but also in the GC-dependent regulation of cerebellar network formation. A study predicted the temporal patterns of gene expression during postnatal GC development by creating pseudotime ordering of developing GCs based on single-nucleus RNA sequencing (snRNA-seq) data (Rosenberg et al., 2018). Among the molecules with differential expression across the pseudotime, those increasing at late stages are likely critical for mature GC functions, but some of them may also contribute to cerebellar network formation, which is actively ongoing in the late postnatal developmental period. Particularly, secreted molecules and membrane molecules are interesting to be tested, considering their potential abilities for cell–cell interactions. Although the temporal patterns of individual gene expression were not analyzed, snRNA-seq was also utilized for the characterization of cell types in the human fetal cerebellum (Aldinger et al., 2021). The study demonstrated the enrichment of neurodevelopmental-disorder risk genes in multiple cell types, including GCPs and GCs, raising the possibility that molecules encoded by the GC-enriched genes may contribute to cerebellar functional development. In addition, gene expression in developmentally synchronized GCs was analyzed by *in vivo* electroporation and translating ribosomal affinity purification (Yang et al., 2016). It was demonstrated that the NuRD chromatin-remodeling complex inactivates activity-dependent genes, such as c-fos or nr4a1, around the time window of GC dendrite morphogenesis, and the inactivation of these genes indeed regulates GC dendrite pruning. Since mature GCs have only 3–5 dendrites, and thus dendrite pruning is a critical step for GC maturation, the regulation of activity-dependent genes and their downstream molecules presumably also affects synaptic formation or cerebellar network formation. Utilizing data derived from different types of gene expression analyses may lead to a deeper understanding of how GCs and their molecules regulate the development of cerebellar networks.

Author contributions

MK and SJ wrote the manuscript draft and made the figures. HP edited the manuscript and figures. YY and KT-Y conceptualized, wrote the manuscript draft, and edited the manuscript. All authors contributed to the article and approved the submitted version.

Funding

This work was supported by the KIST Institutional Program (project no.: 2E32211) and the National Research Foundation of Korea (NRF) grant funded by the Korean Ministry of Science and ICT (NRF grant nos.: 2021R1A2C3009991, 2021R1C1C2007843, and 2022R1A2C2006857).

Acknowledgments

We thank Seul gi Kang, Taehyeong Kim, and Daun Kim for valuable discussions during constructing and writing the manuscript.

Conflict of interest

The authors declare that the research was conducted in the absence of any commercial or financial relationships that could be construed as a potential conflict of interest.

Publisher's note

References

Adachi, T., Miyashita, S., Yamashita, M., Shimoda, M., Okonechnikov, K., Chavez, L., et al. (2021). Notch signaling between cerebellar granule cell progenitors. *eNeuro* 8, ENEURO.0468-20. doi: 10.1523/ENEURO.0468-20.2021

Akins, M. R., and Biederer, T. (2006). Cell–cell interactions in synaptogenesis. *Curr. Opin. Neurobiol.* 16, 83–89. doi: 10.1016/j.conb.2006.01.009

Aldinger, K. A., Thomson, Z., Phelps, I. G., Haldipur, P., Deng, M., Timms, A. E., et al. (2021). Spatial and cell type transcriptional landscape of human cerebellar development. *Nat. Neurosci.* 24, 1163–1175. doi: 10.1038/s41593-021-00872-y

Altman, J. (1982). "Morphological development of the rat cerebellum and some of its mechanisms" in *The Cerebellum—New Vistas*. ed. C.-P. S. L. Palay (Heidelberg: Springer Berlin), 8–49.

Altman, J., and Anderson, W. J. (1971). Irradiation of the cerebellum in infant rats with low-level x-ray: histological and cytological effects during infancy and adulthood. *Exp. Neurol.* 30, 492–509. doi: 10.1016/0014-4886(71)90150-6

Altman, J., Anderson, W. J., and Wright, K. A. (1969). Early effects of x-irradiation of the cerebellum in infant rats: decimation and reconstitution of the external granular layer. *Exp. Neurol.* 24, 196–216. doi: 10.1016/0014-4886(69)90015-6

Altman, J., and Winfree, A. T. (1977). Postnatal development of the cerebellar cortex in the rat. V. Spatial organization of purkinje cell perikarya. *J. Comp. Neurol.* 171, 1–16. doi: 10.1002/cne.901710102

Andrews, P. C., and Dravid, S. M. (2021). An emerging map of glutamate delta 1 receptors in the forebrain. *Neuropharmacology* 192:108587. doi: 10.1016/j.neuropharm.2021.108587

Angenstein, F., Niessen, H. G., Goldschmidt, J., Lison, H., Altrock, W. D., Gundelfinger, E. D., et al. (2007). Manganese-enhanced MRI reveals structural and functional changes in the cortex of bassoon mutant mice. *Cereb. Cortex* 17, 28–36. doi: 10.1093/cercor/bhj121

Armengol, J.-A., and Sotelo, C. (1991). Early dendritic development of Purkinje cells in the rat cerebellum. A light and electron microscopic study using axonal tracing in 'in vitro' slices. *Dev. Brain Res.* 64, 95–114. doi: 10.1016/0165-3806(91)90213-3

Bailly, Y., Rabacchi, S., Sherrard, R. M., Rodeau, J. L., Demais, V., Lohof, A. M., et al. (2018). Elimination of all redundant climbing fiber synapses requires granule cells in the postnatal cerebellum. *Sci. Rep.* 8:10017. doi: 10.1038/s41598-018-28398-7

Baptista, C. A., Hatten, M. E., Blazeski, R., and Mason, C. A. (1994). Cell-cell interactions influence survival and differentiation of purified Purkinje cells in vitro. *Neuron* 12, 243–260. doi: 10.1016/0896-6273(94)90268-2

Baur, D., Bornschein, G., Althof, D., Watanabe, M., Kulik, A., Eilers, J., et al. (2015). Developmental tightening of cerebellar cortical synaptic influx-release coupling. *J. Neurosci.* 35, 1858–1871. doi: 10.1523/JNEUROSCI.2900-14.2015

Beekhof, G. C., Osório, C., White, J. J., Van Zoomeren, S., Van Der Stok, H., Xiong, B., et al. (2021). Differential spatiotemporal development of Purkinje cell populations and cerebellum-dependent sensorimotor behaviors. *elife* 10:e63668. doi: 10.7554/eLife.63668

Ben-Arie, N., Bellen, H. J., Armstrong, D. L., Mccall, A. E., Gordadze, P. R., Guo, Q., et al. (1997). Math1 is essential for genesis of cerebellar granule neurons. *Nature* 390, 169–172. doi: 10.1038/36579

Bilovocky, N. A., Romito-Digiacomo, R. R., Murcia, C. L., Maricich, S. M., and Herrup, K. (2003). Factors in the genetic background suppress the engrailed-1 cerebellar phenotype. *J. Neurosci.* 23, 5105–5112. doi: 10.1523/JNEUROSCI.23-12-05105.2003

Borghesani, P. R., Peyrin, J. M., Klein, R., Rubin, J., Carter, A. R., Schwartz, P. M., et al. (2002). BDNF stimulates migration of cerebellar granule cells. *Development* 129, 1435–1442. doi: 10.1242/dev.129.6.1435

Cadilhac, C., Bachy, I., Forget, A., Hodson, D. J., Jahannault-Talignani, C., Furley, A. J., et al. (2021). Excitatory granule neuron precursors orchestrate laminar localization and differentiation of cerebellar inhibitory interneuron subtypes. *Cell Rep.* 34:108904. doi: 10.1016/j.celrep.2021.108904

Cameron, D. B., Kasai, K., Jiang, Y., Hu, T., Saeki, Y., and Komuro, H. (2009). Four distinct phases of basket/stellate cell migration after entering their final destination (the molecular layer) in the developing cerebellum. *Dev. Biol.* 332, 309–324. doi: 10.1016/j.ydbio.2009.05.575

Carballo, G. B., Honorato, J. R., De Lopes, G. P. F., and Spohr, T. (2018). A highlight on sonic hedgehog pathway. *Cell Commun. Signal* 16:11. doi: 10.1186/s12964-018-0220-7

Carletti, B., Williams, I. M., Leto, K., Nakajima, K., Magrassi, L., and Rossi, F. (2008). Time constraints and positional cues in the developing cerebellum regulate Purkinje cell placement in the cortical architecture. *Dev. Biol.* 317, 147–160. doi: 10.1016/j.ydbio.2008.02.005

Cerminara, N. L., Lang, E. J., Sillitoe, R. V., and Apps, R. (2015). Redefining the cerebellar cortex as an assembly of non-uniform Purkinje cell microcircuits. *Nat. Rev. Neurosci.* 16, 79–93. doi: 10.1038/nrn3886

Chang, C. H., Zanini, M., Shirvani, H., Cheng, J. S., Yu, H., Feng, C. H., et al. (2019). Atoh1 controls primary cilia formation to allow for SHH-triggered granule neuron progenitor proliferation. *Dev. Cell* 48, 184–199.e185. doi: 10.1016/j.devcel.2018.12.017

Chedotal, A., and Sotelo, C. (1993). The 'creeper stage'in cerebellar climbing fiber synaptogenesis precedes the 'pericellular nest'-ultrastructural evidence with parvalbumin immunocytochemistry. *Dev. Brain Res.* 76, 207–220. doi: 10.1016/0165-3806(93)90209-S

Chen, X., Chen, T., Dong, C., Chen, H., Dong, X., Yang, L., et al. (2022). Deletion of CHD8 in cerebellar granule neuron progenitors leads to severe cerebellar hypoplasia, ataxia, and psychiatric behavior in mice. *J. Genet. Genomics* 49, 859–869. doi: 10.1016/j.jgg.2022.02.011

Chen, C., Kano, M., Abeliovich, A., Chen, L., Bao, S., Kim, J. J., et al. (1995). Impaired motor coordination correlates with persistent multiple climbing fiber innervation in PKCγ mutant mice. *Cells* 83, 1233–1242. doi: 10.1016/0092-8674(95)90148-5

Cheng, Y., Sudarov, A., Szulc, K. U., Sgaier, S. K., Stephen, D., Turnbull, D. H., et al. (2010). The engrailed homeobox genes determine the different foliation patterns in the vermis and hemispheres of the mammalian cerebellum. *Development* 137, 519–529. doi: 10.1242/dev.027045

Choi, Y., Borghesani, P. R., Chan, J. A., and Segal, R. A. (2005). Migration from a mitogenic niche promotes cell-cycle exit. *J. Neurosci.* 25, 10437–10445. doi: 10.1523/JNEUROSCI.1559-05.2005

Consalez, G. G., Goldowitz, D., Casoni, F., and Hawkes, R. (2021). Origins, development, and compartmentation of the granule cells of the cerebellum. *Frontiers in Neural Circuits* 14:611841. doi: 10.3389/fncir.2020.611841

Cook, A. A., Jayabal, S., Sheng, J., Fields, E., Leung, T. C. S., Quilez, S., et al. (2022). Activation of TrkB-Akt signaling rescues deficits in a mouse model of SCA6. *Sci. Adv.* 8:eabh3260. doi: 10.1126/sciadv.abh3260

Cordero Cervantes, D., Khare, H., Wilson, A. M., Mendoza, N. D., Coulon-Mahdi, O., Lichtman, J. W., et al. (2023). 3D reconstruction of the cerebellar germinal layer reveals tunneling connections between developing granule cells. Science. *Advances* 9:eadf3471. doi: 10.1126/sciadv.adf3471

Corrales, J. D., Blaess, S., Mahoney, E. M., and Joyner, A. L. (2006). The level of sonic hedgehog signaling regulates the complexity of cerebellar foliation. *Development* 133, 1811–1821. doi: 10.1242/dev.02351

Corrales, J. D., Rocco, G. L., Blaess, S., Guo, Q., and Joyner, A. L. (2004). Spatial pattern of sonic hedgehog signaling through Gli genes during cerebellum development. *Development* 131, 5581–5590. doi: 10.1242/dev.01438

Crepel, F., Delhaye-Bouchaud, N., and Dupont, J. (1981). Fate of the multiple innervation of cerebellar Purkinje cells by climbing fibers in immature control, x-irradiated and hypothyroid rats. *Dev. Brain Res.* 1, 59–71. doi: 10.1016/0165-3806(81)90094-8

Dahmane, N., and Altaba, A. R. I. (1999). Sonic hedgehog regulates the growth and patterning of the cerebellum. *Development* 126, 3089–3100. doi: 10.1242/dev.126.14.3089

De Zeeuw, C. I., Lisberger, S. G., and Raymond, J. L. (2021). Diversity and dynamism in the cerebellum. *Nat. Neurosci.* 24, 160–167. doi: 10.1038/s41593-020-00754-9

Dzubay, J. A., and Otis, T. S. (2002). Climbing fiber activation of metabotropic glutamate receptors on cerebellar Purkinje neurons. *Neuron* 36, 1159–1167. doi: 10.1016/S0896-6273(02)01052-8

Eccles, J.C., Ito, M., and Szentágothai, J. (1967). *The Cerebellum as a Neuronal Machine*. Oxford, England: Springer-Verlag

Elegheert, J., Kakegawa, W., Clay, J. E., Shanks, N. F., Behiels, E., Matsuda, K., et al. (2016). Structural basis for integration of GluD receptors within synaptic organizer complexes. *Science* 353, 295–299. doi: 10.1126/science.aae0104

Elsen, G. E., Juric-Sekhar, G., Daza, R. A. M., and Hevner, R. F. (2013). "Development of cerebellar nuclei" in *Handbook of the Cerebellum and Cerebellar Disorders*. eds. M. Manto, J. D. Schmahmann, F. Rossi, D. L. Gruol and N. Koibuchi (Dordrecht: Springer Netherlands), 179–205.

Ferguson, S. A. (1996). Neuroanatomical and functional alterations resulting from early postnatal cerebellar insults in rodents. *Pharmacol. Biochem. Behav.* 55, 663–671. doi: 10.1016/S0091-3057(96)00253-5

Fink, A. J., Englund, C., Daza, R. A., Pham, D., Lau, C., Nivison, M., et al. (2006). Development of the deep cerebellar nuclei: transcription factors and cell migration from the rhombic lip. *J. Neurosci.* 26, 3066–3076. doi: 10.1523/JNEUROSCI.5203-05.2006

Flora, A., Klisch, T. J., Schuster, G., and Zoghbi, H. Y. (2009). Deletion of Atoh1 disrupts sonic hedgehog signaling in the developing cerebellum and prevents medulloblastoma. *Science* 326, 1424–1427. doi: 10.1126/science.1181453

Goldowitz, D., Cushing, R. C., Laywell, E., D'arcangelo, G., Sheldon, M., Sweet, H. O., et al. (1997). Cerebellar disorganization characteristic of reeler in scrambler mutant mice despite presence of reelin. *J. Neurosci.* 17, 8767–8777. doi: 10.1523/JNEUROSCI.17-22-08767.1997

Hall, A. C., Lucas, F. R., and Salinas, P. C. (2000). Axonal remodeling and synaptic differentiation in the cerebellum is regulated by WNT-7a signaling. *Cells* 100, 525–535. doi: 10.1016/S0092-8674(00)80689-3

Hámori, J., and Somogyi, J. (1983). Differentiation of cerebellar mossy fiber synapses in the rat: a quantitative electron microscope study. *J. Comp. Neurol.* 220, 365–377. doi: 10.1002/cne.902200402

Hashimoto, K., Ichikawa, R., Kitamura, K., Watanabe, M., and Kano, M. (2009a). Translocation of a "winner" climbing fiber to the Purkinje cell dendrite and subsequent elimination of "losers" from the soma in developing cerebellum. *Neuron* 63, 106–118. doi: 10.1016/j.neuron.2009.06.008

Hashimoto, K., and Kano, M. (2013). Synapse elimination in the developing cerebellum. *Cell. Mol. Life Sci.* 70, 4667–4680. doi: 10.1007/s00018-013-1405-2

Hashimoto, K., Yoshida, T., Sakimura, K., Mishina, M., Watanabe, M., and Kano, M. (2009b). Influence of parallel fiber–Purkinje cell synapse formation on postnatal development of climbing fiber–Purkinje cell synapses in the cerebellum. *Neuroscience* 162, 601–611. doi: 10.1016/j.neuroscience.2008.12.037

Hashizume, M., Miyazaki, T., Sakimura, K., Watanabe, M., Kitamura, K., and Kano, M. (2013). Disruption of cerebellar microzonal organization in GluD2 (GluRδ2) knockout mouse. *Frontiers in Neural Circuits* 7:130. doi: 10.3389/fncir.2013.00130

Hatten, M. E., and Heintz, N. (1995). Mechanisms of neural patterning and specification in the development cerebellum. *Annu. Rev. Neurosci.* 18, 385–408. doi: 10.1146/annurev.ne.18.030195.002125

Heckel, D., Brass, N., Fischer, U., Blin, N., Steudel, I., Türeci, O., et al. (1997). cDNA cloning and chromosomal mapping of a predicted coiled-coil proline-rich protein immunogenic in meningioma patients. *Hum. Mol. Genet.* 6, 2031–2041. doi: 10.1093/hmg/6.12.2031

Herrup, K. (1983). Role of staggerer gene in determining cell number in cerebellar cortex. I. Granule cell death is an indirect consequence of staggerer gene action. *Dev. Brain Res.* 11, 267–274. doi: 10.1016/0165-3806(83)90225-0

Herrup, K., and Sunter, K. (1987). Numerical matching during cerebellar development: quantitative analysis of granule cell death in staggerer mouse chimeras. *J. Neurosci.* 7, 829–836. doi: 10.1523/JNEUROSCI.07-03-00829.1987

Hevner, R. F. (2006). From radial glia to pyramidal-projection neuron: transcription factor cascades in cerebral cortex development. *Mol. Neurobiol.* 33, 033–050. doi: 10.1385/MN:33:1:033

Hevner, R. F., Hodge, R. D., Daza, R. A., and Englund, C. (2006). Transcription factors in glutamatergic neurogenesis: conserved programs in neocortex, cerebellum, and adult hippocampus. *Neurosci. Res.* 55, 223–233. doi: 10.1016/j.neures.2006.03.004

Hirai, H., and Launey, T. (2000). The regulatory connection between the activity of granule cell NMDA receptors and dendritic differentiation of cerebellar Purkinje cells. *J. Neurosci.* 20, 5217–5224. doi: 10.1523/JNEUROSCI.20-14-05217.2000

Hirai, H., Pang, Z., Bao, D., Miyazaki, T., Li, L., Miura, E., et al. (2005). Cbln1 is essential for synaptic integrity and plasticity in the cerebellum. *Nat. Neurosci.* 8, 1534–1541. doi: 10.1038/nn1576

Huang, E. J., and Reichardt, L. F. (2001). Neurotrophins: roles in neuronal development and function. *Annu. Rev. Neurosci.* 24, 677–736. doi: 10.1146/annurev.neuro.24.1.677

Hull, C., and Regehr, W. G. (2022). The cerebellar cortex. *Annu. Rev. Neurosci.* 45, 151–175. doi: 10.1146/annurev-neuro-091421-125115

Ibata, K., Kono, M., Narumi, S., Motohashi, J., Kakegawa, W., Kohda, K., et al. (2019). Activity-dependent secretion of synaptic organizer Cbln1 from lysosomes in granule cell axons. *Neuron* 102, 1184–1198.e1110. doi: 10.1016/j.neuron.2019.03.044

Ichikawa, R., Hashimoto, K., Miyazaki, T., Uchigashima, M., Yamasaki, M., Aiba, A., et al. (2016). Territories of heterologous inputs onto Purkinje cell dendrites are segregated by mGluR1-dependent parallel fiber synapse elimination. *Proc. Natl. Acad. Sci.* 113, 2282–2287. doi: 10.1073/pnas.1511513113

Ichikawa, R., Miyazaki, T., Kano, M., Hashikawa, T., Tatsumi, H., Sakimura, K., et al. (2002). Distal extension of climbing fiber territory and multiple innervation caused by aberrant wiring to adjacent spiny branchlets in cerebellar Purkinje cells lacking glutamate receptor δ2. *J. Neurosci.* 22, 8487–8503. doi: 10.1523/JNEUROSCI.22-19-08487.2002

Ito-Ishida, A., Kakegawa, W., Kohda, K., Miura, E., Okabe, S., and Yuzaki, M. (2014). Cbln1 downregulates the formation and function of inhibitory synapses in mouse cerebellar Purkinje cells. *Eur. J. Neurosci.* 39, 1268–1280. doi: 10.1111/ejn.12487

Iulianella, A., Wingate, R. J., Moens, C. B., and Capaldo, E. (2019). The generation of granule cells during the development and evolution of the cerebellum. *Dev. Dyn.* 248, 506–513. doi: 10.1002/dvdy.64

Jaarsma, D., Ruigrok, T. J., Caffé, R., Cozzari, C., Levey, A. I., Mugnaini, E., et al. (1997). Cholinergic innervation and receptors in the cerebellum. *Prog. Brain Res.* 114, 67–96. doi: 10.1016/S0079-6123(08)63359-2

Jensen, P., Smeyne, R., and Goldowitz, D. (2004). Analysis of cerebellar development in math1 null embryos and chimeras. *J. Neurosci.* 24, 2202–2211. doi: 10.1523/JNEUROSCI.3427-03.2004

Jensen, P., Zoghbi, H. Y., and Goldowitz, D. (2002). Dissection of the cellular and molecular events that position cerebellar Purkinje cells: a study of the math1 null-mutant mouse. *J. Neurosci.* 22, 8110–8116. doi: 10.1523/JNEUROSCI.22-18-08110.2002

Joo, W., Hippenmeyer, S., and Luo, L. (2014). Dendrite morphogenesis depends on relative levels of NT-3/TrkC signaling. *Science* 346, 626–629. doi: 10.1126/science.1258996

Kano, M., Hashimoto, K., Kurihara, H., Watanabe, M., Inoue, Y., Aiba, A., et al. (1997). Persistent multiple climbing fiber innervation of cerebellar purkinje cells in mice lacking mGluR1. *Neuron* 18, 71–79. doi: 10.1016/S0896-6273(01)80047-7

Kano, M., Hashimoto, K., Watanabe, M., Kurihara, H., Offermanns, S., Jiang, H., et al. (1998). Phospholipase Cβ4 is specifically involved in climbing fiber synapse elimination in the developing cerebellum. *Proc. Natl. Acad. Sci.* 95, 15724–15729. doi: 10.1073/pnas.95.26.15724

Kano, M., Watanabe, T., Uesaka, N., and Watanabe, M. (2018). Multiple phases of climbing fiber synapse elimination in the developing cerebellum. *Cerebellum* 17, 722–734. doi: 10.1007/s12311-018-0964-z

Kapfhammer, J. P. (2004). Cellular and molecular control of dendritic growth and development of cerebellar Purkinje cells. *Prog. Histochem. Cytochem.* 39, 131–182. doi: 10.1016/j.proghi.2004.07.002

Kashiwabuchi, N., Ikeda, K., Araki, K., Hirano, T., Shibuki, K., Takayama, C., et al. (1995). Impairment of motor coordination, Purkinje cell synapse formation, and cerebellar long-term depression in GluRδ2 mutant mice. *Cells* 81, 245–252. doi: 10.1016/0092-8674(95)90334-8

Kawamura, A., Katayama, Y., Kakegawa, W., Ino, D., Nishiyama, M., Yuzaki, M., et al. (2021). The autism-associated protein CHD8 is required for cerebellar development and motor function. *Cell Rep.* 35:108932. doi: 10.1016/j.celrep.2021.108932

Kim, J. C., Cook, M. N., Carey, M. R., Shen, C., Regehr, W. G., and Dymecki, S. M. (2009). Linking genetically defined neurons to behavior through a broadly applicable silencing allele. *Neuron* 63, 305–315. doi: 10.1016/j.neuron.2009.07.010

Kim, T., Park, H., Tanaka-Yamamoto, K., and Yamamoto, Y. (2023). Developmental timing-dependent organization of synaptic connections between mossy fibers and granule cells in the cerebellum. *Communications Biology* 6:446. doi: 10.1038/s42003-023-04825-y

Komuro, H., and Rakic, P. (1993). Modulation of neuronal migration by NMDA receptors. *Science* 260, 95–97. doi: 10.1126/science.8096653

Konno, K., Matsuda, K., Nakamoto, C., Uchigashima, M., Miyazaki, T., Yamasaki, M., et al. (2014). Enriched expression of GluD1 in higher brain regions and its involvement in parallel fiber–interneuron synapse formation in the cerebellum. *J. Neurosci.* 34, 7412–7424. doi: 10.1523/JNEUROSCI.0628-14.2014

Kullmann, J. A., Trivedi, N., Howell, D., Laumonnerie, C., Nguyen, V., Banerjee, S. S., et al. (2020). Oxygen tension and the VHL-Hif1α pathway determine onset of neuronal polarization and cerebellar germinal zone exit. *Neuron* 106, 607–623.e5. doi: 10.1016/j.neuron.2020.02.025

Kurihara, H., Hashimoto, K., Kano, M., Takayama, C., Sakimura, K., Mishina, M., et al. (1997). Impaired parallel fiber→ Purkinje cell synapse stabilization during cerebellar development of mutant mice lacking the glutamate receptor δ2 subunit. *J. Neurosci.* 17, 9613–9623. doi: 10.1523/JNEUROSCI.17-24-09613.1997

Kusch, V., Bornschein, G., Loreth, D., Bank, JJordan, J., Baur, D., et al. (2018). Munc13-3 is required for the developmental localization of ca(2+) channels to active zones and the Nanopositioning of ca(v)2.1 near release sensors. *Cell Rep.* 22, 1965–1973. doi: 10.1016/j.celrep.2018.02.010

Kuwako, K.-I., Nishimoto, Y., Kawase, S., Okano, H. J., and Okano, H. (2014). Cadherin-7 regulates mossy fiber connectivity in the cerebellum. *Cell Rep.* 9, 311–323. doi: 10.1016/j.celrep.2014.08.063

La Manno, G., Siletti, K., Furlan, A., Gyllborg, D., Vinsland, E., Mossi Albiach, A., et al. (2021). Molecular architecture of the developing mouse brain. *Nature* 596, 92–96. doi: 10.1038/s41586-021-03775-x

Lackey, E. P., Heck, D. H., and Sillitoe, R. V. (2018). Recent advances in understanding the mechanisms of cerebellar granule cell development and function and their contribution to behavior. *F1000 faculty reviews* 7:F1000 Faculty Rev-1142. doi: 10.12688/f1000research.15021.1

Lauder, J. M., Altman, J., and Krebs, H. (1974). Some mechanisms of cerebellar foliation: effects of early hypo-and hyperthyroidism. *Brain Res.* 76, 33–40. doi: 10.1016/0006-8993(74)90511-3

Legué, E., Gottshall, J. L., Jaumouillé, E., Roselló-Díez, A., Shi, W., Barraza, L. H., et al. (2016). Differential timing of granule cell production during cerebellum development underlies generation of the foliation pattern. *Neural Dev.* 11, 1–14. doi: 10.1186/s13064-016-0072-z

Legué, E., Riedel, E., and Joyner, A. L. (2015). Clonal analysis reveals granule cell behaviors and compartmentalization that determine the folded morphology of the cerebellum. *Development* 142, 1661–1671. doi: 10.1242/dev.120287

Lejeune, E., Dortdivanlioglu, B., Kuhl, E., and Linder, C. (2019). Understanding the mechanical link between oriented cell division and cerebellar morphogenesis. *Soft Matter* 15, 2204–2215. doi: 10.1039/C8SM02231C

Leto, K., Arancillo, M., Becker, E. B., Buffo, A., Chiang, C., Ding, B., et al. (2016). Consensus Paper: Cerebellar Development. *Cerebellum* 15, 789–828. doi: 10.1007/s12311-015-0724-2

Leto, K., Bartolini, A., Yanagawa, Y., Obata, K., Magrassi, L., Schilling, K., et al. (2009). Laminar fate and phenotype specification of cerebellar GABAergic interneurons. *J. Neurosci.* 29, 7079–7091. doi: 10.1523/JNEUROSCI.0957-09.2009

Leto, K., Carletti, B., Williams, I. M., Magrassi, L., and Rossi, F. (2006). Different types of cerebellar GABAergic interneurons originate from a common pool of multipotent progenitor cells. *J. Neurosci.* 26, 11682–11694. doi: 10.1523/JNEUROSCI.3656-06.2006

Leto, K., Rolando, C., and Rossi, F. (2012). The genesis of cerebellar GABAergic neurons: fate potential and specification mechanisms. *Front. Neuroanat.* 6:6. doi: 10.3389/fnana.2012.00006

Lewis, P. M., Gritli-Linde, A., Smeyne, R., Kottmann, A., and Mcmahon, A. P. (2004). Sonic hedgehog signaling is required for expansion of granule neuron precursors and patterning of the mouse cerebellum. *Dev. Biol.* 270, 393–410. doi: 10.1016/j.ydbio.2004.03.007

Li, B., Zhu, J.-N., and Wang, J.-J. (2014). Histaminergic afferent system in the cerebellum: structure and function. *Cerebellum & Ataxias* 1:5. doi: 10.1186/2053-8871-1-5

Lorenz, A., Deutschmann, M., Ahlfeld, J., Prix, C., Koch, A., Smits, R., et al. (2011). Severe alterations of cerebellar cortical development after constitutive activation of Wnt signaling in granule neuron precursors. *Mol. Cell. Biol.* 31, 3326–3338. doi: 10.1128/MCB.05718-11

Ma, Y., Smith, D., Hof, P. R., Foerster, B., Hamilton, S., Blackband, S. J., et al. (2008). In vivo 3D digital atlas database of the adult C57BL/6J mouse brain by magnetic resonance microscopy. *Front. Neuroanat.* 2:2008. doi: 10.3389/neuro.05.001.2008

Magdaleno, S., Keshvara, L., and Curran, T. (2002). Rescue of ataxia and preplate splitting by ectopic expression of Reelin in reeler mice. *Neuron* 33, 573–586. doi: 10.1016/S0896-6273(02)00582-2

Mariani, J., Crepel, F., Mikoshiba, K., Changeux, J.-P., and Sotelo, C. (1977). Anatomical, physiological and biochemical studies of the cerebellum from Reeler mutant mouse. *Decennial index* 281, 1–28. doi: 10.1098/rstb.1977.0121

Markwalter, K. H., Yang, Y., Holy, T. E., and Bonni, A. (2019). Sensorimotor coding of vermal granule neurons in the developing mammalian cerebellum. *J. Neurosci.* 39, 6626–6643. doi: 10.1523/JNEUROSCI.0086-19.2019

Matsuda, K., Miura, E., Miyazaki, T., Kakegawa, W., Emi, K., Narumi, S., et al. (2010). Cbln1 is a ligand for an orphan glutamate receptor delta2, a bidirectional synapse organizer. *Science* 328, 363–368. doi: 10.1126/science.1185152

Miale, I. L., and Sidman, R. L. (1961). An autoradiographic analysis of histogenesis in the mouse cerebellum. *Exp. Neurol.* 4, 277–296. doi: 10.1016/0014-4886(61)90055-3

Mikoshiba, K., Nagaike, K., Kohsaka, S., Takamatsu, K., Aoki, E., and Tsukada, Y. (1980). Developmental studies on the cerebellum from reeler mutant mouse in vivo and in vitro. *Dev. Biol.* 79, 64–80. doi: 10.1016/0012-1606(80)90073-1

Miyashita, S., Owa, T., Seto, Y., Yamashita, M., Aida, S., Sone, M., et al. (2021). Cyclin D1 controls development of cerebellar granule cell progenitors through phosphorylation and stabilization of ATOH1. *EMBO J.* 40:e105712. doi: 10.15252/embj.2020105712

Miyata, T., Nakajima, K., Aruga, J., Takahashi, S., Ikenaka, K., Mikoshiba, K., et al. (1996). Distribution of a reeler gene-related antigen in the developing cerebellum: an immunohistochemical study with an allogeneic antibody CR-50 on normal and reeler mice. *J. Comp. Neurol.* 372, 215–228. doi: 10.1002/(SICI)1096-9861(19960819)372:2<215::AID-CNE5>3.0.CO;2-6

Miyata, T., Nakajima, K., Mikoshiba, K., and Ogawa, M. (1997). Regulation of Purkinje cell alignment by reelin as revealed with CR-50 antibody. *J. Neurosci.* 17, 3599–3609. doi: 10.1523/JNEUROSCI.17-10-03599.1997

Miyata, T., Ono, Y., Okamoto, M., Masaoka, M., Sakakibara, A., Kawaguchi, A., et al. (2010). Migration, early axonogenesis, and Reelin-dependent layer-forming behavior of early/posterior-born Purkinje cells in the developing mouse lateral cerebellum. *Neural Dev.* 5:23. doi: 10.1186/1749-8104-5-23

Mody, M., Cao, Y., Cui, Z., Tay, K.-Y., Shyong, A., Shimizu, E., et al. (2001). Genome-wide gene expression profiles of the developing mouse hippocampus. *Proc. Natl. Acad. Sci.* 98, 8862–8867. doi: 10.1073/pnas.141244998

Morrison, M. E., and Mason, C. A. (1998). Granule neuron regulation of Purkinje cell development: striking a balance between neurotrophin and glutamate signaling. *J. Neurosci.* 18, 3563–3573. doi: 10.1523/JNEUROSCI.18-10-03563.1998

Offermanns, S., Hashimoto, K., Watanabe, M., Sun, W., Kurihara, H., Thompson, R. F., et al. (1997). Impaired motor coordination and persistent multiple climbing fiber innervation of cerebellar Purkinje cells in mice lacking Gαq. *Proc. Natl. Acad. Sci.* 94, 14089–14094. doi: 10.1073/pnas.94.25.14089

Oostland, M., and Van Hooft, J. A. (2016). "Serotonin in the cerebellum" in *Essentials of Cerebellum and Cerebellar Disorders: A Primer For Graduate Students*. eds. D. L. Gruol, N. Koibuchi, M. Manto, M. Molinari, J. D. Schmahmann and Y. Shen (Cham: Springer International Publishing), 243–247.

Orvis, G. D., Hartzell, A. L., Smith, J. B., Barraza, L. H., Wilson, S. L., Szulc, K. U., et al. (2012). The engrailed homeobox genes are required in multiple cell lineages to coordinate sequential formation of fissures and growth of the cerebellum. *Dev. Biol.* 367, 25–39. doi: 10.1016/j.ydbio.2012.04.018

Ozol, K., Hayden, J. M., Oberdick, J., and Hawkes, R. (1999). Transverse zones in the vermis of the mouse cerebellum. *J. Comp. Neurol.* 412, 95–111. doi: 10.1002/(SICI)1096-9861(19990913)412:1<95::AID-CNE7>3.0.CO;2-Y

Park, H., Kim, T., Kim, J., Yamamoto, Y., and Tanaka-Yamamoto, K. (2019). Inputs from sequentially developed parallel fibers are required for cerebellar organization. *Cell Rep.* 28, 2939–2954.e5. doi: 10.1016/j.celrep.2019.08.010

Park, H., Yamamoto, Y., and Tanaka-Yamamoto, K. (2021). Refinement of cerebellar network organization by extracellular signaling during development. *Neuroscience* 462, 44–55. doi: 10.1016/j.neuroscience.2020.05.036

Pei, Y., Brun, S. N., Markant, S. L., Lento, W., Gibson, P., Taketo, M. M., et al. (2012). WNT signaling increases proliferation and impairs differentiation of stem cells in the developing cerebellum. *Development* 139, 1724–1733. doi: 10.1242/dev.050104

Penas, C., Maloof, M. E., Stathias, V., Long, J., Tan, S. K., Mier, J., et al. (2019). Time series modeling of cell cycle exit identifies Brd4 dependent regulation of cerebellar neurogenesis. *Nat. Commun.* 10:3028. doi: 10.1038/s41467-019-10799-5

Petzoldt, A. G., and Sigrist, S. J. (2014). Synaptogenesis. *Curr. Biol.* 24, R1076–R1080. doi: 10.1016/j.cub.2014.10.024

Prestori, F., Mapelli, L., and D'angelo, E. (2019). Diverse neuron properties and complex network dynamics in the cerebellar cortical inhibitory circuit. *Front. Mol. Neurosci.* 12:267. doi: 10.3389/fnmol.2019.00267

Rahimi-Balaei, M., Afsharinezhad, P., Bailey, K., Buchok, M., Yeganeh, B., and Marzban, H. (2015). Embryonic stages in cerebellar afferent development. *Cerebellum & ataxias* 2:7. doi: 10.1186/s40673-015-0026-y

Rakic, P., and Sidman, R. (1973). Weaver mutant mouse cerebellum: defective neuronal migration secondary to abnormality of Bergmann glia. *Proc. Natl. Acad. Sci.* 70, 240–244. doi: 10.1073/pnas.70.1.240

Reddy, N. C., Majidi, S. P., Kong, L., Nemera, M., Ferguson, C. J., Moore, M., et al. (2021). CHARGE syndrome protein CHD7 regulates epigenomic activation of enhancers in granule cell precursors and gyrification of the cerebellum. *Nat. Commun.* 12:5702. doi: 10.1038/s41467-021-25846-3

Reeber, S. L., White, J. J., George-Jones, N. A., and Sillitoe, R. V. (2013). Architecture and development of olivocerebellar circuit topography. *Frontiers in neural circuits* 6:115. doi: 10.3389/fncir.2012.00115

Rezai, Z., and Yoon, C. H. (1972). Abnormal rate of granule cell migration in the cerebellum of "weaver" mutant mice. *Dev. Biol.* 29, 17–26. doi: 10.1016/0012-1606(72)90039-5

Rhee, J. K., Park, H., Kim, T., Yamamoto, Y., and Tanaka-Yamamoto, K. (2021). Projection-dependent heterogeneity of cerebellar granule cell calcium responses. *Mol. Brain* 14, 1–17. doi: 10.1186/s13041-021-00773-y

Rice, D. S., and Curran, T. (2001). Role of the reelin signaling pathway in central nervous system development. *Annu. Rev. Neurosci.* 24, 1005–1039. doi: 10.1146/annurev.neuro.24.1.1005

Rico, B., Xu, B., and Reichardt, L. F. (2002). TrkB receptor signaling is required for establishment of GABAergic synapses in the cerebellum. *Nat. Neurosci.* 5, 225–233. doi: 10.1038/nn808

Rocamora, N., García-Ladona, F. J., Palacios, J. M., and Mengod, G. (1993). Differential expression of brain-derived neurotrophic factor, neurotrophin-3, and low-affinity nerve growth factor receptor during the postnatal development of the rat cerebellar system. *Brain Res. Mol. Brain Res.* 17, 1–8. doi: 10.1016/0169-328X(93)90065-W

Rosenberg, A. B., Roco, C. M., Muscat, R. A., Kuchina, A., Sample, P., Yao, Z., et al. (2018). Single-cell profiling of the developing mouse brain and spinal cord with split-pool barcoding. *Science* 360, 176–182. doi: 10.1126/science.aam8999

Ryan, K. E., Kim, P. S., Fleming, J. T., Brignola, E., Cheng, F. Y., Litingtung, Y., et al. (2017). Lkb1 regulates granule cell migration and cortical folding of the cerebellar cortex. *Dev. Biol.* 432, 165–177. doi: 10.1016/j.ydbio.2017.09.036

Saito, S., Matoba, R., Ueno, N., Matsubara, K., and Kato, K. (2002). Comparison of gene expression profiling during postnatal development of mouse dentate gyrus and cerebellum. *Physiol. Genomics* 8, 131–137. doi: 10.1152/physiolgenomics.00077.2001

Sassoè-Pognetto, M., and Patrizi, A. (2017). The Purkinje cell as a model of synaptogenesis and synaptic specificity. *Brain Res. Bull.* 129, 12–17. doi: 10.1016/j.brainresbull.2016.10.004

Scheiffele, P., Fan, J., Choih, J., Fetter, R., and Serafini, T. (2000). Neuroligin expressed in nonneuronal cells triggers presynaptic development in contacting axons. *Cells* 101, 657–669. doi: 10.1016/S0092-8674(00)80877-6

Schiffmann, S. N., Bernier, B., and Goffinet, A. M. (1997). Reelin mRNA expression during mouse brain development. *Eur. J. Neurosci.* 9, 1055–1071. doi: 10.1111/j.1460-9568.1997.tb01456.x

Schilling, K., Oberdick, J., Rossi, F., and Baader, S. L. (2008). Besides Purkinje cells and granule neurons: an appraisal of the cell biology of the interneurons of the cerebellar cortex. *Histochem. Cell Biol.* 130, 601–615. doi: 10.1007/s00418-008-0483-y

Schmidt, H. (2019). Control of presynaptic parallel Fiber efficacy by activity-dependent regulation of the number of occupied release sites. *Front. Syst. Neurosci.* 13:30. doi: 10.3389/fnsys.2019.00030

Shuster, S. A., Wagner, M. J., Pan-Doh, N., Ren, J., Grutzner, S. M., Beier, K. T., et al. (2021). The relationship between birth timing, circuit wiring, and physiological response properties of cerebellar granule cells. *Proc. Natl. Acad. Sci.* 118:e2101826118. doi: 10.1073/pnas.2101826118

Sillitoe, R. V. (2016). Mossy fibers terminate directly within Purkinje cell zones during mouse development. *Cerebellum* 15, 14–17. doi: 10.1007/s12311-015-0712-6

Simat, M., Ambrosetti, L., Lardi-Studler, B., and Fritschy, J. M. (2007). GABAergic synaptogenesis marks the onset of differentiation of basket and stellate cells in mouse cerebellum. *Eur. J. Neurosci.* 26, 2239–2256. doi: 10.1111/j.1460-9568.2007.05846.x

Smeyne, R. J., and Goldowitz, D. (1989). Development and death of external granular layer cells in the weaver mouse cerebellum: a quantitative study. *J. Neurosci.* 9, 1608–1620. doi: 10.1523/JNEUROSCI.09-05-01608.1989

Sotelo, C., and Rossi, F. (2013). "Purkinje cell migration and differentiation" in *Handbook of the Cerebellum and Cerebellar Disorders*. eds. M. Manto, J. D. Schmahmann, F. Rossi, D. L. Gruol and N. Koibuchi (Dordrecht: Springer Netherlands), 147–178.

Stevanovic, M., Drakulic, D., Lazic, A., Ninkovic, D. S., Schwirtlich, M., and Mojsin, M. (2021). SOX transcription factors as important regulators of neuronal and glial differentiation during nervous system development and adult neurogenesis. *Front. Mol. Neurosci.* 14:654031. doi: 10.3389/fnmol.2021.654031

Sudarov, A., and Joyner, A. L. (2007). Cerebellum morphogenesis: the foliation pattern is orchestrated by multi-cellular anchoring centers. *Neural Dev.* 2, 26–22. doi: 10.1186/1749-8104-2-26

Takeda, H., Kameo, Y., Yamaguchi, T., Nakajima, K., and Adachi, T. (2021). Cerebellar foliation via non-uniform cell accumulation caused by fiber-guided migration of granular cells. *Journal of Biomechanical Science and Engineering* 16:516. doi: 10.1299/jbse.20-00516

Takeo, Y. H., Shuster, S. A., Jiang, L., Hu, M. C., Luginbuhl, D. J., Rülicke, T., et al. (2021). GluD2- and Cbln1-mediated competitive interactions shape the dendritic arbors of cerebellar Purkinje cells. *Neuron* 109, 629–644.e628. doi: 10.1016/j.neuron.2020.11.028

Thompson, C. L., Ng, L., Menon, V., Martinez, S., Lee, C.-K., Glattfelder, K., et al. (2014). A high-resolution spatiotemporal atlas of gene expression of the developing mouse brain. *Neuron* 83, 309–323. doi: 10.1016/j.neuron.2014.05.033

Uemura, T., Lee, S. J., Yasumura, M., Takeuchi, T., Yoshida, T., Ra, M., et al. (2010). Trans-synaptic interaction of GluRdelta2 and Neurexin through Cbln1 mediates synapse formation in the cerebellum. *Cells* 141, 1068–1079. doi: 10.1016/j.cell.2010.04.035

Umemori, H., Linhoff, M. W., Ornitz, D. M., and Sanes, J. R. (2004). FGF22 and its close relatives are presynaptic organizing molecules in the mammalian brain. *Cells* 118, 257–270. doi: 10.1016/j.cell.2004.06.025

Van Battum, E., Heitz-Marchaland, C., Zagar, Y., Fouquet, S., Kuner, R., and Chédotal, A. (2021). Plexin-B2 controls the timing of differentiation and the motility of cerebellar granule neurons. *elife* 10:e60554. doi: 10.7554/eLife.60554

Van Der Heijden, M. E., Lackey, E. P., Perez, R., Işleyen, F. S., Brown, A. M., Donofrio, S. G., et al. (2021). Maturation of Purkinje cell firing properties relies on neurogenesis of excitatory neurons. *elife* 10:e68045. doi: 10.7554/eLife.68045

Vaudry, D., Falluel-Morel, A., Leuillet, S., Vaudry, H., and Gonzalez, B. J. (2003). Regulators of cerebellar granule cell development act through specific signaling pathways. *Science* 300, 1532–1534. doi: 10.1126/science.1085260

Wang, L., and Liu, Y. (2019). Signaling pathways in cerebellar granule cells development. *Am J Stem Cells* 8, 1–6.

Wang, X.-T., Zhou, L., Cai, X.-Y., Xu, F.-X., Xu, Z.-H., Li, X.-Y., et al. (2021). Deletion of Mea6 in cerebellar granule cells impairs synaptic development and motor performance. *Frontiers in Cell and Developmental Biology* 8:627146. doi: 10.3389/fcell.2020.627146

Watanabe, H., Fukuda, A., Ikeda, N., Sato, M., Hashimoto, K., and Miyamoto, Y. (2023). Syndecan-3 regulates the time of transition from cell cycle exit to initial differentiation stage in mouse cerebellar granule cell precursors. *Brain Res.* 1807:148317. doi: 10.1016/j.brainres.2023.148317

Wefers, A. K., Haberlandt, C., Tekin, N. B., Fedorov, D. A., Timmermann, A., Van Der Want, J. J., et al. (2017). Synaptic input as a directional cue for migrating interneuron precursors. *Development* 144, 4125–4136. doi: 10.1242/dev.154096

Wen, J., Yang, H. B., Zhou, B., Lou, H. F., and Duan, S. (2013). β-Catenin is critical for cerebellar foliation and lamination. *PLoS One* 8:e64451. doi: 10.1371/journal.pone.0064451

Wetmore, C., Ernfors, P., Persson, H., and Olson, L. (1990). Localization of brain-derived neurotrophic factor mRNA to neurons in the brain by in situ hybridization. *Exp. Neurol.* 109, 141–152. doi: 10.1016/0014-4886(90)90068-4

Wilms, C. D., and Häusser, M. (2015). Reading out a spatiotemporal population code by imaging neighbouring parallel fibre axons in vivo. *Nat. Commun.* 6:6464. doi: 10.1038/ncomms7464

Yacubova, E., and Komuro, H. (2002). Stage-specific control of neuronal migration by somatostatin. *Nature* 415, 77–81. doi: 10.1038/415077a

Yamada, T., Yang, Y., Hemberg, M., Yoshida, T., Cho, H., Murphy, J. P., et al. (2014). Promoter decommissioning by the NuRD chromatin remodeling complex triggers synaptic connectivity in the mammalian brain. *Neuron* 83, 122–134. doi: 10.1016/j.neuron.2014.05.039

Yang, Y., Yamada, T., Hill, K. K., Hemberg, M., Reddy, N. C., Cho, H. Y., et al. (2016). Chromatin remodeling inactivates activity genes and regulates neural coding. *Science* 353, 300–305. doi: 10.1126/science.aad4225

Yasumura, M., Yoshida, T., Lee, S. J., Uemura, T., Joo, J. Y., and Mishina, M. (2012). Glutamate receptor δ1 induces preferentially inhibitory presynaptic differentiation of cortical neurons by interacting with neurexins through cerebellin precursor protein subtypes. *J. Neurochem.* 121, 705–716. doi: 10.1111/j.1471-4159.2011.07631.x

Zanin, J. P., and Friedman, W. J. (2022). p75NTR prevents the onset of cerebellar granule cell migration via RhoA activation. *elife* 11:e79934. doi: 10.7554/eLife.79934

Zhou, P., Porcionatto, M., Pilapil, M., Chen, Y., Choi, Y., Tolias, K. F., et al. (2007). Polarized signaling endosomes coordinate BDNF-induced chemotaxis of cerebellar precursors. *Neuron* 55, 53–68. doi: 10.1016/j.neuron.2007.05.030

Zitnik, G., Chandler, D. J., and Waterhouse, B. D. (2016). "Norepinephrine and synaptic transmission in the cerebellum" in *Essentials of Cerebellum and Cerebellar Disorders: A Primer For Graduate Students*. eds. D. L. Gruol, N. Koibuchi, M. Manto, M. Molinari, J. D. Schmahmann and Y. Shen (Cham: Springer International Publishing), 237–241.

Zong, H., Espinosa, J. S., Su, H. H., Muzumdar, M. D., and Luo, L. (2005). Mosaic analysis with double markers in mice. *Cells* 121, 479–492. doi: 10.1016/j.cell.2005.02.012

Frontiers in
Molecular Neuroscience

Leading research into the brain's molecular structure, design and function

Part of the most cited neuroscience series, this journal explores and identifies key molecules underlying the structure, design and function of the brain across all levels.

Discover the latest Research Topics

See more →

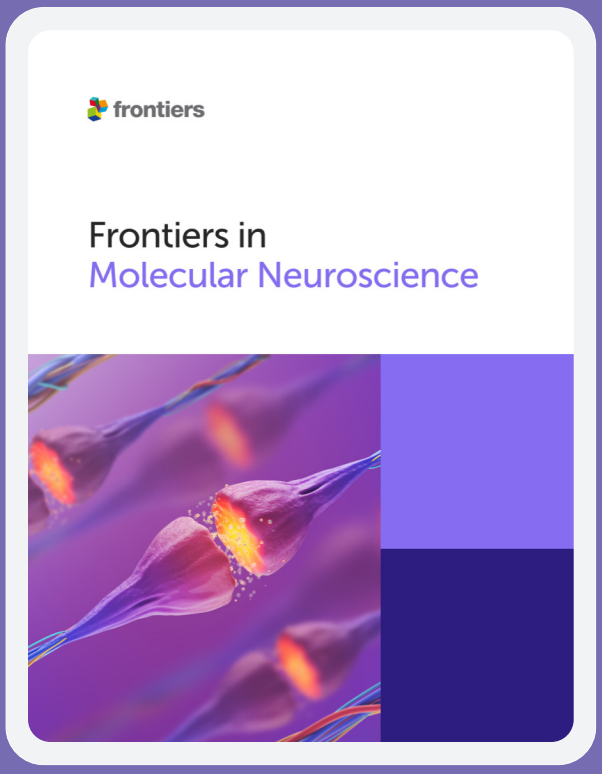

Frontiers

Avenue du Tribunal-Fédéral 34
1005 Lausanne, Switzerland
frontiersin.org

Contact us

+41 (0)21 510 17 00
frontiersin.org/about/contact